Is multiplicity universal? A study of multiplicity in the young moving groups

Submitted by Paul Michael Elliott to the University of Exeter as a thesis for the degree of Doctor of Philosophy in Physics, April 2016

I certify that all material in this thesis which is not my own work has been identified and that no material has previously been submitted and approved for the award of a degree by this or any other University.

Signature:

Abstract

The young moving groups are collections of nearby ($<$200 pc), young (5-150 Myr) pre-main sequence stars; these stars offer us one of the best opportunities to characterise stellar multiplicity, sub-stellar phenomena, disc evolution and planet formation.

Here we present results from a series of multiplicity studies aimed at producing comprehensive multiplicity statistics of the young moving groups. The aim was to compare the derived statistics of the young moving groups to other populations in order to investigate whether the abundance and properties of multiple systems are environment-independent.

We have combined high-resolution spectroscopy, AO-imaging and direct imaging to identify and characterise multiple systems across a huge range of orbital periods (1-10^{10} day). The observational techniques also allow us to constrain the abundance of multiple systems in these populations by calculating detection limits.

We found many similarities (frequency of spectroscopic binaries; frequency, mass-ratio and physical separation of visual binaries) between the young moving groups and both younger and older regions, for multiple systems with physical separations smaller than 1000 au. We did, however, identify a significant number of new wide ($>$1000 au) companions. We reconciled the apparent excess of wide binary systems, when compared to the field population, by arguing that the wide systems are weakly bound and most likely decaying. By comparing the multiplicity statistics in one particular moving group we showed that the dynamical evolution of non-hierarchical protostars could lead to the population of wide binaries we can observe today.

Our results indicate that the majority of low-mass stars form in small groups with 3 or 4 components that undergo significant dynamical evolution. The multiplicity properties of the young nearby moving groups are statistically similar to many other populations, supporting the environment-independent formation of multiple systems.

Contents

List of Figures

List of Tables

Acknowledgements

I am grateful to Dr. Michael West for replying to my rather hopeful email enquiring about a short term project back in 2011, which was really the beginning of my PhD journey. Following on from that, I am indebted to Prof. Amelia Bayo, who accepted a nervous, long-haired undergraduate student to work with her for a mere 5 weeks, before putting up with me for another 3.5 years. I am incredibly grateful and appreciative for all the support and guidance Amelia has given me through my PhD. She has always pushed me to learn more in all disciplines, to be thorough in my science, to look at the bigger picture and to be ambitious. Without her I would not be half the scientist I am today, so thank you. Thank you to to Dr. Claudio Melo for all his words of wisdom both in and out of the field of science that always helped me to put everything into context and kept me *compos mentis* in times of trouble. I am very grateful to Dr. Andrei Tokovinin for the visit in 2015 which pushed me to vastly improve the way I conduct my scientific analysis. Thank you to the University of Exeter (Prof. Isabelle Baraffe) and to ESO (Dr. Claudio Melo) for allowing me to continue on in Chile after my second year had ended. This was a rather unusual move; however, I feel like it was the right decision, and I hope this is reflected in the work presented here.

In a way I have lived many different lives in Chile, however, one continuous entity has been ESO. There is an amazing group of people working there (past and present), and I want to thank a few of them by name here. Thank you to Paulina Jirón for personally taking such good care of us helpless (and at times hopeless) students. Thank you to Dimitri, Tomasz, Kalle, Claudia, Matt, JK, Romain and Big Giacomo for making it so much fun to live and work in Chile. Big thanks to the crazy guys in and out of ESO that are Elyar, Adrien, Oli, Little Giacomo, Liz and Catherine – we had some good times and I hope we will have some more. Thank you to Chile for making my life so amazing for 3.5 years.

Last, but by no means least, I would like to thank my mum, my dad, my sisters and my grandparents. A special thank you to my sisters who have always taken care of their baby brother. If it weren't for my one of my sisters' compulsion to travel to Chile I would never have begun on this journey. And if it weren't for my grandparents' generosity I would never have been able to afford the flight to get there.

I am very lucky to be in the position I'm in and to be surrounded by such amazing people, so thank you all.

Paul Elliott,
13th April 2016

Disclaimer

Parts of this thesis have been previously published as outlined below:

Chapter 2 is an expanded and updated version of the published paper 'Search for associations containing young stars (SACY). V. Is multiplicity universal? Tight multiple systems', Elliott, P.; Bayo, A.; Melo, C. H. F.; Torres, C. A. O.; Sterzik, M.; Quast, G. R., 2014, A&A, 568, A26.

Chapter 3 is an expanded and updated version of the published paper 'Search for associations containing young stars (SACY). VI. Is multiplicity universal? Stellar multiplicity in the range 3-1000 au from adaptive-optics observations', Elliott, P.; Huélamo, N.; Bouy, H.; Bayo, A.; Melo, C. H. F.; Torres, C. A. O.; Sterzik, M. F.; Quast, G. R.; Chauvin, G.; Barrado, D., 2015, A&A, 580, A88.

Chapter 4 is an expanded and updated version of the published paper 'Search for associations containing young stars (SACY). VII. New stellar and sub-stellar candidate members in the young associations', Elliott, P.; Bayo, A.; Melo, C. H. F.; Torres, C. A. O.; Sterzik, M.; Quast, G. R.; Montes, D.; Brahm, R., 2016, A&A, 590, A13.

Chapter 5 is an expanded and updated version of the published paper 'The crucial role of higher-order multiplicity: A case study using the β-Pictoris moving group', Elliott, P. & Bayo, A, accepted for publication in MNRAS, 18 April 2016 [ArXiv ID: 1604.06094]

The data reduction and analysis presented in these papers were performed solely by the author, who also wrote the text in its entirety. The co-authors provided valuable guidance, discussions, critiques and comments along the way.

Signature: 

“Look mum, no hands”

A young boy on a bike, back in the day.

Chapter 1

Introduction

What can the study of stellar multiplicity tell us about how stars form? In a way stars, and stellar multiple systems, are fossils of the star formation process. In the same way that fossils need to form and be found, cleaned and analysed, so do single and multiple stars in a population. It is very important to appreciate that the stars we observe today may have evolved significantly from the time of their birth, similar to the aged fossils hidden on Earth.

Forming them: First of all stars need to form from the vast clouds of dust and gas that make up the interstellar medium. *Finding them:* Once the stars have formed, they need to be observed and linked to a certain population by their colour, magnitude, spectroscopic features and kinematics. Given that many multiple systems are in fact unresolved (due to the pixel scale of instrumentation), finding them is not as straight forward as it may first appear. However, the dedicated study of their variation in colour, brightness and position, sometimes over years, decades and centuries, allows us to confirm their origin and multiple system structure. *Cleaning the data:* Astronomical data does not have infinite precision, and therefore we are always limited by the instruments we use to observe the stars. Additionally, the majority of observational facilities are ground-based, which adds its own atmospheric signature to the data we collect. We reduce the data to the best of our abilities and look for bound companions but below a certain threshold (defined by the physical separation and companion mass), we

have no further knowledge. Therefore our knowledge of the multiple system structure is always an approximation of true physical structure. *Analysing them:* With this population of identified stars and stellar multiple systems we then try to understand what processes could form such a population. The main caveat is that what we observe today is not necessarily the *direct* outcome of star formation. There are many physical processes that can alter the multiplicity properties of a population; it is by no means constant. Our analyses must factor in these processes before we conclude on the formation of these objects.

In this section we[1] hope to summarise the four steps outlined above for the targets that are the main focus of this thesis, multiple systems in the young moving groups. The brief outline of theoretical works regarding the formation and evolution of multiple systems is by no means comprehensive. It, rather, acts to introduce the basic mechanisms, physical scales and potential outcomes of the different processes.

1.1 From cores to stars

The formation of a star involves a huge transformation of scale: from a cloud of density $\rho \sim 10^{-20}\,\mathrm{g\,cm^{-3}}$ transforming eventually to a star of $\rho \sim 1\,\mathrm{g\,cm^{-3}}$, in the case of our Sun (Schulz, 2005). There is a very complex interplay of physical processes that are involved in this transformation, and our understanding of star formation is still very much in progress. One of the outstanding problems is the formation of binary/multiple systems. The mechanisms involved in the formation and evolution of such systems are discussed below.

[1]Throughout this thesis the plural form is used for stylistic reasons. However, the written text is solely the author's and the work presented has been lead by the author, in collaboration with the listed co-authors of each chapter.

1.1.1 Formation of primordial multiple systems

It is generally accepted that almost 50% of low-mass stars are in multiple systems (Duquennoy and Mayor, 1991; Raghavan et al., 2010; Tokovinin, 2014a,b), and this rate of multiplicity is likely even higher at younger ages [Tobin et al., 2016; Chen et al., 2013, Chapter 5]; therefore, we need to understand how these system can form.

The formation of these systems requires fragmentation of the collapsing cloud. These modes can be divided into two types: prompt fragmentation (Boss, 1986) and disc fragmentation (Bonnell and Bate, 1994; Stamatellos and Whitworth, 2009). Prompt fragmentation refers to fragmentation of the collapsing cloud core due to local over-densities (Burkert and Bodenheimer, 1993; Padoan and Nordlund, 2002, 2004; Offner et al., 2010). The typical physical scales of this mode are $\sim$1000 au; however, the initial separations between protostars can be significantly altered via migration. Disc fragmentation takes place in a star-disc system, whereby the disc fragments due to density perturbations. Due to the spatial extent of the disc these companions are formed within $\sim$100 au (Bonnell and Bate, 1994; Hayfield et al., 2011; Zhu et al., 2012).

It is important to emphasise that the typical physical separations and masses of companions can be, and most likely have been, altered significantly between the time of their birth and the T-Tauri[2] stage of evolution. This interplay of many physical processes is extremely complex and is what leads to the somewhat stochastic nature of multiple system formation.

Below we discuss the properties and evolution of close ($\lesssim$100 au) binary systems. Although wide binary systems, formed via prompt fragmentation, are important, the properties of closer systems are more intimately linked because of their accretion history (Bate, 2000; Zhao et al., 2013). Additionally, close companions have the most impact on subsequent evolution, such as proto-planetary disc evolution and planet formation.

[2]Named after the star T Tau, this stage of evolution is when the star has emerged from its parental cloud and is observable at visible wavelengths. The star can still be actively accreting although it has gained almost all of its mass.

1.2 The properties and evolution of close binaries

There are a number of potential formation channels for close binary systems. The closest systems ($<$10 au) cannot form directly via either prompt or disc fragmentation. The smallest separation a primordial binary system could have is $\approx$10 au, due to the size of the first core ($\approx$5 au, Larson, 1969; Vaytet et al., 2012). However, in all observed T-Tauri and main sequence populations there are a significant number of binaries with these separations. The components of these systems must have undergone significant migration to be orbiting at such small separations. The processes responsible for this migration can significantly alter the evolutionary paths of these systems, compared to stars formed in isolation. Below we outline the formation and properties of close binaries and the effect companions can have on subsequent disc evolution.

1.2.1 Formation channels and properties

As mentioned in Section 1.1.1, disc fragmentation is one way to form close binary systems. The closest systems can then evolve from these initial separations via accretion, gravitational torques and dynamical interactions to closer separations (Bate et al., 2002). For example, the dynamical interactions between 3 or more components in an unstable configuration can form an inner binary with a bound tertiary component, or even eject the tertiary component altogether (Reipurth and Mikkola, 2012). This is discussed further in Chapter 5. If a bound system is formed this is also a formation channel for wider multiple systems. Additionally, a stable binary can be perturbed by a third body, another member of the star cluster. Through an exchange interaction, the physical separation of the binary can decrease, thus forming a close a binary system.

The mass-ratios and system configurations formed through the different formation channels can also differ. For example, systems formed via accretion are more likely to be equal mass (Bate, 2000), although more recent simulations including magnetic fields by Zhao et al. (2013) found that this growth via accretion of the secondary was quite severely suppressed. Binaries formed via dynamical interactions could be preferentially

observed in triple system configurations (discussed further in Chapter 5). These processes are taking place simultaneously, and therefore disentangling them observationally is very difficult. However, these close binary systems should reflect the properties of accretion much more closely than wider companions formed via prompt fragmentation.

1.2.2 Effect on subsequent disc evolution

There are two types of discs that can form in binary systems: circumstellar (around one or both components of the system) and circumbinary (one disc around the binary system). Below we consider the form and evolution of both types of discs and their potential to form planets.

1.2.2.1 Circumbinary discs and planets

Circumbinary discs can be found in very close ($\lesssim$1 au) systems. One famous example is the disc around the V4046 Sgr binary (0.04 au separation, 2.4 day period, Quast et al., 2000). This is an actively accreting member of the β-Pictoris moving group with a gaseous disc (Rodriguez et al., 2010). The main features of circumbinary discs from theory are inner cavities with a radii $\sim$2–3 times the semi-major axis (Artymowicz and Lubow, 1994) and density perturbations in discs, induced by the orbit of the binary (Artymowicz and Lubow, 1996; de Val-Borro et al., 2011). These features are yet to be observed in any significant number of systems, firstly due to the small number of known circumbinary disc systems, and secondly because of the current resolution of instruments. However, the Atacama Large Millimeter/submillimeter Array (ALMA)[3] has the power to resolve such features in the future with millimetre interferometric imaging.

The perturbations in the disc manifest themselves as asymmetries in the disc density profile, creating spiral arm features. Ruge et al. (2015) showed that ALMA should be able to resolve these features in close ($<$140 pc) face-on binary systems. Additionally,

[3] `http://www.almaobservatory.org/en/home`

this work showed that the eccentricity and mass-ratio of the system can significantly alter the form of these disc perturbations. Density perturbations can also be induced via other mechanisms such as planet-disc interactions (Gonzalez et al., 2012) and photo-evaporation (Espaillat et al., 2012). Therefore, having a comprehensive understanding of the effect of stellar companions is crucial for a full and comprehensive picture of circumbinary evolution.

Although the protoplanetary disc may be significantly truncated in these systems, there is emerging evidence that the frequency of circumbinary planets may not differ significantly from circumstellar planets. Doyle et al. (2011); Welsh et al. (2012) and Dupuy et al. (2016) all reported circumbinary planet detections, with Welsh et al. (2012) claiming a $\sim$1 % frequency of giant planets in circumbinary systems, although a comprehensive statistical analysis is still missing.

1.2.2.2 Circumstellar discs and planets

Circumstellar discs are found around single stars and wider ($>$1 au) multiple systems. One very interesting case is when the companion is in an orbit of comparable size to the expected size of the protoplanetary disc. In these scenarios, one would expect there should be significant interaction between the two; indeed, previous studies have shown that protoplanetary disc evolution and planet formation in low-mass stars are significantly altered by close companions (Holman and Wiegert, 1999; Jang-Condell et al., 2007; Kraus et al., 2012; Harris et al., 2012).

Artymowicz and Lubow (1994) showed that the outer edge of a circumprimary disc should be truncated at $\approx$1/3 of the semi-major of the binary, in a nearly circular orbit. However, some works have argued that as long as this disc is replenished by the surrounding envelope, that this may not be significant in the evolution of the disc (Bouvier et al., 1997; Mathieu et al., 2000).

One very dramatic effect of a close companion is the disc dispersal timescale. There is an increasing wealth of evidence that suggests that multiple systems with companions

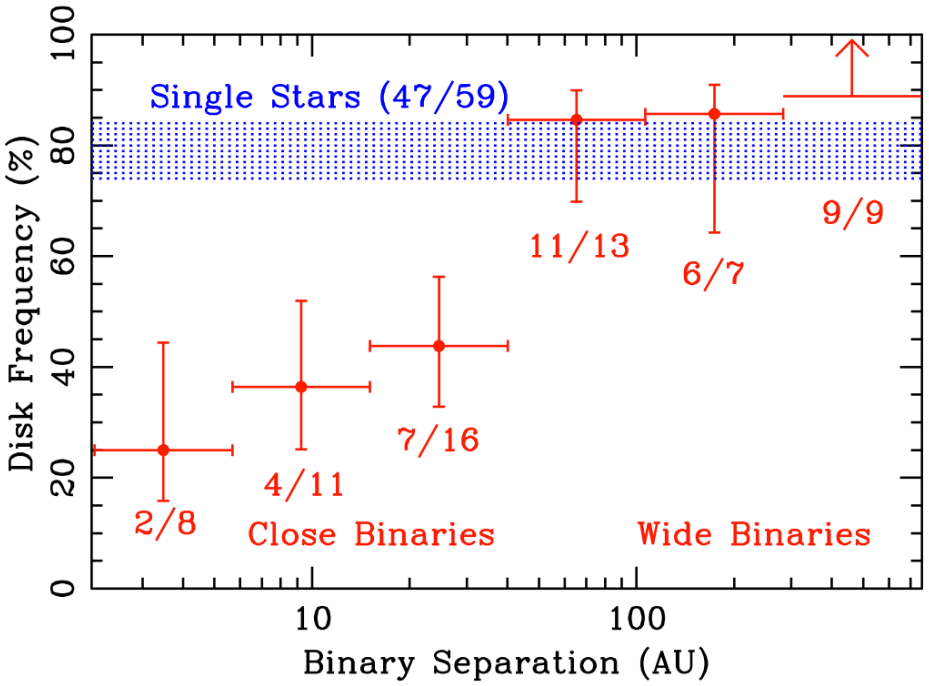

FIGURE 1.1: Binary separation versus disc frequency for binaries in the Taurus-Auriga association (Kraus et al., 2012), used with permission.

$<$100 au disperse their primordial discs much faster than single stars (Kraus et al., 2012; Daemgen et al., 2016). Figure 1.1 is taken from Kraus et al. (2012) and shows the binary separation versus disc frequency for identified multiple systems and single stars in the Taurus region: for systems with companions $\leq$40 au, 40-1000 au and single stars the derived disc frequencies were 39^{+9}_{-7} %, 90^{+3}_{-8} % and 80^{+4}_{-6} %, respectively. They suggest that close binary systems disperse their discs within $\lesssim$1 Myr after the end of the envelope accretion.

The recent work of Rodriguez et al. (2015) studied the effect of multiplicity on debris discs from an *unbiased* sample presented in Phillips et al. (2010). They found that only 1/50 (2%) and 2/61 (3%) systems, with companions between 1-10 and 10-100 au respectively, had dusty discs. For systems with companions between 1000-10,000 au the fraction was 5/22 (23%), and comparable to that of single stars ($\approx$20 %). These results are, again, strong evidence for faster disc dispersal in close binary systems.

Faster disc dispersal in close binary systems could potentially result in a paucity of giant planets due to their formation timescale (although the time scale of gas giants could be much shorter ($<$1 Myr) than previously thought Bitsch et al., 2015). Indeed there is

some observational evidence that this is the case. Wang et al. (2015) showed that, of a sample of giant planet-hosting stars, 0^{+5} % had companions $<$20 au, compared to 34$\pm$8% with companions 20-200 au and 12$\pm$2 % for a control sample. This suggests that planet formation is heavily suppressed for separations $<$20 au, but could play a significant role in the migration of the planets for separations between 20-200 au. However, Jang-Condell (2015) analysed a number of giant planet-hosting binary systems with stellar companions orbiting at $\approx$10-20 au. She showed that even with truncated discs these systems had stable enough conditions to form their planets either via core accretion or disc instability.

The disc dispersal timescale also affects the spin evolution of a star, which is intimately linked with its angular momentum evolution. Stars can interact with their accretion discs through the so-called *disc-locking* mechanism, which prevents them from spinning up, even though they are contracting towards the main-sequence (Bouvier et al., 1997; Gallet and Bouvier, 2013). It must be said that a comprehensive model of angular momentum evolution is extremely complex, and must include the effect of stellar winds and internal processes, that can redistribute angular momentum in the stellar interior[4].

However, considering disc-locking alone, systems with close companions should start spinning up earlier than single stars, and should have faster rotational periods. Analysis from the RACE-OC series of papers (Messina et al., 2010) has shown mixed results so far when comparing spin rates of close binaries and wider companions in the young β-Pictoris moving group (Messina et al., 2014, 2016). Statistical analysis on a larger sample is underway.

1.3 Dynamics of multiple systems in a population

In the previous sections we have concentrated on the birth and evolution of multiple systems, predominantly binaries, but we have not considered the effect of other cluster

[4]For a recent in-depth review of angular momentum evolution in low-mass stars and brown dwarfs see Bouvier et al. (2014)

members. As mentioned at the beginning of this introduction, the multiple systems we observe today are not necessarily in the same configuration as when they were formed. The dominant factor in shaping the properties of the entire populations of stars we observe is N-body dynamics. As stars typically form in large clusters (Lada and Lada, 2003), members formed from different cores are likely to interact to some degree, depending on the spatial density of stars. These interactions can have a variety of outcomes, from member ejection to the formation of hierarchical multiple systems. Understanding the role of N-body dynamics in populations of single and multiple stars is crucial. We need to be able to *reverse engineer* evolved populations to some extent, in order to understand the likely primordial population that initially formed.

Generally speaking, binaries can be divided into two categories: hard and soft (Heggie, 1975; Hills, 1975). Hard binaries are very tightly bound and any encounter with a third body is very unlikely to significantly perturb or destroy the system; soft binaries, on the other hand, are more susceptible to perturbation or destruction from encounters. The destruction of binaries depends on three main quantities: the energy of the binary, the energy of the encounter and the rate of encounters (Reipurth et al., 2014). Therefore, given an approximate calculation of the density of a region and its velocity dispersion, one can calculate the hard-soft boundary and use this to define a *pristine* – free of significant dynamical processing – parameter space of physical separations (Goodwin, 2010). However, the history of the region's density is usually unknown, and this can significantly shift the hard-soft boundary (Parker et al., 2009). That said, it is clear to see that the companions orbiting at the largest separations are the most likely to be disrupted and destroyed.

As well as being disrupted and destroyed by N-body dynamics, multiple systems can also potentially be formed via gravitational capture (Kouwenhoven et al., 2010; Moeckel and Bate, 2010). As the cluster dissolves two members can share extremely similar velocities and form a bound system, and each of these *two* members could themselves be binaries. This mechanism depends on the number of stars in the cluster and the dispersion velocities.

It is also important to reiterate that there can be significant dynamical interactions between components in non-hierarchical primordial triple (or higher-order) systems (Reipurth and Mikkola, 2012), as was mentioned previously in Section 1.2.1. This mechanism can operate very early on in the fragmentation process ($<$0.1 Myr). However, observationally distinguishing between multiple systems formed via the different formation channels is extremely challenging.

From this discussion of the physical processes associated with multiple system formation and destruction, it is easy to see that entire populations need to be studied in order to make any firm conclusions. We therefore need to define a set of derivable properties in order to describe multiplicity.

1.4 Statistics used in multiplicity studies

There are many ways to describe the multiplicity properties of a population. However, there are some standard statistics and distributions that are used in many works (see Duchêne and Kraus, 2013). These properties are referred to and discussed extensively in the work presented here, and therefore deserve a clear definition and outline of their advantages and disadvantages. The reader must keep in mind the limits in parameter space that the properties describe: for example, a population can have different multiplicity frequency (*MF*) values in different physical separation parameter spaces. Where appropriate, the limits of the considered parameter spaces are shown as super- and sub-script descriptions.

1.4.1 Common statistics

Arguably the most basic of the statistics used to describe a population's multiplicity properties are the multiplicity frequency (*MF*), the triple frequency (*TF*) and the companion-star frequency (*CSF*) defined by:

$$MF = \frac{B + T + Qu + Qi + ...}{S + B + T + Qu + Qi + ...} \tag{1.1}$$

$$TF = \frac{T}{S + B + T + Qu + Qi + ...} \tag{1.2}$$

$$CSF = \frac{B + 2T + 3Qu + 4Qi + ...}{S + B + T + Qu + Qi + ...} \tag{1.3}$$

where S, B, T, Qu and Qi represent the number of single, binary, triple, quadruple and quintuple systems, respectively.

In many previous works, and in much of the analysis presented here, the *MF* statistic is used and analysed in more detail than the *CSF*. The *MF* is arguably the most robust multiplicity quantity as it is unaffected by newly resolved components leading to higher-order multiplicity within a system. A system, whether it is a binary or a quintuple, adds a 1 to both the numerator and denominator to the *MF* quantity. Equally, information of higher-order systems is lost within the *MF* quantity. Therefore, given a high level of detection completeness, the *CSF* offers more information about a population's multiplicity.

The *TF* statistic is a probe of higher-order multiplicity (specifically the frequency of triple systems), and is somewhat of a halfway-house between the *MF* and the *CSF* statistics. It is usually only used in imaging studies where the number of triple systems is small but still worthy of comparison.

Better still is a hierarchical breakdown (*HB*) of the type of multiple systems i.e. the relative frequency of binary, triple, quadruple systems in a population, defined by:

$$HB = \frac{S : B : T : Qu : Qi : ...}{S + B + T + Qu + Qi + ...} \tag{1.4}$$

Strictly speaking, this not a statistic but, rather, a description of a population. It is not commonly used in multiplicity works because it relies on a high level of detection

completeness over a large parameter space which is hard to achieve. However, works such as Raghavan et al. (2010); Kraus et al. (2011); Tokovinin (2014a,b) and Tobin et al. (2016) have managed to derive this breakdown due to the extensive detection completeness of their surveys.

1.4.2 Distributions

The common statistics described above only deal with the initial identification of multiple systems within a population, but we however, want to characterise the properties of the systems themselves. Below we outline the distributions that are used to conduct this analysis.

1.4.2.1 Mass-ratio

The mass-ratio ($q = M_b/M_a$) distribution ($f(q)$) describes the distribution of mass in each multiple system, over the entire population. A power law distribution ($f(q) \propto q^{\gamma}$) is usually used to characterise this distribution. Masses of multiple system components are usually model-based due to the timescale of significant orbital motion. However, the mass-ratio quantity is fairly robust; the largest uncertainty comes from further potential unresolved companions.

In higher-order systems the mass-ratio quantity can be defined in several ways, depending on what the definition of the *primary star* is. For example, in a triple system consisting of an inner binary and a wider, tertiary companion, the M_a quantity can either be defined as the total mass of the inner binary or the mass of the more massive component. In the analysis presented here, in order to maintain the mass-ratio quantity between 0 and 1, the *primary star* is defined as the more massive component.

1.4.2.2 Period and physical separation

As mentioned above, for the majority of multiple systems the timescale of significant orbital motion is very large. This makes the determination of a system's period (P) very difficult, and therefore in most cases this quantity is approximated from the system's projected physical separation (a^*). The quantities are related by Kepler's third law:

$$P = \sqrt{a^{*3}/(M_a + M_b)} \tag{1.5}$$

where a^* is the projected physical separation in astronomical units (au), M_a and M_b are the masses of the components in the multiple system in solar masses ($M_\odot$) and P the period of the system in years.

The a^* quantity is an estimation for the orbital semi-major axis (a). On a statistical basis, this estimation should not have a significant effect on the physical separation distributions derived in this work (Brandeker et al., 2006).

The physical separation distribution can be combined with the *MF* and *CSF* quantities by normalising the distribution by the number of systems studied in the population. This way a distinction can be made between a population with the same physical separation distribution form but a higher or lower frequency within the entire studied sample.

1.4.2.3 Eccentricity

The eccentricity (e) of a system is only derivable with multiple observations of a system showing significant orbital motion. For this reason, it is very difficult to produce eccentricity distributions of an entire population of stars, especially when considering wider multiple systems ($a \gtrsim 10$ au, $P \gtrsim 30$ yr). However, it is a very important distribution as it can tell us about the formation, bound / unbound state and dynamical evolution of the multiple system.

The recent work of Tokovinin and Kiyaeva (2016) presented a statistical analysis of the eccentricity distribution based on a comparison between the speed of the relative orbital motion (μ) and the angle (γ) of the orbital motion relative to the vector joining the components. This analysis showed that even for systems with long periods ($P \gtrsim 350$ yr, $a \gtrsim 50$ au) it is possible to study the eccentricities statistically.

In the analysis presented in this work we do not produce eccentricity distributions as there are too few systems with multi-epoch data that would make this quantity derivable[5]. However, it is very important to note their importance, especially in older, higher-order systems where dynamical mechanisms such as the Kozai-cycles with tidal friction (KCTF, Eggleton and Kisseleva-Eggleton, 2006) mechanism can significantly alter orbital parameters.

1.5 State of the art of statistical multiplicity studies

In order to make robust conclusions using the statistics and distributions outlined above we need to study large populations of stars. This allows us to reduce our statistical uncertainties and probe the underlying distributions. Below, we outline the *ideal* properties of a stellar population for a primordial[6] multiplicity study:

1. Volume-limited, large number of stars (ideally $>$1000 stars, for typical statistical uncertainties $<$1 %).
2. Primary stars in the sample have approximately the same mass (in this thesis we are concerned with *solar-type stars* – $\approx$0.2-2.0 $M_{\odot}$).
3. The sample is comprised of stars that have experienced the same environmental effects.

[5] GAIA (Lindegren et al., 2008) is expected to resolve many binary systems with angular separations $>$1-2 mas and produce full orbital solutions.

[6] Primordial refers to the components of a system that formed at the same birth site as opposed to dynamically captured components.

TABLE 1.1: A summary of previous stellar multiplicity studies ordered by the age of the region.

Region	Age (Myr)	Dist. (pc)	Ref.	*N*	Sep. (au)
Various	0.01-0.1	$<$500	Chen et al. (2013)	33	50-5000
Perseus	0.01-0.1	$\approx$250	Tobin et al. (2016)	94	15-10,000
Ophiuchus	0.3	$\approx$140	Ratzka et al. (2005)	158	17-830
Taurus	1-2	$\approx$140	Kraus et al. (2011)	117	3-5000
Taurus	1-2	$\approx$140	Leinert et al. (1993)	104	18-1820
ONC	$<$1	450	Reipurth et al. (2007)	781	62-620
ONC	$<$1	450	Kounkel et al. (2016)	129	100-1000
CrA	1-9	$\approx$130	Köhler et al. (2008)	49	17-774
Cha I	2	160	Lafrenière et al. (2008)	126	16-960
IC 348	2	320	Duchêne (1999)	66	32-2530
η-Cha	6-8	97	Brandeker et al. (2006)	17	5-1300
U Sco	11	145	Köhler et al. (2000)	118	19-870
The field	$\sim$1000	$\leq$22	Duquennoy and Mayor (1991)	164	0.01-100,000
The field	$\sim$1000	$\leq$25	Raghavan et al. (2010)	454	0.01-100,000
The field	$\sim$1000	$\leq$67	Tokovinin (2014a,b)	4847	0.01-100,000

4. Young, *dynamically pristine* region, i.e., the components of multiple systems have had little time to interact with both other components in the multiple system and other members of the star-forming region.

5. Close to the Sun to allow the derivation of orbital parameters (most importantly M_a, M_b, a, P and e) over a large parameter space (1–10^{10} day) and on the shortest possible timescale.

In reality it is often not possible to have all of these properties in one population and therefore one has to make compromises. In Table 1.1 we summarise recent multiplicity works, focussed on solar-type stars.

Table 1.1 shows the various properties and limits of each survey and sample. For example, the recent survey of Tobin et al. (2016) is the largest and most complete multiplicity survey of Class 0 sources. Such surveys have only become possible very recently due to the advent of large millimetre arrays (The Very Large Array (VLA), ALMA) allowing for much higher resolution. However, this survey is still limited to a relatively low number of objects ($<$100 in total) and to physical separations as small

as 15 au. In contrast, the volume-limited sample of Tokovinin (2014a,b) studied 4847 targets in total, down to separations $<$0.01 au, making the statistics extremely robust. However, the history of field objects is not well constrained and the overall population is the result of many different clusters with different dynamical histories. There is always some degree of compromise in the statistical studies, but our knowledge improves as more and more data are collated and compared.

1.5.1 The current status of multiplicity for solar-type stars

Below, we outline the conclusions from previous statistical studies to date along with some remaining open questions. These have been adapted from similar points presented in Duchêne and Kraus (2013), a review of multiplicity.

Conclusions:

- The overall multiplicity properties of a population are set at the pre-main sequence stage or before.
- No single population has a thermal eccentricity distribution, $f(e) = 2e$.
- No single population has a mass-ratio distribution that is compatible with random pairing from the initial mass function (IMF) distribution.
- There does not appear to be a firm upper limit on the separation of two components in a multiple system, although extremely wide systems are rare.

Open questions:

- Are multiplicity properties universal, or do they depend on the native environment?
- How are spectroscopic binaries formed and what is the timescale for this formation?

- How are extremely wide systems formed and what is their fate?
- What effect does multiplicity have on disc evolution and planet formation?

Even now, combining all previous statistical surveys, it is not possible to conclude with certainty whether the multiplicity properties of a population are universal. This is due to the compromises discussed previously in this section. In the work presented here we hope to present a strong case for the universality of the overall multiplicity properties in a population.

Most surveys (excluding the volume-limited surveys conducted for field objects) use only one observing technique to study multiplicity in a specific region. However, multiplicity at the smallest scales (spectroscopic binaries, $a < 1$ au) is not necessarily isolated from multiplicity at the largest scales (common proper motion pairs $\approx$100,000 au). In fact, as discussed previously, they are most likely inherently linked.

The next section describes the origin, progress and current status of the young moving groups (the sample used in the analysis presented in this thesis). We outline the advantages of multiplicity studies using these targets over previously studied young star-forming regions.

1.6 The young moving groups

The young moving groups or young associations are groups of stars that share similar 3D motion but are not necessarily spatially clustered on the sky, due to their proximity (typically $<$100 pc) and age (5-100 Myr). As Torres et al. (2008) highlighted, Orion at 50 pc would cover almost the entire sky. Their age and proximity also mean that they are no longer embedded in their natal cloud, unlike spatially-clustered younger star-forming regions (Taurus, Orion), and they have drifted a significant difference from their original birth site. This drift distance is important for the identification of very wide binaries (see Chapter 4). All of these properties make them ideal for studies of multiplicity, disc evolution and searching for planets.

1.6.1 A brief history

In the late 1970s, and continuing through the 1980s, astronomers started to find so-called *isolated* T-Tauri stars at high galactic latitudes: stars that did not seem to belong to any nearby cloud complexes. Famous examples of such objects are TW-Hya (Herbig, 1978) and V4046-Sgr (a double-lined spectroscopic binary) (Herbig, 1978; de La Reza et al., 1986).

Amongst the first to report that these objects could be kinematically related, due to their similar radial velocities, was de la Reza et al. (1989). Since then, this handful of isolated T-Tauri stars has increased dramatically. In the 1990s the Pico dos Dias survey (PDS) was conducted (Gregorio-Hetem et al., 1992; Torres et al., 1995). Candidates for spectroscopic follow up were reported from identifying optical counterparts to sources in the Infrared Astronomical Satellite (IRAS) point source catalogue. However, this method only identified targets that are still embedded in material from their parental cloud or have strong infrared excess from surrounding circumstellar material: many pre-main sequence objects with ages $>$10 Myr have dissipated the majority of their circumstellar material, and therefore do not show any strong emission at infrared wavelengths.

The census of members dramatically increased with the seminal work of Torres et al. (2006) presenting the Search for Associations Containing Young Stars (SACY) dataset. Candidates were initially identified from a cross-match of X-ray sources[7] (the ROSAT all-sky survey, Voges et al., 1999) with optical sources (HIPPARCOS ESA, 1997, Tycho-2 Høg et al., 2000). They were followed up with high resolution spectroscopy, similar to candidates from the PDS. The spectroscopic observations provide signatures of youth (lithium absorption, H_α emission) and the radial component of the targets' motion. Using the latter, combined with either a photometric distance or parallactic distance and proper motion, one can calculate the 3D galactic velocity of the target (see Figure 5 of

[7]Walter (1986) was one of the first works to show so-called post T-Tauri stars have enhanced X-ray activity.

Torres et al., 2006). In this way, both the youth and kinematics of the objects are studied, which helps to define which moving group[8], if any, a young object belongs to.

There are now hundreds of bonafide members (Kastner et al., 1997; Zuckerman et al., 2004; Torres et al., 2006, 2008; Malo et al., 2013; Murphy and Lawson, 2015) in several distinct moving groups, see Figure 1.2 and Table 1.2.

1.6.2 Advancements in member identification

The methods to identify new members of the young moving groups have also developed significantly. A common theme is the initial identification of candidates from photometry (ultra-violet – Bianchi et al., 2011; visible – GSC, TYC, URAT1: Lasker et al., 2008; Høg et al., 2000; Zacharias et al., 2015; near-infrared – 2MASS: Cutri et al., 2003; mid-infrared – WISE Wright et al., 2010) and proper motion – NOMAD, PPMXL, UCAC4: Zacharias et al., 2005; Roeser et al., 2010; Zacharias et al., 2012). These are then followed up with spectroscopy to identify features consistent with youth and, where possible, compute radial velocities.

One of biggest challenges now is to identify low-mass members of the young moving groups. The initial methods used to identify young stars were very limited in the spectral types of stars they could detect due to the sensitivities of the surveys. If the initial mass function (IMF) of the young moving groups is similar in form (a power-law for masses $> 1\,M_\odot$ (α=-2.35, Salpeter, 1955) and a log-normal (μ=0.2 $M_\odot$, σ=0.6 log($M_\odot$), Chabrier, 2003) for masses smaller than 1 $M_\odot$) to other star-forming regions then there are still hundreds sub-stellar members missing.

Many authors have tried to find these *missing* members, utilising a whole host of available catalogues. In particular, many ($>$200) new late-type ($\geq$M5) candidate members have been identified in the BANYAN All-Sky Survey (BASS) catalogue (Gagné et al., 2015). This survey combined the 2MASS and WISE catalogues with proper motion

[8]Quite often moving groups are referred to as *loose associations* or solely *associations*: these terms are interchangeable in this work.

TABLE 1.2: A summary of the young moving groups studied in this thesis

Ass.	Ass. ID	Age (Myr)	Age ref.	Dist. (pc)	No. of members
AB Dor	ABD	100-150	2,7	49±29	110
Argus	ARG	40-44	1,7	111±47	77
β-Pic	BPC	21-26	1,3,4,7	43±20	73
Carina	CAR	35-45	1,3,7	97±39	50
Columba	COL	35-42	1,3,7	78±25	79
ϵ-Cha	ECH	5-10	1,5,7	106±9	36
Octans	OCT	30-40	1,6,7	111±42	63
Tuc-Hor	THA	33-45	1,3,7	51±10	187
TW Hydrae	TWA	10-12	1,3,7	56±14	27

References. 1: Torres et al. (2006), 2: da Silva et al. (2009), 3: Bell et al. (2015), 4: Binks and Jeffries (2014), 5: Murphy et al. (2013), 6: Murphy and Lawson (2015), 7: Torres et al. in prep.

measurements, outside the plane of the galaxy ($|b| > 15^{\circ}$). High probability candidate members were identified from this list using the statistical tool BANYAN II[9] (Bayesian Analysis for Nearby Young AssociatioNs), which computes membership probabilities based on Bayesian inference. This is a very active area of research and there is a steady stream of works identifying and characterising new very low-mass members. For example, in April 2016 alone, there were 3 independent works with details of potential new members (Weinberger et al., 2016; Kellogg et al., 2016; Schneider et al., 2016).

Kraus et al. (2014) focussed on one specific young moving group, Tuc-Hor, and identified 129 new late-type (SpT = K3-M6) members. The number of bonafide members before that study was 58, therefore significantly increasing the population. Again, the initial candidates were selected from a combination of optical and near-infrared photometry and proper motions, and followed up with spectroscopy.

In part of the analysis presented in this thesis (Chapter 4), we have combined the 2MASS catalogue with proper motion catalogues to identify new members (the majority of which are sub-stellar) around bonafide members. The advantage over many other searches is that the initial candidates are only based on two properties: near-infrared photometry (J, H, K) and proper motion. Thanks to the completeness of the 2MASS

[9] `http://www.astro.umontreal.ca/~gagne/banyanII.php`

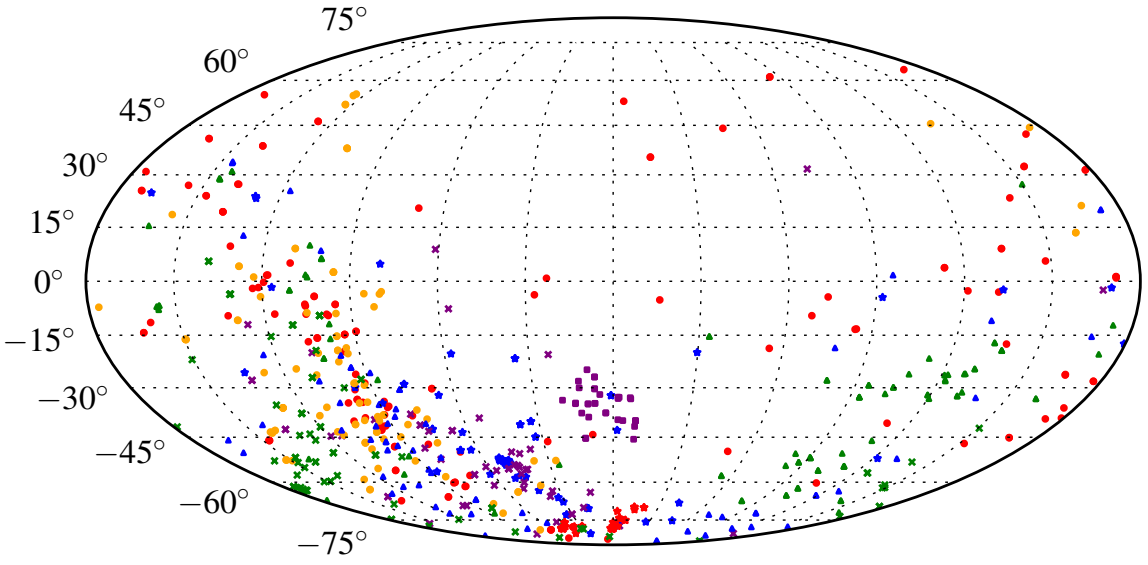

FIGURE 1.2: Spatial distribution of the bonafide and candidate member targets in 9 young moving groups. AB Doradus: red circles, Argus: blue stars, β-Pic moving group: green triangles, Carina: purple crosses, Columba: orange circles, ϵ-Cha: red stars, Octans: blue triangles, Tuc-Hor: green crosses and TW Hydrae: purple squares.

catalogue, this uncovers many new candidate members that would be missed if further cross-matched with other catalogues. However, arguably, it could increase the number of false-positives; this is explored in Chapter 4.

It is difficult and telescope-time consuming to identify and spectroscopically confirm a significant number of these sub-stellar members; however, the community has made a lot of progress in the last decade. A complete census of the young moving groups would enable us to study their spatial structure which is inherently linked to their birth and subsequent dynamical evolution. The precise astrometry from the GAIA mission (Lindegren et al., 2008) will significantly improve this area.

1.6.3 Why study multiplicity in the young moving groups?

The young moving groups are similar to the field population in the way that objects are spatially scattered on the sky and at varying distances. The advantage over the field is that the stars are members of well-defined groups, rather than field stars, whose history is not well constrained. Additionally, these objects are ≈5-150 Myr in age which means that the majority of low-mass stars are still contracting towards the main sequence. This is a very important stage of evolution, including significant angular momentum and disc evolution, see Section 1.2.2. Below, we further motivate using these stars to study multiplicity.

1.6.3.1 Making use of existing data

As mentioned previously, the targets studied in this thesis are ideal for the search and characterisation of circumstellar discs and planets due to their youth and proximity. Owing to this, there is a huge amount of existing observational data on these targets. For example, from previous AO-imaging campaigns searching for companions around young stars, over 300 targets have existing AO-imaging data. We have used this existing data to calculate comprehensive detection limits for our targets. Additionally, given the same instrumental limit in angular resolution, we are able to probe down to smaller physical separations due to the proximity of the stars, compared to nearby ($>$100 pc) star-forming regions.

As mentioned in the previous section, members of the young moving groups are usually confirmed with spectroscopy and radial velocities. With multi-epoch spectroscopy we are sensitive to both single-lined and multiple-lined spectroscopic binary systems. As many authors are interested in spectroscopic characterisation of these objects there is a wealth of multi-epoch data available to us. Additionally, throughout the course of this degree the author has been awarded time to conduct further spectroscopic observations (see Appendix B). In total, over 360 targets have multi-epoch spectroscopy from which we derived radial velocities and detection limits.

1.6.3.2 The ability to probe for wide companions

Another advantage of the proximity of these targets is their projected motion on the sky. For example, the average proper motion of the β-Pictoris moving group is $\mu_{\alpha*,\text{av.}}$ = 50 mas/yr, $\mu_{\delta,\text{av.}}$ = -75 mas/yr. These high values allow us to search for wide companions with a small probability of objects in the field of view sharing the same photometric and kinematic properties. This analysis is presented in Chapter 4. Aside from the field, this is not possible in other star-forming regions due to their spatial density and distance from Earth.

1.6.3.3 Dynamical masses in an unexplored age space

Given that the members of these groups are prime targets for exoplanet searches, accurately determining their masses is crucial. That way we can reduce the uncertainties on the inferred masses of the planets. Additionally, the age range covered by our sample (5-150 Myr) is relatively unexplored in terms of direct comparisons between model-based and direct masses. The majority of young regions with similar ages are much further away than our sample ($>$150 pc), and therefore the timescale to obtain full periods of resolvable binary systems is $\sim$50-100 yr.

We have identified a number of systems in our sample that have orbital periods $<$16 yr. Similar to the analysis presented in Bonnefoy et al. (2009), we have started a series of observations to obtain their orbital solutions (see Appendix B.7 for details). With these solutions we can make comparisons to the masses predicted by evolutionary models such as Baraffe et al. (2015).

1.7 The long-term nature of multiplicity studies

In the discussion above we have tried to motivate the importance of multiplicity in the context of star formation and evolution. We have also discussed how the young moving

groups can play an important role in improving our understanding of this topic. The types of statistical studies embarked upon here are long term projects: this is due to both the volume of data needed for the statistics and the time interval needed to identify and confirm multiple systems. For this reason the work presented in this thesis represents our first steps in terms of studying and understanding multiplicity in the young moving groups. This project is very much ongoing and is being actively pursued by the author and collaborators, as can be seen by a number of observation proposals presented in Appendix B.

1.8 Thesis outline

The remainder of this thesis is divided into the following chapters:

Chapter 2 presents analysis of the abundance and properties of spectroscopic binaries in the young moving groups based on multi-epoch high-resolution spectroscopic observations of 250 targets in the young moving groups. These results are compared with other regions and discussed in the context of universal star formation.

Chapter 3 examines the abundance and properties of visual binaries in the young moving groups based on AO-imaging data for 113 targets in the young moving groups. The statistics and distributions of visual multiple systems in these young moving groups are compared with other regions and discussed in the context of universal star formation.

Chapter 4 presents new stellar and sub-stellar candidate members of the young moving groups identified from a search for wide companions. The technique used to find these companions is described and the candidates' photometric and spectroscopic properties are presented.

Chapter 5 focuses on the multiple system population in the β-Pictoris moving group. Using detection limits from a combination of spectroscopy, AO-imaging and direct imaging (the analyses presented in Chapters 2, 3, and 4) we present evidence for the significant role of higher-order multiple systems in the evolution of a population's multiplicity.

Overall conclusions from the work presented in this thesis and prospects for future analysis are presented in Chapter 6.

Appendix A describes the methods used to handle the large dataset analysed in this thesis. This includes the structure of the database and an example of the object-orientated approach to data manipulation.

Appendix B is a collection of proposals that were awarded telescope time during the course of this thesis (November 2012 to May 2016). The scientific rationales and immediate objectives are presented in their original form.

Appendix C presents a brief summary of an observatory project that was carried out at Paranal observatory in Chile (April to May 2014). The aim of the project was to produce a code to calculate basic statistics of raw FLAMES (a fibre-fed optical spectrograph) *ad hoc*.

Chapters 2, 3 and 4 have been published in *Astronomy and Astrophysics* (Elliott et al., 2014, 2015, 2016), respectively. The full bibliographic information is stated at the beginning of these chapters.

Chapter 5 has been accepted for publication in *Monthly Notices of the Royal Astronomical Society* (Elliott and Bayo, 2016). The full bibliographic information is stated at the beginning of the chapter.

Figure 1.3 presents the reader with a schematic of the observational techniques used in this thesis and the focus of each chapter of analysis. The interferometric and speckle-imaging parameter spaces are hatched, as most targets do not have detection limits in this space. However, as highlighted by the *future work* annotation, this is ongoing (see PIONIER proposal in Appendix B.6).

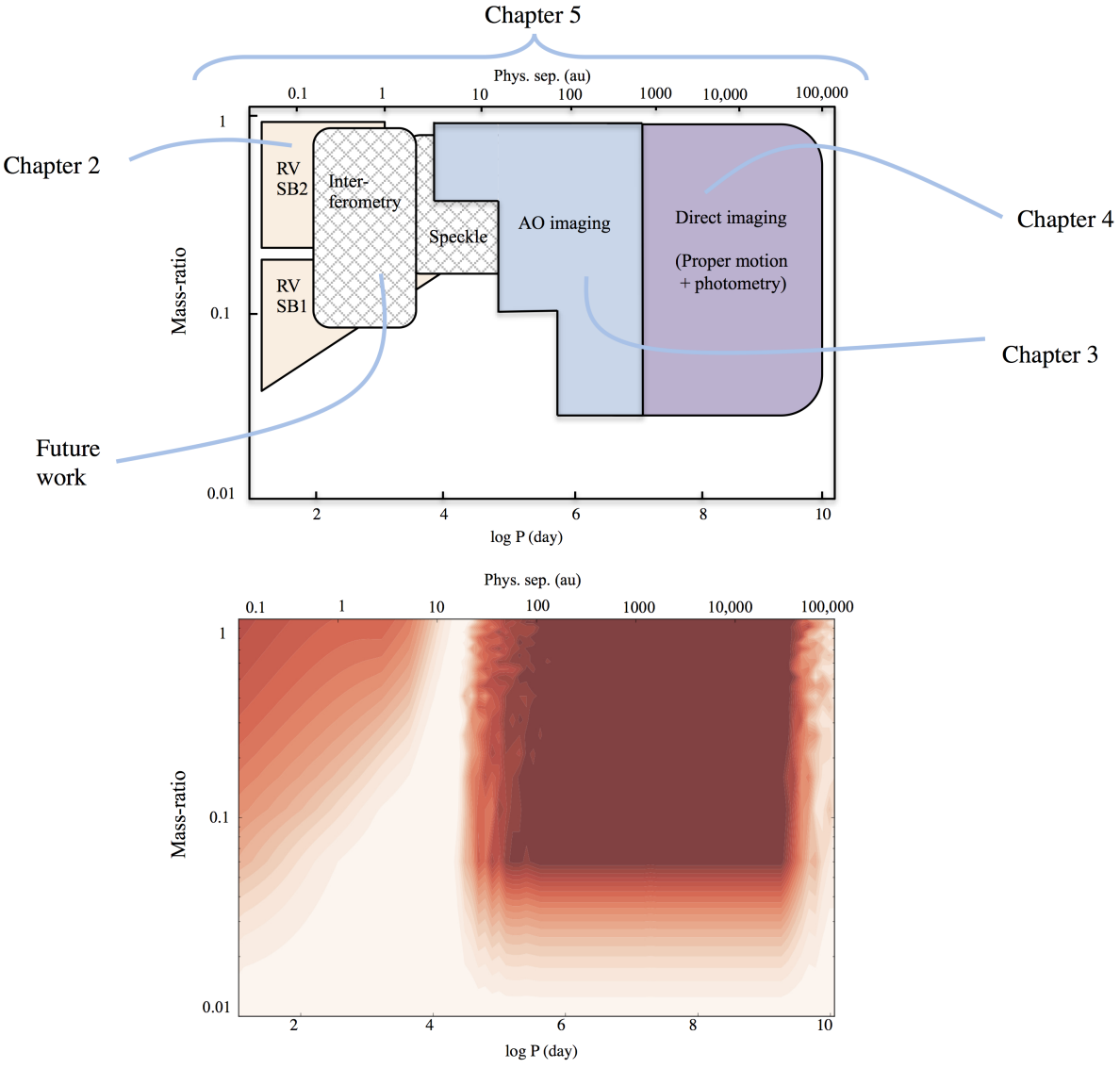

FIGURE 1.3: *Top panel:* Period versus mass-ratio showing the approximate parameter space that each observational technique probes for a typical star in our sample, adapted from Sana and Evans (2011). The parameter space and observational techniques are annotated showing the division of analysis presented in this thesis. *Bottom panel:* An example of detection limits derived in this work from the combination of spectroscopy, AO-imaging and direct imaging techniques for a star (HD 27679) in our sample. Red is 100% probability of companion detection, white 0%.

Chapter 2

Spectroscopic binaries in the young moving groups

Parts of this chapter have been previously published as 'Search for associations containing young stars (SACY). V. Is multiplicity universal? Tight multiple systems', Elliott, P.; Bayo, A.; Melo, C. H. F.; Torres, C. A. O.; Sterzik, M.; Quast, G. R., 2014, A&A, 568, A26. The work is presented here in expanded and updated form.

In this chapter we present analysis of the abundance and properties of spectroscopic binaries in a sub-sample of targets in the young moving groups. We identified single-, double- and triple-lined spectroscopic systems. We found no significant difference between the short period multiplicity fraction (*MF*) of this sub-sample and that of close star-forming regions ($\approx$1-2 Myr) and the field (*MF* $\leq$10%). Our results are consistent with the picture of universal star formation, when compared to the field and close star-forming regions (SFRs). We also comment on the implications of the relationship between increasing multiplicity frequency with the primary mass within the close companion range in relation to star formation.

The chapter is organised as follows. Section 2.1 details the observations and data used in this work. Section 2.2 describes the use of new radial velocity (RV) data to determine

association membership and details the estimation of the mass distribution of the observed sample. Section 2.3 describes the methods employed to find multiple systems within our sample and the methods to account for biases. Section 2.4 presents the results and their significance in relation to star formation. In Section 2.5 the conclusions of this work on multiplicity and future prospects are presented. Section 2.6 shows the spectral type to effective temperature conversion. Section 2.7 notes individual sources. Section 2.8 details the analysis of dubious spectroscopic multiple systems. Section 2.9 details of the individual RV values.

2.1 Observations and data

There were two main sources of high resolution spectroscopy available for analysis:

First, observations performed with the fibre-fed extended range optical spectrograph (FEROS), a high resolution echelle spectrograph ($\lambda/\Delta\lambda$ $\sim$50,000) at La Silla, Chile in two distinct periods: between January 1999 and September 2002 at the 1.5m/ESO telescope (ESO program ID: 67.C-0123) and after October 2002 at the 2.2m telescope (ESO program IDs: 072.C-0393, 077.C-0138). These data were reduced and RV values were calculated for these targets as described in Torres et al. (2006). Out of the total SACY sample used in this analysis, 127 sources have existing RV values from FEROS data and multiplicity flags.

Second, observations performed with the ultraviolet and visual echelle spectrograph (UVES) ($\lambda/\Delta\lambda$ $\sim$40,000 with 1″ slit) at Paranal, Chile with ESO program IDs: 088.C-0506(A) & 089.C-0207(A) between October 2011 and September 2012. In these two programs each source had three separate observations using the standard set-up, a 1″ slit width, which covers the wavelength range 3250-6800 Å. The separation in time between the acquisition of each epoch of data for one source ranges from 1 day to $\sim$ 1 month; the simulations described in Section 2.3.2 help to characterize possible bias from this time sampling.

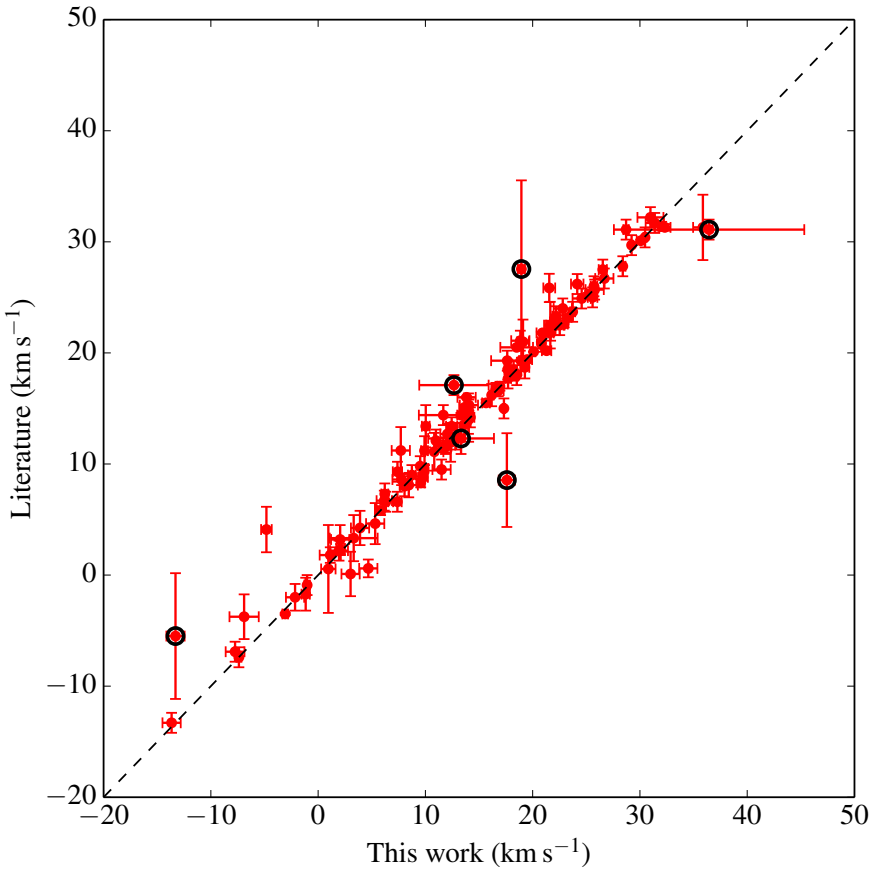

FIGURE 2.1: Average RV values determined in this work versus those from the literature, where values were available for comparison. Error bars represent the standard deviation from the mean value for each source. If uncertainties were not quoted in the literature, the average uncertainty from all other values, 0.90 km s^{-1}, was used. If only one data epoch was available, the overall standard deviation for the SACY targets, 0.89 km s^{-1}, derived in this chapter was used to represent the uncertainty. Black rings indicate identified multiple systems. A line representing a 1:1 relation has been drawn for base comparison.

In addition, for each source, the UVES archive was queried to make use of all available and public data on the SACY targets. All data were reduced using the UVES pipeline recipe *uves_obs_redchain* with the command-line driven utility *esorex* (bias corrected, dark current corrected, flat-fielded, wavelength-calibrated and extracted). This outputs three individual spectra, (in the case of the standard set-up) one spectrum for each CCD chip of the instrument: blue, red upper and red lower (BLUE 3250-4500 Å, REDU 4800-5800 Å, and REDL 5800-6800 Å, respectively).

Association	Ass. ID	Dist. (pc)	N. of Obj.	N. of SBs
AB Doradus	ABD	34±26	53	5
Argus	ARG	106±51	33	0
β-Pic	BPC	31±21	29	4
Carina	CAR	85±35	22	3
Columba	COL	82±30	31	1
ϵ-Cha	ECH	108±9	20	2
Octans	OCT	141±34	13	1
Tuc-Hor	THA	48±7	33	0
TW-Hydrae	TWA	48±13	11	0

TABLE 2.1: Summary of the properties of the moving groups studied in this chapter.

In addition, the VizieR catalogue service was used to look for any existing RV values. A comparison between the archival data and the values calculated in this work is shown in Figure 2.1. The individual values from UVES, FEROS and archival sources is shown in Table 2.4 with their respective uncertainties; the average uncertainty from the literature is 0.9 km s^{-1}.

2.2 Characterising the sample

2.2.1 Revising membership with new radial velocities

Accurately determined RV values are a key ingredient to the convergence method (Torres et al., 2006) used to identify the young association members. The convergence method uses the gamma (systemic) velocity; in the case of single stars, this is equal to the RV. For multiple systems without orbital solutions, there are two cases, with multi-component spectra (SB2/SB3) and without (SB1). For SB2/SB3 systems it is derived from weighting the component RV values, according to their relative flux. For SB1 systems the mean RV value is used with its respective variability induced by further components (certainty of membership for these systems is very difficult without an orbital solution). For multiple systems with orbital solutions it is a known value. Therefore, the

more accurate the RV values and, in the case of multiple systems, the greater phase coverage observed, the more stringent the conditions for membership become.

The large number of RV values calculated in this work was used to revise and refine the member list (da Silva et al., 2009). With this new data any targets that no longer had a high probability of membership were removed from the overall analysis and statistics of the associations (initial members and revised members are shown in Table 2.7). However, as we have conducted useful analysis on these objects, details can be found in Section 2.9.

2.2.2 Mass distribution

The mass distribution was constructed using effective temperatures from da Silva et al. (2009). First, available effective temperatures were used directly with age estimates, as given in Torres et al. (2006), to obtain a model-based mass using isochrones (Baraffe et al., 1998, 2003; Siess et al., 2000), see Section 2.6. The different isochrones were used depending on the temperature range. The median effective temperature for each spectral subclass within each association was used to estimate a value for those targets with a spectral type, as calculated by the method described in Torres et al. (2006), but without an effective temperature value. Linear interpolation was used for those spectral subclasses without any corresponding temperature values from da Silva et al. (2009). In the case of Carina (CAR), effective temperature values for targets of spectral type K3 and later were taken from median values of Tucana-Horologium (THA), which are approximately the same age, and having a much larger population in this spectral type range. Masses were then derived using effective temperatures and isochrones to produce a mass distribution, a shown in Figure 2.2.

To validate this method we derived masses from a calculated bolometric luminosity value using the VOSA tool (Bayo et al., 2008) by assuming a solar metallicity (Viana Almeida et al., 2009) and $log(g)$ between 3.5 and 5. This value is calculated from a fit of the spectral energy distribution (SED). Some 78 sources had poor SED fits due to a lack of available photometry and therefore could not be used any further. The

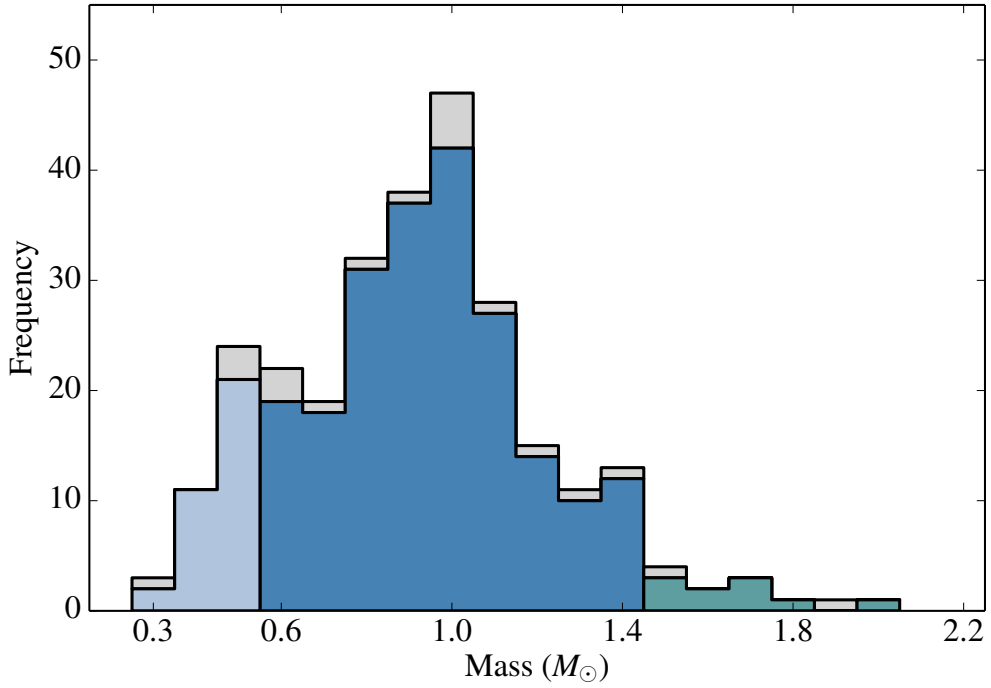

FIGURE 2.2: Mass distribution of all targets used in this work calculated by using available effective temperatures from da Silva et al. (2009) and derived masses using Baraffe et al. (2003) models $< 0.6\,M_\odot$ – light blue, Baraffe et al. (1998) models between masses 0.6-1.4 $M_\odot$ – dark blue, and Siess et al. (2000) models $>1.4\,M_\odot$ – green. The grey represents multiple system primary masses.

calibration of the bolometric luminosity is also based on the distance, which is the largest source of uncertainty. This uncertainty combined with the photometric error count yields a further 65 sources (from $\approx$250) with an error in bolometric luminosity $>$20% of the calculated value. For the remaining sources, we derived the masses with the bolometric luminosity value using the isochrones. The standard deviation in masses derived from the two different methods was 0.07 $M_\odot$. This is a very small and acceptable difference in our model-based masses.

The mass distribution calculated from the effective temperatures was used in this work, as opposed to that calculated from the bolometric luminosity, as it represents our sample more fully.

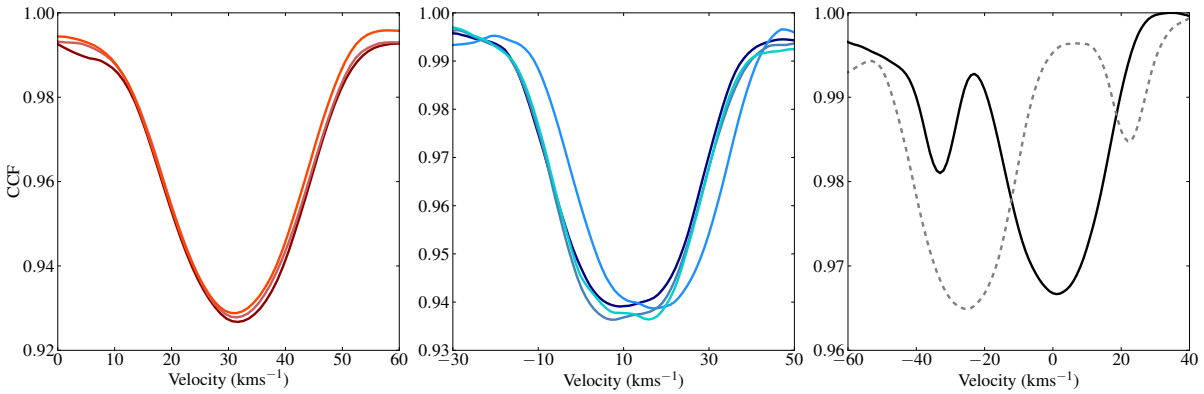

FIGURE 2.3: Resulting CCF profiles from three different sources. *Left Panel:* HD 45270 with no significant variation in RV and standard deviation $< 0.05\,\mathrm{km\,s^{-1}}$ (data epochs: 2007-05-08, 2008-12-05, 2010-09-26). *Central Panel:* HD 104467 a SB1 candidate with significant variation in RV and std dev. $> 2.70\,\mathrm{km\,s^{-1}}$ (data epochs: 2009-03-16, 2010-05-26, 2012-02-24, 2012-03-07). *Right Panel:* HD 155177 a SB2 system, as shown by two clear peaks and temporal movement (data epochs: 2007-04-19, 2012-05-09).

2.3 Identifying multiple systems

To determine the RV values, we computed cross-correlation functions (CCFs) for all reduced spectra with a signal-to-noise ratio greater than 10. To compute the CCF, the observed spectrum is convolved with a CORAVEL-type numerical mask, as described in Queloz (1995). The shape of the CCF function is approximated by a Gaussian profile and, in cases of fast rotation, the Gray rotational profile (Gray, 1976). The RV is the peak of this profile to which the barycentric correction is applied.

For the sake of homogeneity, all CCFs quoted in this paper have been calculated using a K0 mask, including those without a literature spectral type determination. Double-lined spectroscopic systems (SB2s) –and in rare cases, triple-lined spectroscopic systems (SB3s) – are identified visually, displaying two distinct peaks in the outputted CCF. For systems with indications of multiplicity in the CCF profiles, such as two apparently merged components, further analysis was conducted, the details of which can be found in Section 2.8. Examples of the CCF output for these systems and that of a system with no indication of multiplicity are shown in Figure 2.3.

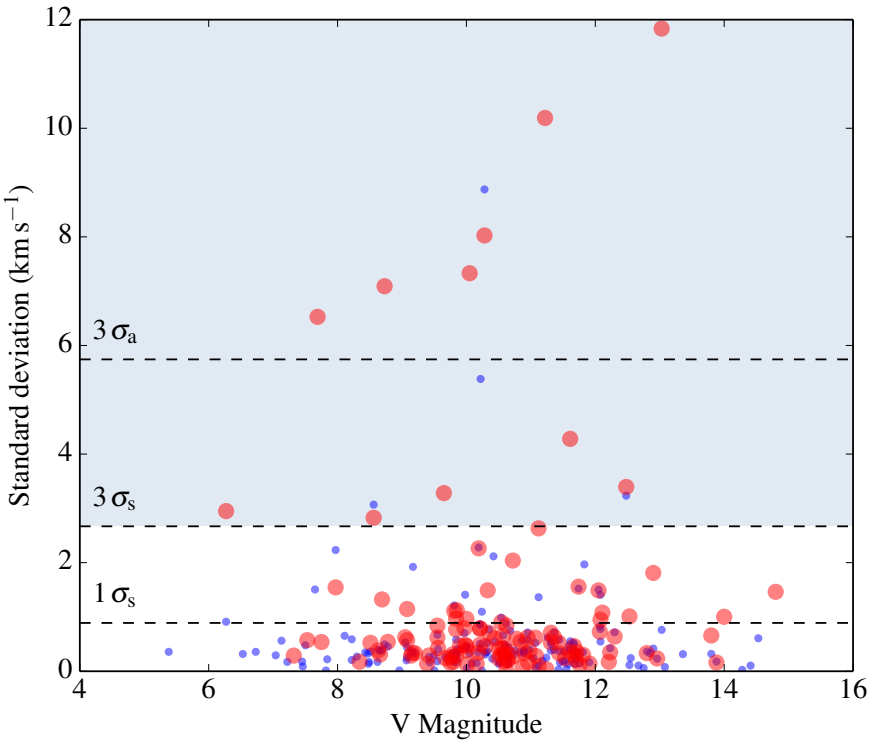

FIGURE 2.4: The standard deviation in RV values for SACY sources, excluding known SB2 systems, as a function of V magnitude. UVES and FEROS values – blue dots and UVES, FEROS and archival data – red circles. The variables, 1 σ_s and 3 σ_s, represent one standard deviation and three standard deviations respectively, for both UVES and FEROS data. The shaded area contains SB1 candidate multiple systems. The variable 3 σ_a, represents three standard deviations including archival data.

Single-lined spectroscopic systems (SB1s) are identified through significant RV variations between different data epochs; the results are shown in Figure 2.4. The shaded area contains all the SB1 candidates; these candidates have significant RV variations; above 3 σ_s (2.70 km s^{-1}), or three standard deviations for the entire dataset. The value of three standard deviations, 3 σ_a, including archival data is also shown for comparison. All candidates above 3 σ_s were investigated further, details can be found in Section 2.7.1.

2.3.1 Sources of uncertainty

The uncertainty in the RV values is calculated from equation (9) of Baranne et al. (1996):

$$\sigma_{\text{meas.}} = \frac{C(T_{\text{eff}})}{D \times S/N} \frac{(1 + 0.2\omega)}{3} \text{ km s}^{-1}, \tag{2.1}$$

where $C(T_{\text{eff}})$ is a constant that depends on both the spectral type of the star and the mask used, which is typically 0.04, ω is the (noiseless) FWHM (km s^{-1}) of the CCF, D is its (noiseless) relative depth, and S/N is the mean signal-to-noise ratio.

This produces a value, which is the internal uncertainty for the measurement of the RV using this CCF method. Due to the very high signal-to-noise ratio in our data (average $\sim$ 100), the contribution of this internal uncertainty is almost negligible. Although the value of $C(T_{\text{eff}})$ is a function of the T_{eff} and the mask used to compute the variation in the temperature range 4000-6000 K, it only changes the value of $C(T_{\text{eff}})$ by $\approx$0.01. When this variation is propagated across the T_{eff}, the output range is not significantly affected. Values are shown in Table 2.6, these typical values of the uncertainty are $\sim$0.01 km s^{-1}. However, the stars in our study are often variable, and this can induce deformities into the CCF (Lagrange et al., 2013) in which this calculation of uncertainty does not account for; it assumes a symmetric CCF profile, and thus, the uncertainty is underestimated in the majority of cases.

A more empirical approach to gauging the level of uncertainty in the measurements is to use the standard deviation of the RV values, as shown in Figure 2.4. This is an *a posteriori* approach, assuming a very small percentage of our candidates are in multiple systems, and that this overall distribution is mainly representing single systems. Previous research in SFRs concerning short period multiplicity of T-Tauri stars has shown that single systems are by far the most abundant 90+% (Melo, 2003; Nguyen et al., 2012) and have used such distributions to estimate empirical uncertainties. The one sigma level in RV variation for all targets with more than one data epoch (excluding known SB2 systems) is 0.89 km s^{-1}, as seen in Figure 2.4.

2.3.2 Accounting for biases

A huge advantage of the SACY dataset is the way in which the sample was compiled from optical counterparts to X-ray sources from the ROSAT all-sky survey. X-ray emission can originate in protostars $\sim 10^4 - 10^5$ yr (Koyama et al., 1996) to post T-Tauri stars $\sim$10 Myr (Walter et al., 1988). In terms of mass this is from sub-stellar (Neuhäuser et al., 1999) to intermediate-mass Herbig Ae/Be stars (Zinnecker and Preibisch, 1994). On this basis, our sample should be relatively free of significant bias for ages and primary masses ($\sim$5-150 Myr and 0.5-3.0 $M_\odot$). However, the sample is not bias-free regarding the characteristics of the secondary components and orbital parameters.

To estimate the completeness of this work, given the sparse and irregular time sampling, in terms of our sensitivity in observing binary systems, probability-detection density maps were created using a set of synthetic binary systems, as described in Section 6.1 of Duquennoy and Mayor (1991) and outlined further below. The primary masses used in these simulations are the mean values of mass bins containing equal numbers of targets (0.6, 0.9 and 1.2 $M_\odot$: 85 targets) taken from the overall mass distribution of the sample, which includes all targets with cross-correlation results not previously identified as SB2 systems.

For each primary mass, a density map as a function of the secondary mass (M_2) and the period (P) of the binary system was constructed. A set of binary systems are generated in this space (M_2/M_1: 0.1 to 1, P: 1 to 1000 day) following certain distributions. The parameters phase at time t=0 ($\phi_{t=0}$), longitude of the ascending mode (ω) and the inclination (i), are randomly drawn from uniform distributions within their respective numerical ranges. The eccentricity (e) values depend on the period of the binary system as follows:

- $P < 8$ day, $e \equiv 0$
- $P \leq 8 < 1000$ day, e is randomly drawn from a normal distribution centred at 0.33 with a standard deviation of 0.03 (Mayor and Mermilliod, 1984).

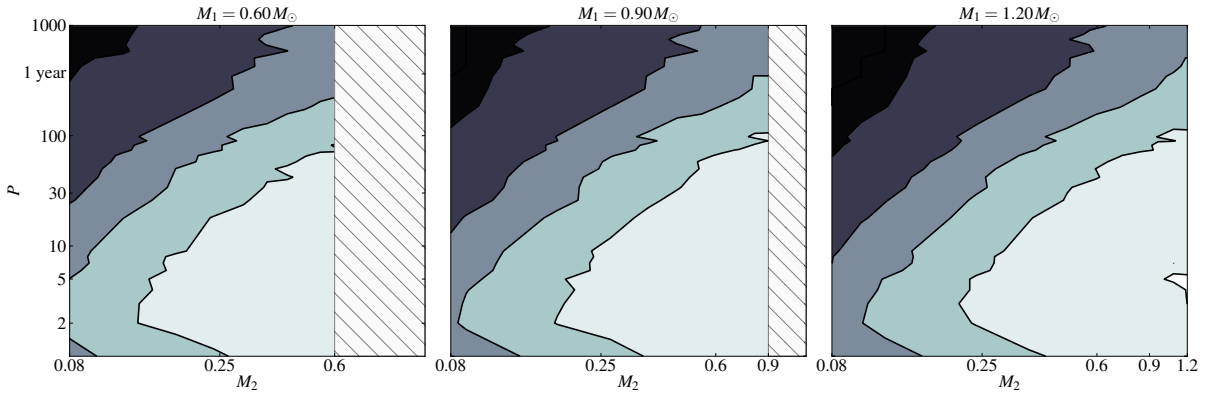

FIGURE 2.5: Probability density maps in (M_2, P) space for three different primary mass stars, 0.60, 0.90, and 1.20 $M_\odot$, periods, P, range from 1-1000 day, and secondary masses, M_2, from 0.1 M_1 − M_1. Probabilities: $<$ 5% – black, 5-39%, 40-59%, 60-74%, 75-90% and $>$ 90% – white.

The semi-amplitude (K) and thus the RV were then calculated through equations (14) and (17) from Halbwachs (2001) using our physical set of data epochs to input the time (t) into the equations. For each object, a set of RVs is produced, and from this, the standard deviation from the mean is calculated. If this calculated value is above the standard deviation of our physical, observed data the system is said to be *observed*; this process is then repeated N times for each (M_2, P) point.

For this range Figure 2.5 shows that the effect of the primary mass of the binary system has little effect on the sensitivity to observe the secondary. For all three primary masses considering a secondary component of 0.1 $M_\odot$, orbital periods of 30 day and 100 day have a $>$75% and $>$60% probability, respectively, of being detected within our dataset.

2.4 Results and discussion

The individual targets classified as multiple systems are shown in Table 2.2, which are identified either as SB1, SB2 or SB3. We then calculated the multiplicity frequency (*MF*) for our sample.

We use the multiplicity frequency, as opposed to the companion star frequency (*CSF*) because the multiplicity frequency is more robust against unobserved higher order

TABLE 2.2: A summary of the basic properties of targets classified as spectroscopic binaries.

ID	Mass ($M_\odot$)	SpT	Ass.	Flag
GSC 09420-00948	0.6	M0	ECH	SB1[a]
HD 104467	1.9	G3	ECH	SB1[a]
V1005 Ori	0.7	M0	BPC	SB1[b]
HD 59169	1.1	G7	ABD	SB1[a]
PX Vir	0.9	K1	ABD	SB1[b]
CD-27 11535	1.0	K5	BPC	SB1[a,b]
AK Pic	1.2	G2	ABD	SB1[b]
GSC 08077-01788	0.6	M0	COL	SB1[a,b]
1RXS J195602.8-320720	0.3	M4	BPC	SB2[a]
V4046-Sgr	1.1	K6	BPC	SB2
HD 155177	1.5	F5	OCT	SB2[a]
BD-20 951	1.0	K1	CAR	SB2
HD 309751	1.1	G5	CAR	SB2
TWA 20*	0.4	M3	TWA	SB2
CD-423328	1.0	K1	CAR	SB2[b,c]
HD 217379	0.6	K7	ABD	SB3
HD 33999	1.3	F8	ABD	SB3

Notes. (*) No longer classified as a member of TWA with new RV data.(a) System has not been previously identified in related SACY work or literature.(b) Targets classified based on variation from literature RV values. (c) Details of the technique to classify this target are described in Section 2.8.

components (Hubber and Whitworth, 2005), whether a multiple system is a binary or a triple system the overall value of *MF* would not be affected. Additionally, given we are only probing SB systems in this part of the analysis the number of higher-order spectroscopic multiple systems is extremely low ($<$10 %).

2.4.0.1 Multiplicity frequency as a function of age

The SACY sample has age determinations calculated in a number of works (Torres et al., 2008; Binks and Jeffries, 2014; Bell et al., 2015), as shown in Table 1.2. There are significant uncertainties for these determinations and different works derive quite

different values in some cases (such as AB Dor 100-150 Myr). However, the relative ages between the associations are less affected and, therefore, are more robust quantities. In other words, it is known that TW-Hydrae is younger than Tucana-Horologium, irrespective of their absolute ages, as seen in da Silva et al. (2009), Figure 3.

If there was a significant relationship between multiplicity and age (between ages $\sim$5-100 Myr) we could observe it. However, as shown in Figure 2.6, we see no such trend, merely scatter across the age range. These results also agree with data from young clusters, Tau-Aur and Cha I with ages 1 Myr and 2 Myr, respectively (Luhman, 2004). In addition to this when considering results from the field within the orbital period range (1-200 day), the frequency, $0.073^{+0.014}_{-0.012}$, is indistinguishable (Duquennoy and Mayor, 1991; Nguyen et al., 2012).

These results can be explained by the minimal N-body dynamical processing for systems with small physical separations ($<$5 au). Such systems are essentially never destroyed (Parker et al., 2009), and if we assume similar numbers of multiple systems are created from population to population initially, we would not expect to see any significant evolution of their abundance.

2.4.0.2 Multiplicity frequency as a function of mass ($< 3\,M_\odot$)

To compare our results in terms of primary mass to previous work, we must define a consistent period and secondary mass range and apply the same correctional techniques. Nguyen et al. (2012) studied the range $P_{\rm min}$=1, $P_{\rm max}$=200 day and $M_{2,\rm min}$=0.08, $M_{2,\rm max}$=0.6 $M_\odot$. The properties of the synthetic binaries used in their simulations are taken from a typical T-Tauri star in their sample; however we have calculated detection probabilities using three primary masses (0.6, 0.9 and 1.2 $M_\odot$) in this analysis.

We can estimate the probability that the multiple system will be in this P and M_2 range from each primary mass M_1 using Bayes' theorem (Bayes and Price, 1763):

$$\mathcal{P}_{M_1}(m,p) = \frac{\sum_{m=M_{2,\rm min}}^{M_{2,\rm max}} \sum_{p=P_{\rm min}}^{P_{\rm max}} \mathcal{M}(m,p)\mathcal{D}(m,p)}{\sum_m \sum_p \mathcal{M}(m,p)\mathcal{D}(m,p)}, \tag{2.2}$$

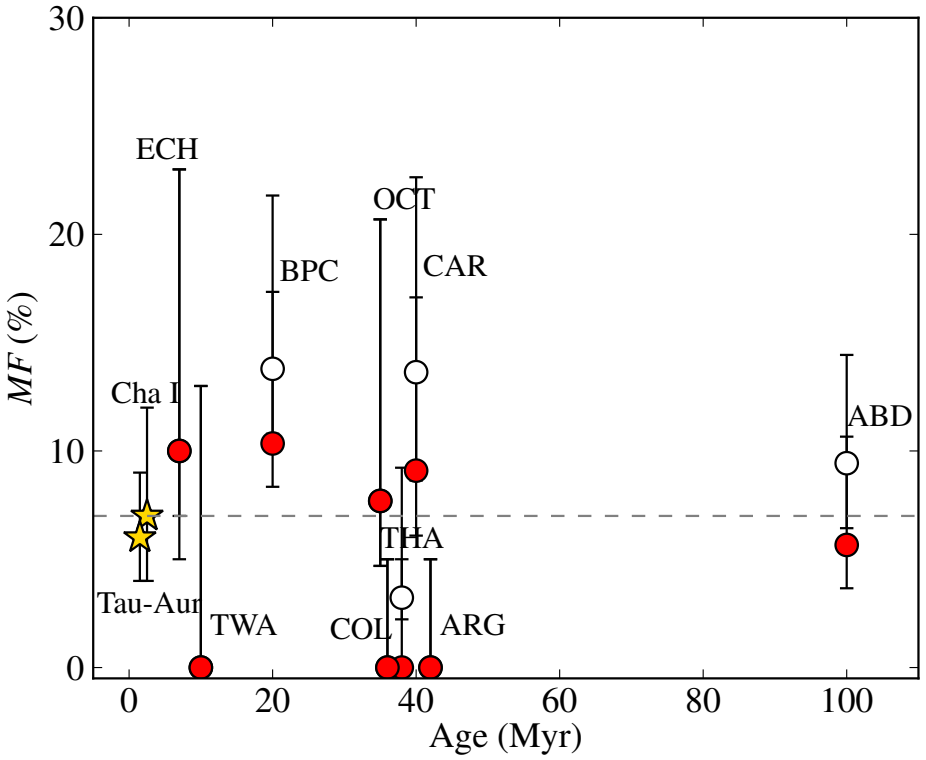

FIGURE 2.6: The frequency of spectroscopic multiple systems from the overall observed sample as a function of age for each of the SACY associations, which are individually labelled. UVES and FEROS data – red, UVES, FEROS and archival data – white, and data from Nguyen et al. (2012) – yellow. Uncertainties were derived from low-number statistics using Equation (A3) from Burgasser et al. (2003). A line representing a 7% frequency is shown.

where $\mathcal{M}(m,p)$ is the prior distribution. In this case the most ignorant prior distribution is used, $\mathcal{M}(m,p) = 1$, and $\mathcal{D}(m,p)$ is the likelihood function from our probability of detection simulations.

We compute the probability for each of our primary masses and use the mean detectability probability to compute a corrected frequency, as below:

$$MF_{\rm correc} = \frac{MF_{\rm obs} \times \mathcal{P}_{M_1}(m,p)}{\frac{1}{N}\sum_{m=M_2,{\rm min}}^{M_2,{\rm max}} \sum_{p=P_{\rm min}}^{P_{\rm max}} \mathcal{D}(m,p)}, \tag{2.3}$$

where $MF_{\rm correc}$ is the corrected frequency, $MF_{\rm obs}$ is the observed frequency, and N is the number of separate detection probabilities from the simulations.

The results of these corrected frequencies are shown in Figure 2.7, along with data from Nguyen et al. (2012). Our mass bins contain equal numbers of targets (85) to eliminate any bias from the frequency of objects in a certain mass range. The results are fully compatible, and the spread in the value of $MF_{\rm correc}$ including the uncertainties is only 7% across the mass range ($\approx$0.2–2.0 $M_\odot$). Additionally, we compared this value to the processed field population and again, find compatible values ($\approx$10%, Raghavan et al., 2010; Tokovinin, 2014b). This result also supports the universality of multiplicity, as the data from a range of different environments (younger denser SFRS, young associations and the field population) is indistinguishable.

As well as comparing the results from SACY to those of younger SFRs, one can look at the form of the corrected frequency with primary mass for the environments. Figure 2.7 shows there is no significant increase or decrease in the corrected frequency as a function of the primary mass. In other words, from our results, it is just as likely to observe a multiple system with a primary mass of $\approx$0.2 $M_\odot$ than one with a primary mass of $\approx$2.0 $M_\odot$. As shown and discussed in Section 2.4.0.3 when higher masses are included the form changes quite dramatically.

2.4.0.3 Multiplicity frequency across a wide mass range

There are two phases of interaction that can shape the multiplicity frequency we observe in populations of stars: (I.) Interactions within the pre-stellar cores ($\leq 10^5$ yr) through accretion, disc interaction and the dynamics of multiple systems (Bate et al., 2002) and (II.) through cluster dynamics, where the interactions between stars that have originated in different pre-stellar cores ($> 10^5$ yr), which can be modelled using N-body simulations (Kroupa, 1995).

Populations that are $\sim$Myr have undergone significant evolution of their parameters already (e.g., mass ratio, separation distribution, and primordial multiplicity frequency). However, the close systems observed in this study ($<$ 10 au) should not have undergone any destructive processing through the second phase described above. Therefore, even across a wide range of ages and environments, we should be probing the

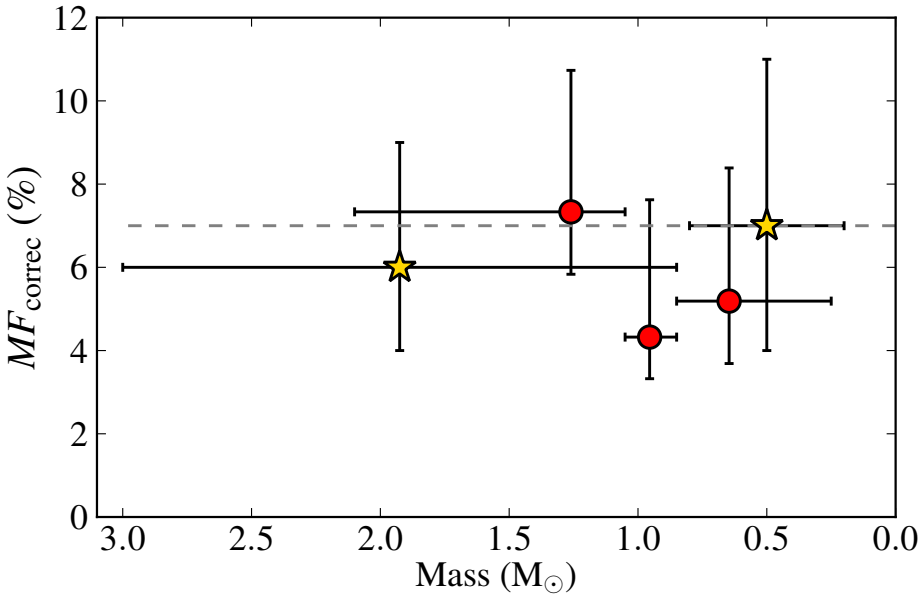

FIGURE 2.7: Multiplicity frequency as a function of primary mass; mass bins are represented with x-axis error bars, the average value for the SACY targets are the red markers. frequencies have been corrected using the techniques outlined in Section 2.4.0.2. The same data (Nguyen et al., 2012) shown in Figure 6 has been transformed from spectral type to mass by assuming an age of 1 Myr and 2 Myr for Tau-Aur and Cha I respectively, using T_{eff} from Luhman (2004) and Sestito et al. (2008) with isochrones explained in Figure 2.2.

multiplicity frequency that is a direct result from the evolution within the separate prestellar cores.

Figure 2.8 shows a compilation of results from this study (in red and white) and from the literature (in blue and gold) for spectroscopic multiplicity frequencies from a range of sources. The apparent exponential form of this function should be considered with caution in this instance, as this compilation lacks thorough refinement, such as a defined consistent orbital period range. It is a qualitative example of the trend of increasing multiplicity frequency with spectral type, and therefore mass, for tightly bound multiple systems. This trend seems to be preserved when considering much wider systems in the field, as seen in Figure 12 of Raghavan et al. (2010).

One potential explanation for this observed relationship in the field relates to the binding energy of the system; however, we would not see a significant relationship for tight

binaries on this basis, (Parker et al. (2009), Section 5.2, interaction time-scale calculations: Nguyen et al. (2012)). As shown in Figure 2.8, there is an increase with mass for these close systems, this is not easily explained with our current understanding of star formation.

The observed physical separation of close systems ($<$10 au) is the result of the evolution of the multiple system's properties. As discussed previously, the size of the first Larson core, a pressure-supported fragment of $\approx$ 5 au (Larson, 1969), does not permit a secondary component to orbit at such a physical separation initially. Bate et al. (2002) shows how these close systems can be formed from wider systems through the processes associated with phase I with dynamical interactions being the dominant mechanism. Kozai cycles with tidal friction (KCTF) (Eggleton and Kisseleva-Eggleton, 2006) is an example of such a dynamical process. This evolution depends on the periods of the primary and tertiary components $P_3(P_3/P_1)$. Given P_1= 1 yr and P_3 = 1000 yr, the time-scale for one cycle is $\sim 10^6$ yr; $> 10^2$ cycles are needed to complete the evolution (Tokovinin et al., 2006). Therefore, one could argue that this evolution is negligible at the PMS stage. However, the periods within the system could be initially much more similar and thus the ratio would be smaller, decreasing the time-scale. On this basis, this mechanism could have an effect even at the PMS stage, producing SB systems.

Bate et al. (2002) conclude that the processes described in phase I favour the production of higher mass multiple systems, which would qualitatively explain the trend shown in Figure 2.8. If these processes are responsible for the systems we observe, there would be other related properties, such as a lack of extreme mass-ratios of the systems and a tendency for wider companions. The second of these properties is investigated in two further chapters of this thesis (Chapters 3 and 5). The mass ratios of identified spectroscopic multiple systems is the subject of further analysis outside of this thesis. We intend to derive the orbital parameters of these systems with further high-resolution spectroscopy, however, this is a long-term project ($\approx$3 yr).

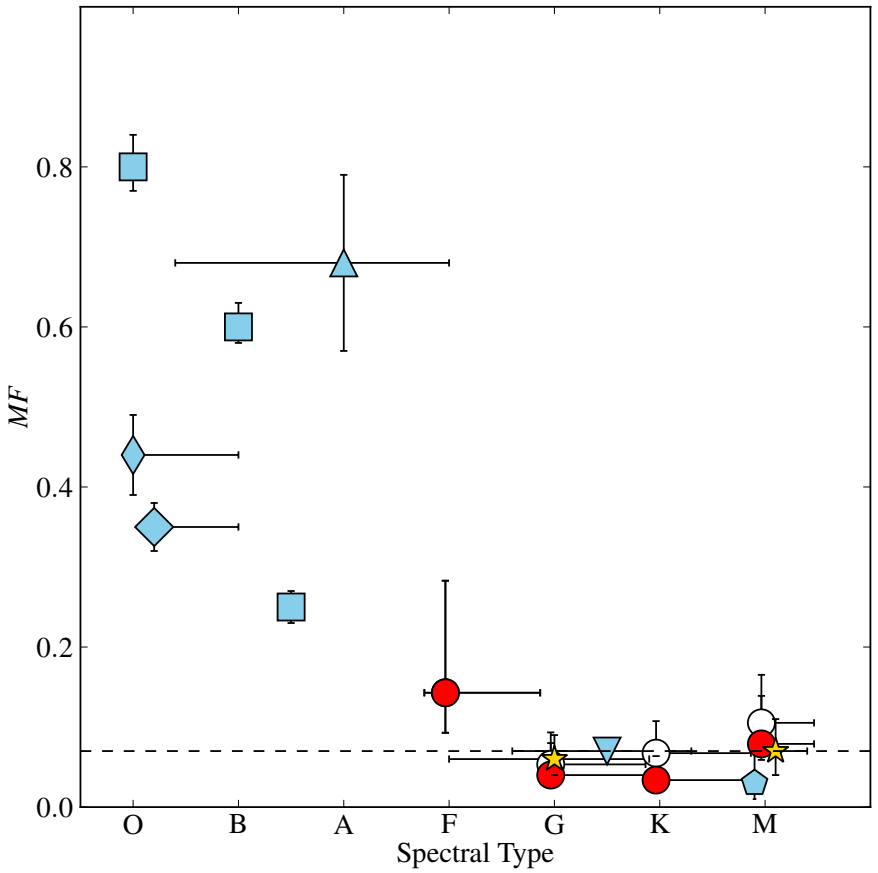

FIGURE 2.8: The spectral type versus the multiplicity frequency for all available SACY data and studies from the literature; the horizontal error bars represent the width of the spectral class bin (symbols in red, white and yellow as described in previous figures). Chini et al. (2012) – filled square, Baines et al. (2006) – filled triangle, Sana and Evans (2011) – filled thin diamond, Sana et al. (2013) – filled diamond, Raghavan et al. (2010) – inverted filled triangle, and Fischer and Marcy (1992) – filled pentagon.

One must also consider the possibility that star formation is not a single universal process. King et al. (2012a) have found significant statistical differences[1] in the multiplicity frequency for binary systems in the 19-100 au range (dynamically unprocessed) between the field and five clusters (Taurus, Upper Scorpius, Corona Australis, Chamaeleon I, and Ophiuchus). They conclude that the star formation process is non-universal and different environments produce different numbers of binaries due to this. However, star formation is a very chaotic process and multiple systems span from 0.01 au - 100,000 au and potentially even wider. The analysis of King et al. (2012a) concentrated on a small physical separation range and should be treated with caution.

[1] see Marks et al. (2014) for an alternative interpretation

In our data presented in Figure 2.6, we find three associations that have no spectroscopic systems from the sample used in our analysis: Argus: 0 / 33 (0^{+7}%), Tucana-Horologium: 0 / 33 (0^{+5}%), and TW-Hydrae: 0 / 11 (0^{+13}%). With our current dataset this means that Argus, Tuc-Hor, and TW-Hydrae have upper limits on the *MF* value of 0.07, 0.05, and 0.13, respectively. However, with more recent spectroscopic observations taken in 2014-2015, and the inclusion of existing archival data these frequencies have been newly calculated as: Argus: 5 / 35 (14%), Tucana-Horologium: 9 / 51 (18%) and TW Hydrae: 4 / 22 (18%).

Due to the stochastic nature of the star formation process it appears that even two populations with statistically similar primordial multiple system distributions could produce different distributions once they have evolved (Parker and Goodwin, 2012). The inclusion of multiple systems across all physical separations (spectroscopic, AO-visual, direct imaging-visual) scales may provide us with the *bigger picture* we need to further our understanding. This is discussed in Chapter 5.

2.5 Conclusions and further work

1. Using our new RV determinations, we have revised the membership of the SACY associations.

2. We have identified seven new multiple systems (SB1s: 5, SB2s: 2) within the SACY sample, as shown in Table 2.2.

3. Within the nine SACY associations studied in this analysis, we have found that there is no significant age dependence on the observed frequency of spectroscopic multiple systems (*MF*).

4. The corrected frequency of spectroscopic multiple systems ($MF_{\rm correc}$) within the mass range $\approx$0.2–2.0 $M_{\odot}$ is compatible with a flat distribution.

5. Our results are consistent, considering frequencies as a function of mass and age, with nearby SFRs and the field, as expected from the picture of universal star formation.

6. The observed frequency of spectroscopic multiple systems sharply declines as a function of spectral type and appears to plateau for later-types. To what spectral types this flat distribution extends still needs to be explored.

This section has analysed the frequency of close multiple systems through spectroscopic techniques. In the next chapter, these results are complemented with AO-assisted direct imaging data.

We have analysed $\approx$ 2700 individual spectra with an average S/N of 100 and succeeded in detecting new spectroscopic systems with our data alone and in combination with catalogue data. From our literature search, we did not fail to detect any systems previously identified as multiple systems. However, there is the possibility that we were not able to identify some multiple systems through our analysis. Our simulations, as seen in Figure 2.5, are one method to try and account for possible biases in our dataset. However, it is important to note that the raw frequencies, as quoted in this chapter, should be treated as lower limits, as 64/250 of our targets have only one RV value.

2.6 Temperature Scale

The way in which the mass distribution (Figure 2.2) of our sample was determined was based on effective temperature values in combination with model predictions. When there was no effective temperature value from da Silva et al. (2009), we used the spectral type of that target as an indication for its effective temperature and took the median value for all available targets with the same spectral type in that age bin. If there were no other targets within that spectral type bin a value was constructed through linear

interpolation, using the nearest earlier- and later-spectral type. Figure 2.9 shows the range of effective temperature and spectral type values.

The spread in effective temperature in each spectral type bin, as shown by the grey shaded areas, is generally small across all three age bins, for example, for the later-types, which is smaller than the spread for younger objects reported in Bayo et al. (2011), which are up to $\pm$ 150 K. The largest apparent spread is for the G3 spectral type bin at $<$20 Myr; it is caused by two values: 4722 K and 5759 K. The result is anomalous, and therefore, any necessary interpolation within the regime G2-G8 was conducted linearly using the two effective temperature values of 5988 K and 5344 K as boundaries, which is in accordance with the trend of the data.

2.7 Notes on individual sources

In Section 2.7.1 we comment on the individual sources that show RV variation above σ_s, 0.89 km s^{-1}. Section 2.7.2 shows the results from an archival search for any existing multiplicity flags. In Section 2.7.3 we comment on the data used to identify SB2 and SB3 systems in this work. Section 2.8 describes further analysis conducted in the cases of potential SB2/SB3 systems to remove false detections from deformities in the CCF profiles.

2.7.1 Archival RV values

Values quoted below, calculated in this analysis, are average values from available UVES and FEROS data; their uncertainties are one standard deviation in the following form: RV $\pm$ σ km s^{-1}.

HD 59169: There are only two available epochs for this object: one is from UVES data and the other is FEROS data producing a value of 34.3$\pm$5.4 km s^{-1}. However, this is a significant change in RV, and therefore, it remains a potential multiple system.

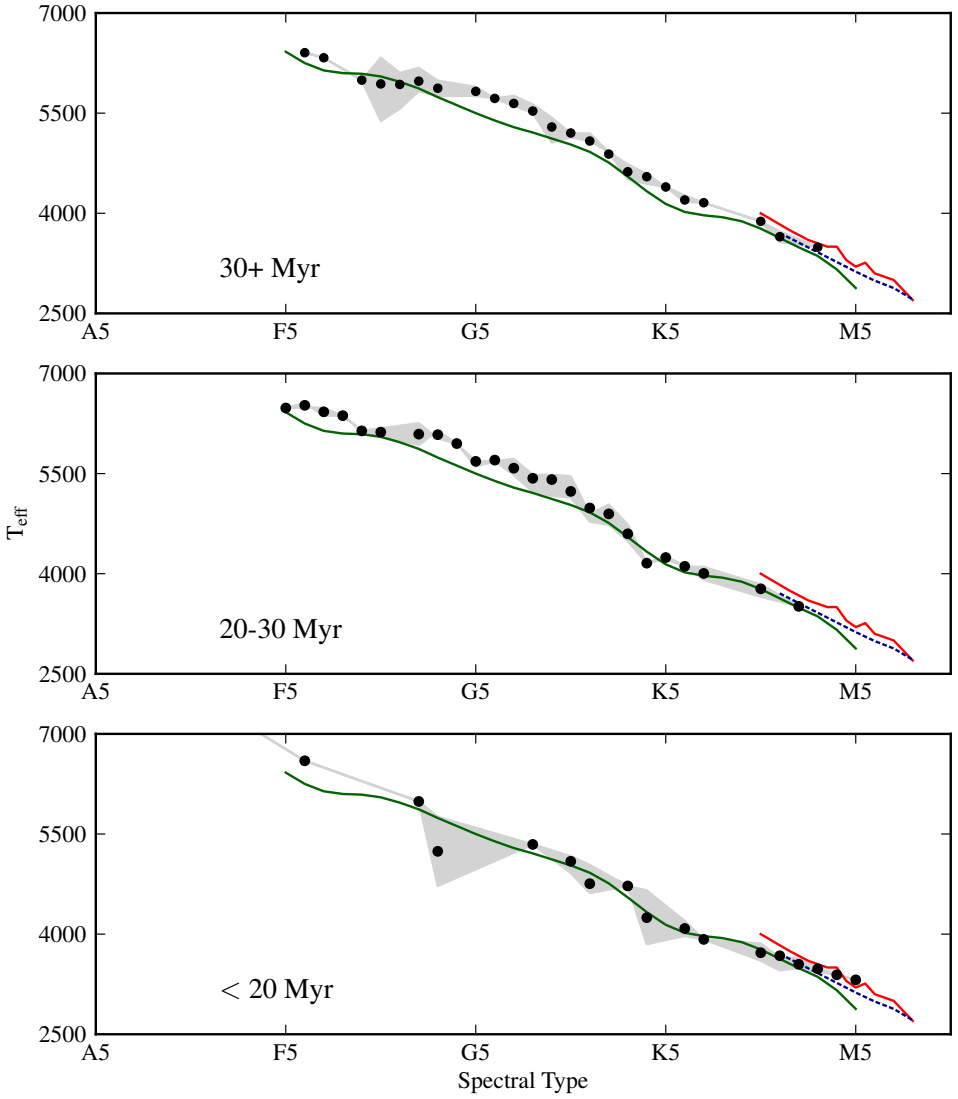

FIGURE 2.9: Spectral type versus the effective temperature for all stars used in this analysis. The stars have been binned in three different age bins, as indicated in each panel. The grey shaded area represents the range of values within each spectral bin; the black marker is the mean value. Also plotted are the results of Pecaut and Mamajek (2013) – green line, Luhman et al. (2003) – dotted blue line, and Bayo et al. (2011) – solid red line for comparison.

AU Mic: There are four data epochs in our own dataset, three from UVES, one from FEROS (-5.1,- 5.2, -4.9, and -4.0 $\mathrm{km\,s^{-1}}$) producing a value of -4.8$\pm$0.5 $\mathrm{km\,s^{-1}}$, which is not a significant variation. If one looks at the values from the literature (1.2$\pm$1.3, 15.6 and -4.5$\pm$1.3 $\mathrm{km\,s^{-1}}$.) there is one value that is significantly different from the others, 15.6. However, after private communication with John E. Gizis, it is apparent that the 1σ uncertainties are $\approx$17 $\mathrm{km\,s^{-1}}$, making this value compatible with all others. Therefore, this target is not considered as a multiple system candidate.

V1005 Ori: This target has a value of 19.0$\pm$0.3 $\mathrm{km\,s^{-1}}$ from three UVES epochs, which is a variation well below 1σ_s. However, there are seven values from the literatures; which when evaluated together show clear RV variability. Therefore, this target is considered a multiple system candidate.

GSC 09420-00948: There are four UVES data epochs for this target, producing a value of 12.7$\pm$3.2 $\mathrm{km\,s^{-1}}$. In combination with this, there are two values from Malaroda et al. (2006): 5.0 and 17.1 $\mathrm{km\,s^{-1}}$. However, these do not have any quoted uncertainties. Because the variation in RV value is larger than σ_s, even without the use of archival data, it remains a potential multiple system.

HD 104467: This target has a value of 13.3$\pm$3.1 $\mathrm{km\,s^{-1}}$ from both UVES and FEROS data. There are also two values from VizieR: 12.3$\pm$1.4 (Torres et al., 2006) and 15.4$\pm$1.0 $\mathrm{km\,s^{-1}}$ (Kharchenko et al., 2007). The values from the literature are consistent with our derived values but this target remains a potential multiple system due to the high standard deviation.

CD-363202: This target only has one observation one from FEROS data, producing a value of 5.2$\pm$0.9 $\mathrm{km\,s^{-1}}$ and one value from the catalogue search, 25.6$\pm$1.0 $\mathrm{km\,s^{-1}}$ (Torres et al., 2006). This is a huge variation in RV; however, it has an extremely high *vsini* value of 170$\pm$17 $\mathrm{km\,s^{-1}}$(Torres et al., 2006), which severely limits the accuracy of the RV determination. For this reason it is not considered as a multiple system candidate.

AK Pic: There are two observations for this target producing a value of 35.9$\pm$0.9 $\mathrm{km\,s^{-1}}$. There are six values from VizieR; four of which have associated uncertainties: 32.3$\pm$0.4,

32.1±0.5, 32.2±1.5, and 28.1±2.1 km s^{-1}. These are more than 3σ, <33.1 km s^{-1}, below our derived value, using their upper uncertainty limits. Therefore, this target is a potential multiple system.

BD+012447: This target only has one value calculated in this work, 7.7±0.9 km s^{-1}. However, there are seven values from VizieR, two of which have associated uncertainties: 8.3±0.2 and 9.1±0.6 km s^{-1}. These values agree with our derived values, and therefore, this target is not considered as a multiple system candidate.

CD-2711535: There are two observations for this target; it has a calculated RV value of -6.9±1.4 km s^{-1}. This standard deviation is well above the average for the sample (0.89 km s^{-1}). There are also two values in VizieR, -6.4±1.0 and -1.1± km s^{-1} from Torres et al. (2006) and Song et al. (2012), respectively. The latter value significantly varies from our derived value, and therefore, this target is considered a potential multiple system.

GJ 3305: This target has three observations. It has a calculated RV value of 23.8±0.5 km s^{-1}. There is one value in VizieR 17.6 km s^{-1} from Reid et al. (1995). However, after private communication with John E. Gizis, it is apparent that the 1σ uncertainties are ≈17 km s^{-1} for this work, and, therefore, this apparent variation is consistent. It is not considered as a member of β-Pic with new RV data from this work. It is a known extremely eccentric multiple system with an eccentricity of 0.06 and a period of 21.5 yr (Delorme et al., 2012; Montet et al., 2015).

BD-211074B: This target has three observations; it has a calculated RV value of 21.6±0.6 km s^{-1}. There are two values from the VizieR 20.0 and 31.7 km s^{-1} from Reid et al. (1995). However, after private communication with John E. Gizis, it is apparent that the 1σ uncertainties are ≈17 km s^{-1} for this work, and therefore, this apparent variation is consistent. Therefore, this target is not considered as a multiple system candidate.

PX Vir: Griffin (2010) determined the spectroscopic orbit of this system (216.48 day). In addition to this, we have one value of -13.3±0.89 km s^{-1}, and there are ten values from the VizieR, of which six have associated uncertainties. There are two values

from Maldonado et al. (2010) that have a huge variation, which are much higher than the level of uncertainty at -13.1±0.1 and -2.6±0.1 km s^{-1}, and agrees with the work of Griffin (2010). Therefore, this target is classified as a multiple system in this work.

GSC 08077-01788: This target has two observations; it has a calculated RV value of 17.6±0.8 km s^{-1}. There are two values from VizieR, (Torres et al., 2006): 24.0±1.0 km s^{-1} and (Kordopatis et al., 2013): -6.9±4.1 km s^{-1} . This is a very large variation, and therefore, this target is considered a multiple system in this work.

2.7.2 Archival multiplicity flags

In addition to querying for any existing RV values, we also queried for multiplicity flags from catalogues using VizieR (Dommanget and Nys (2002); Malkov et al. (2006); Pourbaix et al. (2004); Worley and Douglass (1996)), whether the system has previously been identified to have one or more companions. Out of our sub-sample of the overall SACY sample and probing only the SB systems, we found the previous multiplicity results:

HD 33999: This is a previously known triple-lined system (Dommanget and Nys, 2002) which has been flagged in previous SACY work and identified in this analysis as well.

PX Vir: As discussed in Section 2.7.1, this is a previously identified spectroscopic multiple system which agrees with the variation seen in our catalogue search.

2.7.3 Definite SB2 and SB3 candidates

Below are any details on the data of positively identified SB2 and SB3 candidates; these targets show a clear double peak in the output of the CCF. The literature was also queried to use any potential existing information.

HD 155177: There are four available data epochs for this object over a wide range of dates (2007-04-19, 2008-10-26, 2012-05-09, and 2012-06-14). There are two clear peaks that vary across the data epochs indicating strong it is a binary system. No obvious note of spectroscopic multiplicity in the literature.

HD 33999: As mentioned in Section 2.7.2, this is a previously known triple-lined multiple system.

HD 309751: There is only one epoch of data available for this object (2011-11-20); however, the produced CCF profile is extremely clear to identify it as an SB2 system. Torres et al. (2006) identified this as an SB2 system.

BD-20951: There are two epochs of data for this target (2012-07-17, 2012-07-31). There are two clear peaks in the CCFs, indicating strongly it is a bound binary system, . To the best of our knowledge, there is no note of spectroscopic multiplicity in the literature.

V4046-Sgr: There are a great many data epochs for this object and it is a well known and studied spectroscopic binary system (e.g., Quast et al. (2000); Argiroffi et al. (2012); Donati et al. (2011)).

HD 217379: There is only one epoch of data for this object (2010-05-25). Despite this, the CCF provides a clear result that this is a triple-lined system; the signal-to-noise is $\sim$200, and all three peaks are well above the noise level. Torres et al. (2006) identified this as a triple-lined (SB3) spectroscopic system.

TWA 14: There are two data epochs available for this object (2012-05-22, 2012-06-04). The output of the CCF shows two peaks; however the profiles are merged. The two

peaks have different depths in each data epoch and appear to switch position between the two epochs, indicating it is a bound binary system. Weinberger et al. (2013) and identified Jayawardhana et al. (2006) this as a double-lined (SB2) system.

TWA 20: There are three epochs of data for this target (2012-05-07, 2012-05-22, and 2012-07-03). There are two strong peaks in all of the CCFs from the RED arm of UVES; the blue is very noisy due to the spectral type of the star, M3. In addition, Jayawardhana et al. (2006) identify this is a SB2 system, and therefore, it is classified as an SB2 system in this work; however it is not considered a member of TW-Hydrae with new RV values.

1RXS J195602.8-320720: There is one epoch of data for this target (2011-10-09). The spectral type of the star is M4, and therefore, the CCF output is quite noisy; however, there is a clear second peak above the level of the noise in both the results from the RED arm of UVES. To the best of our knowledge, there is no note of spectroscopic multiplicity in the literature.

2.8 Questionable SB2 and SB3 candidates

TABLE 2.3: Details of all initially flagged potential spectroscopic multiple systems

Target	Spectral Type	MJD	Radial Velocity (RV_1, RV_2) km s^{-1}			Relative	Period[a]	Variability[b]	$vsin(i)$[a]	Association
			REDL	REDU	BLUE	Phase	(days)	Type	km s^{-1}	
CD-423328	K1	56175.398	(9.095, 41.637)	(9.000, 42.705)	(8.283, 39.763)	-	-	rot	-	CAR
		56179.380	(7.480, 38.662)	(8.395, 41.189)	(7.711, 37.067)					
CD-433604	K4	54876.233	(2.708, 34.119)	(2.104, 34.607)	(2.010, 33.134)	0	0.89	-	40.0	ARG
		56175.381	(3.951, 35.856)	(4.654, 37.148)	(3.934, 35.242)	0.717				
		56179.371	(35.742, 4.068)	(37.519, 4.802)	(34.239, 3.361)	0.200				
CD-542644	G5	54898.165	(16.836, 49.248)	(19.884, 52.743)	(16.517, 48.940)	0	1.5	rot	39.50	CAR
		55885.322	(17.599, 49.096)	(21.472, 52.862)	(12.076, 44.050)	0.105				
CP-551885	G5	54898.158	(5.656, 41.220)	(5.431, 41.711)	(4.480, 40.449)	0	0.916	rot	44.0	CAR
		55885.307	(9.909, 43.495)	(8.495, 42.886)	(7.762, 43.320)	0.674				
GSC 09239-01572	K7	55340.108	(-17.435, 17.460)	(-21.218, 18.025)	(-18.301, 17.029)	0	1.536	-	41.0	ECH
		55947.346	(10.446, 42.589)	(11.944, 44.481)	(10.257, 41.772)	0.337				
		55978.336	(-2.790, 28.210)	(-1.960, 31.678)	(2.405, 34.142)	0.513				
		55979.299	(-16.058, 16.753)	(-17.742, 18.181)	(-12.314, 16.757)	0.140				
HD 30051	F2	56138.352	(16.912, 18.734)	(17.352, 19.113)	(13.377, 18.504)	-	-	-	-	THA
		56139.358	(16.623, 17.604)	(15.756, 18.043)	(14.440, 17.640)					
		56140.361	(16.930, 17.758)	(15.124, 17.990)	(13.353, 17.893)					
TYC 7605-1429-1	K4	55461.359	(29.866, 48.461)	(26.870, 46.386)	(31.981, 45.182)	-	0.3514	-	-	ABD
TYC 7627-2190-1	K2	54896.092	(9.368, 38.543)	(7.412, 37.063)	(9.455, 37.343)	0	0.726	-	-	ABD
		55416.402	(17.964, 46.331)	(17.739, 46.579)	(18.739, 45.394)	0.680				
TYC 8594-58-1	G8	54880.184	(-1.595, 23.876)	(-2.748, 23.012)	(-1.593, 22.506)	0	0.982	-	34.1	ARG
		56082.022	(0.5190, 26.313)	(-0.035, 25.474)	(-0.722, 23.995)	0.868				
		56107.997	(-0.819, 25.295)	(-2.022, 23.421)	(-2.078, 22.478)	0.319				

Notes. [(a)] Period values and $vsin(i)$ (Messina et al., 2010, 2011). Relative phase values (relative to our first observation) were computed using the MJD values from each observation and period values. [(b)] Variability Type: **rot**=rotational variability due to the presence of spots (Kiraga, 2012). RV_1 and RV_2 values from two component gaussian fits displayed in the panels within the top row of figures in Section 2.8.

Initially, some targets were flagged as potential multiple systems, as shown in Table 2.3. The targets CD-423328, CD-542644 and CP-551885 have previously been identified as having variable rotational behaviour due to the presence of spots (Kiraga, 2012). However, this does not exclude the possibility that they are multiple systems; therefore, we conduct the same analysis for these targets as for those without any variability flag.

For the targets shown in Table 2.3, we conducted the following analysis to determine whether the deformity could be the solely the result of spots on the surface of the star.

The intensity of Ca II H (3968.5 Å) and Ca II K (3933.7 Å) emission respond to the amount of non-thermal heating of the chromosphere, which can be caused by areas of concentrated magnetic field (Leighton, 1959); therefore, there is a strong link between spot coverage and activity. We can use this to our advantage in our CCF output to differentiate between spots and merged-SB2 components.

We fitted one Gaussian profile to the CCF output, assuming it was a single star, producing a system velocity ($v_{\rm sys}$) and then looked for the specific velocities of the deformities in the profile ($v_{\rm d1}$, v_{d2}, etc.). We then compared the system velocity and deformity velocity values to the line profiles of Ca II H and K; the chromosphere can emit isotropically at the sytem velocity and have components of emission from the strong areas of magnetism, corresponding to the deformity velocities. If the Ca II H and K lines had a multiple-component structure with peaks corresponding to the values of $v_{\rm sys}$ and $v_{\rm d1}$, $v_{\rm d2}$ etc. then it is very likely that the candidate multiple system is a single system with strong activity. If this was not the case but the profiles of Ca II H and K had a multiple component structure, we also checked whether the multiple components had peak values corresponding to a multiple-line fit to the CCF, which assume the system is multiple.

The graphs presented in this section are in the following format. There are four panels for each UVES observation from left to right (1-4).

- *Panel 1:* The CCF output for the BLUE chip of UVES (blue line) and single Gaussian fit (black line). Phase values, ϕ, are shown from Table 2.3 where available.

- *Panel 2:* The residuals from each of the fits, all graphs have the same y-axis range for easy comparison of the goodness of fit. The parameter σ represents the average standard deviation in the residuals from the fit.

- *Panel 3:* The normalised flux of chromospheric line Ca II H, 3968.5 Å, in velocity space (black line); overplotted is the normalised and reversed CCF profile from *Panel 1* (blue dotted line) as well as v_{sys} and $v_{d1,2}$ (red vertical lines).

- *Panel 4* has the same format are *Panel 3* but is at 3933.7 Å, for the chromospheric line Ca II K.

TYC 7605-1429-1: This target was initially identified as a binary candidate due to its abnormal CCF profile. However, TYC 7605-1429-1 only has one epoch of data, which is not conclusive from this analysis, as shown in Figure 2.10. It has an extremely broad component with a FWHM of $\approx$62 km s^{-1}, making the RV determination difficult. Torres et al. (2006) quote a value of 28.6 km s^{-1} which agrees with our derived value of 31.2$\pm$4.0 km s^{-1}. Messina et al. (2010) flagged this target as a single system.

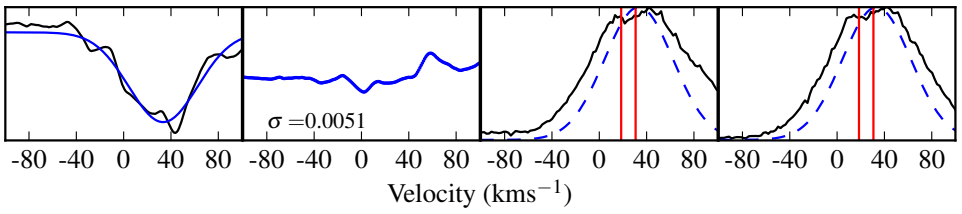

FIGURE 2.10: TYC 7605-1429-1: 2012-09-22.

HD 30051: There are three available epochs for this target, 2012-07-30, 2012-07-31, and 2012-08-01. This is an F2-type star, and therefore, does not have strong chromospheric activity, as shown in the lack of emission in Panels 3 and 4 of Figure 2.11. This star was initially classified as a multiple system due to the two component structure of the CCF profile, which potentially consists of a rapid rotator, producing the broad component with a slower-rotating companion, narrow component. However, there is no significant variation in system velocity (-1.5, -2.1 and, -2.5) between observations,

making it extremely unlikely to be a close binary system with period $>$ 1 day.

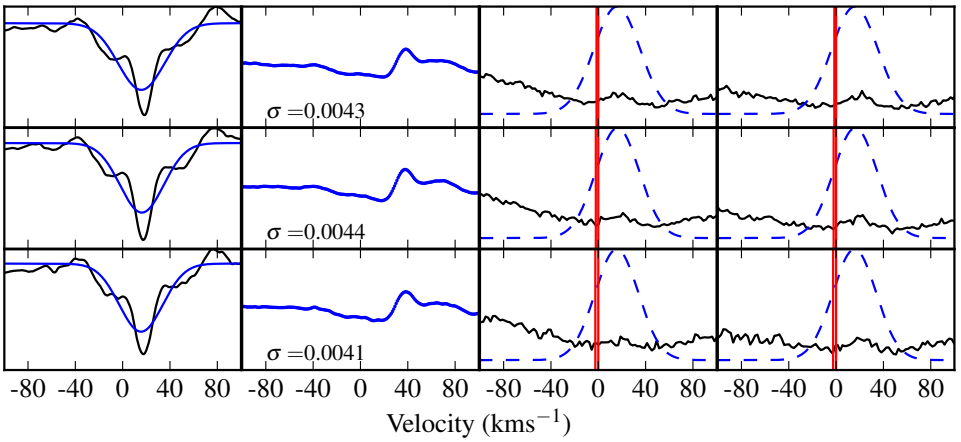

FIGURE 2.11: HD 30051: 2012-07-30, 2012-07-31, and 2012-08-01.

CD-542644: There are two epochs for this target 2009-03-08 and 2011-11-20, as seen in Figure 2.12. The velocities for v_{sys} and v_{d1} do not correspond well to the shape of the line profiles. The CCF profiles are also quite complex, making it hard to determine the correct velocities. Based on this analysis, we do not consider this target a multiple system.

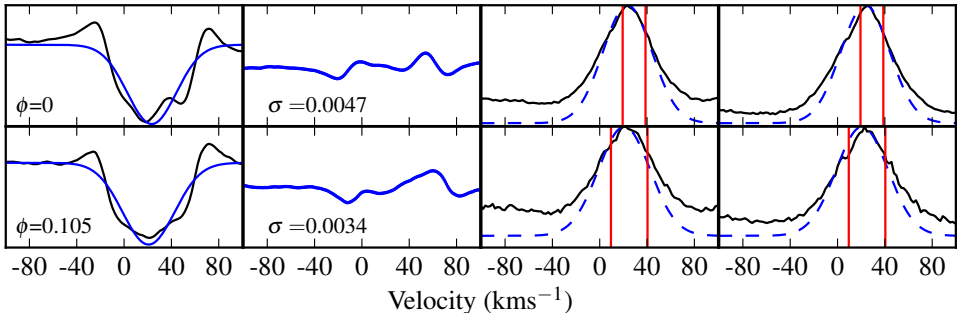

FIGURE 2.12: CD-542644: 2009-03-08, and 2011-11-20.

CP-551885: There are two epochs for this target 2009-03-08 and 2011-11-20, as seen in Figure 2.13. The line profiles displayed in panels 3 and 4 show a clear two component structure. However, the picture we have is confusing; the v_{sys} value agrees well in both epochs; however, v_{d1} does not. Instead, it is one of the velocities fitted using two Gaussians that matches with the secondary peak $\approx$5 km s^{-1}. In addition to

this, if we look at the v_{sys} values, there is no considerable variation: 27.6 (ϕ = 0), 21.5 (ϕ = 0.674) and (Torres et al., 2006) 23.1 km s^{-1} from previous work, assuming the period of rotation is synchronised with the orbital period. Based on these arguments, we do not consider this target a multiple system.

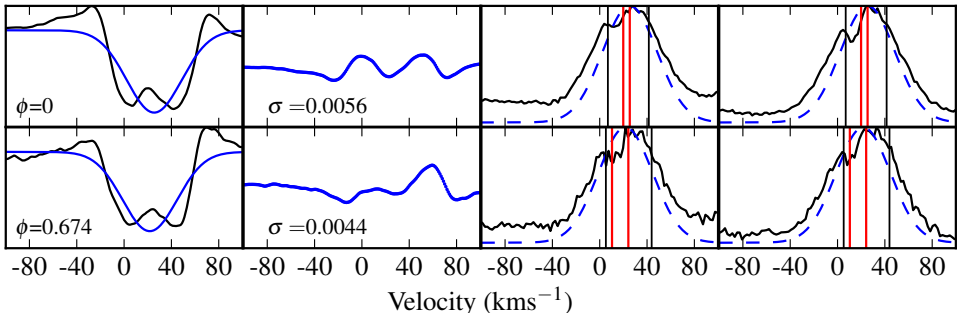

FIGURE 2.13: CP-551885: 2009-03-08, and 2011-11-20.

CD-423328: There are two epochs for this target 2012-09-05 and 2012-09-09, as seen in Figure 2.14. The lines from a two-component Gaussian fit agree with the peaks seen in the profiles of Ca II H and K. Torres et al. (2006) also quote a value of 24.6$\pm$1.0 km s^{-1}, which is hugely different from our value derived from a single Gaussian fit (15.2$\pm$0.1 km s^{-1}). Kiraga (2012) classified this object as rotationally variable due to the presence of spots; however, this does not exclude the possibility that it is a binary system. Due to this line-profile analysis and the variation in RV value, this target is classified as a potential multiple system.

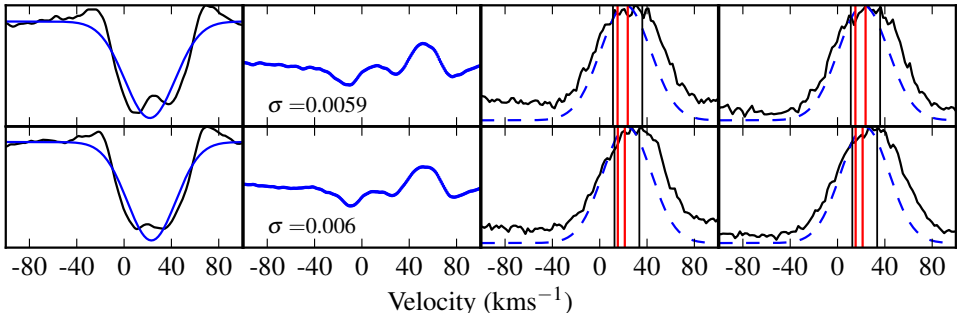

FIGURE 2.14: CD-423328: 2012-09-05, and 2012-09-09.

CD-433604: There are three available epochs for this target, 2009-02-14, 2012-09-05, and 2012-09-09, as seen in Figure 2.15. It is extremely unlikely that it is an SB2 system, as the flux ratio of the two components is variable epoch to epoch (0.97, 0.64, 0.56 respectively). The line profile analysis is inconclusive; epochs 2012-09-05 and 2012-09-09 show a two-component structure in Ca II H and K; however, the derived v_{sys} and v_{d1} values do not correspond to the peaks of these components. The calculated RV values (20.4, 24.1, and 11.0) are extremely variable, but the fits are poor, as seen in panel 2 of Figure 2.15. There is one other existing value (priv. communication, C. A. O. Torres) of 21.4, and therefore, if one considers three of the four values to compute an average, there is no significant variation ($22.0 \pm 1.9\,\mathrm{kms}^{-1}$). At this time, the evidence for multiplicity is not strong enough for us to consider this target as a multiple system.

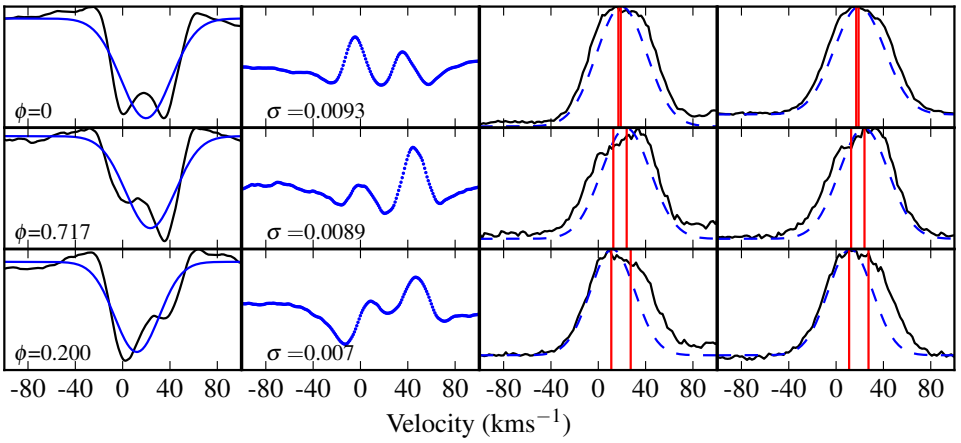

FIGURE 2.15: CD-433604: 2009-02-14, 2012-09-05, and 2012-09-09.

GSC 09239-01572: There are four epochs available for this object, 2010-05-24, 2012-01-21, 2012-02-21, and 2012-02-22. In Figure 2.16, one can see the agreement between the deformity velocities and the line profiles of Ca II H and K is extremely good for all four epochs. On this basis, we conclude that the CCF profile is the result of star spots as opposed to multiplicity.

TYC 7627-2190-1: There are two epochs available for this object: 2009-03-06 and 2010-08-08, as seen Figure 2.17. From the fitting of a single system velocity to the

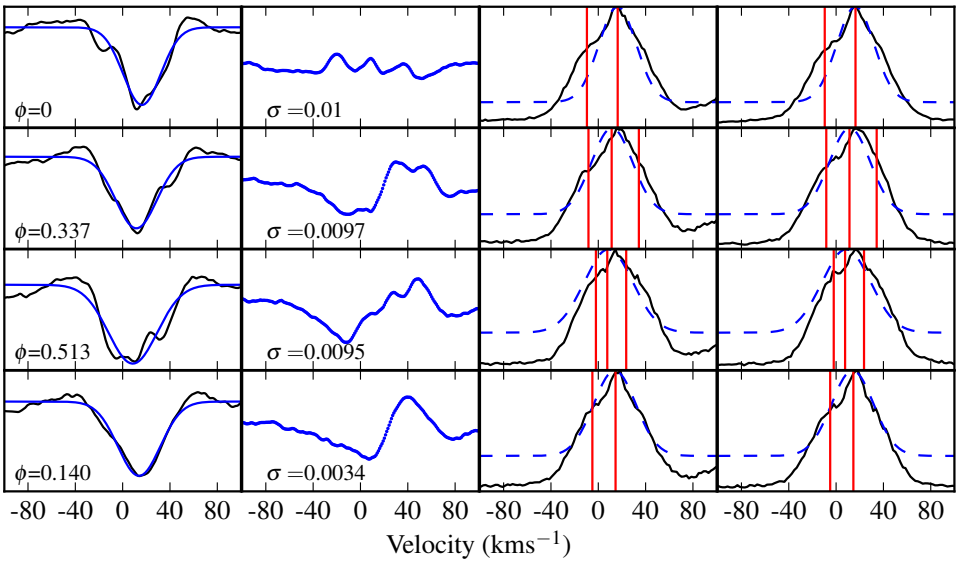

FIGURE 2.16: GSC 09239-01572: 2010-05-24, 2012-01-21, 2012-02-21, and 2012-02-22.

profiles there is no significant variation betwen the observations (25.6 and 27.2). The value of the system velocity is extremely close to that of the deformity velocity; this makes it extremely difficult to see the separate components in this analysis. However, we only have two epochs, and therefore based on this evidence, we do not classify this as a multiple system.

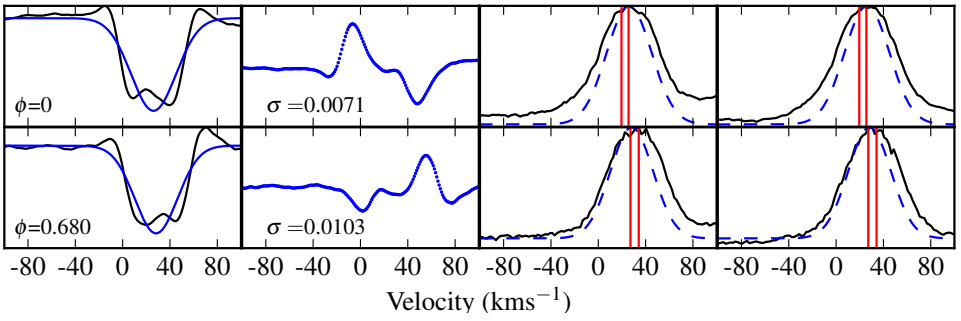

FIGURE 2.17: TYC 7627-2190-1: 2009-03-06, and 2010-08-08.

TYC 8594-58-1: There are three epochs of data for this target: 2009-02-18, 2012-06-04 and 2012-06-29. However, much like TYC7627-2190, the value of the deformity velocity is extremely close to the system velocity, and therefore, seeing the two components

separately is extremely difficult. There is no significant variation in the system velocity between all three epochs (10.8, 8.2, and 10.9, respectively). Figure 2.18 also shows the velocities when fitting the CCF with two Gaussians, as shown as black vertical lines. Neither of these techniques provide strong evidence for or against the multiplicity of the system. Therefore, as it statistically much more likely to be a single system, it is not considered a multiple system in this work.

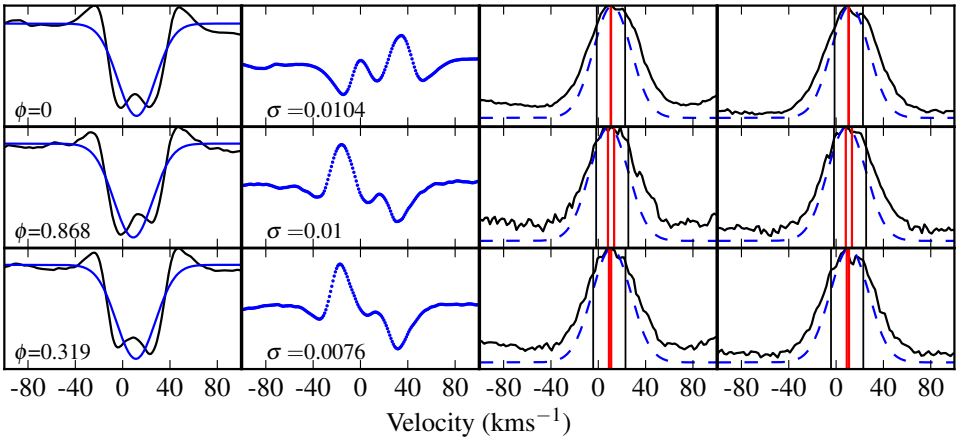

FIGURE 2.18: TYC 8594-58-1: 2009-02-18, 2012-06-04, and 2012-06-29.

2.9 Details of targets and their derived properties

TABLE 2.4: Summary table of all radial velocity values used in this analysis for single and SB1 systems.

ID	RA	DEC	N. of Obs.	RV (km s^{-1})	$\sigma^{1,2}$	Reference[3]
			AB Doradus members			
HD 6569	01:06:26.2	-14:17:47	2	7.55	0.02	
BD-12243	01:20:32.3	-11:28:04	2	10.26	0.35	
CD-46644	02:10:55.4	-46:03:59	1	25.78	0.89	
				25.7	-	t
HD 16760B	02:42:21.0	+38:37:21	1	-3.46	0.89	
HD 16760	02:42:21.3	+38:37:07	1	-3.19	0.89	
HD 17332B	02:47:27.2	+19:22:21	2	4.41	0.65	
HD 17332A	02:47:27.4	+19:22:19	1	3.91	0.89	
				4.5	1.3	a
				4.4	0.2	f
				4.3	0.1	f
				3.76	0.8	g
IS Eri	03:09:42.3	-09:34:47	2	14.46	0.14	
HD 24681	03:55:20.4	-01:43:45	1	18.02	0.89	
HD 25457	04:02:36.7	-00:16:08	2	17.62	0.36	
HD 31652	04:57:22.3	-09:08:00	1	22.61	0.89	
CD-401701	05:02:30.4	-39:59:13	3	28.4	0.25	
				27.8	1.0	j
HD 32981	05:06:27.7	-15:49:30	1	25.64	0.89	
HD 293857	05:11:09.7	-04:10:54	1	20.28	0.89	
HD 35650	05:24:30.2	-38:58:11	4	32.32	0.53	
				31.3	0.3	f
UX Col	05:28:56.5	-33:28:16	2	30.07	0.38	
				30.1	0.1	j
CD-342331	05:35:04.1	-34:17:52	3	30.48	0.14	
				30.4	1.0	j
CD-481893	05:36:55.1	-47:57:48	3	30.98	1.21	
				32.2	0.2	g
				32.2	B	n
UY Pic	05:36:56.9	-47:57:53	3	32.31	0.22	
WX Col	05:37:12.9	-42:42:56	4	31.38	0.18	
TYC 7604-1675-1	05:37:13.2	-42:42:57	2	30.47	0.14	
TYC 4779-394-1	05:38:56.6	-06:24:41	1	22.88	0.89	
CP-19878	05:39:23.2	-19:33:29	2	27.8	0.91	

ID	RA	DEC	N. of Obs.	RV (km s^{-1})	$\sigma^{1,2}$	Reference[3]
TYC 7605-1429-1	05:41:14.3	-41:17:59	1	30.7	0.89	
TZ Col	05:52:16.0	-28:39:25	2	28.71	0.25	
				31.1	1.0	j
BD-131328	06:02:21.9	-13:55:33	1	25.43	0.89	
CD-342676	06:08:33.9	-34:02:55	3	30.47	0.69	
				31.1	1.0	j
CD-352722	06:09:19.2	-35:49:31	3	32.03	0.08	
				31.4	0.4	j
HD 45270	06:22:30.9	-60:13:07	4	31.63	0.32	
AK Pic	06:38:00.4	-61:32:00	2	35.87	0.91	
				32.3	0.35	c
				28.1	-	e
				32.1	0.5	f
				32.2	1.5	g
				28.1	2.1	g
				35.0	1.0	j
CD-611439	06:39:50.0	-61:28:42	1	31.38	0.89	
				31.7	1.0	j
TYC 7627-2190-1	06:41:18.5	-38:20:36	2	28.0	0.8	
GSC 08544-01037*	06:47:53.4	-57:13:32	3	30.0	0.43	
CD-571654	07:10:50.6	-57:36:46	3	29.22	0.14	
				29.7	1.0	j
V429 Gem	07:23:43.6	+20:24:59	2	7.39	0.43	
				9.3	-	b
HD 59169	07:26:17.7	-49:40:51	2	34.29	5.38	
CD-8480	07:30:59.5	-84:19:28	1	23.23	0.89	
				24.2	0.8	j
HD 64982	07:45:35.6	-79:40:08	2	25.66	0.01	
BD+012447	10:28:55.5	+00:50:28	1	7.71	0.89	
				18.3	-	b
				12.7	-	b
				11.8	-	b
				8.4	-	b
				9.9	-	d
				8.3	0.2	f
				9.1	0.6	g
PX Vir	13:03:49.7	-05:09:43	1	-13.3	0.89	
				-10.8	0.3	f
				0.0	-	g
				-13.1	0.08	k
				-2.6	0.09	k
				-13.1	1.7	m
				-9.21	A	n

ID	RA	DEC	N. of Obs.	RV (km s^{-1})	$\sigma^{1,2}$	Reference[3]
				-8.2	-	p
				-5.8	-	p
				7.9	-	q
				0.0	5.0	s
HD 139751	15:40:28.4	-18:41:46	1	-7.6	0.89	
HIP 81084	16:33:41.6	-09:33:12	1	-14.66	0.89	
HD 152555	16:54:08.1	-04:20:25	2	-16.44	0.01	
HD 178085	19:10:57.9	-60:16:20	1	8.45	0.89	
				8.1	1.1	j
TYC 486-4943-1	19:33:03.8	+03:45:40	1	-20.69	0.89	
BD-034778	20:04:49.4	-02:39:20	2	-16.46	0.01	
HD 199058	20:54:21.1	+09:02:24	2	-19.54	0.17	
TYC 1090-543-1	20:54:28.0	+09:06:07	2	-19.18	0.13	
HD 201919	21:13:05.2	-17:29:13	3	-7.39	0.24	
				-7.4	1.0	j
HD 218860	23:11:52.0	-45:08:11	2	9.92	0.32	
				11.2	1.3	j
HD 222575	23:41:54.2	-35:58:39	1	10.83	0.89	
				11.1	1.7	j
HD 224228	23:56:10.5	-39:03:07	4	13.48	0.59	
			Argus members			
CD-292360	05:34:59.2	-29:54:04	3	25.71	0.31	
				26.0	1.0	j
CD-283434	06:49:45.4	-28:59:17	1	26.68	0.89	
				26.7	1.0	j
CD-422906	07:01:53.4	-42:27:56	4	23.73	0.23	
				23.7	1.0	j
CD-482972	07:28:22.0	-49:08:38	1	18.85	0.89	
				21.1	1.0	j
HD 61005	07:35:47.5	-32:12:14	2	22.36	0.21	
CD-483199	07:47:26.0	-49:02:51	5	17.68	0.31	
				18.5	1.0	j
CD-433604	07 48 49.8	-43 27 06	3	22.0	1.91	
TYC 8561-970-1	07:53:55.5	-57:10:07	4	15.85	0.18	
RXS J082952.7-514030	08:29:51.9	-51:40:40	1	16.15	0.89	
PMM 6974	08:34:18.1	-52:15:58	1	15.1	0.89	
TYC 8568-407-1	08:34:20.5	-52:50:05	1	16.88	0.89	
1RXS J083502.7-521339	08:35:01.2	-52:14:01	1	15.4	0.89	
ASAS J083655-5308.5	08:36:55.0	-53:08:34	1	14.67	0.89	

ID	RA	DEC	N. of Obs.	RV (km s^{-1})	$\sigma^{1,2}$	Reference[3]
TYC 8568-2261-1	08:37:51.6	-53:45:46	1	14.58	0.89	
CD-52 2467	08:38:22.9	-52:56:48	1	15.14	0.89	
PMM 686	08:39:22.6	-53:55:06	1	15.18	0.89	
V364 Vel	08:39:53.0	-52:57:57	1	15.26	0.89	
PMM 8415	08:40:16.3	-52:56:29	1	14.79	0.89	
VXR PSPC 22a	08:40:49.1	-53:37:45	1	14.14	0.89	
TYC 8569-3687-1	08:43:00.4	-53:54:08	1	16.13	0.89	
V376 Vel	08:44:05.2	-52:53:17	1	13.61	0.89	
			1	14.74	0.89	
CD-572315	08:50:08.1	-57:45:59	5	11.93	0.86	
				11.7	0.7	j
TYC 8594-58-1	09:02:03.9	-58:08:50	3	10.0	1.53	
BD-202977	09:39:51.4	-21:34:17	1	17.87	0.89	
TYC 9217-641-1	09:42:47.4	-72:39:50	2	6.17	0.72	
				6.7	1.0	j
CD-395833	09:47:19.9	-40:03:10	3	14.87	0.33	
HD 309851	09:55:58.3	-67:21:22	4	7.39	0.4	
				6.6	1.0	j
CD-74673	12:20:34.4	-75:39:29	1	4.68	0.89	
				0.6	0.8	j
CD-75652	13:49:12.9	-75:49:48	5	-1.03	0.26	
				-0.9	1.0	j
HD 129496	14:46:21.4	-67:46:16	1	-11.0	0.89	
NY Aps	15:12:23.4	-75:15:16	4	-3.07	0.26	
				-3.5	0.1	j
CD-529381	20:07:23.8	-51:47:27	1	-13.66	0.89	
				-13.3	1.0	j
			β-Pic members			
HIP 10679	02:17:24.7	+28:44:30	1	5.32	0.89	
				3.9	1.3	a
				5.0	1.3	g
				5.0	0.2	s
GSC 08056-00482	02:36:51.5	-52:03:04	1	13.84	0.89	
				16.0	0.1	j
BD+05378*	02:41:25.9	+05:59:18	1	7.31	0.89	
				10.0	-	n
GJ 3305*	04:37:37.5	-02:29:28	3	23.84	0.47	
				17.6	-	d
V1005 Ori	04:59:34.8	+01:47:01	3	18.95	0.33	

ID	RA	DEC	N. of Obs.	RV (km s^{-1})	$\sigma^{1,2}$	Reference[3]
				39.0	-	b
				32.4	-	b
				18.2	-	b
				37.2	-	d
				18.7	3.3	f
				22.0	5.1	g
				30.5	5.1	s
CD-571054	05:00:47.1	-57:15:25	2	19.48	0.47	
				19.4	0.3	j
BD-211074B	05:06:49.5	-21:35:04	3	21.55	0.55	
				20.0	-	d
				31.7	-	d
BD-211074A	05:06:49.9	-21:35:09	2	21.22	0.31	
TYC 112-917-1	05:20:00.3	+06:13:04	3	18.76	0.13	
TYC 112-1486-1	05:20:31.8	+06:16:11	3	18.52	0.23	
				18.0	-	t
V1311 Ori*	05:32:04.5	-03:05:29	3	23.84	0.55	
AO Men	06:18:28.2	-72:02:41	5	16.18	0.19	
				16.2	1.0	u
TWA 22	10:17:26.9	-53:54:27	2	13.49	0.1	
HD 139084B	15:38:56.8	-57:42:19	1	3.03	0.89	
				0.1	2.0	j
V343 Nor	15:38:57.5	-57:42:27	3	3.32	2.23	
				3.1	0.8	f
				3.6	0.95	g
				4.2	1.4	j
				2.4	-	l
CD-2711535	17:15:03.6	-27:49:40	2	-6.9	1.36	
				-6.4	1.0	j
				-1.1	1.8	r
CD-547336	17:29:55.1	-54:15:49	4	0.95	0.67	
				1.6	1.4	j
				-0.5	3.7	r
HD 164249	18:03:03.4	-51:38:56	1	-0.67	0.89	
GSC 07396-00759	18:14:22.1	-32:46:10	1	-6.05	0.89	
TYC 9073-762-1	18:46:52.6	-62:10:36	3	2.56	0.78	
CD-2613904	19:11:44.7	-26:04:09	1	-9.72	0.89	
HD 181327	19:22:58.9	-54:32:17	3	-0.72	0.29	
TYC 7443-1102-1	19:56:04.4	-32:07:38	2	-6.32	0.04	
1RXS J200136.9-331307	20:01:37.2	-33:13:14	3	-4.64	0.24	
AU Mic	20:45:09.3	-31:20:24	4	-4.82	0.49	
				1.2	1.3	a
				15.6	-	d

ID	RA	DEC	N. of Obs.	RV (km s^{-1})	$\sigma^{1,2}$	Reference[3]
				-4.5	1.3	g
AZ Cap	20:56:02.7	-17:10:54	3	-7.74	0.88	
				-6.9	1.0	j
CP-722713	22:42:48.9	-71:42:21	1	7.78	0.89	
				8.6	0.5	j
WW PsA	22:44:57.8	-33:15:01	3	1.95	0.83	
				2.2	1.0	j
TX PsA	22:45:00.0	-33:15:26	2	2.97	0.32	
BD-136424	23:32:30.9	-12:15:52	3	1.13	0.99	
				1.8	0.7	j
			Carina members			
HD 269620	05:29:27.1	-68:52:05	5	19.27	0.41	
				18.7	1.0	j
HD 42270	05:53:29.3	-81:56:53	3	16.57	0.33	
				16.7	0.6	j
CD-482324	06:28:06.1	-48:26:53	1	24.57	0.89	
				24.9	1.0	j
HD 49855*	06:43:46.2	-71:58:35	4	20.83	0.14	
				20.1	0.5	f
				19.9	0.5	g
				20.7	0.1	j
CD-571709	07:21:23.7	-57:20:37	4	23.32	0.31	
				23.2	0.2	j
CD-423328[a]	07:33:21.2	-42:55:42	2	15.2	0.10	
				24.6	1.0	j
TYC 8557-1251-1	07:55:31.6	-54:36:51	3	21.59	0.37	
				21.8	0.3	j
TYC 8570-1980-1	08:11:09.3	-55:55:56	3	21.47	0.36	
CP-541712	08:37:10.9	-55:18:10	4	20.9	0.24	
CD-612010	08:42:00.4	-62:18:26	4	21.65	0.58	
				22.5	2.1	j
CD-75392	08:50:05.4	-75:54:38	3	17.41	0.49	
TYC 8590-1193-1	08:56:31.5	-57:00:41	3	19.49	1.97	
TYC 8582-3040-1	08:57:45.6	-54:08:37	4	22.12	0.36	
				22.5	0.0	j
CD-494008	08:57:52.2	-49:41:51	4	22.03	0.17	
				23.0	0.2	j
CP-551885	09:00:03.4	-55:38:24	2	25.8	2.55	
				23.1	1.0	j

ID	RA	DEC	N. of Obs.	RV (km s^{-1})	$\sigma^{1,2}$	Reference[3]
CD-552543	09:09:29.3	-55:38:27	4	22.11	0.86	
				22.5	1.0	j
TYC 8174-1586-1	09:11:15.6	-50:14:16	3	22.52	0.35	
				22.5	1.0	j
CD-542644	09:13:16.9	-55:29:03	2	21.15	0.49	
CP-621293	09:43:08.8	-63:13:04	4	20.91	0.55	
				21.8	0.1	j
TYC 8946-872-1*	09:55:15.1	-62:03:32	2	21.8	0.31	
TYC 9217-417-1	09:59:57.7	-72:21:47	3	16.95	0.24	
				17.0	0.4	j
TYC 8962-1747-1	11:08:07.9	-63:41:47	3	17.63	1.5	
				19.3	1.0	j
HD 107722	12:23:29.0	-77:40:51	3	12.5	0.27	
TYC 460-624-1*	18:45:10.3	+06:20:16	2	-25.2	0.21	
HD 189285*	19:59:24.1	-04:32:06	1	-19.41	0.89	
HD 221451*	23:32:19.2	-13:37:18	2	-6.39	0.86	
			Columba members			
CD-52381	01:52:14.6	-52:19:33	7	13.81	0.38	
BD-16351	02:01:35.6	-16:10:01	3	10.03	0.36	
				13.4	1.9	h
CD-44753	02:30:32.4	-43:42:23	2	15.17	2.12	
TYC 8862-19-1	02:58:04.0	-62:41:14	6	16.8	0.49	
				16.6	0.5	j
BD-11648	03:21:49.7	-10:52:18	2	15.12	0.54	
BD-04700	03:57:37.2	-04:16:16	3	18.28	0.46	
BD-15705*	04:02:16.5	-15:21:30	4	15.14	0.14	
HD 26980	04:14:22.5	-38:19:02	5	21.3	0.44	
				20.2	0.3	j
HD 27679	04:21:10.3	-24:32:21	2	21.5	0.16	
CD-431395	04:21:48.7	-43:17:33	4	21.68	0.35	
				22.0	1.0	j
CD-361785	04:34:50.8	-35:47:21	4	22.18	0.35	
				23.3	1.0	j
GSC 08077-01788	04:51:53.0	-46:47:31	2	17.6	0.76	
				23.0	1.0	j
				-6.9	4.1	v
HD 31242N	04:51:53.5	-46:47:13	2	22.0	0.23	
HD 272836	04:53:05.2	-48:44:39	1	22.81	0.89	
				24.0	1.0	j

ID	RA	DEC	N. of Obs.	RV (km s^{-1})	$\sigma^{1,2}$	Reference[3]
TYC 5900-1180-1*	04:58:35.8	-15:37:31	1	23.56	0.89	
BD-08995	04:58:48.6	-08:43:40	3	24.08	0.52	
HD 32372	05:00:51.9	-41:01:07	2	23.17	0.29	
HD 274561	05:28:55.1	-45:34:58	2	24.57	0.16	
BD-191194	05:30:19.1	-19:16:32	1	26.16	0.89	
CD-392075*	05:37:05.3	-39:32:26	3	23.06	0.29	
				23.1	0.6	j
BD-081195	05:38:35.0	-08:56:40	4	24.16	0.58	
				26.2	-	t
CD-382198	05:45:16.3	-38:36:49	4	26.87	0.71	
CD-292531	05:50:21.4	-29:15:21	3	26.54	0.38	
				27.5	1.0	j
HD 40216	05:55:43.1	-38:06:16	2	24.38	0.09	
AB Pic	06:19:12.9	-58:03:16	6	22.94	0.34	
				22.6	0.3	j
CD-402458	06:26:06.9	-41:02:54	4	25.59	0.45	
				25.0	1.0	j
HD 48370	06:43:01.0	-02:53:19	1	23.38	0.89	
CD-363202	06:52:46.8	-36:36:17	1	5.22	0.89	
				25.6	1.0	j
TYC 9178-284-1	06:55:25.2	-68:06:21	3	20.09	0.16	
				20.1	0.1	j
HD 51797	06:56:23.5	-46:46:55	5	25.2	0.31	
				25.2	0.2	j
HD 55279	07:00:30.5	-79:41:46	3	17.59	0.15	
CP-531875*	08:45:52.7	-53:27:28	1	21.82	0.89	
				23.2	1.0	j
V479 Car	09:23:34.9	-61:11:36	5	20.82	0.15	
				20.8	0.4	j
CP-522481	09:32:26.1	-52:37:40	6	21.37	0.56	
HD 298936	10:13:14.6	-52:30:54	4	17.71	0.28	
				17.7	1.0	j
CD-544320*	11:45:51.8	-55:20:46	4	16.01	0.41	
			ϵ-Chamaeleon members			
EG Cha	08:36:56.2	-78:56:46	3	18.22	0.72	
				18.4	1.0	j
EO Cha	08:44:31.9	-78:46:31	3	17.32	0.11	
				15.0	-	o
EQ Cha*	08:47:56.8	-78:54:53	3	22.98	0.77	

ID	RA	DEC	N. of Obs.	RV (km s^{-1})	$\sigma^{1,2}$	Reference[3]
				18.0	-	o
1RXS J091528.1-760856	09:15:29.1	-76:08:47	3	19.1	0.55	
				21.0	2.0	o
1RXS J093455.3-780414	09:34:56.1	-78:04:19	3	16.77	0.61	
1RXS J100515.1-774900	10:05:20.0	-77:48:42	3	16.38	0.06	
DZ Cha	11:49:31.9	-78:51:01	3	14.02	0.42	
				18.0	-	e
				13.4	1.3	j
				12.2	-	o
T Cha	11:57:13.5	-79:21:32	1	14.71	0.89	
GSC 09415-02676*	11:58:26.9	-77:54:45	3	14.47	0.24	
				13.0	2.2	o
HIP 58490	11:59:42.3	-76:01:26	5	13.66	0.51	
				15.1	1.0	j
DX Cha	12:00:05.1	-78:11:35	2	11.51	0.36	
HD 104237-5	12:00:08.3	-78:11:40	2	13.7	0.03	
HD 104237-6	12:00:09.3	-78:11:42	3	13.76	1.41	
HD 104467	12:01:39.1	-78:59:17	5	13.32	3.07	
				12.3	1.4	j
				15.4	1.0	g
GSC 09420- 00948	12:02:03.8	-78:53:01	4	12.66	3.23	
				17.1	-	e
				5.0	-	e
HD 105923	12:11:38.1	-71:10:36	5	14.2	0.37	
				14.2	1.0	j
1RXS J121645.2-775339	12:16:46.0	-77:53:33	4	14.03	0.18	
				14.0	2	o
G92391495	12:19:43.8	-74:03:57	3	13.92	0.08	
GSC 09239-01572	12:20:21.9	-74:07:39	4	12.65	3.26	
CD-74712	12:39:21.3	-75:02:39	9	13.31	0.34	
				14.4	0.2	j
CD-691055	12:58:25.6	-70:28:49	3	12.35	0.7	
				12.8	1.0	j
				11.1	1.5	r
CP-681894	13:22:07.5	-69:38:12	6	11.66	0.76	
				11.6	0.2	j
			Octans members			
CD-58860	04:11:55.6	-58:01:47	4	9.52	0.06	
				9.8	1.0	j

ID	RA	DEC	N. of Obs.	RV (km s^{-1})	$\sigma^{1,2}$	Reference[3]
CD-431451	04:30:27.3	-42:48:47	5	13.17	0.38	
HD 274576	05:28:51.4	-46:28:19	4	12.05	0.66	
				12.7	1.0	j
BD-201111	05:32:29.3	-20:43:33	2	19.36	0.23	
CD-471999	05:43:32.1	-47:41:11	2	11.67	2.28	
				14.4	1.0	j
TYC 7066-1037-1	05:58:11.8	-35:00:49	4	14.52	0.25	
CD-492037	06:03:35.4	-49:11:26	5	12.12	0.19	
CD-303394N	06:40:04.9	-30:33:03	4	14.51	0.17	
CD-303394S	06:40:05.7	-30:33:09	2	14.87	1.1	
TYC 9300-529-1	18:49:45.1	-71:56:58	3	-2.26	0.47	
CP-82784	19:53:56.7	-82:40:42	1	-2.15	0.89	
				-2.0	1.2	j
CD-87121	23:58:17.7	-86:26:24	6	-0.86	1.41	
			Tucana Horologium members			
HD 105	00:05:52.5	-41:45:11	1	2.05	0.89	
				3.2	1.3	a
HD 987	00:13:52.8	-74:41:17	6	9.78	0.45	
				8.8	0.3	f
HD 1466	00:18:26.1	-63:28:39	4	6.23	0.18	
HIP 1993	00:25:14.7	-61:30:48	1	6.06	0.89	
CD-7824	00:42:20.3	-77:47:40	7	11.87	0.51	
				11.5	0.6	j
HD 8558	01:23:21.1	-57:28:50	8	9.56	0.36	
				8.3	0.4	g
HD 9054	01:28:08.6	-52:38:19	3	8.55	0.2	
HD 12039	01:57:49.0	-21:54:05	2	5.83	0.38	
				5.8	0.4	f
HD 13183	02:07:17.9	-53:11:56	11	9.87	0.4	
				9.7	0.3	f
				9.5	0.2	g
HD 13246	02:07:26.1	-59:40:46	6	9.79	0.48	
CD-60416	02:07:32.1	-59:40:21	5	10.59	0.74	
GSC 08491-01194	02:41:47.3	-52:59:31	1	12.85	0.89	
				12.5	1.2	j
CD-58553	02:42:33.0	-57:39:37	5	12.54	0.4	
				12.4	0.1	j
CD-351167	03:19:08.6	-35:07:00	3	13.57	0.11	
				13.5	0.2	j

ID	RA	DEC	N. of Obs.	RV (km s^{-1})	$\sigma^{1,2}$	Reference[3]
CD-461064	03:30:49.1	-45:55:57	1	14.06	0.89	
				15.3	0.5	j
CD-441173	03:31:55.6	-43:59:14	6	15.65	0.36	
				15.5	0.3	j
HD 22705	03:36:53.4	-49:57:29	4	14.34	1.51	
HD 24636	03:48:11.5	-74:41:39	3	13.69	0.56	
BD-12943	04:36:47.1	-12:09:21	2	17.31	0.41	
HD 29615	04:38:43.9	-27:02:02	4	18.92	0.32	
HD 30051*	04:43:17.2	-23:37:42	3	-2.03	0.50	
TYC 8083-455-1	04:48:00.7	-50:41:26	3	18.91	0.2	
				19.3	0.1	j
BD-191062	04:59:32.0	-19:17:42	3	20.12	0.44	
BD-091108	05:15:36.5	-09:30:51	4	20.8	0.34	
				21.0	-	t
CD-302310	05:18:29.0	-30:01:32	4	20.99	0.53	
TYC 8098-414-1	05:33:25.6	-51:17:13	2	18.51	1.52	
				20.5	0.0	j
CD-272520	05:49:06.6	-27:33:56	2	23.0	0.43	
HD 47875	06:34:41.0	-69:53:06	5	15.75	1.92	
GSC 09507-02466*	11:40:16.5	-83:21:00	3	13.06	0.37	
				13.4	0.8	j
HD 202917	21:20:50.0	-53:02:03	6	-1.16	0.39	
				0.1	0.2	f
				-1.6	0.2	g
				-5.3	-	i
				-0.9	0.7	j
				-0.9	A	n
HIP 107345	21:44:30.1	-60:58:39	3	2.09	0.4	
				2.3	0.5	j
HD 207575	21:52:09.7	-62:03:09	3	1.57	0.17	
HD 222259N	23:39:39.1	-69:11:39	6	6.21	0.32	
				7.4	0.2	g
				6.1	0.1	j
				8.3	A	n
HD 222259S	23:39:39.3	-69:11:44	8	7.9	0.17	
TW Hydrae members						
TWA 7	10:42:30.1	-33:40:17	2	11.89	0.37	
TW Hya	11:01:51.9	-34:42:17	2	12.45	0.52	
				13.4	0.8	j

ID	RA	DEC	N. of Obs.	RV (km s^{-1})	$\sigma^{1,2}$	Reference[3]
CD-298887	11:09:13.8	-30:01:40	2	10.98	0.03	
				12.1	1.0	j
TWA 12	11:21:05.5	-38:45:16	2	10.85	0.33	
CD-347390A*	11:21:17.2	-34:46:46	4	10.8	0.43	
				11.3	1.0	j
CD-347390B*	11:21:17.4	-34:46:50	4	11.48	0.4	
				11.6	1.0	j
CD-268632A	11:32:41.2	-26:51:56	2	8.06	0.43	
				8.0	1.0	j
TWA 9B	11:48:23.7	-37:28:49	1	11.51	0.89	
				9.5	B	n
TWA 9A	11:48:24.2	-37:28:49	3	10.39	0.62	
TWA 23	12:07:27.4	-32:47:00	2	10.93	0.1	
CD-397538	12:15:30.7	-39:48:43	3	7.03	0.58	
TWA 16	12:34:56.4	-45:38:07	3	8.74	0.36	
				9.0	-	t
TWA 10	12:35:04.2	-41:36:39	3	6.31	0.23	
				6.6	1.0	j

(*) No longer classified as a member of association with new RV values.

(*a*) RV values from a single-component Gaussian fit; see Section 2.8 for details on target.

(1) Uncertainties for UVES and FEROS data: If more than one observation was available uncertainties were taken to be the standard deviation from the mean value for each target. If there was only one observation the uncertainty has a value of 0.89 km s^{-1}, one standard deviation of the entire sample.

(2) Uncertainties from de Bruijne and Eilers (2012) have values (*A*): the standard errors are generally reliable or (*B*): potential, small, uncorrected, systematic errors.

(3) **References:** a: I/196 (Turon et al., 1993), b: I/306A/ (Ivanov, 2008), c:III/105/ (Andersen et al., 1985), d: III/198/ (Reid et al., 1995), e: III/249/ (Malaroda et al., 2006), f: III/252 (Gontcharov, 2006), g: III/254/ (Kharchenko et al., 2007), h: III/265/ (Siebert et al., 2011), i :J/A+A/423/517/ (Rocha-Pinto et al., 2004), j: J/A+A/460/695/ (Torres et al., 2006), k: J/A+A/521/A12/ (Maldonado et al., 2010), l: J/A+A/530/A138/ (Casagrande et al., 2011), m: J/A+A/531/A8/ (Jenkins et al., 2011), n: J/A+A/546/A61/ (de Bruijne and Eilers, 2012), o: J/A+A/551/A46/ (Lopez Martí et al., 2013), p: J/A+AS/142/275/ (Strassmeier et al.,

2000), q: J/AJ/133/2524/ (White et al., 2007), r: J/AJ/144/8/ (Song et al., 2012), s: J/AZh/83/821/ (Bobylev et al., 2006), t: J/AcA/62/67/ (Kiraga, 2012), u: V/137D/XHIP (Anderson and Francis, 2012), v: III/272/ (Kordopatis et al., 2013).

TABLE 2.5: Summary table of UVES radial velocity values for SB2 and SB3 systems.

ID	RA	DEC	MJD	Ass.	Flux Ratio	RV_1	σ_1	RV_2	σ_2	RV_3	σ_3
BD-20951	04:52:49.5	-19:55:02	56125.4	CAR	0.25	-27.1	0.1	80.2	0.2		
			56139.4			-27.5	0.9	81.9	0.9		
HD 33999	05:12:35.8	-34:28:48	55410.4	ABD	0.70, 0.20	28.7	0.5	-15.7	0.2	59.0	1.0
HD 309751	09:31:44.7	-65:14:53	55885.3	CAR	0.48	-7.4	0.3	53.0	0.6		
TWA 20*	12:31:38.1	-45:58:59	56054.2	TWA	0.79	-50.5	1.8	76.1	2.3		
			56069.2			-47.5	1.5	72.5	1.4		
			56111.1			-47.8	1.2	71.7	1.6		
HD 155177	17:42:09.0	-86:08:05	54209.4	OCT	0.86	12.2	0.3	-21.9	0.6		
			54765.0			7.4	0.9	-7.0	0.7		
			56056.4			-17.2	0.1	31.3	0.3		
			56092.3			15.4	0.5	-7.6	0.5		
V4046-Sgr	18:14:10.5	-32:47:33	53600.0	BPC	0.77	-21.0	0.5	9.3	0.7		
			54237.4			-59.9	0.2	44.1	0.1		
			54238.1			-12.3	1.3	-1.8	1.0		
			54238.3			-31.8	0.2	20.6	0.3		
			54235.3			-53.8	0.3	38.8	0.1		
			54238.4			-43.4	0.1	34.4	0.0		
			54239.4			-17.6	0.4	2.2	0.2		
			54237.1			-37.7	0.3	23.1	0.1		
			54239.2			-22.2	0.1	9.5	0.3		
			53597.1			-58.4	0.2	47.7	0.2		
			54239.1			-32.9	0.3	20.3	0.3		
			54235.4			-43.4	2.9	29.2	2.8		
			54237.2			-49.3	0.1	34.0	0.1		
			54235.2			-59.8	0.1	43.3	0.1		
			54238.2			-20.0	0.1	10.1	0.1		
			53597.0			-58.0	0.3	47.2	0.2		
			53598.0			-51.0	0.2	35.4	0.8		
			53599.0			-20.0	0.1	10.2	0.3		
1RXS J195602.8-320720	19:56:02.9	-32:07:19	55843.1	BPC	0.67	30.0	0.4	-46.2	0.4		
HD 217379	23:00:28.0	-26:18:43	55341.4	ABD	0.62, 0.30	50.0	0.4	-49.7	0.1	5.5	0.4
CD-423328	07:33:21.2	-42:55:42	56175.4	CAR	1.00[a]	36.0	0.6	11.2	0.5		
			56179.4			33.5	0.4	12.5	0.5		

(*) No longer classified as a member of association with new RV values.

(*a*) From CCF profiles in both epochs, it is difficult to accurately compute the flux ratio; however, the two components are very similar, and thus, we assign a value of 1.00.

TABLE 2.6: RV values from each UVES observation available.

ID	RA	DEC	MJD	RV ($km\,s^{-1}$)	$\pm\sigma_{meas.}$
		AB Doradus members			
HD 6569	01:06:26.2	-14:17:47	54749.10	7.6	.004
			55391.42	7.5	.003
BD-12243	01:20:32.3	-11:28:04	54281.37	9.9	.003
			55391.41	10.6	.003
HD 16760B	02:42:21.0	+38:37:21	55415.40	-3.5	.004
HD 16760	02:42:21.3	+38:37:07	55415.40	-3.2	.004
HD 17332B	02:47:27.2	+19:22:21	55415.41	5.1	.003
HD 17332A	02:47:27.4	+19:22:19	55415.41	3.9	.009
IS Eri	03:09:42.3	-09:34:47	54749.14	14.3	.006
			55391.43	14.6	.004
HD 24681	03:55:20.4	-01:43:45	54795.03	18.0	.022
HD 25457	04:02:36.7	-00:16:08	54795.03	18.0	.028
			55391.42	17.3	.020
HD 31652	04:57:22.3	-09:08:00	54784.13	22.6	.004
CD-401701	05:02:30.4	-39:59:13	54309.40	28.6	.003
			55410.38	28.6	.004
HD 32981	05:06:27.7	-15:49:30	55458.30	25.6	.005
HD 293857	05:11:09.7	-04:10:54	54808.11	20.3	.006
HD 35650	05:24:30.2	-38:58:11	54784.25	31.4	.004
			55410.40	32.7	.005
CD-342331	05:35:04.1	-34:17:52	54805.24	30.7	.015
			55410.41	30.4	.015
CD-481893	05:36:55.1	-47:57:48	54805.17	31.7	.016
			55459.25	32.0	.017
UY Pic	05:36:56.9	-47:57:53	54309.41	32.2	.006
			54327.41	32.1	.004
			55459.25	32.6	.006
WX Col	05:37:12.9	-42:42:56	54312.40	31.3	.004
			55398.42	31.2	.019
			55459.25	31.3	.005
TYC 7604-1675-1	05:37:13.2	-42:42:57	54309.42	30.3	.003
TYC 4779-394-1	05:38:56.6	-06:24:41	54814.09	22.9	.005
CP-19878	05:39:23.2	-19:33:29	55416.42	28.7	.025
TYC 7605-1429-1	05:41:14.3	-41:17:59	55461.36	30.7	.145
TZ Col	05:52:16.0	-28:39:25	54814.11	29.0	.024
			55463.25	28.5	.020
BD-131328	06:02:21.9	-13:55:33	54878.03	25.4	.004

ID	RA	DEC	MJD	RV (km s^{-1})	$\pm\sigma_{meas.}$
CD-342676	06:08:33.9	-34:02:55	54226.97	29.8	.006
			55464.25	30.6	.009
CD-352722	06:09:19.2	-35:49:31	54805.34	31.9	.015
HD 45270	06:22:30.9	-60:13:07	54228.98	31.8	.018
			54805.21	31.5	.015
			55465.36	31.2	.011
AK Pic	06:38:00.4	-61:32:00	55466.36	36.8	.021
CD-611439	06:39:50.0	-61:28:42	54805.18	31.4	.005
TYC 7627-2190-1	06:41:18.5	-38:20:36	54896.09	25.6	.049
			55416.40	27.2	.063
GSC 08544-01037*	06:47:53.4	-57:13:32	54773.34	29.6	.005
			55468.33	29.8	.003
CD-571654	07:10:50.6	-57:36:46	54876.22	29.3	.032
			55464.38	29.0	.050
V429 Gem	07:23:43.6	+20:24:59	54893.08	7.0	.006
			55468.38	7.8	.006
HD 59169	07:26:17.7	-49:40:51	55468.39	39.7	.008
CD-8480	07:30:59.5	-84:19:28	54236.98	23.2	.003
HD 64982	07:45:35.6	-79:40:08	54239.99	25.6	.012
			55464.38	25.7	.011
BD+012447	10:28:55.5	+00:50:28	54850.37	7.7	.008
PX Vir	13:03:49.7	-05:09:43	54888.38	-13.3	.004
HD 139751	15:40:28.4	-18:41:46	55340.14	-7.6	.006
HIP 81084	16:33:41.6	-09:33:12	54923.41	-14.7	.005
HD 152555	16:54:08.1	-04:20:25	54906.34	-16.4	.015
			55341.29	-16.5	.018
HD 178085	19:10:57.9	-60:16:20	55341.31	8.4	.030
TYC 486-4943-1	19:33:03.8	+03:45:40	55339.41	-20.7	.004
BD-034778	20:04:49.4	-02:39:20	54783.00	-16.5	.006
			55340.40	-16.5	.006
HD 199058	20:54:21.1	+09:02:24	54783.00	-19.4	.006
			55340.40	-19.7	.011
TYC 1090-543-1	20:54:28.0	+09:06:07	54783.01	-19.0	.012
			55339.41	-19.3	.013
HD 201919	21:13:05.3	-17:29:13	54783.02	-7.5	.005
			55340.40	-7.6	.005
HD 218860	23:11:52.0	-45:08:10	54227.41	9.6	.004
			54760.26	12.7	.004
HD 224228	23:56:10.7	-39:03:08	55341.41	13.1	.004

Argus members

ID	RA	DEC	MJD	RV (km s^{-1})	$\pm\sigma_{meas.}$
CD-292360	05:34:59.2	-29:54:04	54309.41	25.7	.006
			56139.39	26.1	.020
			56140.41	25.3	.011
CD-283434	06:49:45.4	-28:59:17	54234.97	26.7	.004
CD-422906	07:01:53.4	-42:27:56	54234.99	23.4	.004
			56159.40	23.7	.014
			56163.38	23.8	.015
HD 61005	07:35:47.5	-32:12:14	56175.40	22.2	.010
			56179.38	22.6	.013
CD-483199	07:47:26.0	-49:02:51	54876.23	17.8	.037
			54878.04	17.6	.025
			56175.39	17.1	.052
			56179.39	17.9	.025
CD-433604	07:48:49.8	-43:27:06	54876.23	20.4	.056
			56175.38	24.1	.142
			56179.37	11.0	.010
TYC 8561-970-1	07:53:55.5	-57:10:07	54232.01	15.7	.003
			56082.01	15.9	.010
			56162.39	15.7	.008
PMM 7956	08:29:51.9	-51:40:40	54876.26	16.1	.007
PMM 6974	08:34:18.1	-52:15:58	54864.29	15.1	.004
PMM 4280	08:34:20.5	-52:50:05	54876.27	16.9	.022
PMM 6978	08:35:01.2	-52:14:01	54876.28	15.4	.006
PMM 3359	08:36:55.0	-53:08:34	54876.29	14.7	.010
PMM 665	08:37:51.6	-53:45:46	54876.31	14.6	.010
PMM 4362	08:38:22.9	-52:56:48	54876.35	15.1	.017
PMM 686	08:39:22.6	-53:55:06	54880.12	15.2	.007
V364 Vel	08:39:53.0	-52:57:57	54880.14	15.3	.013
PMM 8415	08:40:16.3	-52:56:29	54880.16	14.8	.017
PMM 1142	08:40:49.1	-53:37:45	54878.04	14.1	.006
PMM 756	08:43:00.4	-53:54:08	54878.05	16.1	.012
V376 Vel	08:44:05.2	-52:53:17	54878.06	13.6	.015
V379 Vel	08:45:26.9	-52:52:02	54864.27	14.7	.005
CD-572315	08:50:08.1	-57:45:59	54893.10	13.4	.017
TYC 8594-58-1	09:02:03.9	-58:08:50	54880.18	10.8	.036
			56082.02	8.2	.088
			56108.00	10.9	.068
CD-542644	09:13:16.9	-55:29:03	54898.17	20.8	.037
			55885.32	21.5	.095

ID	RA	DEC	MJD	RV (km s^{-1})	$\pm\sigma_{meas.}$
BD-202977	09:39:51.4	-21:34:17	54240.09	17.9	.005
TYC 9217-641-1	09:42:47.4	-72:39:50	54880.20	5.4	.014
CD-395833	09:47:19.9	-40:03:10	54240.01	14.8	.004
			56097.96	14.5	.011
HD 309851	09:55:58.3	-67:21:22	54227.14	7.3	.012
			54895.22	7.1	.020
			56097.98	8.0	.032
CD-74673	12:20:34.4	-75:39:29	54874.28	4.7	.004
CD-75652	13:49:12.9	-75:49:48	54226.13	-1.0	.063
			54883.33	-1.2	.016
			56134.09	-0.9	.014
			56137.13	-1.4	.031
NY Aps	15:12:23.4	-75:15:16	54905.22	-3.1	.009
			56033.40	-3.5	.017
		β-Pic members			
HIP 10679	02:17:24.7	+28:44:30	54805.16	5.3	.007
BD+05378*	02:41:25.9	+05:59:18	54788.24	7.3	.005
GJ3305*	04:37:37.5	-02:29:28	55846.23	24.4	.038
			55925.24	23.3	.014
			55935.13	23.8	.017
V1005Ori	04:59:34.8	+01:47:01	54808.10	18.8	.013
			55846.30	19.4	.008
			55925.24	18.6	.019
CD-571054	05:00:47.1	-57:15:25	54773.29	19.0	.007
BD-211074B	05:06:49.5	-21:35:04	55846.25	21.8	.034
			55847.27	22.0	.025
			55904.19	20.8	.017
BD-211074A	05:06:49.9	-21:35:09	55846.26	21.5	.013
			55855.36	20.9	.017
TYC 112-917-1	05:20:00.3	+06:13:04	55846.26	19.0	.009
			55925.24	18.7	.010
			55935.15	18.7	.011
TYC 112-1486-1	05:20:31.8	+06:16:11	55846.27	18.4	.020
			55925.25	18.8	.024
			55936.21	18.3	.017
V1311 Ori*	05:32:04.5	-03:05:29	54784.35	23.9	.020
			55846.28	24.5	.020
			55904.18	23.2	.021
AO Men	06:18:28.2	-72:02:41	54805.18	16.1	.009

ID	RA	DEC	MJD	RV (km s^{-1})	$\pm\sigma_{meas.}$
			55846.30	16.5	.026
			55855.35	16.0	.018
			54226.99	16.0	.007
TWA 22	10:17:26.9	-53:54:27	55904.30	13.4	.057
			55968.36	13.6	.051
HD 139084B	15:38:56.8	-57:42:19	55978.37	3.0	.187
V343 Nor	15:38:57.5	-57:42:27	54226.24	5.0	.007
			54906.32	0.2	.010
CD-2711535	17:15:03.6	-27:49:40	55845.05	-8.3	.013
CD-547336	17:29:55.1	-54:15:49	54905.23	1.5	.043
HD 164249	18:03:03.4	-51:38:56	54209.40	-0.7	.017
GSC 07396-00759	18:14:22.1	-32:46:10	55843.05	-6.0	.021
TYC 9073-762-1	18:46:52.6	-62:10:36	55843.06	1.6	.024
CD-2613904	19:11:44.7	-26:04:09	55843.07	-9.7	.011
HD 181327	19:22:58.9	-54:32:17	54226.33	-1.0	.016
			55843.08	-0.8	.034
			55850.07	-0.3	.051
TYC 7443-1102-1	19:56:04.4	-32:07:38	55843.09	-6.4	.010
			55850.07	-6.3	.018
1RXS J200136.9-331307	20:01:37.2	-33:13:14	55843.10	-4.6	.017
			55850.08	-4.4	.010
			56009.36	-5.0	.015
AU Mic	20:45:09.5	-31:20:27	54765.05	-5.1	.018
			55844.10	-5.2	.010
			53608.97	-4.9	.121
AZ Cap	20:56:02.7	-17:10:54	55843.11	-8.2	.017
			55889.03	-8.5	.020
CP-722713	22:42:48.9	-71:42:21	54765.07	7.8	.006
WW PsA	22:44:58.0	-33:15:02	55843.11	1.1	.046
			55850.09	1.6	.074
TX PsA	22:45:00.0	-33:15:26	55850.10	2.7	.277
BD-136424	23:32:30.9	-12:15:52	54760.25	0.7	.009
			55889.06	0.2	.018
		Carina members			
HD 269620	05:29:27.1	-68:52:05	54228.97	19.1	.013
HD 42270	05:53:29.3	-81:56:53	54805.20	16.9	.033
HD 49855*	06:43:46.2	-71:58:35	54805.19	20.8	.011
CD-571709	07:21:23.7	-57:20:37	54215.00	23.2	.005
			55849.31	22.9	.019

ID	RA	DEC	MJD	RV (km s^{-1})	$\pm\sigma_{meas.}$
CD-423328[a]	07:33:21.2	-42:55:42	56175.40	15.1	.130
			56179.38	15.3	.110
TYC 8557-1251-1	07:55:31.6	-54:36:51	55856.32	21.1	.039
TYC 8570-1980-1	08:11:09.3	-55:55:56	55856.32	21.3	.052
CP-541712	08:37:10.9	-55:18:10	54233.02	20.7	.013
			55849.33	20.7	.038
CD-612010	08:42:00.5	-62:18:26	54897.17	21.0	.041
			55856.33	22.1	.158
TYC 8590-1193-1	08:56:31.5	-57:00:41	55885.29	21.0	.012
			55910.18	20.8	.010
TYC 8582-3040-1	08:57:45.6	-54:08:37	54897.18	21.7	.033
			55885.29	21.8	.015
CD-494008	08:57:52.2	-49:41:51	54898.15	22.1	.065
			55885.30	21.8	.032
CP-551885	09:00:03.4	-55:38:24	54898.16	27.6	.078
			55885.31	24.0	.185
CD-552543	09:09:29.4	-55:38:27	54233.03	20.6	.015
			55885.31	22.6	.014
			55910.20	22.4	.008
TYC 8174-1586-1	09:11:15.8	-50:14:15	55885.31	22.2	.023
			55909.30	22.4	.021
CP-621293	09:43:08.8	-63:13:04	54898.19	20.6	.073
			55885.34	20.4	.036
TYC 8946-872-1*	09:55:15.1	-62:03:32	55909.30	22.1	.022
			55933.28	21.5	.019
TYC 9217-417-1	09:59:57.7	-72:21:47	55933.29	16.6	.034
TYC 8962-1747-1	11:08:07.9	-63:41:47	55935.30	16.3	.011
			55981.23	16.8	.010
HD 107722	12:23:29.0	-77:40:51	54906.29	12.8	.056
			55978.35	12.5	.100
			55981.25	12.2	.231
TYC 460-624-1*	18:45:10.3	+06:20:16	55843.06	-25.0	.020
			56009.35	-25.4	.018
HD 189285*	19:59:24.1	-04:32:06	55340.39	-19.4	.007
HD 221451*	23:32:19.2	-13:37:18	55889.06	-7.3	.010
		Columba members			
CD-52381	01:52:14.6	-52:19:33	54254.36	13.7	.011
			54258.42	13.5	.023
			54750.14	13.4	.010
BD-16351	02:01:35.6	-16:10:01	54749.11	10.5	.009

ID	RA	DEC	MJD	RV (km s^{-1})	$\pm\sigma_{meas.}$
			56107.42	9.7	.008
			56116.38	9.9	.009
CD-44753	02:30:32.4	-43:42:23	54749.12	13.1	.007
TYC 8862-19-1	02:58:04.0	-62:41:14	54281.38	16.2	.004
BD-11648	03:21:49.7	-10:52:18	56125.36	14.6	.040
			56141.35	15.7	.045
BD-04700	03:57:37.2	-04:16:16	54755.16	18.4	.014
			56125.37	18.8	.010
			56128.42	17.7	.024
BD-15705*	04:02:16.5	-15:21:30	54765.11	15.0	.008
			56108.42	15.2	.011
			56119.42	15.3	.007
			56125.37	15.0	.006
HD 26980	04:14:22.6	-38:19:02	54288.42	21.3	.016
			54308.42	21.4	.007
HD 27679	04:21:10.3	-24:32:21	54288.41	21.3	.008
			54784.11	21.7	.009
CD-431395	04:21:48.7	-43:17:33	54784.12	22.2	.046
			56125.38	21.8	.019
			56138.33	21.2	.042
CD-361785	04:34:50.8	-35:47:21	56125.38	21.7	.012
			56138.34	22.5	.010
			54308.40	22.1	.003
GSC 08077-01788	04:51:53.0	-46:47:31	54772.23	18.4	.023
			54773.30	16.8	.011
HD 31242N	04:51:53.5	-46:47:13	54309.39	22.2	.010
			54772.21	21.8	.021
HD 272836	04:53:05.2	-48:44:39	54772.22	22.8	.010
TYC 5900-1180-1*	04:58:35.8	-15:37:31	54784.14	23.6	.024
BD-08995	04:58:48.6	-08:43:40	54795.04	24.7	.010
			56144.41	23.5	.007
			56147.39	24.0	.010
HD 32372	05:00:51.9	-41:01:07	54309.39	22.9	.005
HD 274561	05:28:55.1	-45:34:58	54307.41	24.4	.003
BD-191194	05:30:19.1	-19:16:32	54784.25	26.2	.019
CD-392075*	05:37:05.3	-39:32:26	54312.40	23.2	.010
BD-081195	05:38:35.0	-08:56:40	54814.08	24.1	.060
			56144.41	23.2	.029
			56147.40	24.6	.077
			56159.41	24.7	.059
CD-382198	05:45:16.3	-38:36:49	54814.10	25.7	.017
			56139.39	27.4	.045
			56140.42	27.4	.041

ID	RA	DEC	MJD	RV (km s^{-1})	$\pm\sigma_{meas.}$
CD-292531	05:50:21.4	-29:15:21	54805.33	26.5	.008
			56138.42	27.0	.018
			56140.41	26.1	.013
HD 40216	05:55:43.2	-38:06:16	54814.12	24.5	.054
AB Pic	06:19:12.9	-58:03:16	54226.99	22.8	.004
CD-402458	06:26:06.9	-41:02:54	54327.40	25.7	.019
			56144.42	25.1	.006
			56147.40	25.3	.018
HD 48370	06:43:01.0	-02:53:19	54807.35	23.4	.006
TYC 9178-284-1	06:55:25.2	-68:06:21	54214.98	19.9	.004
HD 51797	06:56:23.5	-46:46:55	54234.98	24.9	.011
			54805.34	25.0	.006
HD 55279	07:00:30.5	-79:41:46	54214.02	17.4	.004
V479 Car	09:23:35.0	-61:11:36	54239.98	20.6	.012
			55885.33	20.8	.004
			54843.22	20.7	.007
CP-522481	09:32:26.1	-52:37:40	54240.00	20.9	.008
			54240.00	20.8	.024
			54898.18	21.0	.009
			55885.33	21.5	.012
HD 298936	10:13:14.8	-52:30:54	54223.08	17.8	.009
			55862.36	17.8	.003
			55933.31	17.2	.010
CD-544320*	11:45:51.8	-55:20:46	54884.24	16.2	.003
			55935.30	16.2	.006
			55981.31	15.3	.005
ϵ Chamaeleon members					
EG Cha	08:36:56.2	-78:56:46	55849.32	17.3	.029
			55856.36	19.1	.026
EO Cha	08:44:31.9	-78:46:31	55910.23	17.4	.014
			55932.29	17.4	.011
			55933.22	17.2	.019
EQ Cha*	08:47:56.8	-78:54:53	55910.17	24.0	.049
			55932.30	22.2	.067
			55933.24	22.8	.083
1RXS J091528.1-760856	09:15:29.1	-76:08:47	55910.29	19.1	.020
			55933.25	18.4	.020
			55936.23	19.8	.031
1RXS J093455.3-780414	09:34:56.1	-78:04:19	55910.28	16.0	.069
			55933.27	17.5	.072

ID	RA	DEC	MJD	RV (km s^{-1})	$\pm\sigma_{meas.}$
			55981.21	16.7	.034
1RXS J100515.1-774900	10:05:20.0	-77:48:42	55910.30	16.4	.019
			55933.30	16.3	.021
			55981.23	16.4	.024
DZ Cha	11:49:31.9	-78:51:01	55935.31	14.0	.020
			55981.30	14.5	.020
			55993.17	13.5	.018
T Cha	11:57:13.5	-79:21:32	56049.17	14.7	.028
GSC 09415-02676*	11:58:26.9	-77:54:45	55935.32	14.8	.041
			55977.27	14.4	.017
			55993.19	14.2	.016
HIP 58490	11:59:42.3	-76:01:26	54901.15	14.5	.011
			55340.07	13.6	.009
			55981.25	13.8	.006
			55993.20	13.0	.012
			56009.34	13.3	.011
DX Cha	12:00:05.1	-78:11:35	52663.37	11.8	.017
			54463.33	11.9	.013
HD 104237-5	12:00:08.3	-78:11:40	55979.36	13.7	.050
			55982.34	13.7	.059
HD 104237-6	12:00:09.3	-78:11:42	55993.21	13.4	.053
			56012.32	15.6	.029
			55340.09	12.2	.055
HD 104467	12:01:39.1	-78:59:17	54906.28	11.0	.027
			55342.12	15.9	.041
			55981.26	10.1	.022
			55993.22	11.5	.051
			53453.23	18.0	.016
GSC 09420- 00948	12:02:03.8	-78:53:01	54901.16	18.2	.031
			55977.29	10.4	.024
			55981.27	11.3	.017
			55982.33	10.7	.024
HD 105923	12:11:38.1	-71:10:36	54223.12	13.9	.019
			55342.12	14.0	.014
			55981.25	13.9	.005
			55982.32	14.2	.007
1RXS J121645.2-775339	12:16:46.0	-77:53:33	55947.36	13.9	.027
			55977.29	14.1	.027
			55979.33	13.8	.020
			55981.28	14.3	.029
GSC 09239-01495	12:19:43.8	-74:03:57	55947.34	14.0	.015
			55979.32	13.9	.009
			55981.32	13.9	.023

ID	RA	DEC	MJD	RV (km s^{-1})	$\pm\sigma_{meas.}$
GSC 09239-01572	12:20:21.9	-74:07:39	55340.11	16.4	.097
			55947.35	12.0	.180
			55978.34	8.6	.246
			55979.30	13.6	.197
CD-74712	12:39:21.3	-75:02:39	54226.09	13.4	.012
			54906.30	13.9	.021
			55371.07	13.9	.037
			55978.35	13.2	.017
			55982.26	12.9	.041
CD-691055	12:58:25.6	-70:28:49	55978.36	12.5	.032
			55981.31	11.4	.064
CP-681894	13:22:07.5	-69:38:12	54222.19	10.3	.006
			54877.38	12.1	.018
			55398.07	12.3	.027
			55978.36	10.9	.014
Octans members					
CD-58860	04:11:55.7	-58:01:47	54765.10	9.6	.035
			56108.42	9.5	.026
			56122.42	9.5	.023
CD-431451	04:30:27.3	-42:48:47	54309.38	12.9	.033
			54765.10	12.6	.010
			56108.41	13.2	.024
			56122.41	13.5	.019
HD 274576	05:28:51.4	-46:28:19	54805.17	12.2	.017
			56125.41	10.9	.043
			56138.37	12.4	.039
BD-201111	05:32:29.3	-20:43:33	56140.39	19.1	.057
			56144.39	19.6	.048
CD-471999	05:43:32.1	-47:41:11	56140.38	14.0	.071
TYC 7066-1037-1	05:58:11.8	-35:00:49	54903.11	14.7	.038
			56139.40	14.8	.032
			56140.40	14.3	.018
CD-492037	06:03:35.4	-49:11:26	54214.00	12.3	.004
			54214.00	12.3	.013
			56139.39	12.0	.012
			56140.39	11.8	.003
CD-303394N	06:40:04.9	-30:33:03	54896.08	14.4	.072
			56159.39	14.4	.185
			56161.40	14.8	.124
CD-303394S	06:40:05.7	-30:33:09	56161.40	16.0	.115

ID	RA	DEC	MJD	RV (km s^{-1})	$\pm\sigma_{meas.}$
TYC 9300-529-1	18:49:45.1	-71:56:58	56056.39	-1.6	.054
			56087.39	-2.5	.033
CD-87121	23:58:17.7	-86:26:24	54242.26	0.9	.041
			54765.09	1.2	.053
Tucana-Horologium members					
HD 105	00:05:52.5	-41:45:11	54249.41	2.1	.010
HD 987	00:13:53.0	-74:41:18	54245.42	9.0	.005
HD 1466	00:18:26.1	-63:28:39	54246.42	6.4	.065
			54755.10	5.9	.029
			56087.40	6.3	.041
			56108.39	6.2	.025
HIP 1993	00:25:14.7	-61:30:48	54749.09	6.1	.011
CD-7824	00:42:20.3	-77:47:40	54251.41	11.8	.013
			54755.11	11.0	.011
HD 8558	01:23:21.3	-57:28:51	54251.40	9.6	.010
HD 9054	01:28:08.7	-52:38:19	54252.42	8.3	.005
HD 12039	01:57:49.0	-21:54:05	54281.37	5.4	.014
			56108.40	6.2	.009
HD 13183	02:07:18.1	-53:11:56	54755.16	10.4	.023
HD 13246	02:07:26.1	-59:40:46	54755.15	9.3	.060
CD-60416	02:07:32.2	-59:40:21	54750.15	9.9	.004
GSC 08491-01194	02:41:47.3	-52:59:31	54755.12	12.8	.011
CD-58553	02:42:33.0	-57:39:37	54749.11	11.8	.006
CD-351167	03:19:08.7	-35:07:00	54755.13	13.5	.005
			56107.40	13.5	.009
CD-461064	03:30:49.1	-45:55:57	56107.42	14.1	.011
CD-441173	03:31:55.7	-43:59:14	54749.13	15.0	.010
HD 22705	03:36:53.4	-49:57:29	54281.42	14.1	.033
			56107.40	16.6	.036
			56116.37	14.4	.016
			56125.34	12.4	.054
HD 24636	03:48:11.5	-74:41:39	56108.41	14.5	.115
			56116.38	13.1	.078
			56122.42	13.5	.096
BD-12943	04:36:47.1	-12:09:21	56144.38	16.9	.023
BD-12943	04:36:47.1	-12:09:21	56147.38	17.7	.023
HD 29615	04:38:43.9	-27:02:02	54308.41	19.1	.050
			54765.12	18.5	.037
			56125.39	18.7	.011
			56138.34	19.4	.029

ID	RA	DEC	MJD	RV (km s^{-1})	$\pm\sigma_{meas.}$
HD 30051*	04:43:17.2	-23:37:42	56138.35	-1.5	.138
			56139.36	-2.1	.190
			56140.36	-2.5	.198
TYC 8083-455-1	04:48:00.7	-50:41:26	54772.20	18.8	.013
			56125.40	18.8	.018
BD-191062	04:59:32.0	-19:17:42	54795.05	20.6	.021
			56139.37	20.2	.006
			56140.38	19.5	.014
BD-091108	05:15:36.5	-09:30:51	54892.03	20.3	.025
			56144.40	20.7	.028
			56147.39	21.2	.011
			56159.40	21.0	.026
CD-302310	05:18:29.0	-30:01:32	54805.22	20.6	.004
			56138.36	20.4	.011
			56139.37	21.6	.012
TYC 8098-414-1	05:33:25.6	-51:17:13	56138.36	20.0	.021
CD-272520	05:49:06.6	-27:33:56	56139.41	23.4	.020
			56140.40	22.6	.012
HD 47875	06:34:41.0	-69:53:06	54236.97	16.7	.006
GSC 09507-02466*	11:40:16.6	-83:21:00	53453.19	12.6	.005
			56139.03	13.5	.011
HD 202917	21:20:50.0	-53:02:03	54226.35	-1.6	.007
HIP 107345	21:44:30.1	-60:58:39	54765.06	1.5	.007
HD 207575	21:52:09.7	-62:03:09	54765.07	1.3	.124
			56087.40	1.7	.110
			56092.42	1.6	.065
HD 222259N	23:39:39.3	-69:11:40	54243.35	5.6	.012
HD 222259S	23:39:39.5	-69:11:45	54243.35	7.8	.017
		TW-Hydrae members			
TWA 7	10:42:30.1	-33:40:17	54850.35	11.5	.008
TW Hya	11:01:51.9	-34:42:17	54895.23	11.9	.009
CD-298887	11:09:13.8	-30:01:40	56138.99	10.9	.035
TWA 12	11:21:05.5	-38:45:16	56069.16	11.2	.027
			56097.97	10.5	.034
CD-347390A*	11:21:17.2	-34:46:46	54876.36	11.0	.020
			56082.05	10.2	.026
			56137.98	10.6	.028
CD-347390B*	11:21:17.4	-34:46:50	54864.36	12.0	.009
			56108.05	10.9	.022
			56137.98	11.3	.016

ID	RA	DEC	MJD	RV (km s^{-1})	$\pm\sigma_{meas.}$
CD-268632A	11:32:41.2	-26:51:56	56097.98	7.6	.018
TWA 9B	11:48:23.7	-37:28:49	56138.02	11.5	.019
TWA 9A	11:48:24.2	-37:28:49	54895.24	9.6	.005
			56138.01	10.5	.012
			56139.03	11.1	.013
TWA 23	12:07:27.4	-32:47:00	56138.00	10.8	.077
			56139.01	11.0	.055
CD-397538	12:15:30.7	-39:48:43	54853.37	6.2	.008
			56138.01	7.4	.018
TWA 16	12:34:56.4	-45:38:07	54877.35	9.0	.020
			56111.13	8.2	.022
			56137.99	9.0	.013
TWA 10	12:35:04.2	-41:36:39	54903.14	6.6	.029
			56069.12	6.2	.019
			56109.14	6.1	.034

$^{(*)}$ No longer classified as a member of association with new RV values.

$^{(a)}$ RV values from a single-component Gaussian fit; see Section 2.8 for details on target.

TABLE 2.7: Full member list for the SACY associations.

ID	RA	DEC	V Mag.	X	Y	Z	D	SpT
			AB Doradus members					
HD 36705	05 28 44.4	-65 26 47	13.2	1.2	-12.7	-8.3	15.2	M4
AB Dor	05 28 44.8	-65 26 55	6.88	1.2	-12.7	-8.3	15.2	K0
AK Pic	06 38 00.4	-61 32 00	6.27	0.4	-19.2	-9.1	21.3	G2
BD+012447	10 28 55.5	+00 50 28	9.65	-2.0	-4.1	4.9	6.7	M1
V429 Gem	07 23 43.6	+20 24 59	10.00	23.8	-7.7	7.2	26.0	K5
BD-034778	20 04 49.4	-02 39 20	10.24	52.1	42.3	-21.2	70.4	K1
BD-12243	01 20 32.3	-11 28 04	8.43	-8.6	5.4	-32.8	34.3	G9
BD-131328	06 02 21.9	-13 55 33	10.55	29.1	-24.6	-11.7	39.9	K4
CD-262425	05 44 13.4	-26 06 15	10.88	42.4	-51.5	-31.9	73.9	K2
CD-342331	05 35 04.1	-34 17 52	11.76	37.1	-61.2	-41.1	82.5	K4
CD-342676	06 08 33.9	-34 02 55	10.28	35.9	-63.8	-31.2	79.6	G9
CD-352722	06 09 19.2	-35 49 31	11.08	10.1	-19.4	-9.5	23.8	M1
CD-401701	05 02 30.4	-39 59 13	10.64	14.4	-29.6	-25.0	41.3	K4
CD-46644	02 10 55.4	-46 03 59	11.24	-0.8	-30.1	-65.8	72.4	K3
CD-481893	05 36 55.1	-47 57 48	9.81	-5.7	-20.6	-13.3	25.2	K6
CD-571654	07 10 50.6	-57 36 46	10.50	-3.5	-116.0	-42.6	123.6	G2
CD-611439	06 39 50.0	-61 28 42	9.75	0.4	-20.3	-9.4	22.4	K7
CD-8480	07 30 59.5	-84 19 28	9.98	27.9	-55.4	-30.3	69.0	G9
CP-19878	05 39 23.2	-19 33 29	10.51	46.9	-44.3	-29.1	70.8	K1
GSC 08544-01037*	06 47 53.4	-57 13 32	11.50	-6.8	-125.6	-53.4	136.6	K4
HD 139751	15 40 28.4	-18 41 46	10.44	31.4	-5.9	17.4	36.4	K4
HD 152555	16 54 08.1	-04 20 25	7.82	41.5	10.7	18.7	46.8	G0
HD 159911	17 37 46.5	-13 14 47	10.03	44.2	9.8	7.8	45.9	K4
HD 16760	02 42 21.3	+38 37 07	8.70	37.9	26.0	-16.1	48.7	G2
HD 17332A	02 47 27.4	+19 22 19	7.32	25.1	10.6	-19.6	33.6	G1
HD 17332B	02 47 27.2	+19 22 21	8.11	25.1	10.6	-19.6	33.6	G6
HD 178085	19 10 57.9	-60 16 20	8.34	50.6	-22.3	-26.6	61.4	G1
HD 199058	20 54 21.1	+09 02 24	8.62	38.7	58.4	-28.6	75.7	G5
HD 201919	21 13 05.3	-17 29 13	10.64	25.9	16.1	-24.7	39.2	K6
HD 217379	23 00 28.0	-26 18 43	10.45	12.3	6.7	-30.5	33.6	K7
HD 222575	23 41 54.3	-35 58 40	9.39	18.8	-0.8	-60.8	63.6	G8
HD 224228	23 56 10.7	-39 03 08	8.22	6.0	-1.8	-21.1	22.0	K2
HD 24681	03 55 20.4	-01 43 45	9.05	40.6	-7.9	-33.7	53.4	G8
HD 25457	04 02 36.7	-00 16 08	5.38	14.8	-2.8	-11.3	18.8	F6
HD 25953	04 06 41.5	+01 41 02	7.83	44.7	-7.5	-31.6	55.3	F5
HD 293857	05 11 09.7	-04 10 54	9.26	63.9	-29.6	-31.6	77.2	G8
HD 31652	04 57 22.3	-09 08 00	9.98	63.5	-33.9	-40.7	82.7	G8
HD 32981	05 06 27.7	-15 49 30	9.13	56.7	-41.5	-40.9	81.3	F9

ID	RA	DEC	V Mag.	X	Y	Z	D	SpT
HD 33999	05 12 35.8	-34 28 48	9.37	45.7	-72.5	-58.7	103.9	F8
HD 35650	05 24 30.2	-38 58 11	9.05	-6.7	-13.6	-9.8	18.1	K6
WX Col	05 37 12.9	-42 42 56	9.55	24.0	-60.8	-39.5	76.4	G7
TYC 7604-1675-1	05 37 13.2	-42 42 57	10.65	24.0	-60.8	-39.5	76.4	K1
UY Pic	05 36 56.9	-47 57 53	7.84	-5.7	-20.6	-13.3	25.2	K0
HD 45270	06 22 30.9	-60 13 07	6.53	-0.2	-21.2	-10.7	23.7	G1
HD 59169	07 26 17.7	-49 40 51	10.22	16.0	-106.1	-28.9	111.1	G7
HD 64982	07 45 35.6	-79 40 08	8.96	27.4	-68.2	-33.2	80.6	G0
HD 6569	01 06 26.2	-14 17 47	9.50	-8.2	7.2	-46.1	47.4	K1
HD 99827	11 25 17.7	-84 57 16	7.70	42.0	-70.2	-33.8	88.5	F6
HD 16760B	02 42 21.0	+38 37 21	10.21	37.6	25.8	-16.0	48.3	K2
HIP 81084	16 33 41.6	-09 33 12	11.30	27.3	3.2	12.7	30.3	M0
IS Eri	03 09 42.3	-09 34 47	8.48	22.1	-4.4	-29.9	37.4	G0
LO Peg	21 31 01.7	+23 20 07	9.19	6.3	22.4	-8.5	24.8	K4
HD 209952	22 08 14.0	-46 57 40	1.73	18.6	-3.3	-24.6	31.0	B6
HD 17573	02 49 59.0	+27 15 38	3.61	39.7	20.2	-24.3	50.7	B8
HW Cet	03 12 34.3	+09 44 57	10.46	43.9	7.2	-37.0	57.9	K3
HD 20888	03 17 59.1	-66 55 37	6.03	9.4	-38.1	-38.4	54.9	A3
V577 Per	03 33 13.5	+46 15 27	8.26	29.4	17.1	-4.8	34.3	G5
HD 21845B	03 33 14.0	+46 15 19	11.20	29.4	17.1	-4.8	34.3	M0
HIP 17695	03 47 23.3	-01 58 20	11.54	12.2	-2.1	-10.7	16.4	M3
TYC 91-82-1	04 37 51.5	+05 03 08	11.01	77.7	-15.6	-39.7	88.6	K0
TYC 5899-26-1	04 52 24.4	-16 49 22	11.61	10.5	-7.6	-8.6	15.6	M3
CD-561032N	04 53 30.5	-55 51 32	12.10	-0.9	-8.6	-6.9	11.1	M3
CD-561032S	04 53 31.2	-55 51 37	11.16	-0.9	-8.6	-6.9	11.1	M3
HD 38497	05 45 41.3	-14 46 30	9.52	55.2	-45.0	-27.5	76.3	G3
CD-412076	05 48 30.4	-41 27 30	11.56	19.7	-47.6	-28.4	58.8	K6
CD-352749	06 11 55.7	-35 29 13	10.61	23.4	-44.7	-21.3	54.8	K1
GSC 08894-00426	06 25 56.1	-60 03 27	12.32	-0.3	-21.3	-10.6	23.8	M3
CD-472500	06 38 45.5	-47 14 18	10.14	23.3	-94.2	-38.4	104.4	G5
V372 Pup	07 28 51.4	-30 14 49	10.14	-6.9	-14.0	-1.6	15.7	M1
HD 82879	09 28 21.1	-78 15 35	8.99	45.4	-105.3	-40.4	121.6	F6
HD 160934	17 38 39.6	+61 14 16	10.45	-0.1	28.0	17.7	33.1	K7
HD 181869	19 23 53.2	-40 36 57	3.96	51.3	-2.1	-21.9	55.8	B8
GJ 4231	21 52 10.4	+05 37 36	12.11	11.2	22.1	-17.8	30.5	M3
HIP 110526A	22 23 29.1	+32 27 34	11.45	-0.0	14.0	-5.3	15.0	M3
HIP 110526B	22 23 29.1	+32 27 32	11.55	-0.0	14.0	-5.3	15.0	M3
HIP 114066	23 06 04.8	+63 55 34	10.87	-9.0	22.7	1.4	24.5	M1
HIP 115162	23 19 39.6	+42 15 10	8.94	12.7	46.2	-15.1	50.2	G4
Kap Psc	23 26 56.0	+01 15 20	4.95	2.9	26.8	-38.7	47.2	A0
HD 223352	23 48 55.5	-28 07 49	4.59	9.1	4.3	-41.0	42.2	A0
PX Vir	13 03 49.7	-05 09 43	7.69	7.3	-9.1	18.3	21.7	K1
TYC 4779-394-1	05 38 56.6	-06 24 41	10.91	12.7	-66.2	-45.1	81.1	G8

ID	RA	DEC	V Mag.	X	Y	Z	D	SpT
TYC 486-4943-1	19 33 03.8	+03 45 40	11.15	53.0	46.2	-9.3	70.9	K3
TYC 1090-543-1	20 54 28.0	+09 06 07	11.68	38.5	58.2	-28.4	75.3	K4
TYC 7605-1429-1	05 41 14.3	-41 17 59	12.29	36.9	-86.9	-54.9	109.2	K4
TYC 7627-2190-1	06 41 18.5	-38 20 36	11.08	22.9	-54.7	-19.6	62.5	K2
TY Col	05 57 50.8	-38 04 03	9.60	20.1	-41.7	-22.9	51.6	G6
TZ Col	05 52 16.0	-28 39 25	9.08	43.5	-59.7	-34.0	81.3	G3
UX Col	05 28 56.5	-33 28 16	10.57	25.4	-39.8	-28.2	55.0	K4
			Argus members					
TYC 8561-970-1	07 53 55.5	-57 10 07	11.50	0.6	-138.5	-36.3	143.2	K0
BD-202977	09 39 51.4	-21 34 17	10.22	-21.9	-79.1	34.5	89.0	G9
CD-283434	06 49 45.4	-28 59 17	10.62	-50.9	-84.8	-23.0	101.5	G7
CD-292360	05 34 59.2	-29 54 04	10.53	-34.3	-47.1	-31.8	66.4	K3
CD-395833	09 47 19.9	-40 03 10	10.89	-2.1	-109.4	20.0	111.2	K0
CD-422906	07 01 53.4	-42 27 56	10.64	-26.3	-85.3	-25.8	92.9	K1
CD-433604	07 48 49.8	-43 27 06	11.13	-17.4	-78.8	-12.5	81.7	K4
CD-482972	07 28 22.0	-49 08 38	9.85	-11.9	-75.7	-19.9	79.2	G8
CD-483199	07 47 26.0	-49 02 51	10.56	-12.8	-96.3	-20.2	99.2	G7
CD-529381	20 07 23.8	-51 47 27	10.59	24.5	-5.7	-16.0	29.8	K6
CD-561438	06 11 53.0	-56 19 05	11.32	-9.1	-100.8	-53.0	114.2	K0
CD-572315	08 50 08.1	-57 45 59	10.21	9.2	-105.5	-16.1	107.1	K2
CD-582194	08 39 11.6	-58 34 28	10.18	8.3	-100.0	-18.2	102.0	G5
CD-74673	12 20 34.4	-75 39 29	10.72	25.7	-42.8	-11.4	51.2	K3
CD-75652	13 49 12.9	-75 49 48	9.67	46.9	-63.4	-18.7	81.0	G1
HD 129496	14 46 21.4	-67 46 16	8.78	61.6	-64.9	-11.4	90.2	F7
HD 309851	09 55 58.3	-67 21 22	9.90	31.7	-102.3	-18.9	108.8	G1
HD 61005	07 35 47.5	-32 12 14	8.22	-14.1	-32.2	-3.5	35.3	G8
HD 67945	08 09 38.6	-20 13 50	8.08	-34.8	-60.1	8.5	70.0	F0
AP Col	06 04 52.2	-34 33 36	12.96	-3.7	-6.7	-3.4	8.4	M4
TYC 8568-570-1	08 28 34.6	-52 37 04	10.40	-2.5	-138.2	-19.5	139.6	
TYC 8568-1052-1	08 35 43.7	-53 21 20	12.20	0.5	-137.6	-18.4	138.8	K3
1RXS J083624.5-540101	08 36 24.2	-54 01 06	10.18	2.0	-145.9	-20.3	147.3	G0
PMM 5376	08 37 02.3	-52 46 59	14.30	-0.4	-157.7	-19.7	158.9	
CD-522472	08 38 55.7	-52 57 52	11.04	0.4	-150.4	-18.4	151.5	G2
V365 Vel	08 40 06.2	-53 38 07	10.45	2.1	-152.0	-19.3	153.2	G0
VXR PSPC 18	08 40 18.3	-53 30 29	13.54	1.8	-138.8	-17.4	139.9	K4
HD 74374	08 41 22.7	-53 38 09	9.54	2.3	-143.8	-17.9	144.9	F3
V368 Vel	08 41 57.8	-52 52 14	13.57	0.9	-138.4	-15.9	139.3	K7
HD 74714	08 43 17.9	-52 36 11	9.16	0.7	-154.5	-16.9	155.4	F2
CD-522523	08 43 52.3	-53 14 00	9.76	2.1	-144.4	-16.6	145.4	F5

ID	RA	DEC	V Mag.	X	Y	Z	D	SpT
V377 Vel	08 44 26.2	-52 42 32	11.46	1.4	-169.8	-18.4	170.8	G9
V380 Vel	08 45 39.1	-52 26 00	9.91	1.0	-154.8	-15.9	155.6	F8
PMM 2182	08 45 48.0	-53 25 51	10.22	3.0	-145.9	-16.5	146.9	
CD-621197	09 13 30.3	-62 59 09	10.46	22.1	-114.6	-20.3	118.5	K0
HD 85151A	09 48 43.2	-44 54 08	9.61	2.5	-64.6	7.7	65.1	G7
HD 85151B	09 48 43.4	-44 54 09	10.21	2.5	-64.6	7.7	65.1	G9
CD-65817	09 49 09.0	-65 40 21	10.33	40.1	-143.8	-24.0	151.2	G5
HD 310316	10 49 56.1	-69 51 22	10.82	46.4	-110.5	-19.9	121.5	G8
CP-691432	10 53 51.5	-70 02 16	10.66	61.7	-144.2	-26.1	159.0	G2
CD-427422	12 06 32.9	-42 47 51	10.66	43.4	-96.3	37.0	111.9	K0
HD 145689*	16 17 05.4	-67 56 29	5.95	39.2	-32.4	-11.2	52.1	A6
NY Aps	15 12 23.4	-75 15 16	9.42	32.3	-36.3	-12.9	50.3	G9
VXR PSPC 22a	08 40 49.1	-53 37 45	11.08	2.4	-155.7	-19.6	156.9	G1
ASAS J083655-5308.5	08 36 55.0	-53 08 34	11.51	0.3	-141.2	-18.2	142.4	
TYC 8568-407-1	08 34 20.5	-52 50 05	10.34	-0.9	-150.5	-19.7	151.8	G5
HD 73777	08 37 47.0	-52 52 12	9.66	-0.0	-148.4	-18.4	149.5	F5
VXR PSPC 2b	08 37 55.6	-52 57 11	11.55	0.2	-167.6	-20.9	168.9	G9
CD-52 2467	08 38 22.9	-52 56 48	10.95	0.2	-143.7	-17.8	144.8	
V364 Vel	08 39 53.0	-52 57 57	11.86	0.7	-163.5	-19.7	164.7	K0
V376 Vel	08 44 05.2	-52 53 17	10.85	1.6	-162.1	-18.0	163.1	G3
V379 Vel	08 45 26.9	-52 52 02	12.76	1.6	-137.0	-14.8	137.8	K3
TYC 8568-2261-1	08 37 51.6	-53 45 46	11.35	1.9	-151.2	-20.1	152.5	G8
PMM 686	08 39 22.6	-53 55 06	12.63	2.6	-154.6	-20.4	156.0	
PMM 6974	08 34 18.1	-52 15 58	12.26	-2.1	-143.1	-17.9	144.2	
PMM 6978	08 35 01.2	-52 14 01	12.07	-2.0	-143.2	-17.7	144.3	
TYC 8162-1020-1	08 28 45.6	-52 05 27	10.49	-3.5	-136.7	-18.5	138.0	G6
TYC 8569-3687-1	08 43 00.4	-53 54 08	11.16	3.4	-151.7	-18.8	152.9	G9
PMM 7956	08 29 51.9	-51 40 40	11.62	-4.5	-152.4	-19.7	153.7	
PMM 8415	08 40 16.3	-52 56 29	11.84	0.6	-130.8	-15.6	131.7	G9
TYC 7695-335-1	09 28 54.1	-41 01 19	11.65	-7.9	-147.1	18.8	148.5	K3
TYC 8594-58-1	09 02 03.9	-58 08 50	11.30	15.1	-137.2	-18.6	139.3	G8
TYC 9217-641-1	09 42 47.4	-72 39 50	12.30	50.3	-139.2	-39.0	153.1	K1
			β Pic members					
AO Men	06 18 28.2	-72 02 41	9.80	7.5	-33.2	-18.3	38.6	K4
AU Mic	20 45 09.5	-31 20 27	8.73	7.7	1.7	-5.9	9.8	M1
AZ Cap	20 56 02.7	-17 10 54	10.62	34.0	19.9	-27.6	48.1	K6
BD+05378*	02 41 25.9	+05 59 18	10.27	-27.5	7.0	-31.0	42.0	K6
BD-136424	23 32 30.9	-12 15 52	10.54	4.3	10.5	-25.7	28.1	M0
BD-211074A	05 06 49.9	-21 35 09	10.29	-10.5	-9.6	-9.0	16.8	M1

ID	RA	DEC	V Mag.	X	Y	Z	D	SpT
BD-211074B	05 06 49.5	-21 35 04	11.61	-12.8	-11.7	-10.9	20.5	M3
CD-2613904	19 11 44.7	-26 04 09	10.39	74.1	14.8	-21.3	78.5	K4
CD-2711535	17 15 03.6	-27 49 40	11.12	83.5	-4.0	9.1	84.1	K5
CD-547336	17 29 55.1	-54 15 49	9.55	60.8	-26.0	-12.7	67.3	K1
CD-571054	05 00 47.1	-57 15 25	10.00	-1.5	-21.3	-16.3	26.9	M0
CD-641208	18 45 37.0	-64 51 46	9.90	22.8	-12.8	-11.5	28.6	K5
CP-722713	22 42 48.9	-71 42 21	10.60	19.6	-18.9	-24.5	36.6	K7
GJ 3305*	04 37 37.5	-02 29 28	10.68	-24.0	-8.1	-15.0	29.4	M1
GSC 07396-00759	18 14 22.1	-32 46 10	12.78	98.1	-0.5	-12.5	98.9	M1
1RXS J195602.8-320720	19 56 02.9	-32 07 19	14.2	52.3	8.0	-26.8	59.3	M4
1RXS J200136.9-331307	20 01 37.2	-33 13 14	12.55	54.0	7.5	-29.4	61.9	M1
GSC 08056-00482	02 36 51.7	-52 03 04	12.11	0.5	-15.1	-24.4	28.7	M2
GSC 08350-01924	17 29 20.7	-50 14 53	13.47	61.4	-22.1	-10.0	66.0	M3
V343 Nor	15 38 57.5	-57 42 27	7.97	31.0	-22.7	-1.2	38.4	K0
HD 139084B	15 38 56.8	-57 42 19	14.80	31.0	-22.7	-1.2	38.4	M5
HD 14082	02 17 25.3	+28 44 42	6.99	-28.1	19.8	-20.2	39.9	F5
HD 164249	18 03 03.4	-51 38 56	7.01	44.3	-14.7	-11.6	48.1	F6
HD 181327	19 22 58.9	-54 32 17	7.04	44.4	-13.8	-22.9	51.8	F6
HD 191089	20 09 05.2	-26 13 26	7.22	44.5	12.8	-24.4	52.3	F6
HD 199143	20 55 47.7	-17 06 51	7.35	32.3	18.9	-26.2	45.7	F7
HD 29391	04 37 36.1	-02 28 25	5.22	-24.0	-8.1	-15.0	29.4	F0
HIP 10679	02 17 24.7	+28 44 30	7.75	-28.5	20.1	-20.5	40.5	G2
BD+30397B	02 27 28.1	+30 58 41	12.44	-31.0	20.8	-19.5	42.1	M2
AG Tri	02 27 29.3	+30 58 25	10.12	-31.0	20.8	-19.5	42.1	K6
GJ 3322	05 01 58.8	+09 58 59	11.98	-35.6	-6.6	-12.4	38.3	M3
AF Lep	05 27 04.8	-11 54 03	6.56	-20.4	-13.9	-11.0	27.0	F7
Beta Pic	05 47 17.1	-51 03 59	3.77	-3.4	-16.4	-9.9	19.5	A3
V824 Ara	17 17 25.5	-66 57 04	7.23	24.7	-17.4	-8.8	31.5	G7
HD 155555C	17 17 31.3	-66 57 06	12.82	24.7	-17.4	-8.8	31.5	M3
HD 161460	17 48 33.7	-53 06 43	9.61	63.7	-24.1	-15.4	69.8	K0
HD 164249B	18 03 04.1	-51 38 56	12.5	44.3	-14.7	-11.6	48.1	M2
HD 165189*	18 06 49.9	-43 25 31	5.67	40.4	-7.5	-7.9	41.8	A5
HD 168210	18 19 52.2	-29 16 33	8.89	71.8	4.2	-8.4	72.4	G5
HD 172555	18 45 26.9	-64 52 17	4.78	22.8	-12.8	-11.5	28.6	A6
CD-3116041	18 50 44.5	-31 47 47	11.20	50.7	3.5	-12.4	52.3	M0
TYC 6872-1011-1	18 58 04.2	-29 53 05	11.78	74.7	8.4	-19.4	77.6	M0
Eta Tel	19 22 51.2	-54 25 26	5.02	41.4	-12.7	-21.3	48.3	A0
GJ 799 B	20 41 51.1	-32 26 10	11.09	7.5	1.5	-5.6	9.5	M4
AT Mic	20 41 51.2	-32 26 07	10.99	7.5	1.5	-5.6	9.5	M4
TYC 2211-1309-1	22 00 41.6	+27 15 14	11.43	5.7	42.7	-17.3	46.4	M0
PZ Tel	18 53 05.9	-50 10 50	8.29	46.8	-11.5	-18.3	51.5	G9
TWA 22	10 17 26.9	-53 54 27	14.41	- 3.5	-17.2	0.7	17.2	M5
TX PsA	22 45 00.0	-33 15 26	13.36	9.2	2.0	-17.9	20.2	M5

ID	RA	DEC	V Mag.	X	Y	Z	D	SpT
TYC 112-917-1	05 20 00.3	+06 13 04	11.58	-62.8	-18.5	-20.2	68.5	K4
TYC 112-1486-1	05 20 31.8	+06 16 11	11.68	-64.0	-18.8	-20.3	69.7	K4
TYC 7443-1102-1	19 56 04.4	-32 07 38	11.55	49.5	7.6	-25.4	56.2	M0
TYC 9073-762-1	18 46 52.6	-62 10 36	12.08	42.4	-21.2	-20.4	51.6	M1
V1005 Ori	04 59 34.8	+01 47 01	10.05	-21.3	-6.8	-9.9	24.5	M0
V1311 Ori*	05 32 04.5	-03 05 29	11.44	-34.5	-17.2	-13.3	40.8	M2
V4046 Sgr	18 14 10.5	-32 47 33	10.94	75.7	-0.4	-9.6	76.3	K6
WW PsA	22 44 58.0	-33 15 02	12.07	9.2	2.0	-17.9	20.2	M4
			Carina members					
BD-20951	04 52 49.5	-19 55 02	10.00	-46.2	-37.8	-41.4	72.6	K1
CD-423328	07 33 21.2	-42 55 42	11.42	-28.4	-111.9	-22.6	117.6	K1
CD-482324	06 28 06.1	-48 26 53	10.96	-27.4	-117.0	-52.6	131.2	G9
CD-494008	08 57 52.2	-49 41 51	10.51	-1.0	-108.7	-5.0	108.8	G9
CD-542499	08 59 28.7	-54 46 49	10.08	7.2	-117.9	-11.9	118.7	G5
CD-542644	09 13 16.9	-55 29 03	11.36	13.2	-141.3	-11.8	142.4	G5
CD-552543	09 09 29.4	-55 38 27	10.21	11.1	-124.0	-11.5	125.0	G8
CD-571709	07 21 23.7	-57 20 37	10.73	-2.4	-95.1	-32.3	100.5	K0
CD-612010	08 42 00.5	-62 18 26	10.95	18.9	-133.9	-29.3	138.4	K0
CD-75392	08 50 05.4	-75 54 38	10.59	33.9	-93.3	-35.3	105.4	G9
CP-541712	08 37 10.9	-55 18 10	11.04	5.8	-176.1	-26.6	178.2	G9
CP-551885*	09 00 03.4	-55 38 24	10.83	9.2	-124.9	-13.7	126.0	G5
CP-621293	09 43 08.8	-63 13 04	10.44	17.6	-73.5	-10.2	76.3	G7
HD 107722	12 23 29.0	-77 40 51	8.30	33.1	-54.3	-16.9	65.8	F6
HD 189285*	19 59 24.1	-04 32 06	9.52	42.1	31.3	-16.2	54.9	G7
HD 221451*	23 32 19.2	-13 37 18	8.59	7.9	17.1	-44.6	48.4	G8
HD 269620	05 29 27.1	-68 52 05	9.56	13.5	-82.5	-53.3	99.1	G6
HD 309751	09 31 44.7	-65 14 53	11.33	39.1	-157.6	-28.7	164.9	G5
HD 42270	05 53 29.3	-81 56 53	9.14	21.4	-48.1	-29.0	60.1	K0
HD 49855*	06 43 46.2	-71 58 35	9.06	11.5	-50.8	-25.7	58.1	G7
HD 8813	01 23 25.9	-76 36 42	8.37	18.0	-30.5	-30.1	46.5	G6
CD-65149	03 06 14.5	-65 21 32	10.30	15.4	-65.0	-69.9	96.7	K0
HD 19545	03 07 50.8	-27 49 52	6.18	-20.3	-18.5	-47.2	54.6	A3
HD 22213	03 34 16.4	-12 04 07	8.86	-33.1	-11.7	-40.4	53.5	G7
CD-441533	04 22 45.7	-44 32 52	10.47	-24.3	-66.6	-70.1	99.7	K0
HD 269921	05 38 34.5	-68 53 07	10.28	13.8	-84.8	-53.1	101.0	G7
CD-372984	06 39 46.7	-37 50 10	10.90	-29.1	-67.7	-24.5	77.7	K1
CD-521641	06 41 12.5	-52 07 39	10.83	-13.4	-87.4	-36.8	95.8	K0
HD 48097*	06 42 24.3	+17 38 43	5.20	-41.7	-12.1	4.6	43.7	A2
CD-412572	06 45 37.9	-41 12 41	10.74	-24.6	-69.2	-24.6	77.5	K0

ID	RA	DEC	V Mag.	X	Y	Z	D	SpT
HD 51062	06 53 47.4	-43 06 51	9.23	-26.4	-85.9	-28.8	94.4	G5
HIP 38712	07 55 31.4	+08 51 47	5.85	-31.4	-19.7	12.2	39.0	F2
BD-072388	08 13 51.0	-07 38 25	9.32	-28.2	-33.1	11.2	44.9	K1
CD-532515	08 51 56.4	-53 55 57	11.06	4.9	-130.4	-13.9	131.2	G9
HD 83096*	09 31 24.9	-73 44 49	7.49	27.4	-75.2	-23.1	83.3	F2
HIP 46720B*	09 31 25.2	-73 44 51	10.02	27.4	-75.2	-23.1	83.3	G9
CD-484797	09 33 14.3	-48 48 33	11.72	2.6	-52.1	1.9	52.2	K6
CD-69783	10 41 23.0	-69 40 43	10.27	36.4	-90.0	-16.4	98.5	G8
HD 152598	16 52 58.1	+31 42 06	5.34	13.7	18.5	17.9	29.2	F0
TYC 9486-927-1	21 25 27.5	-81 38 28	11.85	21.7	-25.2	-20.9	39.3	M1
BD-035579	23 09 37.1	-02 25 55	10.99	9.4	32.6	-49.0	59.6	K4
HD 221452*	23 32 22.7	-13 39 07	9.20	8.1	17.4	-45.6	49.5	K0
TYC 460-624-1*	18 45 10.3	+06 20 16	10.76	22.0	17.1	2.1	27.9	M1
TYC 8174-1586-1	09 11 15.8	-50 14 15	11.81	2.6	-115.2	-2.8	115.3	K5
TYC 8557-1251-1	07 55 31.6	-54 36 51	11.44	-6.6	-194.1	-45.8	199.5	G9
TYC 8570-1980-1	08 11 09.3	-55 55 56	11.52	0.9	-145.0	-30.8	148.2	G9
TYC 8582-3040-1	08 57 45.6	-54 08 37	11.71	7.0	-140.9	-13.7	141.7	K2
TYC 8590-1193-1	08 56 31.5	-57 00 41	11.83	16.0	-185.8	-24.6	188.1	K0
TYC 8946-872-1*	09 55 15.1	-62 03 32	12.01	42.1	-171.3	-18.3	177.3	K2
TYC 8962-1747-1	11 08 07.9	-63 41 47	12.05	36.3	-90.7	-5.3	97.8	K6
TYC 9217-417-1	09 59 57.7	-72 21 47	11.70	32.2	-85.2	-22.2	93.7	K4
Columbus members								
TYC 8862-19-1	02 58 04.0	-62 41 14	11.67	11.9	-58.8	-68.6	91.1	K3
TYC 9178-284-1	06 55 25.2	-68 06 21	11.91	14.1	-92.3	-42.9	102.8	K4
BD-191194	05 30 19.1	-19 16 32	9.62	-80.8	-73.3	-53.7	121.6	G6
BD-04700	03 57 37.2	-04 16 16	10.61	-76.5	-19.3	-66.5	103.2	G8
BD-081195	05 38 35.0	-08 56 40	9.84	-63.8	-41.1	-27.9	80.9	G7
BD-08995	04 58 48.6	-08 43 40	10.32	-67.7	-35.7	-42.3	87.4	K0
BD-11648	03 21 49.7	-10 52 18	11.32	-75.2	-21.0	-96.8	124.4	K0
BD-15705*	04 02 16.5	-15 21 30	10.17	-30.6	-16.4	-33.9	48.5	K3
BD-16351	02 01 35.6	-16 10 01	10.33	-26.9	-1.2	-75.6	80.3	K1
CD-292531	05 50 21.4	-29 15 21	11.31	-58.1	-81.0	-47.1	110.2	K0
CD-361785	04 34 50.8	-35 47 21	10.84	-31.1	-49.6	-53.1	79.0	K1
CD-363202	06 52 46.7	-36 36 17	11.22	-34.2	-78.6	-23.8	89.0	K2
CD-382198	05 45 16.3	-38 36 49	10.95	-51.5	-106.3	-65.0	134.8	G9
CD-392075*	05 37 05.3	-39 32 26	9.52	-18.7	-39.7	-25.9	51.0	K1
CD-393026	07 01 51.8	-39 22 04	11.05	-32.5	-88.5	-25.2	97.6	G9
CD-402458	06 26 06.9	-41 02 54	10.00	-31.9	-83.3	-35.9	96.2	K0
CD-431395	04 21 48.7	-43 17 33	10.18	-35.4	-88.4	-95.0	134.5	G7

ID	RA	DEC	V Mag.	X	Y	Z	D	SpT
CD-44753	02 30 32.4	-43 42 23	10.42	-4.2	-21.7	-45.5	50.6	K5
CD-52381	01 52 14.6	-52 19 33	10.89	8.7	-38.8	-75.8	85.6	K2
CD-544320*	11 45 51.8	-55 20 46	10.24	20.9	-47.7	5.8	52.4	K5
CP-522481	09 32 26.1	-52 37 40	10.86	9.3	-99.2	-1.3	99.6	G8
CP-531875*	08 45 52.7	-53 27 28	10.42	3.2	-151.6	-17.2	152.6	G2
GSC 08077-01788	04 51 53.0	-46 47 31	13.03	-18.1	-57.8	-49.9	78.5	M0
HD 26980	04 14 22.6	-38 19 02	9.08	-26.9	-48.7	-58.4	80.7	G3
HD 272836	04 53 05.2	-48 44 39	10.78	-15.3	-57.7	-48.7	77.0	K2
HD 274561	05 28 55.1	-45 34 58	11.45	-23.2	-69.6	-47.7	87.5	K1
HD 27679	04 21 10.3	-24 32 21	9.43	-41.2	-37.3	-51.9	76.0	G2
HD 298936	10 13 14.8	-52 30 54	9.76	9.6	-54.0	3.1	54.9	K3
HD 31242N	04 51 53.5	-46 47 13	9.85	-15.9	-50.8	-43.9	69.0	G5
HD 32309	05 01 25.6	-20 03 07	4.91	-38.9	-32.9	-32.9	60.6	B9
HD 32372	05 00 51.9	-41 01 07	9.50	-25.2	-54.9	-46.6	76.3	G5
HD 40216	05 55 43.2	-38 06 16	7.46	-21.2	-43.7	-24.4	54.4	F7
AB Pic	06 19 12.9	-58 03 16	9.20	-2.2	-41.0	-20.9	46.1	K1
HD 48370	06 43 01.0	-02 53 19	7.92	-26.9	-18.5	-1.8	32.7	G8
HD 51797	06 56 23.5	-46 46 55	9.84	-16.6	-70.0	-24.2	75.9	K0
HD 55279	07 00 30.5	-79 41 46	10.08	19.3	-49.1	-26.0	58.8	K2
V479 Car	09 23 35.0	-61 11 36	10.16	15.7	-85.5	-11.9	87.7	K1
HD 984	00 14 10.2	-07 11 57	7.32	-2.2	17.4	-43.8	47.2	F5
TYC 119-497-1	05 37 46.5	+02 31 26	11.01	-60.5	-24.4	-17.6	67.6	K5
TYC 119-1242-1	05 37 45.3	+02 30 57	10.96	-61.8	-25.0	-18.0	69.1	K5
TYC 4810-181-1	06 31 55.2	-07 04 59	11.80	-74.4	-56.2	-12.3	94.0	K3
AH Lep	05 34 09.2	-15 17 03	8.41	-44.2	-35.2	-25.0	61.8	G3
BD+03480	03 28 15.0	+04 09 48	9.70	-61.8	0.6	-53.5	81.7	G6
BD+08742	04 42 32.1	+09 06 01	11.02	-96.8	-14.3	-42.2	106.6	K0
BD+443670	21 00 47.0	+45 30 10	8.70	3.4	58.1	-0.5	58.2	G2
CD-441568	04 27 20.5	-44 20 39	10.91	-21.0	-56.5	-57.9	83.6	K1
CD-521363	05 51 01.2	-52 38 13	10.61	-17.0	-99.2	-58.6	116.5	G9
CD-53386	02 01 53.7	-52 34 53	11.74	9.5	-51.8	-96.3	109.8	K2
CD-63408	08 24 06.0	-63 34 03	9.87	14.8	-106.3	-28.0	110.9	G5
GSC 08499-00304	03 24 15.0	-59 01 13	12.09	4.3	-60.2	-68.7	91.4	K6
HD 16754	02 39 48.0	-42 53 30	4.74	-5.1	-20.0	-40.5	45.5	A1
HD 21997	03 31 53.6	-25 36 51	6.38	-32.3	-27.0	-58.3	71.9	A3
HD 222439	23 40 24.5	+44 20 02	4.15	-16.7	46.5	-14.8	51.6	B9
HD 23384	03 47 10.6	+51 42 23	6.90	-48.9	30.1	-2.3	57.5	F3
HD 295290	06 40 22.3	-03 31 59	9.00	-50.0	-34.8	-4.3	61.1	K0
HD 30447	04 46 49.5	-26 18 09	7.85	-43.6	-45.7	-49.2	80.1	F3
HD 31647A	04 59 15.4	+37 53 25	4.99	-51.0	11.6	-2.6	52.4	A0
HD 31647B	04 59 15.4	+37 53 30	8.19	-51.0	11.6	-2.6	52.4	G0
HD 35114	05 20 38.0	-39 45 18	7.34	-17.4	-36.2	-26.8	48.3	F6
HD 35841	05 26 36.6	-22 29 24	8.91	-55.6	-56.1	-42.2	89.6	F3

ID	RA	DEC	V Mag.	X	Y	Z	D	SpT
HD 36329	05 29 24.1	-34 30 56	9.18	-31.6	-51.9	-36.5	70.9	G3
HD 37286	05 36 10.3	-28 42 29	6.26	-28.3	-37.1	-24.9	52.9	A2
HD 37484	05 37 39.6	-28 37 35	7.26	-30.5	-40.0	-26.4	56.8	F4
HD 38206	05 43 21.7	-18 33 27	5.73	-50.8	-46.9	-29.5	75.2	A0
HD 38207	05 43 21.0	-20 11 21	8.46	-64.7	-63.4	-39.7	98.9	F2
HD 38397	05 43 35.8	-39 55 25	8.14	-18.7	-41.1	-25.5	51.9	G0
HD 43989	06 19 08.1	-03 26 20	7.91	-41.1	-26.0	-7.5	49.2	F9
HIP 17248	03 41 37.3	+55 13 07	11.34	-29.3	20.0	0.0	35.5	M0
RT Pic	06 00 41.3	-44 53 50	9.09	-14.6	-44.4	-24.2	52.6	G8
TYC 65-1471-1	03 48 58.8	+01 10 54	11.4	-84.6	-10.0	-68.5	109.3	K3
V342 Peg	23 07 28.7	+21 08 03	5.97	-1.5	32.0	-22.9	39.4	A5
TYC 5900-1180-1*	04 58 35.8	-15 37 31	11.15	-97.2	-68.3	-73.8	139.9	G9
			ϵ-Chamaeleon members					
CD-691055	12 58 25.6	-70 28 49	9.97	57.7	-87.1	-14.0	105.4	K0
CD-74712	12 39 21.3	-75 02 39	10.30	55.0	-87.5	-22.3	105.7	K3
CP-681894	13 22 07.5	-69 38 12	10.35	60.9	-85.0	-12.7	105.3	K1
DZ Cha	11 49 31.9	-78 51 01	12.9	46.9	-81.8	-27.7	98.3	M0
EG Cha	08 36 56.2	-78 56 46	11.36	36.7	-89.7	-38.8	104.4	K4
EO Cha	08 44 31.9	-78 46 31	12.53	33.9	-82.5	-35.0	95.8	M0
EQ Cha*	08 47 56.8	-78 54 53	13.92	33.2	-80.1	-33.9	93.1	M2
1RXS J091528.1-760856	09 15 29.1	-76 08 47	12.08	37.9	-98.1	-35.2	110.9	K6
GSC 09239-01495	12 19 43.8	-74 03 57	13.08	52.2	-87.8	-20.5	104.2	M0
GSC 09239-01572	12 20 21.9	-74 07 39	12.85	54.6	-91.7	-21.5	108.9	K7
1RXS J093455.3-780414	09 34 56.1	-78 04 19	14.53	43.3	-100.0	-37.6	115.3	M2
G94010229[a]	10 05 20.0	-77 48 42	12.75	34.2	-75.0	-26.4	86.6	M1
GSC 09415-02676*	11 58 26.9	-77 54 45	14.29	54.0	-93.2	-29.5	111.7	M3
1RXS J121645.2-775339	12 16 46.0	-77 53 33	13.88	57.7	-95.7	-30.3	115.8	M4
GSC 09420-00948	12 02 03.8	-78 53 01	12.48	51.9	-88.2	-29.8	106.6	M0
DX Cha	12 00 05.1	-78 11 35	6.73	55.7	-95.7	-30.9	115.0	A8
HD 104237-5	12 00 08.3	-78 11 40	14.28	55.7	-95.7	-30.9	115.0	M3
HD 104237-6	12 00 09.3	-78 11 42	12.08	55.7	-95.7	-30.9	115.0	K4
HD 104467	12 01 39.1	-78 59 17	8.56	51.4	-87.3	-29.7	105.6	G3
HD 105923	12 11 38.1	-71 10 36	9.16	56.6	-99.2	-17.2	115.5	G8
HIP 58490	11 59 42.3	-76 01 26	11.31	48.7	-85.3	-23.5	101.0	K4
TYC 9245-535-1	12 56 08.4	-69 26 54	12.06	62.3	-94.7	-13.1	114.1	K7
Eps Cha	11 59 37.6	-78 13 19	5.34	53.8	-92.5	-29.9	111.1	B9
GSC 09416-01029	12 04 36.2	-77 31 35	13.81	55.1	-94.2	-29.0	112.9	M2
HIP 42794	08 43 12.2	-79 04 12	6.80	33.0	-79.5	-34.1	92.6	A7

ID	RA	DEC	V Mag.	X	Y	Z	D	SpT
HIP 58410	11 58 35.2	-77 49 31	6.73	52.5	-90.8	-28.6	108.7	A7
Eta Cha	08 41 19.5	-78 57 48	5.46	33.7	-81.8	-35.1	95.2	B8
T Cha	11 57 13.5	-79 21 32	9.85	50.8	-86.8	-30.3	105.0	K0
Octans members								
BD-201111	05 32 29.3	-20 43 33	10.4	-82.4	-79.4	-56.4	127.6	G7
CD-303394N	06 40 04.9	-30 33 03	9.84	-72.4	-123.7	-40.1	148.8	F6
CD-303394S	06 40 05.7	-30 33 09	10.24	-80.9	-138.2	-44.8	166.3	F9
CD-431451	04 30 27.3	-42 48 47	10.75	-35.7	-85.8	-87.8	127.8	G9
CD-471999	05 43 32.1	-47 41 11	10.19	-38.8	-138.7	-85.9	167.7	G0
CD-492037	06 03 35.4	-49 11 26	11.18	-33.0	-139.5	-75.4	162.0	K0
CD-58860	04 11 55.7	-58 01 47	10.01	-1.5	-74.2	-70.5	102.4	G6
CD-66395	06 25 12.4	-66 29 10	10.92	14.2	-125.8	-65.3	142.4	K0
CD-72248	05 06 50.6	-72 21 12	10.91	32.3	-130.8	-89.5	161.7	K0
CD-87121	23 58 17.7	-86 26 24	9.98	56.3	-83.8	-59.7	117.3	G8
CP-82784	19 53 56.8	-82 40 42	10.87	80.9	-93.2	-68.0	140.9	K1
HD 155177	17 42 09.0	-86 08 05	8.88	76.1	-100.8	-61.4	140.4	F5
HD 274576	05 28 51.4	-46 28 19	10.57	-33.0	-105.3	-72.1	131.8	G6
CP-791037	19 47 03.9	-78 57 43	11.16	107.4	-106.6	-84.7	173.4	G8
TYC 9300-891-1	18 49 48.7	-71 57 10	11.43	125.1	-94.2	-75.0	173.6	K0
TYC 7066-1037-1	05 58 11.8	-35 00 49	11.24	-57.2	-103.1	-56.0	130.5	G9
TYC 9300-529-1	18 49 45.1	-71 56 58	11.59	138.0	-104.0	-82.7	191.6	K0
Tucana Horologium members								
AF Hor	02 41 47.3	-52 59 31	12.21	0.8	-22.4	-34.6	41.2	M2
BD-091108	05 15 36.5	-09 30 51	9.79	-60.1	-35.6	-33.4	77.4	G5
BD-12943	04 36 47.1	-12 09 21	9.86	-49.0	-26.9	-39.6	68.5	K0
BD-191062	04 59 32.0	-19 17 42	10.65	-41.9	-34.2	-35.1	64.5	K3
CD-272520	05 49 06.6	-27 33 56	10.22	-40.4	-52.6	-30.9	73.2	G9
CD-302310	05 18 29.0	-30 01 32	11.66	-34.3	-45.4	-35.7	67.2	K4
CD-351167	03 19 08.7	-35 07 00	11.12	-13.0	-19.5	-36.9	43.7	K7
CD-441173	03 31 55.7	-43 59 14	10.90	-8.4	-24.9	-35.9	44.5	K6
CD-461064	03 30 49.1	-45 55 57	9.55	-6.8	-24.5	-34.2	42.6	K3
CD-58553	02 42 33.0	-57 39 37	10.98	3.9	-28.2	-38.8	48.1	K5
CD-60416	02 07 32.2	-59 40 21	10.68	7.1	-24.4	-36.2	44.2	K5
CD-7824	00 42 20.3	-77 47 40	10.21	21.2	-32.0	-31.4	49.6	K3
HIP 1993	00 25 14.7	-61 30 48	11.47	15.6	-19.7	-36.4	44.2	M0

ID	RA	DEC	V Mag.	X	Y	Z	D	SpT
HD 16978	02 39 35.4	-68 16 01	4.12	10.5	-30.7	-33.4	46.6	B9
HD 105	00 05 52.5	-41 45 11	7.53	10.4	-5.4	-37.6	39.4	G0
HD 12039	01 57 49.0	-21 54 05	8.66	-10.7	-3.4	-39.2	40.8	G4
HD 12894	02 04 35.1	-54 52 54	6.46	5.2	-23.9	-41.1	47.8	F4
HD 13183	02 07 18.1	-53 11 56	8.63	4.3	-24.9	-44.4	51.1	G7
HD 13246	02 07 26.1	-59 40 46	7.50	7.1	-24.4	-36.2	44.2	F7
HD 1466	00 18 26.1	-63 28 39	7.45	15.6	-19.3	-33.3	41.5	F8
HD 17250	02 46 14.6	+05 35 33	7.88	-36.1	8.0	-39.8	54.3	F8
HD 20121AB	03 12 25.8	-44 25 11	6.40	-6.5	-22.3	-35.7	42.6	F5
HD 202917	21 20 50.0	-53 02 03	8.69	29.9	-8.5	-29.6	42.9	G7
HD 20385	03 16 40.7	-03 31 49	7.48	-32.8	-2.9	-36.6	49.2	F5
HD 207575	21 52 09.7	-62 03 09	7.22	28.2	-16.0	-31.6	45.3	F5
HD 207964	21 55 11.4	-61 53 12	6.56	28.7	-16.3	-32.7	46.5	F4
HD 222259S	23 39 39.5	-69 11 45	8.49	21.0	-23.3	-33.2	45.7	G6
HD 222259N	23 39 39.3	-69 11 40	9.84	21.0	-23.3	-33.2	45.7	K3
HD 22705	03 36 53.4	-49 57 29	7.65	-4.6	-26.8	-33.7	43.3	G2
HD 24636	03 48 11.5	-74 41 39	7.13	14.3	-40.4	-32.9	54.0	F3
HD 29615	04 38 43.9	-27 02 02	8.47	-29.6	-31.4	-36.0	56.2	G3
HD 30051*	04 43 17.2	-23 37 42	7.12	-36.8	-34.1	-39.2	63.7	F2
HD 32195	04 48 05.2	-80 46 45	8.14	20.8	-47.6	-31.9	61.0	F7
HD 47875	06 34 41.0	-69 53 06	9.17	11.1	-60.9	-31.2	69.3	G4
HD 8558	01 23 21.3	-57 28 51	8.51	10.6	-23.1	-42.5	49.5	G7
HD 9054	01 28 08.7	-52 38 19	9.07	5.6	-15.0	-32.2	36.0	K1
HD 987	00 13 53.0	-74 41 18	8.78	19.5	-26.5	-29.9	44.5	G8
HIP 107345	21 44 30.1	-60 58 39	11.61	29.0	-15.2	-31.6	45.5	M0
TYC 9344-293-1	23 26 10.7	-73 23 50	11.83	21.8	-25.0	-30.3	44.9	M0
CD-53544	02 41 46.8	-52 59 52	10.22	0.8	-22.4	-34.6	41.2	K6
CD-86147	23 27 49.4	-86 13 19	9.29	28.8	-41.9	-30.1	59.1	G8
ASAS J015220-5950.4	01 52 18.3	-59 50 17	12.57	7.2	-20.5	-31.8	38.5	M2
1RXS J100104.1-791314	10 01 08.8	-79 13 08	13.30	30.5	-64.7	-24.6	75.6	M0
HD 24071	03 48 35.9	-37 37 12	4.79	-15.7	-27.4	-39.7	50.7	A1
HD 25042	04 00 32.0	-41 44 54	8.36	-12.8	-29.2	-36.6	48.5	G3
HD 2884	00 31 32.7	-62 57 30	4.36	14.6	-19.5	-33.6	41.5	B9
HD 2885	00 31 33.5	-62 57 56	4.77	15.0	-20.1	-34.6	42.7	A2
HD 3003	00 32 43.9	-63 01 53	5.07	15.9	-21.5	-36.8	45.5	A0
HD 3221	00 34 51.2	-61 54 58	9.61	14.9	-20.2	-36.0	43.9	K4
HD 53842	06 46 13.5	-83 59 30	7.46	21.9	-44.6	-25.5	55.8	F5
HIP 1910	00 24 09.0	-62 11 04	11.49	16.6	-20.9	-37.6	46.1	M0
HD 86356	09 51 50.7	-79 01 38	10.20	29.5	-64.0	-24.4	74.6	K0
TYC 9507-2466-1*	11 40 16.6	-83 21 00	11.56	35.5	-59.7	-26.4	74.3	K4
TYC 8083-455-1	04 48 00.7	-50 41 26	11.53	-8.9	-40.8	-34.9	54.4	K7
TYC 8098-414-1	05 33 25.6	-51 17 13	11.74	-8.8	-43.0	-28.3	52.2	K7

ID	RA	DEC	V Mag.	X	Y	Z	D	SpT
HD 193924	20 25 38.9	-56 44 06	1.91	42.4	-14.7	-31.7	54.9	B2
			TW-Hydrae members					
HD 14228	02 16 30.6	-51 30 43	3.56	2.1	-22.9	-41.2	47.2	B8
TWA 27	12 07 33.4	-39 32 54	19.95	20.1	-45.7	20.7	54.0	M8
CD-337795	11 31 55.3	-34 36 27	12.12	11.6	-43.6	21.5	50.0	M2
TWA 3A	11 10 27.9	-37 31 52	12.57	7.0	-33.7	13.3	36.9	M4
TWA 3B	11 10 27.8	-37 31 53	13.07	7.0	-33.7	13.3	36.9	M4
HD 96819	11 08 44.0	-28 04 50	5.43	5.8	-48.0	27.4	55.6	A1
HD 98800	11 22 05.3	-24 46 40	9.42	5.5	-37.3	25.2	45.3	K5
TWA 11A	12 36 01.0	-39 52 10	5.78	33.3	-58.4	28.4	73.0	A0
TWA 11B	12 36 00.6	-39 52 16	12.8	31.5	-55.2	26.8	69.0	M2
TWA 26	11 39 51.1	-31 59 21	20.5	10.0	-35.6	20.0	42.0	M8
TWA 5B	11 31 55.4	-34 36 29	20.4	11.6	-43.6	21.5	50.0	M8
TW Hya	11 01 51.9	-34 42 17	11.07	7.7	-50.4	21.6	55.4	K6
TWA 10	12 35 04.2	-41 36 39	12.96	26.7	-46.9	20.9	57.9	M2
TWA 12	11 21 05.5	-38 45 16	12.85	14.7	-58.1	22.8	64.1	M1
CD-347390A*	11 21 17.2	-34 46 46	11.46	11.5	-51.0	23.9	57.5	M1
CD-347390B*	11 21 17.4	-34 46 50	11.96	11.5	-51.0	23.9	57.5	M1
TWA 14	11 13 26.5	-45 23 43	12.8	24.9	-89.9	23.5	96.2	M0
TWA 16	12 34 56.4	-45 38 07	12.8	37.2	-64.7	23.0	78.1	M1
CD-298887	11 09 13.8	-30 01 40	11.43	5.7	-40.7	21.7	46.5	M2
TWA 23	12 07 27.4	-32 47 00	12.67	17.9	-43.4	26.2	53.8	M3
CD-397538	12 15 30.7	-39 48 43	11.44	21.5	-45.1	20.7	54.1	M1
TWA 7	10 42 30.1	-33 40 17	11.65	2.3	-29.9	12.1	32.3	M2
CD-268632A	11 32 41.2	-26 51 56	12.23	7.9	-37.1	24.4	45.1	M3
TWA 8B	11 32 41.2	-26 52 09	15.3	7.7	-36.3	23.9	44.1	M5
TWA 9A	11 48 24.2	-37 28 49	11.26	22.2	-63.3	29.5	73.3	M1
TWA 9B	11 48 23.7	-37 28 49	14.0	22.2	-63.3	29.5	73.3	M1

Notes. $^{(*)}$ No longer classified as a member of association with new RV values. $^{(a)}$ No SIMBAD entry within 5 arcseconds.

Chapter 3

Visual binaries in the young moving groups

Parts of this chapter have been previously published as 'Search for associations containing young stars (SACY). VI. Is multiplicity universal? Stellar multiplicity in the range 3-1000 au from adaptive-optics observations', Elliott, P.; Huélamo, N.; Bouy, H.; Bayo, A.; Melo, C. H. F.; Torres, C. A. O.; Sterzik, M. F.; Quast, G. R.; Chauvin, G.; Barrado, D., 2015, A&A, 580, A88. The work is presented here in expanded and updated form.

In this chapter we use adaptive-optics (AO)-imaging data for 113 targets in the young moving groups to derive multiplicity frequencies, mass-ratio, and physical separation distributions in a consistent parameter space, and compare our results to other PMS populations and the field. We identified multiple systems using co-moving proper-motion analysis for targets with multi-epoch data, and using contamination estimates in terms of mass-ratio and physical separation for targets with single-epoch data. We have explored a wide range of projected separations ($a \approx$3–1000 au) and mass-ratios (q$\approx$0.1–1). We identified 31 multiple systems (28 binaries and 3 triples). Analysis from Chapter 2 indicated that the underlying multiple system distribution of the young associations and the young star-forming region (SFR) Taurus are statistically similar, supporting the idea that these two populations formed in a similar way. In this work, we show further similarities between the two populations: flat mass-ratio distributions

and statistically similar *MF* and *TF* values. We also compared the SACY sample to the field (in the separation range of 19-100 au), finding that the two distributions are indistinguishable, suggesting a similar formation mechanism.

This chapter is organised as follows: Section 3.1 describes the target selection. Section 3.2 details the observations, data reduction, and the sensitivity limits, as well as the literature analysis. Section 3.3 outlines the methods used to identify bound multiple systems and the uncertainty estimations. Section 3.4 describes how we derived the multiplicity properties of our sample. Section 3.5 presents the statistical analysis of the built distributions and comparisons to other populations. Section 3.6 states the main conclusions of this chapter and prospects. Section 3.7 provides tables summarising all the targets studied in this chapter and the multiple systems identified in populations other than the 9 young moving groups.

3.1 Sample definition

The starting point for our sample selection was based on the census by Torres et al. (2006). For the southern targets two additional criteria were followed: (i) we only consider stars with spectral types later than G5, in order to increase the contrast between the primary and the possible companion candidate, and (ii) the right ascension (RA) should be obtainable from Paranal observatory when our service observations were conducted (periods 77, 81, 88, and 89). The northern targets also followed criterion (i) and were also observed according to their visibility during the two runs at the Lick observatory in 2008 and 2009.

Later on, the membership of several targets was revised based on new data (e.g. new RV values derived from high-resolution spectra, Chapter 2). This revision allowed us to eliminate contamination within the sample from interlopers. From the 201 SACY targets observed originally with AO, 113 are now confirmed SACY members, while 88 have been rejected.

The bulk of this work is focused on the 113 confirmed SACY members, and the specific details of the sample are provided below (summarised in Table 3.1). However, for completeness with our original observations, we also provide details on the 88 non-SACY targets, including their observational parameters and a summary of the identified multiple systems, in Tables J1[1] and 3.7, respectively.

3.1.1 Filtered coherent sample for this work

Table 3.1 provides the census of the 113 confirmed SACY members (once the additional data from Chapter 2 have been included to identify interlopers) studied in this work. We have included two K magnitude values: the original value from the 2MASS survey, K (2M), and our estimated K (M_1). From our observations (with a narrow field of view that does not allow for a robust flux calibration), we can only obtain relative photometry and therefore we use 2MASS magnitudes for calibration. We denoted our estimated magnitude, K (M_1), and it only differs from the original 2MASS value in the case of a detection of a new companion (previously unresolved) within the 2MASS PSF. The typical PSF width for 2MASS is $\approx 2''$and, in some cases, multiple components can be found within this angular distance. To estimate the photometry of the primary and components we weighted the 2MASS value according to the observed flux ratio. In the next sections, the primary masses have been calculated using this value, and the age value included in Table 3.2 with the evolutionary tracks of Baraffe et al. (1998).

Finally, we note that all the targets in this sample have PM values from the UCAC4 catalogue (Zacharias et al., 2012). Precise PMs allow us to determine whether identified companions are co-moving with the primary source.

[1] Due to the number of columns (34) in this Table we have not included it in this manuscript. The table can be located using the online VizieR query service and Table ID: *J/A+A/580/A88/tableb1*

TABLE 3.1: All SACY targets observed and analysed in this chapter. The distance values are kinematic, derived from the convergence method (Torres et al., 2006).

ID	RA	DEC	K (2M)	K (M_1)	Ass.	Dist.	M_1
	hh:mm:ss.s	dd:mm:ss	(mag.)	(mag.)		(pc)	($M_\odot$)
CD-45 14955B	23:11:53.6	-45:08:00	8.85	8.85	ABD	49.3	0.56
GJ 9809	23:06:04.8	+63:55:34	6.98	6.98	ABD	24.5	0.61
HD 1405	00:18:20.9	+30:57:22	6.51	6.51	ABD	27.3	0.78
HD 160934	17:38:39.6	+61:14:16	6.81	6.81	ABD	33.1	0.8
HD 201919	21:13:05.2	-17:29:12	7.58	7.58	ABD	39.5	0.72
HD 222575	23:41:54.2	-35:58:39	7.62	7.62	ABD	63.6	0.96
HD 24681	03:55:20.4	-01:43:45	7.25	7.25	ABD	53.3	0.96
LP 745-70	16:33:41.6	-09:33:11	7.55	7.55	ABD	30.3	0.59
TYC 486-4943-1	19:33:03.7	+03:45:39	8.66	8.66	ABD	72.0	0.77
V* PX Vir	13:03:49.6	-05:09:42	5.51	5.51	ABD	21.7	0.9
HD 152555	16:54:08.1	-04:20:24	6.36	6.36	ABD	46.8	1.13
GJ 885 A	23:00:27.9	-26:18:42	6.27	6.75	ABD	32.7	0.81
Wolf 1225	22:23:29.1	+32:27:34	6.05	6.77	ABD	15.1	0.48
BD-03 4778	20:04:49.3	-02:39:20	7.92	8.06	ABD	71.5	0.91
GJ 4231	21:52:10.4	+05:37:35	7.38	8.2	ABD	30.6	0.5
TYC 91-82-1	04:37:51.4	+05:03:08	8.65	8.86	ABD	87.6	0.82
CD-52 9381	20:07:23.7	-51:47:27	7.39	7.39	ARG	29.4	0.59
2MASS J05200029+0613036	05:20:00.2	+06:13:03	8.57	8.57	BPC	67.8	0.67
BD-13 6424	23:32:30.8	-12:15:51	6.57	6.57	BPC	27.9	0.7
CD-31 16041	18:50:44.4	-31:47:47	7.46	7.46	BPC	53.2	0.87
CD-54 7336	17:29:55.0	-54:15:48	7.36	7.36	BPC	68.4	1.06
CPD-72 2713	22:42:48.9	-71:42:21	6.89	6.89	BPC	37.3	0.81
GSC 07396-00759	18:14:22.0	-32:46:10	8.54	8.54	BPC	95.2	0.93
HD 161460	17:48:33.7	-53:06:43	6.78	6.78	BPC	71.0	1.2
Smethells 20	18:46:52.5	-62:10:36	7.85	7.85	BPC	52.4	0.73
TYC 6872-1011-1	18:58:04.1	-29:53:04	8.02	8.02	BPC	82.6	0.99
V* TX PsA	22:45:00.0	-33:15:25	7.79	7.79	BPC	20.1	0.19
V* V4046 Sgr	18:14:10.4	-32:47:34	7.25	7.25	BPC	76.9	1.15
V* WW PsA	22:44:57.9	-33:15:01	6.93	6.93	BPC	20.1	0.35
GJ 3322	05:01:58.7	+09:58:59	6.37	6.8	BPC	37.8	0.85
CD-26 13904	19:11:44.6	-26:04:08	7.37	7.77	BPC	78.9	1.03

ID	RA hh mm ss	DEC dd mm ss	K (2M) (mag.)	K (M_1) (mag.)	Ass.	Dist. (pc)	M_1 ($M_\odot$)
CD-27 11535	17:15:03.6	-27:49:39	7.38	8.06	BPC	87.3	1.01
GSC 08350-01924	17:29:20.6	-50:14:53	7.99	8.65	BPC	66.3	0.63
2MASS J05203182+0616115	05:20:31.8	+06:16:11	8.57	8.7	BPC	71.0	0.66
2MASS J08110934-5555563	08:11:09.3	-55:55:56	9.4	9.4	CAR	129.0	0.84
2MASS J08521921-6004443	08:52:19.2	-60:04:44	9.37	9.37	CAR	163.9	1.04
2MASS J08563149-5700406[(a)]	08:56:31.4	-57:00:40	9.76	9.76	CAR	191.6	0.94
BD-03 5579	23:09:37.1	-02:25:55	7.82	7.82	CAR	63.0	0.85
CD-44 1533	04:22:45.6	-44:32:51	8.58	8.58	CAR	103.7	0.91
CD-49 4008	08:57:52.1	-49:41:50	8.64	8.64	CAR	102.9	0.89
CD-53 2515	08:51:56.4	-53:55:56	8.75	8.75	CAR	137.1	1.13
CD-54 2499	08:59:28.7	-54:46:49	8.4	8.4	CAR	109.5	1.08
CD-55 2543	09:09:29.3	-55:38:27	8.4	8.4	CAR	115.2	1.12
CD-61 2010	08:42:00.4	-62:18:26	8.83	8.83	CAR	121.4	0.93
CD-69 783	10:41:23.0	-69:40:43	8.38	8.38	CAR	86.5	0.87
HD 107722	12:23:29.0	-77:40:51	7.14	7.14	CAR	59.0	1.05
HD 309751	09:31:44.7	-65:14:52	8.36	8.36	CAR	141.6	1.2
HD 8813	01:23:25.8	-76:36:42	6.79	6.79	CAR	46.5	0.92
TYC 8174-1586-1	09:11:15.8	-50:14:14	9.5	9.5	CAR	117.2	0.79
TYC 8557-1251-1	07:55:31.6	-54:36:50	9.19	9.19	CAR	123.0	0.86
TYC 8582-3040-1[(a)]	08:57:45.6	-54:08:36	9.35	9.35	CAR	143.2	0.89
TYC 8962-1747-1	11:08:07.9	-63:41:47	8.29	8.29	CAR	88.2	0.9
TYC 9217-417-1	09:59:57.6	-72:21:47	8.69	8.69	CAR	83.6	0.8
TYC 9486-927-1	21:25:27.4	-81:38:27	7.34	7.34	CAR	36.3	0.71
HD 22213	03:34:16.3	-12:04:07	6.79	6.97	CAR	52.4	0.94
BD-07 2388	08:13:50.9	-07:38:24	6.92	7.4	CAR	42.6	0.77
2MASS J09131689-5529032	09:13:16.8	-55:29:03	8.36	8.61	CAR	131.7	1.15
CD-57 1709	07:21:23.7	-57:20:37	8.7	8.7	CAR	100.5	0.87
CPD-62 1293	09:43:08.8	-63:13:04	8.6	8.82	CAR	69.4	0.7
2MASS J08371096-5518105	08:37:10.9	-55:18:10	9.38	9.38	CAR	180.8	1.11
2MASS J03573723-0416159	03:57:37.2	-04:16:15	8.75	8.75	COL	106.5	0.89
2MASS J09322609-5237396	09:32:26.0	-52:37:39	8.84	8.84	COL	101.9	0.85
BD+08 742	04:42:32.0	+09:06:00	9.12	9.12	COL	105.6	0.81
BD-11 648[(a)]	03:21:49.6	-10:52:17	9.26	9.26	COL	128.1	0.86
CD-36 1785	04:34:50.7	-35:47:21	8.59	8.59	COL	80.1	0.8

ID	RA hh mm ss	DEC dd mm ss	K (2M) (mag.)	K (M_1) (mag.)	Ass.	Dist. (pc)	M_1 ($M_\odot$)
HD 26980	04:14:22.5	-38:19:01	7.62	7.62	COL	80.7	1.12
HD 27679	04:21:10.3	-24:32:20	7.81	7.81	COL	78.0	0.94
HD 31242	04:51:53.5	-46:47:13	8.16	8.16	COL	68.1	0.82
TYC 9178-284-1	06:55:25.1	-68:06:21	8.94	8.94	COL	108.3	0.86
V* V479 Car	09:23:34.9	-61:11:35	7.96	7.96	COL	87.7	1.07
2MASS J02303239-4342232	02:30:32.4	-43:42:23	7.23	7.57	COL	51.3	0.81
V* V1221 Tau	03:28:14.9	+04:09:47	7.44	8.01	COL	81.5	0.92
2MASS J08240598-6334024	08:24:05.9	-63:34:02	8.13	8.18	COL	118.6	1.2
HD 272836	04:53:05.1	-48:44:38	8.24	8.34	COL	78.6	0.84
BD-16 351	02:01:35.6	-16:10:00	7.96	8.43	COL	80.9	0.83
2MASS J04272050-4420393	04:27:20.4	-44:20:39	8.56	8.7	COL	86.2	0.81
CD-43 1395	04:21:48.6	-43:17:32	8.42	9.16	COL	141.0	0.93
2MASS J11594226-7601260	11:59:42.2	-76:01:26	8.3	8.3	ECH	101.0	0.98
2MASS J12194369-7403572	12:19:43.6	-74:03:57	8.86	8.86	ECH	108.9	0.78
2MASS J12392124-7502391	12:39:21.2	-75:02:39	7.78	7.78	ECH	108.6	1.2
CD-69 1055	12:58:25.5	-70:28:49	7.55	7.55	ECH	106.7	1.2
HD 104467	12:01:39.1	-78:59:16	6.85	6.85	ECH	106.5	1.2
V* DZ Cha	11:49:31.8	-78:51:01	8.49	8.49	ECH	102.7	0.91
V* MP Mus	13:22:07.5	-69:38:12	7.29	7.29	ECH	106.1	1.2
HD 105923	12:11:38.1	-71:10:36	7.18	7.26	ECH	117.1	1.2
TYC 9245-535-1	12:56:08.3	-69:26:53	7.99	8.34	ECH	119.3	1.14
2MASS J12202177-7407393	12:20:21.7	-74:07:39	8.37	8.4	ECH	114.8	1.07
2MASS J05581182-3500496	05:58:11.8	-35:00:49	9.38	9.38	OCT	105.8	0.77
2MASS J06400573-3033089	06:40:05.7	-30:33:08	8.7	8.7	OCT	162.4	1.2
CD-58 860	04:11:55.6	-58:01:47	8.36	8.36	OCT	87.1	0.88
CD-66 395	06:25:12.3	-66:29:10	9.0	9.0	OCT	126.1	0.91
HD 271037[(a)]	05:06:50.5	-72:21:11	8.67	8.67	OCT	145.8	1.19
BD-18 4452A	17:13:11.6	-18:34:25	6.48	6.48	OCT	16.7	0.51
CD-30 3394A	06:40:04.9	-30:33:03	8.59	8.59	OCT	162.4	1.2
CD-47 1999	05:43:32.1	-47:41:10	8.64	8.68	OCT	166.7	1.2
BD-20 1111	05:32:29.3	-20:43:33	8.7	8.7	OCT	129.7	1.1
HD 274576	05:28:51.3	-46:28:19	8.81	8.92	OCT	117.1	0.89
2MASS J04302731-4248466	04:30:27.3	-42:48:46	8.73	9.42	OCT	122.8	0.82
2MASS J06033540-4911256	06:03:35.4	-49:11:25	9.08	9.81	OCT	173.8	0.89

ID	RA hh mm ss	DEC dd mm ss	K (2M) (mag.)	K (M_1) (mag.)	Ass.	Dist. (pc)	M_1 ($M_\odot$)
2MASS J05490656-2733556	05:49:06.5	-27:33:55	8.25	8.25	THA	74.3	0.86
ASAS J051536-0930.8	05:15:36.4	-09:30:51	8.08	8.08	THA	77.5	0.91
BD-12 943	04:36:47.1	-12:09:20	7.76	7.76	THA	62.3	0.88
BD-19 1062	04:59:32.0	-19:17:41	8.07	8.07	THA	64.1	0.83
CD-35 1167	03:19:08.6	-35:07:00	7.72	7.72	THA	44.6	0.72
CD-46 1064	03:30:49.0	-45:55:57	7.1	7.1	THA	42.2	0.84
CD-53 544	02:41:46.8	-52:59:52	6.76	6.76	THA	41.4	0.9
CD-78 24	00:42:20.3	-77:47:39	7.53	7.53	THA	50.1	0.83
TYC 8098-414-1	05:33:25.5	-51:17:13	8.16	8.16	THA	51.6	0.68
TYC 9344-293-1	23:26:10.7	-73:23:49	7.94	7.94	THA	44.2	0.65
HD 22705	03:36:53.4	-49:57:28	6.14	6.18	THA	43.3	1.04
CD-44 1173	03:31:55.6	-43:59:13	7.47	7.58	THA	44.0	0.75
TYC 8083-455-1	04:48:00.6	-50:41:25	7.92	8.25	THA	54.8	0.7
2MASS J05182904-3001321	05:18:29.0	-30:01:32	8.3	8.41	THA	66.2	0.76

Notes. [(a)] Targets excluded from statistical analysis due to the quality of their sensitivity curves, see Figure 3.5.

3.2 Observations and data reduction

3.2.1 Southern Targets: NACO data

We had four sets of observations in service mode dedicated to collecting data on SACY sources with NAOS-CONICA, an adaptive optics system and near-IR camera at the very large telescope (VLT). The first epoch of data was taken between March–August 2006 (077.C-0483), and 76 targets were observed (seeing $\approx$0.9″). The 40 objects (out of the 76) identified to have potential companions were re-observed (seeing $\approx$0.7″) between March–June 2008 (081.C-0825). We had two additional programs to observe

TABLE 3.2: Summary of the properties and frequency of visual multiple systems identified for the SACY associations studied in this chapter.

Name	ID	Dist. (pc)	Age (Myr)	N. of observed[(a)] objects	N. of VBs[(b)] (this work)	$MF_{3-1000\,au}$[(c)] (%)
AB Doradus	ABD	34±26	100	16 (16)	5	31^{+13}_{-9}
Argus	ARG	106±51	40	1	0	-
β–Pic MG	BPC	31±21	20	17 (17)	5	29^{+13}_{-8}
Carina	CAR	85±35	40	26 (24)	5	21^{+10}_{-5}
Columba	COL	82±30	40	17 (16)	6	38^{+13}_{-10}
ϵ–Cha	ECH	108±9	8	10 (10)	2	20^{+17}_{-7}
Octans	OCT	141±34	40	11 (10)	5	50^{+14}_{-14}
Tuc–Hor	THA	48±7	40	14 (14)	3	21^{+14}_{-5}

Notes. [(a)] Effective number used to calculate *MF* values shown in parentheses.[(b)] Systems either confirmed from PM analysis or high probability ($\geq$95% detections) based on single-epoch data. [(c)] In the separation range 3-1000 au considering observed targets with sensitivities $\geq$95% of our sample.

other members of the SACY associations in 2011 and 2012 (088.C-0506, and 089.C-0207), and we observed 60 and 25 targets (seeing $\approx$1.0″), respectively (see Table 3.6 for details on individual sources).

All the targets are bright enough (V $<$ 16 mag or K $<$ 13 mag) to be used as AO reference stars. For the majority of the stars, we used the visible wave-front sensor (VIS WFS). For the reddest objects we used the IR WFS with the N90C10 dichroic, which sends 90% of the light to NAOS and 10% to the infrared detector. Since all the sources are very bright in the near-IR, the observations with the VIS WFS were performed with intermediate- and narrow-band filters to avoid saturation of the primary star. The first selection of filters was IB 2.21 (λ_0, $\Delta\lambda$=2.21, 0.06 μm) and NB 2.17 (λ_0, $\Delta\lambda$=2.17, 0.023 μm). During the observations, the IB 2.21 filter showed strong optical ghosts that prevented us from detecting companions in some particular regions of the detector. Therefore, we replaced it with the IB 2.27 (λ_0, $\Delta\lambda$=2.27, 0.06 μm) filter. The observations with the IR WFS were performed with the broad band K_s filter (λ_0, $\Delta\lambda$=2.18, 0.35 μm). All the observations from 2006 and 2008 used the S27 objective, which provides a field

of view (FoV) of $27.6'' \times 27.6''$. The data from 2011 and 2012 used the S13 objective, with a FOV of $14'' \times 14''$.

We observed each object using a jitter sequence to remove the sky contribution and to correct for bad pixels. The sky emission was estimated from the median image of all offsets positions. The average total exposure time for each source was $\approx$12 minutes. We reduced the data using the recommended *eclipse* ESO software (Devillard, 1997) and the *esorex* driven interface *gasgano*. Dark subtraction, bad pixel correction, and flat-field correction were applied to each frame prior to aligning and stacking.

To derive accurate astrometry of the potential companions, we derived the plate scale and orientation on the infrared detector, using archival observations of the astrometric field θ^1 Ori C (McCaughrean and Stauffer, 1994), and the astrometric binaries IDS 2150 and IDS 22141 (van Dessel and Sinachopoulos, 1993); see Chauvin et al. (2012) for details. The values measured in different epochs are displayed in Table 3.3. For each target, we have adopted the plate scale and orientation closest to the date of observation.

A summary of the NACO observations is provided in Table 3.4.

3.2.2 Northern Targets: Lick data

To observe the 40 northern targets in our sample, we used the adaptive optics facility at the Lick Observatory Shane 3 m telescope (Gavel et al., 2002) between 14–18 July 2008 and 8–9 July 2009.

In 2008 the conditions were relatively good, although not photometric, with an average seeing between $0.8''$ and $1.1''$ in the visible, at the zenith. The targets were all bright enough to be used as a reference for the wave-front sensor. All of the targets were observed using the K_s filter, which provides the best compromise between the AO performances and the sensitivity to faint and red companions.

TABLE 3.3: Detector plate scales ($s \pm \sigma_s$) and true north orientations ($t \pm \sigma_t$)

Obs. date	Plate scale (mas / pix)	True north[a] (deg)	Target
		NACO	
24/04/2006	27.01±0.05	-0.08±0.14	θ^1 Ori C
26/08/2006	27.02±0.05	-0.12±0.20	θ^1 Ori C
06/04/2008	27.01±0.05	-0.36±0.14	θ^1 Ori C
10/06/2008	27.01±0.05	-0.39±0.15	IDS 2150, θ^1 Ori C
15/11/2011	13.27±0.05	-0.47±0.14	θ^1 Ori C
04/07/2012	13.27±0.05	-0.78±0.20	IDS 22141
		Lick	
15/07/2008	75.7±0.1	+1.80±0.30	HIP 66225
09/07/2009	75.7±0.2	-0.30±0.20	HIP 66225

Notes. [(a)] This value is subtracted from the measured position angle (PA).

When a clear companion was detected in the images, an additional H band (and sometimes J band) image was acquired to provide colour information. All observations were performed using a dither pattern to efficiently remove cosmic rays, bad pixels and accurately compute the sky. The data were processed using *Eclipse*, including dark subtraction, flat-field correction, sky subtraction, frame registration, and stacking. A Hipparcos binary (HIP 66225, Gontcharov, 2006) was observed every night to be used as an astrometric calibrator and derive an accurate plate scale and plate position angle on the sky (see Table 3.3).

The 2009 observations aimed at obtaining second epoch images of the 21 targets with companion candidates detected in the first epoch images. Conditions were poorer, with a seeing of $\approx 1.5''$ and some cirrus. As we were most interested in deriving accurate astrometry, the observations were performed in a single band (using the K_s filter). The same observing strategy (five point dither pattern) and processing steps were applied. The same astrometric reference was used to calibrate the plate scale and position angle of the camera (see Table 3.3).

A description of the Lick data used in this chapter is included in Table 3.4.

TABLE 3.4: A summary of all AO-imaging data used in this chapter. The number of observations refers to the number of reduced images as opposed to separate objects, i.e., an object can be counted twice if it was re-observed.

Instrument	FOV (arcsec)	Filter	λ_0 (μm)	$\Delta\lambda$ (μm)	No. of Obs.
NACO	14×14	K_s	2.18	0.35	91
	28×28	K_s	2.18	0.35	53
	28×28	IB 2.27	2.27	0.06	82
	28×28	IB 2.21	2.21	0.06	11
	28×28	NB 2.17	2.17	0.02	12
Lick	20×20	K_s	2.15	0.32	70
	20×20	H	1.66	0.30	14
	20×20	J	1.24	0.27	2

3.2.3 Archival data and literature search

We queried the ESO archive for related NACO data for objects that were observed only once in our service campaigns. This way, we could utilise a second epoch to determine if the detected companion candidates are co-moving. In total 64 objects had multi-epoch observations. In addition to this, we queried the CDS for object-type determinations and multiplicity flags for all 201 targets studied in this chapter, (see Table 3.6). For objects previously identified as multiple systems, we checked whether the companions' properties were within the parameter space of our observations, which in turn, tests the completeness of our work. As a result, we did not find any previously identified systems in this parameter space which we failed to detect.

3.2.4 Observational detection limits

Figure 3.1 shows the average contrast in the selected filters as a function of the angular separation from the primary star for both the NACO (using the S13 and S27 objectives) and Lick data. On average, we reach $\Delta K_s = 7$ mag and $\Delta K_s = 4$ mag at an angular separation of $0.5''$, for the NACO and Lick data, respectively. For an age of 30 Myr (the average age of the SACY associations) and a primary mass of $1.0\,M_\odot$, these

differences in magnitude correspond to masses of $\sim$15 M_{Jup} and $\sim$0.10 $M_{\odot}$ (dashed lines in Figure 3.1), using the evolutionary tracks from Baraffe et al. (1998).

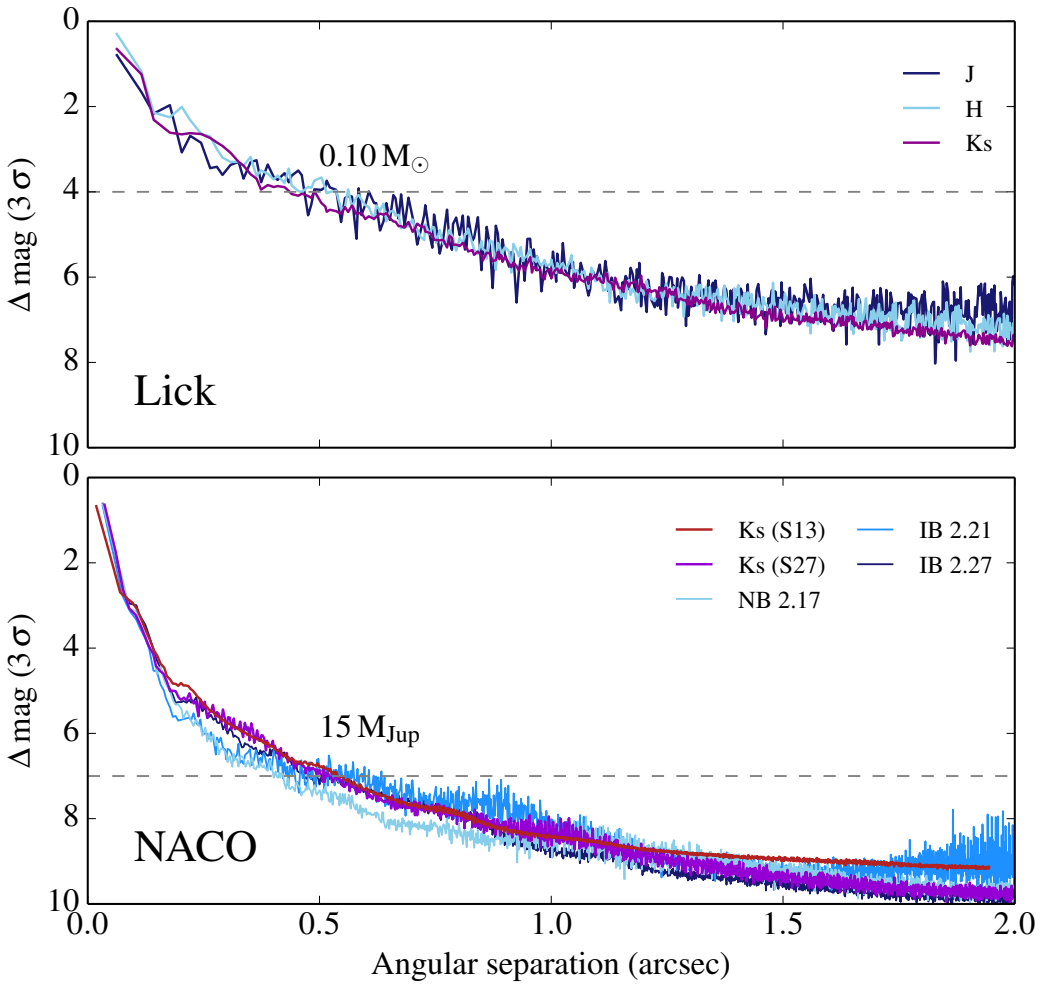

FIGURE 3.1: The average sensitivity limit in all filters for both NACO and Lick data. The limits were computed from the 3σ root-mean squared (RMS) of the PSF radial profile for each target, and then averaged within each filter. The K_s filter for the NACO data is displayed for the S13 and S27 objective. The dashed lines represent our mass limits at 0.″5, according to Baraffe et al. (1998) evolutionary tracks, assuming an average age of 30 Myr and a primary mass of 1 $M_{\odot}$.

3.3 Identifying multiple systems

In order to identify multiple systems in our sample, we first identified all the point sources within the FoV of each target. Then, we determined the astrometry and photometry of these sources, and used these parameters to determine whether the identified point sources are bound companions or background objects. We provide all the details in the next subsections.

3.3.1 Initial source detection

Combining the NACO data and Lick data, we have imaged a total of 201 targets. In order to identify companions in our images, we first need to identify all possible point sources in the FoV. We used the source extraction software SExtractor (Bertin and Arnouts, 1996) to perform the source identification. Only detections of sources with 5 or more pixels with values $\geq 3\sigma$ were considered (where σ is the standard deviation of the background signal).

We visually checked each image to (i) confirm whether the detection was from a true point source as opposed to, for example, an optical ghost and (ii) search for potential severely blended binaries (with component separations $\sim$4 pixel) that had been detected as one source. With the catalogues of point sources for each observation we then modelled the PSFs using the software PSFEx in conjunction with SExtractor. For the majority of observations, the primary targets were used to model the PSF. In the case that the primary target was resolved into a close binary, either further components in the FOV (as close to the centre of the image as possible) were used, or another bright target observed during the same night with the same instrumental setup and as close in time as possible. Figure 3.2 shows a typical example of a blended object originally detected as a single source. The centre and the photometric aperture as derived by SExtractor are represented by the black circle and black ellipse, respectively. Through the modelling of the PSF we were able to extract the astrometry

and photometry for the two components, whose centres and FWHMs are shown by the red crosses and dashed circles, respectively.

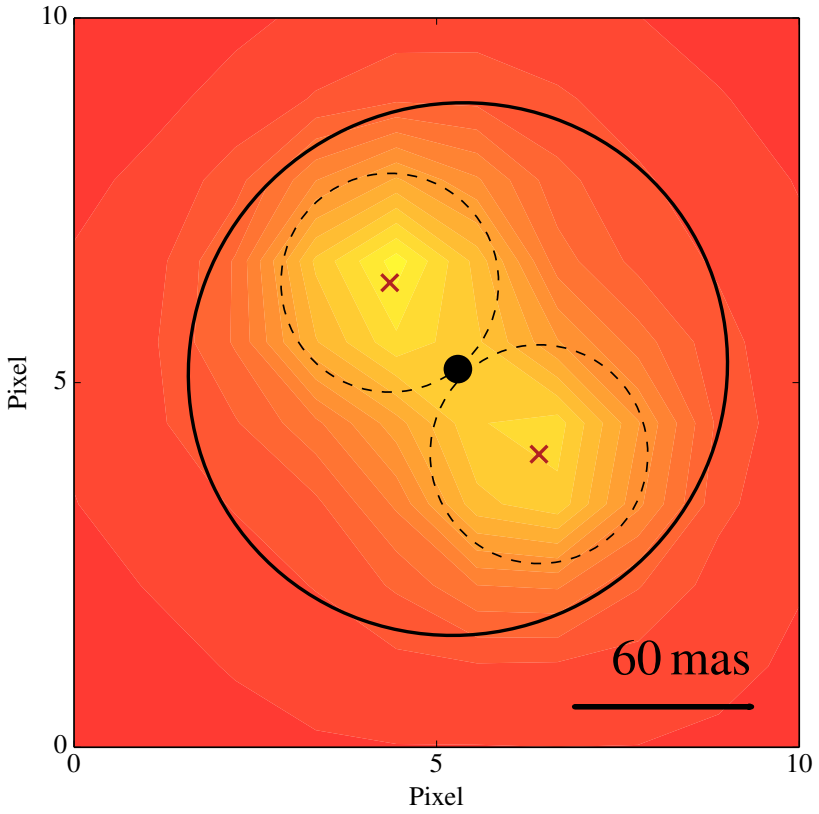

FIGURE 3.2: A section of the NACO image for target CD-30 3394B, showing two partially resolved components. The black solid-lined ellipse is the aperature applied by SEXTRACTOR and the black filled circle the centre of the ellipse. The red crosses and black dashed circles indicate the centre and FWHM of the model PSF extracted from the primary CD-30 3394A, using PSFEX for each source.

3.3.2 Relative photometry

Our observations did not include photometric calibrator fields and, therefore, we can only perform relative photometry in our images. However, the vast majority of our targets were imaged in the K_s band, so we can make use of the available 2MASS K_s values (Skrutskie et al., 2006). In the cases where we discovered multiple components within the original PSF of 2MASS, we weighted the magnitudes according to the flux ratios of the components. These values are provided in the fifth column of Table 3.1,

as K(M_1), and have been used to compute the mass ratio of the multiple systems using evolutionary tracks (Baraffe et al., 1998), and the age estimation from Table 3.2.

3.3.3 Relative astrometry

For every point source detected in each observation, we calculated the angular separation from the primary in detector coordinates and then applied the appropriate pixel scale and true north correction value (Table 3.3). In the case of non-blended sources, we have used the parameters from the aperture extraction, while for severely blended sources we have used the ones coming from PSF modelling. We have performed both types of extractions (aperture and PSF) on a small number of targets and confirmed that, for non-blended sources, the resultant photometry and astrometry is consistent within the uncertainties. We then employed a different method to determine whether the detected point sources are bound companions or not, depending on the availability of multiple epochs.

3.3.3.1 Uncertainties

The main source of uncertainty comes from the temporal and spatial variability of the atmospheric conditions. The uncertainties for the angular separation, $\rho(x, y) \pm \sigma_\rho$, and position angle, $\theta(x, y) \pm \sigma_\theta$, were derived using equations 3.1 and 3.2, using the appropriate plate-scale and true north correction values. Table J1 lists the parameters and their uncertainties of the multiple systems identified for each observation.

$$\sigma_\rho = \left[\left(\frac{\partial \rho}{\partial x} \sigma_x \right)^2 + \left(\frac{\partial \rho}{\partial y} \sigma_y \right)^2 \right]^{\frac{1}{2}} \tag{3.1}$$

where $\sigma_x = x\,\sigma_s$, $\sigma_y = y\,\sigma_s$ and σ_s is the uncertainty in the plate scale.

$$\sigma_\theta = \left[\left(\frac{\partial \theta}{\partial x} \sigma_x \right)^2 + \left(\frac{\partial \theta}{\partial y} \sigma_y \right)^2 + \sigma_t^2 \right]^{\frac{1}{2}} \tag{3.2}$$

where σ_t is the uncertainty in the true north correction.

3.3.3.2 Multi-epoch data

To assess whether a pair of point sources are bound, and not a projection effect, we computed their relative motion and compared it to the motion one would expect for a background object. The PM values were taken from UCAC4 (Zacharias et al., 2012). We then combined this with the parallactic motion, and produced the total relative motion one would expect to see if the point source were a background, stationary object (see Chauvin et al., 2005). An example is shown in Figure 3.3. We would expect a bound companion to show negligible movement with respect to the primary between our multi-epoch observations, and this is our criterion for binary identification. In those cases in which the PM of the source did not produce significant motion, given the time difference between observations, we used the criterion described in Section 3.3.3.3.

3.3.3.3 Single-epoch data

For those targets with only one epoch of data (NACO data using S13 camera) we could use their properties, to provide statistical constraints on how likely is the source to be bound. One way to do that is to estimate the potential contamination from background sources given the target's galactic co-ordinates, and the limiting magnitude of the observations. However, galactic models such as Robin et al. (2003) have a limited resolution and, given our small FOV ($13'' \times 13''$), this method only provides a very rough estimate of the level of contamination. To avoid this limitation we decided to use our available multi-epoch data to assist in the classification of our single-epoch data.

We classified our own multi-epoch detections as either bound companions or background sources from PM analysis, see Section 3.3.3.2. We then used two additional sources of data. Firstly, Wahhaj et al. (2013), a high-contrast direct imaging survey for giant planets. We converted the H-band photometry into mass-ratios using the evolutionary tracks of Baraffe et al. (2003) and the ages quoted in the work. Secondly, we

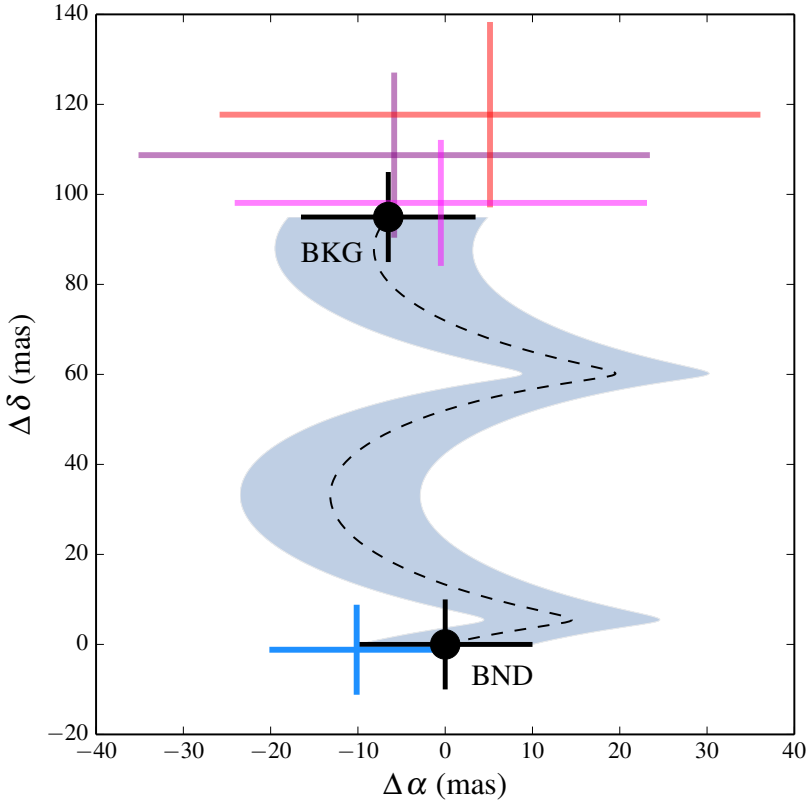

FIGURE 3.3: The relative movement of four point sources, in RA and DEC, for two observations of GSC 08350-01924. The black dotted line and black markers represent the motion one would expect from a background (BKG) source with respect to the primary, and the shaded area represents the error space. The dark blue marker represents a source showing no significant relative motion, consistent with a bound (BND) companion at 0.3″. The other coloured markers represent three background sources detected at separations of 10.5, 13.2 and 14.2″ from the primary.

used the data from Daemgen et al. (2015), a multiplicity survey in Taurus conducted in K_s-band. From these two works, we only used sources classified by PM analysis (in total, 246 classified sources).

We then pseudo-randomly split this classified data: 2/3 as a training set, 1/3 a test set. Using support vector machines (SVM)[2], we determined the optimum soft-boundary in the physical separation-mass-ratio space that splits bound and background sources. On average, we reached a completeness and contamination rate of $>$80% and $<$10% respectively, when classifying our test set. With this classifier we then calculated the probability that our single-epoch sources are bound ($P_{\rm BND}$) or background ($P_{\rm BKG}$). In

[2]see Chapter 9 of Ivezić et al. (2014) for many applications of this technique in classification of astronomical objects such as differentiating variable and non-variable MS-stars using photometric colours.

this instance, there are only two labels: either bound or background and as a result, $P_{\text{BND}} = 1 - P_{\text{BKG}}$. We repeated this procedure 1000 times and took the median result to account for the variations induced by different training and test datasets. The individual probabilities (P_{BND}) of these companion candidates with their respective properties are shown in Table 3.5.

To test whether this technique produces realistic probabilities, we calculated the bound probabilities for the 35 companions already confirmed by PM analysis. The median bound probability was ≈99%.

Figure 3.4 shows the graphical result of this procedure. There is a clear trend towards high mass-ratio, closely-separated sources being bound (as one would expect), very few bound sources lie in the parameter space mainly populated by background sources.

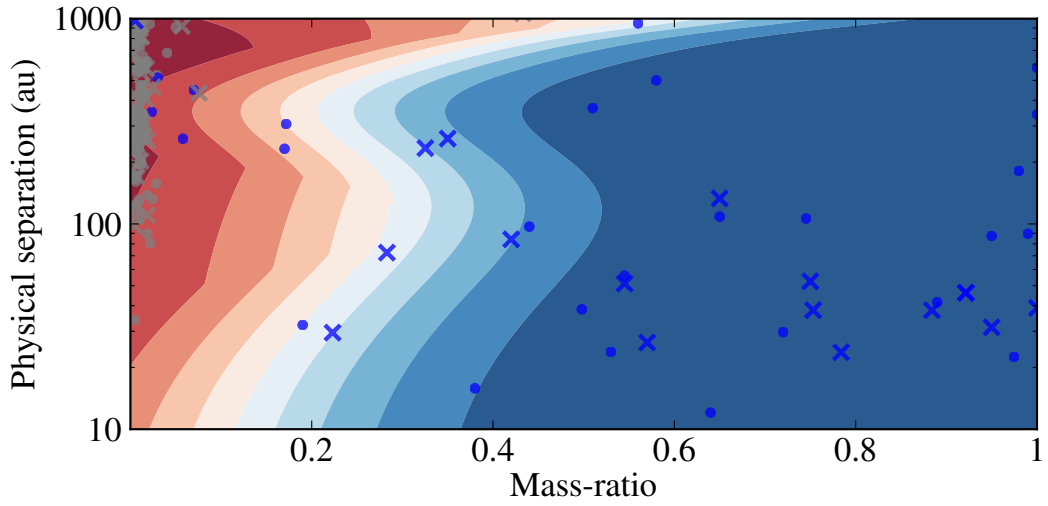

FIGURE 3.4: The probability of identifying a bound system from 100–0% in intervals of 10% from blue to red in physical separation–mass-ratio parameter space. The circles and crosses represent the training and test set, respectively. Blue markers represent bound companions, and grey markers unbound companions.

3.4 Results

We have identified 31 potential multiple systems (28 binaries and 3 triples) from 113 confirmed SACY targets. Of these 31 systems, 7 have been confirmed by PM analysis and 24 have a bound-probability $\geq$95%[3] (see Section 3.3.3.3). A summary of the physical properties of the multiple systems is included in Table 3.5.

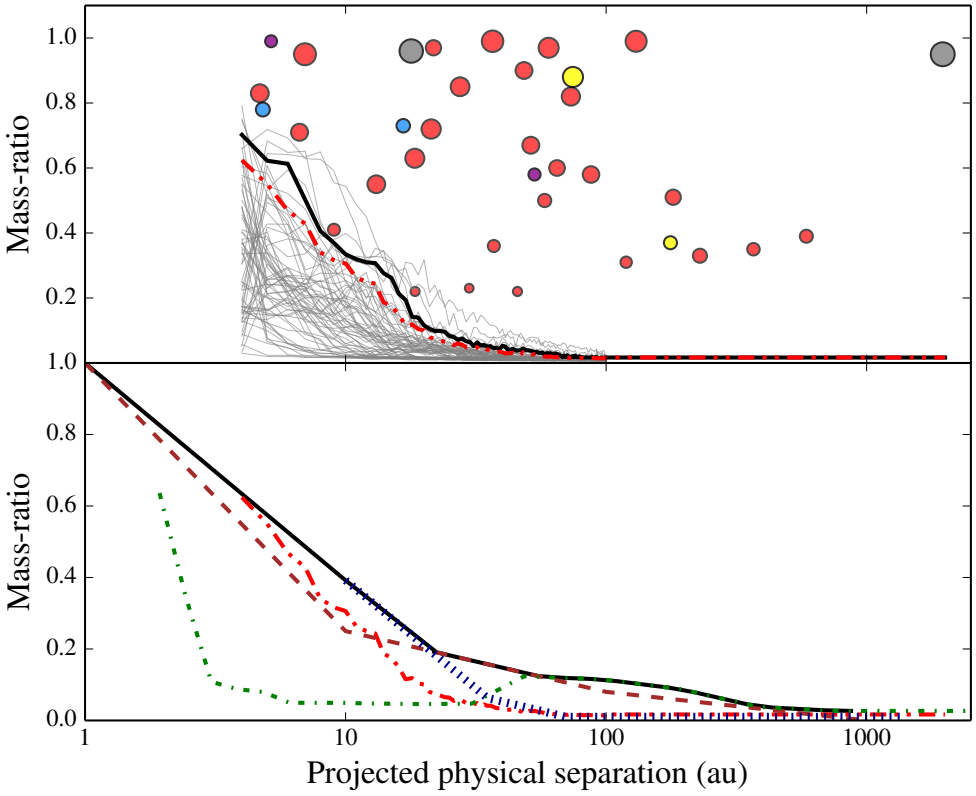

FIGURE 3.5: *Top panel:* The physical projected separations versus mass-ratio for identified multiple systems. The filled red markers represent binary companions, the other coloured markers are components of triple systems with matching colours for the secondary and tertiary. The size of the marker is proportional the companion's mass. The grey lines represent the sensitivity limits for the individual targets. The red and black lines represent the 90% and 95% detections limits for the whole sample, respectively. *Bottom Panel:* The 95% detection limits for four studies, red: this work, blue: Daemgen et al. (2015), green: Kraus et al. (2011) and brown: Raghavan et al. (2010), used for analysis in Section 3.5.

[3]Based on this statistical analysis there is a 57% probability that all 24 systems are bound from the product sum of their respective probabilities.

We have followed the multiple component designations described in Tokovinin (2005), where systems are described by individual components and *super* components. For example, a triple system composed of a binary system orbiting the primary (brightest) star would have the following designations: ”A, B, *” and ”Ba, Bb, B” following increasing hierarchy. In such cases, there are two entries in Table 3.5, one to describe ”A, Ba” and the other ”Ba, Bb”.

The analysis presented in the following subsections considers the 31 identified multiple systems from 8 SACY associations (outlined in Table 3.2). We note that have also identified 28 multiple systems in the sample of non-SACY members. A summary of these systems' properties can be found in Table 3.7.

We have defined two ranges of physical separations in our analysis, derived from the sample sensitivities displayed in Figure 3.5. The first, 3-1000 au, is the most extensive, considering 109 from the 113 observed targets, and including all the 34 companion detections (28 binaries and 3 triples). We define another as 10-1000 au, that will allow us to compare our results with other studies. For this parameter space, we again consider 109 observed targets but only 27 companions detections (25 binaries and 1 triple).

3.4.1 Multiplicity frequencies

In this chapter we consider the following quantities: multiplicity frequency (*MF*), companion star frequency (*CSF*) and triple frequency (*TF*) – the number of triple systems in the population.

We have identified 31 multiple systems from observations of 113 confirmed SACY targets. Therefore, we estimate a raw multiplicity frequency ($MF_{\rm raw}$) of $27.4^{+4.5}_{-3.8}$%, and a raw companion star frequency ($CSF_{\rm raw}$) of $30.1^{+4.6}_{-3.9}$%. However, as mentioned previously, these frequencies include companions that would not be detected around all of the targets due to different contrasts and distances (see Figure 3.5). When we remove

these targets, we derive a multiplicity frequency of $MF_{3-1000\,au}$=28.4$^{+4.7}_{-3.9}$% in the separation range 3-1000 au. All of our companion detections are above 95% sensitivity curve and therefore we do not disregard any of them in our calculation.

3.4.1.1 Higher-order multiple systems

Considering the higher-order systems separately (3 triple systems) we derive a triple frequency of $TF_{3-1000\,au}$=2.8$^{+2.5}_{-0.8}$% in the separation range of 3-1000 au. It is interesting to note that 2 of the 3 triple systems identified in this work have secondary components at very small separations (4.8 and 5.2 au), that are only detectable due to the proximity of the systems (31 and 17 pc).

3.4.1.2 Multiplicity frequency and primary mass

We analysed the effect of the primary mass on the multiplicity frequency within our sample for the 109 systems in the separation range 3-1000 au. We binned our data according to the Freedman-Diaconis rule, which is suited for non-Gaussian distributions (bin width$\approx$0.1 $M_\odot$). The results are shown in Figure 3.6. The large uncertainties for masses of 0.25, 0.35 and 0.45 $M_\odot$ are a result of the low-number fractions, 0/1, 0/1 and 1/1, respectively.

3.4.2 Mass-ratios

We calculated the mass-ratios (q) of our multiple systems in two ways, to test the effect of using primary mass values derived with different methods. We note that, in the case of triple systems composed of a primary component A and an outer orbiting binary (Ba, Bb), the mass-ratio of the component Ba is derived as be M_{Ba}/M_A:

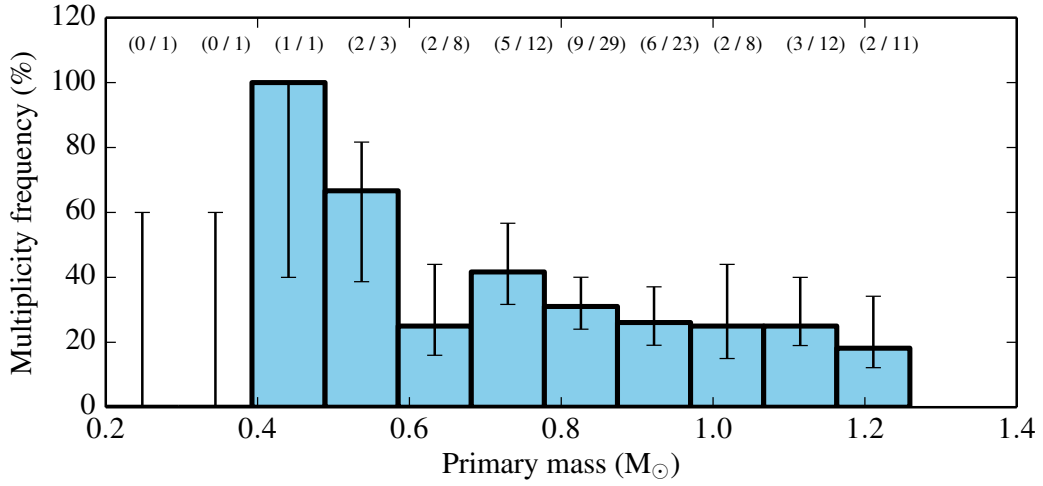

FIGURE 3.6: Primary mass versus multiplicity frequency for systems in the separation range 3-1000 au. The data is binned according to the Freedman-Diaconis rule. The fractions are shown by each mass bin.

(i) We derived primary mass values (M_1) from absolute magnitudes using kinematic distances (D) and ages with the evolutionary tracks of Baraffe et al. (1998). We then calculated the companion masses from ΔK values and computed the mass-ratios (the normalised cumulative distribution function (CDF) is shown by the red line in Figure 3.7).

(ii) We used the ΔK values of our components for a range of K_1 values, which is equivalent to a range of model-based M_1 values for the given age of the system (0.8-1.2 $M_\odot$, according to the evolutionary tracks of Baraffe et al., 1998). To obtain the uncertainty, we calculated the standard deviation of the mass-ratio as a function of the primary mass for a given system. We then computed 100 mass-ratio distributions composed of pseudo-random realisations of each mass-ratio value and its uncertainty. We binned the data in 0.01 steps and took the average and standard deviation producing a smoothed, normalised CDF, shown by the black dots and shaded areas (dark and light: 1σ and 3σ) of Figure 3.7, respectively.

The values and uncertainties used in further analysis (shown in Table 3.5) are obtained using method (ii) in order provide realistic uncertainties given that, at this time, the masses are model-based.

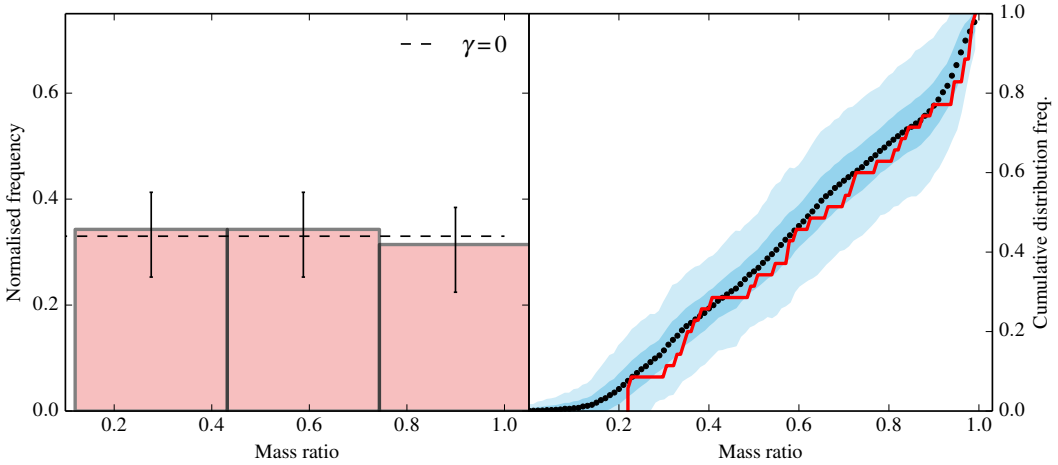

FIGURE 3.7: *Left panel*: Normalised frequency of mass-ratios. The dashed line represents a power-law function with index $\gamma = 0$. *Right panel:* The cumulative frequency distribution of mass-ratios using the two methods outlined in Section 3.4.2. Method (i) The red line represent the derived mass ratios. Method (ii) The black dots, dark and light blue-coloured area represent the average, 1 σ and 3 σ variation in frequency from 100 realisations of the mass ratio, respectively.

The mass distribution is usually described using a power law index, γ. We derive a value of $\gamma = -0.04 \pm 0.14$ using linear regression of 1000 pseudo-random realisations of the mass-ratio distribution considering their respective uncertainties.

3.4.3 Physical separations

We calculated the physical separations of the multiple systems using the kinematic distances shown in Table 3.1, and the average angular separation from our observations. The top panel of Figure 3.5 shows the physical separation versus mass-ratio for the 31 SACY multiple systems, considering both multiple-epoch and single-epoch observations with probabilities $\geq$95%). The size of the markers represents the companion's mass. In addition to this, the detection limits are shown for each multiple system (grey lines) and 90% and 95% detection limits for the entire observed sample in red and black, respectively. This calculation demonstrates the powerful nature of the SACY dataset when observed with AO-imaging: we can probe very small physical projected separations across our sample down to low mass-ratios.

In addition to this, we generated separation distributions in two ranges. Firstly, 10-1000 au, for SACY, Taurus (Kraus et al., 2011; Daemgen et al., 2015) and the field (Raghavan et al., 2010), see Figure 3.8. Secondly, 19-100 au, for SACY, Taurus (only Kraus et al., 2011) and the field (see Figure 3.9). The first separation range was chosen to maximise the number of comparable systems due to different observational techniques. The second, to make the same comparison that was made in King et al. (2012a).

First of all, we created 90% sensitivity curves for each study in terms of mass-ratio and physical separation (shown by the coloured lines in the bottom panel of Figure 3.5), using the available published data. In the case of Raghavan et al. (2010), we used the sensitivity curve from Figure 11 of that paper. Then, we defined the master sensitivity curve as the upper boundary of all the individual curves (shown by the black solid line in the bottom panel of Figure 3.5). We then only consider systems with parameters above this curve.

To perform this analysis we used kernel density estimations (KDEs), see Scott (2009) for details. This technique minimises features induced by bin phase. The results for the two separation ranges are shown in the left panels of Figures 3.8 and 3.9. The plots shows the KDE from SACY in red, Taurus in blue and green, and the field in gold with 95% confidence intervals (CIs) shown by the respective-coloured shaded areas. The CIs were calculated by considering the distribution of densities for each physical separation from 10^5 bootstrap iterations of the KDE. To see the differences between the distributions more clearly we have plotted them in the form of cumulative frequency distributions (CDFs) in the right panels of Figures 3.8 and 3.9.

The low-density nature of Taurus makes it very interesting to compare to our associations, as they most likely formed in a low-density environment too. We use both the work of Kraus et al. (2011) and Daemgen et al. (2015) since both samples are complementary. The statistical sample defined in Daemgen et al. (2015) consists of 10 members from the extended Taurus region ($\sim$20 Myr) and 5 from the young Taurus region ($\sim$2 Myr), totalling 15 multiple systems. That of Kraus et al. (2011) only considers

the young region and in our defined parameter space, this produces a sample of 50 multiple systems for comparison.

The field represents a far more processed population of stars from a range of initial environments and, therefore, provides a mixed sample of evolved multiple systems. The number of comparable systems in the field within our defined parameter range is 123.

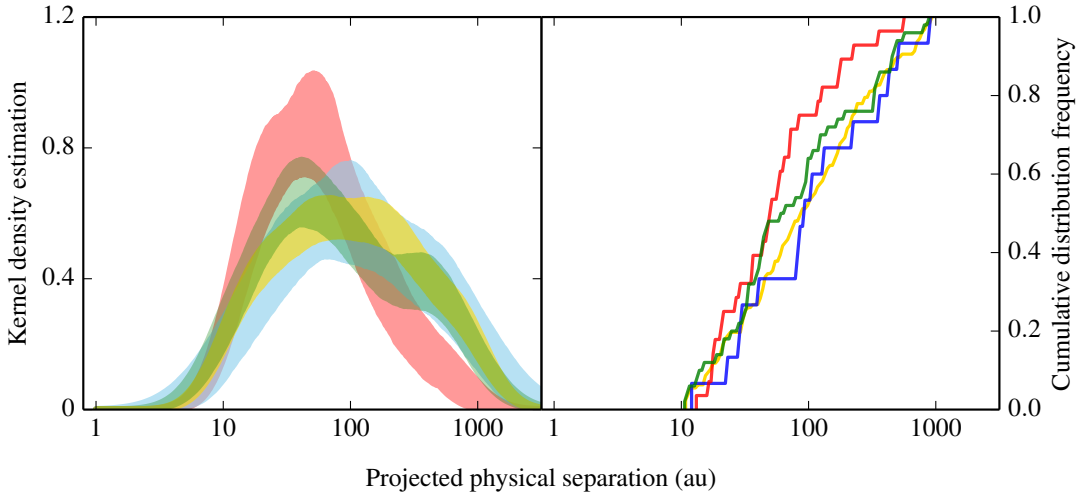

FIGURE 3.8: *Left:* Red, green, blue and gold shaded areas represent the 68% confidence intervals for the kernel density estimation (KDE) for SACY, Taurus (Kraus et al., 2011), Taurus (Daemgen et al., 2015) and the field (Raghavan et al., 2010) respectively. The multiple systems considered are all above the master sensitivity curve defined in the bottom panel of Figure 3.5 and in the separation range 10-1000 au. *Right:* The cumulative distribution frequencies for the same systems.

Firstly, we tested the effect of primary mass on the separation distribution as the studies we are considering probe slightly different primary mass ranges.

We performed a set of simulations using 10,000 synthetic binaries with primary masses between 0.2-1.4 $M_{\odot}$. We performed two sets of simulations which differed by their mass-ratio distribution. In the first case, we considered the mass-ratio distribution as uniform across all primary masses. In the second simulation we adopt the information from Figure 5 of Kraus et al. (2011) as priors. In the range M_1: 0.7-1.4 $M_{\odot}$ the mass-ratio distribution as uniform. For the range M_1: 0.2-0.7 $M_{\odot}$ there is a preference for more equal mass-ratio systems for lower primary masses. We created a probability function

for the secondary masses, and pseudo-randomly chose mass-ratio values from this distribution.

The period values were drawn from the log-normal distribution defined in Raghavan et al. (2010), μ=5.03 and σ=2.28 log (day). We then fitted the separation distributions with log-normal distribution and evaluated their parameters. When comparing the two sets of simulations, we see that the peaks of the separation distributions are shifted to smaller separations for the lightest primary masses: mean values of 30 au in the first case, and 60 au in the second case. However, this difference is not significant given the separation range we are considering (10-1000 au) There is also no significant difference resulting from the mass-ratio distributions.

Based on this result, we have compared separations distributions of field stars in the mass range of 0.7-1.4 $M_\odot$, and SACY objects in the mass range of 0.2-1.2 $M_\odot$.

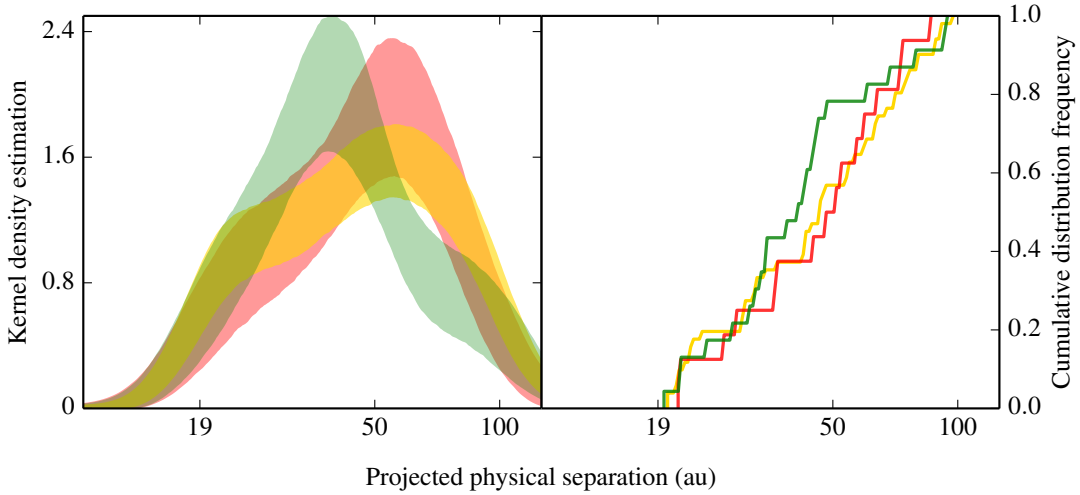

FIGURE 3.9: *Left:* Red, green and gold shaded areas represent the 68% confidence intervals for the kernel density estimation (KDE) of multiple systems for SACY, Taurus (Kraus et al., 2011) and the field(Raghavan et al., 2010), respectively. The multiple systems considered are all above the master sensitivity curve defined in the bottom panel of Figure 3.5 and in the separation range 19-100 au. *Right:* The cumulative distribution frequencies for the same systems.

Our comparison between the three populations is shown in Figure 3.8. The shape of the SACY distribution differs from those of the other populations at a 1 σ level (68% CIs are represented by the coloured filled areas in left panel of Figure 3.8). The distribution

departs in form from the other populations at ≈50-100 au. Potentially, this departure for wider systems is the result of a bias in the way we classify our objects as bound, favouring close-in systems, using the method described in Section 3.3.3.3. However, to check this, we included companions regardless of their probabilities and the resultant distribution still differed from the other populations at a 1 σ level for the widest systems.

3.5 Discussion

The SACY sample offers a unique opportunity to study multiplicity among young stars down to very small physical separations. Currently, it is not known whether all these associations shared a common origin, due to limitations on the accuracy of their galactic motion[4]. Whether these associations share a common origin or not, it is likely that these groups resulted from *sparse* star formation whereby ∼100 stars were formed in each group. Therefore, by studying these targets we are obtaining crucial information regarding this mode of star formation. In this analysis we present the results assuming a common formation mechanism, i.e. grouping the data together in some cases from all associations and looking for relationships in physical parameters (i.e. primary mass, physical separation).

3.5.1 Frequency of multiple systems

The triple frequency is $TF_{3-1000\,\mathrm{au}}=2.8^{+2.5}_{-0.8}$% in the separation range 3-1000 au. If we consider the range 10-1000 au, we derive the value $TF_{10-1000\,\mathrm{au}}=0.9^{+2.0}_{-0.3}$%. The value from Daemgen et al. (2015) in Taurus, $TF_{10-1000\,\mathrm{au}}=1.8^{+4.2}_{-1.5}$%, is comparable within the uncertainties.

The multiplicity frequency for SACY is $MF_{3-1000\,\mathrm{au}}=28.4^{+4.7}_{-3.9}$% in the separation range 3-1000 au across the primary mass range 0.2-1.2 $M_{\odot}$. To compare to the work of Daemgen et al. (2015) in the Taurus SFR, we consider the separation range 10-1000 au and

[4]The GAIA mission (Lindegren et al., 2008) will provide extremely precise astrometry for members of such associations, with expected accuracies of 7-25 μas.

derive a multiplicity frequency of $MF_{10-1000\,\mathrm{au}}$=25.7$^{+4.8}_{-3.7}$%. The multiplicity frequency for Taurus in that parameter space is $MF_{10-1000\,\mathrm{au}}$=26.3$^{+6.6}_{-4.9}$%, so the two values agree very well within the uncertainties. However, if we limit the primary mass of our targets the result is slightly different, as discussed below.

As shown by King et al. (2012b,a), collating studies from Taurus, ρ-Ophiuchus, Chamaeleon I, IC 348 and the ONC, and additionally the work of Kraus et al. (2011); Daemgen et al. (2015) studying Taurus, the multiplicity frequency of Taurus is marginally higher ($\approx$1 σ) than that of other SFRs. In order to make a comparison between Taurus (Daemgen et al., 2015), SACY and the field (Raghavan et al., 2010) we have selected targets in the separation range 10-1000 au and the primary mass range $\geq$0.7 $\mathrm{M}_{\odot}$. In the case of SACY the primary mass range is 0.7-1.2 $\mathrm{M}_{\odot}$ for Taurus and for the field it is 0.7-1.4 $\mathrm{M}_{\odot}$. The resultant multiplicity frequencies ($MF_{10-1000\,\mathrm{au},\,\mathrm{M}_1\geq0.7}$) are shown in the bottom panel of Figure 3.10. The result of SACY (23.2$^{+4.8}_{-3.7}$%) agrees with the field (28.9$^{+3.0}_{-2.9}$%) and marginally disagrees with Taurus (37.9$^{+9.5}_{-7.9}$%) at $\approx$1 σ level. Based on these results, within this range, there is marginal evidence that the Taurus region has a higher frequency of multiple systems than SACY and the field. However, when considering systems across a much wider separation range it appears that, at least in the case of the β-Pic moving group, that the young associations have a higher frequency of multiple systems, see Chapter 5.

Kroupa and Bouvier (2003) showed how environments such as Taurus are insufficient at binary disruption and, therefore, their high *MF* values are due to their binary populations being more pristine than that of heavily processed populations. We would therefore expect, assuming similar primordial multiple system distributions, to see the same effect in the young associations. The analysis presented in Chapter 5 supports this idea. As there is no disagreement between SACY and the field for the systems discussed in this chapter, assuming common primordial multiple distributions, it suggests that few multiple systems have been destroyed by dynamical processing in this range.

In contrast to the general trend of high multiplicity in low-density SFRs and associations, Brandeker et al. (2006) found an absence of multiple systems with separations

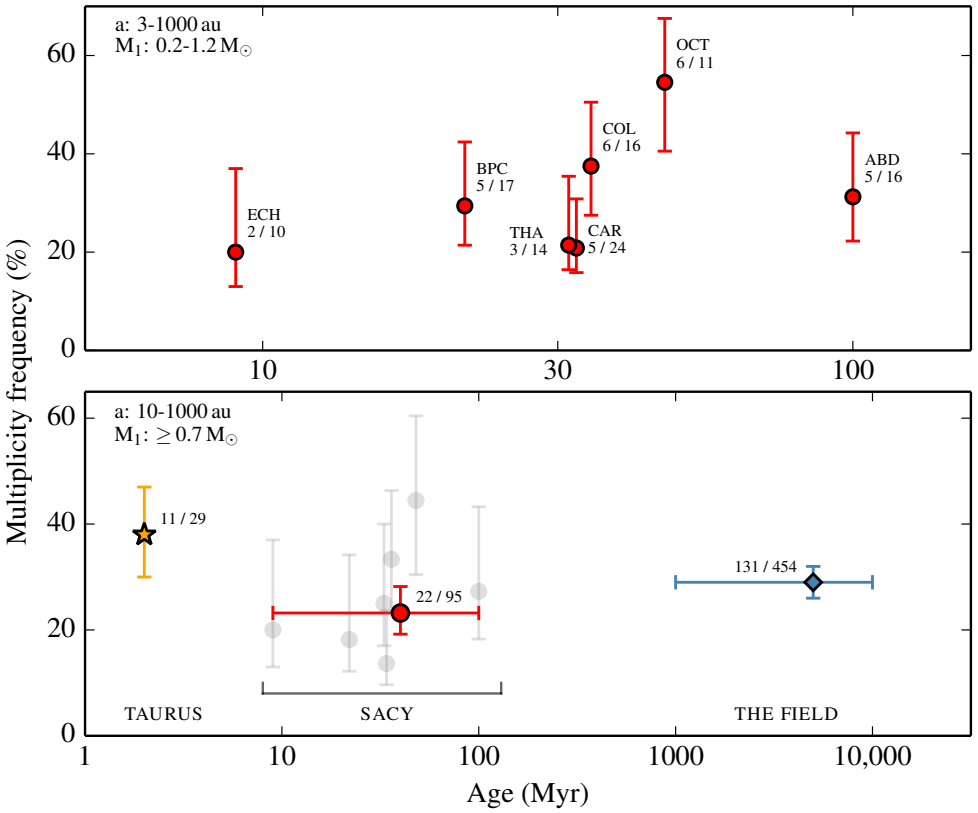

FIGURE 3.10: Age versus multiplicity frequency. *Top panel:* In the separation and primary mass range 3-1000 au and 0.2-1.2 $M_{\odot}$, respectively. *Bottom panel:* In the separation and primary mass range range 10-1000 au and 0.7-1.4 $M_{\odot}$, respectively. Data from (Daemgen et al., 2015, Taurus) and (Raghavan et al., 2010, the field) are shown by the star and diamond marker, respectively. Argus (ARG) has been omitted as only 1 object was observed.

$>$20 au in the young (6-8 Myr, Jilinski et al., 2005) cluster η Chamaeleontis. This survey of 17 targets used NACO observations similar to those presented in this chapter, probing similar targets and mass-ratio systems. They found a probability $<10^{-4}$ that η Chamaeleontis and TW-Hydrae share the same parent multiple system distribution. Although η Chamaeleontis is denser than the associations presented in this thesis, the authors conducted analysis to disregard dynamical processing as the cause of such a result, finding a collision time-scale 3000 times that of the cluster age. The frequency of spectroscopic systems (SBs) in η Chamaeleontis is statistically similar to that of the young associations (Riviere-Marichalar et al., 2015a), $\approx$10%. The physical separations of these SBs are so tight that they should be free of dynamical processing

and therefore similarities between regions support the idea of statistically similar binary populations. However, the discs in η Chamaeleontis are long-lived (Sicilia-Aguilar et al., 2009), considering its age, with respect to other young regions. Therefore, at this time, it is still not clear whether the differences in multiplicity frequency between this cluster and other low-density SFRs and associations, are the result of dynamical processing or stem from environment-dependent star formation.

However, since there is a general trend of high multiplicity frequency with low-density environments, it is likely that, at least in some part, it stems from the lack of dynamical processing compared to stars in populations such as the field (Lada and Lada, 2003).

3.5.1.1 What is the effect of the primary mass on the frequency?

It is common in many populations to observe an increase in multiplicity frequency with primary mass (see Figure 12 of Raghavan et al., 2010). We also noted the same relationship among the tightest multiple systems, i.e. spectroscopic binaries (Chapter 2). However, this is considering a very large mass range, from spectral types O-M. We have investigated whether this relationship is also observable within our sample of stars (primary mass range 0.2-1.2 $M_{\odot}$.)

Figure 3.6 shows the result of binning our data in terms of primary mass for the 109 targets with $\geq$95% sensitivity from Figure 3.5). There is no observed trend of increasing multiplicity frequency with primary mass. There is a slight disagreement between some mass bins ($\approx$1 σ) but only in the case of very low numbers ($\leq$ 3). The most reliable mass bins (with more than 10 objects) show no tendency of higher frequency with primary mass. This is in agreement with the results of Kraus et al. (2011) and Daemgen et al. (2015) within the same primary mass range.

3.5.2 The impact of a flat mass-ratio distribution

Duchêne and Kraus (2013) compiled observations and discussed how random pairing

from the IMF (Chabrier, 2003) does not agree with the derived observational mass-ratio distributions for primary masses of $\sim$1-10 $M_{\odot}$. The mass-ratio power-law index is a much steeper function of the mass for lower-mass primaries ($\leq 0.5\,M_{\odot}$).

The mass-ratio distribution derived for the SACY sub-sample in this chapter (power-law index γ=-0.04 ± 0.14), agrees with the compilation of observational results in Duchêne and Kraus (2013), in the primary mass range of $\approx$0.2-1.2 $M_{\odot}$ (see left panel of Figure 3.7). The derived γ values in this range are very close to 0, i.e. flat distributions. With these observations we are not sensitive to more extreme mass-ratio systems (smaller than 0.2) at close-separations. To investigate whether the power-law index continues to be flat in this primary mass range, we need to observe our sample with more sensitive techniques, such as extreme high-contrast imaging or sparse-aperture masking (Evans et al., 2012). Finding sub-stellar objects around newly identified members of the young moving groups is the subject of a proposal submitted to SPHERE/VLT in March 2016.

3.5.3 Is there dynamical evolution within the SACY sample?

Another great advantage of the SACY sample is the range of PMS ages that we can probe ($\sim$10-100 Myr). This allows us to search for any potential dynamical evolution within the sample on these time scales.

Figure 3.10 shows the multiplicity frequency for systems in the separation range 3-1000 au. If we consider the youngest and oldest associations, ϵ-Cha (ECH) and AB Dor (ABD), we do not see significant differences in the multiplicity frequency. Given the number of observations we have at this time, we are limited by low-number statistics. To investigate this further, we need to observe more systems in each association to build up larger samples. Given that there is only one association (Octans) that does not agree with the other seven, we assume a statistically similar primordial multiple system distribution for all associations. See Appendix B.4 for details on a proposal that was awarded time to double the number of objects in the Octans association with

NACO/VLT data. Observations are scheduled for execution between April and October 2016.

Although the parameters of such systems may evolve on a time-scale of 10-100 Myr (see below) it is very unlikely that the systems will be entirely destroyed. Most of the destruction of multiple systems occurs very early on, within a few crossing times of the clusters ($<$1 Myr, Parker et al., 2009) and, therefore, at the age of the associations studied here this process has long ended.

As mentioned above, we can also investigate the relationship between the projected physical separation and the age of the systems. Although the frequency of systems has not significantly evolved, it is possible that we can observe significant differences in the system parameters. To check this, we performed a KS test for three sets of ages: a) $<$30, b) 30-50, c) $>$50 Myr. The age groups were comprised of 7, 23, 6 companions, respectively. The KS test produced one significant result; the distributions of b) and c) are very unlikely to be resultant from two different parental distributions (KS statistic: 0.18, p-value: 0.99). This statistical similarity implies there is no significant dynamical evolution of the physical separations on this time-scale (30-100 Myr). Due to the insignificant results from the other KS tests we cannot discern whether or not the other age-grouped samples agree or not.

3.5.4 Comparing physical separation distributions

As discussed previously our current understanding of multiple system formation invokes two formation channels; (i) fragmentation of the collapsing proto-stellar core, systems $\geq$1000 au (Bodenheimer and Burkert, 2001) (ii) via gravitational instability and fragmentation of the proto-stellar accretion disc of the primary star, systems $\leq$100 au (Toomre, 1964). If one of these two formation channels is dominant, one would expect to see a relative over- or under-abundance of systems between the two separation ranges, assuming that within our age range there is no significant evolution of the physical separations (see Section 3.5.3).

Therefore, one interpretation of the over-abundance of multiple systems with separations $<$100 au, a total of 21 systems, compared to wider systems, a total of 8, is that formation channel (ii) is dominant for multiple systems in our sample. Although as mentioned previously the additional physical mechanisms such as dissipative interactions during the accretion phase may *blur* the scales of two modes of fragmentation by the T-Tauri phase.

Another interpretation is that the original density of the SACY associations was much higher than the present day density. This high-density environment would have dynamically processed many of the wider systems $>$100 au early-on and, therefore, would lead to an observed relative under-abundance in this separation range. However, this original density would have to be extremely high to account for such extreme processing. In addition to this, the *MF* value of SACY is large and similar to that of Taurus which is an indication that the binary population has not been heavily processed.

TABLE 3.5: A summary of the properties of multiple systems identified in this chapter.

ID	Sep. ($''$)	PA (deg)	Dist. (pc)	Phys. sep (au)	ΔK (mag.)	Comp.	Prob.[a]	Pop.	M_1 ($M_\odot$)	M_2 ($M_\odot$)	q	σ_q
GJ 4231	0.16	298.4	30.6	4.8	0.58	A, B	.99	ABD	0.5	0.39	0.78	0.2
GJ 4231	0.54	0.4	30.6	16.6	0.70	A, C	.99	ABD	0.5	0.36	0.73	0.2
TYC 91-82-1	0.74	110.4	87.6	64.8	1.67	A, B	.99	ABD	0.82	0.49	0.6	0.13
BD-03 4778	2.53	208.5	71.5	180.9	2.19	A, B	-	ABD	0.91	0.46	0.51	0.12
Wolf 1225	1.44	232.7	15.1	21.7	0.07	A, B	-	ABD	0.48	0.47	0.99	0.2
HD 217379	2.24	239.0	32.7	73.2	0.63	A, B	.99	ABD	0.81	0.67	0.82	0.18
HD 152555	3.79	58.0	46.8	177.4	3.89	A, B	.77	ABD	1.13	0.28	0.25	0.07
GJ 3322	1.36	149.5	37.8	51.4	0.78	A, B	.99	BPC	0.85	0.57	0.67	0.18
GSC 08350-01924	0.73	19.9	66.3	48.4	0.17	A, B	-	BPC	0.63	0.56	0.9	0.19
2MASS J05203182+0616115	0.42	235.0	71.0	29.8	2.19	A, B	.96	BPC	0.66	0.15	0.23	0.05
CD-27 11535	0.08	278.8	87.3	7.0	0.17	A, B	-	BPC	1.01	0.97	0.95	0.2
CD-26 13904	0.27	81.8	78.9	21.3	0.93	A, B	-	BPC	1.03	0.74	0.72	0.21
2MASS J09131689-5529032	0.14	128.7	131.7	18.4	1.48	A, B	.99	CAR	1.15	0.72	0.63	0.09
CD-57 1709	5.84	220.5	100.5	586.9	2.28	A, B	.96	CAR	0.87	0.34	0.39	0.15
2MASS J08371096-5518105	5.72	23.5	180.8	1034.2	3.79	A, B	.38	CAR	1.11	0.18	0.16	0.04
HD 22213	1.67	281.1	52.4	87.5	1.87	A, B	.99	CAR	0.94	0.54	0.58	0.14
BD-07 2388	0.11	328.6	42.6	4.7	0.62	A, B	.99	CAR	0.77	0.64	0.83	0.21
CPD-62 1293	0.13	344.9	69.4	9.0	1.62	A, B	.98	CAR	0.7	0.28	0.41	0.14
V* V1221 Tau	0.92	134.3	81.5	74.6	0.57	A, B	.99	COL	0.92	0.81	0.88	0.15
V* V1221 Tau	2.17	320.7	81.5	176.6	2.5	A, C	.96	COL	0.92	0.34	0.37	0.11
2MASS J08240598-6334024	0.17	288.2	118.6	20.7	3.141	A, B	.98	COL	1.2	0.34	0.29	0.05
2MASS J08240598-6334024	6.38	140.5	118.6	756.6	3.358	A, C	.29	COL	1.2	0.29	0.25	0.04
2MASS J04272050-4420393	0.43	179.9	86.2	37.1	2.15	A, B	.96	COL	0.81	0.29	0.36	0.15
2MASS J02303239-4342232	0.13	294.7	51.2	6.7	1.09	A, B	.99	COL	0.81	0.57	0.71	0.22
BD-16 351	0.34	311.4	80.9	27.5	0.66	A, B	.99	COL	0.83	0.71	0.85	0.2
CD-43 1395	0.26	324.6	141.0	36.7	0.02	A, B	.99	COL	0.93	0.92	0.99	0.16
HD 272836	1.52	358.2	78.5	119.4	2.492	A, B	.96	COL	0.84	0.26	0.31	0.13
HD 105923	1.96	145.1	116.9	229.1	2.81	A, B	-	ECH	1.2	0.39	0.33	0.02
2MASS J12202177-7407393	0.23	3.7	114.8	26.4	3.91	A, B	.48	ECH	1.07	0.08	0.07	0.02
TYC 9245-535-1	0.11	9.3	119.3	13.1	1.06	A, B	.99	ECH	1.14	0.63	0.55	0.1
CD-30 3394A	12.06	116.7	162.4	1958.5	0.5	A, Ba	.82	OCT	1.2	1.14	0.95	0.08
CD-30 3394A	0.11	43.2	162.4	17.9	0.18	Ba, Bb	.99	OCT	1.14	1.10	0.96	0.14
HD 274576	3.14	15.8	117.1	367.7	2.51	A, B	.95	OCT	0.89	0.31	0.35	0.12
2MASS J04302731-4248466	0.49	193.4	122.8	60.2	0.13	A, B	.99	OCT	0.82	0.8	0.97	0.2
BD-20 1111	4.01	301.0	129.7	520.1	3.56	A, Ba	.43	OCT	1.11	0.21	0.19	0.05
BD-20 1111[b]	0.07	340.0	129.7	9.1	0.46	Ba, Bb	.98	OCT	0.21	0.18	0.86	0.14
CD-47 1999	0.22	321.5	166.7	36.7	3.56	A, B	.81	OCT	1.2	0.3	0.25	0.04
2MASS J06033540-4911256	0.75	90.0	173.8	130.4	0.06	A, B	.99	OCT	0.89	0.88	0.99	0.18
BD-18 4452	3.18	190.7	16.7	53.1	0.81	A, B	-	OCT	0.51	0.29	0.58	0.13
BD-18 4452	0.31	349.4	16.7	5.2	0.01	Ba, Bb	-	OCT	0.29	0.28	0.99	0.2
TYC 8083-455-1	1.06	347.8	54.8	58.1	1.15	A, B	.98	THA	0.7	0.35	0.5	0.14
2MASS J05182904-3001321	0.69	76.5	66.2	45.7	2.48	A, B	.97	THA	0.76	0.17	0.22	0.07
CD-44 1173	0.42	83.4	44.0	18.5	2.44	A, B	.96	THA	0.75	0.17	0.22	0.07
HD 22705	2.71	89.2	43.3	117.3	3.39	A, B	.52	THA	1.04	0.22	0.21	0.06

Notes. [a] Probabilities are shown unless system was confirmed by co-moving proper motion analysis.[b] Ba, Bb has a probability $>$0.95, however, currently there is no information regarding its membership and is therefore not included in further analysis.

3.5.5 Universality of multiple systems

Using a compilation of multiplicity surveys, King et al. (2012a,b) claimed that binary (multiple system) formation is not the same everywhere, and that star formation is not a single universal process. This conclusion was partly based on the significant differences found in the CDF between young populations and field stars, in the separation range of 19-100 au. They claim that, in this particular separation range, these systems should not be dynamically processed and therefore their CDFs should be indistinguishable, independent of their age and initial environment. However, Marks et al. (2014) dispute many of the results and claims of King et al. (2012a). They argue that if different initial densities are considered for the analysed SFRs, then the resultant multiple system properties are compatible with a single universal star formation process. In fact, the separation range 19-100 au is potentially not pristine, and in the case of Taurus, the comparable pristine range is only $\approx$20-30 au.

For the sake of comparison, we have also produced a separation distribution in the range 19-100 au, comparing 16 SACY systems, 23 Taurus systems, and 48 field systems. The results are shown in Figure 3.9. We note that we excluded data from Daemgen et al. (2015), as in this separation range only seven systems were available for comparison.

We find that the SACY and field distributions are statistically indistinguishable within the CIs. We also performed a KS test which produced a p-value of 0.995, which is highly significant, this means it is very unlikely that the two distributions are realisations of different parent distributions. If the separation range of 19-100 au is considered a pristine range, this result is a strong indication that the stars born in the field and those born in associations form in a similar way.

In the case of Taurus, the distribution shows a different shape, and has a p-value of 0.30 and 0.24 when compared to SACY and the field, respectively. However, the p-values are not significant and therefore we cannot rule out that it is a realisation of the same parent distribution.

SACY and Taurus share many similar multiplicity properties (similar $MF_{10-1000\,\mathrm{au}}$ and $TF_{10-1000\,\mathrm{au}}$ values, a flat mass-ratio distribution).

However, their respective separation distributions differ in both in the 10-1000 au and the 19-100 au range and additionally their $MF_{10-1000\,\mathrm{au},\,M_1\geq 0.7}$ are marginally discrepant. If one population had been more heavily dynamically processed than the other, we would expect to see differences in both their *MF* values and their separation distributions. We do see tentative differences in both quantities, implying that Taurus has experienced less dynamical processing than the young associations.

From the analysis presented in this chapter, the significance of the differences between the populations is still low ($\approx 1\,\sigma$), and therefore further data and analysis is needed to clarify whether these differences are physical or merely an effect of low-number statistics. One way to approach this problem is to focus on imaging a large number of targets in a pristine separation range. However, calculating this pristine range can be problematic due to unknown initial densities. Once again, the recently launched ESA mission, GAIA, will put important constraints on the galactic velocities of members with accurate astrometry. This will provide much better constraints on the initial densities of such associations.

Another approach is to collect data across a wider range of physical separations to span as much parameter space as possible. This is the subject of the analysis presented in Chapter 5.

3.6 Conclusions

In this chapter we have presented multiplicity statistics of the SACY associations from AO-observations. We have derived multiplicity properties of our sample from observations of 113 targets in the mass range 0.2-1.2 $\mathrm{M}_{\odot}$. We compared these derived properties to other populations searching for statistical similarities and / or differences.

Our observed sample consisted of 201 targets: 113 confirmed SACY members and 88 targets belonging to other populations (both from the field and PMS regions). As discussed in Section 3.2, these 88 targets were not included in our analysis. The parameters from individual observations can be found in Table J1, and a summary of the identified multiple systems in Table 3.7.

From this analysis of the 113 confirmed SACY members our main conclusions can be summarised as follows:

1. We have identified 31 multiple systems (28 binaries, 3 triples) from observations of 113 targets.

2. Out of these 31 systems, 7 were identified from co-moving proper motion analysis, and 24 from contamination likelihood based on the component's parameters (with probabilities $\geq$0.95).

3. The multiplicity frequency and triple frequency for SACY, in the separation range 3-1000 au, are $MF_{3-1000\,\mathrm{au}}$=$28.4^{+4.7}_{-3.9}$% and $TF_{3-1000\,\mathrm{au}}$=$2.8^{+2.5}_{-0.8}$%, respectively.

4. In the separation range 10-1000 au and for primary masses $\geq$0.7 $M_\odot$ the multiplicity frequency ($MF_{10-1000\,\mathrm{au},\,M_1\geq0.7}$) of SACY ($23.2^{+4.8}_{-3.7}$%) is similar to the field ($28.9^{+3.0}_{-2,9}$%) and discrepant at a 1 σ level to Taurus ($37.9^{+9.5}_{-7.9}$%).

5. The multiplicity frequency is not a function of the primary mass, within the primary mass range of 0.2-1.2 $M_\odot$.

6. There is no evidence of dynamical destruction of multiple systems in the age range of 10-100 Myr.

7. There is evidence that the multiple systems' physical separations do not evolve significantly on the time-scale 30-100 Myr.

8. The mass-ratio distribution (power-law index γ=-0.04 ± 0.14) is compatible with a uniform distribution (γ=0).

9. The separation distribution of the young associations and the field are indistinguishable in the separation range 19-100 au, suggesting a similar formation mechanism (if we assume this separation range is free of dynamical processing).

3.7 Properties of observed targets

TABLE 3.6: Properties of all targets analysed in this chapter.

ID	RA	DEC	V	K_s	SpT	μ_α	μ_δ	Plx	Population	Simbad Class.	Lit. Flag[a]	SACY Flag[d]
	hh:mm:ss.s	dd:mm:ss	(mag.)	(mag.)		(mas)	(mas)	(pc)				
HD 1405	00 18 20.9	+30 57 22	8.86	6.51	K2V	143.7	-171.5	~	ABD	RS*		
HD 24681	03:55:20.4	-01:43:45	9.05	7.25	G5	46.2	-90.2	~	ABD	*		
TYC 91-82-1	04:37:51.4	+05:03:08	11.01	8.65	~	18.50	-59.30	~	ABD	*		AB
V* PX Vir	13:03:49.6	-05:09:42	7.69	5.51	G5V	-191.13	-218.73	46.10	ABD	BY*		SB1
LP 745-70	16:33:41.6	-09:33:11	11.24	7.55	K9V	-70.05	-177.52	32.60	ABD	PM*	A*F[1]	
HD 160934	17:38:39.6	+61:14:16	10.45	6.81	K7Ve	-23.30	47.71	30.19	ABD	Fl*	AB[6] ,A*D, Aa,Ab[1]	
TYC 486-4943-1	19:33:03.7	+03:45:39	11.15	8.66	~	18.0	-65.5	~	ABD	*		
BD-03 4778	20:04:49.3	-02:39:20	10.24	7.92	~	28.6	-71.7	~	ABD	Ro*		AB
HD 201919	21:13:05.2	-17:29:12	10.64	7.58	K6Ve	76.5	-144.1	~	ABD	Ro*		
GJ 4231	21:52:10.4	+05:37:35	21.11	7.38	M2.4V	119.17	-150.29	32.79	ABD	Fl*	AB, C	
GJ 885 A	23:00:27.9	-26:18:42	10.48	6.27	(K7V)M+~	113.2	-169.2	~	ABD	*i*		SB3
GJ 9809	23:06:04.8	+63:55:34	10.87	6.98	M0.3V	171.46	-58.55	40.81	ABD	Fl*	A*Y,Za*m[1]	
CD-45 14955B	23:11:53.6	-45:08:00	13.8	8.85	M3Ve	85.2	-84.7	19.7	ABD	*i*		
HD 222575	23:41:54.2	-35:58:39	9.39	7.62	G8V	69.49	-67.53	15.70	ABD	Ro*		
HD 199058	20:54:21.0	+09:02:23	8.62	6.96	G5	37.2	-56.9	~	ABD[10]	*		
TYC 1090-543-1	20:54:28.0	+09:06:06	11.68	8.82	~	34.4	-58.6	~	ABD[10]	V*		
HD 189285	19:59:24.1	-04:32:06	9.43	7.84	G5	14.2	-55.8	~	ABD[10]	*		
V* PW And	00:18:20.8	+30:57:22	8.81	6.39	K2V	143.7	-171.5	~	ABD[18]	RS*		
V* LO Peg	21:31:01.7	+23:20:07	9.19	6.38	K5-7V	133.38	-145.24	40.32	ABD[18]	BY*	AB,AC[1]	
BD+41 4749	23:19:39.5	+42:15:09	8.93	7.22	G0	77.52	-66.90	19.94	ABD[18]	*		
HD 152555	16:54:08.1	-04:20:24	7.82	6.36	F8/G0V	-37.25	-114.05	21.40	ABD	*	AB	
Wolf 1225	22:23:29.0	+32:27:32	11.45	6.05	M1V	255.3	-207.8	~	ABD, PMG[12]	*i*	AB[3]	AB
CD-52 9381	20:07:23.7	-51:47:27	10.5	7.39	K6Ve	88.9	-146.2	~	ARG	Ro*		
GJ 3322	05:01:58.7	+09:58:59	11.98	6.37	M3V	12.09	-74.41	30.12	BPC	Ro*	AB[4]	AB
2MASS J05200029+0613036	05:20:00.2	+06:13:03	11.58	8.57	K3	5.5	-37.8	~	BPC	TT*		
2MASS J05203182+0616115	05:20:31.8	+06:16:11	11.68	8.57	K3	12.4	-38.8	~	BPC	TT*		AB
CD-27 11535	17:15:03.6	-27:49:39	11.12	7.38	K5Ve	-9.30	-48.30	~	BPC	Ro*		AB, SB1
GSC 08350-01924	17:29:20.6	-50:14:53	13.47	7.99	M3Ve	-5.0	-54.7	~	BPC	*		AB
CD-54 7336	17:29:55.0	-54:15:48	9.55	7.36	K1V	-7.0	-63.1	~	BPC	Ro*		
HD 161460	17:48:33.7	-53:06:43	9.61	6.78	K0IV	-5.60	-53.30	~	BPC	Ro*		
V* V4046 Sgr	18:14:10.4	-32:47:34	10.94	7.25	K5V	2.1	-54.5	~	BPC	BY*		SB2
GSC 07396-00759	18:14:22.0	-32:46:10	12.78	8.54	M1Ve	7.3	-39.9	~	BPC	Em*		
Smethells 20	18:46:52.5	-62:10:36	12.08	7.85	M1Ve	13.7	-82	~	BPC	pr*		

ID	RA	DEC	V mag.	K_s mag.	SpT	μ_α	μ_δ	Plx	Population	Simbad Class.	Lit. Flag[a]	SACY Flag[d]
CD-31 16041	18:50:44.4	-31:47:47	11.2	7.46	K8Ve	10.6	-77.8	~	BPC	Ro*	A*J[1]	
TYC 6872-1011-1	18:58:04.1	-29:53:04	11.78	8.02	M0Ve	6.7	-42.9	~	BPC	Ro*		
CD-26 13904	19:11:44.6	-26:04:08	10.39	7.37	K4V(e)	18.9	-44.2	~	BPC	pr*	AB[2]	AB
CPD-72 2713	22:42:48.9	-71:42:21	10.6	6.89	K7Ve	94.1	-54.4	~	BPC	Ro*		
V* WW PsA	22:44:57.9	-33:15:01	12.07	6.93	M4IVe	184.76	-119.76	42.84	BPC	BY*	A[3]	
V* TX PsA	22:45:00.0	-33:15:25	13.36	7.79	M5IVe	183	-118	~	BPC	Fl*	B[3]	
BD-13 6424	23:32:30.8	-12:15:51	10.5	6.57	M0Ve	139.20	-83.40	~	BPC	Ro*		
HD 8813	01:23:25.8	-76:36:42	8.46	6.79	G6V	100.16	-20.93	21.52	CAR	pr*		
HD 22213	03:34:16.3	-12:04:07	8.86	6.79	G8V	80.7	-35.4	~	CAR	Ro*		AB
CD-44 1533	04:22:45.6	-44:32:51	10.47	8.58	K0V	32.0	2.8	~	CAR	Ro*		
CD-57 1709	07:21:23.7	-57:20:37	10.73	8.7	K0V	-1.6	22.1	~	CAR	Ro*		AB
TYC 8557-1251-1	07:55:31.6	-54:36:50	11.44	9.19	G9V	-4.1	10.3	~	CAR	Ro*		
2MASS J08110934-5555563	08:11:09.3	-55:55:56	11.52	9.4	G8V(e)	-3.5	15.1	~	CAR	pr*		
BD-07 2388	08:13:50.9	-07:38:24	9.32	6.92	K0	-25.3	-45.2	~	CAR	Ro*		AB
2MASS J08371096-5518105	08:37:10.9	-55:18:10	11.04	9.38	G9V	-7.4	18.0	~	CAR	pr*		AB?
CD-61 2010	08:42:00.4	-62:18:26	10.95	8.83	K0V	-11.3	15.9	~	CAR	Ro*		
CD-53 2515	08:51:56.4	-53:55:56	11.06	8.75	G9V	-11.6	12.7	~	CAR	Ro*		
2MASS J08521921-6004443	08:52:19.2	-60:04:44	11.48	9.37	K0V	-2.8	12.0	~	CAR	pr*		
2MASS J08563149-5700406	08:56:31.4	-57:00:40	11.83	9.76	K0V(e)	-14.7	6.0	~	CAR	pr*		
TYC 8582-3040-1	08:57:45.6	-54:08:36	11.71	9.35	K2IV(e)	-13.1	8.6	~	CAR	Ro*		
CD-49 4008	08:57:52.1	-49:41:50	10.5	8.64	G9V	-23.00	15.40	~	CAR	Ro*		
CD-54 2499	08:59:28.7	-54:46:49	10.08	8.4	G5IV	-18.3	15.2	~	CAR	Ro*		
CD-55 2543	09:09:29.3	-55:38:27	10.21	8.4	G8V	-13.2	14.8	~	CAR	Ro*		
TYC 8174-1586-1	09:11:15.8	-50:14:14	11.81	9.5	K5Ve	-19.45	7.42	~	CAR	Ro*		
2MASS J09131689-5529032	09:13:16.8	-55:29:03	11.36	8.36	G5V(e)	-13.8	14.8	~	CAR	pr*		AB
HD 309751	09:31:44.7	-65:14:52	11.33	8.36	G3V	-12.40	19.00	~	CAR	pr*		SB2
CPD-62 1293	09:43:08.8	-63:13:04	10.44	8.6	G6V	-34.9	25.0	~	CAR	Ro*		AB
TYC 9217-417-1	09:59:57.6	-72:21:47	11.7	8.69	K4Ve	-24.2	29.0	~	CAR	Ro*		
CD-69 783	10:41:23.0	-69:40:43	10.27	8.38	G8V(e)	-30.0	24.4	~	CAR	Ro*		
TYC 8962-1747-1	11:08:07.9	-63:41:47	12.07	8.29	M0Ve	-33.2	7.2	~	CAR	Ro*		
HD 107722	12:23:29.0	-77:40:51	8.24	7.14	F6V	-65.1	10.8	~	CAR	TT*		
TYC 9486-927-1	21:25:27.4	-81:38:27	11.85	7.34	M1Ve	63.4	-110.0	~	CAR	Ro*		
BD-03 5579	23:09:37.1	-02:25:55	10.99	7.82	K4Ve	57.5	-47.4	~	CAR	Ro*		
CPD-53 1875	08:45:52.7	-53:27:28	10.42	8.77	G2V	-13.8	7.7	~	CAR[10]	Ro*		AB
CPD-55 1885	09:00:03.3	-55:38:24	10.83	9.01	G5V	-12.7	16.4	~	CAR[10]	Ro*		
Ass Cha T 2-21	11:06:15.4	-77:21:56	11.42	6.42	G5Ve	-16.5	-0.5cm	~	CHA I	pr*	D+w[9]	
2MASS J12571172-7640111	12:57:11.7	-76:40:11	15.0	8.4	M0e	10	-32	~	CHA II[11]	Y*O		AB
BD-16 351	02:01:35.6	-16:10:00	10.34	7.96	~	57.1	-29.7	~	COL	Ro*		AB
2MASS J02303239-4342232	02:30:32.4	-43:42:23	10.37	7.23	K5V(e)	80.5	-14.9	~	COL	pr*		AB
BD-11 648	03:21:49.6	-10:52:17	11.63	9.26	G9	~	~	~	COL	Ro*		

ID	RA	DEC	V mag.	K_s mag.	SpT	μ_α	μ_δ	Plx	Population	Simbad Class.	Lit. Flag[a]	SACY Flag[d]
V* V1221 Tau	03:28:14.9	+04:09:47	9.7	7.44	G6V+K3v...	34.4	-45.0	~	COL	BY*	AB, C	
2MASS J03573723-0416159	03:57:37.2	-04:16:15	10.72	8.75	~	~	~	~	COL	Ro*		
HD 26980	04:14:22.5	-38:19:01	9.08	7.62	G3V	41.78	1.40	12.42	COL	Ro*		
HD 27679	04:21:10.3	-24:32:20	9.43	7.81	G2V	40.0	-9.1	~	COL	pr*		
CD-43 1395	04:21:48.6	-43:17:32	10.18	8.42	G7V	20.4	5.6	~	COL	Ro*		AB
2MASS J04272050-4420393	04:27:20.4	-44:20:39	10.91	8.56	K1V(e)	31.3	2.2	~	COL	pr*		AB
CD-36 1785	04:34:50.7	-35:47:21	10.84	8.59	K1Ve	34.8	-1.6	~	COL	Ro*		
BD+08 742	04:42:32.0	+09:06:00	11.19	9.12	G5V:	27.60	-25.50	~	COL	*		
HD 31242	04:51:53.5	-46:47:13	9.85	8.16	G5V	32.7	14.2	~	COL	Ro*		SB1
HD 272836	04:53:05.1	-48:44:38	10.72	8.24	K2V(e)	30.8	17.0	~	COL	Ro*		
TYC 9178-284-1	06:55:25.1	-68:06:21	11.91	8.94	K4Ve	2.7	20.2	~	COL	Ro*		
2MASS J08240598-6334024	08:24:05.9	-63:34:02	9.87	8.13	G5V	-15.6	22.4	~	COL	pr*	AB, C	
V* V479 Car	09:23:34.9	-61:11:35	10.16	7.96	K1V(e)	-28.30	17.98	11.36	COL	BY*		
2MASS J09322609-5237396	09:32:26.0	-52:37:39	10.86	8.84	G8V(e)	-16.5	10.9	~	COL	pr*		
HD 174656	18:53:05.9	-36:10:22	9.87	7.28	K0IV(e)	0.20	-21.40	~	CRA	Ro*	AB[2]	
V* DZ Cha	11:49:31.8	-78:51:01	12.0	8.49	M0Ve	-38.0	-8.3	~	ECH	Or*		
2MASS J11594226-7601260	11:59:42.2	-76:01:26	11.31	8.3	K4Ve	-40.5	-5.83	9.89	ECH	TT*		
HD 104467	12:01:39.1	-78:59:16	8.56	6.85	G3V(e)	-42.8	-4.0	~	ECH	TT*		SB1
HD 105923	12:11:38.1	-71:10:36	9.16	7.18	G8V	-38.9	-8.3	~	ECH	Ro*		AB
2MASS J12194369-7403572	12:19:43.6	-74:03:57	12.5	8.86	M1	-42.1	-11.7	~	ECH	TT*		
2MASS J12202177-7407393	12:20:21.7	-74:07:39	12.0	8.37	M1V	-41.0	-6.5	~	ECH	TT*		AB?
2MASS J12392124-7502391	12:39:21.2	-75:02:39	10.3	7.78	K3Ve	-43.6	-11.1	~	ECH	TT*		
TYC 9245-535-1	12:56:08.3	-69:26:53	12.06	7.99	K7Ve	-33.6	-7.6	~	ECH	Ro*		AB
CD-69 1055	12:58:25.5	-70:28:49	9.67	7.55	K0Ve	-43.1	-18.7	~	ECH	Ro*		
V* MP Mus	13:22:07.5	-69:38:12	9.75	7.29	K1Ve	-40.80	-23.30	~	ECH	TT*		
2MASS J12375231-5200055	12:37:52.2	-52:00:05	10.68	6.02	M3V(e)	-1032.41	30.39	103.18	HYA[12]	pr*		
2MASS J22420163+0946091	22:42:01.6	+09:46:09	11.99	8.26	K6Ve	17.27	30.22	26.73	HYA[12]	pr*		
2MASS J23350028+0136193	23:35:00.2	+01:36:19	9.59	6.04	K7V	341.31	25.50	52.56	IC2391[12]	pr*[(c)]	A*F,BC[1]	
TYC 8639-1114-1	11:55:42.9	-56:37:31	12.11	8.04	M0Ve	-45.4	-6.0	~	LCC	Ro*		AB
TYC 8978-3494-1	12:12:48.8	-62:30:31	12.13	7.96	K7Ve	-36.4	-16.4	~	LCC	Ro*		AB
TYC 8637-1558-1	12:16:01.1	-56:14:07	11.22	7.96	K5Ve	-42.7	-10.3	~	LCC	Ro*		
CD-62 657	12:28:25.3	-63:20:58	9.08	7.33	G7V	-34.9	-11.3	~	LCC	Ro*		
CPD-63 2367	12:36:38.9	-63:44:43	9.69	7.37	K2V	-37.8	-9.7	~	LCC	Ro*	A*P[1]	
2MASS J12474824-5431308	12:47:48.2	-54:31:30	11.82	8.05	M0Ve	-41.5	-11.0	~	LCC	pr*		
HD 112245	12:56:09.4	-61:27:25	9.63	7.26	K0Ve	-52.5	-14.7	~	LCC	Ro*		AB
TYC 9012-1005-1	13:44:42.7	-63:47:49	11.04	7.74	K4Ve	-44.9	-20.8	~	LCC	Ro*	A,Z*r,A*Y[1]	
CPD-64 1859	12:19:21.6	-64:54:10	9.87	7.4	K3V	-40.20	-10.20	~	LCC[15]	Ro*		
TYC 7846-833-1	15:56:44.0	-42:42:29	11.88	8.27	K6IVe	-13.7	-16.6	~	LUP	Ro*		AB, C
CD-33 11275	16:35:22.4	-33:28:53	11.42	8.08	K4Ve	-16.8	-33.8	~	LUP	Ro*		AB, C
CD-58 860	04:11:55.6	-58:01:47	10.01	8.36	G6V	-7.9	38.2	~	OCT	Ro*		

ID	RA	DEC	V mag.	K_s mag.	SpT	μ_α	μ_δ	Plx	Population	Simbad Class.	Lit. Flag[a]	SACY Flag[d]
2MASS J04302731-4248466	04:30:27.3	-42:48:46	10.75	8.73	G9V(e)	2.6	20.8	~	OCT	pr*		AB
HD 271037	05:06:50.5	-72:21:11	10.91	8.67	K0IV	-7.0	24.7	~	OCT	Ro*		
HD 274576	05:28:51.3	-46:28:19	10.5	8.81	G6V	-10.3	22.6	~	OCT	Ro*		AB
BD-20 1111	05:32:29.3	-20:43:33	10.4	8.7	~	-8.3	12.0	~	OCT	*		Ba, Bb ?
CD-47 1999	05:43:32.1	-47:41:10	10.19	8.64	G0V	-10.0	15.0	~	OCT	Ro*		AB?
2MASS J05581182-3500496	05:58:11.8	-35:00:49	11.24	9.38	G9V	-12.7	13.0	~	OCT	pr*		
2MASS J06033540-4911256	06:03:35.4	-49:11:25	11.18	9.08	K0Ve	-9.3	8.3	~	OCT	pr*		AB
CD-66 395	06:25:12.3	-66:29:10	10.87	9.0	K0IV	-18.40	24.40	~	OCT	Ro*		
2MASS J06400573-3033089	06:40:05.7	-30:33:08	10.24	8.7	F9V	-12.60	7.70	~	OCT	pr*	AB[2]	
BD-18 4452	17:13:11.6	-18:34:25	10.86	6.48	M0Ve	39.0	-88.7	~	OCT	pr*	AB[1]	A, Ba, Bb
CD-30 3394	06:40:04.9	-30:33:03	9.83	8.59	F6V	-18.3	7.0	~	OCT	*		A, Ba, Bb
V* BO Mic	20:47:45.0	-36:35:40	9.39	6.79	K3V(e)	11.42	-75.87	19.16	PMG[12]	BY*		
V* V1002 Sco	16:12:40.5	-18:59:28	9.81	7.49	K6e	-11.70	-22.20	~	RHO	Or*	AB,Aa[1]	AB
2MASS J16141107-2305362	16:14:11.0	-23:05:36	10.5	7.46	K2IV	-11.9	-22.9	~	RHO	TT*	A*G,Aa,Ab[1]	
HD 147808	16:24:51.3	-22:39:32	9.5	7.08	G9IVe	-13.4	-20.0	~	RHO	TT*	AB,Aa,Ab[1]	
V* V896 Sco	16:25:38.4	-26:13:54	11.75	7.52	M	~	~	~	RHO	Or*		AB
2MASS J16312019-2430009	16:31:20.1	-24:30:00	10.69	7.09	K3e	-5.1	-28.8	~	RHO	SB*	AB	AB, C
V* V877 Sco	16:33:41.9	-25:23:34	10.66	7.95	K4IVe	-2.4	-25.4	~	RHO	bL*		
2MASS J16471358-1514275	16:47:13.5	-15:14:27	12.02	8.04	M0Ve	-5	-11	~	RHO[17]	TT*		AB
2MASS J16482187-1410427	16:48:21.8	-14:10:42	14.79	7.86	~	~	~	~	RHO[17]	Y*O		AB
CD-78 24	00:42:20.3	-77:47:39	10.21	7.53	K3Ve	79.5	-32.1	~	THA	Ro*		
CD-53 544	02:41:46.8	-52:59:52	10.22	6.76	K6Ve	97.5	-13.7	~	THA	Ro*		
CD-35 1167	03:19:08.6	-35:07:00	11.0	7.72	K7Ve	89.2	-20.3	~	THA	Ro*		
CD-46 1064	03:30:49.0	-45:55:57	9.79	7.1	K3V	87.2	-5.0	~	THA	Ro*		
CD-44 1173	03:31:55.6	-43:59:13	10.9	7.47	K6Ve	90.9	-5.0	~	THA	Ro*		AB
HD 22705	03:36:53.4	-49:57:28	7.65	6.14	G2V	89.74	0.29	23.07	THA	*i*	AB,AC[1]	AB
BD-12 943	04:36:47.1	-12:09:20	9.86	7.76	~	45.9	-20.4	~	THA	Ro*		
TYC 8083-455-1	04:48:00.6	-50:41:25	11.53	7.92	K7Ve	64.3	16.6	~	THA	Ro*		AB
BD-19 1062	04:59:32.0	-19:17:41	10.61	8.07	~	42.6	-10.0	~	THA	Ro*		
ASAS J051536-0930.8	05:15:36.4	-09:30:51	9.82	8.08	G5	31.4	-20.4	~	THA	TT*		
2MASS J05182904-3001321	05:18:29.0	-30:01:32	11.66	8.3	K4Ve	37.7	4.3	~	THA	pr*		AB
TYC 8098-414-1	05:33:25.5	-51:17:13	11.74	8.16	K7Ve	54.1	16.6	~	THA	Ro*		
2MASS J05490656-2733556	05:49:06.5	-27:33:55	10.22	8.25	G9V	30.90	-4.70	~	THA	pr*		
TYC 9344-293-1	23:26:10.7	-73:23:49	11.83	7.94	M0Ve	71.5	-66.5	~	THA	Ro*		
HD 30051	04:43:17.2	-23:37:42	7.12	6.02	F2/3IV/V	50.25	-11.84	15.73	THA[19]	*		
CD-46 10045	15:25:11.6	-46:59:12	10.08	7.78	G9V	-49.63	-21.24	15.46	UCL	**	AB[3]	AB
V* KW Lup	15:45:47.6	-30:20:55	9.28	6.46	K2V	-69.11	-98.40	24.78	UCL[16]	BY*		AB
2MASS J15594951-3628279	15:59:49.5	-36:28:27	10.36	8.03	K3e	-16.21	-51.01	15.40	US	pr*		
V* V857 Ara	17:18:14.6	-60:27:27	9.48	7.53	G8V	-54.62	-91.04	16.97	US, THA[16]	BY*		AB
TYC 6234-1287-1	17:26:56.5	-16:31:34	11.59	7.83	K4Ve	-10.1	-39.0	~	US?[13]	Ro*		AB, SB2?

ID	RA	DEC	V mag.	K_s mag.	SpT	μ_α	μ_δ	Plx	Population	Simbad Class.	Lit. Flag[a]	SACY Flag[d]
2MASS J09551508-6203324	09:55:15.0	-62:03:32	12.01	9.66	K2V	-15.3	4.1	~	N	pr*		
BD+01 3657	18:22:17.2	+01:42:25	10.2	6.86	K6Vke	84.65	-18.29	37.28	N	Ro*		
HD 83096	09:31:24.8	-73:44:49	7.3	6.17	F1V	-35.40	32.44	11.98	N	**		
HD 154361	17:05:08.4	-01:47:10	9.5	6.81	K0	75.7	-44.2	~	N	cC*		
TYC 438-902-1	18:03:17.8	+04:48:26	10.3	8.01	K2	-11.8	-27.0	~	N	Ro*		
TYC 458-290-1	18:31:59.1	+05:40:19	10.82	8.85	~	31.8	-5.9	~	N	Ro*[b]		
TYC 460-624-1	18:45:10.2	+06:20:15	10.76	6.81	~	-38.0	-83.7	~	N	Ro*		
TYC 1026-1952-1	18:47:25.5	+08:41:07	12.1	8.97	~	-11.1	-18.2	~	N	Ro*		AB
BD+01 3828	18:57:19.4	+01:20:33	9.56	7.79	G0	27.4	-0.9	~	N	*i*	AB[2]	
HD 176898	19:02:17.0	+02:44:21	9.19	7.16	G	24.6	-30.2	~	N	*		
TYC 490-110-1	19:31:34.9	+05:56:07	11.13	7.73	K3III	22.2	2.8	~	N	Ro*		AB
TYC 482-1106-1	19:36:04.3	+03:25:48	10.43	8.33	~	3.0	-24.7	~	N	Ro*		
TYC 1062-1904-1	19:47:39.1	+09:29:36	11.81	8.85	~	26.3	13.2	~	N	*		
TYC 1058-1925-1	19:51:13.3	+08:42:19	10.48	8.13	~	11.1	-17.5	~	N	*		AB
TYC 5188-193-1	20:35:27.1	-07:06:54	11.59	10.78	~	16.2	-14.6	~	N	*		
HD 199602	20:58:32.5	-08:50:22	9.19	6.4	K0	-31.9	-56.1	~	N	*		
TYC 538-573-1	21:01:24.5	+05:42:12	11.55	9.39	~	18.7	-3.3	~	N	V*		AB
TYC 553-84-1	21:56:22.0	+05:17:48	10.68	6.9	~	-8.2	-6.3	~	N	*		
CCDM J00002+0146AB	00:00:12.2	+01:46:17	10.78	7.93	G9IV	44.10	-22.90	~	N	**	A[2]	AB, SB3
TYC 1-1187-1	00:09:21.7	+00:38:06	11.88	8.71	K4Ve	119.4	-29.7	~	N	Ro*		SB2
HD 531	00:09:51.6	+08:27:11	9.35	7.57	G6V+G7V	56.21	-11.41	13.11	N	**	AB[3]	AB
GJ 3029	00:21:37.2	-46:05:33	12.22	7.45	M3Ve	-302.66	-360.97	51.80	N	Fl*		
BD+07 85	00:38:59.2	+08:28:41	10.09	7.2	K4Ve	100.9	-48.9	~	N	Ro*		
2MASS J01452133-3957204	01:45:21.3	-39:57:20	11.39	7.59	M1V	279.02	131.42	33.84	N	pr*	AB[7]	
BD-21 332	01:53:11.3	-21:05:43	11.73	7.14	M2Ve	271.4	72.5	~	N	Ro*	SB2[8]	
GJ 3148 A	02:16:41.1	-30:59:18	12.05	7.13	M3Ve	683.07	250.88	69.81	N	Fl*	AB[3]	
2MASS J14110874-6155469	14:11:08.7	-61:55:47	10.8	6.92	M1Ve	147.9	-51.0	~	N	pr*		
2MASS J15011648-4339311	15:01:16.5	-43:39:31	10.8	6.07	M3Ve	98.0	26.9	~	N	pr*		SB2
2MASS J15104047-5248189	15:10:40.4	-52:48:19	12.26	6.85	M2V(e)	-145.3	-167.5	~	N	pr*		AB, SB3
2MASS J15240033-7054096	15:24:00.3	-70:54:09	11.93	7.77	M1Ve	-145.1	-128.2	~	N	pr*		SB2
CD-24 12794	16:43:56.9	-25:08:36	11.26	7.42	K6Ve	8.7	-50.7	~	N	Ro*		
TYC 6242-104-1	17:21:56.0	-20:10:51	13.22	9.15	K5Ve	-11.7	-13.7	~	N	Ro*		
V* V2384 Oph	17:42:30.3	-28:44:55	9.03	7.32	G5V	-2.83	-40.87	12.82	N	bL*		
HIP 96515	19:37:08.7	-51:34:00	12.29	7.96	M1Ve	91.07	-21.94	22.79	N	Al*	AB[4]	AB, SB2
GJ 781.1 A	20:07:44.9	-31:45:14	13.08	7.4	M4Ve	286.55	-750.5	67.08	N	Fl*	AB[3]	SB2
HIP 106043	21:28:44.4	-47:15:42	12.2	8.29	M1Ve	-16.42	-58.10	27.94	N	Ro*		
GJ 841 A	21:57:41.2	-51:00:22	10.5	5.88	M2Ve	-35.66	-377.25	62.61	N	Fl*	AB[3]	
BD+02 4456	21:59:59.9	+03:02:24	10.35	7.89	K0IV	63.80	-3.20	~	N	Ro*		SB2
2MASS J22023015-0406117	22:02:30.1	-04:06:11	10.06	7.97	K2V	29.9	-13.4	~	N	pr*		
V* CS Gru	22:15:35.2	-39:00:50	9.32	7.09	K0V	94.36	-39.79	17.84	N	BY*		SB1

ID	RA	DEC	V mag.	K_s mag.	SpT	μ_α	μ_δ	Plx	Population	Simbad Class.	Lit. Flag[a]	SACY Flag[d]
HD 212781	22:26:53.2	-00:50:39	10.46	8.34	K0V(e)	-4.30	-48.00	~	N	Ro*		AB, SB1
HIP 113001	22:53:05.9	+07:28:19	11.72	7.94	K6Ve	59.38	-79.98	19.62	N	Ro*		SB2
TYC 572-382-1	22:56:49.5	+02:35:39	10.29	8.08	K1IV	-14.2	-18.0	~	N	Ro*		AB
2MASS J23045301+0632003	23:04:53.0	+06:32:00	10.99	8.18	K1Ve	-14.8	-23.4	~	N	pr*		
2MASS J23085046+0000528	23:08:50.4	+00:00:52	10.5	8.62	G8V	16.8	-7.1	~	N	pr*		
TYC 584-343-1	23:21:56.3	+07:21:32	10.97	8.94	K0V	21.50	-2.50	~	N	Ro*		AB
V* BS Psc	23:52:24.3	-00:55:59	10.76	8.95	G7V	19.90	-12.30	~	N	BY*		
CD-36 14261	20:36:08.3	-36:07:11	11.73	7.17	M3Ve	11.4	40.3	~	N	Ro*		

References. (1) Mason et al. (2001); (2) Dommanget and Nys (2002); (3) Turon et al. (1993); (4) Dommanget and Nys (2000); (5) Anderson and Francis (2012); (6) Gliese and Jahreiß (1991); (7) Bergfors et al. (2010); (8) Shkolnik et al. (2010); (9) Kraus and Hillenbrand (2007); (10) Messina et al. (2010); (11) Alcalá et al. (2008); (12) Montes et al. (2001); (13) Aarnio et al. (2008); (14) Riedel et al. (2014); (15) Mamajek et al. (2006); (16) Song et al. (2012); (17) Sartori et al. (2003); (18) López-Santiago et al. (2006); (19) Zuckerman et al. (2011); (20) Zuckerman et al. (2004); (21) Schlieder et al. (2012b)

Notes. [(a)] Formats as 'A*Y' signifies multiple components AB, AC, ..., AY [(b)] Note in SIMBAD to potential component within 30″ [(c)] Note in SIMBAD for triple system identified by Malogolovets et al. (2007) [(d)] SB systems denote spectroscopic binary systems identified in Torres et al. (2008); Elliott et al. (2014).

TABLE 3.7: A summary of the properties of non-SACY multiple systems identified in this chapter.

ID	Ang. sep. ($''$)	PA (deg.)	Dist. (pc)	Phys. sep (au)	ΔK (mag.)	Comp.	Prob.	Pop.	q	σ_q
				PMS populations						
CPD-53 1875	0.21	288.6	-	-	2.18	A, B	0.91	CAR[1]	0.27	0.08
2MASS J12571172-7640111	0.28	150.1	-	-	0.69	A, B	-	CHAII[2]	0.61	0.05
HD 112245	2.56	169.4	66.0	168.9	2.48	A, B	-	LCA, C	0.22	0.12
TYC 8978-3494-1	0.43	41.2	72.5	31.2	0.13	A, B	-	LCA, C	0.93	0.2
TYC 8639-1114-1	0.84	305.6	79.0	66.4	0.42	A, B	-	LCA, C	0.80	0.2
CD-33 11275	0.18	252.9	123.7	22.3	0.04	A, B	-	LUP	1.03	0.2
CD-33 11275	1.78	3.7	123.7	220.2	0.54	A, C	-	LUP	0.67	0.13
TYC 7846-833-1	0.2	192.5	139.7	27.9	0.76	A, B	-	LUP	0.58	0.11
TYC 7846-833-1	6.0	19.8	139.7	837.9	2.47	A, C	-	LUP	0.17	0.04
V* V896 Sco	0.87	20.9	125.0	108.7	1.68	A, B	-	RHO	0.30	0.05
V* V1002 Sco	0.12	156.0	138.7	16.6	1.58	A, B	0.89	RHO	0.32	0.03
2MASS J16312019-2430009	0.32	170.4	103.4	33.1	2.98	A, B	-	RHO	0.12	0.05
2MASS J16312019-2430009	4.48	12.1	103.4	463.2	0.33	A, C	-	RHO	0.79	0.14
2MASS J16471358-1514275	0.35	60.5	-	-	1.15	A, B	-	RHO[3]	0.44	0.05
2MASS J16482187-1410427	1.01	252.2	-	-	1.93	A, B	-	RHO[3]	0.26	0.05
CD-46 10045	0.62	334.5	67.9	42.1	0.07	A, B	-	UCL	0.96	0.2
V* V857 Ara	0.2	194.2	-	-	2.45	A, B	-	US	0.19	0.06
TYC 6234-1287-1	1.51	245.2	-	-	0.21	A, B	-	US?[4]	0.88	0.05
				Other						
HIP 96515	8.58	224.0	-	-	6.36	A, B	-	N, Field	-	-
HD 212781	5.34	77.3	-	-	4.71	A, B	-	N, Field	-	-
TYC 1026-1952-1	6.99	58.6	-	-	3.76	A, B	-	N, Field	-	-
TYC 572-382-1	3.07	53.5	-	-	2.68	A, B	-	N, Field	-	-
TYC 490-110-1	2.42	180.3	-	-	2.45	A, B	-	N, Field	-	-
TYC 538-573-1	6.19	25.3	-	-	2.27	A, B	-	N, Field	-	-
TYC 584-343-1	5.08	228.5	-	-	1.53	A, B	-	N, Field	-	-
2MASS J15104047-5248189	0.47	294.7	-	-	1.14	A, B	-	N, Field	-	-
CCDM J09314-7345AB	0.95	133.1	-	-	0.62	A, B	0.99	N, Field	-	-
TYC 1058-1925-1	0.76	236.1	-	-	0.17	A, B	-	N, Field	-	-
CCDM J00002+0146AB	1.81	262.9	-	-	0.16	A, B	-	N, Field	-	-
HD 531	5.21	275.9	-	-	0.05	A, B	-	N, Field	-	-

Notes. (1) Messina et al. (2010); (2) Alcalá et al. (2008); (3) Sartori et al. (2003); (4) Aarnio et al. (2008)

Chapter 4

Finding new members of the young moving groups as wide companions

Parts of this chapter have been previously published as 'Search for associations containing young stars (SACY). VII. New stellar and sub-stellar candidate members in the young associations', Elliott, P.; Bayo, A.; Melo, C. H. F.; Torres, C. A. O.; Sterzik, M.; Quast, G. R.; Montes, D.; Brahm, R., 2016, A&A, 590, A13. The work is presented here in expanded and updated form.

In this analysis we searched the field of view of 542 previously identified members of the young associations to identify wide / extremely wide (1000-100,000 au in physical separation) companions using near-infrared photometry and proper motions. We collated further photometry and spectroscopy from the literature and conducted our own high-resolution spectroscopic observations for a sub-sample of candidate members. We identified 84 targets (45: 0.2-1.3 $M_\odot$, 17: 0.08-0.2 $M_\odot$, 22: $<$0.08 $M_\odot$) in our analysis. For 33 of these 84 we were able to further assess their membership using a variety of properties (X-ray emission, UV excess, H_α, lithium and K I equivalent widths, radial velocities, and CaH indices). We derive a success rate of 76–88% for this technique based on the consistency of these properties. Given the predicted masses of the

majority of these new candidate members and their proximity, high-contrast imaging techniques would facilitate the search for new low-mass planets.

This chapter is arranged as follows. Section 4.1 explains how the sample for this chapter was formed. Section 4.2 details our technique for identifying new members. Section 4.3 outlines the sources where we gathered additional information. Section 4.4 describes the high resolution spectra we analysed for a sub-sample of identified targets. Section 4.5 discusses the properties of the candidates we identified. Section 4.6 concludes this analysis evaluating the success of the technique. Section 4.7 discusses the compatibility of specific newly identified sources. Section 4.8 details previously identified wide multiple systems. Section 4.9 shows colour-magnitude diagrams for all 9 young moving groups with candidate members. Section 4.10 lists the properties of the 542 members used in this chapter.

4.1 The sample

We collated high-probability members from a collection of prominent moving group works to date [Torres et al., 2008; Zuckerman et al., 2011; Malo et al., 2014; Kraus et al., 2014; Elliott et al., 2014 – Chapter 2, Murphy and Lawson, 2015] which cover a wide range of spectral types (B2-M5) and ages ($\sim$5-150 Myr), totalling 542 targets in 9 associations. A summary of the associations can be found in Table 4.1. We did not put any constraints on the mass of the known members as we want to maximise our sample size. However, we are limited in sensitivity to wide companions depending on the position of the source on the sky, its proper motion and density of objects in the field of view (FoV), as discussed in Section 4.2. The targets that make up the sample and their basic properties are listed in Table 4.6.

TABLE 4.1: A summary of the targets and their membership studied in this chapter.

Ass.	Ass. ID	No. of objects
AB Dor	ABD	105
Argus	ARG	77
β-Pic	BPC	69
Carina	CAR	48
Columba	COL	78
ϵ-Cha	ECH	24
Octans	OCT	62
Tuc-Hor	THA	56
TW Hydrae	TWA	23

4.2 Searching for new members as very wide companions

To identify very wide companions we used the point source catalogue of 2MASS (Cutri et al., 2003) for near-infrared photometry (*J*, *H*, *K*). We combined this with proper motions from NOMAD, PPMXL and UCAC4 (Zacharias et al., 2005; Roeser et al., 2010; Zacharias et al., 2012, respectively).

One aim of this search was to produce robust detection limits of our entire sample out to 100,000 au in physical separation from the known member. These limits will be used in further work to produce comprehensive statistics of all 9 young moving groups. We first calculated the angular query needed to achieve a physical search radius out to 100,000 au using the distance to the source (either from parallax ESA (1997); van Leeuwen (2007) or derived kinematically using the convergence method, i.e. Torres et al., 2006). We then converted the apparent magnitude of any sources in the FoV into absolute magnitude, assuming the known member's distance. Using the available photometry (*J*, *H*, *K*) we constructed colour-magnitude diagrams (*H*-*K*, *K* and *J*-*K*, *K*) for each FoV. We used the evolutionary tracks of (Baraffe et al., 2015) (with the age of the association that the member belongs to). We then used the photometry with derived statistical uncertainties and kinematic criteria (detailed below) to classify potential companions.

4.2.1 Computing statistical photometric uncertainties

The three photometric bands of 2MASS (*J*, *H*, *K*) do not offer a very wide range of colours to distinguish young objects from contamination. Additionally proper motion values are only projected motions and therefore the distance to the object can be a severe limiting factor. For those reasons we took the time to produce photometric criteria that would limit the number of false-positives whilst attempting to minimise the possibility of true companion rejection.

First of all we computed the standard deviation of the difference between the colour of the isochrone and 2MASS photometry for each object, for the entire sample. The values were $\sigma_{\mathrm{H-K}}$=0.06 mag. and $\sigma_{\mathrm{J-K}}$=0.16 mag. for the colours *H*-*K* and *J*-K, respectively. This provided an estimate of the difference between the models and the observations. We used the generous criteria of 2σ for both colours, however the source must agree in both of these colours to be classified as a potential companion.

The colour and the magnitude are related quantities and therefore an offset in magnitude can dramatically affect the agreement in colour. An unresolved (equal-mass) companion can affect the magnitude of a source by upto $\approx$0.8 mag. We therefore adopted this value as our upper uncertainty on the absolute magnitude. The effect of unresolved companions is asymmetric with respect to the magnitude i.e. it only ever increases this value. For the lower limit we computed the average difference (0.15 mag.) between the isochrone and the known member, in the cases that the known member was fainter than its isochrone, again we used 2σ as our criterion.

To test the effectiveness of our derived criteria we performed the analysis on a subset of the primary sources in our sample. Of 198 primaries, 188 were initially identified correctly. Of the ten sources that were not identified, seven were known sources with 2 or more components in their photometry (such as HD 217379, identified as a triple-lined spectroscopic binary in Chapter 2. These are rare cases, however we do not want to exclude any sources (companions also have a small probability of being in an SB3 configuration) and therefore we increased the upper limit on the magnitude (1.2 mag.). With this new criterion we identified 195 / 198 of our primaries. Of the three

sources (T Cha, CP-681894, TWA 22) that were still not identified, two have near-infrared photometric excesses (T Cha is a well known disc system (Weintraub, 1990) and CP-681894 shows strong H_α emission and K-band excess, indicative of accretion (Schütz et al., 2005). The other target, TWA 22 is a very tight, near equal-mass binary system (Bonnefoy et al., 2009). Using the resolved photometry this system would have been classified correctly. However, with the unresolved 2MASS photometry the system appears too red for its magnitude. Due to its proximity ($\approx$18 pc) and its age (10-20 Myr) the effect of the unresolved companion is exaggerated, however such young, nearby, low-mass (system mass: 220$\pm$21 $M_{Jup.}$) systems are very rare in our sample. Therefore, we proceeded with the criteria described above.

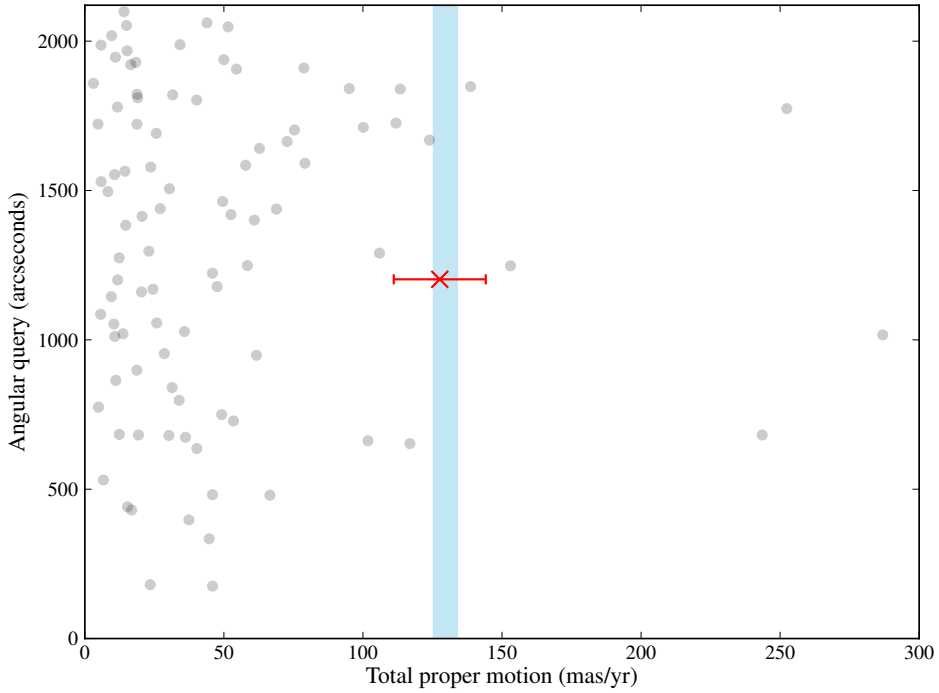

FIGURE 4.1: A graphical demonstration of our contamination / detection method for target Kap Psc (distance: 50 pc). The red marker is the one proper motion compatible source (with 3σ uncertainties), the grey markers incompatible sources. The blue shaded space is the 3σ boundary of primary target's proper motion. The extent of the angular query is 2000″, equivalent to 100,000 au at 50 pc.

This may induce a small bias in the way that we search for our companions i.e. we could potentially exclude sources with strong infrared excess. However, only 3 / 198 were not classified due to their excess (1.5%). Additionally the frequency of primordial discs for

the ages of the young associations is very low. For example, at 5 Myr the frequency is $\approx$10 % and for populations older than 10 Myr $<$5 %, (see Figure 1 of Mamajek, 2009). Furthermore this effect will be less and less prominent as the mass of the companion decreases. Andrews et al. (2013) showed that, for a sample of stars with spectral types earlier than M8.5 in Taurus, the disc mass decreases with the stellar mass. If we consider this in terms of infrared photometry the excess scales with the luminosity of the object, i.e. a significant excess, considering the same detection threshold, is less likely for a lower mass star. Furthermore, if we assume a flat-mass ratio, as observed in many regions (including close –$\approx$10-1000 au–visual binaries in the young associations, Elliott et al., 2015) this bias becomes even less significant.

4.2.2 Finding companions with near-IR photometry and proper motions

Any source that met the criteria described above was classified as a potential companion within the FoV. We then cross-matched all of these sources with the catalogues of UCAC4, PPMXL and NOMAD (in that order of preference based on uncertainties, completeness and catalogue-catalogue agreement) to collect the proper motion values.

Finding physical extremely-wide companions is limited by the projected motion of the target on the sky. In most cases we do not have access to parallax or radial velocity values, only proper motion - which is intrinsically linked to its distance. Additionally the target's galactic position is a limiting factor i.e. targets close to the galactic plane (and close to the Sun) are likely to have a high number of sources in their FoV, increasing the false-positive probability even with the imposed photometric constraints. Our targets are of different ages, at different distances and spatial positions and therefore there are many competing factors in estimating the contribution of contamination. We treated the contamination of each source individually; to find potential companions and also derive the maximum angular separation space we could probe. This method provides us with detection limits in angular separation which is crucial for our broader statistical analysis, presented in Chapter 5 and in future work (Elliott et al. in prep.).

For sources with low / intermediate proper motion ($<$20 mas) the chance of contamination increases significantly. In many works authors decide to use a hard cut-off (i.e. only considering sources with proper motions above a certain, somewhat arbitrary, threshold). However, information on the population can be lost as a source with intermediate proper motion is not analysed at all. Below is a description of the method we employed to maximise the physical separation space we can query without significant contamination.

Figure 4.1 graphically demonstrates our method for a primary target in our sample. The total proper motion, the x-axis, is defined as $\sqrt{\mu_{\alpha,*}^2 + \mu_{\delta}^2}$. Therefore, two sources may share the same total proper motion, however, not the same angle of projected motion. It is this angle that distinguishes proper motion-compatible sources (red markers) from incompatible sources (grey markers).

All markers in Figure 4.1 are sources with compatible 2MASS photometry. The grey markers show sources with an incompatible proper motion vector ($\geq 3\sigma$ discrepancy), the red marker (at $\approx$1200″, 57,000 au) with a compatible proper motion vector and the blue shaded area is 3σ proper motion space of the primary target. The total queried FoV is equivalent to 100,000 au. We use the point at which the total proper motion of the primary crosses any region in the parameter space with 2 or more incompatible sources as our maximum angular separation. This is a very conservative estimate but proved very powerful. If the total proper motion of the primary never crosses any such regions we set our sensitivity to a radial physical distance of 100,000 au, as in Figure 4.1.

Figure 4.2 shows a summary of the photometry (V, J, H, K) and proper motion of the potential companion from Figure 4.1. The agreement in the colour V-K is generally quite poor and is discussed more thoroughly in Section 4.5.8.

For the inner angular query we use the limit given by the PSF of 2MASS ($\approx$3″) which relates to a physical inner limit of 18–570 au for our nearest and furthest sources, respectively.

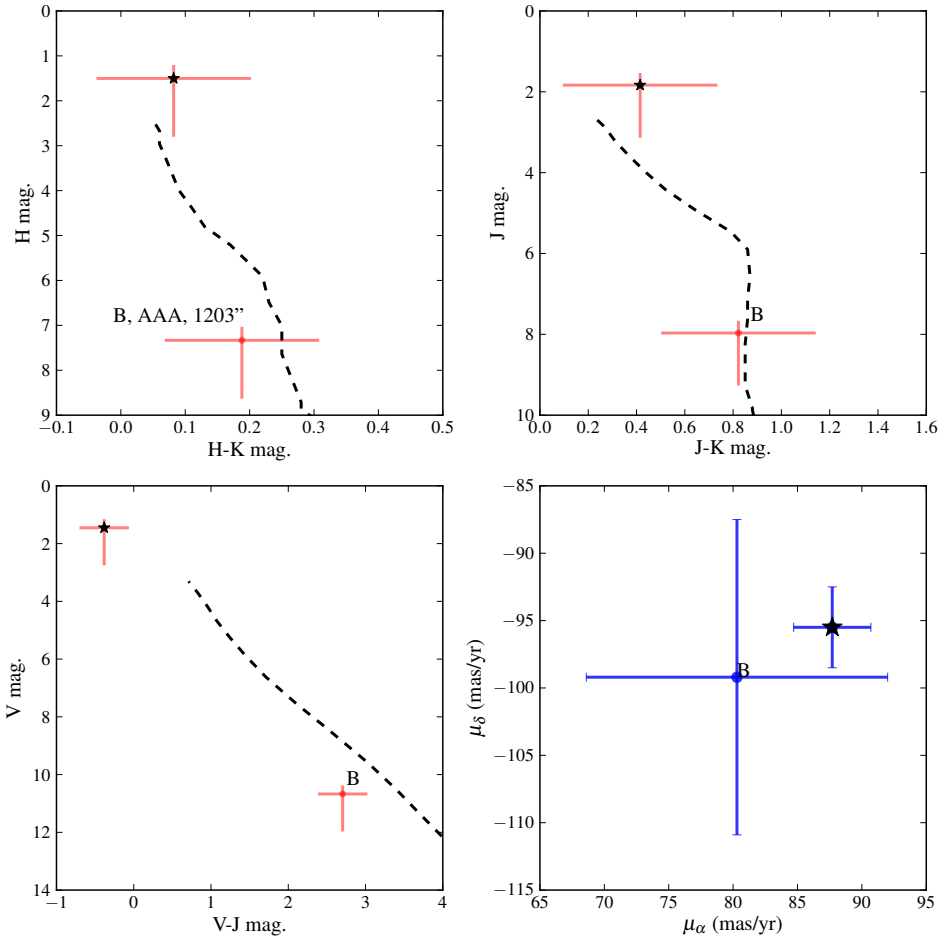

FIGURE 4.2: *Top left, top right and bottom left panels:* Colour-magnitude diagrams for Kap Psc+2MASS J23270114+0055200 in (*H*-*K*, *K*), (*J*-*K*, *K*) and (*V*-*J*, *V*), respectively. The text next to the marker indicates the component designation, the quality flags of the 2MASS photometry and the angular separation from the primary. The dotted lines are the evolutionary tracks of Baraffe et al. (2015) using the age of the moving group. *Bottom right panel*: Proper motion values of the primary and companion.

4.3 Further information from catalogues and the literature

Table 4.2 summarises the catalogues and works we cross-matched our sample with to gain further photometry, spectroscopy, kinematics and information of multiplicity. Where the cross-match was successful we collated any available notes of the source from the works. We also compared our results to other works that have focussed on very wide companions to stars in the moving groups (Kastner et al., 2011, 2012; Scholz

et al., 2005; Looper et al., 2010; Feigelson et al., 2006; Alonso-Floriano et al., 2015). A detailed comparison of these targets can be found in Section 4.8. Additionally we queried Simbad (Wenger et al., 2000) for each object to collate any noteworthy features, analysis and further parameters available.

4.3.1 Photometry from the Catalina survey

We used the Catalina survey (Drake et al., 2009), aimed at identifying optical transients, covering 33,000 deg^2 of the sky, to analyse optical photometric variability. We cross-matched our sample with the second data release via the online multi-object search service[1]. From this cross-match there were 235 matches. This was significantly reduced to 55 matches, considering objects fainter than 13 mag. to avoid saturation. We checked the light curves of all 55 of these objects for any signs of variability using a Lomb-Scargle periodogram via the ASTROML python package (Vanderplas et al., 2012) and derived *V* magnitudes based on the median value of those data (for objects with 3 or more epochs of data, see Figure 4.3 for an example). However, the median values we derived were, in most cases, much higher (0.5-1.0 mag.) than those catalogued in NOMAD and URAT1. This discrepancy is most likely down to the transformation from unfiltered photometry to *V* magnitudes. In this analysis we do not use the median magnitudes derived from Catalina photometry due to this large discrepancy. However, any variability or periodicity seen in an objects light curve is included as a flag in Table J2[2] and is discussed further in Section 4.5.8.

4.3.2 Previous searches for members of young associations

Some of the works listed in Table 4.2 and additionally other works are specifically concerned with identifying new members of the young associations. Below we note any overlap between our identified objects and other works. We are interested in not only

[1] `http://nesssi.cacr.caltech.edu/cgi-bin/getmulticonedb_release2.cgi`

[2] Due to the number of columns (43) in this table we have not included it in this manuscript. The table can be located using the online VizieR query service and Table ID: *J/A+A/590/A13/appene*.

TABLE 4.2: Surveys and catalogues cross-matched with the sample presented in this chapter.

Code	Reference	Parameters
NO04	Nordström et al. (2004)	RV
BA12	Bailey et al. (2012)	RV
EL14	Elliott et al. (2014), Chapter 2	RV
MA14	Malo et al. (2014)	RV, H_α, Li, L_x
RAVE	Kordopatis et al. (2013)	RV
DE15	Desidera et al. (2015)	RV, Li
RO13	Rodriguez et al. (2013)	RV, H_α, Li, NaI
RI06	Riaz et al. (2006)	RV,H_α,L_x/L_{bol},CaH1,2,3
BE15	Bell et al. (2015)	*V* mag.
IPHAS	Barentsen and et al. (2014)	H_α
GALEX	Bianchi et al. (2011)	NUV, FUV mag.
URAT1	Zacharias et al. (2015)	*R*,*B*,*V* mag.
CATA	Drake et al. (2009)	*V* mag. (+ variability)
ASAS	Pojmanski (2002)	*V* mag. (+ variability)
RO13	Rodriguez et al. (2013)	RV
SH12	Shkolnik et al. (2012)	RV
SC12	Schlieder et al. (2012b)	RV, SpT
SPM4	Girard et al. (2011)	*B*,*V* mag.
RE09	Reiners and Basri (2009)	RV, Li presence
RI15	Riviere-Marichalar et al. (2015b)	RV, H_α
M013	Moór et al. (2013)	RV, Li, H_α,L_x/L_{bol}
GO06	Gontcharov (2006)	RV, *V* mag.
DE12	de Bruijne and Eilers (2012)	RV
FR13	Frith et al. (2013)	RV
MO08	Morin et al. (2008)	RV
LO10	Looper et al. (2010)	RV
KH07	Kharchenko et al. (2007)	RV
HO91	Hoffleit and Jaschek (1991)	RV
LE13	Lépine et al. (2013)	H_α, CaH2,3
MO01a	Montes et al. (2001)	RV
LO06	López-Santiago et al. (2006)	RV, Li
MA10	Maldonado et al. (2010)	RV
WISE	Wright et al. (2010)	*W*1, *W*2, *W*3, *W*4
RI14	Riedel et al. (2014)	*V* mag.
VI56	Vyssotsky (1956)	*V* mag.
ME06	Mermilliod (2006)	*V* mag.
LA01	Lawson et al. (2001)	*V* mag.
KH09	Kharchenko et al. (2009)	*V* mag.
NOMAD	Zacharias et al. (2005)	*B*,*V*, *R* mag.
WDS	Mason et al. (2001)	Multiplicity
MA13	Malo et al. (2013)	RV,H_α,Li
GSC	Lasker et al. (2008)	*B*,*U*,*V* mag.
TYC	Høg et al. (2000)	*B*,*V* mag.
3XMM	Xmm-Newton Survey Science Centre (2013)	X-ray: flux
CHAN	Evans et al. (2010)	X-ray: flux
BSC	Voges et al. (1999)	X-ray: counts, HR
FSC	Voges et al. (2000)	X-ray: counts, HR

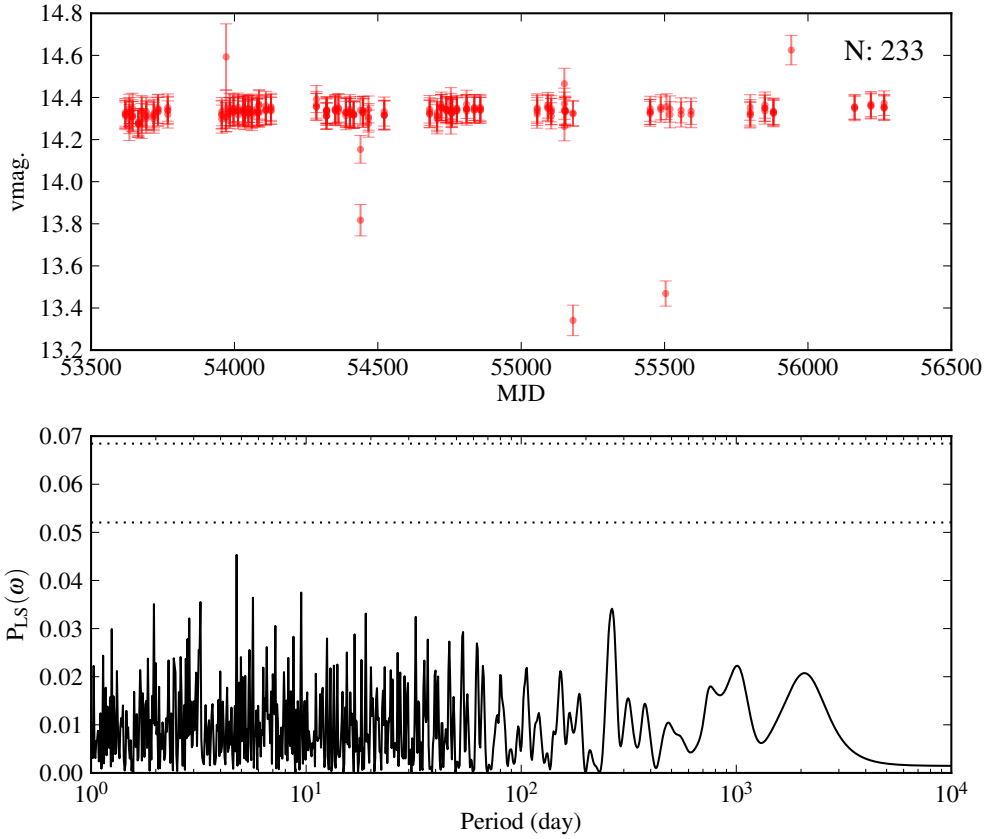

FIGURE 4.3: *Top panel:* The light curve of optical magnitudes for a candidate member in our sample (2MASS J02103888-4557248), N is the total number of data points. *Bottom panel:* The Lomb-Scargle periodogram for the data presented in the top panel. The dashed lines represent the levels of significance: 1 σ and 5 σ.

confirming the youth of the objects but additionally to analyse their radial velocity agreement with their associated known member.

- Malo et al. (2013): There were two objects identified here that are in common (2MASS J01034210+4051158, 2MASS J21100535-1919573). Both objects have compatible radial velocity values with their associated primary stars.

- Gagné et al. (2015): We found one object in common (2MASS J11020983-3430355), which was also identified in Teixeira et al. (2008) and is discussed in more detail in Section 4.8. This object has compatible radial velocity with its associated primary.

- Shkolnik et al. (2012): There were 3 objects in common (2MASS J01034210+4051158, 2MASS J04373746-0229282, 2MASS J12573935+3513194). The radial velocity values were consistent with their primary stars for the first two sources. The third source is a spectroscopic binary and therefore its radial velocity is not consistent with its associated primary star, see Section 4.7. Due to a lack of data its system velocity cannot be derived at this time.

- Schlieder et al. (2012b): We found one object in common (2MASS J05015665+0108429) which has compatible radial velocity with its associated primary.

- Rodriguez et al. (2013): We found one object in common (2MASS J02105345-4603513) which is most likely a spectroscopic binary. The target has an incompatible radial velocity and is discussed in more detail in Section 4.7.

- Kraus et al. (2014): Although we included the bonafide member list from this analysis we did not include identified candidate members. There was one successful match with these candidate members (2MASS J00302572-6236015). This source has compatible radial velocity with its associated primary.

- Alonso-Floriano et al. (2015): The authors identified 36 potential wide binaries, 16 of these systems only had one stellar component previously classified as a member of the β-Pic moving group. In this analysis we recovered 15/16 of these new identifications. The one detection we did not recover we conclude is not a physical wide companion (V4046 Sgr – GSC 07396-00759), see Section 4.8 for details.

4.4 Spectroscopic parameters and observations

High-resolution optical spectra allow us to compute radial velocity values and look for signatures of youth. In the following analysis we computed EWs for the gravity-sensitive

atomic alkali lines of K I (7699 Å) and NaI (8194.8 Å), see Martin (1997), H_α – associated with activity and lithium, used as an age indicator – Barrado y Navascués et al. (1999); Binks and Jeffries (2014).

To produce the spectroscopic quantities described above we used the line-fitting method described in Bayo et al. (2011). This automatic line measurement procedure has been improved and includes a local pseudo-continuum iterative identification process and Monte Carlo solutions on the latter to take into account the normalisation contribution to the uncertainties of the line measurements.

4.4.1 Existing observations

We searched the public archives of 4 high resolution spectrographs (UVES/VLT, FEROS/2.2m, HARPS/3.6m, HIRES/KECK). We found one HARPS spectrum for target 2MASS J23485048-2807157 (Prog. ID: 92.C-0224) and one HIRES spectrum for target 2MASS J02455260+0529240 (Prog. ID: U033Hr). The radial velocities were computed using a binary mask (SpT: K0) to produce a cross-correlation function (CCF) as described in Queloz (1995) and Chapter 2. The spectroscopic quantities are shown in Table 4.3. We could not compute EWs for Na I or K I for the HARPS observation due to the wavelength coverage of the spectrum (3780–6910 Å).

4.4.2 New observations

To further classify identified candidates we obtained new high resolution spectra using HERMES/Mercator and FEROS/2.2 m. The details of the observations are presented below.

HERMES: Spectroscopic observations were obtained at the 1.2 m Mercator Telescope at the *Observatorio del Roque de los Muchachos* (La Palma, Spain) on 14-18 December 2015 with HERMES, High Efficiency and Resolution Mercator Echelle Spectrograph (Raskin et al., 2011). Using the high resolution mode (HRF), the spectral

resolution is 85000 and the wavelength range is from λ3800 Å to λ8750 Å approximately. All the obtained *echelle* spectra were reduced with the automatic pipeline (Raskin et al., 2011) for HERMES. We were limited to brighter targets to keep the integration times below 2000 seconds for a signal-to-noise ratio (SNR) $\geq$30 at 6500 Å. When the observations were taken we were not aware that 3 / 4 of these targets had existing radial velocity values. However, with the newly obtained spectra we were able to compare our values to those of the literature, increase our sensitivity to single-lined spectroscopic binaries and additionally calculate EWs of spectral lines.

FEROS: We observed 5 newly identified candidate members using FEROS on 25-12-2015. These observations were taken with the standard FEROS setup (2″fibre aperture, R$\sim$48,000, 3600-9200 Å) in OBJCAL mode, using the ThAr+Ne lamp for simultaneous wavelength calibration. The targets were faint (V$\approx$13-14.8 mag.) and therefore the SNR was low ($\leq$20). To calculate accurate radial velocities for these spectra we used a dedicated pipeline built from a modular code (CERES, Brahm et al. in prep.) capable of processing data in a homogeneous and optimal way coming from different echelle spectrographs. A description of a similar pipeline developed for the Coralie spectrograph can be found in Jordán et al. (2014). This FEROS pipeline is able to achieve a long term RV precision of 5 m/s in the high SNR limit. In the case of low SNR data ($\sim$20), its optimal extraction routine, coupled to the careful treatment of systematics allow it to obtain RV precisions of $\sim$20-30 m/s. In order to increase the accuracy of the wavelength solution, the bluest ($\lambda < 3900$ Å)and reddest ($\lambda > 6700$ Å) orders are not used. Some features such as the NaI and K I doublets are in the reddest orders and therefore are unavailable in these 1D reduced spectra. For calculation of all EWs and indices from molecular bands we used the standard reduced products from the MIDAS pipeline. Unfortunately the low SNR of our observations prevented us from continuum identification and extraction in several wavelengths regions. One of these regions was Li I (6708 Å) which is affected by a strong Ar emission line originated from the contiguous comparison fibre. We therefore do not analyse the Li I region from these FEROS spectra.

A summary of the observations and derived spectroscopic properties are shown in Table 4.3 for the HERMES and FEROS observations.

4.5 Properties of candidates from our search

Discussions of individual objects with discrepant/dubious spectroscopic parameters (denoted by a ”N” or ”?” in *Member?* column of Table 4.4) can be found in Section 4.7. The detailed spectroscopic, kinematic and photometric properties of all identified targets and their respective references can be found in Table J2. For a brief summary of the 84 targets identified in this analysis and their membership status see Table 4.4. Below we compare individual kinematic, spectroscopic and photometric properties of identified targets with our original sample and other young sources to assess the success of our method.

Spectral types were calculated by converting effective temperatures using the relationship for pre-main sequence stars from Pecaut and Mamajek (2013). The effective temperatures were derived from fitting the SEDs (produced using the VOSA tool Bayo et al., 2008) with the evolutionary models of Baraffe et al. (2015).

TABLE 4.3: Summary of targets and their derived properties for high resolution spectra analysed in this analysis.

2MASS ID	RV ($km\,s^{-1}$)	Na I (8194.8) (Å)	K I (7699) (Å)	H_α (Å)	Li I (mÅ)	T_{eff} (K)	SpT	SpT ref.	Obs.
01334282-0701311	-14.934±0.003	0.26±0.01	0.17±0.01	2.00±0.11	64±3	5830	G1	1	HERMES
01373545-0645375	11.689±0.002	0.329±0.026	0.210±0.003	1.202±0.101	101±10	5200	G6	2	HERMES
03281095+0409075	10.952±0.667	0.146±0.048	0.196±0.044	2.727±0.329	124±16	5900	F6	2	HERMES
04373746-0229282	22.047±0.031	1.052±1.162	0.769±0.034	-2.142±0.127	61±23	3750	M1.1	3	HERMES
01354915-0753470	6.487±0.029	0.69±0.09	0.69±0.05	-0.06±0.02	...	3500	M4	4	FEROS
03074909-2750467	16.512±0.171	1.21±0.08	1.21±0.13	-12.80±1.11	...	3500	M4	4	FEROS
04515223-4640497	51.188±0.019	0.35±0.03	0.49±0.05	-0.03±0.01	...	4800	K6	4	FEROS
07013945-4231370	24.339±0.025	-0.001±0.002	0.45±0.07	0.33±0.22	...	4300	K4	4	FEROS
08371456-5517343	81.314±0.019	-0.15±0.07	0.001±0.001	0.70±0.10	...	4850	K9	4	FEROS
23485048-2807157	7.430±0.032	...	...	1.63±0.17	140±10	5200	G8	2	HARPS
02455260+0529240	88.502±0.053	...	0.912±0.039	-2.462±0.216	...	3100	M1	2	HIRES

References. 1: Gray et al. (2006), 2: T_{eff} conversion from VOSA spectral energy distribution (Bayo et al., 2008), 3: Shkolnik et al. (2012), 4: estimation from FEROS data reduction.

4.5.1 Identification of existing members as wide companions

Using our method we identified known members of the moving groups as potential wide companions to other known members in our sample. This effectively reduced our sample size of primaries, from 581 to 567. We used these sources to check whether our method based on 2MASS photometry and proper motion is consistent for sources with derived photometric distances and galactic velocities. Table 4.5 summarises the results and notes any companions to the sources that could affect their photometry ($<3''$) and therefore their distance estimation. The uncertainties on the galactic velocities are $\sim$1 kms^{-1}. To quantify the agreement between components in these 14 cases we first calculated the standard deviation of (U, V, W) galactic velocities for the known members in each association. We compared this to the magnitude of the differences between the galactic velocities grouped as in Table 4.5. We found that 13/14 targets had dispersions below the standard deviation of their respective association, the left panel of Figure 4.4 shows this result graphically. Additionally, the right panel shows the photometric distances derived between the primary and its associated companion for all 14 systems. These two results are a very good indication that these targets do in fact form physically wide multiple systems rather than being the result of a projection effect due to the spatial density of stars. The formation, abundance and dynamical evolution of wide binaries in the young associations is discussed in Chapter 5. We do not refer to these targets as *identified in this analysis*, they form part of the *original sample* in any discussion presented here.

4.5.2 Radial velocities

In Figure 4.5 we show a comparison of radial velocities between targets identified in this analysis (companions) and their associated known member for the 23 targets with both measurements. If these companions did form very wide binary systems with their associated known member we would expect a 1:1 relation between the two quantities, within uncertainties. As can be seen, we do indeed see this relation for the majority of targets (18/23). As these targets share the same proper motion and radial velocity, by

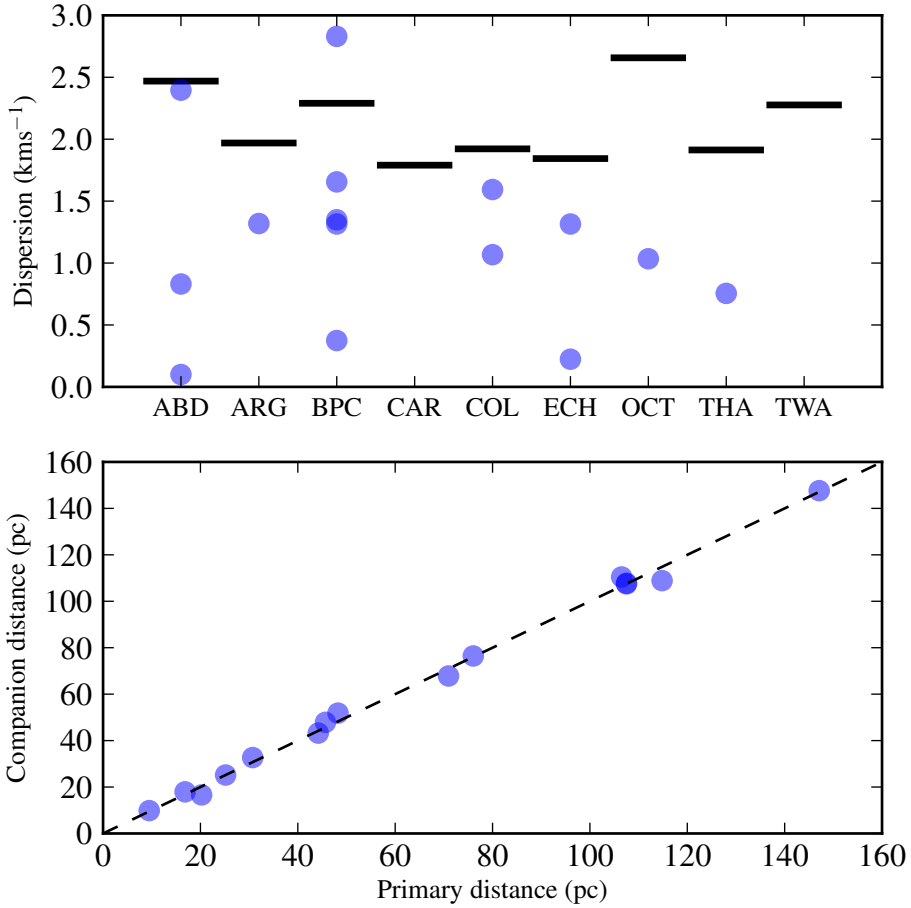

FIGURE 4.4: *Top panel*: The black markers represent the absolute value of the standard deviation in galactic velocities (U, V, W) for each association. The blue markers are the absolute difference between companions and their associated primary star, shown in Table 4.5. *Bottom panel*: The photometric distances derived from the convergence method for companions and their associated known member.

assuming the same distance, they share the same galactic velocity. Some of the known members are part of spectroscopic binary systems, these are indicated by crosses in Figure 4.5. The plotted radial velocities of the known members are the gamma (system) velocities and therefore the effect of the spectroscopic component has been accounted for. The quality of this correction depends on how much of the orbital phase has been covered by previous radial velocity observations. However, as shown by the agreement between the values this does not have a significant effect. The suspected single-lined spectroscopic binary 2MASS J02105345-4603513 is highlighted by an open black circle and discussed, along with the other four discrepant targets in Section 4.7.

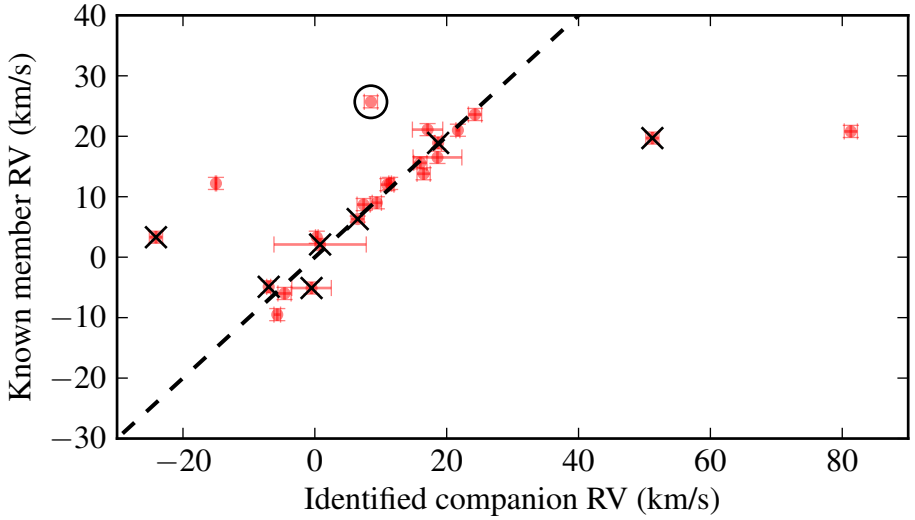

FIGURE 4.5: Radial velocity of identified targets in this analysis versus radial velocity our their associated known member. The dotted line represents a 1:1 relation in the quantities. Crosses indicate the presence the known member is a spectroscopic binary (plotted radial velocity is the system(gamma) velocity). The open circle represents the suspected single-lined spectroscopic binary 2MASS J02105345-4603513.

4.5.3 Identification of young objects combining GALEX, 2MASS and WISE photometry

Some previous works have focussed on identifying new late-type members (M0-M5) detecting their predicted enhanced UV emission (Shkolnik et al., 2012; Rodriguez et al., 2013). The convective envelopes of these low-mass stars stars combined with their differential rotation produces strong magnetic dynamos. These dynamos lead to enhanced chromospheric and coronal activity which increases UV emission and X-ray emission (see Section 4.5.4), respectively.

Rodriguez et al. (2011) combined near-IR photometry with UV emission to identify young, late-type (M0-M5) stars in Upper Scorpius and TW-Hydrae. The dotted lined-box in Figure 4.6 shows the criteria imposed Rodriguez et al. (2013) to identify new members using NUV and infrared photometry. We have plotted identified candidates and known members that have all the necessary photometry (NUV, J, $W1$ and $W2$).

The few identified targets that have photometry in all four bands are either compatible i.e. candidate young M dwarfs within the boxed area or consistent with previous members of earlier spectral type. Additionally, three of the targets matching this criteria have X-ray detections. These sources have the largest L_x/L_{bol} values shown in Figure 4.7 (smaller than -3) for targets identified in this analysis. Objects matching the criteria are noted in Table 4.4. Note the success rate of this technique, as derived in Rodriguez et al. (2013), was $\approx$75%.

4.5.4 X-ray sources

The original SACY sample was constructed from optical counterparts to X-ray bright sources from the ROSAT all-sky survey (BSC, Voges et al., 1999). We additionally queried the faint X-ray catalogue of ROSAT (FSC, Voges et al., 2000), the serendipitous source catalogue of XMM (3XMM, Xmm-Newton Survey Science Centre, 2013) and the Chandra source catalogue (CSC, Evans et al., 2010).

4.5.4.1 X-ray emission

3XMM is the most recent serendipitous source catalogue from pointed observed using XMM-Newton. Using Figure 8 of Watson et al. (2009) (2XMM catalogue) the lower limit of X-ray flux (0.2-2.0 keV) ranges between $10^{-15} - 10^{-14}$ erg cm^{-2} s^{-1}, depending on the sky coverage. On average the XMM catalogue provides fluxes one order of magnitude fainter than ROSAT (Voges et al., 1999). We cross-matched our detections with 3XMM for sources within 6″– an upper search radius encompassing >99% of positional uncertainties, see Figure 11 of Watson et al. (2009). We additionally searched the Chandra source catalogue (Evans et al., 2010) for sources within 5″using the CSCview[3] program to access data in the 0.2-2.0 keV energy regime. Our search yielded 5 sources with X-ray data (3: XMM, 1: FSC, 3: BSC, 1: CSC).

[3] http://cda.cfa.harvard.edu/cscview/

In the case of ROSAT data we converted the count rate and hardness-ratio (HR1) to X-ray flux using the formulation of Fleming et al. (1995), these values are for energies in the range 0.1-2.4 keV. For CSC and XMM data the fluxes are available in the catalogues directly and we used the energies in the range 0.2-2.0 keV to calculate total fluxes for an approximately equal comparison to fluxes derived from ROSAT data. We converted the fluxes to luminosities assuming the distance to the target was that of its associated known member.

We calculated bolometric luminosities of our targets using the VOSA tool (Bayo et al., 2008) which collates multi-band photometry from many reliable catalogues and fits both evolutionary models and black-body curves. The values were calculated based on best-fit atmospheric models (Allard et al., 2012) using available photometry and are listed in Table J2. For the 9 members identified in this analysis with available X-ray data we calculated the X-ray to bolometric luminosity ratio (Lx/L_{bol}). Three additional sources had a previously calculated values from Riaz et al. (2006) and Rodriguez et al. (2013) which we also used. The results are presented in Figure 4.7.

TABLE 4.4: Basic properties and membership status of identified targets.

2MASS identifier	Dist. [a] (pc)	SpT	V (mag.)	K (mag.)	Mass ($M_\odot$)	$\mu_{\alpha,*}$ (mas/yr)	μ_δ (mas/yr)	Ass.	Quantity [b]	Ref.	Mem? [c]
00341993+2528147	49.9	M4	...	10.7	0.23	90.7 ± 4.1	-105.3 ± 4.1	ABD			...
01034210+4051158	29.6	K7	12.9	8.5	0.41	132.0 ± 8.0	-164.0 ± 8.0	ABD	H_α, X, CaH, UV	1, 5	Y
02103888-4557248	73.7	K5	14.6	11.4	0.25	48.2 ± 1.6	-1.5 ± 1.6	ABD	Fl	5	...
02105345-4603513	73.7	M4	15.2	10.3	0.44	53.2 ± 1.8	-10.2 ± 1.8	ABD	RV, X, UV	2	Y?
02123342+2356379	36.6	M4	17.0	11.0	0.12	131.0 ± 8.0	-158.0 ± 8.0	ABD			...
02484213+2716185	50.7	M5	18.8	13.8	0.04	62.4 ± 5.2	-127.3 ± 5.2	ABD			...
03331403+4615194	34.3	F5	11.8	7.6	0.63	64.7 ± 4.0	-172.4 ± 3.6	ABD	RV, H_α, CaH	14	Y
04080429+0143548	55.3	K9	14.5	10.9	0.23	29.9 ± 4.6	-88.7 ± 5.2	ABD			...
04575034-0652070	45.0	M2	15.6	11.3	0.14	41.3 ± 4.3	-103.1 ± 5.2	ABD			...
05060187-1543564	78.9	M1	...	14.1	0.05	18.7 ± 4.0	-50.2 ± 4.1	ABD			...
05105505-0410563	76.9	M4	15.9	10.8	0.38	19.0 ± 3.4	-54.4 ± 3.7	ABD			...
05274075-0930438	21.9	M3	...	9.7	0.14	61.6 ± 5.1	-172.7 ± 5.1	ABD			...
05454276-1450198	75.8	M4	...	13.6	0.06	10.7 ± 4.1	-51.6 ± 4.1	ABD			...
07285117-3015527	15.7	M4	13.4	8.1	0.25	-45.7 ± 3.4	17.2 ± 3.5	ABD	RV	9	Y
07435039-7940252	80.6	K9	16.2	12.4	0.15	-6.7 ± 3.8	49.3 ± 3.9	ABD			...
07453522-7940136	80.6	F5	12.1	8.9	0.82	-16.5 ± 2.5	42.2 ± 2.5	ABD			...
09281506-7815223	116.5	F5	8.6	7.7	0.22	-25.8 ± 1.1	21.9 ± 1.1	ABD			...
12573935+3513194	19.3	M4	13.0	8.0	0.33	-281.8 ± 3.6	-147.0 ± 6.7	ABD	RV, CaH, H_α	4, 14	Y?
17360095-1320580	46.3	M0	15.3	11.7	0.11	-4.1 ± 6.0	-108.7 ± 6.3	ABD			...
23270114+0055200	47.2	K5	14.0	10.6	0.23	80.3 ± 3.9	-99.2 ± 3.9	ABD			...
23485048-2807157	42.2	G8	9.1	7.1	0.87	99.2 ± 0.9	-100.9 ± 1.7	ABD	RV, Li, H_α, X	5	Y
23514340+3127045	42.8	M4	14.1	9.5	0.38	96.5 ± 3.3	-86.6 ± 3.6	ABD	UV	5	Y
03262220+2313122	16.9	M4	16.4	10.7	0.04	247.0 ± 8.0	-96.0 ± 8.0	ARG	Fl	5	...
06494841-2858025	120.8	M4	15.6	11.5	0.30	-15.7 ± 4.3	20.0 ± 4.3	ARG			...
07013945-4231370	101.0	K4	13.9	10.9	0.38	-9.9 ± 1.1	34.6 ± 1.1	ARG	KI, RV, H_α	5	Y
07283006-4908589	82.8	F8	8.8	7.6	1.18	-25.4 ± 0.8	48.8 ± 1.3	ARG	RV, Li	5, 6	Y
08374680-5252307	152.3	K2	14.5	12.3	0.28	1.7 ± 1.9	6.2 ± 1.8	ARG			...
09394669-2133023	93.3	M5	18.0	14.4	0.04	-41.4 ± 4.0	15.8 ± 4.0	ARG			...
01334282-0701311	24.0	G1	5.8	4.3	0.97	175.2 ± 1.0	-82.3 ± 1.0	BPC	RV, Li	5, 16	N
01354915-0753470	37.9	M4	13.8	9.8	0.13	88.6 ± 5.1	-42.2 ± 5.1	BPC	H_α, KI, RV	5	Y?
01373545-0645375	24.0	G6	7.7	5.8	0.89	171.3 ± 1.0	-98.5 ± 1.0	BPC	X, RV, Li, H_α	5, 15, 16	Y
02160734+2856530	39.5	M2	15.7	11.6	0.04	92.9 ± 3.1	-64.0 ± 3.2	BPC			...
04373746-0229282	29.4	M1	10.6	6.4	0.78	45.9 ± 1.3	-63.6 ± 1.2	BPC	Li, RV, CaH, H_α, KI, X	1, 4	Y
05015665+0108429	24.2	M4	12.9	7.7	0.28	33.2 ± 2.2	-89.1 ± 3.1	BPC	X, RV, CaH, H_α	5, 7, 14	Y
05195327+0617258	71.0	M5	18.3	12.4	0.05	13.7 ± 4.0	-38.1 ± 4.0	BPC	X	5	Y
14141700-1521125	30.2	M3	15.6	8.8	0.18	-117.4 ± 8.0	-196.6 ± 8.0	BPC	UV	5	Y
17483374-5306118	71.0	M2	13.7	9.3	0.47	-2.5 ± 2.0	-51.7 ± 2.0	BPC			...
18011138-5125594	48.1	M0	14.8	11.3	0.07	-9.8 ± 5.2	-84.5 ± 5.1	BPC			...
18420483-5554126	51.9	M4	15.1	9.9	0.20	13.4 ± 3.5	-73.9 ± 3.7	BPC	H_α, X, CaH, UV	1, 5	Y
18480637-6213470	52.4	F6	7.3	6.1	1.26	16.1 ± 2.0	-80.3 ± 2.0	BPC	Li, RV	8	Y
18580464-2953320	82.6	M3	12.8	8.8	0.75	15.4 ± 2.4	-45.6 ± 2.4	BPC	RV	8	Y
19223409-5429181	48.3	M0	14.0	10.7	0.10	32.0 ± 2.4	-87.8 ± 2.5	BPC			...
20085122-2740536	48.0	M3	16.3	11.8	0.05	40.4 ± 4.0	-61.7 ± 4.0	BPC			...
20321797-2600432	48.3	M5	18.6	13.0	0.01	50.0 ± 4.9	-70.1 ± 4.9	BPC			...
21100461-1920302	32.6	M4	13.1	7.6	0.47	87.0 ± 1.4	-94.4 ± 3.1	BPC	RV, UV	5, 9	Y
21212446-6654573	30.2	G9	9.0	6.4	0.84	90.5 ± 1.0	-90.9 ± 1.6	BPC	X, RV	5, 17	Y?
02590322-4232450	103.3	M3	15.0	10.3	0.52	41.1 ± 2.3	0.0 ± 1.5	CAR	UV	5	Y
03074909-2750467	54.6	M4	12.5	10.2	0.24	59.6 ± 5.3	-16.4 ± 17.6	CAR	RV	5	Y
08371456-5517343	180.8	K9	13.9	10.3	0.79	-7.9 ± 1.8	9.7 ± 1.9	CAR	H_α, RV	5	N
09594633-7227360	83.6	M2	15.8	12.0	0.13	-37.4 ± 3.4	23.0 ± 3.4	CAR			...
01525509-5222266	83.4	M1	17.0	12.4	0.09	52.6 ± 7.0	-7.5 ± 7.0	COL			...
02005969-1608428	80.9	M4	18.0	13.9	0.04	51.1 ± 4.9	-25.0 ± 4.9	COL			...
02015050-1614575	80.9	M2	16.7	13.7	0.04	50.0 ± 3.8	-30.6 ± 3.8	COL			...

2MASS identifier	Dist. [a] (pc)	SpT	V (mag.)	K (mag.)	Mass ($M_\odot$)	$\mu_{\alpha,*}$ (mas/yr)	μ_δ (mas/yr)	Ass.	Quantity [b]	Ref.	Mem? [c]
03212872-1048588	128.1	M3	...	13.7	0.08	24.7 ± 4.0	-28.2 ± 4.0	COL			...
03255277-3601161	107.5	M4	15.4	10.6	0.47	33.9 ± 2.8	-4.1 ± 2.8	COL			...
03281095+0409075	81.5	F6	8.8	7.2	1.26	46.7 ± 0.7	-37.0 ± 0.8	COL	RV, Li	5	Y
03400260+5441003	35.4	M5	17.7	12.0	0.04	102.0 ± 4.0	-109.2 ± 4.0	COL			...
03471077+5138276	57.5	M2	15.6	11.8	0.09	60.1 ± 3.7	-67.5 ± 3.8	COL			...
04423261+0905471	105.6	M3	15.8	11.0	0.37	31.7 ± 3.9	-41.3 ± 3.9	COL			...
04515223-4640497	68.1	K6	14.3	11.7	0.13	27.7 ± 2.5	17.1 ± 2.6	COL	H_α, RV	5	N
05005830-4100023	76.3	M4	14.7	9.6	0.54	32.6 ± 1.5	9.6 ± 2.8	COL			...
05301939-1916161	115.1	K2	...	9.1	0.86	17.8 ± 3.1	-0.6 ± 2.3	COL			...
05374880+0233088	70.8	M3	14.2	9.5	0.52	16.8 ± 3.7	-44.6 ± 4.0	COL			...
09151348-7605020	117.5	K2	9.4	6.9	1.17	-31.2 ± 1.0	23.3 ± 1.0	ECH			...
12201867-7417202	114.8	M0	15.0	11.6	0.07	-39.5 ± 3.1	7.7 ± 3.0	ECH			...
02174439+3330409	34.5	M3	16.3	11.8	0.05	44.8 ± 4.1	-52.5 ± 4.1	OCT			...
06251922-6630435	126.1	M2	16.4	12.1	0.22	-13.0 ± 3.8	25.4 ± 3.3	OCT			...
17420077-8608464	132.0	K5	12.9	9.6	0.80	9.2 ± 1.2	-25.5 ± 1.2	OCT			...
23315208+1956142	6.1	M4	10.3	5.3	0.26	543.2 ± 1.6	-44.6 ± 1.6	OCT	H_α, RV, CaH, X	5, 10, 14	Y
00230961-6139143	44.6	M3	16.7	12.2	0.04	79.8 ± 2.7	-49.3 ± 2.6	THA			...
00302572-6236015	42.5	M4	12.2	7.5	0.71	95.2 ± 0.9	-48.0 ± 0.9	THA	Li, H_α, RV	11	Y
02455260+0529240	54.3	M1	13.4	9.2	0.41	71.9 ± 2.9	-41.5 ± 3.0	THA	RV, UV	5	N
03153814-0339004	49.2	M3	16.8	12.1	0.05	65.4 ± 4.2	-47.4 ± 4.2	THA			...
03365153-4957314	43.3	K5	12.4	9.8	0.20	124.5 ± 2.2	-75.7 ± 2.1	THA			...
03484041-3738198	50.7	M2	13.3	8.7	0.51	79.0 ± 1.1	-4.5 ± 1.1	THA	X, RV	5, 12	Y
04354718-1210374	62.3	M3	...	12.0	0.08	58.0 ± 4.8	-26.4 ± 4.2	THA			...
04485254-5043145	54.8	M3	16.9	12.2	0.06	43.6 ± 5.3	19.0 ± 5.0	THA			...
05154763-0931041	77.5	M5	17.8	14.0	0.03	39.5 ± 5.6	-8.0 ± 5.6	THA			...
06350229-6951519	68.4	K2	11.9	8.6	0.72	21.8 ± 1.5	41.6 ± 1.4	THA	RV	9	Y
11020983-3430355	51.0	M8	21.2	11.9	0.02	-77.0 ± 9.5	-19.5 ± 9.5	TWA	H_α, CaH	13	Y
11130416-4516056	96.2	M0	15.7	11.7	0.08	-41.0 ± 3.2	4.0 ± 3.0	TWA	Fl	5	...
12073145-3310222	53.8	K9	14.5	11.0	0.06	-62.7 ± 1.8	-32.3 ± 1.4	TWA	Fl	5	...
12090628-3247453	53.8	M1	16.1	12.0	0.02	-68.1 ± 2.0	-40.2 ± 2.7	TWA			...
12354893-3950245	73.0	M5	12.1	8.9	0.42	-48.6 ± 1.7	-21.3 ± 1.6	TWA	X	5	Y

Notes. [a] Distance taken from the bonafide member which the target is associated with.[b] Optical flaring from Catalina photometry (Fl) is not used to asses the membership of targets.[c] Based on quantities listed in column *Quantity*: consistent radial velocity (RV), H_α EW (H_α), Li absorption (Li), X-ray emission (X), UV/IR photometric criteria discussed in Section 4.5.3: UV, CaH indices (CaH). Those systems with either a flag of "?" or "N" are discussed in Section 4.7.

References. 1: Riaz et al. (2006), 2: Rodriguez et al. (2013), 3: Kharchenko et al. (2007), 4: Shkolnik et al. (2012), 5: this analysis, 6: Desidera et al. (2015), 7: Schlieder et al. (2012b), 8: Moór et al. (2013), 9: Kordopatis et al. (2013), 10: Morin et al. (2008), 11: Kraus et al. (2014), 12: Hoffleit and Jaschek (1991), 13: Kordopatis et al. (2013), 13: Scholz et al. (2005), 14: Lépine et al. (2013), 15: Delorme et al. (2012), 16: Gontcharov (2006), 17: Torres et al. (2006)

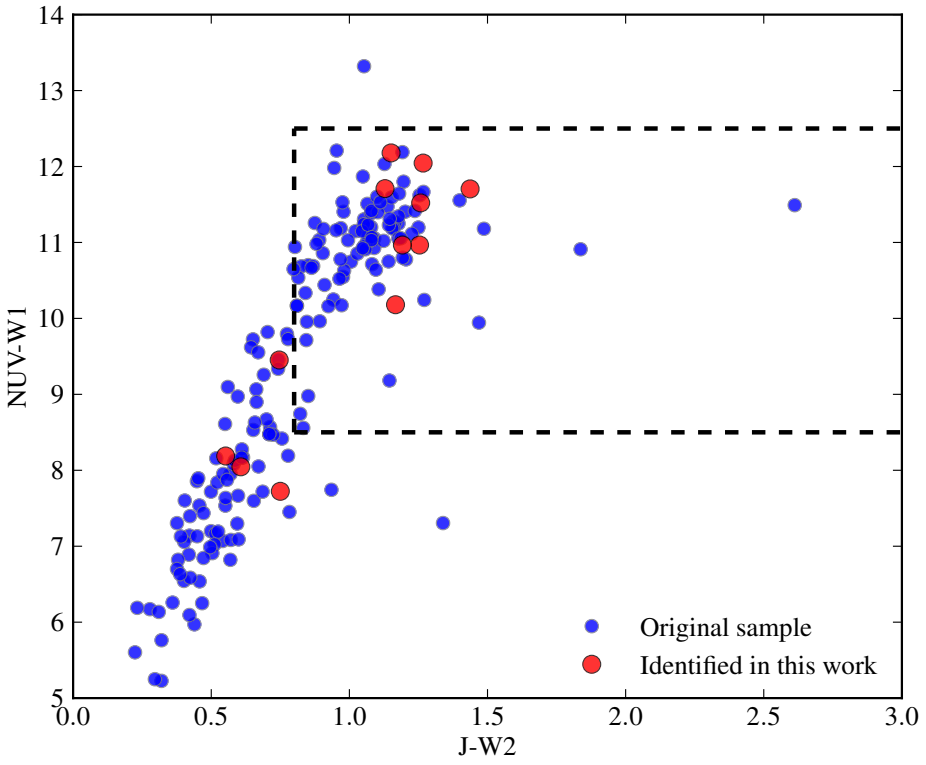

FIGURE 4.6: Colour-colour diagram for *J*-*W*2, NUV-*W*2 for new (red) and known (blue) members of the moving groups. The boxed area represents the criteria described in Rodriguez et al. (2013) used to classify potential young M dwarfs.

Typical values for young (<100 Myr) sources are 10^{-5} – 10^{-3}, with saturation at $\approx 10^{-3}$ (Riaz et al., 2006; Zuckerman et al., 2004). One source (GJ 3305 AB) was identified previously as an X-ray bright, wide component (66″) to HD 29391 by Feigelson et al. (2006). The ratio we calculate in this analysis is in agreement with that derived previously.

Ten of the twelve sources are clearly consistent as they have ratios of -3.5 or lower. The target at (5.9, -4.3) is a proposed member of AB Doradus (2MASS J23485048-2807157), given its colour and age (estimates range from 100-145 Myr for the moving group) it is still not ruled out as a young source from analysis of its X-ray emission (see Figure 4 of Zuckerman et al. (2004)). Additionally it has strong lithium absorption and consistent radial velocity with its associated primary. The remaining source (2MASS J05195327+0617258, at 2.0, -3.8) has a very low estimated mass (0.05 $M_{\odot}$) and is a

proposed member of the β-Pic moving group. We did not find any additional information on this object, however its calculated ratio is still consistent with being a young member.

4.5.4.2 X-ray non-detections

Using the all sky ROSAT surveys (RASS, Voges et al., 1999, 2000) we also investigated non-detections based on expected Lx/L_{bol} values for young sources. As shown in Figure 4 of Zuckerman et al. (2004) young sources with a B-V colour $>$0.7 mag have Lx/L_{bol} values larger than -3.5. From our analysis, Figure 4.7, we see the majority of sources also have values -3.5 or larger. We used the bolometric luminosities calculated using VOSA (Bayo et al., 2008) for the 50 sources in the colour range B-V$>$0.7 mag. to calculate expected X-ray fluxes (f_x =L_{bol} $\times$ $10^{-3.5}/4\pi D^2$) based on this ratio. The detection limit of RASS is $\approx 2\times10^{-13}$ erg s^{-1} (Schmitt et al., 1995), 44/50 targets had predicted fluxes below this limit. For the six sources with apparent non-detections we re-queried the RASS catalogues, extending the search radius beyond the positional error. Two of the six had nearby detections that were extremely extended, causing the positional offset of the source to lie within the radius of the detection which could account for an apparent non-detection in this region. We do not use the further 4 non-detections as a further youth constraint of the objects as one cannot be certain if these are reliable non-detections from the catalogue data. For reference, the BSC catalogue has sky coverage of 92% at a brightness limit of 0.1 cts s^{-1} (Voges et al., 1999).

4.5.5 Gravity-sensitive features

We were able to calculate Na I and K I EWs for 11 objects from our spectroscopic observations. Figure 4.8 shows the results for the EWs of K I for objects identified here and objects studied in Shkolnik et al. (2011) – a work focussed on identifying nearby ($<$25 pc) young M-dwarfs. We only show objects classified as M0 or later, the region where K I EWs distinguish between younger and older populations. All four objects

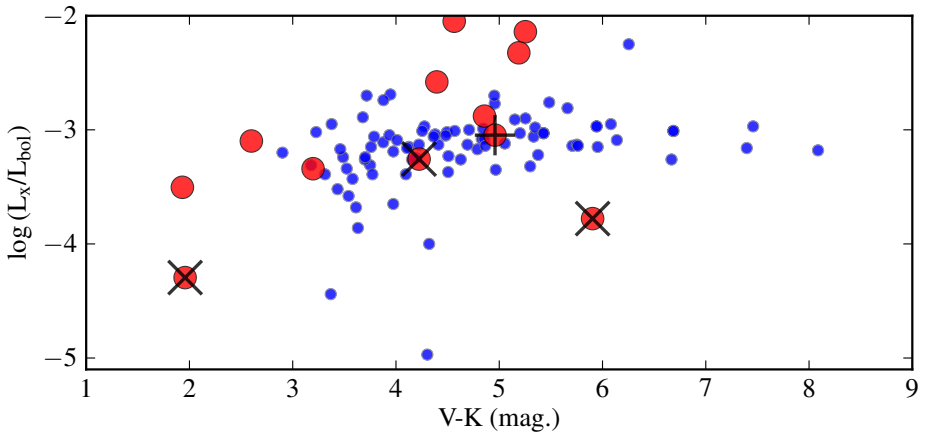

FIGURE 4.7: *V*-*K* colour versus log (Lx/L_{bol}) for the original sample (blue) and for targets identified in this analysis (red). The crosses represent targets identified as close ($<$0.3″) binaries, the luminosities are not corrected for unresolved components. The plus symbols represent sources with a variability flag in the 3XMM catalogue.

have EWs consistent with youth, including the radial velocity-discrepant target 2MASS J02455260+0529240.

Given the SNR and wavelength coverage of the available spectroscopic observations we could only estimate EWs of Na I (8194.8 Å) for spectral types earlier than ≈M2. Slesnick et al. (2006) verified that the Na I strength saturates for spectral types earlier than M2. Additionally the work of Schlieder et al. (2012a) verified that this feature is only useful for colours $V-K \geq 5$. We therefore have not used this quantity in assessing the membership status of these objects. The values are listed in Table 4.3 for reference.

The visible spectra of M dwarfs are dominated by molecular bands (titanium oxide: TiO and calcium hydride: CaH). Mould (1976) showed that these bands are gravity-sensitive. To quantify the strength of these bands Reid et al. (1995) defined a series of band indices including CaH2 are CaH3. These indices measure the ratio of on-band to off-band flux. We were unable to calculate these spectral indices using our own high-resolution spectra due to low SNR. However, we have collated values from other works the result of which are shown in Figure 4.9. The dotted and solid lines represent the lower envelopes of indices for BPC and ABD, respectively. There is a large amount of

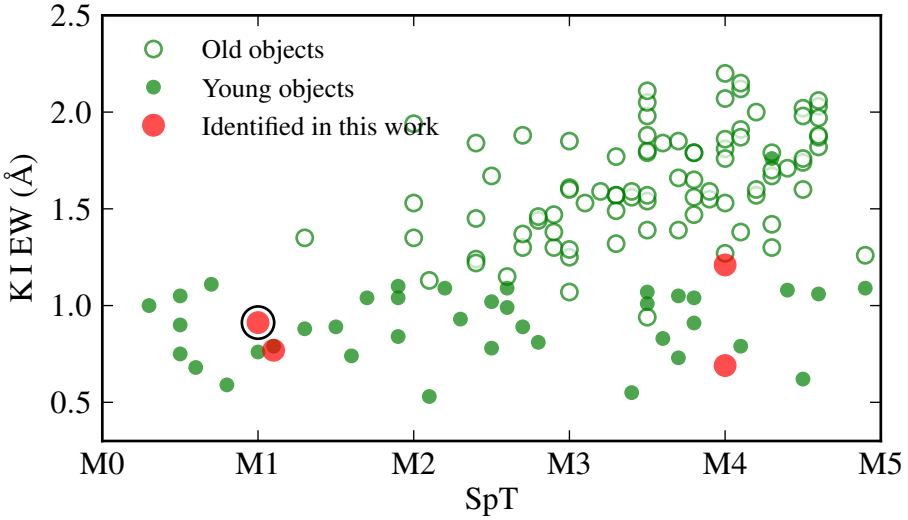

FIGURE 4.8: Spectral type versus EW of K I. Green open and filled circles are for old and young objects from Shkolnik et al. (2011), respectively. Red filled circles are objects identified in this analysis. The black open circle represents the RV-discrepant target 2MASS J02455260+0529240.

scatter for both indices (≈0.1). However, all the objects identified in this analysis have consistent CaH2 and CaH3 indices by comparison with known members.

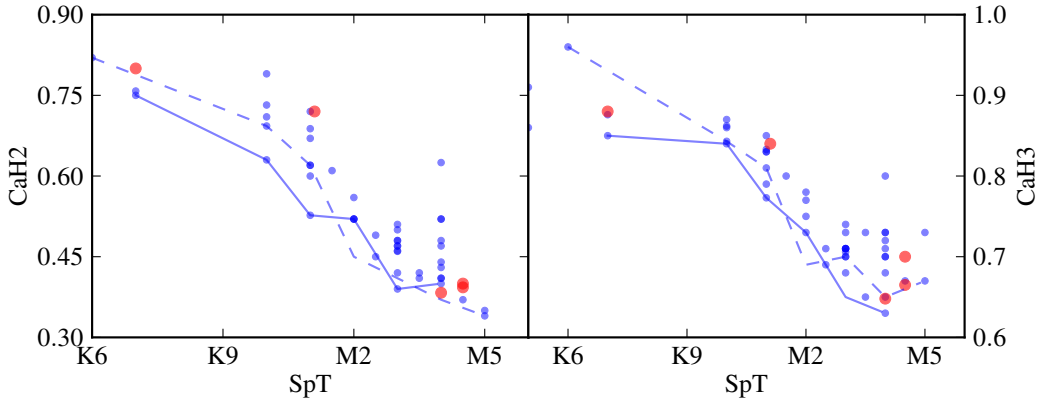

FIGURE 4.9: *Left panel:* Spectral type versus CaH2 index for the original sample (blue) and members identified in this analysis (red). *Right panel*: Same as left, but for CaH3 index. The solid and dotted lines represent the lower envelopes of ABD and BPC, respectively.

4.5.6 H_α emission

H_α emission can be used as an indication of youth, however, one has to keep in mind this feature can also be observed in older, main sequence stars. Furthermore, the EW of H_α is a function of the spectral type of the star at a given age e.g. Stauffer et al. (1997). In Figure 4.10 we show the spectral type versus H_α EW for the original sample and targets identified in this analysis. Additionally we show the lower envelope of EWs for the original sample of ABD and, similar to Figure 6 of Kraus et al. (2014), show the lower envelope derived in Stauffer et al. (1997) (for the young open clusters IC 2391 and IC 2602, 25-35 Myr). We have grouped the objects by age (ARG, CAR, COL, OCT, THA all have age estimates $\approx$30-40 Myr and are hence, plotted together). The envelopes act as an approximate lower boundary, as a function of age, to classify the object as having compatible H_α properties.

There is one object (2MASS J01354915-0753470) that has a discrepant EW, it is discussed in more detail in Section 4.7.

4.5.7 Lithium abundance

If the mass of PMS star is $\approx$0.06 $M_\odot$ or greater its core temperature will eventually reach $\approx$3 MK and burn lithium (Chabrier et al., 1996). The time-scale to reach this temperature is mass dependent and once reached, the lithium is depleted rapidly as the mixing time-scale is very short in convective stars.

The lithium depletion boundary (LDB) method is based on observing at which luminosity, for a given population, this lithium burning occurs. It is a very powerful technique to calculate the ages of young stars (Soderblom et al., 2014). One of its main advantages is that it is less model-dependent than other techniques (Bildsten et al., 1997; Jeffries and Naylor, 2001). lithium EWs can also provide accurate relative ages by comparing the abundance between different groups of stars (see Figure 3 of da Silva et al., 2009). However, one must be cautious as even for young ages there is a large dispersion in

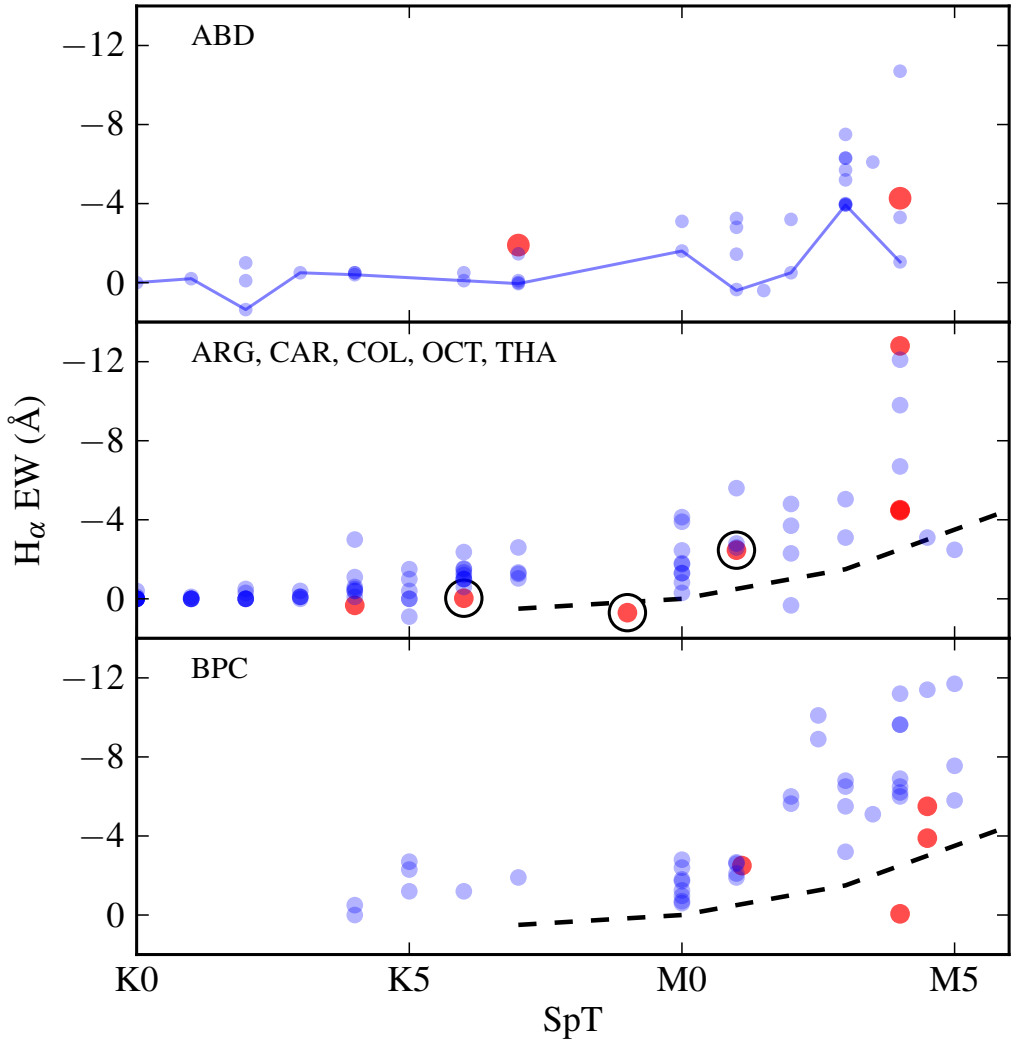

FIGURE 4.10: Spectral type versus H_α EW for the original sample (blue) and objects identified in this analysis (red). The black rings represent objects with discrepant radial velocities. The blue and black-dotted lines are the lower envelopes of EWs for the original sample of ABD members and from Stauffer et al. (1997), respectively.

the Li EWs which could be attributed to activity. Bayo et al. (2011) showed that measurements for the same object at different epochs and EWs between objects of the same spectral type can be significantly different.

In Figure 4.11 we plot the *V*-*K* colour of the target versus the EW of lithium for both detections and non-detections, 10 in total. Additionally we show the region of lithium depletion (Li/Li$_0$ $\leq$0.1) calculated using the evolutionary models of Baraffe et al. (2015).

There are two ways to classify targets as having consistent lithium measurements; one

from the empirical abundances from known members, the other from a comparison to the evolutionary models. All of our detections / non-detections are consistent with the models and empirical abundances.

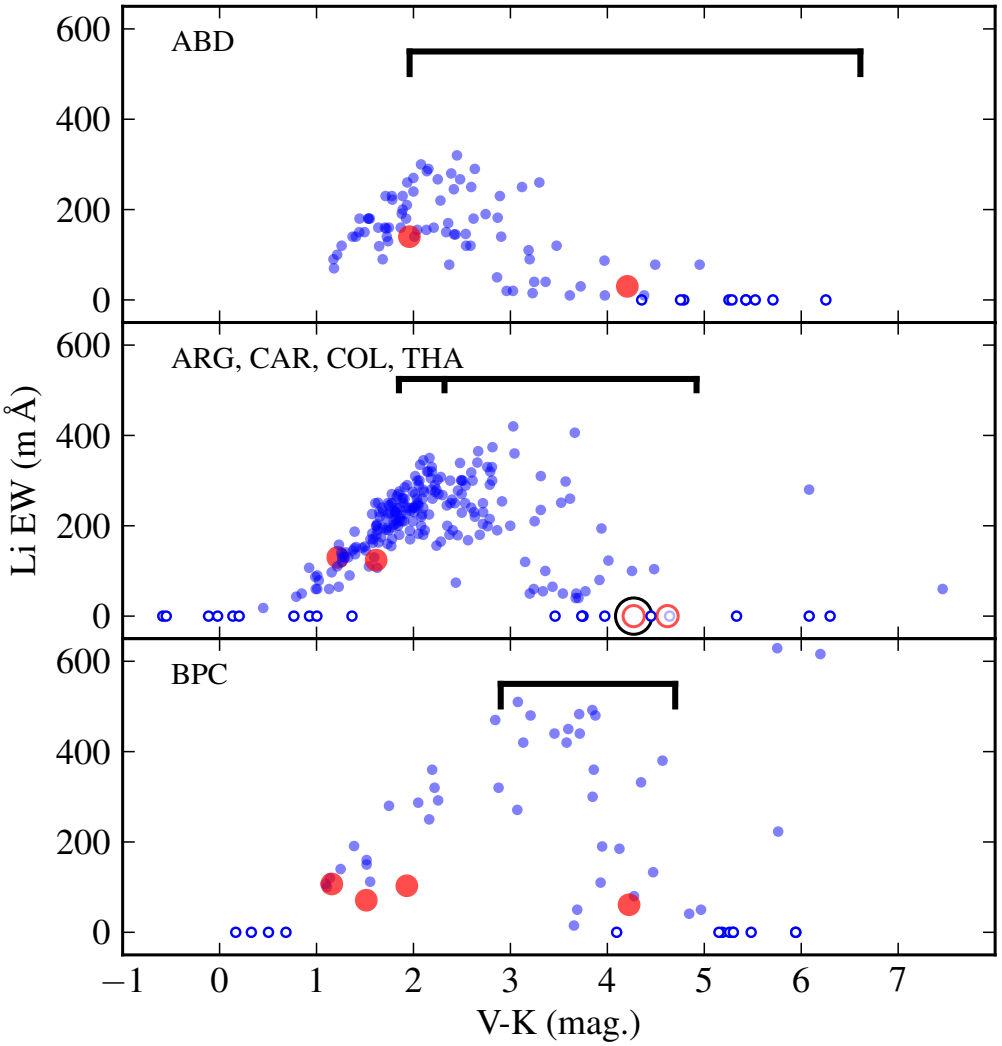

FIGURE 4.11: *V-K* magnitude versus Li EW for original sample (blue) and targets identified in this analysis (red). Filled and open markers represent detections and non-detections, respectively. Black open circles represent sources classified as non-members ("N") in Table 4.4. The black lines encompass regions of lithium depletion ($Li/Li_0 \leq 0.1$) using the models of Baraffe et al. (2015). For the middle panels there are two minima corresponding to ages of 30 and 40 Myr.

TABLE 4.5: Known members from our original sample that have been identified as wide companions to other known members.

ID	Dist. (pc)	(U, V, W) (kms^{-1})	Comps.
HD 104467	106.5	-11.6, -18.9, -10.2	SB
GSC 09420-00948	110.5	-11.6, -18.7, -10.3	
GSC 09239-01572	114.8	-11.5, -19.9, -8.2	0.3″
GSC 09239-01495	108.8	-10.9, -21, -8.6	
HD 21423	107.5	-13.0, -22.4, -5.2	
CD-36 1289	107.5	-13.7, -21.1, -5.8	
HD 21434	107.8	-12.2, -21.9, -5.7	0.2″
GJ 140	16.9	-24.3, -14, -6.5	3″
GJ 140 C	17.9	-24.1, -13.9, -5.2	
HD 199058	76.0	-6.2, -27.9, -13.3	0.5″
TYC 1090-543-1	76.4	-6.4, -27.2, -13.7	
TYC 112-1486-1	71.0	-13, -15.4, -8.2	0.4″
TYC 112-917-1	67.8	-13.2, -15.5, -8.5	
Eta Tel	47.7	-9.1, -15.5, -8.3	
HD 181327	50.6	-10.1, -16.4, -8.2	
HD 199143	45.7	-7.9, -13.9, -10.9	1.1″
AZ Cap	47.9	-10.1, -15, -9.5	2.2″
HD 217343	32.0	-2.9, -25.3, -14.2	
HD 217379	30.0	-3.8, -27.5, -14.5	1.9″+SB
HD 196982	9.5	-9.8, -15.8, -9.6	
AU Mic	9.8	-10.8, -16.6, -9.9	2.9″
UY Pic	23.9	-7.0, -28.1, -14.6	
CD-48 1893	24.2	-7.0, -28.2, -14.6	
TYC 9300-891-1	147.6	-12.0, -2.8, -9.5	1″
TYC 9300-529-1	147.0	-11.5, -3.7, -9.6	
BD-21 1074A	20.2	-11, -15.6, -9.4	
BD-21 1074B	16.6	-12.2, -15.3, -8.3	0.8″
HD 13246	44.2	-9.2, -20.3, -1.5	SB
CD-60 416	43.2	-9.0, -20.5, -0.8	

4.5.8 Optical magnitudes

From our compilation of optical photometric values it is clear that catalogue-catalogue variations in both V and R magnitude can be very significant ($>$ 2 mag.). If these magnitudes were used as a further mode of classification for our objects we could be omitting viable candidates due to an apparent photometric mismatch which is not necessarily associated with the sources membership status. These apparent variations in magnitudes could be induced by physical phenomena such as flaring (Montes et al., 2005) at the time of observation, from blending of multiple sources or purely poor measurement accuracy. Additionally, optical magnitudes are not available for all of our targets (for example, 18 sources have no V mag., 35 sources have only one source of V mag.). Figure 4.12 demonstrates how the variation in apparent optical magnitudes translates into large uncertainties in colour and absolute magnitude for existing and new members of the β-Pic moving group. Data points with no uncertainties only have one optical magnitude value. It is interesting to note that many of the identified members lie closer to the zero-age main sequence (ZAMS) than to their respective isochrone. This could be an indication that some of the identified targets in this analysis are from the older field population. Further spectroscopic observations will allow us to conclude whether these targets are young. Colour-magnitude diagrams of the remaining 8 associations are in Section 4.9.

As mentioned in Section 4.3.1 we checked all sources with Catalina photometry for any signs of optical flaring that could be associated with variable strong activity (Montes et al., 2005). We found 4 / 36 identified targets in this analysis, with Catalina photometry, showed significant flaring. We classify significant flaring as 2 or more observations with values 3 times the standard deviation of all data. None of these 4 objects have optical spectra to connect the photometric flare with strong, variable activity. For that reason, this quantity is not used to assess the membership of the target but, it is noted in Table 4.4.

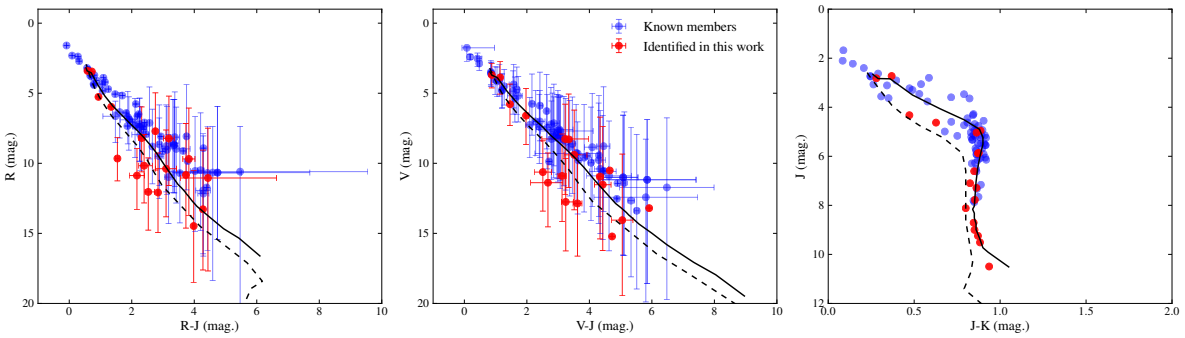

FIGURE 4.12: *Left and middle panel:* Colour-magnitude diagrams (*R*-*J*, *R*) and (*V*-*J*, *V*) for known (blue) and newly proposed (red) members of the β-Pic association. The uncertainties are derived using the upper and lower boundaries of the *R* and *V* magnitude values, respectively, compiled from our photometric search. In most cases those markers without uncertainties only have one magnitude value. *Right panel:* Colour-magnitude diagram (*J*-*K*, *J*) for known and newly proposed members. The solid and dotted line is the isochrone of Baraffe et al. (2015) using the age of the association and the zero-age main sequence (ZAMS), respectively.

4.5.9 Revised mass function of the young associations

As mentioned previously, the original works aiming to derive censuses of the young associations suffered from large incompleteness for masses $<1\,M_{\odot}$. However, recent work has significantly improved members in this mass range.

Figure 4.13 shows the IMF, when considering all 9 young associations as one overall population. This figure includes targets from the original sample, targets identified in this analysis (a pseudo-random sample of all 84 targets multiplied by the success rate), high-probability targets from Gagné et al. (2015) and *consistent* targets (based on RV, H_{α} and/or Li) from Kraus et al. (2014). Although the work of Kraus et al. (2014) was only focused on the Tucana-Horologium association it significantly increased the number of potential members from 62 to 191 and therefore even in the context of all nine associations still makes a large difference to the IMF (note the log-scale of Figure 4.13).

The most considerable improvement from analysis presented in this analysis is for stars with masses $\lesssim 0.5\,M_{\odot}$. We are sensitive to low mass objects as our initial selection criteria is only based on 2MASS photometry and proper motions. Many other works, such as Rodriguez et al. (2013), use more extensive selection criteria, but at the cost

of severely limiting the number of sources with photometry in multiple bands. This is highlighted by Figure 4.6 that shows only 13 of 84 sources (15%) had photometry in both GALEX and WISE.

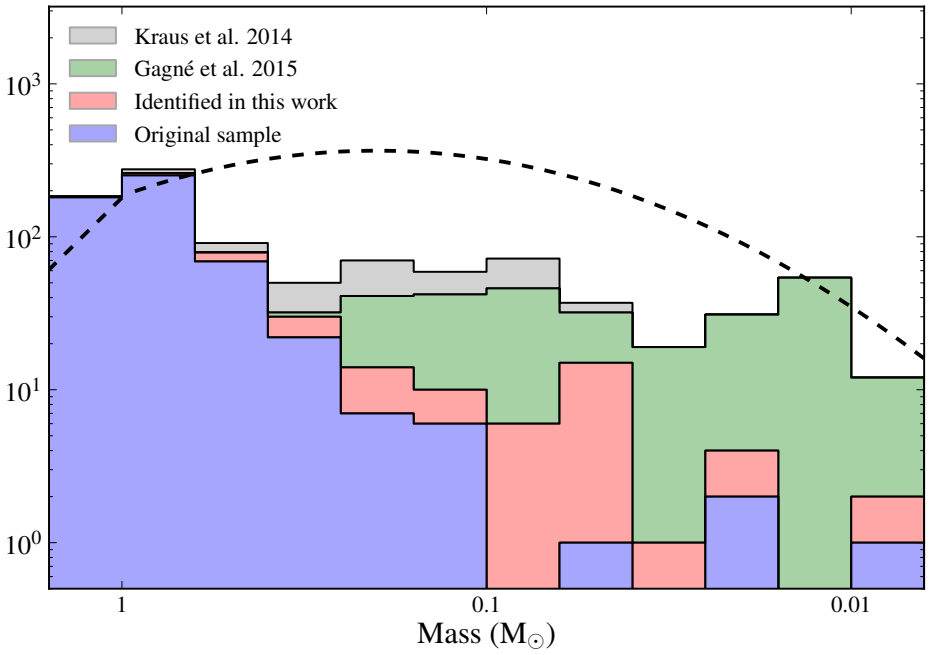

FIGURE 4.13: Mass function of the 9 young moving groups for objects identified in this analysis (red), Gagné et al. (2015) (green), Kraus et al. (2014) (grey) and the original sample (blue). A power-law is fitted for masses $> 1\,M_\odot$ (α=-2.35, Salpeter, 1955) and a log-normal (μ=0.2 $M_\odot$, σ=0.6 log($M_\odot$)) for masses smaller than 1 $M_\odot$ (Chabrier, 2003).

4.6 Conclusions

We have identified 84 targets (43: 0.2-1.3 $M_\odot$, 16: 0.08-0.2 $M_\odot$, 25: $<$0.08 $M_\odot$) in this analysis using our sample of 542 high-probability members. 33 / 84 sources have spectroscopic parameters either derived here or taken from previous works listed in Table 4.2. Of these 33 sources, 4 sources have inconsistent parameters and 4 have questionable parameters. We can therefore derive a success rate of $\approx$ 76–88% using this technique. Additionally only 10 / 33 have been identified in previous works concerned with young associations. Thanks to the collation of numerous parameters we

were able to find and use existing additional information from mid/high resolution spectra and X-ray observations to successfully complement our photometric–proper motion search for new members. Note that the targets with existing additional information, on which the success rate is derived, are generally brighter in magnitude (average in V: 12.2 mag. compared to 15.1 mag) and earlier spectral type (average K7 compared to M0) than those currently without further photometric and spectroscopic information. Therefore the derived success rate is only an approximation at this time and should be treated in that way. In the future we aim to take mid/high resolution spectra of all the targets identified in this analysis that currently have no spectroscopic information. We have been awarded time for UVES/VLT observations to take place between April-October 2016, see Appendix B.5. With this we can better assess the youth and kinematics of the objects.

As expected by our success rate so far, if many of these new members are confirmed they could have big implications for the formation and dynamical evolution of stars in loose associations. Our initial results are broadly consistent with the mechanism proposed by Reipurth and Mikkola (2012) whereby preferentially lower-mass components in 3-body systems are ejected from the stellar cores soon after birth. These components collectively form *unfolding* triple systems (potentially in the process of disintegrating to unbound systems). The majority of these wide companions would therefore be associated with tight inner binaries (tightening of the inner binary from angular momentum exchange as the third body is ejected). An evaluation of this mechanism using the β-Pic moving group is presented in Chapter 5.

Regardless of whether these targets form wide multiple systems or not, if their youth is confirmed, they would make up an ideal sample for the characterisation of low-mass objects and the search for warm planets around nearby stars. New instruments such as SPHERE/VLT (Beuzit et al., 2008) and GPI/GEMINI (Macintosh et al., 2014) have been designed for the purpose of detecting and characterising planets using high-contrast imaging techniques. For a strehl ratio of $\approx$70% or better in H band, the limiting magnitudes for SPHERE and GPI are R $<$13 mag. and I$<$10 mag., respectively. From our

sample of identified candidates in this analysis, 24 have *R* magnitudes brighter than the limit of SPHERE. Fifteen of these have been classified as members (denoted by "Y" in Table 4.4) based on further photometric and spectroscopic quantities, and nine of these fifteen are M-dwarfs. We have therefore, based on this initial work alone, identified crucial new targets to search for warm planets around nearby young stars.

In March 2016 we submitted a proposal to observe 10 newly identified members of the young moving groups using SPHERE/VLT. If this proposal is successful observations will most likely take place in December 2016.

4.7 Notes on compatibility of individual sources

Identified targets with discrepant / dubious properties (denoted by either "N" or "Y?" in Table 4.4) are discussed below. We combine all available indicators of youth in the discussion to assess their potential membership. Note that uncertainties of radial velocity values quoted are 1.0 kms^{-1} in the case of measurements performed by the SACY team. This is not a measurement uncertainty but rather it is the average variation seen in single stars from using the CCF technique on optical spectra (see Chapter 2 for details).

2MASS J02105345-4603513: The radial velocity of this target with its associated known member are incompatible 25.7$\pm$1 and 8.5$\pm$1 kms^{-1}. However, the evidence that these two sources form a young wide binary is strong. It is identified as a multiple system in the WDS catalogue (ID: 02109-4604, observations 1977-2000), McCarthy and White (2012) and Rodriguez et al. (2013). However, due to the angular separation (21.5″) there is no observable orbital motion on this time-scale. The proper motion values match within 1 sigma (total proper motions: 54.4$\pm$3.1 and 54.2$\pm$2.5 mas/yr) and additionally the photometry is compatible in *V*, *J*, *H* and *K*. 2MASS J02105345-4603513 also shows strong X-ray emission (L_x/L_{bol}=-2.88) and UV excess. It is very likely that 2MASS J02105345-4603513 is a spectroscopic binary and the radial velocity value

calculated by Rodriguez et al. (2013) is not the system velocity. For those reasons we conclude 2MASS J02105345-4603513 is a most likely a young source.

2MASS J12573935+3513194: The radial velocities of this target with its associated known member borderline agree (2-3 σ) within measurement uncertainties (-9.5$\pm$1.0 and -5.7$\pm$0.5 kms^{-1}), however both components have been identified as spectroscopic binaries. The separation between the two components is relatively small (16.2″) and the photometry matches well for *V*, *J*, *H* and *K*. 2MASS J12573935+3513194 shows strong H_α emission (-4.27) indicating it is young. Additionally the proper motion of the components are both extremely high and agree within uncertainties (total proper motion: 303.9$\pm$2.8 and 317.8$\pm$7.6 mas/yr).

2MASS J01334282-0701311: Initially identified as part of a triple system. The components have radial velocities -15$\pm$0.1 (HR 448), 11.4$\pm$0.2 (2MASS J01334282-0701311) and 12.2$\pm$1 kms^{-1} (G 271-110), respectively. The lowest mass component (G 271-110) in the this system is the original known member from Malo et al. (2014). The highest mass component (HR 448) is a well documented target with extensive radial velocity coverage and therefore this discrepancy is unlikely to arise from variation induced by spectroscopic companion.

2MASS J21212446-6654573: There are two epochs of data for this target, however one radial velocity has huge uncertainties (-24.1$\pm$1 and 6.4$\pm$14.8 kms^{-1}). Torres et al. (2006) also noted this component as a potential spectroscopic binary. The proper motions do not agree within 3σ however, the magnitudes of the values are very large, 142.4$\pm$1.9 and 128.3$\pm$1.9 mas/yr, respectively. The field of view is not crowded and positions of the targets are well outside the galactic plane (galactic longitude and latitude: 326.596, -39.1878) making a chance alignment improbable. The system is also identified as a multiple system (with no additional notes) in the WDS catalogue, with 7 observations between 1835-2000. The photometry of both components matches very

well in V, J, H and K.

2MASS J04515223-4640497: This target has a hugely discrepant radial velocity with its associated known member (51.2±1.0 and 23±1.0 kms^{-1}). It has small emission in H_α (EW: -0.32 Å). Due to its discrepant radial velocity it is not classified as a potential member.

2MASS J08371456-5517343: This target has a hugely discrepant radial velocity with its associated known member (81.3±1.0 and 20.8±1.0 kms^{-1}) and low proper motion magnitude (12.5±2.6 mas/yr). It has absorption in H_α therefore there is no evidence it is a young member.

2MASS J01354915-0753470: This target has consistent radial velocity (6.3±0.5 and 6.5±1.0 kms^{-1}) and very large and consistent proper motion (104.7±2.8 and 98.1±7.2) with its associated known member, both agree within 1 sigma. The calculated K I EW is consistent with youth, however it does not show H_α emission. Given its V-K colour this makes the youth of the object questionable.

2MASS J02455260+0529240: The calculated radial velocity is hugely discrepant with its associated known member (88.5 and 4.3 kms^{-1}) and there is no sign of a spectroscopic companion to account for such a discrepancy. The total proper motions are large and agree within 1 sigma (83.0±4.2 and 87.6±0.9 mas/yr). However, due to RV value, it is not considered as a potential member.

4.8 Previously identified extremely wide companions

Below we present previous detections of potential wide binary systems in the young associations. We discuss whether these systems were recovered in the analysis presented here and the reasons for why or why not.

T Cha – 2MASS J11550485-7919108: This system was first identified in Kastner et al. (2012). In our analysis we did not recover the system as the H-K colour is incompatible ($<$0.03 mag. beyond criterion, see Figure 4.14). As discussed previously at the youngest ages ($\approx$10 Myr) our technique is weaker as infrared excesses are more likely and therefore the companion is less likely to be classified as possibly physical. However, this effect is unlikely to induce any strong bias in our statistics. Kastner et al. (2012) show 2MASS J11550485-7919108 has a modest infrared excess (K-$W3$ $\sim$0.8) which is why it was not recovered here. The system is classified as a potential wide binary system due to the detailed analysis performed by Kastner et al. (2012) - including H_α, X-ray and lithium EW analysis and the recent work of Montet et al. (2015).

V4046 Sgr – GSC 07396-00759: First identified in Kastner et al. (2011), this companion does have compatible photometry and kinematics using our method. However, many other sources in the field of view also match the criteria (see Figure 4.15) and therefore our upper angular limit is set much smaller (10″) than the angular separation of this candidate companion (2.82'). It is also noteworthy that the kinematic distances are not compatible between the two sources 76.9 and 95.1 pc, respectively. Furthermore Kastner et al. (2011) argues that GSC 07396-00759 would itself have to be a spectroscopic multiple system (of approximately equal mass) to account for the discrepancy in magnitudes. However, spectroscopic analysis does not support this. From 3 separate epochs of data there is no evidence for a companion. The radial velocities are -5.7, -5.0 and -5.7 kms^{-1} (σ=0.3 kms^{-1}) from Torres et al. (2006) and this analysis, well below the criterion for multiplicity (σ $>$3 kms^{-1}). For these reasons the system is not included in our statistics.

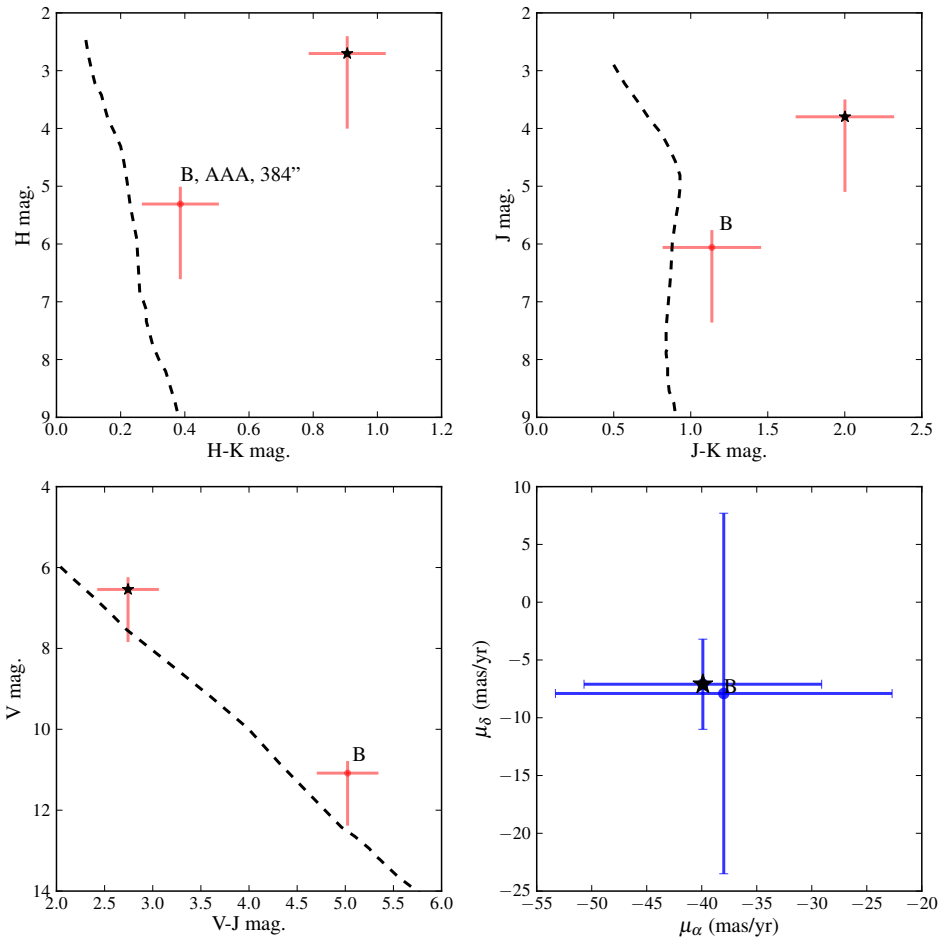

FIGURE 4.14: A photometric and kinematic summary of 2MASS J11550485-7919108.

TWA 1 – 2MASS J11020983-3430355: This system was first identified in Scholz et al. (2005). The system is also recovered here. Figure 4.16 shows that 2MASS J11020983-3430355 is the only source with both compatible photometry and kinematics in the field of view. Furthermore the work of Scholz et al. (2005) used spectroscopic analysis to show the source is consistent with being a member of the TW Hydrae moving group. The system is therefore included in our statistics.

TWA 30 – 2MASS J11321822-3018316: This system was first identified in Looper et al. (2010). The system was also recovered here, however, initially it was discarded due to the extremely large uncertainties on the proper motion (14.3 mas/yr). The work of

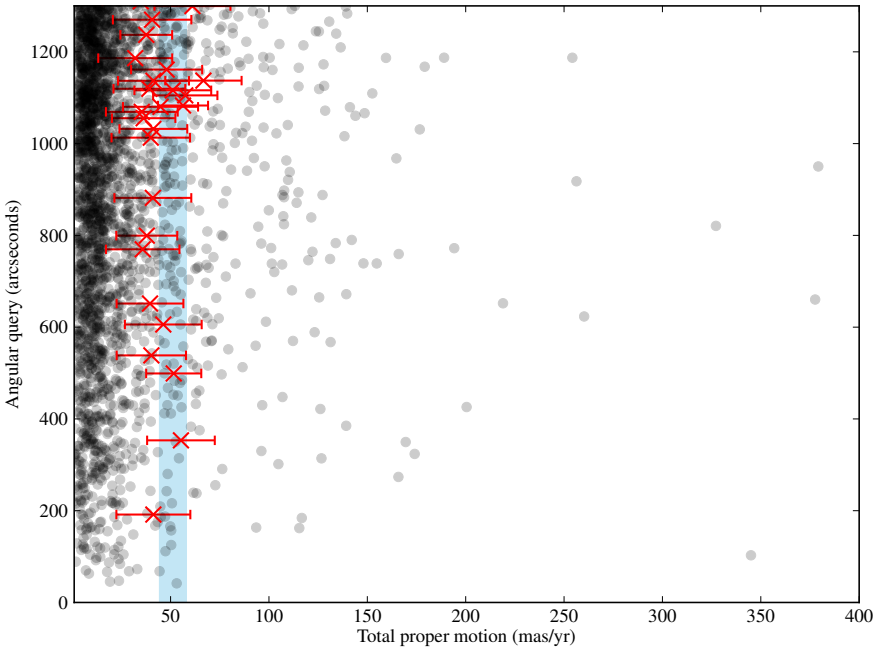

FIGURE 4.15: The considered field of view for V4046 Sgr. The markers are the same as in Figure 4.1

Looper et al. (2010) produced much more accurate proper motion values (uncertainties 9 mas/yr) and a radial velocity value ($12\pm3\,\mathrm{kms}^{-1}$), showing its galactic velocity is compatible with that of TWA 30 – (-10.2, -18.3, -4.9) compared with (-11.7, -19.7, -4.1) for TWA 30. Furthermore their spectroscopic analysis showed the source has features consistent with being a young object, member of the TW Hydrae moving group. For these reasons it is included in our statistics.

51 Eri – 2MASS J04373746-0229282: This system was first identified in Feigelson et al. (2006). It is also recovered in our analysis. The work of Feigelson et al. (2006) concludes that these two objects are very likely a physical pair. In recent work Montet et al. (2015) calculated the system velocity of 2MASS J04373746-0229282, itself a close binary, as $20.8\pm0.2\,\mathrm{kms}^{-1}$. The radial velocity of 51 Eri is $21.0\pm1.2\,\mathrm{kms}^{-1}$, therefore the two components of the wide binary system are consistent.

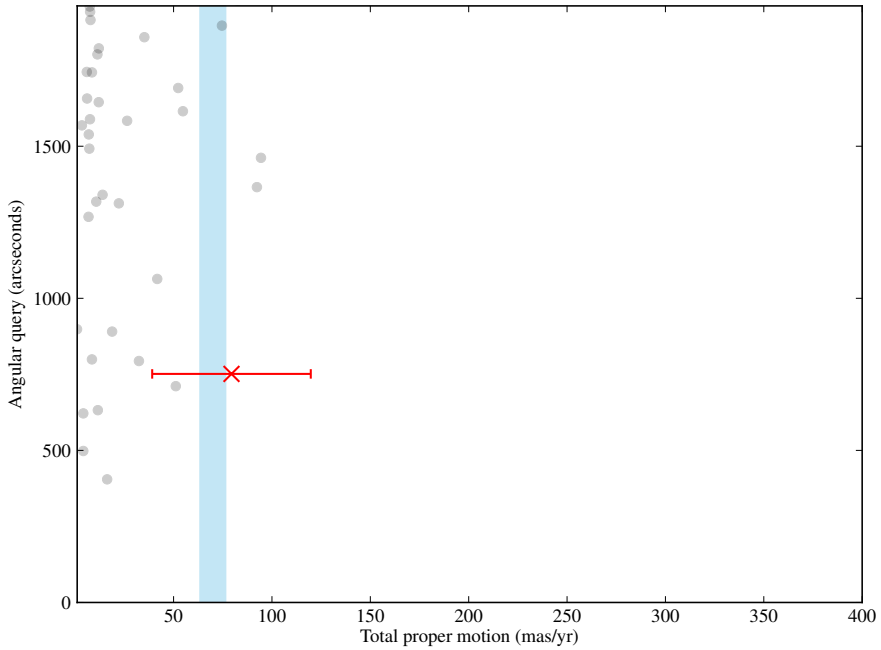

FIGURE 4.16: The considered field of view for TWA 1. The markers are the same as in Figure 4.1. 2MASS J11020983-3430355 is the only source with compatible proper motion.

4.9 Colour-magnitude diagrams for new candidates

Below are colour-magnitude diagrams (in the same format as Figure 4.2) for the remaining 8 associations.

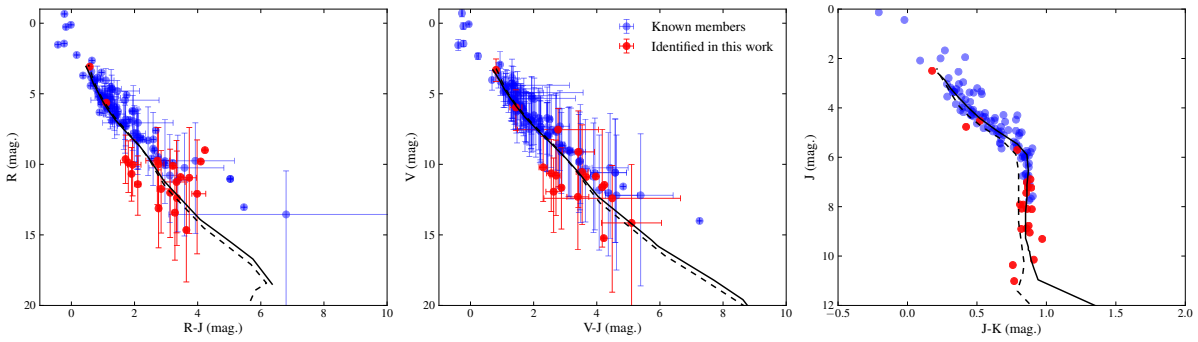

FIGURE 4.17: Colour-magnitude diagrams for the AB Doradus association

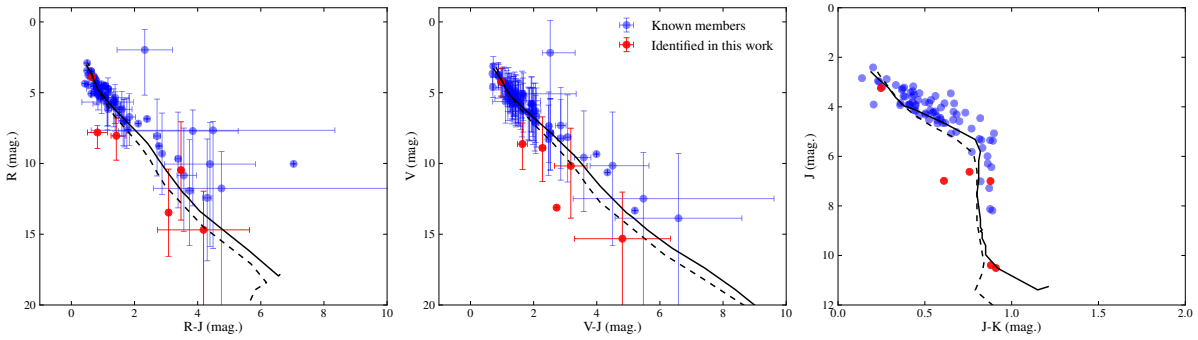

FIGURE 4.18: Colour-magnitude diagrams for the Argus association.

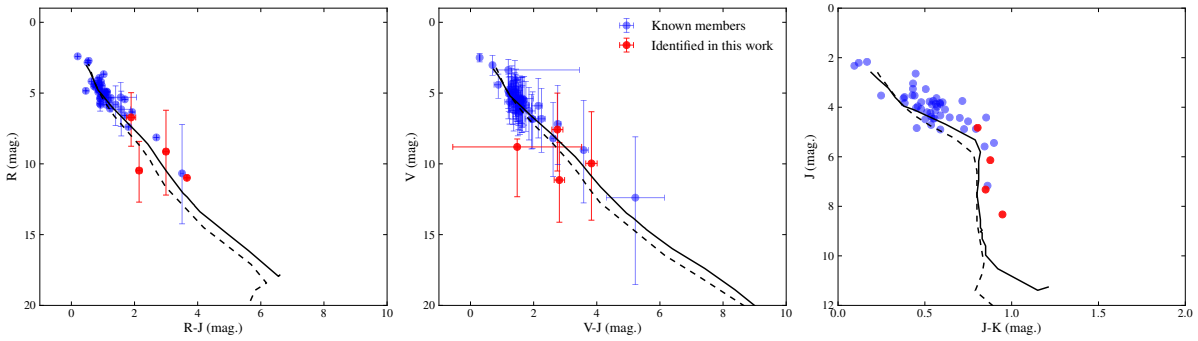

FIGURE 4.19: Colour-magnitude diagrams for the Carina association.

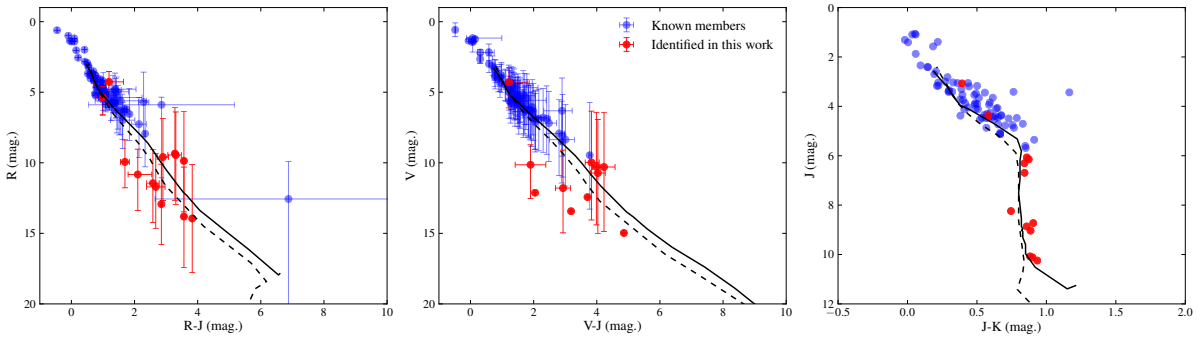

FIGURE 4.20: Colour-magnitude diagrams for the Columba association.

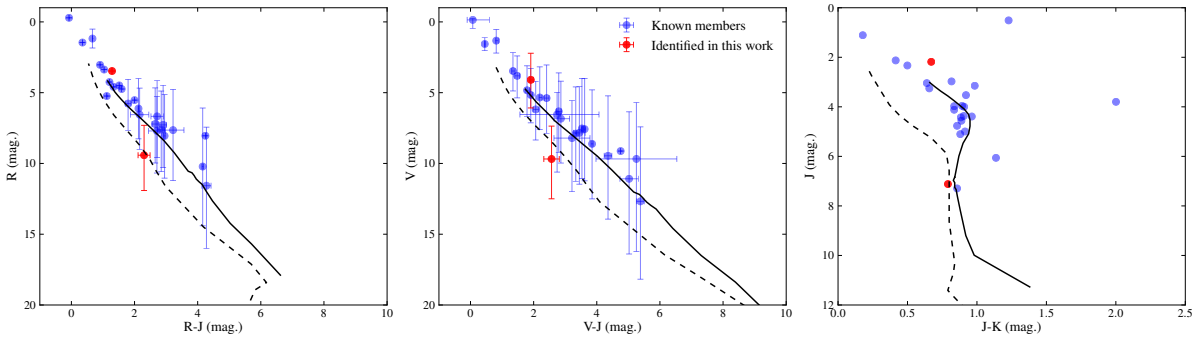

FIGURE 4.21: Colour-magnitude diagrams for the ϵ-Cha association.

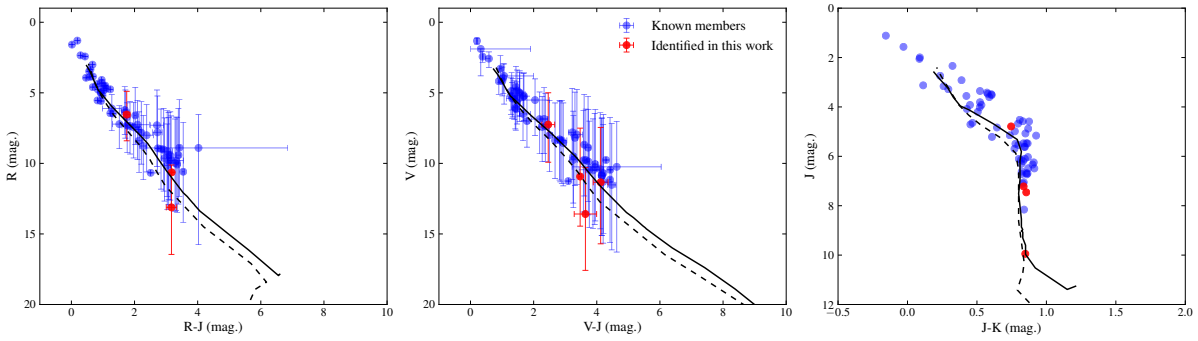

FIGURE 4.22: Colour-magnitude diagrams for the Octans association.

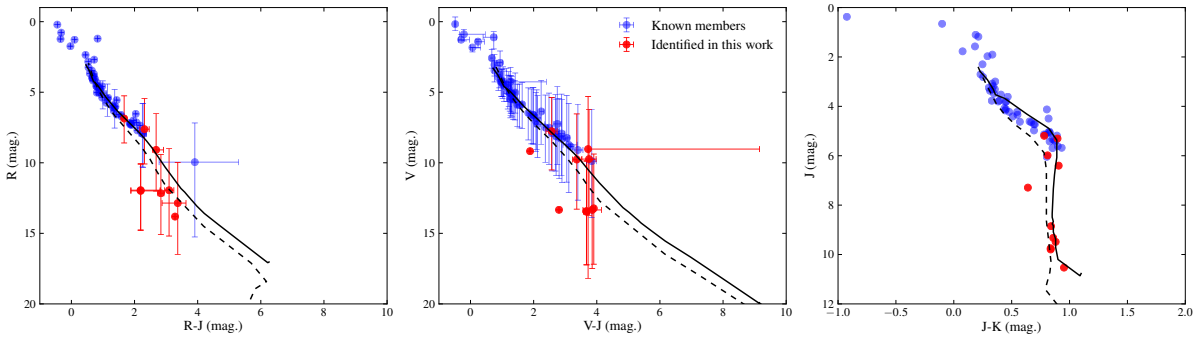

FIGURE 4.23: Colour-magnitude diagrams for the Tucana-Horologium association.

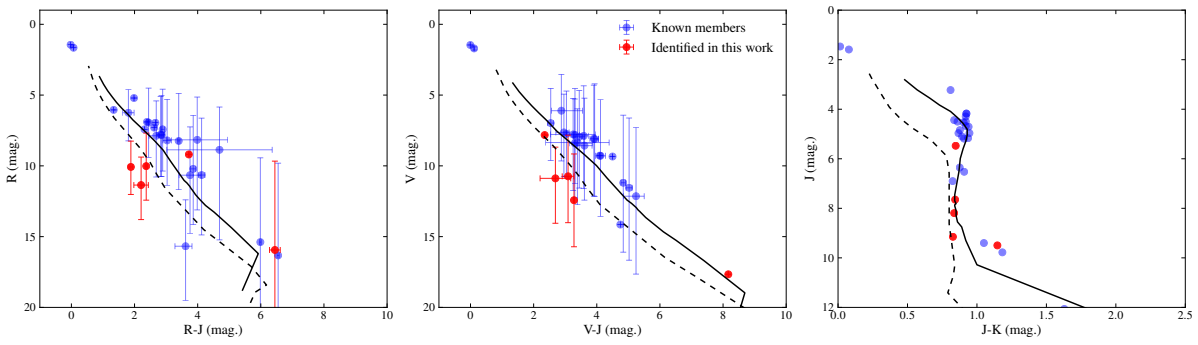

FIGURE 4.24: Colour-magnitude diagrams for the TW Hydrae association.

4.10 Properties of sample

TABLE 4.6: Basic properties of the sample used in this chapter.

ID	RA hh:mm:ss.s	DEC dd:mm:ss.s	Dist. (pc)	*J* (mag.)	*H* (mag.)	*K* (mag.)	$\mu_{\alpha,*}$ (mas/yr)	μ_δ (mas/yr)	Mem ref.
			ABD						
PW And	00:18:20.9	+30:57:22.0	27.3	7.0	6.5	6.4	144.4±1.0	-170.8±0.9	1
V493 And AB	00:34:8.4	+25:23:50.0	49.9	8.5	7.8	7.7	81.5±1.8	-97.6±1.1	3
HD 4277	00:45:50.9	+54:58:40.0	52.7[(a)]	6.6	6.4	6.4	95.6±1.0	-76.9±1.0	1
HIP 4967	01:03:40.1	+40:51:29.0	29.6[(a)]	8.1	7.5	7.3	126.7±0.7	-167.2±0.8	1
HD 6569	01:06:26.2	-14:17:47.0	47.4[(a)]	7.9	7.4	7.3	99.8±1.6	-91.8±2.5	1
BD-12 243	01:20:32.3	-11:28:4.0	34.3[(a)]	7.0	6.7	6.5	112.0±2.3	-137.7±1.3	1
HS Psc	01:37:23.2	+26:57:12.0	37.4	8.4	7.8	7.6	120.2±0.9	-126.5±1.4	3
CD-46 644	02:10:55.4	-46:03:59.0	73.7	9.3	8.8	8.6	53.3±2.5	-10.8±1.8	1, 5
HD 13482	02:12:15.4	+23:57:29.0	36.6[(a)]	6.2	5.8	5.7	127.1±1.0	-160.4±1.0	1
HD 16760 b	02:42:21.0	+38:37:21.0	48.4[(a)]	8.4	7.9	7.8	107.0±8.0	-102.8±8.0	1
HD 16760	02:42:21.3	+38:37:7.0	48.8[(a)]	7.4	7.1	7.0	76.7±2.2	-108.3±2.3	1
HD 17332 b	02:47:27.2	+19:22:21.0	33.6[(a)]	6.0	5.7	5.6	117.8±2.5	-160.3±2.5	1
HD 17332 a	02:47:27.4	+19:22:19.0	33.6[(a)]	5.9	5.6	5.5	117.8±1.0	-160.3±1.0	1
HD 17573	02:49:59.0	+27:15:38.0	50.7[(a)]	3.7	3.8	3.9	66.8±1.0	-116.5±1.0	1, 2
IS Eri	03:09:42.3	-09:34:47.0	37.4[(a)]	7.2	6.8	6.7	88.8±1.3	-112.7±1.5	1
HW Cet	03:12:34.3	+09:44:57.0	57.5	8.6	8.1	8.0	60.8±0.8	-88.2±1.1	1
HD 20888	03:17:59.1	-66:55:37.0	54.9[(a)]	5.8	5.8	5.7	57.3±1.0	13.6±1.0	1, 2
V577 Per	03:33:13.5	+46:15:27.0	34.3[(a)]	6.8	6.5	6.4	61.8±9.9	-173.8±5.1	1
HIP 17695	03:47:23.3	-01:58:20.0	16.4[(a)]	7.8	7.2	6.9	178.6±2.2	-278.2±3.1	1
HD 24681	03:55:20.4	-01:43:45.0	53.3	7.7	7.4	7.3	43.4±0.8	-90.7±1.1	1
HD 25457	04:02:36.7	-00:16:8.0	18.8[(a)]	4.7	4.3	4.2	149.0±1.0	-253.0±1.0	1
HD 25953	04:06:41.5	+01:41:2.0	55.3[(a)]	6.9	6.7	6.6	37.1±0.6	-94.4±0.8	1
2MASS J04141730-0906544	04:14:17.3	-09:06:54.4	23.8	9.6	9.1	8.8	95.1±5.0	-141.0±5.0	3
TYC 91-82-1	04:37:51.5	+05:03:8.0	87.6	9.2	8.8	8.6	20.8±0.9	-58.9±1.2	1
LP 776-25	04:52:24.4	-16:49:22.0	16.3	7.7	7.1	6.9	118.9±8.0	-211.9±8.0	1, 3
CD-56 1032 N	04:53:30.5	-55:51:32.0	11.1	7.8	7.2	6.9	88.2±42.5	85.8±12.6	1
CD-56 1032 S	04:53:31.2	-55:51:37.0	11.1[(a)]	7.2	6.6	6.3	133.1±1.4	68.0±1.4	1
2MASS J04571728-0621564	04:57:17.3	-06:21:56.0	45.0	9.5	8.8	8.6	22.9±1.9	-99.1±2.5	3
HD 31652	04:57:22.3	-09:08:0.0	82.4	8.8	8.4	8.4	12.9±1.3	-50.8±1.6	1
CD-40 1701	05:02:30.4	-39:59:13.0	41.3	8.7	8.2	8.1	33.6±0.8	-21.9±0.8	1
HD 32981	05:06:27.7	-15:49:30.0	78.9	8.0	7.8	7.7	16.3±1.3	-44.0±1.6	1
HD 293857	05:11:9.7	-04:10:54.0	76.9	7.8	7.5	7.4	18.1±1.3	-57.6±2.2	1
HD 33999	05:12:35.8	-34:28:48.0	101.4	7.6	7.3	7.2	8.1±0.8	-16.8±1.2	1
HD 35650	05:24:30.2	-38:58:11.0	18.1[(a)]	6.7	6.1	5.9	42.2±0.9	-57.0±1.1	1
NLTT 15049	05:25:41.7	-09:09:12.0	21.9	8.5	7.9	7.6	39.2±8.0	-188.4±8.0	3
HD 36705 b	05:28:44.4	-65:26:47.0	15.2	8.2	7.7	7.3	0.0±0.0	0.0±0.0	1
AB Dor	05:28:44.8	-65:26:55.0	15.2[(a)]	5.3	4.8	4.7	33.2±1.0	150.8±1.0	1
UX Col	05:28:56.5	-33:28:16.0	54.1	8.4	7.9	7.8	10.5±0.7	-32.3±0.7	1
CD-30 2476	05:33:18.6	-30:33:27.0	132.9	10.4	10.1	9.9	0.1±1.0	-14.3±0.9	1
CD-34 2331	05:35:4.1	-34:17:52.0	80.5	9.8	9.2	9.1	5.8±0.8	-20.0±0.9	1
UY Pic	05:36:56.9	-47:57:53.0	25.2[(a)]	6.4	5.9	5.8	25.3±1.0	0.0±1.0	1
WX Col	05:37:12.9	-42:42:56.0	76.4[(a)]	8.1	7.7	7.7	-12.6±4.7	1.5±2.2	1
2MASS J05385663-0624410	05:38:56.6	-06:24:41.0	114.5	9.6	9.2	9.1	5.6±1.8	-37.3±1.4	1
CP-19 878	05:39:23.2	-19:33:29.0	70.2	8.7	8.2	8.1	4.5±1.6	-44.5±1.5	1
2MASS J05411433-4117585	05:41:14.3	-41:17:59.0	127.3	9.8	9.3	9.1	1.5±1.2	-6.4±1.4	1
CD-26 2425	05:44:13.4	-26:06:15.0	72.3	9.2	8.6	8.5	16.6±1.3	-27.8±1.5	1
HD 38497	05:45:41.3	-14:46:30.0	75.8	7.4	7.1	7.1	-0.1±1.6	-46.8±1.6	1
CD-41 2076	05:48:30.4	-41:27:30.0	65.3	9.2	8.5	8.4	0.6±1.3	-11.7±1.2	1
TZ Col	05:52:16.0	-28:39:25.0	81.3[(a)]	7.9	7.6	7.5	3.3±0.9	-26.8±0.8	1
TY Col	05:57:50.8	-38:04:3.0	50.1	8.1	7.7	7.6	12.6±1.4	-16.9±1.1	1
BD-13 1328	06:02:21.9	-13:55:33.0	39.7	8.4	7.9	7.8	-8.3±1.0	-91.1±1.0	1

ID	RA	DEC	Dist.	J	H	K	$\mu_{\alpha,*}$	μ_{δ}	Mem ref.
	hh:mm:ss.s	dd:mm:ss.s	(pc)	(mag.)	(mag.)	(mag.)	(mas/yr)	(mas/yr)	
CD-34 2676	06:08:33.9	-34:02:55.0	77.5	8.7	8.3	8.2	3.7±0.8	-19.3±0.9	1
CD-35 2722	06:09:19.2	-35:49:31.0	25.0	7.9	7.3	7.0	-5.0±0.9	-55.1±0.9	1, 3
CD-35 2749	06:11:55.7	-35:29:13.0	59.8	8.8	8.3	8.2	-7.6±2.0	-20.7±1.0	1
HD 45270	06:22:30.9	-60:13:7.0	23.7[(a)]	5.4	5.2	5.0	-11.3±1.0	64.2±1.0	1
GSC 08894-00426	06:25:56.1	-60:03:27.0	12.2	8.1	7.5	7.2	-23.5±1.5	110.5±1.4	1
AK Pic	06:38:0.4	-61:32:0.0	21.3[(a)]	5.1	4.7	4.5	-50.1±1.0	72.7±1.0	1
CD-47 2500	06:38:45.5	-47:14:18.0	114.7	9.1	8.7	8.7	-4.4±0.8	0.7±1.4	1
CD-61 1439	06:39:50.0	-61:28:42.0	22.4[(a)]	7.3	6.6	6.5	-23.8±1.0	77.8±1.8	1
2MASS J06411849-3820360	06:41:18.5	-38:20:36.0	64.7	9.5	8.9	8.8	-9.9±1.2	-16.5±1.0	1
CD-57 1654	07:10:50.6	-57:36:46.0	133.3	9.4	9.0	8.9	-7.7±0.9	7.9±0.8	1
V429 Gem	07:23:43.6	+20:24:59.0	25.7	7.6	7.0	6.9	-67.8±2.9	-231.1±3.5	1
HD 59169	07:26:17.7	-49:40:51.0	111.1[(a)]	8.4	8.0	7.9	-24.7±6.0	-3.1±1.9	1
V372 Pup	07:28:51.4	-30:14:49.0	15.7[(a)]	6.6	6.0	5.7	-130.9±8.0	-131.4±8.0	1
CD-84 80	07:30:59.5	-84:19:28.0	67.4	8.4	8.0	7.9	-11.6±1.3	55.1±1.0	1
HD 64982	07:45:35.6	-79:40:8.0	80.6[(a)]	7.9	7.7	7.6	-11.5±2.0	65.2±7.0	1
HD 82879	09:28:21.1	-78:15:35.0	116.5	8.1	7.9	7.8	-25.8±1.0	18.0±1.4	1
CD-45 5772	10:07:25.2	-46:21:50.0	69.5	8.8	8.2	8.1	-50.1±1.3	-31.3±0.9	1
2MASS J10121768-0344441	10:12:17.7	-03:44:44.1	7.9[(a)]	5.9	5.3	5.0	-150.7±2.6	-241.4±3.3	3
BD+01 2447	10:28:55.5	+00:50:28.0	6.7	6.2	5.6	5.3	-602.3±8.0	-731.9±8.0	1
HD 99827	11:25:17.7	-84:57:16.0	88.5[(a)]	6.7	6.6	6.5	-48.4±1.0	12.0±1.0	1
2MASS J11254754-4410267	11:25:47.5	-44:10:27.0	51.0	10.3	9.8	9.5	-83.9±2.6	-57.0±7.7	3
2MASS J12194808+5246450	12:19:48.1	+52:46:45.0	28.0[(a)]	8.3	7.6	7.5	-171.4±1.0	-121.2±1.2	3
2MASS J12574030+3513306	12:57:40.3	+35:13:30.6	19.3[(a)]	7.4	6.7	6.6	-264.0±1.9	-150.6±2.1	3
PX Vir	13:03:49.7	-05:09:43.0	21.7[(a)]	6.1	5.7	5.5	-191.1±1.0	-218.7±1.0	1
L 264-18	15:24:48.5	-49:29:47.0	23.5	8.2	7.5	7.3	-120.8±8.0	-241.0±8.0	1
HD 139751	15:40:28.4	-18:41:46.0	36.4[(a)]	7.7	7.1	6.9	-79.0±4.5	-157.3±1.6	1
HIP 81084	16:33:41.6	-09:33:12.0	30.3[(a)]	8.4	7.8	7.5	-65.8±1.3	-179.4±1.4	1
HD 152555	16:54:8.1	-04:20:25.0	46.8[(a)]	6.7	6.5	6.4	-37.2±1.1	-112.9±0.7	1
HD 159911	17:37:46.5	-13:14:47.0	46.3	7.6	7.0	6.8	-16.8±1.4	-124.9±1.6	1
HD 160934	17:38:39.6	+61:14:16.0	33.1[(a)]	7.6	7.0	6.8	-19.2±0.7	46.7±0.7	1
HD 178085	19:10:57.9	-60:16:20.0	61.4[(a)]	7.2	7.0	6.9	11.3±1.2	-98.6±1.2	1
HD 181869	19:23:53.2	-40:36:57.0	55.8[(a)]	4.2	4.2	4.2	31.5±1.0	-120.3±1.0	1, 2
TYC 486-4943-1	19:33:3.8	+03:45:40.0	72.0	9.3	8.8	8.7	16.0±1.6	-66.2±1.5	1
BD-03 4778	20:04:49.4	-02:39:20.0	71.5	8.5	8.0	7.9	27.2±1.1	-72.1±1.9	1
2MASS J20465795-0259320	20:46:58.0	-02:59:32.0	47.5	9.1	8.4	8.3	53.0±2.5	-109.5±1.7	3
HD 199058	20:54:21.1	+09:02:24.0	76.0	7.4	7.0	7.0	35.3±1.0	-58.4±0.6	1
TYC 1090-543-1	20:54:28.0	+09:06:7.0	76.4	9.5	8.9	8.8	36.4±2.7	-57.3±1.8	1
HD 201919	21:13:5.3	-17:29:13.0	39.5	8.3	7.7	7.6	73.9±0.8	-144.4±0.8	1, 3
LO Peg	21:31:1.7	+23:20:7.0	24.8[(a)]	7.1	6.5	6.4	134.4±0.8	-145.2±0.8	1
GJ 4231	21:52:10.4	+05:37:36.0	30.6[(a)]	8.2	7.6	7.4	109.8±1.5	-150.0±2.0	1, 3
HD 209952	22:08:14.0	-46:57:40.0	31.0[(a)]	2.0	2.0	2.0	126.7±1.0	-147.5±1.0	1, 2
HIP 110526a	22:23:29.1	+32:27:34.0	15.1[(a)]	6.9	6.3	6.1	251.3±8.0	-207.6±8.0	1
HIP 110526b	22:23:29.1	+32:27:32.0	15.1	6.9	6.3	6.1	251.3±8.0	-207.6±8.0	1
HD 217343	23:00:19.3	-26:09:14.0	30.7[(a)]	6.3	6.0	5.9	110.0±1.0	-160.1±1.0	1
HD 217379A	23:00:28.0	-26:18:43.0	32.7[(a)]	7.0	6.4	6.3	113.6±8.0	-162.2±8.0	1
HIP 114066	23:06:4.8	+63:55:34.0	24.5[(a)]	7.8	7.2	7.0	172.7±1.0	-57.8±1.4	1
HD 218860 S	23:11:52.1	-45:08:11.0	49.3[(a)]	7.5	7.1	7.0	85.3±1.0	-93.3±1.0	1
HIP 115162	23:19:39.6	+42:15:10.0	50.2[(a)]	7.6	7.3	7.2	78.4±0.5	-65.4±0.6	1
Kap Psc	23:26:56.0	+01:15:20.0	47.2[(a)]	5.3	5.0	4.9	87.7±1.0	-95.5±1.0	1, 2
LTT 9582	23:32:0.2	-39:17:37.0	23.1	8.9	8.3	8.0	193.4±17.9	-	3
								178.4±17.9	
HD 222575	23:41:54.3	-35:58:40.0	63.6[(a)]	8.1	7.8	7.6	70.0±0.9	-66.3±1.0	1
HD 223352	23:48:55.5	-28:07:49.0	42.2[(a)]	4.8	4.6	4.5	100.8±1.0	-105.3±1.0	1, 2
1RXS J235133.3+312720	23:51:33.7	+31:27:23.0	42.8	9.8	9.2	9.0	106.6±1.7	-87.9±3.8	3
HD 224228	23:56:10.7	-39:03:8.0	22.0[(a)]	6.5	6.0	5.9	205.1±1.9	-186.5±2.1	1
			ARG						
FT Psc	00:50:33.2	+24:49:0.0	28.8[(a)]	8.0	7.3	7.1	198.0±5.1	-14.0±5.4	3

ID	RA	DEC	Dist.	J	H	K	$\mu_{\alpha,*}$	μ_{δ}	Mem ref.
	hh:mm:ss.s	dd:mm:ss.s	(pc)	(mag.)	(mag.)	(mag.)	(mas/yr)	(mas/yr)	
2MASS J03033668-2535329	03:03:36.7	-25:35:32.9	38.6[(a)]	8.0	7.3	7.1	213.2±8.0	94.5±8.0	3
HIP 15844 a	03:24:6.5	+23:47:6.0	16.9[(a)]	7.1	6.5	6.3	217.2±8.0	-129.2±8.0	1
HIP 15844 c	03:24:12.9	+23:46:19.0	17.9	8.3	7.7	7.5	199.0±8.0	-112.0±8.0	1
2MASS J04132663-0139211	04:13:26.6	-01:39:21.1	26.2	9.4	8.8	8.5	131.3±7.4	-9.5±3.0	3
CD-29 2360	05:34:59.2	-29:54:4.0	74.9	8.7	8.2	8.0	17.1±0.6	33.1±1.5	1
AP Col	06:04:52.2	-34:33:36.0	8.4	7.7	7.2	6.9	-118.9±5.9	-91.3±5.8	1
CD-56 1438	06:11:53.0	-56:19:5.0	118.6	9.8	9.3	9.2	-2.5±0.9	38.3±1.0	1
TYC 155-2167-1	06:41:9.3	+04:47:19.0	82.3	9.5	8.8	8.7	-7.9±2.2	-9.9±0.8	1
CD-28 3434	06:49:45.4	-28:59:17.0	120.8	9.1	8.7	8.6	-11.3±0.9	20.8±0.8	1
CD-42 2906	07:01:53.4	-42:27:56.0	101.0	9.2	8.7	8.6	-13.8±0.7	35.5±0.7	1
CD-48 2972	07:28:22.0	-49:08:38.0	82.8	8.5	8.1	8.1	-26.7±1.0	44.4±1.0	1
HD 61005	07:35:47.5	-32:12:14.0	35.3[(a)]	6.9	6.6	6.5	-58.8±0.8	74.0±0.7	1
CD-48 3199	07:47:26.0	-49:02:51.0	103.9	9.3	8.9	8.8	-22.4±2.1	36.1±0.9	1
CD-43 3604	07:48:49.8	-43:27:6.0	86.5	8.9	8.3	8.2	-26.8±1.3	39.6±1.0	1
2MASS J07535548-5710073	07:53:55.5	-57:10:7.0	145.7	10.3	9.8	9.7	-18.3±1.2	26.9±1.0	1
HD 67945	08:09:38.6	-20:13:50.0	77.0	7.4	7.2	7.2	-37.8±1.3	20.4±1.5	1
PMM 5314	08:28:34.6	-52:37:4.0	142.7	9.7	9.6	9.5	-24.1±1.0	22.7±1.5	1
PMM 7422	08:28:45.6	-52:05:27.0	141.4	9.3	9.1	8.9	-22.6±1.0	24.6±0.9	1
PMM 7956	08:29:51.9	-51:40:40.0	157.7	9.8	9.4	9.2	-23.0±1.1	18.8±0.9	1
PMM 6974	08:34:18.1	-52:15:58.0	147.4	10.5	10.0	9.9	-22.6±2.0	23.0±0.9	1
PMM 4280	08:34:20.5	-52:50:5.0	154.8	9.2	8.9	8.8	-21.0±0.9	22.5±0.9	1
PMM 6978	08:35:1.2	-52:14:1.0	147.3	10.4	9.9	9.8	-23.3±0.9	22.3±0.9	1
PMM 2456	08:35:43.7	-53:21:20.0	141.1	10.3	9.7	9.6	-23.6±1.8	24.3±1.3	1
PMM 351	08:36:24.2	-54:01:6.0	149.2	9.2	8.9	8.8	-24.4±2.0	20.7±1.3	1
PMM 3359	08:36:55.0	-53:08:34.0	144.8	10.1	9.7	9.6	-23.1±0.9	23.6±1.0	1
PMM 5376	08:37:2.3	-52:46:59.0	161.9	11.4	10.7	10.5	-20.8±1.4	20.9±1.4	1
PMM 4324	08:37:47.0	-52:52:12.0	152.3	8.8	8.6	8.5	-22.4±1.0	22.0±1.0	1
PMM 665	08:37:51.6	-53:45:46.0	154.8	10.1	9.7	9.6	-21.1±1.2	22.7±1.7	1
PMM 4336	08:37:55.6	-52:57:11.0	141.0	9.9	9.4	9.3	-21.2±0.9	17.9±1.0	1
PMM 4362	08:38:22.9	-52:56:48.0	147.3	9.8	9.4	9.4	-23.5±0.9	22.4±0.8	1
PMM 4413	08:38:55.7	-52:57:52.0	154.2	9.1	8.8	8.7	-22.3±0.9	21.6±0.9	1
CD-58 2194	08:39:11.6	-58:34:28.0	102.2	8.9	8.5	8.4	-32.7±1.0	35.4±1.0	1
PMM 686	08:39:22.6	-53:55:6.0	158.1	10.6	10.0	9.9	-21.3±1.6	21.7±1.6	1
V364 Vel	08:39:53.0	-52:57:57.0	167.4	10.3	9.9	9.8	-21.1±1.0	19.3±1.0	1
V365 Vel	08:40:6.2	-53:38:7.0	155.5	9.3	9.0	8.9	-20.0±1.4	23.4±1.3	1
PMM 8415	08:40:16.3	-52:56:29.0	133.8	10.2	9.7	9.6	-25.7±1.2	24.9±1.1	1
PMM 1759	08:40:18.3	-53:30:29.0	141.8	11.1	10.4	10.2	-26.2±1.7	21.2±1.7	1
PMM 1142	08:40:49.1	-53:37:45.0	159.2	9.7	9.4	9.3	-18.4±1.2	23.6±1.2	1
PMM 1174	08:41:22.7	-53:38:9.0	146.8	8.7	8.5	8.5	-23.6±1.9	22.7±1.2	1
V368 Vel	08:41:57.8	-52:52:14.0	141.5	11.1	10.4	10.3	-24.0±1.2	23.9±1.3	1
PMM 756	08:43:0.4	-53:54:8.0	154.6	9.8	9.4	9.3	-23.5±1.1	20.4±1.1	1
PMM 5811	08:43:17.9	-52:36:11.0	157.9	8.4	8.3	8.2	-21.3±1.1	21.6±1.1	1
PMM 2888	08:43:52.3	-53:14:0.0	147.3	8.8	8.7	8.6	-25.5±1.1	20.2±1.3	1
PMM 2012	08:43:59.0	-53:33:44.0	136.8	10.2	9.8	9.7	-20.9±1.4	12.7±1.4	1
V376 Vel	08:44:5.2	-52:53:17.0	165.5	9.6	9.3	9.2	-21.3±1.4	19.7±1.0	1
PMM 1373	08:44:10.2	-53:43:34.0	142.8	10.4	10.0	9.8	-24.8±1.5	10.6±1.5	1
V377 Vel	08:44:26.2	-52:42:32.0	173.3	10.0	9.6	9.6	-21.4±1.3	17.5±1.0	1
V379 Vel	08:45:26.9	-52:52:2.0	139.9	10.7	10.2	10.1	-25.2±1.1	23.4±1.1	1
V380 Vel	08:45:39.1	-52:26:0.0	137.8	8.9	8.7	8.6	-20.8±0.9	22.0±1.0	1
PMM 2182	08:45:48.0	-53:25:51.0	152.8	9.1	8.9	8.8	-26.3±1.0	18.5±2.1	1
CD-57 2315	08:50:8.1	-57:45:59.0	107.2	8.6	8.1	8.0	-34.1±2.0	31.0±1.0	1
2MASS J09020394-5808497	09:02:3.9	-58:08:50.0	138.1	9.9	9.5	9.4	-24.2±1.3	26.2±1.3	1
CD-62 1197	09:13:30.3	-62:59:9.0	116.1	8.9	8.4	8.3	-34.1±1.1	27.4±1.0	1
TYC 7695-335-1	09:28:54.1	-41:01:19.0	153.0	9.8	9.3	9.1	-28.7±1.1	13.6±1.1	1
BD-20 2977	09:39:51.4	-21:34:17.0	93.3	8.8	8.5	8.4	-50.0±0.9	7.8±0.9	1
TYC 9217-641-1	09:42:47.4	-72:39:50.0	143.8	10.4	10.0	9.8	-30.1±1.3	18.9±1.3	1
CD-39 5833	09:47:19.9	-40:03:10.0	113.4	9.4	9.0	8.9	-40.6±1.2	16.3±1.6	1
HD 85151a	09:48:43.2	-44:54:8.0	65.9	8.0	7.7	7.6	-68.4±8.0	33.5±3.0	1
HD 85151b	09:48:43.4	-44:54:9.0	65.9	8.0	7.7	7.6	3.9±7.6	1.6±3.7	1
CD-65 817	09:49:9.0	-65:40:21.0	134.9	9.1	8.8	8.7	-31.4±7.6	16.1±6.9	1

ID	RA	DEC	Dist.	J	H	K	$\mu_{\alpha,*}$	μ_{δ}	Mem ref.
	hh:mm:ss.s	dd:mm:ss.s	(pc)	(mag.)	(mag.)	(mag.)	(mas/yr)	(mas/yr)	
HD 309851	09:55:58.3	-67:21:22.0	105.1	8.7	8.4	8.3	-42.4±0.9	25.7±1.2	1
2MASS J10142048-8138423	10:14:20.5	-81:38:42.0	125.7	10.0	9.3	9.1	-37.0±1.3	18.5±2.3	1
HD 310316	10:49:56.1	-69:51:22.0	115.0	8.8	8.4	8.3	-43.5±1.2	13.5±0.9	1
CP-69 1432	10:53:51.5	-70:02:16.0	147.1	9.4	9.2	9.0	-32.6±1.3	12.1±1.0	1
HD 103742	11:56:42.3	-32:16:5.0	33.7[(a)]	6.5	6.2	6.1	-166.1±1.0	-7.7±1.0	1
CD-42 7422	12:06:32.9	-42:47:51.0	106.9	9.2	8.7	8.6	-50.3±1.3	-2.5±1.0	1
CD-74 673	12:20:34.4	-75:39:29.0	50.1	8.6	8.1	7.9	-109.4±2.0	4.2±1.1	1
CD-75 652	13:49:12.9	-75:49:48.0	77.1	8.4	8.0	8.0	-62.2±1.0	-31.5±1.9	1
2MASS J13591045-1950034	13:59:10.4	-19:50:3.4	10.7	8.3	7.8	7.4	-552.7±8.0	-183.1±8.0	3
HD 129496	14:46:21.4	-67:46:16.0	84.8	7.8	7.5	7.4	-47.6±1.4	-39.7±1.0	1
NY Aps	15:12:23.4	-75:15:16.0	50.3[(a)]	7.8	7.5	7.4	-75.6±1.4	-73.5±1.2	1
2MASS J18083702-0426259	18:08:37.0	-04:26:25.9	167.5[(a)]	5.8	5.2	4.9	-8.6±1.3	-15.7±1.2	3
CD-52 9381	20:07:23.8	-51:47:27.0	29.4	8.2	7.6	7.4	85.9±0.7	-143.9±0.7	1, 3
2MASS J20531465-0221218	20:53:14.7	-02:21:21.8	37.9	9.3	8.7	8.4	186.8±8.0	15.7±8.0	3
2MASS J23205766-0147373	23:20:57.7	-01:47:37.3	41.0	9.4	8.8	8.5	168.6±8.0	26.2±8.0	3
2MASS J23581366-1724338	23:58:13.7	-17:24:33.8	39.1	8.3	7.7	7.4	222.6±4.1	12.8±1.5	3
			BPC						
2MASS J00172353-6645124	00:17:23.5	-66:45:12.0	36.3	8.6	7.9	7.7	102.9±1.0	-15.0±1.0	3
GJ 3076	01:11:25.4	+15:26:21.0	19.3	9.1	8.5	8.2	192.0±8.0	-130.0±8.0	3
Barta 161 12	01:35:13.9	-07:12:52.0	37.9	9.0	8.4	8.1	93.0±1.7	-48.0±2.2	3, 5
G 271-110	01:36:55.1	-06:47:38.0	24.0	9.7	9.1	8.9	172.6±8.0	-84.2±8.0	3
HIP 10679	02:17:24.7	+28:44:30.0	40.0[(a)]	6.6	6.4	6.3	98.2±1.0	-67.4±1.0	1
HD 14082	02:17:25.3	+28:44:42.0	39.5[(a)]	6.0	5.8	5.8	94.3±1.0	-72.2±1.0	1
BD+30 397 b	02:27:28.1	+30:58:41.0	42.4	8.8	8.1	7.9	81.5±4.6	-69.1±3.2	1
AG Tri	02:27:29.3	+30:58:25.0	42.4[(a)]	7.9	7.2	7.1	80.4±0.9	-70.1±1.3	1
EXO 0235.2-5216	02:36:51.7	-52:03:4.0	28.6	8.4	7.8	7.5	102.2±0.8	1.2±0.8	1, 3
HD 29391	04:37:36.1	-02:28:25.0	29.4[(a)]	4.7	4.8	4.5	44.2±1.0	-64.4±1.0	1
V1005 Ori	04:59:34.8	+01:47:1.0	24.2[(a)]	7.1	6.5	6.3	37.5±0.8	-93.5±0.9	1
CD-57 1054	05:00:47.1	-57:15:25.0	26.9[(a)]	7.1	6.4	6.2	35.5±0.9	74.4±0.9	1
HIP 23418aa	05:01:58.8	+09:58:59.0	37.8[(a)]	7.2	6.7	6.4	17.2±8.0	-82.0±8.0	1, 3
BD-21 1074b	05:06:49.5	-21:35:4.0	20.2	7.0	6.4	6.1	33.1±2.7	-33.2±2.0	1, 3
2MASS J05200029+0613036	05:20:0.3	+06:13:4.0	67.8	9.3	8.7	8.6	9.4±1.9	-34.7±2.1	1
RX J0520.5+0616	05:20:31.8	+06:16:11.0	71.0	9.2	8.7	8.6	9.5±1.8	-32.8±2.1	1
2MASS J05241914-1601153	05:24:19.1	-16:01:15.0	26.8	8.7	8.1	7.8	16.0±2.5	-34.8±3.5	3
AF Lep	05:27:4.8	-11:54:3.0	27.0[(a)]	5.3	5.1	4.9	17.7±1.0	-49.5±1.0	1
Beta Pic	05:47:17.1	-51:03:59.0	19.5[(a)]	3.7	3.5	3.5	4.7±1.0	83.1±1.0	1
2MASS J06131330-2742054	06:13:13.3	-27:42:5.4	29.2	8.0	7.4	7.1	-13.1±1.6	-0.3±1.3	3
AO Men	06:18:28.2	-72:02:41.0	38.6[(a)]	7.5	7.0	6.8	-6.4±0.9	76.4±0.8	1
2MASS J09133435-7550099	09:13:34.4	-75:50:10.0	62.7	11.9	11.3	11.0	0.0±0.0	0.0±0.0	1
TWA22	10:17:26.9	-53:54:27.0	17.6	8.6	8.1	7.7	-177.0±3.3	-10.3±3.3	1
2MASS J14142141-1521215	14:14:21.4	-15:21:21.5	30.2[(a)]	7.4	6.8	6.6	-141.1±2.3	-187.9±4.6	3
V343 Nor	15:38:57.5	-57:42:27.0	38.4[(a)]	6.4	6.0	5.9	-43.6±2.0	-95.6±1.5	1
CD-27 11535	17:15:3.6	-27:49:40.0	87.3	8.2	7.5	7.4	-5.2±0.8	-43.6±0.8	1
V824 Ara	17:17:25.5	-66:57:4.0	31.5[(a)]	5.3	4.9	4.7	-21.8±1.0	-136.9±1.0	1
HD 155555 c	17:17:31.3	-66:57:6.0	31.5	8.5	7.9	7.6	-11.0±2.0	-143.0±2.0	1
GSC 08350-01924	17:29:20.7	-50:14:53.0	66.3	8.9	8.2	8.0	-5.8±1.5	-62.7±5.1	1, 3
CD-54 7336	17:29:55.1	-54:15:49.0	68.4	7.9	7.5	7.4	-9.8±3.2	-60.0±1.7	1
HD 161460	17:48:33.7	-53:06:43.0	71.0	7.3	6.9	6.8	-3.6±1.0	-58.4±1.3	1
HD 164249	18:03:3.4	-51:38:56.0	48.1[(a)]	6.2	6.0	5.9	4.0±1.0	-86.5±1.0	1
V4046 Sgr	18:14:10.5	-32:47:33.0	76.9	8.1	7.4	7.2	5.5±1.2	-50.9±1.9	1, 3
GSC 07396-00759	18:14:22.1	-32:46:10.0	95.2	9.4	8.8	8.5	1.9±5.7	-41.2±2.6	1, 3
HD 168210	18:19:52.2	-29:16:33.0	72.4[(a)]	7.5	7.2	7.1	3.5±1.4	-46.4±1.5	1
2MASS J18420694-5554254	18:42:6.9	-55:54:25.0	51.9	9.5	8.8	8.6	9.7±12.1	-81.2±2.8	3
HD 172555	18:45:26.9	-64:52:17.0	28.6[(a)]	4.4	4.3	4.3	32.5±1.0	-148.8±1.0	1
CD-64 1208	18:45:37.0	-64:51:46.0	28.6	6.9	6.3	6.1	25.9±8.0	-184.2±8.0	1
Smethells 20	18:46:52.6	-62:10:36.0	52.4	8.7	8.0	7.9	13.6±1.4	-79.4±1.4	1, 3
CD-31 16041	18:50:44.5	-31:47:47.0	53.2	8.3	7.7	7.5	16.4±1.6	-72.8±1.1	1, 3

ID	RA	DEC	Dist.	J	H	K	$\mu_{\alpha,*}$	μ_{δ}	Mem ref.
	hh:mm:ss.s	dd:mm:ss.s	(pc)	(mag.)	(mag.)	(mag.)	(mas/yr)	(mas/yr)	
PZ Tel	18:53:5.9	-50:10:50.0	51.5[a]	6.9	6.5	6.4	19.1±1.1	-81.8±1.1	1
TYC 6872-1011-1	18:58:4.2	-29:53:5.0	82.6	8.9	8.2	8.0	12.2±1.3	-45.7±2.5	1, 3
CD-26 13904	19:11:44.7	-26:04:9.0	78.9	8.1	7.6	7.4	17.9±1.4	-45.0±1.9	1
Eta Tel	19:22:51.2	-54:25:26.0	48.3[a]	5.1	5.1	5.0	25.6±1.0	-82.7±1.0	1
HD 181327	19:22:58.9	-54:32:17.0	51.8[a]	6.2	6.0	5.9	24.0±1.0	-81.8±1.0	1
2MASS J19233820-4606316	19:23:38.2	-46:06:32.0	72.2	9.1	8.4	8.3	17.2±1.0	-55.0±1.1	3
2MASS J19312434-2134226	19:31:24.3	-21:34:22.6	26.0	8.7	8.1	7.8	58.7±6.2	-109.5±2.3	3
UCAC3 116-474938	19:56:2.9	-32:07:19.0	58.4	9.0	8.3	8.1	35.2±1.8	-59.9±1.5	1, 3
TYC 7443-1102-1	19:56:4.4	-32:07:38.0	56.3	8.7	8.0	7.8	31.9±1.4	-65.1±1.2	1, 3
2MASS J20013718-3313139	20:01:37.2	-33:13:14.0	63.4	9.2	8.5	8.2	27.0±3.2	-58.6±2.0	1, 3
HD 190102	20:04:18.1	-26:19:46.0	46.8[a]	7.0	6.7	6.6	32.3±1.0	-75.1±1.0	1
HD 191089	20:09:5.2	-26:13:26.0	52.3[a]	6.3	6.1	6.1	39.2±1.0	-68.3±1.0	1
2MASS J20100002-2801410	20:10:0.0	-28:01:41.0	48.0	8.7	8.0	7.7	40.7±3.0	-62.0±1.7	3
2MASS J20333759-2556521	20:33:37.6	-25:56:52.1	48.3	9.7	9.1	8.9	52.8±1.7	-75.9±1.3	3
AT Mic S	20:41:51.1	-32:26:10.0	9.5	5.8	5.2	4.9	286.2±8.0	-377.2±8.0	1
AT Mic N	20:41:51.2	-32:26:7.0	9.5[a]	5.8	5.2	4.9	269.3±8.0	-365.7±8.0	1
2MASS J20434114-2433534 A	20:43:41.1	-24:33:53.0	45.1	8.6	8.0	7.8	57.2±1.2	-70.2±1.8	3
2MASS J20434114-2433534 B	20:43:41.1	-24:33:53.0	45.1	8.6	8.0	7.8	57.2±1.2	-70.2±1.8	1
AU Mic	20:45:9.5	-31:20:27.0	9.8	5.4	4.8	4.5	287.8±3.7	-359.0±3.7	1
HD 199143	20:55:47.7	-17:06:51.0	45.7[a]	6.2	5.9	5.8	58.8±1.0	-62.8±1.0	1
AZ Cap	20:56:2.7	-17:10:54.0	47.9	7.8	7.2	7.0	57.6±1.1	-59.9±1.2	1, 3
GSC 06354-00357	21:10:5.3	-19:19:57.0	32.6	8.1	7.4	7.2	0.0±0.0	0.0±0.0	1
2MASS J21100535-1919573	21:10:5.3	-19:19:57.0	32.6	8.1	7.4	7.2	89.0±0.9	-89.9±1.8	3
TYC 2211-1309-1	22:00:41.6	+27:15:14.0	46.6	8.6	7.9	7.7	74.9±1.2	-16.8±0.5	1, 3
CP-72 2713	22:42:48.9	-71:42:21.0	37.3	7.8	7.1	6.9	92.7±0.8	-51.1±0.8	1, 3
WW PsA	22:44:58.0	-33:15:2.0	20.1[a]	7.8	7.2	6.9	178.7±1.0	-123.0±2.0	1
TX PsA	22:45:0.0	-33:15:26.0	20.1	8.7	8.1	7.8	171.1±1.3	-125.2±4.3	1
2MASS J23301341-2023271	23:30:13.4	-20:23:27.1	16.2[a]	7.2	6.6	6.3	314.5±8.0	-208.1±8.0	3
BD-13 6424	23:32:30.9	-12:15:52.0	27.9	7.5	6.8	6.6	137.4±1.0	-81.0±1.0	1, 3
			CAR						
HD 8813	01:23:25.9	-76:36:42.0	46.5[a]	7.2	6.9	6.8	99.0±0.8	-18.7±0.9	1
WISE J025901.49-423220.4	02:59:1.5	-42:32:20.0	103.3	12.2	11.7	11.4	39.9±4.1	-6.9±4.4	1
CD-65 149	03:06:14.5	-65:21:32.0	90.0	8.6	8.2	8.0	42.6±1.3	7.1±0.8	1
HD 19545	03:07:50.8	-27:49:52.0	54.6[a]	5.9	5.9	5.8	66.3±1.0	-19.1±1.0	1, 2
HD 22213	03:34:16.4	-12:04:7.0	52.4	7.3	7.0	6.8	75.6±2.3	-34.3±1.5	1
CD-45 1384	04:03:53.4	-44:39:32.0	109.1	9.0	8.6	8.5	32.0±1.1	1.2±1.1	1
CD-44 1533	04:22:45.7	-44:32:52.0	103.7	9.0	8.7	8.6	31.2±0.9	4.0±0.9	1
BD-20 951	04:52:49.5	-19:55:2.0	72.4	8.0	7.5	7.3	38.7±0.9	-15.6±0.9	1
HD 269620	05:29:27.1	-68:52:5.0	91.2	8.4	8.2	8.1	21.1±1.4	28.3±1.2	1
AT Col	05:37:5.3	-39:32:26.0	66.2	7.9	7.5	7.3	31.1±1.3	8.0±1.3	1
HD 269921	05:38:34.5	-68:53:7.0	90.8	8.9	8.4	8.4	18.8±1.1	29.5±1.3	1
HD 42270	05:53:29.3	-81:56:53.0	54.0	7.5	7.0	6.9	28.6±1.2	64.2±1.2	1
CD-48 2324	06:28:6.1	-48:26:53.0	141.8	9.5	9.1	9.0	7.3±1.2	11.6±1.2	1
CD-37 2984	06:39:46.7	-37:50:10.0	75.3	9.3	8.8	8.7	11.3±0.7	9.6±0.8	1
CD-52 1641	06:41:12.5	-52:07:39.0	99.2	9.1	8.5	8.5	7.5±0.8	18.9±0.8	1
CD-41 2572	06:45:37.9	-41:12:41.0	80.7	9.2	8.8	8.7	11.4±1.8	10.1±1.7	1
HD 51062	06:53:47.4	-43:06:51.0	94.4[a]	7.5	7.2	7.1	5.5±3.6	11.0±0.9	1
CD-57 1709	07:21:23.7	-57:20:37.0	100.5	9.2	8.8	8.7	0.8±1.0	22.1±0.8	1
CD-42 3328	07:33:21.2	-42:55:42.0	125.1	9.9	9.6	9.4	-2.9±1.0	9.1±0.9	1
CD-60 1850	07:43:42.9	-61:07:17.0	91.0	9.2	8.7	8.5	2.2±1.3	26.4±1.3	1
HIP 38712	07:55:31.4	+08:51:47.0	39.0[a]	5.1	5.0	5.0	-7.4±1.0	-89.9±1.0	1
TYC 8557-1251-1	07:55:31.6	-54:36:51.0	123.0	9.8	9.3	9.2	-1.7±1.2	16.5±2.5	1
2MASS J08110934-5555563	08:11:9.3	-55:55:56.0	129.0	9.9	9.5	9.4	-5.9±1.0	15.7±1.2	1
BD-07 2388	08:13:51.0	-07:38:25.0	42.6	7.6	7.1	6.9	-23.7±1.5	-46.0±1.1	1
CD-38 4458	08:26:10.0	-39:02:5.0	142.8	9.0	8.7	8.6	-6.4±1.1	7.2±1.1	1
CP-54 1712	08:37:10.9	-55:18:10.0	180.8	9.8	9.4	9.4	-5.9±1.0	10.6±1.8	1
CD-61 2010	08:42:0.5	-62:18:26.0	121.4	9.4	9.0	8.8	-10.2±0.8	18.6±0.8	1

ID	RA	DEC	Dist.	J	H	K	$\mu_{\alpha,*}$	μ_{δ}	Mem ref.
	hh:mm:ss.s	dd:mm:ss.s	(pc)	(mag.)	(mag.)	(mag.)	(mas/yr)	(mas/yr)	
CD-75 392	08:50:5.4	-75:54:38.0	91.4	9.3	8.8	8.7	-15.1±1.5	33.1±0.9	1
CD-53 2515	08:51:56.4	-53:55:57.0	137.1	9.3	8.9	8.7	-11.7±1.0	11.3±1.0	1
2MASS J08521921-6004443	08:52:19.2	-60:04:44.0	163.9	9.9	9.5	9.4	-6.5±1.6	13.2±1.3	1
2MASS J08563149-5700406	08:56:31.5	-57:00:41.0	191.6	10.3	9.9	9.8	-8.2±1.4	8.9±2.7	1
TYC 8582-3040-1	08:57:45.6	-54:08:37.0	143.2	9.9	9.5	9.3	-11.9±1.8	10.4±2.3	1
CD-49 4008	08:57:52.2	-49:41:51.0	102.9	9.1	8.8	8.6	-17.3±0.9	10.9±0.8	1
CD-54 2499	08:59:28.7	-54:46:49.0	109.5	8.8	8.5	8.4	-15.9±1.3	14.0±1.2	1
CD-55 2543	09:09:29.4	-55:38:27.0	115.2	8.8	8.5	8.4	-14.8±1.4	14.8±1.8	1
TYC 8174-1586-1	09:11:15.8	-50:14:15.0	117.2	10.2	9.6	9.5	-15.9±8.3	10.7±2.3	1
CD-54 2644	09:13:16.9	-55:29:3.0	131.7	8.9	8.5	8.4	-15.0±1.9	10.3±1.9	1
HD 309751	09:31:44.7	-65:14:53.0	141.6	8.8	8.5	8.4	-13.1±1.8	14.6±1.2	1
CD-48 4797	09:33:14.3	-48:48:33.0	47.0	8.9	8.3	8.1	-46.6±1.4	23.0±1.6	1, 3
CP-62 1293	09:43:8.8	-63:13:4.0	69.4	9.0	8.7	8.6	-33.1±1.1	26.9±1.0	1
TYC 9217-417-1	09:59:57.7	-72:21:47.0	83.6	9.5	8.9	8.7	-28.3±1.1	27.8±1.0	1
BD-19 3018	10:27:37.3	-20:27:11.0	60.2	8.4	8.0	7.9	-51.5±1.2	-24.5±3.0	1
CD-69 783	10:41:23.0	-69:40:43.0	86.5	8.9	8.5	8.4	-33.5±1.6	19.5±1.6	1
TYC 8962-1747-1	11:08:7.9	-63:41:47.0	88.2	9.1	8.5	8.3	-37.1±1.9	8.3±1.9	1
HD 107722	12:23:29.0	-77:40:51.0	59.0	7.4	7.2	7.1	-65.7±0.9	11.8±0.9	1
HD 152598	16:52:58.1	+31:42:6.0	29.2[(a)]	4.7	4.5	4.6	-90.8±1.0	-17.3±1.0	1
TYC 9486-927-1	21:25:27.5	-81:38:28.0	36.3	8.2	7.6	7.3	58.9±1.5	-109.4±1.0	1
BD-03 5579	23:09:37.1	-02:25:55.0	63.0	8.6	8.0	7.8	55.7±1.8	-45.1±1.6	1
			COL						
HD 984	00:14:10.2	-07:11:57.0	47.2[(a)]	6.4	6.2	6.1	102.8±1.0	-66.4±1.0	1, 2
BD+17 232	01:37:39.4	+18:35:33.0	65.1	7.5	6.9	6.7	68.6±0.8	-47.3±0.6	1
CD-52 381	01:52:14.6	-52:19:33.0	83.4	9.1	8.5	8.4	51.3±1.2	-6.7±1.1	1
BD-16 351	02:01:35.6	-16:10:1.0	80.9	8.6	8.1	8.0	53.5±1.5	-30.3±1.9	1
CD-53 386	02:01:53.7	-52:34:53.0	106.9	9.2	8.7	8.6	38.5±2.0	-10.0±1.4	1
CD-44 753	02:30:32.4	-43:42:23.0	51.3	8.0	7.4	7.2	80.3±0.9	-13.3±0.9	1, 3, 5
HD 16754	02:39:48.0	-42:53:30.0	45.5[(a)]	4.7	4.6	4.5	88.2±1.0	-17.8±1.0	1, 2
TYC 8862-19-1	02:58:4.0	-62:41:14.0	92.6	9.6	9.0	8.9	40.5±1.5	5.5±1.0	1
BD-11 648	03:21:49.7	-10:52:18.0	128.1	9.8	9.4	9.3	31.0±1.2	-14.5±1.6	1
GSC 08499-00304	03:24:15.0	-59:01:13.0	92.9	9.5	8.9	8.7	37.5±1.1	9.6±1.1	1, 3
CD-36 1289	03:25:51.9	-35:56:26.0	107.5	8.6	8.2	8.1	34.6±1.0	-1.8±1.0	1
HD 21423	03:25:55.8	-35:55:15.0	107.5[(a)]	6.2	6.2	6.2	36.3±1.0	-4.4±1.0	1
HD 21434	03:25:59.0	-35:57:30.0	107.8	6.7	6.6	6.6	34.2±2.0	-5.1±2.0	1
V1221 Tau	03:28:15.0	+04:09:48.0	81.5	8.0	7.6	7.4	46.9±0.9	-33.8±0.7	1
HD 21997	03:31:53.6	-25:36:51.0	71.9[(a)]	6.2	6.1	6.1	53.9±1.0	-14.9±1.0	1
HIP 17248	03:41:37.3	+55:13:7.0	35.4[(a)]	8.3	7.6	7.5	95.7±0.8	-119.2±1.0	1, 2
HD 23384	03:47:10.6	+51:42:23.0	57.5[(a)]	6.2	6.1	6.1	60.2±1.0	-74.6±1.0	1
TYC 65-1471-1	03:48:58.8	+01:10:54.0	111.1	8.9	8.4	8.3	33.6±1.0	-20.9±0.8	1
BD-04 700	03:57:37.2	-04:16:16.0	106.5	9.2	8.8	8.8	33.7±1.3	-18.0±1.4	1
HD 26980	04:14:22.6	-38:19:2.0	80.7[(a)]	7.9	7.7	7.6	38.6±0.9	3.0±0.8	1
HD 27679	04:21:10.3	-24:32:21.0	78.0	8.2	7.9	7.8	38.3±0.9	-6.9±1.1	1
CD-43 1395	04:21:48.7	-43:17:33.0	141.0	8.9	8.5	8.4	20.5±0.9	4.9±1.0	1
2MASS J04240094-5512223	04:24:0.9	-55:12:22.0	66.4	9.8	9.2	8.9	42.4±2.1	17.2±2.1	1, 3, 5
CD-44 1568	04:27:20.5	-44:20:39.0	86.2	9.2	8.7	8.6	32.5±1.1	4.6±1.1	1
CD-36 1785	04:34:50.8	-35:47:21.0	80.1	9.3	8.8	8.6	33.4±0.9	0.4±0.9	1
BD+08 742	04:42:32.1	+09:06:1.0	105.6	9.6	9.2	9.1	26.7±0.8	-27.8±1.1	1
HD 30447	04:46:49.5	-26:18:9.0	80.1[(a)]	7.1	7.0	6.9	30.5±1.1	-2.4±1.8	1
2MASS J04515303-4647309	04:51:53.0	-46:47:31.0	77.5	9.8	9.1	8.9	30.5±1.5	12.2±1.5	1, 3, 5
HD 31242 N	04:51:53.5	-46:47:13.0	68.1	8.5	8.2	8.2	33.5±1.1	16.1±1.3	1
HD 272836	04:53:5.2	-48:44:39.0	78.6	8.9	8.4	8.2	29.3±0.9	14.9±0.9	1
BD-08 995	04:58:48.6	-08:43:40.0	86.8	8.8	8.5	8.3	25.2±1.3	-22.4±1.2	1
HD 31647 b	04:59:15.4	+37:53:30.0	52.4	7.0	5.9	5.9	46.3±2.5	-97.8±2.5	1
HD 31647 a	04:59:15.4	+37:53:25.0	52.4[(a)]	4.9	5.0	4.9	46.3±1.0	-97.8±1.0	1, 2
HD 32372	05:00:51.9	-41:01:7.0	76.3[(a)]	8.1	7.9	7.8	33.4±0.8	10.7±0.9	1
HD 32309	05:01:25.6	-20:03:7.0	60.6[(a)]	5.0	5.0	5.0	36.4±1.0	-16.5±1.0	1, 2

ID	RA	DEC	Dist.	J	H	K	$\mu_{\alpha,*}$	μ_{δ}	Mem ref.
	hh:mm:ss.s	dd:mm:ss.s	(pc)	(mag.)	(mag.)	(mag.)	(mas/yr)	(mas/yr)	
AS Col	05:20:38.0	-39:45:18.0	48.3[a]	6.4	6.2	6.1	38.4±1.0	13.1±1.0	1
CD-43 1846	05:26:23.0	-43:22:36.0	84.7[a]	8.1	7.9	7.8	21.2±1.3	10.3±2.9	1
HD 35996	05:26:24.0	-43:22:33.0	71.4[a]	7.4	7.3	7.2	23.8±1.2	12.9±1.0	1
HD 35841	05:26:36.6	-22:29:24.0	94.0	8.0	7.8	7.8	18.0±0.8	-7.9±1.0	1
HD 274561	05:28:55.1	-45:34:58.0	86.8	9.6	9.1	9.0	19.2±1.0	13.8±1.0	1
HD 36329	05:29:24.1	-34:30:56.0	70.9[a]	7.3	7.1	6.9	25.8±0.8	5.9±0.8	1
AG Lep	05:30:19.1	-19:16:32.0	115.1	8.4	8.0	7.9	14.1±1.5	-7.3±1.2	1
AH Lep	05:34:9.2	-15:17:3.0	61.3	7.2	7.0	6.9	26.4±1.3	-24.1±1.2	1, 2
HD 37286	05:36:10.3	-28:42:29.0	52.9[a]	6.0	5.9	5.9	25.8±1.0	-3.0±1.0	1, 2
HD 37484	05:37:39.6	-28:37:35.0	56.8[a]	6.5	6.3	6.3	24.3±1.0	-4.1±1.0	1, 2
TYC 119-1242-1	05:37:45.3	+02:30:57.0	70.8	9.0	8.4	8.3	18.6±3.7	-39.8±2.0	1
TYC 119-497-1	05:37:46.5	+02:31:26.0	67.0	9.0	8.4	8.2	21.8±2.4	-41.4±1.3	1
BD-08 1195	05:38:35.0	-08:56:40.0	82.0	8.5	8.1	8.0	16.7±0.9	-22.3±1.6	1
CD-34 2406	05:42:34.3	-34:15:42.0	89.8	9.2	9.0	8.7	14.6±1.5	7.0±0.9	1
HD 38207	05:43:21.0	-20:11:21.0	86.3	7.7	7.5	7.5	17.4±1.4	-6.2±1.5	1
HD 38206	05:43:21.7	-18:33:27.0	75.2[a]	5.8	5.8	5.8	18.9±1.0	-14.0±1.0	1
HD 38397	05:43:35.8	-39:55:25.0	55.3[a]	7.1	6.8	6.8	25.8±1.1	13.1±1.2	1, 2
CD-38 2198	05:45:16.3	-38:36:49.0	134.1	9.6	9.2	9.1	10.7±1.1	5.7±1.7	1
CD-29 2531	05:50:21.4	-29:15:21.0	107.8	9.6	9.2	9.1	11.6±1.0	2.1±0.8	1
CD-52 1363	05:51:1.2	-52:38:13.0	110.5	9.1	8.7	8.6	10.1±1.5	17.2±0.9	1
HD 40216	05:55:43.2	-38:06:16.0	54.4[a]	6.5	6.3	6.2	20.5±1.0	9.3±1.0	1
RT Pic	06:00:41.3	-44:53:50.0	52.6[a]	7.7	7.4	7.3	17.4±0.9	21.3±0.9	1, 2
V1358 Ori	06:19:8.1	-03:26:20.0	49.2[a]	6.8	6.6	6.6	10.4±0.4	-43.3±0.4	1
AB Pic	06:19:12.9	-58:03:16.0	46.1[a]	7.6	7.1	7.0	16.2±0.8	45.7±0.8	1
CD-40 2458	06:26:6.9	-41:02:54.0	94.5	8.5	8.2	8.0	5.0±1.2	11.3±1.3	1
TYC 4810-181-1	06:31:55.2	-07:04:59.0	87.5	9.8	9.2	9.1	7.0±2.0	-19.2±1.6	1
HD 295290	06:40:22.3	-03:31:59.0	60.2	7.4	7.0	7.0	3.4±1.0	-37.9±0.7	1
HD 48370	06:43:1.0	-02:53:19.0	34.1	6.7	6.4	6.3	14.5±0.6	-71.0±1.1	1
HD 49855	06:43:46.2	-71:58:35.0	58.1[a]	7.7	7.4	7.3	4.6±0.9	60.9±0.8	1
CD-36 3202	06:52:46.7	-36:36:17.0	101.5	9.4	8.9	8.7	-1.6±0.9	6.2±0.8	1
TYC 9178-284-1	06:55:25.2	-68:06:21.0	108.3	9.7	9.1	8.9	1.2±1.0	26.4±1.4	1
HD 51797	06:56:23.5	-46:46:55.0	77.7	8.4	7.9	7.8	-1.6±1.0	18.5±0.9	1
HD 55279	07:00:30.5	-79:41:46.0	58.8[a]	8.3	7.8	7.7	1.9±0.9	59.8±0.9	1
CD-39 3026	07:01:51.8	-39:22:4.0	119.9	9.9	9.4	9.3	-0.1±0.8	7.9±0.8	1
CD-63 408	08:24:6.0	-63:34:3.0	118.6	8.6	8.2	8.1	-13.7±1.1	18.2±1.6	1
V479 Car	09:23:35.0	-61:11:36.0	87.7[a]	8.6	8.1	8.0	-24.5±2.5	12.7±1.3	1
CP-52 2481	09:32:26.1	-52:37:40.0	101.9	9.4	9.0	8.8	-26.8±1.5	6.9±2.0	1
HD 298936	10:13:14.8	-52:30:54.0	50.5	7.9	7.4	7.2	-60.9±1.5	13.9±0.8	1
BD+44 3670	21:00:47.0	+45:30:10.0	57.8	7.3	7.0	6.9	39.2±1.1	8.6±0.5	1, 2
TYC 1158-1185-1 S	22:42:48.8	+13:30:54.0	50.2	8.6	8.0	8.0	72.8±1.3	-41.0±1.5	1
TYC 1158-1185-1 N	22:42:48.9	+13:30:53.0	50.2	8.6	8.0	8.0	72.8±1.3	-41.0±1.5	1, 3
V342 Peg	23:07:28.7	+21:08:3.0	39.4[a]	5.4	5.3	5.2	107.9±1.0	-49.6±1.0	1, 2
HD 222439	23:40:24.5	+44:20:2.0	51.6[a]	4.6	4.6	4.6	80.7±1.0	-18.7±1.0	1, 2
			ECH						
EG Cha	08:36:56.2	-78:56:46.0	108.7	8.2	7.5	7.3	-26.8±1.0	25.2±1.1	1
RX J0902.9-7759	09:02:51.3	-77:59:35.0	100.0	10.1	9.5	9.2	-33.9±1.7	22.0±1.7	1
2MASS J09053087-8134572	09:05:30.9	-81:34:57.0	93.9	12.2	11.6	11.3	-35.2±9.6	27.2±9.6	1
2MASS J09152912-7608471	09:15:29.1	-76:08:47.0	117.5	9.3	8.7	8.5	-28.2±1.3	18.7±1.4	1
2MASS J09345604-7804193	09:34:56.1	-78:04:19.0	121.6	9.8	9.1	8.9	-27.5±1.4	18.3±1.3	1
RX J1005.3-7749	10:05:20.0	-77:48:42.0	91.6	9.8	9.1	8.9	-44.4±1.9	10.1±1.9	1
DZ Cha	11:49:31.9	-78:51:1.0	102.7	9.4	8.7	8.5	-41.1±4.3	-9.4±1.7	1, 3
T Cha	11:57:13.5	-79:21:32.0	107.5	9.0	7.9	7.0	-39.9±3.6	-7.1±1.3	1
EE Cha	11:58:35.2	-77:49:31.0	108.7[a]	6.3	6.2	6.1	-42.0±1.0	-9.1±1.0	1
Eps Cha	11:59:37.6	-78:13:19.0	111.1[a]	5.0	5.0	5.0	-41.2±1.0	-8.5±1.0	1
HIP 58490	11:59:42.3	-76:01:26.0	101.0[a]	9.1	8.5	8.3	-39.5±1.5	-6.1±1.8	1
2MASS J12000511-7811346	12:00:5.0	-78:11:34.0	111.1	5.8	5.2	4.6	-39.0±1.0	-5.7±1.0	1
DX Cha	12:00:5.1	-78:11:35.0	115.0[a]	5.8	5.2	4.6	-39.0±1.0	-5.7±1.0	1

ID	RA	DEC	Dist.	J	H	K	$\mu_{\alpha,*}$	μ_{δ}	Mem ref.
	hh:mm:ss.s	dd:mm:ss.s	(pc)	(mag.)	(mag.)	(mag.)	(mas/yr)	(mas/yr)	
HD 104467	12:01:39.1	-78:59:17.0	106.5	7.3	7.0	6.8	-40.7±1.1	-5.5±1.0	1
2MASS J12020369-7853012	12:02:3.8	-78:53:1.0	110.5	9.2	8.5	8.3	-39.0±5.3	-5.8±1.7	1
2MASS J12043615-7731345	12:04:36.2	-77:31:35.0	116.9	9.8	9.1	8.9	-36.8±1.6	-1.7±1.6	1
HD 105923	12:11:38.1	-71:10:36.0	117.1	7.7	7.3	7.2	-36.9±1.7	-8.1±1.1	1
2MASS J12164593-7753333	12:16:46.0	-77:53:33.0	116.3	10.1	9.5	9.2	-36.1±1.6	-9.9±1.6	1
2MASS J12194369-7403572	12:19:43.8	-74:03:57.0	108.9	9.7	9.0	8.9	-40.1±1.9	-6.6±1.9	1
RX J1220.4-7407	12:20:21.9	-74:07:39.0	114.8	9.3	8.6	8.4	-37.8±1.8	-6.1±1.8	1
CD-74 712	12:39:21.3	-75:02:39.0	108.6	8.4	8.0	7.8	-38.9±1.5	-13.7±1.6	1
TYC 9245-535-1	12:56:8.4	-69:26:54.0	119.3	8.9	8.2	8.0	-34.9±2.6	-15.3±3.3	1
CD-69 1055	12:58:25.6	-70:28:49.0	106.7	8.2	7.7	7.5	-39.4±1.6	-17.4±1.1	1
MP Mus	13:22:7.5	-69:38:12.0	106.1	8.3	7.6	7.3	-39.1±1.2	-19.9±1.6	1
			OCT						
2MASS J00530603-8250259	00:53:6.0	-82:50:25.9	129.0	10.1	9.5	9.3	22.2±1.2	22.1±1.2	4
CD-50 245	00:55:25.3	-49:56:57.0	65.6	8.7	8.4	8.3	38.2±1.3	27.8±1.1	1
CD-46 287	01:01:16.7	-45:56:37.0	78.0	9.4	8.9	8.7	32.0±0.8	21.9±1.7	1
HIP 10670	02:17:18.9	+33:50:50.0	34.5[a]	3.8	3.9	4.0	45.7±1.0	-52.2±1.0	1
CD-41 702	02:29:0.3	-41:07:33.0	59.9	9.0	8.5	8.3	23.1±1.0	34.8±0.9	1
HIP 16095	03:27:18.7	+12:44:7.0	87.7[a]	6.3	6.3	6.3	10.4±1.0	-7.6±1.0	1
2MASS J03302115-6412207	03:30:21.1	-64:12:20.7	121.0	12.1	11.5	11.3	8.7±6.2	26.0±6.1	4
HD 23208	03:42:39.8	-20:32:44.0	50.3[a]	7.7	7.3	7.2	3.2±1.6	26.4±1.6	1
2MASS J04085395-7203535	04:08:54.0	-72:03:53.5	89.0	10.8	10.2	9.9	-4.6±2.2	38.6±2.0	4
HIP 19496	04:10:35.8	+25:21:45.0	98.0[a]	8.2	8.0	7.9	2.8±0.7	-19.5±0.5	1
2MASS J04105436-6924209	04:10:54.4	-69:24:20.9	89.0	11.4	10.8	10.5	-4.8±3.2	36.0±3.3	4
CD-58 860	04:11:55.7	-58:01:47.0	87.1	8.8	8.5	8.4	-4.0±1.4	32.8±2.4	1
2MASS J04224274-6137581	04:22:42.7	-61:37:58.1	98.0	11.7	11.1	10.9	-4.3±2.5	31.1±2.4	4
CD-43 1451	04:30:27.3	-42:48:47.0	122.8	9.3	8.9	8.7	0.3±0.8	19.2±0.8	1
EX Eri	04:46:25.7	-28:05:15.0	56.2[a]	5.8	5.7	5.7	-4.5±1.0	17.5±1.0	1
2MASS J04593927-3426546	04:59:39.3	-34:26:54.6	86.0	11.2	10.5	10.2	-14.7±1.8	21.8±1.8	4
2MASS J05015289-6101308	05:01:52.9	-61:01:30.8	120.0	11.5	10.9	10.6	-7.2±2.3	24.4±2.2	4
2MASS J05060048-4545196	05:06:0.5	-45:45:19.6	116.0	12.0	11.4	11.2	-9.5±3.0	20.1±3.9	4
CD-72 248	05:06:50.6	-72:21:12.0	145.8	9.2	8.8	8.7	-6.1±1.1	21.3±1.2	1
2MASS J05181994+0829132	05:18:20.0	+08:29:13.0	88.3	9.6	9.0	8.9	-6.3±2.1	-9.9±1.2	1
2MASS J05184173-4907129	05:18:41.7	-49:07:12.9	136.0	11.2	10.5	10.4	-12.1±1.6	13.6±1.6	4
HD 274576	05:28:51.4	-46:28:19.0	117.1	9.3	8.9	8.8	-11.3±1.0	19.5±1.1	1
2MASS J05321635-4132446	05:32:16.4	-41:32:44.6	141.0	11.4	10.7	10.5	-5.4±5.1	17.6±16.9	4
BD-20 1111	05:32:29.3	-20:43:33.0	129.7	9.1	8.7	8.7	-9.8±1.3	8.3±1.5	1
2MASS J05410719-2409179	05:41:7.2	-24:09:17.9	111.0	10.9	10.3	10.2	-8.1±1.6	11.0±1.6	4
CD-47 1999	05:43:32.1	-47:41:11.0	166.7	9.0	8.8	8.6	-8.2±0.9	14.5±0.8	1
2MASS J05541279-4044059	05:54:12.8	-40:44:5.9	143.0	12.5	11.8	11.6	-11.3±5.6	11.1±5.3	4
2MASS J05581182-3500496	05:58:11.8	-35:00:49.0	105.8	9.8	9.5	9.4	-14.6±1.0	17.2±1.2	1
2MASS J05584222-5639409	05:58:42.2	-56:39:40.9	138.0	11.8	11.2	11.0	-11.1±2.7	18.7±2.6	4
2MASS J06002910-5531015	06:00:29.1	-55:31:1.5	126.0	11.8	11.2	10.9	-12.6±2.8	15.4±2.7	4
CD-49 2037	06:03:35.4	-49:11:26.0	173.8	9.7	9.2	9.1	-10.1±3.7	13.2±2.4	1
2MASS J06055373-2541242	06:05:53.7	-25:41:24.2	110.0	11.7	11.1	10.8	-13.4±2.5	14.9±2.8	4
2MASS J06124600-3836083	06:12:46.0	-38:36:8.3	85.0	11.7	11.1	10.9	-23.5±3.2	18.3±3.1	4
2MASS J06204718-3619482	06:20:47.2	-36:19:48.2	116.0	10.0	9.4	9.2	-15.5±1.5	12.6±1.5	4
2MASS J06205027-7905195	06:20:50.3	-79:05:19.5	130.0	10.7	10.1	9.8	-16.6±1.9	22.1±1.8	4
CD-66 395	06:25:12.4	-66:29:10.0	126.1	9.5	9.1	9.0	-12.8±1.4	22.1±1.3	1
CD-30 3394N	06:40:4.9	-30:33:3.0	137.1	8.8	8.6	8.6	-16.1±1.6	10.3±1.2	1
CD-30 3394S	06:40:5.7	-30:33:9.0	137.1	8.8	9.2	8.7	-13.4±1.4	9.3±1.2	1
2MASS J06434892-5130461	06:43:48.9	-51:30:46.1	140.0	12.0	11.3	11.1	-15.6±2.2	18.2±2.4	4
2MASS J06555474-4046498	06:55:54.7	-40:46:49.8	132.0	11.7	11.1	10.9	-17.5±3.1	9.9±2.9	4
2MASS J07402971-7148232	07:40:29.7	-71:48:23.0	168.9	9.7	9.2	9.1	-15.2±1.8	12.4±2.2	1
2MASS J08145586-7613014	08:14:55.9	-76:13:1.4	139.0	11.2	10.5	10.4	-22.9±1.9	10.1±1.9	4
2MASS J16405331-7234127	16:40:53.3	-72:34:12.7	134.0	12.7	12.1	11.9	-17.4±-5.7	8.7±8.7	4
BD-18 4452N	17:13:11.6	-18:34:25.0	16.7	7.3	6.7	6.5	44.0±3.5	-67.1±4.4	1
2MASS J17214553-8026396	17:21:45.5	-80:26:39.6	162.0	12.3	11.7	11.5	8.2±4.2	-20.9±4.5	4

ID	RA	DEC	Dist.	J	H	K	$\mu_{\alpha,*}$	μ_{δ}	Mem ref.
	hh:mm:ss.s	dd:mm:ss.s	(pc)	(mag.)	(mag.)	(mag.)	(mas/yr)	(mas/yr)	
2MASS J17325153-7336111	17:32:51.5	-73:36:11.1	167.0	10.6	10.0	9.8	9.1±1.9	-20.4±1.8	4
HD 155177	17:42:9.0	-86:08:5.0	132.0	7.9	7.7	7.6	11.5±1.1	-22.5±0.9	1
BD+01 3657	18:22:17.2	+01:42:25.0	26.8[a]	7.6	7.0	6.9	83.2±0.9	-19.8±0.5	1
2MASS J18494869-7157100	18:49:48.7	-71:57:10.0	147.1	9.3	8.9	8.7	7.9±3.6	-16.5±5.4	1
CP-79 1037	19:47:3.9	-78:57:43.0	150.8	9.8	9.4	9.3	16.1±3.4	-14.3±1.7	1
CP-82 784	19:53:56.8	-82:40:42.0	132.7	9.2	8.8	8.6	21.3±0.9	-13.2±0.9	1
2MASS J19545336-6450090	19:54:53.4	-64:50:9.0	166.0	10.7	10.0	9.8	15.8±2.1	-13.8±2.2	4
2MASS J19545407-6450343	19:54:54.1	-64:50:34.3	181.0	11.2	10.5	10.3	16.9±2.3	-9.1±2.3	4
2MASS J20293579-6317079	20:29:35.8	-63:17:7.9	140.0	10.8	10.2	10.0	23.4±1.7	-12.3±1.6	4
2MASS J20410187-7813502	20:41:1.9	-78:13:50.2	157.0	11.4	10.8	10.6	23.0±6.2	-5.1±5.4	4
HIP 102218	20:42:40.6	-10:58:11.0	67.6[a]	6.9	6.7	6.7	37.0±1.1	-6.2±1.3	1
HD 197157	20:44:2.3	-51:55:15.0	24.2[a]	3.9	3.7	3.8	155.9±1.0	-53.6±1.0	1
CD-33 15436	21:11:55.2	-32:58:37.0	54.8	8.9	8.4	8.3	61.3±0.8	-11.5±1.2	1
2MASS J22540018-7807039	22:54:0.2	-78:07:3.9	99.0	10.6	9.9	9.8	37.0±2.0	11.0±2.0	4
HK Aqr	23:08:19.6	-15:24:36.0	31.6[a]	8.0	7.3	7.1	107.7±1.7	-19.3±1.0	1
EQ Peg B	23:31:52.6	+19:56:14.0	6.1	7.1	6.6	6.3	-78.1±6.3	108.4±6.3	1
CD-87 121	23:58:17.7	-86:26:24.0	109.3	8.5	8.1	8.0	26.4±1.0	16.0±0.8	1
			THA						
HD 105	00:05:52.5	-41:45:11.0	39.4[a]	6.5	6.2	6.1	97.5±1.0	-76.3±1.0	1
HD 987	00:13:53.0	-74:41:18.0	44.5[a]	7.4	7.1	7.0	78.1±1.3	-51.3±1.3	1
HD 1466	00:18:26.1	-63:28:39.0	41.5[a]	6.5	6.2	6.1	89.4±1.0	-59.5±1.0	1
HIP 1910	00:24:9.0	-62:11:4.0	43.7[a]	8.4	7.7	7.5	82.6±2.7	-51.1±0.8	1, 5
CT Tuc	00:25:14.7	-61:30:48.0	44.6[a]	8.6	7.9	7.7	84.7±1.9	-54.8±1.2	1, 5
HD 2884	00:31:32.7	-62:57:30.0	41.5[a]	4.7	4.7	4.5	83.6±1.0	-54.8±1.0	1
HD 2885	00:31:33.5	-62:57:56.0	42.5[a]	4.3	4.2	4.1	94.0±1.0	-46.3±1.0	1
HD 3003	00:32:43.9	-63:01:53.0	45.5[a]	5.1	5.2	5.0	86.7±1.0	-50.3±1.0	1
HD 3221	00:34:51.2	-61:54:58.0	43.9[a]	7.3	6.7	6.5	83.7±1.3	-50.2±0.8	1, 5
CD-78 24	00:42:20.3	-77:47:40.0	50.1	8.2	7.7	7.5	77.6±0.9	-30.4±1.2	1, 5
HD 8558	01:23:21.3	-57:28:51.0	49.5[a]	7.2	6.9	6.8	89.1±0.8	-38.9±0.7	1
CC Phe	01:28:8.7	-52:38:19.0	36.0[a]	7.4	6.9	6.8	103.7±0.7	-44.1±0.7	1
2MASS J01521830-5950168	01:52:18.3	-59:50:17.0	37.9	8.9	8.3	8.1	109.2±1.8	-25.7±1.8	1, 3, 5
DK Cet	01:57:49.0	-21:54:5.0	40.8[a]	6.9	6.6	6.5	103.9±0.9	-47.8±0.9	1
HD 12894	02:04:35.1	-54:52:54.0	47.8[a]	5.7	5.5	5.4	75.7±1.0	-25.1±1.0	1
HD 13183	02:07:18.1	-53:11:56.0	51.1[a]	7.3	7.0	6.9	88.2±1.4	-23.5±1.1	1
HD 13246	02:07:26.1	-59:40:46.0	44.2	6.5	6.3	6.2	91.1±1.0	-18.3±1.0	1
CD-60 416	02:07:32.2	-59:40:21.0	43.2	8.3	7.7	7.5	94.4±1.9	-21.8±1.8	1, 5
HD 14228	02:16:30.6	-51:30:43.0	47.2[a]	4.0	4.0	4.1	90.7±1.0	-22.0±1.0	1
HD 16978	02:39:35.4	-68:16:1.0	46.6[a]	4.4	4.4	4.3	86.8±1.0	-0.2±1.0	1
CD-53 544	02:41:46.8	-52:59:52.0	41.4	7.6	6.9	6.8	97.4±1.3	-13.1±1.1	1, 3, 5
CD-58 553	02:42:33.0	-57:39:37.0	48.5	8.6	8.0	7.8	82.7±0.9	-8.3±1.7	1, 3, 5
HD 17250	02:46:14.6	+05:35:33.0	54.3[a]	6.9	6.6	6.5	75.4±0.8	-44.6±0.5	1, 2
HD 20121 a	03:12:25.8	-44:25:11.0	42.6[a]	5.1	4.9	4.8	82.7±1.0	-2.6±1.0	1, 2
HD 20385	03:16:40.7	-03:31:49.0	49.2[a]	6.5	6.2	6.1	78.6±1.0	-43.8±1.0	1
CD-35 1167	03:19:8.7	-35:07:0.0	44.6	8.6	7.9	7.7	86.4±1.3	-21.0±1.0	1, 3, 5
CD-46 1064	03:30:49.1	-45:55:57.0	42.2	7.8	7.3	7.1	88.8±1.2	-5.0±1.1	1
CD-44 1173	03:31:55.7	-43:59:14.0	44.0	8.3	7.7	7.5	85.0±1.4	-8.2±1.9	1, 3, 5
HD 22705	03:36:53.4	-49:57:29.0	43.3[a]	6.5	6.3	6.1	89.7±1.0	0.3±1.0	1
HD 24636	03:48:11.5	-74:41:39.0	54.0[a]	6.4	6.2	6.1	63.5±1.0	24.9±1.0	1, 2
HD 24701	03:48:35.9	-37:37:13.0	50.7[a]	3.9	4.6	4.8	75.8±1.0	-10.7±1.0	1, 2
HD 25042	04:00:32.0	-41:44:54.0	48.5[a]	7.2	6.9	6.9	69.1±0.9	1.2±1.8	1
BD-15 705	04:02:16.5	-15:21:30.0	52.9	8.2	7.7	7.6	66.7±1.5	-28.2±1.3	5
BD-12 943	04:36:47.1	-12:09:21.0	62.3	8.3	7.9	7.8	50.4±2.7	-22.7±1.5	1
HD 29615	04:38:43.9	-27:02:2.0	56.2[a]	7.3	7.0	6.9	49.7±1.7	-9.7±1.3	1
TYC 8083-455-1	04:48:0.7	-50:41:26.0	54.8	8.7	8.1	7.9	53.1±2.1	15.7±2.3	1, 3, 5
HD 32195	04:48:5.2	-80:46:45.0	61.0[a]	7.2	7.0	6.9	46.2±0.8	41.6±0.9	1
BD-19 1062	04:59:32.0	-19:17:42.0	64.1	8.8	8.2	8.1	43.7±0.9	-13.4±1.0	1
BD-09 1108	05:15:36.5	-09:30:51.0	77.5	8.5	8.2	8.1	31.7±1.2	-20.0±1.3	1

ID	RA	DEC	Dist.	J	H	K	$\mu_{\alpha,*}$	μ_δ	Mem ref.
	hh:mm:ss.s	dd:mm:ss.s	(pc)	(mag.)	(mag.)	(mag.)	(mas/yr)	(mas/yr)	
CD-30 2310	05:18:29.0	-30:01:32.0	66.2	9.1	8.4	8.3	37.4±0.9	1.6±1.0	1
TYC 8098-414-1	05:33:25.6	-51:17:13.0	51.6	9.0	8.4	8.2	43.8±2.1	25.1±2.1	1, 3, 5
CD-27 2520	05:49:6.6	-27:33:56.0	74.3	8.8	8.4	8.3	26.0±1.2	3.2±1.1	1
HD 47875	06:34:41.0	-69:53:6.0	68.4	7.8	7.4	7.3	18.7±1.1	40.9±1.3	1
HD 53842	06:46:13.5	-83:59:30.0	55.8[(a)]	6.6	6.4	6.3	19.7±1.0	61.6±1.0	1
HD 86356	09:51:50.7	-79:01:38.0	74.5	8.6	8.1	8.0	-26.7±0.8	38.1±0.8	1
2MASS J10010873-7913074	10:01:8.8	-79:13:8.0	75.1	10.1	9.4	9.2	-25.7±1.5	38.5±1.6	1
2MASS J11401658-8321003	11:40:16.6	-83:21:0.0	74.2	9.3	8.7	8.6	-41.6±1.1	27.5±1.1	1
HD 193924	20:25:38.9	-56:44:6.0	54.9[(a)]	2.3	2.5	2.5	6.9±1.0	-86.0±1.0	1
HD 202917	21:20:50.0	-53:02:3.0	42.9[(a)]	7.4	7.0	6.9	30.1±1.0	-94.5±1.0	1
HIP 107345	21:44:30.1	-60:58:39.0	46.5[(a)]	8.8	8.1	7.9	39.6±2.4	-91.9±1.8	1, 5
HD 207575	21:52:9.7	-62:03:9.0	45.3[(a)]	6.4	6.1	6.0	44.0±1.0	-92.0±1.0	1
HD 207964	21:55:11.4	-61:53:12.0	46.5[(a)]	5.2	5.2	4.9	44.5±1.0	-91.1±1.0	1
2MASS J22021626-4210329	22:02:16.3	-42:10:33.0	44.6	8.9	8.2	8.0	50.4±1.0	-90.9±1.5	3, 5
TYC 9344-293-1	23:26:10.7	-73:23:50.0	44.2	8.8	8.2	7.9	72.9±1.0	-67.4±1.0	1, 3, 5
CD-86 147	23:27:49.4	-86:13:19.0	58.4	8.0	7.6	7.5	54.7±0.9	-42.2±0.9	1
DS Tuc	23:39:39.5	-69:11:45.0	45.7[(a)]	7.1	6.8	6.7	82.9±1.8	-78.8±4.0	1
			TWA						
CE Ant	10:42:30.1	-33:40:17.0	34.5	7.8	7.1	6.9	-114.9±8.7	-18.7±4.7	1
TW Hya	11:01:51.9	-34:42:17.0	51.0[(a)]	8.2	7.6	7.3	-68.7±1.8	-13.1±1.2	1
HD 96819	11:08:44.0	-28:04:50.0	55.6[(a)]	5.3	5.4	5.2	-72.8±1.0	-22.2±1.0	1
CD-29 8887	11:09:13.8	-30:01:40.0	46.5	7.6	6.9	6.7	-88.4±1.0	-21.2±0.8	1
TWA 3A	11:10:27.9	-37:31:52.0	36.4	7.7	7.0	6.8	-105.9±0.9	-17.3±1.0	1
V1215 Cen	11:13:26.5	-45:23:43.0	96.2	9.4	8.7	8.5	-43.9±1.4	-7.4±1.4	1, 3
V1217 Cen	11:21:5.5	-38:45:16.0	64.1	9.0	8.3	8.1	-66.6±1.5	-11.7±1.5	1, 3
V547 Hya	11:21:17.2	-34:46:46.0	55.6	8.4	7.7	7.5	-85.4±0.9	39.9±1.0	1
TV Crt	11:22:5.3	-24:46:40.0	43.1[(a)]	6.4	5.8	5.6	-88.8±1.6	-32.6±5.0	1
CD-33 7795	11:31:55.3	-34:36:27.0	50.0	7.7	7.0	6.7	-79.6±0.8	-22.6±0.9	1, 3
TWA5 b	11:31:55.4	-34:36:29.0	50.0	7.7	7.0	6.7	-79.6±0.8	-22.6±0.9	1
TWA30 a	11:32:18.3	-30:19:52.0	45.5	9.6	9.0	8.8	-87.8±1.3	-25.2±1.3	3
V549 Hya	11:32:41.2	-26:52:9.0	38.6	9.8	9.3	9.0	-95.3±2.2	-28.6±4.7	1
V550 Hya	11:32:41.2	-26:51:56.0	42.7	8.3	7.7	7.4	-99.2±6.2	-32.2±6.2	1
TWA26	11:39:51.1	-31:59:21.0	38.2	12.7	12.0	11.5	-96.0±11.6	-40.3±11.6	1
V1239 Cen	11:48:24.2	-37:28:49.0	70.6[(a)]	8.7	8.0	7.8	-44.2±1.8	-18.0±0.9	1
TWA23	12:07:27.4	-32:47:0.0	53.8	8.6	8.0	7.8	-70.4±1.4	-29.7±1.1	1, 3
TWA27	12:07:33.4	-39:32:54.0	52.3	13.0	12.4	11.9	-80.1±17.9	-15.1±17.9	1
V1249 Cen	12:15:30.7	-39:48:43.0	54.1	8.2	7.5	7.3	-73.2±0.8	-27.7±0.8	1, 3
TWA32	12:26:51.4	-33:16:13.0	68.1	10.7	10.1	9.8	-61.6±2.0	-23.0±4.9	1
TWA16	12:34:56.4	-45:38:7.0	78.1	9.0	8.3	8.1	-47.5±1.3	-20.2±0.8	1
V1252 Cen	12:35:4.2	-41:36:39.0	61.7	9.1	8.5	8.2	-70.1±1.1	-28.9±1.1	1, 3
TWA11a	12:36:1.0	-39:52:10.0	73.0[(a)]	5.8	5.8	5.8	-56.7±1.0	-25.0±1.0	1

Notes. [(a)] Distances from parallax measurements

References. 1: SACY works (Torres et al., 2008, Elliott et al., 2014 – Chapter 2), 2: Zuckerman et al. (2011), 3: Malo et al. (2014), 4: Murphy and Lawson (2015), 5: Kraus et al. (2014).

Chapter 5

The crucial role of higher-order multiplicity in the formation of the widest binaries

Parts of this chapter have been accepted for publication in the Monthly Notices of the Royal Astronomical Society (18 April 2016) [ArXiv ID: 1604.06094] as 'The crucial role of higher-order multiplicity: A case study using the β-Pictoris moving group', Elliott, P. & Bayo, A. The work is presented here in expanded and updated form.

The "in-situ" formation of very wide binaries is hard to explain as their physical separations are beyond the typical size of a collapsing cloud core ($\approx$5000-10,000 au). Here we investigate the formation process of such systems. We compute population statistics such as the multiplicity frequency (*MF*), companion-star frequency (*CSF*) and physical separation distribution of companions in the β-Pictoris moving group (BPMG). We compare previous multiplicity studies in younger and older regions and show that the dynamic evolution of a young population with a high degree of primordial multiplicity can lead to a processed separation distribution, similar to the field population. The evolution of outer components is attributed to the dynamical unfolding of higher-order (triple) systems; a natural consequence of which is the formation of wide binaries. We

find a strong preference for wide systems to contain three or more components ($>$1000 au: 11 / 14, 10,000 au: 6 / 7). We argue that the majority of wide binaries identified in young moving groups are primordial. Under the assumption that stellar populations, within our galaxy, have statistically similar primordial multiplicity, we can infer that the paucity of wide binaries in the field is the result of dynamical evolution.

This chapter is organised as follows. Section 5.1 introduces wide binary formation. Section 5.2 explains how we assembled our sample for this analysis. Section 5.3 explains how we calculated the detection limits. Section 5.4 discusses the sample's completeness. In Section 5.5 we present analysis to define wide binary systems. Section 5.6 presents the results of the analysis in this chapter. In Section 5.7 we outline a model for the dynamical evolution of triple systems. In Section 5.8 we discuss the current limitations of this analysis and finally in Section 5.9 we present the conclusions.

5.1 Introduction

The formation of very wide multiple systems ($>$10,000 au) is hard to explain with our current theory of star formation because companions have separations beyond the limit imposed by the original hydrostatic clump size (5000-10,000 au, Benson and Myers, 1989; Motte et al., 1998; Pineda et al., 2011). Therefore, in-situ formation seems extremely improbable, and either these systems are primordial but have migrated (Reipurth and Mikkola, 2012), or are non-primordial altogether (originating from different birth sites and after becoming gravitationally bound, Kouwenhoven et al., 2010). To differentiate between the two scenarios we need to derive statistical properties of populations and their wide binaries, i.e. Tokovinin et al. (2006); Tokovinin (2015), and compare these with theoretical predictions of different formation mechanisms.

In this chapter we use the multiplicity census of the Perseus region (Tobin et al., 2016), the β-Pictoris moving group (hereafter, BPMG) and the field population (Raghavan et al., 2010; Tokovinin, 2014a,b) to analyse the role of higher-order multiple systems in the formation of wide binaries and population multiplicity.

Due to the long periods of wide multiple systems ($\gtrsim$30,000 yr) detecting significant orbital motion is not possible on short ($<$100 yr) time-scales. In fact we cannot directly determine whether components are gravitationally bound. Therefore, components are usually identified as co-moving proper motion pairs, e.g., Caballero (2010), but a high false-positive rate limits the identification to nearby sources in uncrowded fields. In Chapter 4 we identified 84 potential wide multiple systems in young nearby associations Torres et al. (2006, 2008); Malo et al. (2014) using 2MASS photometry, proper motions and additional spectroscopic/photometric properties. The high number of identified wide binary systems prompted the analysis of their formation presented in this chapter.

5.2 Sample

Reipurth and Mikkola (2012) suggested the young moving groups to be ideal populations to identify wide binaries formed by the dynamical unfolding of triple systems, thanks to their age ($\approx$10-100 Myr) and the distance travelled from their original birth site ($\sim$5-10 pc), see Section 5.5. From the analysis presented in Chapter 4 we chose the BPMG in particular because of its optimal properties for wide binary analysis. The large average proper motions ($\overline{\mu_\alpha}$ = 50 mas/yr, $\overline{\mu_\delta}$ = -75 mas/yr) allowed us to derive separation limits $>$20,000 au for a significant number (49) of systems. Due to its age (21-26 Myr, Barrado y Navascués et al., 1999; Torres et al., 2006; Binks and Jeffries, 2014; Bell et al., 2015) and proximity (average distance 43 pc) many systems (38 / 49) have been imaged previously using high-contrast techniques, looking for low-mass companions. Additionally, almost all (42/49) systems have multi-epoch spectroscopy from works such as Malo et al. (2014) and Chapter 2.

Thus, the sample studied in this chapter comprises 49 single and multiple stellar systems in the BPMG. See Table 5.1 for full references.

5.3 Companion detections and detection probabilities

To study the abundance of multiple systems across a large parameter space in our sample we need both: detections of companions, and constrained parameter space for non-detections. We have combined radial velocity (RV) values, high contrast imaging and direct imaging / proper motion to estimate our detection probabilities. Detection limits from RV measurements were derived using multi-epoch observations following Tokovinin (2014a). For high-contrast imaging we converted the angular separation versus contrast, to physical separation versus mass-ratio, using the target's distance and the evolutionary models of Baraffe et al. (2015). We used the detection limits described in Chapter 4; combining 2MASS photometry (Cutri et al., 2003) and proper motions (UCAC4, PPMXL, NOMAD: Zacharias et al., 2012; Roeser et al., 2010; Zacharias et al., 2005), for the widest parameter space ($\gtrsim$3″, $\gtrsim$130 au). Details of the exact steps in the calculation of detection probabilities can be found in Appendix A.2.1.

Figure 5.1 shows the average detection probabilities for our sample (contour map) in combination with the companion detections (star markers). Our observed multiplicity properties should not be significantly affected by our completeness, as discussed in the following section. Details of the targets and the multiple systems studied in this chapter can be found in Tables 5.1 and 5.2, respectively.

5.4 Detection completeness

We did not attempt to *correct* our statistics with our detection probabilities, however, below we justify why this should not significantly affect our results.

In this analysis before averaging the detection probabilities over the sample, as in Figure 5.1, we first consider whether a companion is likely to inhabit the parameter space based on stability arguments. Tokovinin (2014b) showed that the region of instability (for triple and higher-order systems), based on the ratio of periods in the system is between certain values ($4.7 < P_L/P_S < 47$). We use the mid-value (26) of this criterion

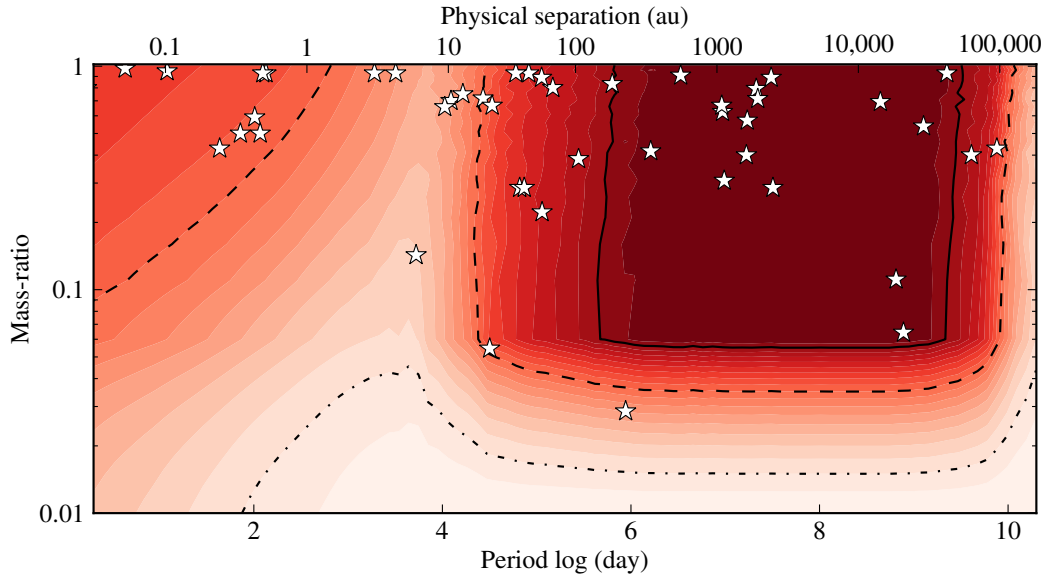

FIGURE 5.1: Average detection probabilities (contours from red, 100% to white, 0%) and detected companions (white stars) in the physical separation versus mass-ratio space for the 49 systems. The solid, dashed and dash-dotted lines encompass areas with detection probabilities $\geq$ 90%, 50% and 10%, respectively.

to mask regions of detection probability space using previously identified companions in the system. For example, if a system has a companion with a period of 100 day then we mask the region 4–2600 day. Masking in this case means setting a detection probability of 1. This is because we use these probabilities to predict where the *missing* companions would be and we have indirectly probed this space with our stability arguments. We repeated this for all objects to create a new set of detection probability arrays. We then averaged these detection probabilities over the mass-ratio in each period bin because there is no significant evidence that the mass-ratio is a function of period (Reggiani and Meyer, 2013; Tokovinin, 2014b).

Figure 5.2 shows our results based on the period distribution of systems in our sample. We used kernel density estimations (KDEs) to perform this analysis which reduces the phase effect when binning data, see Scott (2009) for details.

The grey dotted and dash-dotted lines are the median detection probabilities with and without dynamical constraints, respectively. This Figure shows that although we are very insensitive in regions $\approx 10^4$ day, due to identified companions in the systems, the likely number of missing companions is not very significant. The red dashed line and

blue line are the KDEs of the raw sample and the *corrected* sample (KDE / detection probability), respectively. We then integrated these curves to calculate the quantitative difference in *CSF* values. The difference was $\approx$15% i.e. the derived *CSF* value derived in this chapter is most likely $\approx$1.17 as opposed to 1.02. This increase would not significantly affect any conclusions presented in this chapter, in fact this value would put our results in even better agreement with the Class 0 *CSF* value from Tobin et al. (2016), see Section 5.6.1 for details.

TABLE 5.1: Observtional properties of β-Pictoris targets studied in this chapter.

ID	Comp.[a]	Common ID	R.A. hh:mm:ss.s	DEC. dd:mm:ss	Dist. (pc)	V (mag.)	K (mag.)	Mem. ref.	2MASS lim. ($''$)	AO refs.	RV refs.
BPC 10	A	V1005 Ori	04:59:34.8	+01:47:01.0	25.9	10.11	6.26	28	4000	3, 2, 8, 12, 17, 19, 24	9, 1, 12
BPC 10	B	2MASS J05015665+0108429	05:01:56.7	+01:08:43.0	25.9	12.87	7.68	11	4000		
BPC 12	A	HIP 23418aa	05:01:58.8	+09:58:59.0	33.2	11.67	6.37	20, 28	1000	10	
BPC 14	A	BD-21 1074b	05:06:49.5	-21:35:04.0	20.2	11.30	6.11	20, 28	6000	8	12, 9, 12
BPC 16	B	2MASS J05200029+0613036	05:20:00.3	+06:13:04.0	67.8	11.42	8.57	28	600	10	9
BPC 16	A	RX J0520.5+0616	05:20:31.8	+06:16:11.0	71.0	11.64	8.57	28	600	10	9
BPC 16	C	2MASS J05195327+0617258	05:19:53.3	+06:17:26.0	71.0	18.31	12.41	11	600		
BPC 19	A	Beta Pic	05:47:17.1	-51:03:59.0	19.4	3.85	3.53	28	4500	7, 26, 3, 29	
BPC 2	A	GJ 3076	01:11:25.4	+15:26:21.0	19.3	13.96	8.21	20	5000		20
BPC 22	A	TWA22	10:17:26.9	-53:54:27.0	17.6	13.89	7.69	28	5500	12, 7, 2	9, 12
BPC 26	A	V824 Ara	17:17:25.5	-66:57:04.0	31.4	6.86	4.70	28	3100	23, 7, 2, 19, 24	25
BPC 26	B	HD 155555 c	17:17:31.3	-66:57:06.0	31.4	12.89	7.63	28	3100	3	
BPC 28	A	GSC 08350-01924	17:29:20.7	-50:14:53.0	66.3	12.96	7.99	20, 28	350	10	
BPC 3	A	Barta 161 12	01:35:13.9	-07:12:52.0	37.9	13.43	8.08	20, 16	2500		20
BPC 3	B	2MASS J01354915-0753470	01:35:49.2	-07:53:47.0	37.9	13.79	9.81	11	2500		
BPC 30	A	HD 161460	17:48:33.7	-53:06:43.0	71.0	8.99	6.78	28	600	10, 7	22
BPC 30	B	2MASS J17483374-5306118	17:48:33.8	-53:06:12.0	71.0	13.65	9.27	11	600		
BPC 31	A	HD 164249	18:03:03.4	-51:38:56.0	48.1	7.01	5.91	28	2000	7, 26	12, 9, 11, 12
BPC 31	C	2MASS J18011138-5125594	18:01:11.3	-51:26:00.0	48.1	14.79	11.27	11	2000		
BPC 36	A	2MASS J18420694-5554254	18:42:06.9	-55:54:25.0	51.9	13.54	8.58	20	500		20
BPC 36	B	2MASS J18420483-5554126	18:42:04.8	-55:54:13.0	51.9	15.11	9.85	11	500		
BPC 37	A	HD 172555	18:45:26.9	-64:52:17.0	28.5	4.80	4.30	28	3500	7, 3, 2, 29, 26, 24	
BPC 37	B	CD-64 1208	18:45:37.0	-64:51:46.0	28.5	9.97	6.10	28	3500	24, 7, 2, 19	22
BPC 39	B	Smethells 20	18:46:52.6	-62:10:36.0	52.4	12.20	7.85	20, 28	2000	10, 3	27, 9
BPC 39	A	2MASS J18480637-6213470	18:48:06.5	-62:13:47.0	52.4	7.29	6.14	11	2000		
BPC 4	B	HIP 10679	02:17:24.7	+28:44:30.0	27.3	7.78	6.26	28	2500	3, 5	25
BPC 4	A	HD 14082	02:17:25.3	+28:44:42.0	34.5	7.04	5.79	28	2500		25
BPC 4	C	2MASS J02160734+2856530	02:16:07.3	+28:56:53.0	34.5	15.74	11.61	11	2500		
BPC 41	A	PZ Tel	18:53:05.9	-50:10:50.0	51.5	8.42	6.37	28	1900	3, 24, 19	12, 12
BPC 42	A	TYC 6872-1011-1	18:58:04.2	-29:53:05.0	82.6	11.73	8.02	20, 28	300	10	11
BPC 42	B	2MASS J18580464-2953320	18:58:04.6	-29:53:32.0	82.6	12.85	8.76	11	300		
BPC 43	A	CD-26 13904	19:11:44.7	-26:04:09.0	78.9	10.24	7.37	28	600	10	9, 11
BPC 44	A	Eta Tel	19:22:51.2	-54:25:26.0	48.2	5.17	5.01	28	2000	23, 18, 3, 6, 29	
BPC 44	B	HD 181327	19:22:58.9	-54:32:17.0	51.8	7.05	5.91	28	2000	7, 3	9, 12
BPC 47	B	UCAC3 116-474938	19:56:02.9	-32:07:19.0	58.4	13.27	8.11	20, 28	1800	3, 4	27, 20, 11
BPC 47	A	TYC 7443-1102-1	19:56:04.4	-32:07:38.0	56.3	11.78	7.85	20, 28	1800	8, 3, 4	27, 9, 11
BPC 52	C	AU Mic	20:45:09.5	-31:20:27.0	9.8	8.80	4.53	28	10000	23, 15, 2, 8, 17, 14, 3, 5, 24	12, 9, 1, 12

ID	Comp.	Common ID	R.A. hh:mm:ss.s	DEC. dd:mm:ss	Dist. (pc)	V (mag.)	K (mag.)	Mem. ref.	2MASS lim. ($''$)	AO refs.	RV refs.
BPC 52	B	AT Mic S	20:41:51.1	-32:26:10.0	9.5	10.89	4.94	28	10500	24, 2, 19	1, 12
BPC 52	A	AT Mic N	20:41:51.2	-32:26:07.0	10.2	10.89	4.94	28	10500	23, 15, 2, 3, 19, 24	1, 12
BPC 55	A	2MASS J20434114-2433534 A	20:43:41.1	-24:33:53.0	45.1	14.45	7.76	20	2200		20
BPC 55	B	2MASS J20434114-2433534 B	20:43:41.1	-24:33:53.0	45.1	14.45	7.76	28	2200		20
BPC 57	A	HD 199143	20:55:47.7	-17:06:51.0	45.7	7.33	5.81	28	1200	23, 21	
BPC 57	B	AZ Cap	20:56:02.7	-17:10:54.0	45.7	10.62	7.04	20, 28	1500	23, 24, 19	9
BPC 6	B	BD+30 397 b	02:27:28.1	+30:58:41.0	40.0	12.39	7.92	28	2400	5	11
BPC 6	A	AG Tri	02:27:29.3	+30:58:25.0	40.0	10.15	7.08	28	2400	5	11, 1
BPC 63	A	WW PsA	22:44:58.0	-33:15:02.0	23.6	12.10	6.93	28	4800	8	9, 20, 1
BPC 63	B	TX PsA	22:45:00.0	-33:15:26.0	20.1	13.35	7.79	28	4800	8, 10, 3	9, 1
BPC 65	C	G 271-110	01:36:55.1	-06:47:38.0	29.5	...	8.86	20	4100	4	
BPC 65	B	2MASS J01373545-0645375	01:37:35.4	-06:45:38.0	24.0	7.68	5.75	11	4100	14, 24, 17	12
BPC 65	A	2MASS J01334282-0701311	01:33:42.8	-07:01:31.0	29.5	5.77	4.26	11	4100		27
BPC 68	A	2MASS J14142141-1521215	14:14:21.4	-15:21:21.5	30.2	10.39	6.60	20	3200	7	27, 20
BPC 68	B	2MASS J14141700-1521125	14:14:17.0	-15:21:13.0	30.2	15.60	8.82	11	3200		
BPC 69	B	2MASS J21212873-6655063	21:21:28.7	-66:55:06.3	30.2	10.66	7.01	20	3200		
BPC 69	A	2MASS J21212446-6654573	21:21:24.5	-66:54:57.0	30.2	9.00	6.40	11	3200	15	
BPC 70	A	2MASS J20100002-2801410	20:10:00.0	-28:01:41.0	48.0	15.13	7.73	20	2700	4	20
BPC 70	B	2MASS J20085122-2740536	20:08:51.1	-27:40:54.0	48.0	16.27	11.78	11	2700		
BPC 8	A	EXO 0235.2-5216	02:36:51.7	-52:03:04.0	28.6	12.07	7.50	20, 28	3500	23, 6	27, 20
BPC 9	A	HD 29391	04:37:36.1	-02:28:25.0	29.4	5.22	4.54	28	3400	26, 3, 13	
BPC 9	B	2MASS J04373746-0229282	04:37:37.5	-02:29:28.0	29.4	10.64	6.41	11	3400	8, 15	27, 9, 1, 12

Bailey et al. (2012): 1, Biller et al. (2007): 2, Biller et al. (2013): 3, Bowler et al. (2015): 4, Brandt et al. (2014): 5, Chauvin et al. (2003): 6, Chauvin et al. (2010): 7, Delorme et al. (2012): 8, Elliott et al. (2014) – Chapter 2: 9, Elliott et al. (2015) – Chapter 3: 10, Elliott et al. (2016) – Chapter 4: 11, Elliott et al. in prep.: 12, Heinze et al. (2010): 13, Janson et al. (2013): 14,Kasper et al. (2007): 15, Kraus et al. (2014): 16, Lafrenière et al. (2007): 17, Lowrance et al. (2005): 18, Masciadri et al. (2005): 19, Malo et al. (2014): 20, Metchev and Hillenbrand (2009): 21, Messina et al. (2010): 22, Neuhäuser et al. (2003): 23,Nielsen and Close (2010): 24, Nordström et al. (2004): 25, Rameau et al. (2013): 26, Kordopatis et al. (2013): 27,Torres et al. (2006): 28, Vigan et al. (2012): 29

[a]The "ID" column + "Comp." column is a unique identifier for resolved targets. This unique identifier links this Table to Table 5.2, this avoids any confusion for targets with multiple unresolved components.

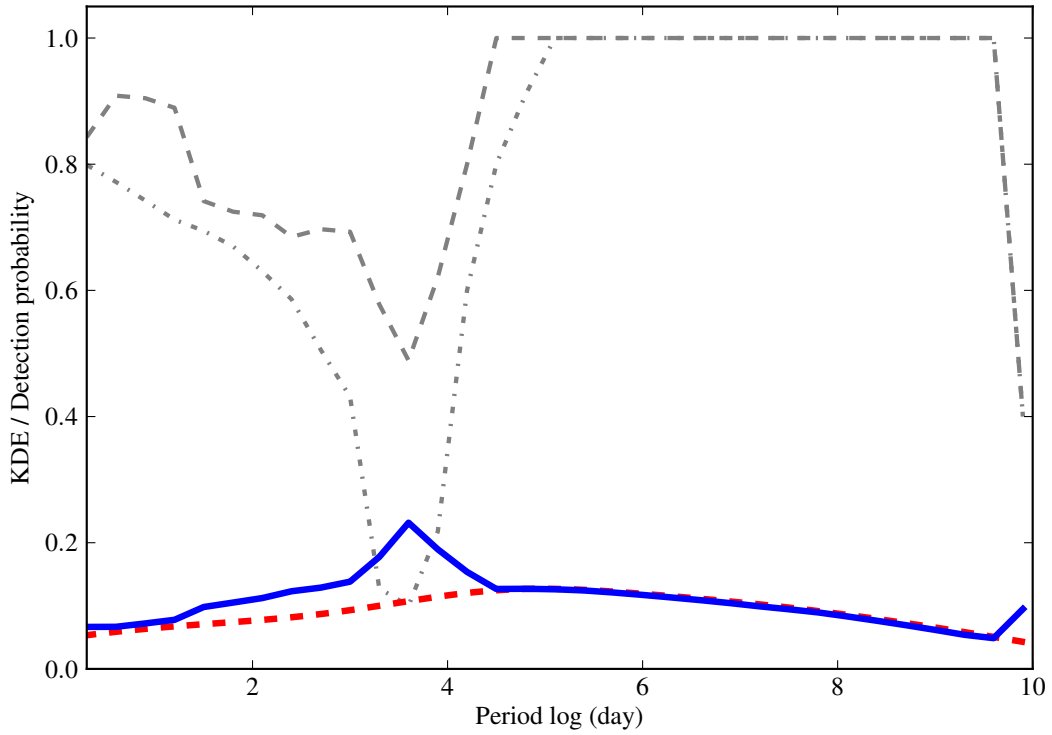

FIGURE 5.2: Kernel density estimations for the period versus companion-star frequency. The dashed and dash-dotted grey lines represent median detection probabilities (averaged over mass-ratio) with and without dynamical stability considerations, respectively. The red dashed line is the raw sample analysed in the body of this chapter and the blue line is the detection-probability *corrected* distribution.

5.5 Defining wide multiple systems in the young moving groups

Wide components are usually identified from the galactic motion (the quantity used, at least in initial identification, is proper motion) they share with their associated primary. With the proper motion, radial velocity and either a photometric or kinematic distance, the 3D kinematics can be derived. However, young moving group members are also classified on this basis, i.e. looking for collections of objects sharing the same galactic motion. Therefore we need to clarify what is a component in a multiple system and what is *another* moving group member.

To investigate this we looked at the different scales of physical clustering within the

BPMG. We cannot use projected separations from spatial positions for this analysis as the proximity of the stars means the group has significant depth (in galactic co-ordinates: X≈160, Y≈100, Z≈45 pc). We can, however, use the derived photometric distances to known members and perform queries in a 3-dimensional volume. This is similar to the analysis presented in Larson (1995) and Bate et al. (1998) where the authors identified a break in the density of objects as a function of angular separation in various star-forming regions, including Taurus (58″, ≈8000 au). However, as the distance to Taurus is larger (≈140 pc) an angular query was used, assuming a fixed distance to all sources.

For our analysis we queried a 30 pc volume around each bonafide member of the BPMG using the derived X, Y and Z galactic positions. We calculated the magnitude of the distance difference $\sqrt{(X_1 - X_2)^2 + (Y_1 - Y_2)^2 + (Z_1 - Z_2)^2}$ between the considered bonafide member and any other member in this volume. For wide components that share statistically similar radial velocities and proper motions and without X, Y and Z values, the distance magnitude was computed from the angular separation of the components and the distance to the bonafide member.

We collected all of these distance magnitudes together and then calculated the volume density of stars (ρ) in shells of 0.25 log (pc) using the spatial volume and dividing by the total number of stars. Figure 5.3 shows the result of this procedure. We consider two potential physical clustering scales: at 1 pc (left panel) and between 0.02-0.2 pc, where there is an apparent paucity of members (right panel). For each scenario we have fitted, using linear-regression, two power-laws, considering where the potential break occurs. The left panel shows that fitting the data considering a break at ≈1 pc results in two power-laws that do intercept at ≈1 pc. The right panel shows that considering a break between 0.02-0.2 pc does not affect the fitted power law of the inner region significantly (-2.9 compared to -3.0 in left panel), however, the slope of the outer region is significantly altered (-1.8 compared to -1.2). The point of interception also occurs closer to 1 pc as opposed to between 0.02-0.2 pc. This apparent break in the typical spatial density of members in BPMG is evidence that the population of identified wide companions (100,000 au and smaller) is not just a continuation of clustering down to

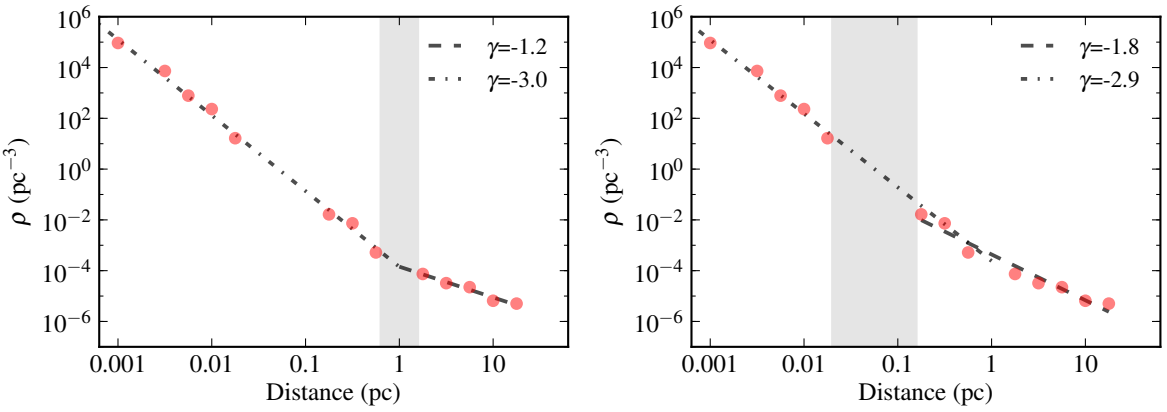

FIGURE 5.3: The volume density of members in the BPMG (red markers), densities have been calculated in annuli of 0.25 log(pc). Black dotted and dot-dashed lines represent power laws fitted to the data for breaks at 1 pc (left panel) and between 0.02-0.2 pc (right panel). The grey shaded areas represent the physical distances of the considered breaks in self-similarity.

smaller scales. These wide companions form a distinct population, their separation distribution is a result of a different physical process.

It must be said that the moving groups are far from complete and, therefore, it is hard to produce a definitive answer at this time as to the true physical clustering scale, especially given the paucity of sources between 0.02-0.2 pc. However, our analysis supports the break in physical clustering occurring beyond 100,000 au (≈0.5 pc).

5.6 Results

In the following section we present analysis using the multiplicity frequency (*MF*) and the companion-star frequency (*CSF*), equations 1.1 and 1.3.

Additionally we use the physical separation (a proxy for the semi-major axis) versus *CSF* which allows us to investigate the dynamical evolution of multiple systems.

TABLE 5.2: The properties of multiple systems used in this chapter.

ID	Comp.	Struc.	Hier.	M1 ($M_\odot$)	M2 ($M_\odot$)	Sep. (au)	Type[a]	Ref.
BPC 10	B	A, B, *	L1	0.70	0.30	81044	Cpm	EL16
BPC 10	A	Aa, Ab, A	L11	0.70	0.30	0.26	s	EL14
BPC 12	A	A, B, *	L1	0.50	0.40	46	v	HIP
BPC 12	A	Aa, Ab, A	L11	1.00	0.95	0.10	S	DE99
BPC 14	B	A, B, *	L1	0.60	0.50	122	v	WDS
BPC 14	A	Ba, Bb, B	L12	0.30	0.20	13	v	WDS
BPC 16	C	A, B, *	L1	0.70	0.70	39269	Cpm	EL16
BPC 16	A	Aa, Ab, A	L11	0.70	0.20	28	v	EL15
BPC 19	A	A, B, *	L1	1.40	0.01	7.78	v	WDS
BPC 2	A	A, B, *	L1	0.10	0.07	5.79	v	WDS
BPC 22	A	A, B, *	L1	0.10	0.10	1.76	v	WDS
BPC 26	B	A, B, *	L1	1.30	0.40	1065	v	AF15
BPC 26	A	Aa, Ab, A	L11	1.30	1.04	0.94	s	WDS
BPC 28	A	A, B, *	L1	0.63	0.56	48	v	EL15
BPC 3	A	Aa, Ab, A	L1	0.20	0.20	0.38	s	MA14
BPC 30	A	Aa, Ab, A	L1	1.30	1.27	0.71	s	ME10
BPC 31	B	Aa, Ab, A	L1	1.20	0.50	323	v	WDS
BPC 36	B	A, B, *	L1	0.50	0.20	1138	Cpm	WDS
BPC 37	B	A, B, *	L1	0.50	0.70	2035	v	WDS
BPC 37	B	Ba, Bb, B	L12	0.70	0.10	5.71	v	WDS
BPC 37	B	Ba1, Ba2, Ba	L121	0.70	0.70	0.86	s	ME10
BPC 39	A	A, B, *	L1	1.30	0.70	28894	v	AF15
BPC 39	A	Aa, Ab, A	L11	1.30	0.65	1.57	s	MO13
BPC 4	B	Aa, Ab, A	L1	1.10	1.00	390	v	WDS
BPC 41	A	A, B, *	L1	1.10	0.06	21	v	WDS
BPC 41	A	Aa, Ab, A	L11	1.10	0.65	1.54	s	NO04
BPC 42	B	A, B, *	L1	0.90	0.80	2290	Cpm	AF15
BPC 43	A	A, B, *	L1	1.03	0.74	21	v	EL15
BPC 44	B	A, B, *	L1	1.40	0.09	20072	Cpm	WDS
BPC 44	B	Aa, Ab, A	L11	1.40	0.04	203	v	WDS
BPC 47	B	A, B, *	L1	0.70	0.40	1488	Cpm	WDS
BPC 47	B	Ba, Bb, B	L12	0.40	0.30	11	v	WDS
BPC 47	B	Ba1, Ba2, Ba	L121	0.40	0.40	0.56	s	MA14
BPC 52	C	A, B, *	L1	0.50	0.20	44377	Cpm	EL16
BPC 52	C	Ba, Bb, B	L12	0.20	0.20	27	Cpm	WDS
BPC 55	B	A, B, *	L1	0.60	0.60	4.51	v	MA13
BPC 55	A	Aa, Ab, A	L11	0.60	0.30	1.35	s	ELPP
BPC 57	B	A, B, *	L1	1.30	0.90	14764	Cpm	WDS
BPC 57	A	Aa, Ab, A	L11	0.90	0.20	50	v	WDS
BPC 57	B	Ba, Bb, B	L12	1.30	0.50	100	v	WDS
BPC 6	B	A, B, *	L1	0.80	0.50	894	Cpm	AF15
BPC 63	B	A, B, *	L1	0.30	0.20	681	Cpm	SO02
BPC 65	C	Ba, Bb, B	L12	0.90	0.10	14635	Cpm	WDS
BPC 68	B	A, B, *	L1	0.70	0.20	1905	Cpm	WDS
BPC 68	A	Aa, Ab, A	L11	0.70	0.20	33	v	WDS
BPC 69	A	Aa, Ab, A	L1	0.80	0.80	0.30	s	TO06
BPC 70	A	Aa, Ab, A	L1	0.70	0.70	34	v	WDS
BPC 8	A	Aa, Ab, A	L1	0.40	0.20	0.29	s	ELPP
BPC 9	B	A, B, *	L1	1.40	1.11	1957	Cpm	FE06
BPC 9	B	Ba, Bb, B	L12	0.67	0.44	8.83	V	MO15

[a]Cpm: Common proper motion companion, s: spectroscopic binary without orbital solution, S: spectroscopic binary with orbital solution, v: visual binary without orbital solution, V: visual binary with orbital solution. HIP: Perryman et al. (1997), DE99: Delfosse et al. (1999), WDS: Mason et al. (2001), SO02: Song et al. (2002), NO04: Nordström et al. (2004), Torres et al. (2006), ME10: Messina et al. (2010), BA12: Bailey et al. (2012), MA13: Malo et al. (2013), MA14: Malo et al. (2014), EL14: Elliott et al. (2014) – Chapter 2, EL15: Elliott et al. (2015) – Chapter 3, AF15: Alonso-Floriano et al. (2015), MO15: Montet et al. (2015), EL16: Elliott et al. (2016) – Chapter 4, ELPP: Elliott et al. in prep.

5.6.1 Linking multiplicity: young - old populations

The *MF* and *CSF* of the BPMG, shown in row four of Table 5.3, are incompatible with that of the older field population, at $> 5\sigma$ level. In contrast, our derived quantities are compatible with those of extremely young Class 0 sources from the work of Chen et al. (2013) (a ≈50-5000 au) and Tobin et al. (2016) (a ≈15-10,000 au). However, we are sensitive to a much wider range of physical separations. Therefore, the apparent conservation of the *MF* and *CSF* values between these regions can be interpreted as an evolution of the separation distribution. Assuming all considered regions have statistically similar primordial multiple system populations (Kroupa, 2011), we investigate if significant dynamical evolution from Class 0 (Perseus), to Class I/II/III (Taurus), to Class III (BPMG), to main sequence (the field) populations can explain the derived quantities.

The top panel of Figure 5.4 shows the *CSF* as a function of physical separation for Class 0 objects in Perseus (Tobin et al., 2016). We chose the Tobin et al. (2016) sample as our main comparison to Class 0 sources as opposed to Chen et al. (2013) because of its completeness and focus on one specific region, the Perseus region. The main limitation of the observations of Perseus is the angular resolution (0.″065, ≈15 au, grey line). However, we would not expect to find components smaller than this separation due to the opacity limit, where the compression becomes approximately adiabatic, of the initial cores (≈5 au, Larson, 1969). If components have undergone significant dynamical evolution at this stage already (as suggested by Reipurth et al., 2010) and are brought within this limit they would most likely have merged. Additionally systems with separations greater than ∼5,000-10,000 au at these young ages, are unlikely primordial (originating from different birth sites). We cannot assess whether components are gravitationally bound however, as in Tobin et al. (2016), we treat all identified components within 10,000 au as bound systems. The second panel shows the distribution for the Taurus region (3-5000 au). We see that there is a wealth of systems with separations $<$10 au and the overall number of multiple systems is still very high.

TABLE 5.3: A summary of the type and fraction of multiple systems samples analysed in this chapter. S:B:T:Qu:Qi:Se represent system components from Equation 1.4.

Sample	Ref.	S:B:T:Qu:Qi:Se	Total	*MF*[a]	*CSF*[a]
Class 0 regions	1	36:43:15:6:0:0	33	$0.64^{+0.09}_{-0.05}$	$0.91^{+0.15}_{-0.09}$
Perseus	2	43:23:17:7:7:3	30	$0.57^{+0.06}_{-0.11}$	$1.20^{+0.27}_{-0.32}$
Taurus	3	41:43:10:3:0:1	117	$0.59^{+0.04}_{-0.04}$	$0.78^{+0.09}_{-0.07}$
BPMG	4	35:35:24:6:0:0	49	$0.65^{+0.06}_{-0.02}$	$1.02^{+0.14}_{-0.06}$
BPMG (10,000 au)	4	44:42:11:3:0:0	57	$0.56^{+0.07}_{-0.05}$	$0.73^{+0.12}_{-0.08}$
BPMG (1000 au)	4	52:38:10:0:0:0	63	$0.48^{+0.06}_{-0.07}$	$0.58^{+0.08}_{-0.09}$
The field	5	56:33:8:3:0:0	454	$0.44^{+0.01}_{-0.02}$	$0.58^{+0.01}_{-0.04}$
The field	6	54:33:8:4:1:0	4847	$0.46^{+0.01}_{-0.01}$	$0.65^{+0.01}_{-0.01}$

[a] 1σ confidence intervals from 1000 bootstrapped samples. Note, bootstrapped uncertainties are indistinguishable from those calculated using binomial statistics for *MF* values in the majority of cases.
1: Chen et al. (2013), 2: Tobin et al. (2016), 3: Kraus et al. (2011), 4: this chapter, 5: Raghavan et al. (2010), 6: Tokovinin (2014b)

For comparison with the BPMG (middle panel of Figure 5.4) we assume all wide systems are primordial.There is another mechanism to produce wide (non-primordial) systems (Kouwenhoven et al., 2010; Moeckel and Bate, 2010), which is discussed in Section 5.8. At the same time as there being a wealth of systems with separations $<$10 au in our sample there are also many objects with large separations (1000-100,000 au). This *stretching* of the initial separation distribution to both smaller separations and larger separations implies intense dynamical evolution.

5.6.2 The role of unfolding higher-order systems

Reipurth and Mikkola (2012) described a potential physical mechanism for the formation of wide and very wide binaries ($\geq$1,000 au); through the dynamical *unfolding* of primordial triple systems. The mechanism predicts:

- A preference for wide binaries to be in triple systems

- These systems will have high ($>$0.9) eccentricities.
- The majority of wide components will be low-mass (these systems are likely unstable and therefore their lifetime is $<$100 Myr)

We note that although there should be a preference for wide binary systems to be in triple systems we would not expect to find all systems in this configuration due to previous mergers. Additionally that we cannot assess the eccentricity of the wide components. This problem is discussed in more detail in Section 5.8.

5.6.2.1 Higher-order multiplicity in wide systems?

We found that for systems with companions $>$1000 au and $>$10,000 au, 11 / 14 ($0.79^{+0.07}_{-0.14}$) and 6 / 7 ($0.86^{+0.05}_{-0.21}$) were part of triple or higher-order systems, respectively. In contrast, for systems with no components $>$1000 au we found 4 / 19 ($0.21^{+0.12}_{-0.06}$) systems were higher-order systems. *The fraction of higher-order multiple systems is clearly a function of the physical separation.*

Additionally we looked at the separations of the inner components of the 11 systems (8 triples, 3 quadruples, i.e. 14 inner components) with companions $>$1000 au. Of these 14, 11 had separations smaller than the inner peak identified of the separation distribution found in the Perseus region by Tobin et al. (2016). Again, this supports the theory of migration via the interaction of multiple components.

Although there is no evidence for higher-order multiplicity amongst the 3 binary systems (BPC 36,42,65) that have components $>$1000 au, that does not necessarily negate the possibility, as few of the components have been observed with AO-imaging and have multi-epoch radial velocity data, see Table 5.1.

5.6.2.2 Masses and mass-ratios

We studied the mass distribution within the 10 higher-order multiple systems with wide components. For the triple systems we compared the mass-ratios of the inner binaries

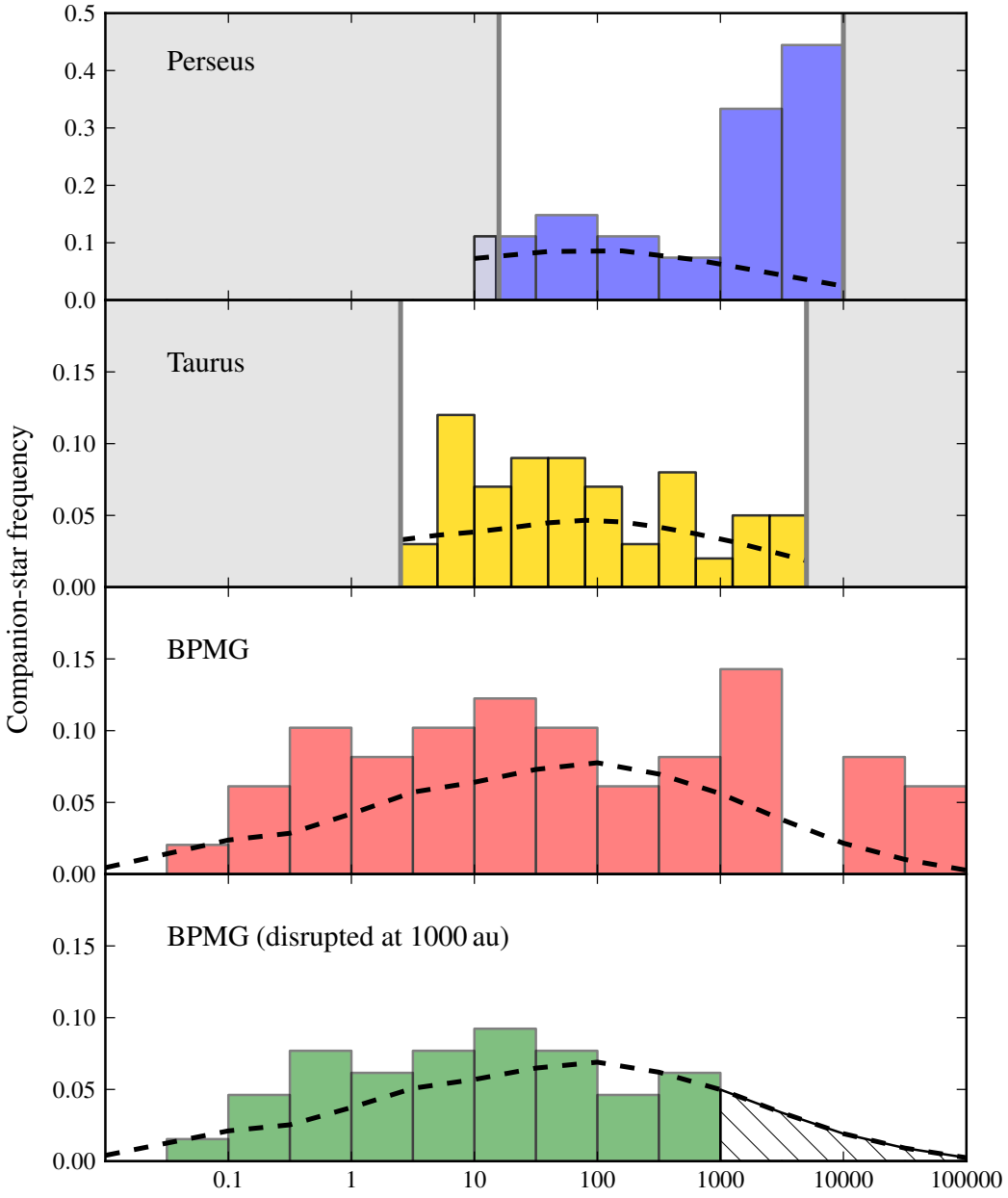

FIGURE 5.4: Physical separation versus CSF for four different samples. *Top:* Perseus (15-10,000 au, Tobin et al., 2016), *second:* Taurus (3-5000 au, Kraus et al., 2011), *third:* The BPMG sample, *bottom:* The BPMG sample, disrupted at 1000 au. The log-normal field distribution derived in Raghavan et al. (2010) is over-plotted (black dotted line) in all panels. Grey shaded areas represent parameter spaces not probed.

and outer components. In the case of the quadruple systems we compared the mass-ratios of each sub-system and each component with that of the primary. In neither case we found a significant relationship between the system configuration and absolute mass nor the mass-ratio. Our derived mass-ratio distribution was statistically similar to a power-law with $\gamma = 0$ i.e. a flat distribution in the range 0.1-1.0.

5.6.3 Disruption of higher-order systems

In the framework of Reipurth and Mikkola (2012) we estimated the survival rate of the identified triple systems, given their mass distribution.

Similar to Figure 3 of Reipurth and Mikkola (2012) we compared the mass sum of the inner binary (M_a + M_b) to the mass of the outer companion (M_c) for wide triple systems. We show our results in Figure 5.5: star markers are BPMG triple systems with at least one companion $>$1000 au, grey dots are field stars (Tokovinin, 2014b) meeting the same criterion. Firstly we see that all BPMG systems are in the *dominant binary* (red shaded area) regime. Secondly, we see that 5 / 8 of these systems occupy a parameter space mostly uninhabited by very wide field systems. Reipurth and Mikkola (2012) show that most systems in this parameter space are unstable and are disrupted between the ages of 10-100 Myr. Therefore, our results imply that the majority of wide triple systems in the BPMG are in the process of disintegrating/decaying without external influence.

To investigate if the disruption of higher-order multiple systems in our sample could "bridge-the-gap" between young populations rich in multiplicity and the older processed field population we artificially disrupted our higher-order multiple systems at two physical separation limits (1000 au and 10,000 au)[1]. The first limit is a somewhat arbitrary definition of a wide binary, the second is an approximation for the size of a hydrostatic clump. We then calculated the *MF* and *CSF*, considering systems with components

[1]The multiplicity properties derived using a disruption separation anywhere between 3000-10,000 au are unaffected.

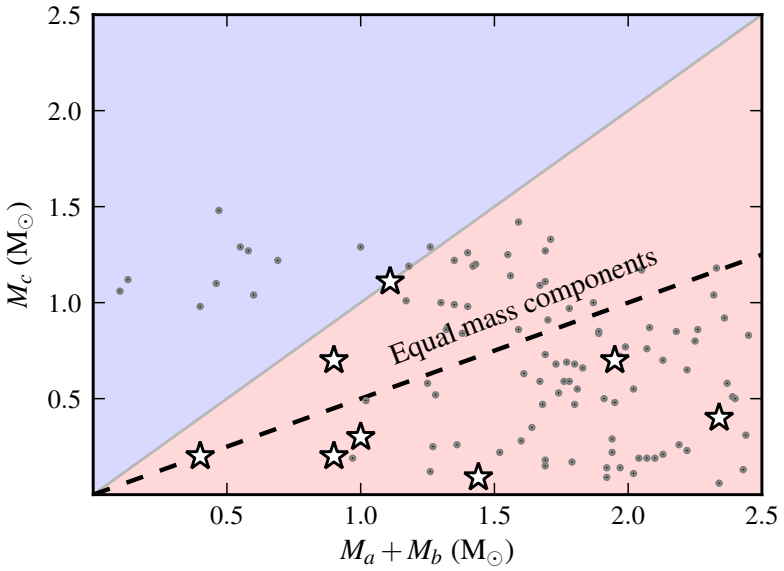

FIGURE 5.5: Inner binary (M_a + M_b) versus outer component (M_c) masses for BPMG (stars) and field (Tokovinin (2014b), grey dots) wide systems. The blue and red shaded areas highlight the dominant single and binary regimes, respectively. The dotted line describes equal mass component systems (Ma = Mb = Mc).

wider than these limits as *separate* systems.The results are shown in Table 5.3. Considering the limit at 10,000 au, the *MF* and *CSF* values are within 2 σ and 1 σ, respectively, of the field population (higher in value). For the limit at 1000 au both the *MF* and *CSF* values are within 1σ (the *CSF* now lower in value). In the same line, the *MF* and *CSF* values of Taurus are compatible with the disruption of systems at 10,000 au in the BPMG sample. This suggests that the majority of primordial systems with separations somewhere between 1000-10,000 au and beyond have been destroyed or decayed in older populations.

We also compared the *CSF*, as a function of physical separation distribution, for: the original BPMG sample, the BPMG sample disrupted at 1000 au and 10,000 au and the field. The results are shown in Figure 5.6. We split our samples at the mean of the field distribution (≈50 au) and compared the different populations. We would expect the distribution of inner separations to be very similar already at the age of the BPMG, as demonstrated in Chapters 2 and 3.

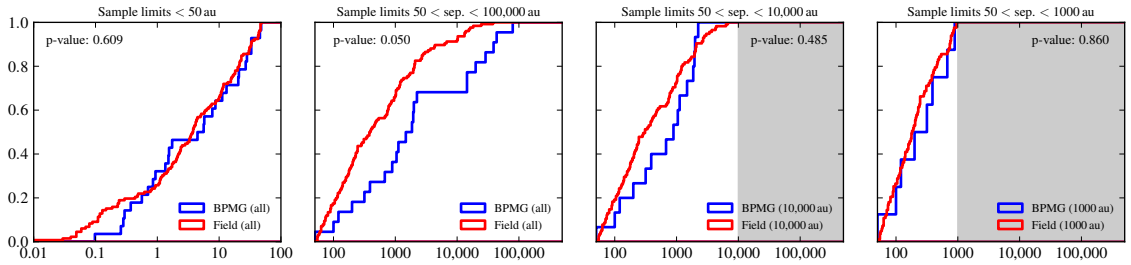

FIGURE 5.6: Cumulative separation distributions for four different samples. Labels above each plot indicate the physical separation range. The p-value calculated from the Kolmogorov-Smirnov test is shown in each panel. Field systems from from Raghavan et al. (2010).

We can reject the null hypothesis when comparing the field with the original BPMG sample (p-value 0.028, second panel of Figure 5.6) for separations $>$50 au, i.e. these distributions are not likely to be realisations of the same parent distribution. However, if we compare the BPMG sample disrupted at 1000 and 10,000 au (3rd and 4th panel of Figure 5.6) to the field, we calculate p-values of 0.860 and 0.485, respectively (non rejection).

The recent work of Parker and Meyer (2014) suggested that the primordial binary population is similar to the population we observe today and has undergone little dynamical processing. Along with many previous works, Parker and Meyer (2014) have focussed on binaries as opposed to higher-order multiple systems. However, our results indicate that the disruption of primordial higher-order systems significantly shapes older, more processed populations, such as the field. We outline a simple model for the contribution of unfolding triple systems to the separation distribution in a population in Section 5.7.

5.7 A model for the dynamical evolution of triple systems

Below we collect together the physical mechanisms discussed in the previous sections, along with additional physics, to briefly outline the separation evolution of higher-order (in this case, specifically triple) systems in a population. Our simplified model is shown

in Figure 5.7 in 3 stages.

Stage I: We approximate the initial distribution of separations within clumps using the identified bimodal distribution of Tobin et al. (2016) (peaks; 75 and 3000 au). These peaks have been attributed with typical scales for disc ($\sim$100 au, Zhu et al., 2012) and core ($\sim$1000 au, Offner et al., 2010) fragmentation. No multiple systems can inhabit the hatched region for separations $<$10 au due to the size of the first Larson core (a pressure supported fragment) ($\approx$5 au, Larson, 1969). The second hatched region beyond $\approx$5000-10,000 au represents the initial size of the hydrostatic clump (Benson and Myers, 1989; Motte et al., 1998; Pineda et al., 2011), i.e. by definition a primordial multiple system at this stage cannot have components beyond this separation.

Stage II: The inner peak both broadens and shifts to closer separations through the exchange of angular momentum with the outer component (components are now in a hierarchical configuration, although potentially unstable, as Reipurth and Mikkola, 2012). This is supported by the conservation of the *MF* and *CSF* quantities in larger separation ranges for Class 0 sources (15-10,000 au, Tobin et al., 2016), Class I/I-I/III sources (3-5000 au, Kraus et al., 2011) and Class III sources ($\approx$0.01-100,000 au, this chapter). Additional migration to closer separations can also occur through gas-induced orbital decay (Bate et al., 2002; Korntreff et al., 2012; Bate, 2012). Concurrently, through angular momentum exchanges, the outer components move to wider separations. These wide components (red shaded area) are weakly bound, and some will be in the process of decaying (so-called *unfolding*: Reipurth and Mikkola, 2012) without any external influence. Others may be dynamically disrupted / destroyed by external dynamics i.e. stellar encounters within a cluster. Our analysis in Section 5.6.3 indicates that most systems are in the process of decaying without external influence. However, as this process is still taking place at the age of the BPMG, there is still a significant population of wide systems.

Stage III: In loose low-density environments, such as the BPMG, the resultant distribution is double peaked. The inner peak is at a smaller separation than the original 75 au ($\approx$4 au for the higher-order multiple systems in our sample). The outer peak ($\approx$8000 au

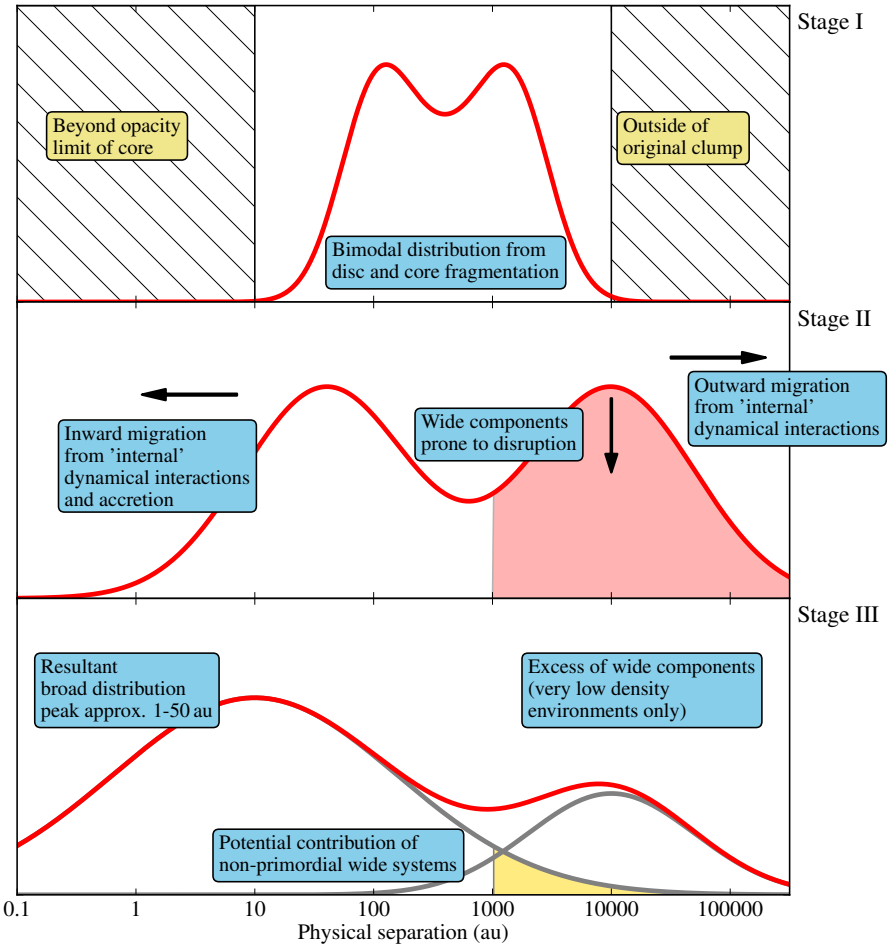

FIGURE 5.7: A simplified model of the dynamical evolution of separations within a population of primordial triple systems. Regions of interest are annotated and processes are described in detail in the text (Section 5.7).

in our sample) is smaller as some components have unfolded and decayed completely, reducing the number of triples. However, a significant population still remains, due to the lack of external dynamical perturbations. We have highlighted the region (gold shaded area) where non-primordial wide multiple systems can be formed during the cluster dissolution phase (Kouwenhoven et al., 2010, discussed in Section 5.8). In the case of higher-density and older ($\approx$100 Myr) environments, the secondary peak is mostly destroyed and the contribution of primordial triple systems to the overall distribution is small/negligible.

5.8 Discussion and limitations

We have shown that the dynamical evolution of primordial higher-order multiple systems can reconcile the multiplicity properties of Perseus, Taurus, BPMG and the field. Below we discuss the current limitations and prospects.

The mechanism of Kouwenhoven et al. (2010) and Moeckel and Bate (2010) is a potential route to produce wide, non-primordial binaries in the cluster dissolution phase. However, this mechanism predicts only one or two wide binaries ($>$1000 au) in a population of the size studied here, compared to the 14 identified. Additionally we have shown how the decay of primordial higher-order systems can "bridge-the-gap" between young and old populations. We do not claim the mechanism of Kouwenhoven et al. (2010) is ineffective, rather that it is not the dominant mechanism in our sample. However, one also has to consider that binary formation and destruction is very stochastic. N-body simulations of clusters with very similar initial conditions can produce resultant distributions with different forms (Parker and Goodwin, 2012). Therefore, we must conduct similar analysis on other nearby young moving groups in order to see if those populations also have similar multiplicity properties to the BPMG.

A parameter that would help to determine the formation mechanism of wide multiple systems is their eccentricity (e). A natural consequence of the Reipurth and Mikkola (2012) mechanism is a distribution peaked at high eccentricities. Whereas the mechanism of Kouwenhoven et al. (2010) predicts a flatter eccentricity distribution, see their Figure 10. Tokovinin and Kiyaeva (2016) recently showed that wide binaries in the field do not have a thermal eccentricity distribution and therefore are unlikely products of either formation scenario. Given the predicted periods of very wide systems ($\gtrsim$Myr) determining their eccentricities is extremely challenging. However, the GAIA mission (Lindegren et al., 2008) will provide extremely accurate astrometry (7-25 μas) that can help. Face-on multiple systems of total mass 1 $M_{\odot}$, at 40 pc, and with 20,000 au separation, will have detectable movement at 3σ level using GAIA astrometry within 1 yr.

The work of Reipurth and Mikkola (2012) used only three bodies within the original clump to study the formation of wide binaries. However, the initial multiplicity is likely to be a spectrum, which indeed is observed in young regions (Chen et al., 2013, Tobin et al., 2016) where clumps contain up to six components. Higher-order systems would be responsible for an even more chaotic start for components within the clump, likely resulting in more ejections. Further studies of nearby young regions with instruments such as ALMA and the VLA will provide further insight into the initial distributions of hydrostatic cores. These can then be used as realistic starting points of N-body simulations and *evolved* into older dynamically processed populations.

5.9 Conclusions

- Similar *CSF* values between the very young sources of Perseus and the BPMG can be explained by dynamical evolution of the separation distribution of multiple systems.
- The high fraction of wide ($>$1000 au, 11 / 14) and very wide ($>$10,000 au, 6 / 7) systems in higher-order configurations supports the mechanism of Reipurth and Mikkola (2012).
- There is no significant mass-ratio trend among inner and outer components in wide higher-order systems.
- The separation distribution of the field and the BPMG (for separations $>$50 au) are not realisations of the same parent distribution (p-value 0.03).
- The decay of primordial higher-order (triple and higher-order) systems can link multiplicity in young regions to dynamically processed populations such as the field, in opposition to the more static framework of Parker and Meyer (2014).
- The abundance and configuration of the wide systems in the BPMG favours the Reipurth and Mikkola (2012) mechanism over that of Kouwenhoven et al. (2010).

Chapter 6

Conclusions

In the introduction to this thesis we outlined some important open questions regarding multiplicity. We re-state them below.

- Are multiplicity properties universal, or do they depend on the native environment?
- How are spectroscopic binaries formed and what is the timescale for this formation?
- How are extremely wide systems formed and what is their fate?
- What effect does multiplicity have on disc evolution and planet formation?

These questions, especially the first, are very profound and to have conclusive answers still requires further work. However, in this thesis we have, at least in part, addressed the first three of these questions. Below we summarise how the analysis presented in this manuscript has addressed each of these questions and what steps we are taking for future analysis.

Are multiplicity properties universal?

We have presented a whole host of results that support the universality of multiple systems throughout this thesis, by comparing various derived properties with other populations (spectroscopic binaries: abundance, visual binaries: abundance, occurrence in triple systems, mass-ratio, separation distribution, wide binaries: abundance, higher-order configuration, mass-ratio). We reconciled the apparent excess of very wide companions in the young groups compared to the field by comparing the abundance of multiple systems to the very young region of Perseus, assuming significant dynamical interaction and migration. This analysis indicates that the majority of low-mass stars form in small groups of 3 or 4 components before dynamical interactions facilitate significant migration.

A full statistical analysis of the young moving groups is under way and will be presented in future work. This analysis will include newly obtained observations and make extensive use of the database outlined in Appendix A for $\approx$600 young targets.

Overall there is still a lot of work, both theoretical and observational, to be done to answer this question. From a theoretical point view, the role of magnetic fields needs to be explored further, as early results indicate they can significantly affect accretion rates and resultant mass-ratios (Zhao et al., 2013). Another potential property that could affect multiplicity properties is the opacity of molecular gas. Bate (2014) investigated this by performing simulations of gas with different opacities, corresponding to a range in metallicity of 0.01-3 $Z_{\odot}$. He found no significant statistical differences in the multiplicity properties, indicating that gas opacity does not play a strong role in observed statistical properties.

Observationally we are starting to see great progress of Class 0 multiplicity e.g., Chen et al. (2013) and Tobin et al. (2016). Further studies making use of millimetre facilities such as the VLA and ALMA are likely to somewhat revolutionise our understanding of primordial multiplicity thanks to their high resolution. In the closest star-forming regions ALMA can resolve physical separations $<$10 au. It will also be able to dramatically increase our knowledge of more distant, *typical* star-forming regions such as Orion. In

addition to these studies of very young regions, for the T-Tauri stage and older populations, as ever, it is a case of increasing sample sizes and detection limits. With recent developments in instrumentation we can extend detections of companions down to lower masses including sub-stellar and even planetary mass objects. Such efforts are long-term projects, however, significant progress is being made.

How are spectroscopic binaries formed and what is the time-scale for this formation?

In Figure 5.7 we showed a schematic for the evolution of triple systems in a population. In this framework the outcome is a population of hierarchical wide binary multiple systems; tight inner binaries with wide companions. This is a potential formation channel for spectroscopic binaries. We found that 8/12 (67%) of the spectroscopic binaries were in higher-order multiple systems. This is indicative of a preference for spectroscopic binaries to be found in triple of higher-order systems, similar to the results of Tokovinin et al. (2006) (63%). However, it also appears that spectroscopic binaries can also form without higher-order components in the system. The formation process is likely a combination of orbital shrinkage via accretion and dynamical interactions (Bate et al., 2002).

Our results along with many other studies (Raghavan et al., 2010; Nguyen et al., 2012; Tokovinin, 2014b) indicate that the timescale of formation is shorter than $\approx$1 Myr. Tokovinin et al. (2006) showed that the properties of spectroscopic binaries with tertiary companions can evolve over long timescales, but the overall abundance after 1 Myr is unchanged. In order to probe the timescale of formation, again, facilities such as ALMA will be invaluable. The apparent theoretical limit of fragmentation ($\approx$5 au) can be probed for the closest star-forming regions to look for closely separated ($\lesssim$10 au) binaries that would violate this limit. Thanks to the commissioning of the longest baselines, the high resolving power of ALMA has recently been demonstrated, for the protoplanetary disc of HL Tau; resolving features as small as 3.5 au (ALMA Partnership et al., 2015). From our results; the agreement between the *CSF* in the β-Pic moving group and that of

Perseus (Tobin et al., 2016), the formation timescale is somewhere between 0.1 Myr - 1 Myr.

How are extremely wide systems formed and what is their fate?

The analysis presented in Chapter 5 supports the mechanism of Reipurth and Mikkola (2012); wide binaries are the result of dynamical interactions between components of non-hierarchical protostar systems, in the young moving groups. These results are based on small number statistics but combined with the rate of higher-order multiplicity in young Class 0 regions the results are promising. The higher-order multiplicity of 50 identified wide binary systems is the subject of a proposal submitted for observations to take place between October-April 2016/17.

Regarding the fate of these systems, this analysis indicates that many of the identified systems are in the process of decaying. By the time these systems are $\approx$100 Myr in age they will disintegrate, without external perturbation from other stars. A possible comparison for future analysis is with the AB Doradus moving group (100-150 Myr), to see if there is a significantly lower number of wide binary systems, compared to the younger β-Pic moving group population.

Distinguishing between the different formation channels of wide binaries is extremely challenging due to the limitations of observability. Potentially the eccentricities of these wide systems could shed light on their formation mechanism, but, due to the long orbital periods of very wide systems periods and current instrumentation, we are severely limited to deriving the eccentricities of closer companions. GAIA (Lindegren et al., 2008) could potentially help with the derivation of eccentricities of such wide systems. Due to its extremely high astrometric accuracy (7-25 μas) significant orbital motion of even extremely wide binaries could be detected. The final data release of GAIA, with the highest astrometric accuracy, is scheduled for 2022.

What effect does multiplicity have on disc evolution and planet formation?

This question has not been directly addressed in this thesis, however, in the introduction we have briefly discussed the theoretical and observational results that show the significant effect of companions on disc evolution and planet formation. This field of research is still very much in its infancy but it is advancing fast.

In the future we will combine our multiplicity knowledge with both disc detections and planet detections for these young objects. We are yet to perform a statistical analysis comparing multiplicity properties with disc properties of the young moving groups, similar to that of Rodriguez et al. (2015). However, we have much of the information needed for such an analysis compiled and have applied for further observations of newly identified targets. We want to study both the abundance and properties of these discs. The properties of the dusty discs can be probed with mid-infrared spectroscopy (observations have already been taken), to look for differences in dust evolution in multiple and single star systems.

We also want to extend this analysis of disc properties to planet formation and abundance. We plan to do this by combining observations taken with deep AO imagers such as SPHERE/VLT (Beuzit et al., 2008) and GPI/GEMINI (Macintosh et al., 2014) and near-infrared spectrographs such as CSHELL/IRTF (Anglada-Escudé et al., 2012), GIANO/TNG (Oliva et al., 2006) and CRIRES+/VLT (Dorn et al., 2014). Up until very recently observational studies searching for planets around young stars have been limited to AO imaging techniques. However, there have been advancements in near-infrared spectrographs and reduction techniques, which facilitate exoplanet detections around young, active stars via radial velocity jitter. This is demonstrated in the recent works Gagné et al. (2016) and Carleo et al. (2016). The long-term radial velocity precisions are estimated at 5-10 ms^{-1} which would allow super Earth detections in the habitable zone of young mid-M dwarfs.

By combining all of this information together we can make strong links between multiplicity, disc evolution and planet formation/abundance for these young stars.

Appendix A

Handling and manipulating large datasets

The analysis presented in this thesis is based on a large number of objects. Firstly, it is important to handle the data in such a way that the statistics that are produced are free of user-induced errors. Secondly, this analysis is part of a larger ongoing project and, therefore, it is very important that this data is accessible and stored correctly. The data structure and methods that produce the statistics need to be able to handle newly incorporated data efficiently.

In August 2015 I spent one week at the Cerro Tololo Inter-American Observatory (CTIO) in La Serena, Chile, working with Dr. Andrei Tokovinin[1]. Dr. Tokovinin has published a huge number of papers based on the statistics of multiple systems in the nearby field population. Two of the most recent papers (Tokovinin, 2014a,b) are based on the statistics of over 4800 stars and, therefore, he is extremely experienced with the data structure and techniques needed to handle such large datasets and produce statistics.

This visit highlighted the importance of data organisation and structure and drove me to start building my own database, with a basic structure similar to that shared with

[1] http://www.ctio.noao.edu/~atokovin/

me by Dr. Tokovinin. The database I created uses the Structured Query Language[2] (SQL), combined with methods created in python[3]. This combination is very effective and allows fast access to, and easy manipulation of, the data.

Below I outline the structure of the database, based on that of Dr. Tokovinin's own IDL structures, and an example of one method that calculates the detection probability for companions around a target.

A.1 Database structure

Figure A.1 shows the basic structure of the database. The *ncomp* table is in bold text because this is the table where the unique identifier is introduced. The unique identifier is a combination of a system id such as "BPC_10", for a member of the β-Pic moving group, and a component, for both single and multiple systems, such as "_A", making "BPC_10_A". The unique identifier applies to a *resolved* target in our sample. In this case resolved means resolved by typical all sky surveys (2MASS – Cutri et al., 2003, WISE Wright et al., 2010, TYCHO – Høg et al., 2000). A consequence of that, is that one unique identifier may actually refer to an *unresolved* multiple system, for example, a spectroscopic binary. However, one wants to keep the information of the multiple system separate from the observational information. That is because the information of the system is physical, such as the period and the mass of the components.

The data in each table shown in Figure A.1 is outlined below.

- *assoc*: The name of each association with an age estimation that is used in model-based masses of targets.
- *ncomp*: Observational information of resolved targets in our sample such as its co-ordinates, proper motion, magnitude, spectroscopic emission features, membership status.

[2] `http://www.w3schools.com/sql/`
[3] `https://www.python.org/`

- *2m_sources*: Basic properties of all 2MASS sources within a field of a view equivalent to 100,000 au, given the target's distance. There can be 10,000s of entries for one target.
- *wds_local*: A local version of the WDS (Mason et al., 2001) catalogue containing previous potential detections and notes.
- *systems*: Properties of all identified multiple systems including flags for unconfirmed systems.
- *excess*: Individual photometric entries at multiple wavelengths to investigate potential non-photospheric emission around stars.
- *detec*: Detection limits for targets from either spectroscopic, AO-imaging or direct imaging data.
- *individ_ao*: Individual AO-imaging data contrast curves (magnitude versus angular separation) for each separate observation.
- *individ_rv*: Individual radial velocities with modified Julian dates for each previous observation.

The information in the sample is constantly evolving, for example, with new age estimations of the associations, new observations of individual targets and new detections of companions. Therefore, the stored data and the statistics produced need to be easily manipulated. The structure outlined above combined with the custom methods developed in python makes this process quick and simple. Below is an example one particular method that is used to calculate the detection probabilities. This example highlights both the complexity of the method *behind the scenes* and how simply it is executed by the user.

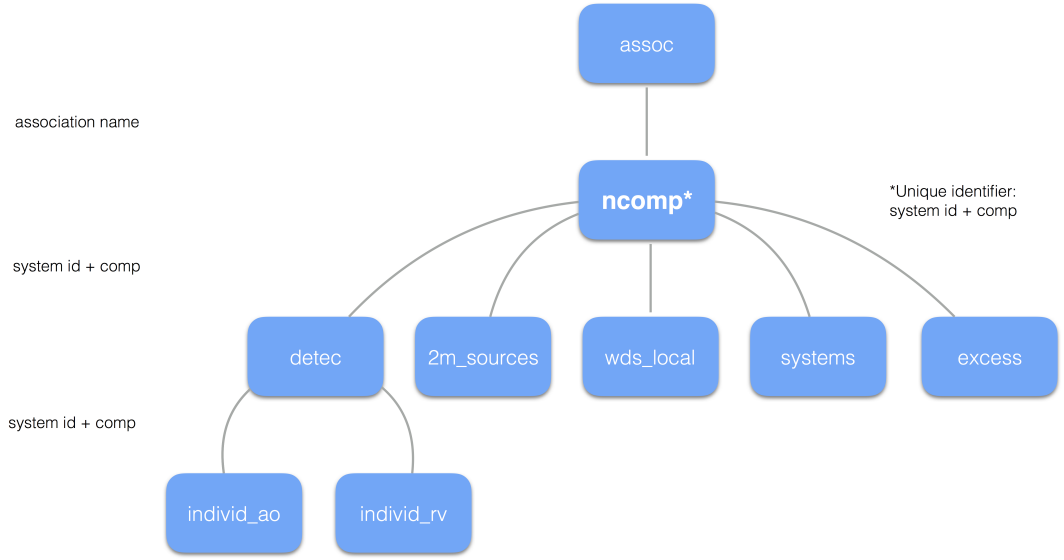

FIGURE A.1: The basic structure of the SQL database created to handle the data presented in this thesis and ongoing work. The boxes represent the tables and have their respective names. The labels on the left show the column that links the data from one table to the other.

A.2 Object-orientated approach to data manipulation

Many of the techniques used in the statistical analysis are repeatable from object to object. In other words, no aspect of the analysis needs to be *tweaked* in any special way, and, therefore, exactly the same steps of analysis can be applied to each target. Using object-orientated custom methods in python in combination with SQL one can execute complex analysis with very little user input.

First a class of object was created which, for the database used here, is called *System_mss*. This refers to one multiple stellar system (mss), which can contain more than one resolved component. An instance of this class is created by giving the system id of one specific system as a string. A series of self-built methods then act upon this instance and perform different tasks. An example of one such task is discussed below.

A.2.1 A breakdown of the detection probability method

The text below shows the python code needed for the execution of the *master_prob* method on the system ”BPC_16_A”. The definition of the object and execution is only two lines of python code. Therefore, it is easy to see that to perform this task on every single system in the database, it is simply a case of looping over all possible system ids and components.

```
obj = System_mss("BPC_16") % object instance
obj.master_prob("A", "plot_name.pdf") % execution on comp.  A
```

Figure A.2 shows a breakdown of the *master_prob* method that calculates the probability of detecting a companion on a grid of mass-ratio (q) values from 0.01-1 and periods (p) 1-10^{10} day. This method needs quite a lot of parameters from different tables in the database to produce the final output; an array of periods, mass-ratios and detection probabilities. Below I outline how this method operates. Figure A.2 showing a schematic of the steps involved.

prob_sb: First of all the individual radial velocities (rv) and their respective modified Julian dates (mjd) are collected. From these, the N, T and sigma parameters are calculated, where N is the number of observations, T is the time between the first and the last observation and sigma is the standard deviation of all rv values. These parameters are combined with the primary mass (m1) parameter from the ncomp table. The formulae defined in Tokovinin (2014a) are used to calculate the probability of detection, using these parameters and many thousands of simulated binaries. An array of p, q and probability is outputted.

prob_ao: The individual AO detections are collected from the *individ_ao* table. These detections are always stored as two arrays of 5 elements, one array for the angular separations (sep 1, 2, 3, 4, 5) and one for the delta magnitude (dm 1, 2, 3, 4, 5) value, along with the wavelength (wlen) of observation. First of all, for each observation, the delta magnitude values are combined. As the delta magnitudes can refer to different wavelengths of observation these delta magnitudes are all converted to the K_s band

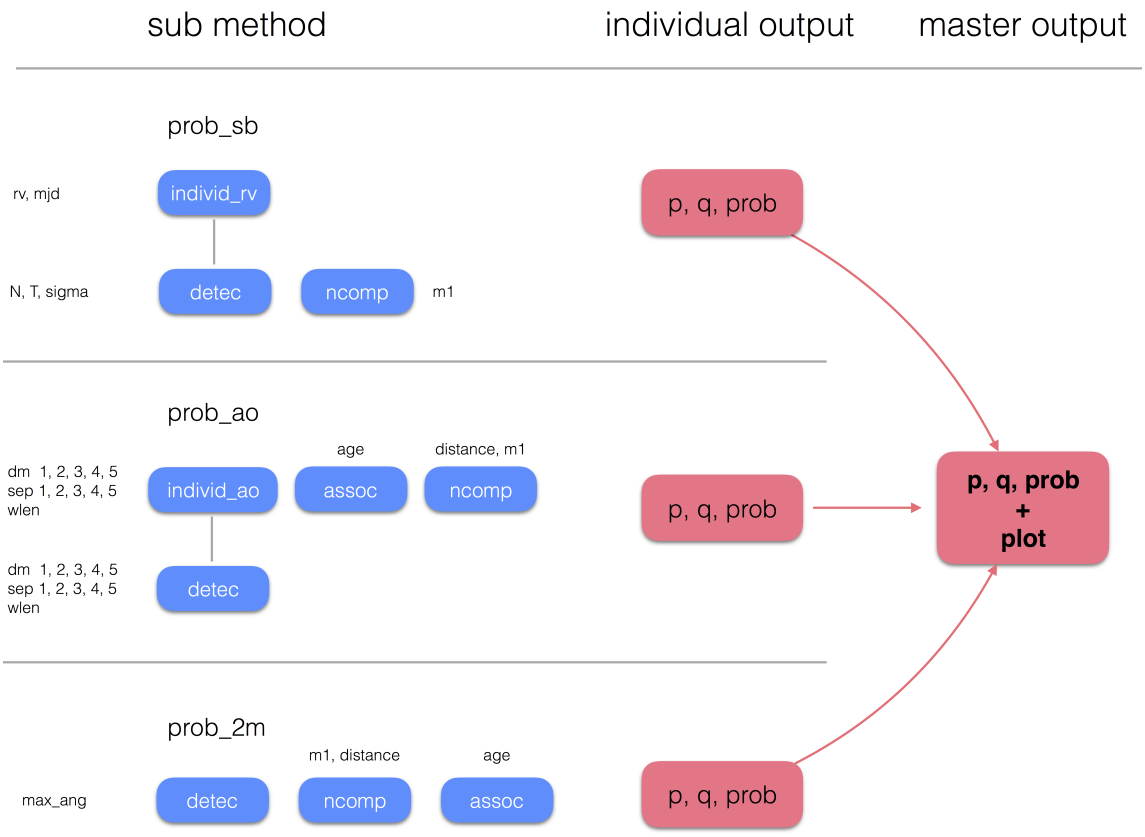

FIGURE A.2: Structure of *master_prob* python method. Blue and red boxes represent tables and outputs, respectively. Labels next to each table refer to the parameters collected and used in the method. See text in Section A.2.1 for further details.

using the evolutionary models of Baraffe et al. (2015) and distance of the system from the *ncomp* table. From these individual arrays a master array is created that is the deepest (has the highest contrast) observation at each element of angular separation. This is the array that is then stored in the *detec* table. This array is retrieved and combined with the primary mass value from the *ncomp* table. Using thousands of simulated binaries (by converting their masses to magnitudes) and *observing* them with the master contract curve, an array of p, q and probability is outputted.

prob_2m: The max_ang parameter is retrieved from the *detec* table. This parameter was derived using the analysis presented in Chapter 4 and is the angular separation to which we defined our sensitivity to wide visual companions. As this analysis was based on 2MASS photometry the 10 σ limits (J=15.8, H=15.1, K=14.3, Cutri et al., 2003) were used in the calculation. These values were combined with the evolutionary

models of Baraffe et al. (2015), and distance to the target, to calculate the minimum mass of a detectable companion. This information is then combined with the primary mass value and again, thousands of simulated binaries are *observed*. An array of p, q, and probability is outputted.

The arrays outputted from *prob_sb*, *prob_ao* and *prob_2m* are combined using the equation:

$$\text{prob}_{\text{all}} = 1 - \prod^{i}(1 - \text{prob}_i) \tag{A.1}$$

where prob_i is the probability from the individual technique, i.e. either from spectroscopy, AO-imaging or direct imaging.

This is very important in the cases where the target is close enough that the parameters of detectable companions from AO-imaging and spectroscopy can overlap. Additionally, for almost every object, the direct imaging and AO-imaging parameter spaces overlap (typically where the AO observational field of view is $>3''$). Therefore, the resultant probability needs to reflect the probability given the information from two observational sources. For objects that do not have detection limits from one (or potentially all) techniques described above, an array of zeros is outputted i.e. a zero probability of detection.

The master output (prob_{all}) is then stored in the *detec* table and a plot is made for each target (see Figure 1.3 for an example).

For every system id + component in our database we have an individual detection probability and this is crucial for producing our statistics. These detection probabilities can be averaged, thanks to all the probabilities being calculated on the same grid of period and mass-ratio values. Therefore, producing population detection probabilities across 10 orders of magnitude in period (1-10^{10} day) and from mass-ratios 0.01 to 1 is very simple (see Figure 5.1 for an example). Additionally, updating the detection probabilities is merely a case of adding the data to tables *individ_rv* and *individ_ao* and re-running the method on those particular objects.

Appendix B

Successful proposals

This Appendix collates the observational proposals written by the author of this thesis[1] (during Nov 2012–April 2016) that were rewarded telescope time. Before each proposal we present the scientific goal, the instrument (and telescope) and the total amount of observation time. We then include the *scientific rationale* and *immediate objectives* of each proposal in their original format.

[1]The proposal *Determining dynamical masses of nearby pre-main sequence multiple stellar systems* was submitted by Amelia Bayo as PI although the scientific case was adapted from a science case written by the author of this thesis. This is due to allocation of telescope time from Chilean institutions.

B.1 P93, NACO & UVES

Title: Is multiplicity universal?

Scientific goal: Collect more high resolution spectra and AO imaging data of confirmed young moving group members

Instrument / **Telescope**: NACO/VLT, UVES/VLT

Number of hours: 10.3, 21.2

European Organisation for Astronomical Research in the Southern Hemisphere

OBSERVING PROGRAMMES OFFICE • Karl-Schwarzschild-Straße 2 • D-85748 Garching bei München • e-mail: opo@eso.org • Tel.: +49 89 320 06473

APPLICATION FOR OBSERVING TIME PERIOD: **93A**

Important Notice:

By submitting this proposal, the PI takes full responsibility for the content of the proposal, in particular with regard to the names of CoIs and the agreement to act according to the ESO policy and regulations, should observing time be granted.

1. Title Category: **C–7**

Is Multiplicity Universal?

2. Abstract / Total Time Requested

Total Amount of Time:

The multiplicity surveys conducted during the last couple of decades have revealed that the fraction of multiple systems among the T-Tauri stars is similar or 2 times higher than that of Main Sequence (MS) stars by Duquennoy & Mayor, but what is dominant effect for these fractions in young Pre-MS stars: mass, age or environment? Preliminary results of the close-companion frequency of the SACY sample show no relationship with spectral type, i.e. mass, differing greatly to their young higher-mass equivalents. Coeval loose associations show a dramatic difference in frequency, Columba having potentially 0^{+4}%, compared to that of Carina, 14^{+9}_{-4}%. These preliminary conclusions challenge the universality of the multiple system fraction among young stars. We propose continuing towards a comprehensive multiplicity frequency of the SACY associations, taking full advantage of the proximity of these targets, by probing a continuous range of orbital separations.

3.

Run	Period	Instrument	Time	Month	Moon	Seeing	Sky	Mode	Type
A	93	UVES	21.2h	any	n	n	THN	s	
B	93	NACO	10.3h	any	n	1.0	THN	s	

4.

Number of nights/hours	Telescope(s)	Amount of time
a) already awarded to this project:	UT2/UT4	90h/33h during P88 and P89
b) still required to complete this project:	UT2	10h

5. Special remarks:

Excellent filler for bad weather conditions. This proposal is part of Ph.D. thesis (*Is Multiplicity Universal?*, Paul Elliott) which started in November 2012.

6. Principal Investigator: pelliott

6a. Co-investigators:

C.	Torres	1599
C.	Melo	1261
N.	Huelamo	1456
M.	Sterzik	1261

Following CoIs moved to the end of the document ...

7. Description of the proposed programme

A – Scientific Rationale:

It is now accepted that multiplicity is a product of star formation, however the processes creating these primordial multiple systems are currently not well understood. Previous work such as Duquennoy & Mayor (1991) focused on older, Main Sequence (MS), dynamically evolved stars in the solar neighborhood. However, with such a sample, we cannot be certain if we are observing multiple systems created from dynamical encounters or those that were created at birth; we need to not only study younger populations (∼10 Myr), but study them in a range of environments in order to disentangle the two processes and observe environmental effects.

In the last couple of decades sensitive infra-red detectors have allowed multiplicity studies focused on younger populations of stars (e.g., Ghez et al. 1993, 1997; Leinert et al. 1993; Kraus & Hillenbrand, 2007). These surveys revealed that the binary fraction of T-Tauri stars is similar or 2 times higher than that of MS stars (Duchêne 1999; Duchêne et al. 2007) and multiplicity frequency increases with primary mass (Raghavan et al. 2010; Kouwenhoven et al. 2007). However, these results have been obtained from the population of young clusters. These young clusters are normally located at distances larger than ∼100pc (in some cases much larger) and still embedded in their parental clouds. Both effects put caveats and biases in the determination of the true multiplicity fractions, potentially leading to incompleteness and difficult cluster-cluster comparisons. We need to try and better constrain this observable as a function of mass, age and environment; *is multiplicity universal?*

What is the SACY sample and how can it help? In 2001 our team undertook the titanic task of carrying out spectroscopic observations of 1500 late-type, potentially young stellar optical counterparts of ROSAT X-ray sources. Five years later, the SACY (Search for Associations Containing Young stars) survey (Torres et al. 2006, 2008) has changed our vision of local star formation. Nine young (age∼1-70 Myr), nearby (d∼20-110pc) associations (containing ∼450 stars) have been identified. Due to their proximity, we can probe a continuous range of orbital separations using spectroscopic techniques and AO-imaging to obtain a comprehensive multiplicity fraction for these young stars. Their range of ages provides us with invaluable laboratories to study recent star formation, and in addition to this, their low spatial density makes dynamical encounters extremely improbable; *we can probe primordial multiplicity.*

Multiplicity trend as a function of mass: With data collected along several periods, our group is conducting a systematic multiplicity study of these 9 young associations. We are obtaining very interesting preliminary results regarding the close-companion frequency, derived from existing UVES and FEROS data (shown in the left panel of Fig. 1, and compared to other populations). This fraction is the combination of both multiple-lined spectroscopic (SB2) systems (where two, or more, peaks are seen in the cross-correlation function, 15 systems) and single-lined spectroscopic (SB1) systems (from large radial velocity (RV) variations between different data epochs, 4 systems) for all 9 associations. These results, after accounting for biases, imply that close-companion multiplicity is *not* a function of spectral type i.e. mass, in this range. This differs significantly when compared to higher mass stars where studies have shown much greater fractions as well as a strong dependence on mass, see the left panel of Fig. 1 (Chini et al. 2012) for close-companion multiplicity.

Multiplicity with environment and age: If multiplicity is in fact universal, i.e. onsets at the earliest stages of star formation, we would expect that a loose collection of stars of approximately the same age would have statistically indistinguishable fractions of multiple systems. The right panel of Figure 1, however, shows how different the fractions can be with coeval low spatial-density populations (Columba (COL), Carina (CAR) and Tucana-Horologium (THA) are ∼30 Myr). COL currently shows 0^{+4}% of multiple systems which appears anomalous when compared to all other 8 associations. Such a result implies there are other factors at play between coeval groups of stars causing variability in the multiplicity fraction. However we must be very careful when dealing with low number statistics which leads us to the next point:

The need for further data: Run A of this proposal is mainly concerned with Columba (COL) and AB Doradus (ABD) - see the right panel of Fig. 1, highlighted with crosses. As mentioned above it is crucial for us to obtain more data of COL to better constrain this null multiplicity rate. Observing 11 targets (9 of which currently only have one/zero data epochs (vastly limiting analysis) from the total 44 previously observed members of COL would greatly improve our statistics on this anomalous association. ABD is the oldest of our associations (∼70Myr) and should show us that the close-companion frequency is not significantly affected by age, as the majority of data in the right panel of Fig. 1 shows. We can investigate this using the high number of sources in ABD (∼80 solar spectral type pre-main sequence stars). With new data we can probe 25 new targets for SB1 systems from RV variations and vastly improve our ability to see SB2 systems from 30 targets. Run B is concerned with the remaining targets that are possible to observe with NACO, in order to maximise this unique dataset. So far, data from Eta Chamaeleon (ECH) and β Pictoris (BPC) has been analysed in search of visual companions. The results show a possible 15 and 50 visual companions respectively, ranging from ∼10-300 M_{Jup}. Although the AO part of the work is very preliminary NACO is the perfect instrument to carry it out, therefore this last set of observations is really necessary before its imminent removal from UT4.

Multiplicity across a continuous range of orbital separations: Consider an idealised binary system of two $1M_{\odot}$ stars at 70 pc (the average distance for the SACY sample), eccentricity=0, vrad=10kms^{-1}. AO, NACO with an angular resolution of <0.4″, FOV 27″x 27″, gives a separation range of **28 - 700 A.U**. Spectroscopic, UVES using 3 times the velocity accuracy, for this work, of ∼1kms^{-1} gives a separation range of **4 - 45 A.U.**

7. Description of the proposed programme and attachments

Description of the proposed programme (continued)

P91 comments The OPC commented that no analysis had been conducted on the existing data. Since P91, work is fully underway, the preliminary results are discussed and presented (Fig. 1) in this proposal, and a paper of close-companion frequency is in preparation. Once complete, the data of visual companions (NACO data) will be analysed more fully and combined to produce the overall multiplicity frequency of the SACY sample.

References

Duquennoy & Mayor 1991, A&A 248, 485
Ghez et al. 1993, AJ 106, 2005
Ghez et al. 1997, ApJ 481, 378
Leinert et al. 1993, A&A 278, 129.
Kraus & Hillenbrand, 2007, ApJ, 662, 413
Duchêne 1999, A&A 341, 547
Duchêne et al. 2007, A&A 476, 229
Shatsky & Tokovinin, 2002, A&A, 382, 92
Raghavan et al. 2010, ApJS, 190, 1
Kobulnicky & Fryer 2007, ApJ, 670, 747
Kouwenhoven et al. 2007, A&A, 474, 77
Torres et al. 2006, A&A 460, 695
Torres et al. 2008, Handbook of Star Forming Regions, Volume II, The Southern Sky ASP Monograph Publications, Vol. 5, ed. Bo Reipurth, 757
Chini et al. 2012, MNRAS, 424, 1925

B – Immediate Objective:

Here we propose to carry out AO-assisted observations and multiple spectroscopic visits to make a complete census of the binary population

Run A - UVES: In total we need 3 separate data epochs, therefore we propose to take up to 3 high-resolution spectra of each target, depending on the number of existing obsrvations, in this period. Radial velocities and $V \sin i$ will be determined by applying the cross-correlation technique to these spectra as calculated for the previous data. Objects showing a double-lined cross-correlation function or showing significant radial velocity variations will be selected for a further radial velocity follow up in order to derive orbital parameters.

Run B - NACO: We propose to obtain high-angular resolution observations of the SACY sample **not yet found in the NACO archive**, for 31 targets, observable on even periods from Paranal. The main goal is to take diffraction-limited observations of the targets in order to look for new stellar companion candidates. The targets have been selected based on the following criteria: i) be members of one SACY association, ii) have $d \lesssim 100$ pc; iii) be younger than Pleaides (i.e., 100Myr) based on its Li content; iv) spectral type later than G5 and V>9; v) not observed in a similar survey (e.g., by Zuckermann et al. 2004 or Masciadri et al. 2005. They will be observed in the K-band with NACO. They are all bright enough to be used as reference stars. We will use the S27 objective which provides a FOV of $27'' \times 27''$, sufficient to find companions up to distances up to $\sim 10''$from the central source. We will also use the S13 objective for the brightest targets to avoid saturation. We will integrate a total of 5-10 minutes on-source, to reach ΔK deep enough to look for stellar companions. An astrometric calibrator (Θ^1 Ori C) will be observed to calibrate the plate scale and orientation of CONICA.

Attachments (Figures)

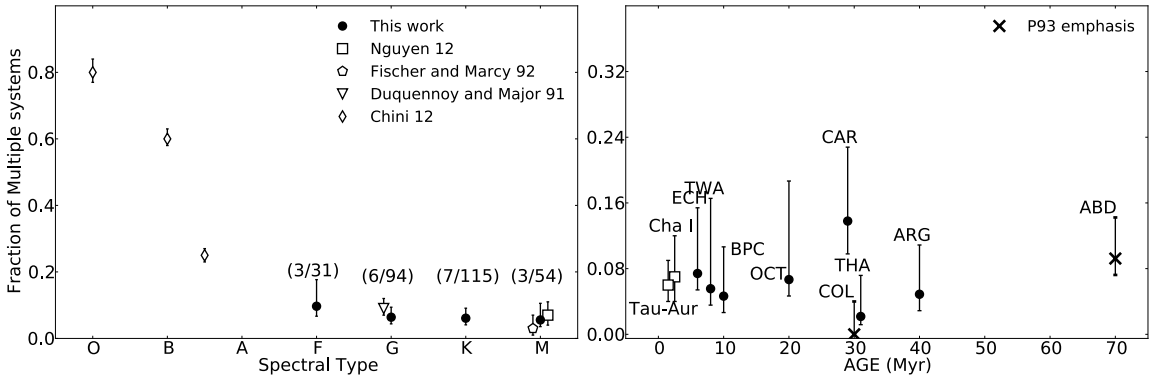

Fig. 1: Left Panel: The multiplicity fraction for the SACY sample (filled circles); High mass stars (O-B), Chini et al. 2012; Nearby solar type stars, Duquennoy & Mayor 1991; Nearby M Dwarfs, Fischer & Marcy 92; Nearby star-forming regions, Nguyen 2012, as a function of spectral type, O-M. The explicit fraction of multiple systems in each mass bin is shown for the SACY data. Right Panel: The multiplicity fraction as a function of age for the SACY associations and nearby star-forming regions, Nguyen 2012, crosses indicate associations with many observation targets in this proposal.

B.2 P95, UVES

Title: Are there true differences in the fraction of spectroscopic binaries within the SACY sample?

Scientific goal: Collect more high resolution spectra to investigate differences in spectroscopic binary fractions

Instrument / **Telescope**: UVES/VLT

Number of hours: 75.7

European Organisation for Astronomical Research in the Southern Hemisphere

OBSERVING PROGRAMMES OFFICE • Karl-Schwarzschild-Straße 2 • D-85748 Garching bei München • e-mail: opo@eso.org • Tel.: +49 89 320 06473

APPLICATION FOR OBSERVING TIME PERIOD: **95A**

Important Notice:

By submitting this proposal, the PI takes full responsibility for the content of the proposal, in particular with regard to the names of CoIs and the agreement to act according to the ESO policy and regulations, should observing time be granted.

1. Title Category: **C–7**

Are there true differences in the fraction of spectroscopic binaries within the SACY sample?

2. Abstract / Total Time Requested

Total Amount of Time:

Characterising the fraction and properties of multiple systems in a stellar population can tell us a great deal about the environment in which they formed. If populations of stars form in a similar way across a wide parameter space we would not expect to find significant differences in their multiplicity properties. The most ideal populations to test this hypthesis are young (∼10 Myr) to probe more directly the outcome of star formation, with little effect of N-body dynamics. We have recently derived the fraction of spectroscopic binaries (SBs) in the SACY associations (Elliott et al. 2014). We found that some associations have 0^{+4}% of SBs where others have 14^{+9}_{-4}%. We propose to investigate whether this discrepancy arises from low-number statistics or reflects a true difference in the binary populations. Additionally we will complete the spectroscopic observations of SACY and increase the number of targets with both UVES and adaptics optics-assisted data by ∼20%.

3.

Run	Period	Instrument	Time	Month	Moon	Seeing	Sky	Mode	Type
A	95	UVES	58.0h	any	n	n	THN	s	
B	95	UVES	17.7h	any	n	n	THN	s	

4.

Number of nights/hours	Telescope(s)	Amount of time
a) already awarded to this project:	UT2/UT4	33h: P88 and P89, 21.2h: P93
b) still required to complete this project:		

5. Special remarks:

Excellent filler for bad weather conditions.
This proposal is part of Ph.D. thesis (*Is multiplicity universal?*, Paul Elliott) which started in November 2012.

6. Principal Investigator: pelliott

6a. Co-investigators:

A.	Bayo	1842
C.	Melo	1261
C.	Torres	1599
N.	Huelamo	1456

Following CoIs moved to the end of the document ...

7. Description of the proposed programme

A – Scientific Rationale:

It is now observationally confirmed that multiplicity is a product of star formation, and, therefore, studying and characterising multiplicity properties can tell us a lot about how the stars formed. However, processes that create these primordial multiple systems and the relationship with the primary mass are currently not well understood. Works such as Raghavan et al. 2010; Tokovinin 2014 focus on older, main sequence (MS), dynamicaly evolved stars in the solar neighbourhood. With such a sample we cannot be certain if we are observing multiple systems created from dynamical encounters or those that were created at birth; we need to not only study younger populations (∼10 Myr), but study them in a range of environments in order to disentangle the two processes and observe environmental effects.

In the last couple of decades sensitive infra-red detctors have allowed multiplicity studies focused on younger populations of stars (e.g., Ghez et al. 1993, 1997; Leinert et al. 1993; Kraus & Hillenbrand, 2007). These surveys revealed that the binary fraction of T-Tauri stars is similar or 2 times higher than that of MS stars (Duchêne 1999; Duchêne et al. 2007) and multiplicity fraction ($F_{\rm m}$) increases with primary mass (Raghavan et al 2010; Kouwenhoven et al. 2007). However, these results have been obtained from the population of young clusters. These young clusters are normally located at distances larger than ∼100 pc (in some cases much larger) and still embedded in their parental clouds. Both effects put caveats (extinction, sensitivity) in the determination of the true $F_{\rm m}$, potentially leading to incompleteness and difficult comparisons between clusters. We need to better constrain $F_{\rm m}$ as a function of mass, age and environment; *is multiplicity universal?*

What is the SACY sample and how can it help? In 2001 our team undertook the titanic task of carrying out spectroscopic observations of 1500 late-type, potentialy young stellar optical counterparts of ROSAT X-ray sources (Torres et al. 2006; 2008). Nine young (age∼1-70 Myr), nearby (d∼20-110 pc) loose associations (containing ∼450 stars) have been identified. These populations have stars all over the southern sky; tens of degrees can contain less than 100 members, however they do not belong to any nearby cloud regions. Due to their proximity, we can probe a continuous range of orbital separations using spectroscopic (Elliott et al. 2014), interferometric and AO-imaging (Elliott et al. in prep.) techniques to obtain a comprehensive multiplicity fraction for these young stars; breaking down the barrier between observational techniques to provide the systems' properties i.e. their masses and orbital separations. Their range of ages provides us with invaluable laboratories to study recent star formation, and in addition to this, their low spatial density makes dynamical encounters extremely improbable. The SACY sample is a truly unique dataset to produce comprehensive statistics of pre-MS stars; *we can probe primordial multiplicity.*

Current results with high-resolution spectra: We have recently refined the membership list of the SACY associations and determined the fraction of spectroscopic binaries (SBs) using previous UVES/FEROS observations, archival data and available data/information in the literature (Elliott et al. 2014), see Fig. 2 for fractions of each association. We found the fraction of SBs is statistically indistinguishable from the fraction found in the field and nearby star-forming regions (SFRs) (Nguyen et al. 2012), as we would expect if these stars formed in similar environments. However, from Fig. 2 it is clear that by no means is the fraction of spectroscopic systems constant for all nine associations, *are the differences just the result of low-number statistics?* There are three associations that have no known spectroscopic binary systems using all available high resolution spectra available the fractions are currently: Argus: 0/33, Tuc-Hor: 0/33 and TW-Hydrae: 0/11.

How do the proposed observations help us? The observations we propose here could produce a highly significant difference between some associations (i.e. β-Pic moving group and Argus) if some of these associations truly have no SBs. On the other hand it could reconcile these three associations with the other six, producing a much more uniform distribution of the fraction of SBs in the SACY associations as we would expect from the similar environment in which the stars formed. The objects presented in Run A currently do not have any high-resolution spectra available and therefore at this time we cannot say anything at all about whether they are SBs. They make up approximately 25% of our overall sample, which is a huge proportion of our targets missing from our spectroscopic census. In addition to those objects, the objects presented in run B have partial data available (1 or 2 previous observations) however for those with only 1 observation our sensitivity to SB1 systems is 0% and from previous work 50% of SBs we identified were of type SB1 (Elliott et al. 2014). We are currently missing a substantial part of data if we wish to derive accurate fractions of SB systems for these populations of pre-MS stars.

Breaking down the observational barrier: We are not only interested in the fraction of SB systems; we want to characterise the multiplicity of the whole sample. Analysis of visual binaries (VBs), using NACO/Lick AO-imaging, is in its final stages. The observations proposed here would add another 40 targets to have both high-res. spectra and AO-assisted imaging which would increase the sample observed using both methods by ∼ 20%. The statistics produced from our AO analysis will be combined with our analysis of SBs in conjunction with interferometric data. This will cover systems from ∼0.1 au - 1000 au and where available, this orbital range will be *continuously covered.* Using our derived average fractions of SBs and VBs and those expected in SFRs (King et al. 2012) we will have ∼40 SBs and ∼150 VBs in our pre-MS population. Such a substantial number of close-by characterised pre-MS multiple systems, with a range of masses is invaluable to the community of star formation and planetary research.

7. Description of the proposed programme and attachments

Description of the proposed programme (continued)

References:

Raghavan et al. 2010, ApJS, 190, 1
Tokovinin 2014, AJ, 147, 86
Ghez et al. 1993, AJ 106, 2005
Ghez et al. 1997, ApJ 481, 378
Leinert et al. 1993, A&A 278, 129
Kraus & Hillenbrand, 2007, ApJ, 662, 413
Duchêne 1999, A&A 341, 547
Duchêne et al. 2007, A&A 476, 229
Kouwenhoven et al. 2007, A&A, 474, 77
Torres et al. 2006, A&A 460, 695
Torres et al. 2008, Handbook of Star Forming Regions, Volume II, 757
Elliott et al. 2014, A&A, 568, A26
Nguyen et al. 2012, ApJ, 745, 119
King et al. 2012, MNRAS, 421, 2025

B – Immediate Objective:

Run A: Here we propose to carry out multiple spectroscopic visits for those SACY targets that currently have no high-resolution spectroscopic data. In total we need 3 separate data epochs to have good sensitivity to spectroscopically bound systems, of both type SB1 and SB2.

Run B: We propose to carry out observations for those targets currently with only 1 or 2 observations in order to increase our sensitivity to longer-period spectroscopic systems (SB1 systems; Fig. 1, middle panel) and potentially missed SB2 systems from previous observations with poor phase coverage.

RVs and $v \sin(i)$ will be determined by applying the cross-correlation technique to these spectra, Fig. 1. Objects showing a double-lined cross-correlation function (Fig. 1, right panel) or showing significant RV variations (Fig. 1, middle panel) will be selected for a further radial velocity follow up in order to derive orbital parameters.

Attachments (Figures)

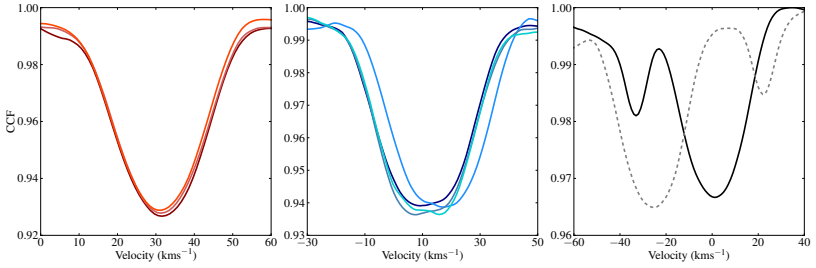

Fig. 1 Examples of the cross-correlation output for three different types of systems, within each panel the different lines represent different data epochs. *Left*: a single system (no significant variation), *middle*: an SB1 system (significant temporal variation), *right*: an SB2 system, two clear peaks indicating two sources of flux with different RV values.

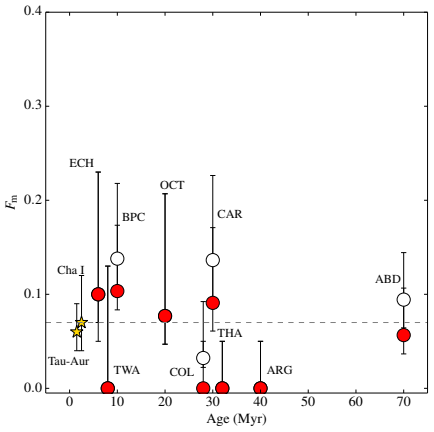

Fig. 2 The SB fraction as a function of age for the SACY sample. Fractions derived using our UVES/FEROS observations are red, those derived additionally using literature values are white, fractions of SFRs are gold.

B.3 P96, NACO

Title: Is multiplicity universal? Confirming visual pre-main sequence binaries in the SACY associations

Scientific goal: Obtain a second epoch of AO imaging data for previously identified candidate multiple systems

Instrument / **Telescope**: NACO/VLT

Number of hours: 11.3

European Organisation for Astronomical Research in the Southern Hemisphere

OBSERVING PROGRAMMES OFFICE • Karl-Schwarzschild-Straße 2 • D-85748 Garching bei München • e-mail: opo@eso.org • Tel.: +49 89 320 06473

APPLICATION FOR OBSERVING TIME PERIOD: **96A**

Important Notice:

By submitting this proposal, the PI takes full responsibility for the content of the proposal, in particular with regard to the names of CoIs and the agreement to act according to the ESO policy and regulations, should observing time be granted.

1. Title Category: **C–7**

Is multiplicity universal? Confirming visual pre-main sequence binaries in the SACY associations

2. Abstract / Total Time Requested

Total Amount of Time:

Characterising the nature of multiple systems in a given population of stars can tell us a great deal about their initial conditions. If populations of stars form in a similar way across a wide parameter space we would not expect to find significant differences in their multiplicity properties. The most ideal populations to study are young ($\lesssim$100 Myr) and have low stellar density; to probe more directly the outcome of star formation, with little effect of N-body dynamics. We have recently derived the properties (multiplicity fractions, mass-ratios, physical separations) of a statistical sample of visual multiple systems in the SACY associations. However, many of the these bound systems are not confirmed, their classification is based on statistical analysis of their observables. This can lead to mis-classification which leads to significantly different derived properties and conclusions about our sample. To produce a robust results we need to confirm identified sources using proper motion analysis.

3.

Run	Period	Instrument	Time	Month	Moon	Seeing	Sky	Mode	Type
A	96	NACO	6.1h	any	n	1.0	THN	s	
B	96	NACO	5.2h	any	n	1.2	THN	s	

4.

Number of nights/hours	Telescope(s)	Amount of time
a) already awarded to this project:	UT2/UT4	33h during P88 and P89
b) still required to complete this project:	UT1	50h

5. Special remarks:

Run B is an excellent filler program as the required seeing is only $\approx$1.2″.
This proposal is part of Ph.D. thesis (*Is multiplicity universal?*, Paul Elliott) which started in November 2012 and has a planned defence date in early 2016.

6. Principal Investigator: pelliott

6a. Co-investigators:

N.	Huelamo	1456
A.	Bayo	1842
C.	Melo	1261
C.	Torres	1599

Following CoIs moved to the end of the document ...

7. Description of the proposed programme

A – Scientific Rationale:

It is now observationally confirmed that multiplicity is a product of star formation, and, therefore, studying and characterising multiplicity properties can tell us a lot about how the stars formed. However, processes that create these primordial multiple systems are currently not well understood. Works such as [1] and [2] focus on older, main sequence (MS), dynamically evolved stars in the solar neighbourhood. With such a sample we are observing multiple systems that have been severely dynamically processed and therefore the population's properties and abundances do not reflect the original outcome of star formation. For studies of primordial multiplicity we need to study young ($\lesssim$100 Myr), low-density populations.

In the last couple of decades sensitive infra-red detctors have allowed multiplicity studies focused on younger populations of stars (e.g. [3],[4],[5],[6],[7]). These surveys revealed that the binary fraction of T-Tauri stars is similar or 2 times higher than that of MS stars ([8]) and multiplicity fraction ($F_{\rm m}$) increases with primary mass ([9],[1]). However, these results have been obtained from the population of young clusters. These young clusters are normally located at distances larger than $\sim$100 pc (in some cases much larger) and still embedded in their parental clouds. Both effects put caveats (extinction, sensitivity) on the determination of the true $F_{\rm m}$, potentially leading to incompleteness and difficult comparisons between clusters. We need to better constrain $F_{\rm m}$ as a function of mass, age and environment; *is multiplicity universal?*

What is the SACY sample and how can it help? In 2001 our team undertook the titanic task of carrying out spectroscopic observations of 1500 late-type, potentialy young stellar optical counterparts of ROSAT X-ray sources ([10], [11]). Nine young (age$\sim$5-100 Myr), nearby (d$\sim$20-110 pc) loose associations (containing $\sim$450 stars) have been identified. These populations have stars all over the southern sky; tens of degrees can contain less than 100 members, however they are not associated with cloud regions. Due to their proximity, we can probe a continuous range of orbital separations using spectroscopic ([12]), interferometric and AO-imaging (Elliott et al. submitted) techniques to obtain comprehensive multiplicity statistics for these young stars; breaking down the barrier between observational techniques to provide the systems' physical properties (mass-ratios and orbital separations). Their range of ages provides us with invaluable laboratories to study recent star formation, and in addition to this, their low spatial density means they have undergone little dynamical processing. The SACY sample is a truly unique dataset to produce comprehensive statistics of PMS stars; *we can probe primordial multiplicity.*

Current project status: We have determined the fraction of spectroscopic binaries (SBs) in the SACY associations ([12]). We found the fraction of SBs is statistically indistinguishable from the fraction found in the field and nearby star-forming regions (SFRs). Such systems have incredibly high binding energy and therefore are essentially free of dynamical processing. This result supports the idea that these populations had statistically similar primordial binary populations (in separation range $\sim$0.01-1 au). We have now extended this analysis to visual systems (Elliott et al. submitted) in the separation range 3-1000 au, however, we need to confirm our identified multiple systems to improve our derived statistics.

Results with AO-assisted data: We have analysed NACO data (from P77, P81, P88 and P89). The data taken in P81 was the second epoch for P77 targets, and therefore we used astrometic analysis to determine whether sources are bound, as shown in Figure 2. However, the targets imaged in P89 were not follow-up observations of P88 targets and therefore we could only base our bound-probability estimate on the properties of confirmed and rejected bound systems from previous runs. From the analysis of our data so far, we have identified many similarities between SACY and the SFR Taurus, indicative of similar primordial binary distributions. The multiplicity fractions are 25% and 26% for SACY and Taurus, respectively, for systems in the separation range 10-1000 au. This is a factor $\approx$1.5 higher than the field, due to the low-density nature of these environments. We also find a flat mass-ratio distribution in line with results from Taurus ([6, [7]).

Current limitations of statistics: The set of identified multiple systems is dominated by single-epoch data and therefore potentially we are mis-classifying companions as bound / not-bound. To highlight this, in Figure 3 we show the separation distributions for SACY, and 3 other populations, considering companions with probabilities (p) $\geq$0.95 and $\geq$0.50. If we only consider systems with p$\geq$0.95 our distribution is very narrow, double peaked and differs at $\sim 2\,\sigma$ level to the other populations. However, considering systems with p$\geq$ 0.50 the distribution is single peaked and agrees with the 3 other distributions. These two distributions lead to completely different conclusions about the physical nature of multiple systems in SACY. **The only way we can confirm our single-epoch detections is with a further epoch, to analyse the relative astrometry of the companions.**

B – Immediate Objective: We propose to obtain a second epoch of high-angular resolution data for visual binary candidates in the SACY sample. The selected targets have multiple point sources around the primary target, potential bound systems, identified from previous NACO observations in P88 and P89. Our targets are nearby and have high proper motions and given the difference in time (now 3 yr) the relative astrometric motion of the sources will be large ($\sim$10 times larger than measurement uncertainties), the example in Figure 2 shows the successful application of this method for data separated by <2 yr. The targets will be observed in the K_s band with NACO. They are all bright enough to be used as reference stars. We will use the S13 objective which

7. Description of the proposed programme and attachments

Description of the proposed programme (continued)

provides a FOV of 13 $''$ × 13$''$, sufficient to find image all previous identified sources. We will integrate for 5-10 minutes on-source, to reach ΔK_s deep enough to identify sub-stellar companions, see Figure 1.
We split our targets into two runs according to the angular separation (ρ) of the sources in the FOV (A: ρ <0.5$''$, B: $\rho \geq$0.5$''$). This way we can loosen the constraints on the seeing (from 1.0 to 1.2$''$) for targets in run B.
An astrometric calibrator (Θ^1 Ori C) will be observed to calibrate the plate scale and orientation.

References: [1] Raghavan et al. 2010, ApJS, 190, 1 [2] Tokovinin 2014, AJ, 147, 86 [3] Ghez et al. 1993, AJ 106, 2005 [4] Ghez et al. 1997, ApJ 481, 378 [5] Leinert et al. 1993, A&A 278, 129 [6] Kraus et al. 2011, ApJ 731, 8 [7] Daemgen et al. 2015, ApJ 799, 155 [8] Duchêne et al. 2007, A&A 476, 229 [9] Kouwenhoven et al. 2007, A&A, 474, 77 [10] Torres et al. 2006, A&A 460, 695 [11] Torres et al. 2008, Handbook of Star Forming Regions, Volume II, 757 [12] Elliott et al. 2014, A&A, 568, A26 [13] Baraffe et al. 1998, A&A, 337, 403

Attachments (Figures)

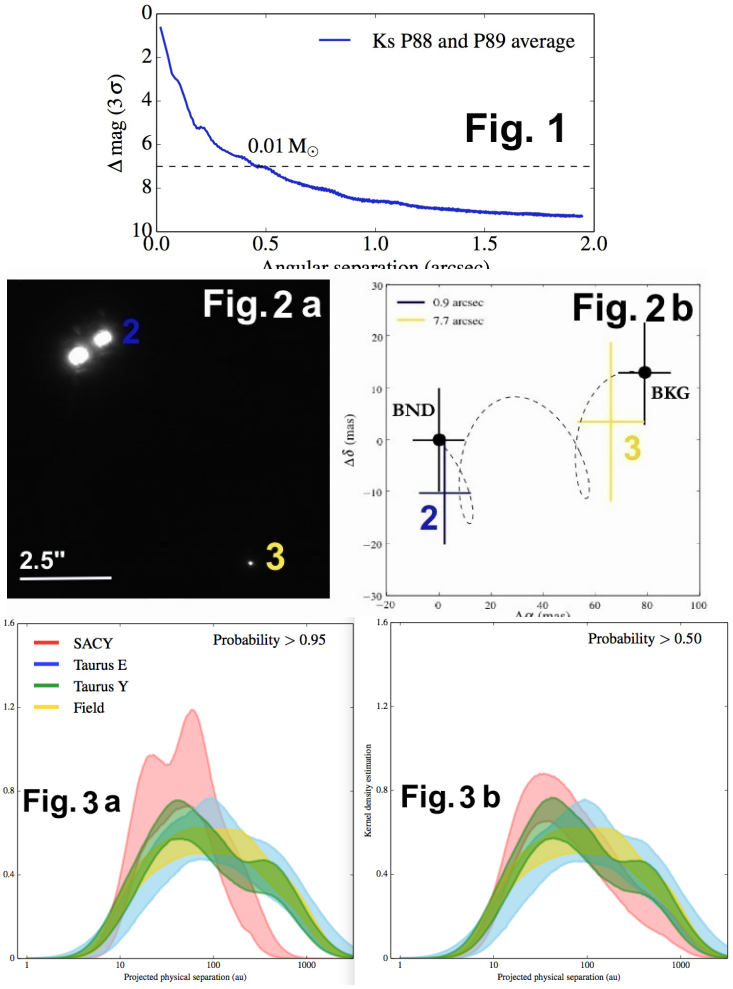

Figure 1: The average sensitivity in the K_s band for observations of target from P88 and P89. The dotted line represents the mass of a potential companion using an average SACY target (distance: 70 pc, abs. K_s: 3.5 mag, age: 30 Myr.) as the central source and the evolutionary tracks of [13].
Figure 2a: One epoch of NACO data for a target that has two additional point sources in its FOV, labelled 2 and 3.
Figure 2b: The black markers and dotted line represent the relative movement from the central source one would expect from a background source from observation 1-2. Source 2 shows no relative movement, meaning it is a bound (BND) companion whereas source 3 shows movement compatible with that of a background (BKG) source.
Figure 3a: Separation distribution for 4 populations; SACY, Taurus E (extended population of Taurus, age ∼20 Myr, [7]), Taurus Y (young population, age ∼2 Myr, [6]) and the Field ([1]), considering companions with probabilities ≥ 0.95 for SACY.
Figure 3b: The same as Figure 3a, however, considering companions with probabilities ≥0.50.

B.4 P97, NACO

Title: Peculiar multiplicity or incomplete census? Looking for companions around newly identified members in the Octans association

Scientific goal: Investigate the apparent over-abundance of visual multiple systems in the Octans young moving group

Instrument / **Telescope**: NACO/VLT

Number of hours: 12.4

European Organisation for Astronomical Research in the Southern Hemisphere

OBSERVING PROGRAMMES OFFICE • Karl-Schwarzschild-Straße 2 • D-85748 Garching bei München • e-mail: opo@eso.org • Tel.: +49 89 320 06473

APPLICATION FOR OBSERVING TIME PERIOD: **97A**

Important Notice:

By submitting this proposal, the PI takes full responsibility for the content of the proposal, in particular with regard to the names of CoIs and the agreement to act according to the ESO policy and regulations, should observing time be granted.

1. Title Category: **C–7**

Peculiar multiplicity or incomplete census? Looking for companions around newly identified members in the Octans association

2. Abstract / Total Time Requested

Total Amount of Time:

Stellar multiplicity is intimately linked to the processes of star formation and different environments could alter the resulting multiplicity properties. With this proposal we want to confirm whether we are witnessing this effect or if our previous multiplicity results in the Octans were dominated by low number statistics. So far we have conducted an analysis of tight (<1 au) and wider visual systems (10-1000 au) in 9 loose associations (collections of pre-main sequence stars) in our solar neighbourhood. One of the most interesting yet under-studied of these associations is Octans. We recently discovered it has an unusually high number of visual binaries, however this is based on low numbers. Here we propose observations that would increase the number of objects with AO data by >300% (from 11 to 49). These observations would allow us to determine whether Octans really has an unusual multiple system population and additionally provide resolved photometry for age/distance determination.

3. Run	Period	Instrument	Time	Month	Moon	Seeing	Sky	Mode	Type
A	97	NACO	12.4h	any	n	1.2	THN	s	

4. Number of nights/hours Telescope(s) Amount of time

a) already awarded to this project:

b) still required to complete this project:

5. Special remarks:

Excellent filler program as the required seeing is only ≈1.2″.

6. Principal Investigator: pelliott

6a. Co-investigators:

S.	Murphy	1139
A.	Bayo	1842
C.	Melo	1261
C.	Torres	1599

7. Description of the proposed programme

A – Scientific Rationale: Multiple systems are a natural outcome of star formation processes since we find significant numbers in young (1-2 Myr) star-forming regions (SFRs) such as Taurus, 42±8% ([1]) as well as in the older field population, ≈50% ([2,3]). Therefore, one can assume that key ingredients of those processes are hard-coded in the final multiple products, and differences in, for example, multiplicity rates of populations, could point towards different natal conditions. These differences dilute with time (due to dynamical processing), so one should look at the youngest possible populations.

One problem of studying PMS multiple systems in their typical cradle environments (nearby embedded clusters) is the lack of overlapping parameter space from sample to sample due to differing distances and extinction properties of the clusters that are generally studied. An alternative population of stars that can be used is the **SACY** sample (Search for Associations Containing Young stars), originally presented in [4] and [5], and with recent revised and updated solutions (Torres et al. 2015, in prep). This sample is made up of nine distinct associations of stars. In total, ≈450 stars, <200 pc in distance, between the ages of 10-100 Myr and free of extinction. These loose associations most likely formed in low-density environments and therefore make a good comparison to denser SFRs. The members are extremely nearby and allow a very large orbital parameter space to be probed when combining different observational techniques (spectroscopy, interferometry, AO- and direct imaging) with little effect from N-body dynamics due to their youth.

Project status: One of the most interesting yet under-studied of the nine associations is the Octans association (distance range: 80-180 pc, age: ≈40 Myr). In [6], [7] we recently derived the fraction of spectroscopic binaries (SBs) and the fraction and physical parameters of visual binaries (VBs) in the SACY sample, respectively. The Octans association has a compatible SB fraction with the other associations and that of the field and the SFR Taurus, as we would expect from a universal model of star formation. However, in [7] we found that Octans has a high VB fraction in the range 3-1000 au (55%). In Figure 1 we show the individual multiplicity fractions (MFs) for each association. Additionally we show the $1\,\sigma$ MF space (blue shaded area) considering all associations together except Octans. There is a $2.6\,\sigma$ discrepancy between the MF of Octans and that of the other populations grouped together. It is this discrepancy that we want to investigate further.

Why we need these observations: We are investigating whether or not stellar populations always have statistically similar initial multiple system distributions. This question is directly linked to the hypothesis of star formation being a universal process. These nearby associations (<200 pc) offer us the opportunity to fully characterise (across many orders of magnitude; 10^{-2}–10^{5} au) the multiple system population. Therefore, we need to investigate any significant discrepancies between populations to make sure they are not just effects of low number statistics but real products of their star formation history. At the moment, the number of members the statistics for Octans were derived on is small (11) and therefore *we need larger numbers to confirm whether this is a truly physical over-abundance or not.*

New data for Octans: [8] recently doubled the number of known members in this association from ≈30 to 60 stars using spectroscopy to derive spectral types, kinematics, youth signatures (Lithium equivalent width, H_α) and identify spectroscopic binaries (SBs). A colour-magnitude diagram (CMD) of Octans members is shown in Figure 2. Several of the K- and M-type members from [8] are suspected binaries, based on their elevated position near the equal mass binary locus, or broad (but still unresolved in $R \approx 7000$ spectra) cross-correlation functions. In this proposal we aim to observe the remaining original members currently without AO imaging and the newly discovered members (red markers in Figure 2) with NACO. This would significantly increase the observed number of systems from 11 to 49. These observations will:

a) Vastly improve our multiplicity statistics for this association and allow us to see if the over-abundance of VBs is real or not (reduction of statistical uncertainties from 14% to 5%).

b) Provide resolved photometry for newly discovered tight multiple systems.

How will these observations specifically help us: [8] derived the kinematic distances for newly identified Octans sources using the convergence method ([4]) and then combined these distances with photometry to produce an HR diagram for the new and previously identified members (Figure 2). The ages of PMS populations are very hard to constrain and the HR diagram is a very powerful tool in this analysis, especially by comparing to isochrones from theoretical models ([9]). Since the resolution of 2MASS is ≈2″, we are currently blind to companions in multiple systems within 260 au of the primary (2″× 130 pc = 260 au). Given the peak of physical separations in the SACY associations is ≈50 au ([7]) and that we have discovered 6/11 stars in Octans are multiple systems already (all 6 of those detections were within 2″of the primary) *it is very likely that the photometry for many sources in Figure 2 is in fact blended with a close companion.* If these components are near equal-mass the actual magnitude of the primary can be up to ≈0.75 mag fainter (e.g. for Octans target 2MASS J06033540–4911256 in [7] we calculated a resolved K magnitude of 9.81 mag compared to 9.08 mag from 2MASS). With improved knowledge of the binary population and resolved photometry for many new VB systems we can better populate the HR diagram of Octans. With this we will obtain a more robust age estimate that we can compare with other dating techniques such as the lithium depletion boundary.

References: [1] King et al. 2012, MNRAS, 427, 2636 [2] Raghavan et al. 2010, ApJS, 190, 1 [3] Tokovinin 2014, AJ,

7. Description of the proposed programme and attachments

Description of the proposed programme (continued)

147, 86 [4] Torres et al. 2008, Handbook of Star Forming Regions, Volume II, 757 [5] Torres et al. 2006, A&A, 460, 695 [6] Elliott et al. 2014, A&A, 568, A26 [7] Elliott et al. 2015, A&A, 580, A88 [8] Murphy & Lawson 2015, MNRAS, 447, 1267 [9] Baraffe et al. 2015, A&A, 577, A42

B – Immediate Objective: We propose to obtain AO direct imaging NACO data for previously unobserved members of Octans (members from [4], [5], Torres et al. 2015 in prep. and [8]).
The targets will be observed in the K_s band with NACO. All the targets are bright enough (V $<$ 16 mag. or K$<$13 mag.) to be used as AO reference stars. For the reddest objects we will use the IR WFS with the N90C10 dichroic, otherwise we will use the visible wave-front sensor (VIS WFS). We will use the S13 objective which provides a field of view of 13 $''$ $\times$ 13$''$ and integrate for 5-10 minutes on-source, to reach ΔK_s deep enough to identify stellar/sub-stellar companions ($\Delta K_s \approx$6 mag. at 0.3$''$).
An astrometric calibrator (Θ^1 Ori C) will be observed to calibrate the plate scale and orientation.

Attachments (Figures)

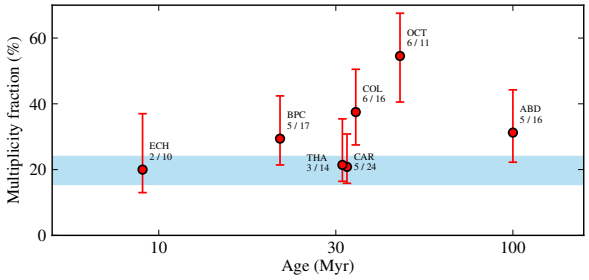

Figure 1: Age versus multiplicity frequency, for the separation and primary mass range 3-1000 au and 0.2-1.2 $M_\odot$, respectively. The blue shaded area represents the 1 σ uncertainty of the multiplicity fraction considering all associations as one population excluding Octans.

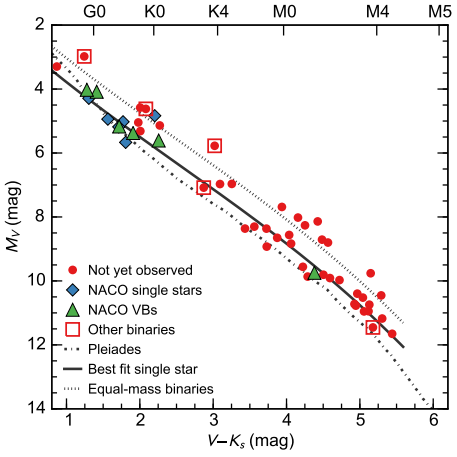

Figure 2: CMD of Octans members. The solid line is a cubic fit from [8], ostensibly tracing single stars or high mass ratio binaries. The dotted line (0.75 mag. brighter) shows the presumed position of equal-mass binary systems. NACO data of single and identified multiple systems from [7] is shown as diamonds and triangles.

B.5 P97, UVES

Title: Investigating the widest binaries in young moving groups: Is there an over-abundance?

Scientific goal: Spectroscopic confirmation of wide companion candidates identified from our photometric + proper motion search

Instrument / **Telescope**: UVES/VLT

Number of hours: 8.7

European Organisation for Astronomical Research in the Southern Hemisphere

OBSERVING PROGRAMMES OFFICE • Karl-Schwarzschild-Straße 2 • D-85748 Garching bei München • e-mail: opo@eso.org • Tel.: +49 89 320 06473

APPLICATION FOR OBSERVING TIME PERIOD: **97A**

Important Notice:

By submitting this proposal, the PI takes full responsibility for the content of the proposal, in particular with regard to the names of CoIs and the agreement to act according to the ESO policy and regulations, should observing time be granted.

1. Title Category: **C–7**

Investigating the widest binaries in young moving groups: Is there an over-abundance?

2. Abstract / Total Time Requested

Total Amount of Time:

Stellar multiplicity is a key aspect to understand star formation in general. Several aspects are still open regarding multiplicity, one of them is what is the widest separation that two objects formed from a unique core can hold in the first Myr's of evolution? So far we have conducted analysis on tight systems (<1 au) and wider visual systems (3-1000 au) in a loose associations (nearby collections of PMS stars believed to have formed together) in our solar neighbourhood. We have recently developed a simple methodology to query public surveys for photometry (2MASS) and proper motions (UCAC4, PPMXL and NOMAD) to identify wide binaries. From this query we have identified 27 wide (500-10,000 au) candidate companions around bona-fide members of loose associations. To confirm the youth and membership of these wide binary companions we require 2 epochs of high resolution spectroscopy.

3.

Run	Period	Instrument	Time	Month	Moon	Seeing	Sky	Mode	Type
A	97	UVES	8.7h	any	n	1.4	THN	s	

4. Number of nights/hours Telescope(s) Amount of time

a) already awarded to this project:

b) still required to complete this project:

5. Special remarks:

This proposal is part of Ph.D. thesis (Is multiplicity universal?, Paul Elliott) which started in November 2012 and has a planned defence date in 2016.

6. Principal Investigator: pelliott

6a. Co-investigators:

A.	Bayo	1842
C.	Melo	1261
C.	Torres	1599

7. Description of the proposed programme

A – Scientific Rationale: Multiple stellar systems can be found in many different populations in our galaxy. For example, 46±2% solar-like field stars ([1], [2]) have at least one companion. We also find significant numbers in younger star-forming regions (SFRs) such as Taurus, 42±8% ([3]) indicating that a large number of multiple systems are the outcome of star formation. Therefore the study of young, pre-main sequence (PMS), multiple systems can provide us with clues about star formation processes.

One problem of studying PMS multiple systems in their typical cradle environments (nearby embedded clusters) is the lack of overlapping parameter space from sample to sample due to differing distances and extinction properties of the clusters that are generally studied. An alternative population of stars that can be used is the **SACY** sample (Search for Associations Containing Young stars), presented in [4] (to be updated in Torres et al. 2015, in prep). This sample is a collection of ≈450 stars <150 pc in distance, between the ages of 10-100 Myr, free of extinction. These loose associations most likely formed in low-density environments and therefore make a good comparison to denser SFRs. The members are extremely nearby and allow a very large orbital parameter space to be probed when combining different observational techniques (spectroscopy, interferometry, AO- and direct imaging) with little effect from N-body dynamics due to their youth.

Project status: So far we have identified spectroscopic binaries (SBs) ([5]) and close (3-1000 au) visual binaries (VBs) ([6]) in the SACY sample. We have produced robust statistics and derived many properties of the sample (SB fraction, VB fraction, VB fraction with primary mass, physical separation and mass-ratio distribution). We have compared our results to other PMS populations such as Taurus and the older, more processed population, the field. We found many similarities between the SACY sample and Taurus, however we are currently limited to small portions of parameter space due to observational techniques. We are now in the process of collating all the available detections / detection limits (from spectroscopy, interferometry, AO-imaging) in the literature and performing our own direct imaging analysis (using 2MASS and the proper motion catalogues UCAC4, PPMXL and NOMAD) to continuously probe 10 orders of magnitude (1-10^{10} day) in orbital period space for as many stars as possible. With these results we will give complete answers to the questions on how many and at which separations multiple systems occur in the SACY sample, a proxy for the larger/more general question of what multiple systems look like in all environments.

Identifying new wide binary candidates: Our direct imaging and kinematic analysis lead us to identify new candidate members in these loose associations. In this analysis we query a field of view (FoV) around every source in our sample equivalent to 10,000 au in physical separation, (the angular query depends on the target's distance). We then created two HR diagrams H-K, K and J-K, K (see Figure 1) to test if the photometry is compatible with the theoretical isochrone ([7]) and the target's age based on its membership to an association ([4], [8]). The uncertainties on the photometry were derived statistically from our overall sample of primary stars (Elliott et al. in prep.). If a target has compatible photometry we then query UCAC4, PPMXL and NOMAD for proper motion values to test if they are also compatible with the primary source within 3σ limits. Figure 1 shows an example for a target in our sample, the green marker shows the companion that has compatible photometry and proper motion and the black markers incompatible sources in the FoV. This query produced 33 compatible sources from an original 9,000 sources in the FoV. Of these 33 sources 6 already had high resolution spectroscopy and all 6 have compatible radial velocities and youth signatures. We are therefore confident that our simple method has a low false-positive rate. In this proposal we plan to observe the visible targets currently without high resolution spectroscopy.

What would these observations tell us? The purpose of this proposal is twofold. Firstly, to characterise potential companions in the wide binary parameter space (500-10,000 au). In the field the separation distribution is approximately Gaussian and peaks at separations <100 au. However, there are theories that postulate that in young loose associations one would expect to see a relative over-abundance of systems in this region due to their youth and initial low-density ([9]), see Figure 2. If this over-abundance were to be observed it would have huge consequences regarding star formation and dynamical evolution. We therefore need as much information as possible for such systems and to eliminate false positives.
Secondly, we can potentially confirm new PMS members in these loose associations, improving their census.

What specific information do we get from these observations? Currently without high resolution spectroscopy we cannot characterise the youth nor the full kinematics of these objects. We therefore propose 2 UVES observations for each target that will provide us with this information, specifically: radial velocities which holds vital kinematic information as mentioned previously (we need two separated by ∼ months in order to identify potential movement from a companion, i.e. a single-lined spectroscopic system), lithium equivalent widths (6708 Å) which is related to youth and both permitted and forbidden emission lines. These emission lines trace activity, accretion and mass-loss processes. Specifically, permitted emission lines of He I (6678 Å) and Hα (6563 Å) are characteristics of classical T Tauri stars and trace accretion processes, although they are also known to be signposts of chromospheric activity ([10, 11, 12, 13]). They can be used with empirical calibrations to assess youth in the critical M-type range ([14]). Forbidden emission lines of [OI] (5577, 6300, 6364 Å), [SII] (6717, 6731 Å) and [NII] (6548, 6581 Å) have been attributed in the literature to low density regions such

7. Description of the proposed programme and attachments

Description of the proposed programme (continued)

as winds, and are therefore a tracer of the mass-loss process ([15, 16, 17]).
References: [1] Raghavan et al. 2010, ApJS, 190, 1 [2] Tokovinin 2014, AJ, 147, 86 [3] King et al. 2012, MNRAS, 427, 2636 [4] Torres et al. 2008, Handbook of Star Forming Regions, Volume II, 757 [5] Elliott et al. 2014, A&A, 568, A26 [6] Elliott et al. 2015, A&A, 580, A88 [7] Baraffe et al. 2015, A&A, 577, A42 [8] Torres et al. 2006, A&A, 460, 695 [9] Reipurth & Mikkola 2012, Nature, 492, 221 [10] Natta, A. et al. 2002, A&A, 393, 597 [11] Testi, L. et al. 2002, ApJ, 571, L155 [12] Barrado y Navascués, D. & Martín, E. L. 2003, AJ, 126, 2997 [13] White, R. J. & Basri, G. 2003, ApJ, 582, 1109 [14] Schmidt et al. 2015, AJ, 149, 158 [15] Shu, F. H. et al. & Lizano, S. 1994, ApJ, 429, 797 [16] Hartmann, L.et al. 1994, ApJ, 426, 669 [17] Hartmann, L. 1999, Physics Today, 52, 60

B – Immediate Objective: We propose to obtain 2 epochs of high resolution spectra for newly identified candidate members in loose associations using the red arm of UVES with cross disperser CD#3 (5000-7050 Å, covering the lithium and emission line regions). We will derive spectral types, radial velocities, lithium and emission-line equivalent widths and confirm whether or not these sources are compatible with the membership properties of their primary stars and parent populations.

Attachments (Figures)

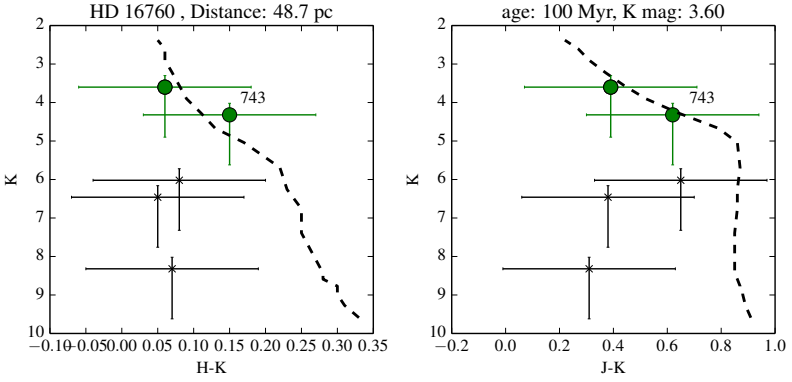

Figure 1: *Left panel*: H-K vs. K magnitude for sources in the FoV of HD 16760. The circular markers represent sources with both compatible proper motion and colours. Their projected physical separation is shown in au (743), the crosses are likely unrelated sources (not fulfilling one or more of the two criteria). The dotted black line is the isochrone from [7] for the estimated age of the primary, given its association membership. *Right panel*: Same as left, but for J-K, K magnitude.

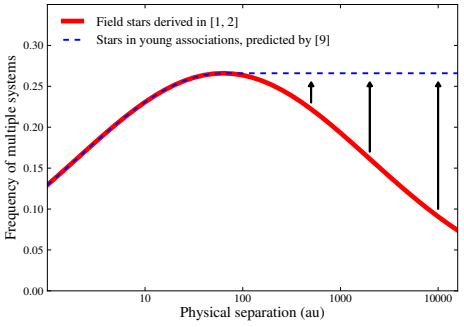

Figure 2. The distribution of multiple systems in the field and predicted by [9] in young moving groups. The arrows indicate the space that the current observations would probe and their diagnostic capabilities.

B.6 P97, PIONIER & NACO

Title: Complete multiplicity survey of pre-main sequence stars: connecting the dots with VLTI/PIONIER and NACO/SAM

Scientific goal: To search for companions in a parameter space only accessible using interferometric techniques around bona-fide members of the young moving groups

Instrument / **Telescope**: PIONIER/VLT, NACO/VLT

Number of hours: 28, $\approx$38

European Organisation for Astronomical Research in the Southern Hemisphere

OBSERVING PROGRAMMES OFFICE • Karl-Schwarzschild-Straße 2 • D-85748 Garching bei München • e-mail: opo@eso.org • Tel.: +49 89 320 06473

APPLICATION FOR OBSERVING TIME PERIOD: **97A**

Important Notice:

By submitting this proposal, the PI takes full responsibility for the content of the proposal, in particular with regard to the names of CoIs and the agreement to act according to the ESO policy and regulations, should observing time be granted.

1. Title Category: **C–7**

Complete multiplicity survey of pre-main sequence stars: connecting the dots with VLTI/PIONIER and NACO/SAM.

2. Abstract / Total Time Requested

Total Amount of Time:

Characterising the multiplicity properties of stellar populations provides us with many clues related to star formation. However, complete studies across large parameter spaces are hard to obtain. Fortunately we have a collection (≈500 stars) of pre-main sequence stars on our doorstep. This population is ideal as they originated in low-density regions and have undergone little dynamical processing in their lifetime. Their proximity allow us to probe a continuous range of physical separations once spectroscopy, interferometry and adaptive-optics imaging are combined, which is not possible for more distant populations. We propose VLTI/PIONIER and NACO/SAM observations to "bridge the gap" between spectroscopy and AO-imaging. This will yield detections of new companions, robust confirmation of single stars and potentially resolve spectroscopic binaries. All detections and non-detections will be used to produce statistics of this population in relation to star formation.

3.

Run	Period	Instrument	Time	Month	Moon	Seeing	Sky	Mode	Type
A	97	PIONIER	28h	any	n	1.2	THN	s	
B	97	NACO	4n	sep	n	0.8	THN	v	

4. Number of nights/hours Telescope(s) Amount of time

a) already awarded to this project:

b) still required to complete this project:

5. Special remarks:

This proposal is part of Ph.D. thesis (Is multiplicity universal?, Paul Elliott) which started in November 2012 and has a planned defence date in 2016.

The proposed observations would link the two previously published results of Elliott et al. 2014 (spectroscopy) and Elliott et al. 2015 (AO-imaging), bringing the whole thesis together.

6. Principal Investigator: pelliott

6a. Co-investigators:

S.	Ertel	1261
X.	Haubois	1261
A.	Bayo	1842
C.	Melo	1261

Following CoIs moved to the end of the document ...

7. Description of the proposed programme

A – Scientific Rationale: It is now observationally confirmed that multiplicity is a product of star formation. Therefore, studying and characterising multiplicity properties can tell us a lot about how the stars formed. However, processes that create these primordial multiple systems are currently not well understood. Works such as [1] and [2] focus on older, main sequence (MS), dynamically processed stars in the solar neighbourhood. With such a sample one can only constrain the architecture of multiple systems that have originated from a range of environments and have been severely dynamically processed. These populations provide robust statistics however the population's properties and abundances do not reflect the original outcome of star formation. For studies of primordial multiplicity we need to study young ($\lesssim$100 Myr), low-density populations.

In the last couple of decades sensitive infra-red detectors have allowed multiplicity studies focused on younger populations of stars (e.g. [3],[4],[5],[6],[7]). These surveys revealed that the binary fraction of T-Tauri stars is similar or 2 times higher than that of MS stars ([8]) and multiplicity fraction ($F_{\rm m}$) increases with primary mass ([9],[1]). However, these results have been obtained from the population of young clusters which have many problems. These young clusters are located at distances larger than $\sim$100 pc (in some cases much larger) and still embedded in their parental clouds. Both effects put caveats (extinction, sensitivity, angular resolution) on the determination of the true multiplicity properties, leading to a reliance on incompleteness factors. We need to better constrain multiplicity properties as a function of mass, age and environment; *is multiplicity universal?*

What is the SACY sample and how can it help? In 2001 our team undertook the titanic task of carrying out spectroscopic observations of 1500 late-type, potentially young stellar optical counterparts of ROSAT X-ray sources ([10], [11]). Nine young (age$\sim$5-100 Myr), nearby (d$\sim$10-200 pc) loose associations (containing $\sim$450 stars) have been identified from the original 1500, this is the SACY (Search for Associations Containing Young stars) sample. The stars in these populations are distributed all over the southern sky; tens of degrees can contain less than 100 members, and they are not associated with cloud regions. Due to their proximity, we can probe a continuous range of physical projected separations using spectroscopic (<1 au, [12]), long baseline interferometry (0.001-0.1 au), sparse aperture masking (SAM) (0.05-5 au), AO imaging (3-1000 au, [13]), and direct imaging (>200 au) and produce comprehensive multiplicity statistics for these young stars. This combination of techniques breaks down the observational barrier, i.e., instead of purely labelling systems as spectroscopic binaries (SBs) or visual binaries (VBs) we can provide the systems' physical properties (Single observation: model-based masses, mass ratios, physical separations. Multi-epoch observations: inclinations, dynamical masses and orbits). Their range of ages provides us with invaluable laboratories to study recent star formation, and in addition to this, their low spatial density ($\ll$1 star / pc^3) means they have undergone little dynamical processing. The SACY sample is a truly unique dataset to produce comprehensive statistics of PMS stars; *we can probe primordial multiplicity.* Once primordial multiplicity is well understood, it can be used as initial conditions for n-body simulations that will try to reproduce the environments of denser star-forming regions (SFRs) where in fact most stars form.

Current project status: So far we have determined the properties of SBs and VBs in the SACY associations ([12], [13]). We have found many similarities (mass-ratio and physical separation distribution, binary frequency, triple frequency) between these associations and more typical low-density SFRs such as Taurus. This result supports the idea that these populations had statistically similar primordial multiple system populations. We are currently extending this analysis to include information on the entire sample of stars including all available detections / non-detections in the literature. However, for the vast majority of stars the problem still remains that without interferometric observations there are still unreachable angular separations. The left panel of Figure 1 highlights how dramatically the interferometric observations can change our detection probability (blue is 0% probability of detection, red 100%), adopting the limits of [14] - a multiplicity study of massive O and B type stars. Without these observations we cannot release the full potential of this youthful sample of stars.

Previous studies using interferometry: The science case of [14] is very different to that presented here, however, they demonstrated how powerful using both PIONIER and SAM is for detecting companions, see right panel of Figure 1 for individual detections and derived limits. Utilising both of these techniques we can "bridge the gap" between spectroscopy and direct AO-imaging. We have already analysed NACO data for 113 objects in our sample and are currently compiling all available detections and detection limits in the literature (sample size: 300-400 objects).

Detections and non-detections: Assuming a field-like distribution ([1,2]) of multiple systems we would expect a detection rate of $\approx$30% for the observations proposed here. However, both the detections and non-detections are equally useful for our science case. Non-detections when combined with radial velocity and AO-imaging provide us with very good constraints on the target's multiplicity (see Figure 1 for detection probability for one target) and therefore we can identify truly single stars (when we combine information from other observational techniques). Covering this parameter space continuously also provides extremely precious detection limits which, when producing statistics using maximum likelihood estimation (MLE) technique for different models, are vital (see appendix of [2]).

Choosing a representative sample for observations: The sample of targets presented here has primary masses in the range 0.8-1.2 $M_\odot$, estimated using the evolutionary tracks of [15]. We have chosen the targets

7. Description of the proposed programme and attachments

Description of the proposed programme (continued)

blindly with respect to their multiplicity i.e. they could be part of wider multiple systems, spectroscopic binaries or thought to be single stars. This is to avoid any inherent bias in our statistics. Our sample size is 28 targets; a compromise between large numbers to derive meaningful statistics and time constraints. We chose this primary mass range as it is representative of our overall sample (250 targets have primary masses in this range). Narrowing the range of primary masses is crucial because the fraction of stars with at least one companion (the multiplicity fraction) is a strong function of primary mass, ranging from 20% to 100% for M stars and O stars, respectively (see Figure 1 of [16]). Therefore, one can only derive meaningful statistics with a constraint on the primary mass. Assuming a 30% detection rate we would derive multiplicity fractions in this parameter space to approximately 8% accuracy, and any deviation from this is a result in itself, tracing the dynamical evolution of multiple systems in the field population. We can apply the derived fractions to the majority of our sample.

B – Immediate Objective:
We propose to obtain interferometric data for a sub-sample (28 targets) of the SACY dataset with PIONIER and NACO/SAM. The targets have been selected based on their RA and DEC, magnitude (all brighter than 7 mag. in H) and primary mass estimation (0.8-1.2 $M_{\odot}$), for reasons explained in the previous section.
These observations should yield a detection rate of ≈30% (assuming a field-like distribution [1,2]) in a parameter space that is unreachable with spectroscopy or AO-imaging techniques. We will be able to calculate multiplicity fractions in this currently unexplored parameter space to an accuracy of 8% and also derive robust detection limits which can be applied to our overall sample (continuously covering 7 orders of magnitude of physical separation).

The proposed observations when combined with existing data using other observational techniques would provide the best multiplicity constraints on a PMS population of solar-mass stars to date. Only the study of young associations offers the opportunity to derive complete multiplicity statistics for a PMS population across such a wide parameter space. The derived statistics would provide insights into the formation of these nearby, young, low-density associations.

References: [1] Raghavan et al. 2010, ApJS, 190, 1 [2] Tokovinin 2014, AJ, 147, 86 [3] Ghez et al. 1993, AJ 106, 2005 [4] Ghez et al. 1997, ApJ 481, 378 [5] Leinert et al. 1993, A&A 278, 129 [6] Kraus et al. 2011, ApJ 731, 8 [7] Daemgen et al. 2015, ApJ 799, 155 [8] Duchêne et al. 2007, A&A 476, 229 [9] Kouwenhoven et al. 2007, A&A, 474, 77 [10] Torres et al. 2006, A&A 460, 695 [11] Torres et al. 2008, Handbook of Star Forming Regions, Volume II, 757 [12] Elliott et al. 2014, A&A, 568, A26 [13] Elliott et al. 2015, A&A, 580, A88 [14] Sana et al. 2014, ApJ, 215, 15 [15] Baraffe et al. 2015, A&A, 577, A42 [16] Duchêne & Kraus 2013, ARAA, 51, 269 [17] Lacour et al. 2011, A&A, 532, A72

Attachments (Figures)

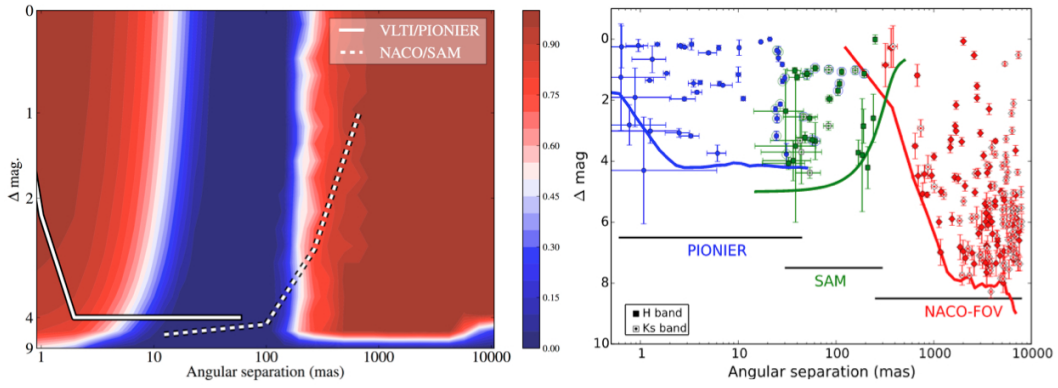

Figure 1: *Left panel*: The probability of companion detection for a target in our sample (blue = 0%, red 100%) using spectroscopy, AO- and direct imaging data. The white solid and dotted line represent the detection limits derived in [14], and also shown in the right panel, for PIONIER and SAM, respectively. *Right panel*: Individual detections and detection limits from using PIONIER, SAM (NACO) and direct imaging (NACO) from the work [14] (originally their Figure 7).

B.7 CNTAC 2016A, MagAO

Title: Determining dynamical masses of nearby pre-main sequence multiple stellar systems

Scientific goal: To gain another epoch of accurate astrometry and photometry for 2 low-mass tight binaries

Instrument / **Telescope**: MagAO/Clay (Las Campanas)

Number of hours: 0.4 nights (4.3)

Semester 2016A

CHILEAN NATIONAL TAC

Prop. #:

Deadline: October 13, 2015, 13:59

Panel: G

Submit your proposal at http://www.das.uchile.cl/cntac/form_prop_cntac.php

1. Title

Determining dynamical masses of nearby pre-main sequence multiple stellar systems

2. Abstract

We have a collection (∼500 stars) of pre-main sequence (PMS) stars on our doorstep that are yet to be fully characterized in terms of their multiplicity; this is the SACY sample. In a recent work we identified 38 visual multiple systems (with ages between 10-100 Myr) from NACO data of 113 of the targets in SACY.
A subset of these systems, five systems, have estimated orbital periods small enough to be fully characterized on the time-scale of yrs (we have already observed orbital motion in some systems in 2 yr).
With this proposal, a pilot study, we seek to further constraint the orbits of two of those systems. From the orbital solutions we will be able to calculate the system mass which when combined with multi-wavelength photometry and resolved high resolution spectroscopy will provide five new benchmark systems for comparisons with theoretical PMS models.
In particular, we propose MagAO observations to obtain another epoch of data to constrain, in total, 50% orbital phase coverage and provide color information using J, H, Ks and L' photometric bands for two PMS low-mass binaries.

3a. Number of requested nights, or hours, on each telescope/radiotelescope (see also #15)

CTIO

Blanco	SOAR	1.5m	1.3m	0.9m	LCO-GTN	PROMPT	KASI	SARA

LCO

Baade	Clay	du Pont	Swope	Warsaw
	0.4n			

3b. Instrument(s) requested/ Minimum time requested

MagAO/0.4n

National Telescopes

Arma zones	Danish	EULER	REM	TAROT	ESO-Schmidt	TRA-PPIST	MPG 2.2m	mini-TAO

Radio

ASTE	NAN-TEN2		

4. Principal investigator **Status (A,S,V):** A

◁ **Name** Amelia Bayo

e-mail[a] amelia.bayo@uv.cl

Phone (+56 32) 250 8426

Institute Universidad de Valparaiso

Address Instituto de Física y Astronomía, Universidad de Valparaíso, Chile

[a]Institutional e-mail required

5. Co-investigators (names and institutions)

◁ Paul Elliott (ESO, Chile / University of Exeter)
◁ Claudio Cáceres, (UV, Chile)
Claudio Melo (ESO, Chile)
Carlos Torres (MCT, Brazil)
Nuria Huélamo (ESAC, Spain)
Hervé Bouy (ESAC, Spain)

12. Description of the programme (1 page of text and up to 2 pages for references, tables and figures.)

A) Scientific rationale Multiple stellar systems are abundant in our galaxy. For example, ∼50% of solar-like field stars ([1], [2]) have at least one companion. Binaries provide the only model independent means to estimate stellar masses, which are among the most fundamental parameters in stellar astrophysics. Currently the mass-luminosity (M/L) relationship is a huge limitation for a number of topics such as the initial mass function (IMF) and exoplanet population studies. We need more binaries providing direct mass measurements in order to calibrate the M/L relationship as a function of age, where the PMS stage is a particularly uncertain territory.
Our PMS parent sample: The SACY sample (Search for Associations Containing Young stars), originally presented in [4], and with recent revised and updated solutions (Torres et al. 2015, in prep) is a collection (∼500 stars) of nearby (<200 pc) young (10-100 Myr) stars, free of extinction. Due to the proximity of these targets a very large and continuous orbital parameter space can be probed when combining different observational techniques (spectroscopy, interferometry, AO- and direct imaging), which is not possible for more distant regions (>200 pc). A dedicated proposal for interferometric observations has been submitted in this period to bridge the gap between the two studies described below. This population is ideal for statistical studies and more focussed target studies such as this one.
Project status: So far we have identified spectroscopic binaries (SBs) ([5]) and close (10-1000 au) visual binaries (VBs) ([6]) in the SACY sample. We have produced robust statistics and derived many properties of the sample (SB fraction, VB fraction, physical separation and mass-ratio distributions). We have compared our results to other PMS populations such as Taurus and the older field population and generally found good agreement between the regions. We are investigating those features that do not agree in dedicated proposals submitted to not-CNTAC facilities.

B) Scientific aim **Following up identified close VBs to get dynamical masses**: In [6] we analyzed NACO data for 113 members of the SACY sample and identified 44 companions around 38 stars. As mentioned previously, one of the great advantages of the SACY sample is its proximity and, therefore, there is a subset of identified systems that should show observable orbital motion on the time-scale of ∼ yr. *This opens up the doorway for astrometric monitoring; to obtain their full orbital solutions.* In this proposal we aim to obtain new MagAO observations for two out of five visual binaries identified in [6], for which we estimate noticeable orbital motion in our observing timeline, in order to further cover the orbital phase of these valuable systems. We selected systems with periods <16 yr and at least two previous observations so that the full orbital solutions can be determined in the near future. Fig. 1 shows an example of one of our targets displaying orbital motion (a change in position angle of 50°) between epochs just 2 yr apart.
What data is currently available and what else do we need: We have checked the archives of NACO, NIRC2 (Keck observatory) and UVES, cross-matched with [4] and [5] and searched the literature. Table 1 shows the data we recovered. We have elected to perform the proposed observations in four bands to provide resolved color information. We will require ∼7 epochs of data in total to obtain the full orbital solution (not necessarily multiple bands). Here we propose to gather the third epoch of the two (out of five) systems achievable within the time slot for Chilean time.The orbits of VBs provide the system mass (m_1+m_2), not individual component masses (see Fig. 2, originally from [8]). With photometry in multiple bands we can compare system masses derived from resolved photometry in numerous near-IR bands (IR observations calibrated with age and distance values) to direct system masses calculated from the orbital solution. We will also make use of existing unresolved high resolution spectra (4000-7000 Å range) with two goals. Firstly, radial velocity (RV) estimates provide further constraints on the orbital fit (we already have these estimates for multiple epochs). Secondly, we can use multicomponent fitting (similar to [11]) to derive individual spectral types, effective temperatures and log(g) using the effectively extinction-free spectral library of the young region Collinder 69 [12] and models. We must note that our multi-component fitting doesn't have the limitation of unknown multiplicity since we have resolved the components in our AO images (if there is no significant improvement in the fit with two components of different fundamental parameters we know it is an equal mass system).
The need for direct masses of PMS stars: As mentioned previously, stellar evolutionary codes are still far from accurate predictions of masses (highest empirical accuracy ∼5% using eclipsing binary systems), especially at low masses (<0.6 $M_\odot$), see Figs. 5, 6 and 7 of [13] for examples of evolutionary traces with and without magnetic fields. As most PMS stars reside in clusters (>140 pc in distance) very few PMS binaries with orbital solutions exist due to the long orbital periods. Most VBs with orbital solutions are nearby main sequence field stars. The targets proposed here are therefore extremely valuable and full orbital solutions combined with spectroscopy will provide very good young calibrators for comparison with PMS stellar evolution theory, as in the work of [8].
Future observations: The observations proposed here will not provide sufficient coverage to derive the full orbital solution for our systems. However, they will help to constrain the parameters of the orbit, vastly helping to plan future observations and additionally providing resolved photometry in 4 bands (J, H, Ks, L) for all systems. In the future we will apply for additional data (also on the three targets not overvable in this period of Chilean time) to further constrain and produce the full orbital solution.
In short: We propose to obtain AO direct imaging MagAO data for previously identified young multiple stellar systems to improve the existing orbital phase coverage. The targets will be observed in 4 bands (J, H, Ks, L') with the Clio2 imager. All the targets are bright enough (V < 12 mag.) to be used as AO reference stars. We will use the narrow camera (field of view: 16" × 8" and integrate for 5-10 minutes on-source.).

References

1 Raghavan et al. 2010, ApJ, 190, 1

2 Tokovinin 2014, AJ, 147, 86

3 King et al. 2012, MNRAS, 427, 2636

4 Torres et al. 2008, Handbook of Star Forming Regions, Volume II, 757

5 Elliott et al. 2014, A&A, 568, A26

6 Elliott et al. 2015, A&A, 580, A88

7 Baraffe et al. 2015, A&A, 577, A42

8 Bonnefoy et al. 2009, A&A, 506, 799

9 Dupuy et al. 2009, ApJ, 706, 328

10 Jodar et al. 2013, MNRAS, 429, 859

11 Burgasser et al. 2010, 710, 1142

12 Bayo et al. 2011, 2011, 536, A63

13 Malo et al. 2014, ApJ, 792, 37

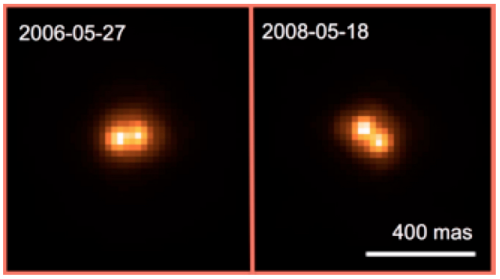

Figure 1: Two epochs of data NACO data for CD-27 11535. This is one of the new systems presented in [6]. Note how the system shows significant orbital motion in just two years (the change in position angle is roughly 50 degrees).

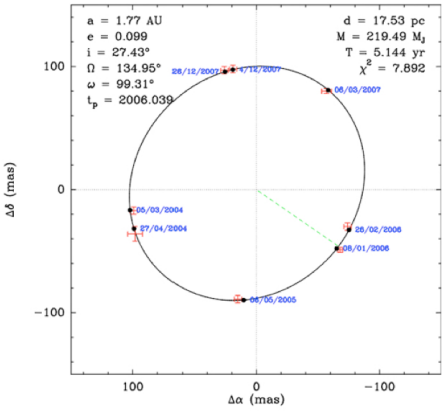

Figure 2: Orbital solution for TWA 22AB, taken from [8]. The astrometry was calculated from multiple NACO observations. We propose to carry out a similar analysis with the requested MagAO data.

ID	Period (yr)	Age (Myr)	Mass:m_1,m_2 ($M_\odot$)	Previous AO obs.	Phase coverage w.r.t. Feb/Mar 2016	AO obs. band	AO obs. ref.	High res. spectra
2MJ023032	14.6	35	0.81,0.57	2010,2012	0.36, 0.25	J, H, Ks, Kp, Lp	A, [5]	2
CD-27 11535	15.6	22	1.01,0.97	2008,2012	0.50, 0.23	IB 2.27, Ks	A, [5]	2
GJ 4231	11.4	100	0.50,0.39	2008,2012	0.65, 0.32	J, Kp, Ks	[9], A	2
BD-18 4452 B	15.5	38	0.29,0.28	2006,2008	0.63, 0.50	NB 2.17, IB 2.27	[5], [5]	1
CD-53 544	5.9	33	0.51,0.51	2007,2008	0.41, 0.23	Ks, Lp	[5], [5]	3

Table 1. Full sample of five targets with predicted significant orbital motion within our observing time line. Only two are easily doable during the four-night Chilean-time slot of the semester with MAGAO. Notes. A: Keck archive

Appendix C

Paranal observatory project

In April 2014 I spent one week at the Paranal observatory in Chile. The aim of this visit was to work with the instrument scientist for FLAMES/VLT (Dr. Dimitri Gadotti) and create a code that could estimate the signal-to-noise ratio and, produce basics statistics of FLAMES/VLT (in MEDUSA mode) data as observations were being taken, a so-called *on-the-fly* estimation. Below I outline the FLAMES instrument and typical observational data. I then describe exactly how the code estimates the statistics on the raw observational data.

C.1 An outline of FLAMES/VLT instrument

The FLAMES[1] instrument (Pasquini et al., 2002) is a multi-object intermediate and high-resolution optical spectrograph mounted on UT2 at the Paranal observatory. It can either feed the UVES or GIRAFFE spectrograph and, in this project the data being analysed was that of GIRAFFE. This spectrograph is medium–high resolution ($R \sim$5500-65000) in the wavelength range 3700–9000 Å. For this spectrograph there are a number of different modes depending on the goal of the observations. The most commonly used is the fibre-fed MEDUSA mode. In this mode up to 132 fibres can be

[1] http://www.eso.org/sci/facilities/paranal/instruments/flames.html

used for simultaneous observations of targets within a 25′ diameter field of view. This is ideal for spectroscopic observations of clusters (minimum angular separation of targets 11″), such as the large VLT-FLAMES Tarantula survey (Evans et al., 2011).

GIRAFFE has a 2000 x 4000 pixel CCD with separate spectra from individual fibres spanning the x-direction and wavelength dispersion in the y-direction. Due to the alignment between the wavelength dispersion and its x position on the chip it is very simple to crudely *identify* separate spectra. This is very useful in producing the statistical estimates as explained in the next section.

C.2 Calculating statistics of the raw data

Below is a breakdown of the code explaining exactly how the estimates are made. References are made to Figure C.1 which shows the graphical output of the code for the user.

- First of all the code attempts to identify spectra resulting from individual fibres on the CCD. It does this by using the bias value to try and distinguish between areas of the CCD that have no astronomical signal (in other words a count approximately equal to the level of the bias) and areas with significantly higher counts.
- The median value of each collection (with significant signal) of pixels is then taken, on the condition that the signal spans at least 2-3 pixels (i.e. it is not a spurious signal).
- The code iterates around certain bias thresholds and compares the number of identified fibres to the number of expected fibres from the observational setup. This information is outputted to the terminal for the user so they can see the comparison for themselves. Additionally, a summary of the number of identified fibres is shown in panel 4 of Figure C.1. Performing this procedure ensures that spectra on the CCD that lie very close in x-direction still have a chance of being

differentiated rather than counted as 1 very wide spectrum which could affect the resultant statistics. The raw pixel counts are shown in the panel 2 of Figure C.1.

- Now for each identified fibre, the central region (pixel values 1500-2500 in the y-direction) is selected. A cut of this region on the CCD is shown in panel 3 of Figure C.1. This region is then chunked by 50 pixel intervals and the mean and standard deviation is calculated in each chunk.

- The median value of the calculated mean and standard deviation values is taken. This is to avoid strong emission lines being included that could skew the statistics significantly. The resultant values are shown in panel 1 of Figure C.1.

- Users are normally concerned with the signal-to-noise around the central region and therefore, the code also displays a more detailed analysis of this area of the CCD. Five *representative* fibres are found by looking at the average value within each fibre and taking 5 fibres around the median of this.

- Then, as before, the central region (1500-2500 in the y-direction is chunked in 50 pixel intervals). Instead of averaging over this region as before, the signal-to-noise in each 50 pixel interval is displayed to the user, and a second-order polynomial is fitted to the data. This gives the user an immediately viewable estimation, see panel 5 of Figure C.1.

The code was used at the Paranal observatory over a one year period until a change in python version prevented further use.

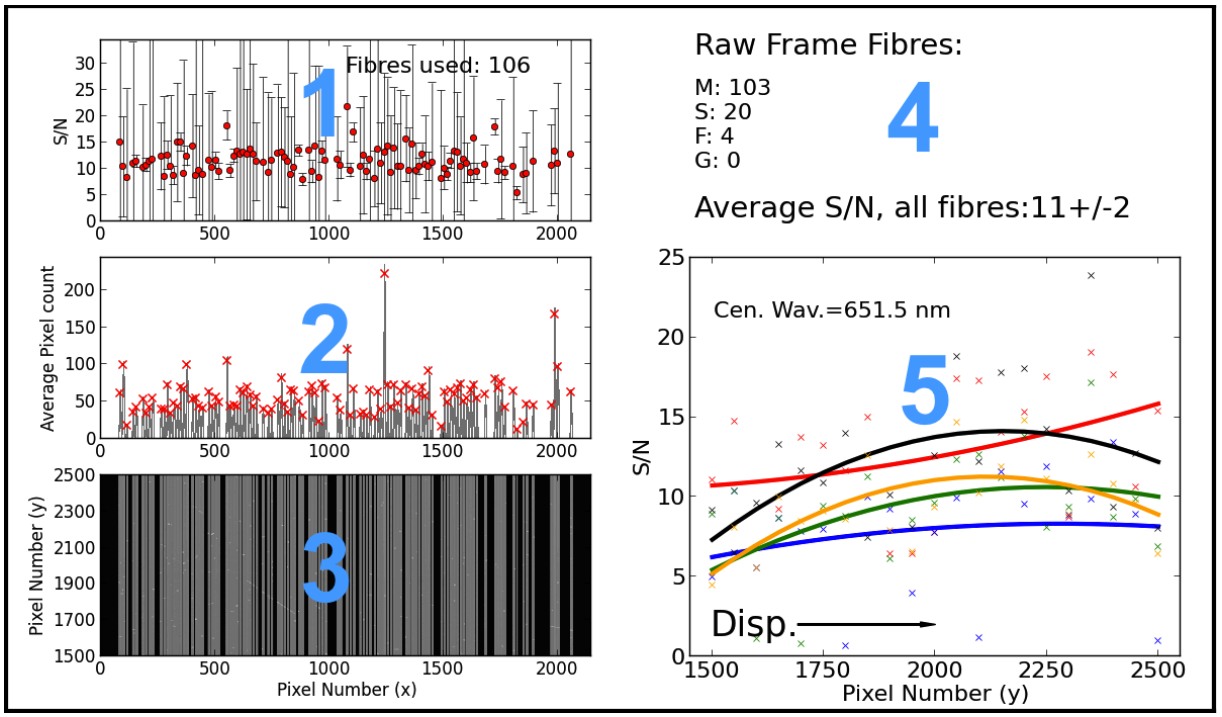

FIGURE C.1: An example of the graphical output showing estimations the signal-to-noise of raw FLAMES/VLT data in MEDUSA mode.

Bibliography

Aarnio, A. N., Weinberger, A. J., Stassun, K. G., Mamajek, E. E., and James, D. J. (2008). A Survey for A Coeval, Comoving Group Associated with HD 141569. *AJ*, 136:2483–2492.

Alcalá, J. M., Spezzi, L., Chapman, N., Evans, II, N. J., Huard, T. L., Jørgensen, J. K., Merín, B., Stapelfeldt, K. R., Covino, E., Frasca, A., Gandolfi, D., and Oliveira, I. (2008). The Spitzer c2d Survey of Large, Nearby, Interstellar Clouds. X. The Chamaeleon II Pre-Main-Sequence Population as Observed with IRAC and MIPS. *ApJ*, 676:427–463.

Allard, F., Homeier, D., and Freytag, B. (2012). Models of very-low-mass stars, brown dwarfs and exoplanets. *Royal Society of London Philosophical Transactions Series A*, 370:2765–2777.

ALMA Partnership, Brogan, C. L., Pérez, L. M., Hunter, T. R., Dent, W. R. F., Hales, A. S., Hills, R. E., Corder, S., Fomalont, E. B., Vlahakis, C., Asaki, Y., Barkats, D., Hirota, A., Hodge, J. A., Impellizzeri, C. M. V., Kneissl, R., Liuzzo, E., Lucas, R., Marcelino, N., Matsushita, S., Nakanishi, K., Phillips, N., Richards, A. M. S., Toledo, I., Aladro, R., Broguiere, D., Cortes, J. R., Cortes, P. C., Espada, D., Galarza, F., Garcia-Appadoo, D., Guzman-Ramirez, L., Humphreys, E. M., Jung, T., Kameno, S., Laing, R. A., Leon, S., Marconi, G., Mignano, A., Nikolic, B., Nyman, L.-A., Radiszcz, M., Remijan, A., Rodón, J. A., Sawada, T., Takahashi, S., Tilanus, R. P. J., Vila Vilaro, B., Watson, L. C., Wiklind, T., Akiyama, E., Chapillon, E., de Gregorio-Monsalvo, I., Di Francesco, J., Gueth, F., Kawamura, A., Lee, C.-F., Nguyen Luong, Q., Mangum, J., Pietu, V., Sanhueza, P., Saigo, K., Takakuwa, S., Ubach, C., van Kempen, T., Wootten, A., Castro-Carrizo, A., Francke, H., Gallardo, J., Garcia, J., Gonzalez, S., Hill, T., Kaminski, T., Kurono, Y., Liu, H.-Y., Lopez, C., Morales, F., Plarre, K., Schieven, G., Testi, L., Videla, L., Villard, E., Andreani, P., Hibbard, J. E., and Tatematsu, K. (2015). The 2014 ALMA Long Baseline Campaign: First Results from High Angular Resolution Observations toward the HL Tau Region. *ApJ*, 808:L3.

Alonso-Floriano, F. J., Caballero, J. A., Cortés-Contreras, M., Solano, E., and Montes, D. (2015). Reaching the boundary between stellar kinematic groups and very wide binaries. III. Sixteen new stars and eight new wide systems in the β Pictoris moving group. *A&A*, 583:A85.

Andersen, J., Nordstrom, B., Ardeberg, A., Benz, W., Mayor, M., Imbert, M., Martin, N., Prevot, L., Lindgren, H., and Maurice, E. (1985). Radial velocities of southern stars

obtained with the photoelectric scanner CORAVEL. III - 790 late-type bright stars. *A&AS*, 59:15–36.

Anderson, E. and Francis, C. (2012). XHIP: An extended hipparcos compilation. *Astronomy Letters*, 38:331–346.

Andrews, S. M., Rosenfeld, K. A., Kraus, A. L., and Wilner, D. J. (2013). The Mass Dependence between Protoplanetary Disks and their Stellar Hosts. *ApJ*, 771:129.

Anglada-Escudé, G., Plavchan, P., Mills, S., Gao, P., García-Berríos, E., Lewis, N. S., Sung, K., Ciardi, D., Beichman, C., Brinkworth, C., Johnson, J., Davison, C., White, R., and Prato, L. (2012). Design and Construction of Absorption Cells for Precision Radial Velocities in the K Band Using Methane Isotopologues. *PASP*, 124:586–597.

Argiroffi, C., Maggio, A., Montmerle, T., Huenemoerder, D. P., Alecian, E., Audard, M., Bouvier, J., Damiani, F., Donati, J.-F., Gregory, S. G., Güdel, M., Hussain, G. A. J., Kastner, J. H., and Sacco, G. G. (2012). The Close T Tauri Binary System V4046 Sgr: Rotationally Modulated X-Ray Emission from Accretion Shocks. *ApJ*, 752:100.

Artymowicz, P. and Lubow, S. H. (1994). Dynamics of binary-disk interaction. 1: Resonances and disk gap sizes. *ApJ*, 421:651–667.

Artymowicz, P. and Lubow, S. H. (1996). Mass Flow through Gaps in Circumbinary Disks. *ApJ*, 467:L77.

Bailey, III, J. I., White, R. J., Blake, C. H., Charbonneau, D., Barman, T. S., Tanner, A. M., and Torres, G. (2012). Precise Infrared Radial Velocities from Keck/NIRSPEC and the Search for Young Planets. *ApJ*, 749:16.

Baines, D., Oudmaijer, R. D., Porter, J. M., and Pozzo, M. (2006). On the binarity of Herbig Ae/Be stars. *MNRAS*, 367:737–753.

Baraffe, I., Chabrier, G., Allard, F., and Hauschildt, P. (2003). Evolutionary models for low mass stars and brown dwarfs at young ages. In Martín, E., editor, *Brown Dwarfs*, volume 211 of *IAU Symposium*, page 41.

Baraffe, I., Chabrier, G., Allard, F., and Hauschildt, P. H. (1998). Evolutionary models for solar metallicity low-mass stars: mass-magnitude relationships and color-magnitude diagrams. *A&A*, 337:403–412.

Baraffe, I., Homeier, D., Allard, F., and Chabrier, G. (2015). New evolutionary models for pre-main sequence and main sequence low-mass stars down to the hydrogen-burning limit. *A&A*, 577:A42.

Baranne, A., Queloz, D., Mayor, M., Adrianzyk, G., Knispel, G., Kohler, D., Lacroix, D., Meunier, J.-P., Rimbaud, G., and Vin, A. (1996). ELODIE: A spectrograph for accurate radial velocity measurements. *A&AS*, 119:373–390.

Barentsen and et al. (2014). VizieR Online Data Catalog: IPHAS DR2 Source Catalogue (Barentsen+, 2014). *VizieR Online Data Catalog*, 2321:0.

Barrado y Navascués, D., Stauffer, J. R., Song, I., and Caillault, J.-P. (1999). The Age of beta Pictoris. *ApJ*, 520:L123–L126.

Bate, M. R. (2000). Predicting the properties of binary stellar systems: the evolution of accreting protobinary systems. *MNRAS*, 314:33–53.

Bate, M. R. (2012). Stellar, brown dwarf and multiple star properties from a radiation hydrodynamical simulation of star cluster formation. *MNRAS*, 419:3115–3146.

Bate, M. R. (2014). The statistical properties of stars and their dependence on metallicity: the effects of opacity. *MNRAS*, 442:285–313.

Bate, M. R., Bonnell, I. A., and Bromm, V. (2002). The formation of close binary systems by dynamical interactions and orbital decay. *MNRAS*, 336:705–713.

Bate, M. R., Clarke, C. J., and McCaughrean, M. J. (1998). Interpreting the mean surface density of companions in star-forming regions. *MNRAS*, 297:1163–1181.

Bayes, M. and Price, M. (1763). An Essay towards Solving a Problem in the Doctrine of Chances. By the Late Rev. Mr. Bayes, F. R. S. Communicated by Mr. Price, in a Letter to John Canton, A. M. F. R. S. *Royal Society of London Philosophical Transactions Series I*, 53:370–418.

Bayo, A., Barrado, D., Stauffer, J., Morales-Calderón, M., Melo, C., Huélamo, N., Bouy, H., Stelzer, B., Tamura, M., and Jayawardhana, R. (2011). Spectroscopy of very low mass stars and brown dwarfs in the Lambda Orionis star forming region. I. Enlarging the census down to the planetary mass domain in Collinder 69. *A&A*, 536:A63.

Bayo, A., Rodrigo, C., Barrado Y Navascués, D., Solano, E., Gutiérrez, R., Morales-Calderón, M., and Allard, F. (2008). VOSA: virtual observatory SED analyzer. An application to the Collinder 69 open cluster. *A&A*, 492:277–287.

Bell, C. P. M., Mamajek, E. E., and Naylor, T. (2015). A self-consistent, absolute isochronal age scale for young moving groups in the solar neighbourhood. *MNRAS*, 454:593–614.

Benson, P. J. and Myers, P. C. (1989). A survey for dense cores in dark clouds. *ApJS*, 71:89–108.

Bergfors, C., Brandner, W., Janson, M., Daemgen, S., Geissler, K., Henning, T., Hippler, S., Hormuth, F., Joergens, V., and Köhler, R. (2010). Lucky Imaging survey for southern M dwarf binaries. *A&A*, 520:A54.

Bertin, E. and Arnouts, S. (1996). SExtractor: Software for source extraction. *A&AS*, 117:393–404.

Beuzit, J.-L., Feldt, M., Dohlen, K., Mouillet, D., Puget, P., Wildi, F., Abe, L., Antichi, J., Baruffolo, A., Baudoz, P., Boccaletti, A., Carbillet, M., Charton, J., Claudi, R., Downing, M., Fabron, C., Feautrier, P., Fedrigo, E., Fusco, T., Gach, J.-L., Gratton, R., Henning, T., Hubin, N., Joos, F., Kasper, M., Langlois, M., Lenzen, R., Moutou,

C., Pavlov, A., Petit, C., Pragt, J., Rabou, P., Rigal, F., Roelfsema, R., Rousset, G., Saisse, M., Schmid, H.-M., Stadler, E., Thalmann, C., Turatto, M., Udry, S., Vakili, F., and Waters, R. (2008). SPHERE: a 'Planet Finder' instrument for the VLT. In *Ground-based and Airborne Instrumentation for Astronomy II*, volume 7014 of *Society of Photo-Optical Instrumentation Engineers (SPIE) Conference Series*, page 701418.

Bianchi, L., Herald, J., Efremova, B., Girardi, L., Zabot, A., Marigo, P., Conti, A., and Shiao, B. (2011). GALEX catalogs of UV sources: statistical properties and sample science applications: hot white dwarfs in the Milky Way. *Ap&SS*, 335:161–169.

Bildsten, L., Brown, E. F., Matzner, C. D., and Ushomirsky, G. (1997). Lithium Depletion in Fully Convective Pre-Main-Sequence Stars. *ApJ*, 482:442–447.

Biller, B. A., Close, L. M., Masciadri, E., Nielsen, E., Lenzen, R., Brandner, W., McCarthy, D., Hartung, M., Kellner, S., Mamajek, E., Henning, T., Miller, D., Kenworthy, M., and Kulesa, C. (2007). An Imaging Survey for Extrasolar Planets around 45 Close, Young Stars with the Simultaneous Differential Imager at the Very Large Telescope and MMT. *ApJS*, 173:143–165.

Biller, B. A., Liu, M. C., Wahhaj, Z., Nielsen, E. L., Hayward, T. L., Males, J. R., Skemer, A., Close, L. M., Chun, M., Ftaclas, C., Clarke, F., Thatte, N., Shkolnik, E. L., Reid, I. N., Hartung, M., Boss, A., Lin, D., Alencar, S. H. P., de Gouveia Dal Pino, E., Gregorio-Hetem, J., and Toomey, D. (2013). The Gemini/NICI Planet-Finding Campaign: The Frequency of Planets around Young Moving Group Stars. *ApJ*, 777:160.

Binks, A. S. and Jeffries, R. D. (2014). A lithium depletion boundary age of 21 Myr for the Beta Pictoris moving group. *MNRAS*, 438:L11–L15.

Bitsch, B., Lambrechts, M., and Johansen, A. (2015). The growth of planets by pebble accretion in evolving protoplanetary discs. *A&A*, 582:A112.

Bobylev, V. V., Goncharov, G. A., and Bajkova, A. T. (2006). The OSACA database and a kinematic analysis of stars in the solar neighborhood. *Astronomy Reports*, 50:733–747.

Bodenheimer, P. and Burkert, A. (2001). Formation of Wide Binaries by Fragmentation. In Zinnecker, H. and Mathieu, R., editors, *The Formation of Binary Stars*, volume 200 of *IAU Symposium*, page 13.

Bonnefoy, M., Chauvin, G., Dumas, C., Lagrange, A.-M., Beust, H., Desort, M., Teixeira, R., Ducourant, C., Beuzit, J.-L., and Song, I. (2009). The young, tight, and low-mass binary TWA22AB: a new calibrator for evolutionary models?. Orbit, spectral types, and temperature. *A&A*, 506:799–810.

Bonnell, I. A. and Bate, M. R. (1994). The Formation of Close Binary Systems. *MNRAS*, 271.

Boss, A. P. (1986). Protostellar formation in rotating interstellar clouds. V - Nonisothermal collapse and fragmentation. *ApJS*, 62:519–552.

Bouvier, J., Matt, S. P., Mohanty, S., Scholz, A., Stassun, K. G., and Zanni, C. (2014). Angular Momentum Evolution of Young Low-Mass Stars and Brown Dwarfs: Observations and Theory. *Protostars and Planets VI*, pages 433–450.

Bouvier, J., Rigaut, F., and Nadeau, D. (1997). Pleiades low-mass binaries: do companions affect the evolution of protoplanetary disks? *A&A*, 323:139–150.

Bowler, B. P., Liu, M. C., Shkolnik, E. L., and Tamura, M. (2015). Planets around Low-mass Stars (PALMS). IV. The Outer Architecture of M Dwarf Planetary Systems. *ApJS*, 216:7.

Brandeker, A., Jayawardhana, R., Khavari, P., Haisch, Jr., K. E., and Mardones, D. (2006). Deficit of Wide Binaries in the η Chamaeleontis Young Cluster. *ApJ*, 652:1572–1584.

Brandt, T. D., Kuzuhara, M., McElwain, M. W., Schlieder, J. E., Wisniewski, J. P., Turner, E. L., Carson, J., Matsuo, T., Biller, B., Bonnefoy, M., Dressing, C., Janson, M., Knapp, G. R., Moro-Martín, A., Thalmann, C., Kudo, T., Kusakabe, N., Hashimoto, J., Abe, L., Brandner, W., Currie, T., Egner, S., Feldt, M., Golota, T., Goto, M., Grady, C. A., Guyon, O., Hayano, Y., Hayashi, M., Hayashi, S., Henning, T., Hodapp, K. W., Ishii, M., Iye, M., Kandori, R., Kwon, J., Mede, K., Miyama, S., Morino, J.-I., Nishimura, T., Pyo, T.-S., Serabyn, E., Suenaga, T., Suto, H., Suzuki, R., Takami, M., Takahashi, Y., Takato, N., Terada, H., Tomono, D., Watanabe, M., Yamada, T., Takami, H., Usuda, T., and Tamura, M. (2014). The Moving Group Targets of the SEEDS High-contrast Imaging Survey of Exoplanets and Disks: Results and Observations from the First Three Years. *ApJ*, 786:1.

Burgasser, A. J., Kirkpatrick, J. D., Reid, I. N., Brown, M. E., Miskey, C. L., and Gizis, J. E. (2003). Binarity in Brown Dwarfs: T Dwarf Binaries Discovered with the Hubble Space Telescope Wide Field Planetary Camera 2. *ApJ*, 586:512–526.

Burkert, A. and Bodenheimer, P. (1993). Multiple Fragmentation in Collapsing Protostars. *MNRAS*, 264:798.

Caballero, J. A. (2010). Reaching the boundary between stellar kinematic groups and very wide binaries . II. α Librae + KU Librae: a common proper motion system in Castor separated by 1.0 pc. *A&A*, 514:A98.

Carleo, I., Sanna, N., Gratton, R., Benatti, S., Bonavita, M., Oliva, E., Origlia, L., Desidera, S., Claudi, R., and Sissa, E. (2016). High precision radial velocities with GIANO spectra. *Experimental Astronomy*.

Casagrande, L., Schönrich, R., Asplund, M., Cassisi, S., Ramírez, I., Meléndez, J., Bensby, T., and Feltzing, S. (2011). New constraints on the chemical evolution of the solar neighbourhood and Galactic disc(s). Improved astrophysical parameters for the Geneva-Copenhagen Survey. *A&A*, 530:A138.

Chabrier, G. (2003). Galactic Stellar and Substellar Initial Mass Function. *PASP*, 115:763–795.

Chabrier, G., Baraffe, I., and Plez, B. (1996). Mass-Luminosity Relationship and Lithium Depletion for Very Low Mass Stars. *ApJ*, 459:L91.

Chauvin, G., Lagrange, A.-M., Beust, H., Bonnefoy, M., Boccaletti, A., Apai, D., Allard, F., Ehrenreich, D., Girard, J. H. V., Mouillet, D., and Rouan, D. (2012). Orbital characterization of the β Pictoris b giant planet. *A&A*, 542:A41.

Chauvin, G., Lagrange, A.-M., Bonavita, M., Zuckerman, B., Dumas, C., Bessell, M. S., Beuzit, J.-L., Bonnefoy, M., Desidera, S., Farihi, J., Lowrance, P., Mouillet, D., and Song, I. (2010). Deep imaging survey of young, nearby austral stars . VLT/NACO near-infrared Lyot-coronographic observations. *A&A*, 509:A52.

Chauvin, G., Lagrange, A.-M., Dumas, C., Zuckerman, B., Mouillet, D., Song, I., Beuzit, J.-L., and Lowrance, P. (2005). Giant planet companion to 2MASSW J1207334-393254. *A&A*, 438:L25–L28.

Chauvin, G., Thomson, M., Dumas, C., Beuzit, J.-L., Lowrance, P., Fusco, T., Lagrange, A.-M., Zuckerman, B., and Mouillet, D. (2003). Adaptive optics imaging survey of the Tucana-Horologium association. *A&A*, 404:157–162.

Chen, X., Arce, H. G., Zhang, Q., Bourke, T. L., Launhardt, R., Jørgensen, J. K., Lee, C.-F., Foster, J. B., Dunham, M. M., Pineda, J. E., and Henning, T. (2013). SMA Observations of Class 0 Protostars: A High Angular Resolution Survey of Protostellar Binary Systems. *ApJ*, 768:110.

Chini, R., Hoffmeister, V. H., Nasseri, A., Stahl, O., and Zinnecker, H. (2012). A spectroscopic survey on the multiplicity of high-mass stars. *MNRAS*, 424:1925–1929.

Cutri, R. M., Skrutskie, M. F., van Dyk, S., Beichman, C. A., Carpenter, J. M., Chester, T., Cambresy, L., Evans, T., Fowler, J., Gizis, J., Howard, E., Huchra, J., Jarrett, T., Kopan, E. L., Kirkpatrick, J. D., Light, R. M., Marsh, K. A., McCallon, H., Schneider, S., Stiening, R., Sykes, M., Weinberg, M., Wheaton, W. A., Wheelock, S., and Zacarias, N. (2003). 2MASS All-Sky Catalog of Point Sources (Cutri+ 2003). *VizieR Online Data Catalog*, 2246:0.

da Silva, L., Torres, C. A. O., de La Reza, R., Quast, G. R., Melo, C. H. F., and Sterzik, M. F. (2009). Search for associations containing young stars (SACY). III. Ages and Li abundances. *A&A*, 508:833–839.

Daemgen, S., Bonavita, M., Jayawardhana, R., Lafrenière, D., and Janson, M. (2015). Sub-stellar Companions and Stellar Multiplicity in the Taurus Star-forming Region. *ApJ*, 799:155.

Daemgen, S., Elliot Meyer, R., Jayawardhana, R., and Petr-Gotzens, M. G. (2016). The frequency of accretion disks around single stars: Chamaeleon I. *A&A*, 586:A12.

de Bruijne, J. H. J. and Eilers, A.-C. (2012). Radial velocities for the HIPPARCOS-Gaia Hundred-Thousand-Proper-Motion project. *A&A*, 546:A61.

de La Reza, R., Quast, G., Torres, C. A. O., Mayor, M., Meylan, G., and Llorente de Andres, F. (1986). Simultaneous UV-optical observations of isolated T-Tauri stars: The V4046 SGR CASE. In Rolfe, E. J., editor, *New Insights in Astrophysics. Eight Years of UV Astronomy with IUE*, volume 263 of *ESA Special Publication*, pages 107–111.

de la Reza, R., Torres, C. A. O., Quast, G., Castilho, B. V., and Vieira, G. L. (1989). Discovery of new isolated T Tauri stars. *ApJ*, 343:L61–L64.

de Val-Borro, M., Gahm, G. F., Stempels, H. C., and Pepliński, A. (2011). Modelling circumbinary gas flows in close T Tauri binaries. *MNRAS*, 413:2679–2688.

Delfosse, X., Forveille, T., Beuzit, J.-L., Udry, S., Mayor, M., and Perrier, C. (1999). New neighbours. I. 13 new companions to nearby M dwarfs. *A&A*, 344:897–910.

Delorme, P., Lagrange, A. M., Chauvin, G., Bonavita, M., Lacour, S., Bonnefoy, M., Ehrenreich, D., and Beust, H. (2012). High-resolution imaging of young M-type stars of the solar neighbourhood: probing for companions down to the mass of Jupiter. *A&A*, 539:A72.

Desidera, S., Covino, E., Messina, S., Carson, J., Hagelberg, J., Schlieder, J. E., Biazzo, K., Alcalá, J. M., Chauvin, G., Vigan, A., Beuzit, J. L., Bonavita, M., Bonnefoy, M., Delorme, P., D'Orazi, V., Esposito, M., Feldt, M., Girardi, L., Gratton, R., Henning, T., Lagrange, A. M., Lanzafame, A. C., Launhardt, R., Marmier, M., Melo, C., Meyer, M., Mouillet, D., Moutou, C., Segransan, D., Udry, S., and Zaidi, C. M. (2015). The VLT/NaCo large program to probe the occurrence of exoplanets and brown dwarfs in wide orbits. I. Sample definition and characterization. *A&A*, 573:A126.

Devillard, N. (1997). The eclipse software. *The Messenger*, 87:19–20.

Dommanget, J. and Nys, O. (2000). The visual double stars observed by the Hipparcos satellite. *A&A*, 363:991–994.

Dommanget, J. and Nys, O. (2002). VizieR Online Data Catalog: CCDM (Catalog of Components of Double and Multiple stars) (Dommanget+ 2002). *VizieR Online Data Catalog*, 1274:0.

Donati, J.-F., Gregory, S. G., Montmerle, T., Maggio, A., Argiroffi, C., Sacco, G., Hussain, G., Kastner, J., Alencar, S. H. P., Audard, M., Bouvier, J., Damiani, F., Güdel, M., Huenemoerder, D., and Wade, G. A. (2011). The close classical T Tauri binary V4046 Sgr: complex magnetic fields and distributed mass accretion. *MNRAS*, 417:1747–1759.

Dorn, R. J., Anglada-Escude, G., Baade, D., Bristow, P., Follert, R., Gojak, D., Grunhut, J., Hatzes, A., Heiter, U., Hilker, M., Ives, D. J., Jung, Y., Käufl, H.-U., Kerber, F., Klein, B., Lizon, J.-L., Lockhart, M., Löwinger, T., Marquart, T., Oliva, E., Origlia, L., Pasquini, L., Paufique, J., Piskunov, N., Pozna, E., Reiners, A., Smette, A., Smoker, J., Seemann, U., Stempels, E., and Valenti, E. (2014). CRIRES+: Exploring the Cold Universe at High Spectral Resolution. *The Messenger*, 156:7–11.

Doyle, L. R., Carter, J. A., Fabrycky, D. C., Slawson, R. W., Howell, S. B., Winn, J. N., Orosz, J. A., Prˇ sa, A., Welsh, W. F., Quinn, S. N., Latham, D., Torres, G., Buchhave, L. A., Marcy, G. W., Fortney, J. J., Shporer, A., Ford, E. B., Lissauer, J. J., Ragozzine, D., Rucker, M., Batalha, N., Jenkins, J. M., Borucki, W. J., Koch, D., Middour, C. K., Hall, J. R., McCauliff, S., Fanelli, M. N., Quintana, E. V., Holman, M. J., Caldwell, D. A., Still, M., Stefanik, R. P., Brown, W. R., Esquerdo, G. A., Tang, S., Furesz, G., Geary, J. C., Berlind, P., Calkins, M. L., Short, D. R., Steffen, J. H., Sasselov, D., Dunham, E. W., Cochran, W. D., Boss, A., Haas, M. R., Buzasi, D., and Fischer, D. (2011). Kepler-16: A Transiting Circumbinary Planet. *Science*, 333:1602.

Drake, A. J., Djorgovski, S. G., Mahabal, A., Beshore, E., Larson, S., Graham, M. J., Williams, R., Christensen, E., Catelan, M., Boattini, A., Gibbs, A., Hill, R., and Kowalski, R. (2009). First Results from the Catalina Real-Time Transient Survey. *ApJ*, 696:870–884.

Duchêne, G. (1999). Binary fraction in low-mass star forming regions: a reexamination of the possible excesses and implications. *A&A*, 341:547–552.

Duchêne, G. and Kraus, A. (2013). Stellar Multiplicity. *ArXiv e-prints*.

Dupuy, T. J., Kratter, K. M., Kraus, A. L., Isaacson, H., Mann, A. W., Ireland, M. J., Howard, A. W., and Huber, D. (2016). Orbital Architectures of Planet-hosting Binaries. I. Forming Five Small Planets in the Truncated Disk of Kepler-444A. *ApJ*, 817:80.

Duquennoy, A. and Mayor, M. (1991). Multiplicity among solar-type stars in the solar neighbourhood. II - Distribution of the orbital elements in an unbiased sample. *A&A*, 248:485–524.

Eggleton, P. P. and Kisseleva-Eggleton, L. (2006). A Mechanism for Producing Short-Period Binaries. *Ap&SS*, 304:75–79.

Elliott, P. and Bayo, A. (2016). The crucial role of higher-order multiplicity in wide binary formation: A case study using the β-Pictoris moving group. *MNRAS*.

Elliott, P., Bayo, A., Melo, C. H. F., Torres, C. A. O., Sterzik, M., and Quast, G. R. (2014). Search for associations containing young stars (SACY). V. Is multiplicity universal? Tight multiple systems. *A&A*, 568:A26.

Elliott, P., Bayo, A., Melo, C. H. F., Torres, C. A. O., Sterzik, M. F., Quast, G. R., Montes, D., and Brahm, R. (2016). Search for associations containing young stars (SACY) VII. New stellar and substellar candidate members in the young associations. *ArXiv e-prints*.

Elliott, P., Huélamo, N., Bouy, H., Bayo, A., Melo, C. H. F., Torres, C. A. O., Sterzik, M. F., Quast, G. R., Chauvin, G., and Barrado, D. (2015). Search for associations containing young stars (SACY). VI. Is multiplicity universal? Stellar multiplicity in the range 3-1000 au from adaptive-optics observations. *A&A*, 580:A88.

ESA, editor (1997). *The HIPPARCOS and TYCHO catalogues. Astrometric and photometric star catalogues derived from the ESA HIPPARCOS Space Astrometry Mission*, volume 1200 of *ESA Special Publication*.

Espaillat, C., Ingleby, L., Hernández, J., Furlan, E., D'Alessio, P., Calvet, N., Andrews, S., Muzerolle, J., Qi, C., and Wilner, D. (2012). On the Transitional Disk Class: Linking Observations of T Tauri Stars and Physical Disk Models. *ApJ*, 747:103.

Evans, C. J., Taylor, W. D., Hénault-Brunet, V., Sana, H., de Koter, A., Simón-Díaz, S., Carraro, G., Bagnoli, T., Bastian, N., Bestenlehner, J. M., Bonanos, A. Z., Bressert, E., Brott, I., Campbell, M. A., Cantiello, M., Clark, J. S., Costa, E., Crowther, P. A., de Mink, S. E., Doran, E., Dufton, P. L., Dunstall, P. R., Friedrich, K., Garcia, M., Gieles, M., Gräfener, G., Herrero, A., Howarth, I. D., Izzard, R. G., Langer, N., Lennon, D. J., Maíz Apellániz, J., Markova, N., Najarro, F., Puls, J., Ramirez, O. H., Sabín-Sanjulián, C., Smartt, S. J., Stroud, V. E., van Loon, J. T., Vink, J. S., and Walborn, N. R. (2011). The VLT-FLAMES Tarantula Survey. I. Introduction and observational overview. *A&A*, 530:A108.

Evans, I. N., Primini, F. A., Glotfelty, K. J., Anderson, C. S., Bonaventura, N. R., Chen, J. C., Davis, J. E., Doe, S. M., Evans, J. D., Fabbiano, G., Galle, E. C., Gibbs, II, D. G., Grier, J. D., Hain, R. M., Hall, D. M., Harbo, P. N., (Helen He, X., Houck, J. C., Karovska, M., Kashyap, V. L., Lauer, J., McCollough, M. L., McDowell, J. C., Miller, J. B., Mitschang, A. W., Morgan, D. L., Mossman, A. E., Nichols, J. S., Nowak, M. A., Plummer, D. A., Refsdal, B. L., Rots, A. H., Siemiginowska, A., Sundheim, B. A., Tibbetts, M. S., Van Stone, D. W., Winkelman, S. L., and Zografou, P. (2010). The Chandra Source Catalog. *ApJS*, 189:37–82.

Evans, T. M., Ireland, M. J., Kraus, A. L., Martinache, F., Stewart, P., Tuthill, P. G., Lacour, S., Carpenter, J. M., and Hillenbrand, L. A. (2012). Mapping the Shores of the Brown Dwarf Desert. III. Young Moving Groups. *ApJ*, 744:120.

Feigelson, E. D., Lawson, W. A., Stark, M., Townsley, L., and Garmire, G. P. (2006). 51 Eridani and GJ 3305: A 10-15 Myr old Binary Star System at 30 Parsecs. *AJ*, 131:1730–1739.

Fischer, D. A. and Marcy, G. W. (1992). Multiplicity among M dwarfs. *ApJ*, 396:178–194.

Fleming, T. A., Molendi, S., Maccacaro, T., and Wolter, A. (1995). The Einstein Extended Medium-Sensitivity Survey Second Epoch: Results for the Stars. *ApJS*, 99:701.

Frith, J., Pinfield, D. J., Jones, H. R. A., Barnes, J. R., Pavlenko, Y., Martin, E. L., Brown, C., Kuznetsov, M. K., Marocco, F., Tata, R., and Cappetta, M. (2013). A catalogue of bright ($K < 9$) M dwarfs. *MNRAS*, 435:2161–2170.

Gagné, J., Faherty, J. K., Cruz, K. L., Lafreniére, D., Doyon, R., Malo, L., Burgasser, A. J., Naud, M.-E., Artigau, É., Bouchard, S., Gizis, J. E., and Albert, L. (2015). BANYAN. VII. A New Population of Young Substellar Candidate Members of Nearby Moving Groups from the BASS Survey. *ApJS*, 219:33.

Gagné, J., Plavchan, P., Gao, P., Anglada-Escude, G., Furlan, E., Davison, C., Tanner, A., Henry, T. J., Riedel, A. R., Brinkworth, C., Latham, D., Bottom, M., White, R., Mills, S., Beichman, C., Johnson, J. A., Ciardi, D. R., Wallace, K., Mennesson, B., von Braun, K., Vasisht, G., Prato, L., Kane, S. R., Mamajek, E. E., Walp, B., Crawford, T. J., Rougeot, R., Geneser, C. S., and Catanzarite, J. (2016). A High-Precision NIR Survey for RV Variable Low-Mass Stars. *ArXiv e-prints*.

Gallet, F. and Bouvier, J. (2013). Improved angular momentum evolution model for solar-like stars. *A&A*, 556:A36.

Gavel, D. T., Max, C. E., Olivier, S. S., Bauman, B. J., Pennington, D. M., Macintosh, B. A., Patience, J., Brown, C. G., Danforth, P. M., Hurd, R. L., Gates, E. L., Severson, S. A., and Lloyd, J. P. (2002). Science with laser guide stars at Lick Observatory. In Tyson, R. K., Bonaccini, D., and Roggemann, M. C., editors, *Adaptive Optics Systems and Technology II*, volume 4494 of *Society of Photo-Optical Instrumentation Engineers (SPIE) Conference Series*, pages 336–342.

Girard, T. M., van Altena, W. F., Zacharias, N., Vieira, K., Casetti-Dinescu, D. I., Castillo, D., Herrera, D., Lee, Y. S., Beers, T. C., Monet, D. G., and López, C. E. (2011). The Southern Proper Motion Program. IV. The SPM4 Catalog. *AJ*, 142:15.

Gliese, W. and Jahreiß, H. (1991). Preliminary Version of the Third Catalogue of Nearby Stars. Technical report.

Gontcharov, G. A. (2006). Radial velocities of 35495 Hipparcos stars in a common system. *Astronomical and Astrophysical Transactions*, 25:145–148.

Gonzalez, J.-F., Pinte, C., Maddison, S. T., Ménard, F., and Fouchet, L. (2012). Planet gaps in the dust layer of 3D protoplanetary disks. II. Observability with ALMA. *A&A*, 547:A58.

Goodwin, S. P. (2010). Binaries in star clusters and the origin of the field stellar population. *Philosophical Transactions of the Royal Society of London Series A*, 368:851–866.

Gray, D. F. (1976). *The observation and analysis of stellar photospheres*.

Gray, R. O., Corbally, C. J., Garrison, R. F., McFadden, M. T., Bubar, E. J., McGahee, C. E., O'Donoghue, A. A., and Knox, E. R. (2006). Contributions to the Nearby Stars (NStars) Project: Spectroscopy of Stars Earlier than M0 within 40 pc-The Southern Sample. *AJ*, 132:161–170.

Gregorio-Hetem, J., Lepine, J. R. D., Quast, G. R., Torres, C. A. O., and de La Reza, R. (1992). A search for T Tauri stars based on the IRAS point source catalog. *AJ*, 103:549–563.

Griffin, R. F. (2010). Spectroscopic binary orbits from photoelectric radial velocities - Paper 212: HD 113449, HD 113762, HD 113880, and HD 119944. *The Observatory*, 130:125–142.

Halbwachs, J.-L. (2001). Présentation générale des étoiles doubles. *Ecole de Goutelas*, 23:1.

Harris, R. J., Andrews, S. M., Wilner, D. J., and Kraus, A. L. (2012). A Resolved Census of Millimeter Emission from Taurus Multiple Star Systems. *ApJ*, 751:115.

Hayfield, T., Mayer, L., Wadsley, J., and Boley, A. C. (2011). The properties of pre-stellar discs in isolated and multiple pre-stellar systems. *MNRAS*, 417:1839–1852.

Heggie, D. C. (1975). Binary evolution in stellar dynamics. *MNRAS*, 173:729–787.

Heinze, A. N., Hinz, P. M., Sivanandam, S., Kenworthy, M., Meyer, M., and Miller, D. (2010). Constraints on Long-period Planets from an L'- and M-band Survey of Nearby Sun-like Stars: Observations. *ApJ*, 714:1551–1569.

Herbig, G. H. (1978). *Can Post-T Tauri Stars Be Found?*, page 171.

Hills, J. G. (1975). Encounters between binary and single stars and their effect on the dynamical evolution of stellar systems. *AJ*, 80:809–825.

Hoffleit, D. and Jaschek, C. (1991). *The Bright star catalogue*.

Høg, E., Fabricius, C., Makarov, V. V., Urban, S., Corbin, T., Wycoff, G., Bastian, U., Schwekendiek, P., and Wicenec, A. (2000). The Tycho-2 catalogue of the 2.5 million brightest stars. *A&A*, 355:L27–L30.

Holman, M. J. and Wiegert, P. A. (1999). Long-Term Stability of Planets in Binary Systems. *AJ*, 117:621–628.

Hubber, D. A. and Whitworth, A. P. (2005). Binary star formation from ring fragmentation. *A&A*, 437:113–125.

Ivanov, G. A. (2008). Catalogue of stars with high-proper motions - version 2. *Kinematika i Fizika Nebesnykh Tel*, 24:480.

Ivezić, Ž., Connolly, A., Vanderplas, J., and Gray, A. (2014). *Statistics, Data Mining and Machine Learning in Astronomy*. Princeton University Press.

Jang-Condell, H. (2015). On the Likelihood of Planet Formation in Close Binaries. *ApJ*, 799:147.

Jang-Condell, H., Mugrauer, M., and Schmidt, T. (2007). Constraints on Planet Formation in Close Binary Systems. In *American Astronomical Society Meeting Abstracts*, volume 39 of *Bulletin of the American Astronomical Society*, page 872.

Janson, M., Brandt, T. D., Moro-Martín, A., Usuda, T., Thalmann, C., Carson, J. C., Goto, M., Currie, T., McElwain, M. W., Itoh, Y., Fukagawa, M., Crepp, J., Kuzuhara, M., Hashimoto, J., Kudo, T., Kusakabe, N., Abe, L., Brandner, W., Egner, S., Feldt, M., Grady, C. A., Guyon, O., Hayano, Y., Hayashi, M., Hayashi, S., Henning, T., Hodapp, K. W., Ishii, M., Iye, M., Kandori, R., Knapp, G. R., Kwon, J., Matsuo, T., Miyama, S., Morino, J.-I., Nishimura, T., Pyo, T.-S., Serabyn, E., Suenaga, T.,

Suto, H., Suzuki, R., Takahashi, Y., Takami, M., Takato, N., Terada, H., Tomono, D., Turner, E. L., Watanabe, M., Wisniewski, J., Yamada, T., Takami, H., and Tamura, M. (2013). The SEEDS Direct Imaging Survey for Planets and Scattered Dust Emission in Debris Disk Systems. *ApJ*, 773:73.

Jayawardhana, R., Coffey, J., Scholz, A., Brandeker, A., and van Kerkwijk, M. H. (2006). Accretion Disks around Young Stars: Lifetimes, Disk Locking, and Variability. *ApJ*, 648:1206–1218.

Jeffries, R. D. and Naylor, T. (2001). The Lithium Depletion Boundary as a Clock and Thermometer. In Montmerle, T. and André, P., editors, *From Darkness to Light: Origin and Evolution of Young Stellar Clusters*, volume 243 of *Astronomical Society of the Pacific Conference Series*, page 633.

Jenkins, J. S., Murgas, F., Rojo, P., Jones, H. R. A., Day-Jones, A. C., Jones, M. I., Clarke, J. R. A., Ruiz, M. T., and Pinfield, D. J. (2011). Chromospheric activities and kinematics for solar type dwarfs and subgiants: analysis of the activity distribution and the AVR. *A&A*, 531:A8.

Jilinski, E., Ortega, V. G., and de la Reza, R. (2005). On the Origin of the Very Young Groups η and ϵ Chamaeleontis. *ApJ*, 619:945–947.

Jordán, A., Brahm, R., Bakos, G. Á., Bayliss, D., Penev, K., Hartman, J. D., Zhou, G., Mancini, L., Mohler-Fischer, M., Ciceri, S., Sato, B., Csubry, Z., Rabus, M., Suc, V., Espinoza, N., Bhatti, W., de Val-Borro, M., Buchhave, L., Csák, B., Henning, T., Schmidt, B., Tan, T. G., Noyes, R. W., Béky, B., Butler, R. P., Shectman, S., Crane, J., Thompson, I., Williams, A., Martin, R., Contreras, C., Lázár, J., Papp, I., and Sári, P. (2014). HATS-4b: A Dense Hot Jupiter Transiting a Super Metal-rich G star. *AJ*, 148:29.

Kasper, M., Apai, D., Janson, M., and Brandner, W. (2007). A novel L-band imaging search for giant planets in the Tucana and β Pictoris moving groups. *A&A*, 472:321–327.

Kastner, J. H., Sacco, G. G., Montez, R., Huenemoerder, D. P., Shi, H., Alecian, E., Argiroffi, C., Audard, M., Bouvier, J., Damiani, F., Donati, J.-F., Gregory, S. G., Güdel, M., Hussain, G. A. J., Maggio, A., and Montmerle, T. (2011). GSC 07396-00759 = V4046 Sgr C[D]: A Wide-separation Companion to the Close T Tauri Binary System V4046 Sgr AB. *ApJ*, 740:L17.

Kastner, J. H., Thompson, E. A., Montez, R., Murphy, S. J., Bessell, M. S., and Sacco, G. G. (2012). 2M1155-79 (= T Chamaeleontis B): A Low-mass, Wide-separation Companion to the nearby, "Old" T Tauri Star T Chamaeleontis. *ApJ*, 747:L23.

Kastner, J. H., Zuckerman, B., Weintraub, D. A., and Forveille, T. (1997). X-ray and molecular emission from the nearest region of recent star formation. *Science*, 277:67–71.

Kellogg, K., Metchev, S., Gagné, J., and Faherty, J. (2016). The Nearest Isolated Member of the TW Hydrae Association is a Giant Planet Analog. *ApJ*, 821:L15.

Kharchenko, N. V., Piskunov, A. E., Schilbach, E., Roeser, S., Scholz, R.-D., and Zinnecker, H. (2009). VizieR Online Data Catalog: Integrated BVJHKs for 650 open clusters (Kharchenko+, 2009). *VizieR Online Data Catalog*, 350:40681.

Kharchenko, N. V., Scholz, R.-D., Piskunov, A. E., Röser, S., and Schilbach, E. (2007). Astrophysical supplements to the ASCC-2.5: Ia. Radial velocities of 55000 stars and mean radial velocities of 516 Galactic open clusters and associations. *Astronomische Nachrichten*, 328:889.

King, R. R., Goodwin, S. P., Parker, R. J., and Patience, J. (2012a). Testing the universality of star formation - II. Comparing separation distributions of nearby star-forming regions and the field. *MNRAS*, 427:2636–2646.

King, R. R., Parker, R. J., Patience, J., and Goodwin, S. P. (2012b). Testing the universality of star formation - I. Multiplicity in nearby star-forming regions. *MNRAS*, 421:2025–2042.

Kiraga, M. (2012). ASAS photometry of ROSAT sources (Kiraga, 2012). *VizieR Online Data Catalog*, 1206:20067.

Köhler, R., Kunkel, M., Leinert, C., and Zinnecker, H. (2000). Multiplicity of X-ray selected T Tauri stars in the Scorpius-Centaurus OB association. *A&A*, 356:541–558.

Köhler, R., Neuhäuser, R., Krämer, S., Leinert, C., Ott, T., and Eckart, A. (2008). Multiplicity of young stars in and around R Coronae Australis. *A&A*, 488:997–1006.

Kordopatis, G., Gilmore, G., Steinmetz, M., Boeche, C., Seabroke, G. M., Siebert, A., Zwitter, T., Binney, J., de Laverny, P., Recio-Blanco, A., Williams, M. E. K., Piffl, T., Enke, H., Roeser, S., Bijaoui, A., Wyse, R. F. G., Freeman, K., Munari, U., Carrillo, I., Anguiano, B., Burton, D., Campbell, R., Cass, C. J. P., Fiegert, K., Hartley, M., Parker, Q. A., Reid, W., Ritter, A., Russell, K. S., Stupar, M., Watson, F. G., Bienaymé, O., Bland-Hawthorn, J., Gerhard, O., Gibson, B. K., Grebel, E. K., Helmi, A., Navarro, J. F., Conrad, C., Famaey, B., Faure, C., Just, A., Kos, J., Matijevič, G., McMillan, P. J., Minchev, I., Scholz, R., Sharma, S., Siviero, A., de Boer, E. W., and Žerjal, M. (2013). The Radial Velocity Experiment (RAVE): Fourth Data Release. *AJ*, 146:134.

Korntreff, C., Kaczmarek, T., and Pfalzner, S. (2012). Towards the field binary population: influence of orbital decay on close binaries. *A&A*, 543:A126.

Kounkel, M., Megeath, S. T., Poteet, C. A., Fischer, W. J., and Hartmann, L. (2016). An HST Survey for 100-1000 AU Companions around Young Stellar Objects in the Orion Molecular Clouds: Evidence for Environmentally Dependent Multiplicity. *ArXiv e-prints*.

Kouwenhoven, M. B. N., Goodwin, S. P., Parker, R. J., Davies, M. B., Malmberg, D., and Kroupa, P. (2010). The formation of very wide binaries during the star cluster dissolution phase. *MNRAS*, 404:1835–1848.

Koyama, K., Hamaguchi, K., Ueno, S., Kobayashi, N., and Feigelson, E. D. (1996). Discovery of Hard X-Rays from a Cluster of Protostars. *PASJ*, 48:L87–L92.

Kraus, A. L. and Hillenbrand, L. A. (2007). The Role of Mass and Environment in Multiple-Star Formation: A 2MASS Survey of Wide Multiplicity in Three Young Associations. *ApJ*, 662:413–430.

Kraus, A. L., Ireland, M. J., Hillenbrand, L. A., and Martinache, F. (2012). The Role of Multiplicity in Disk Evolution and Planet Formation. *ApJ*, 745:19.

Kraus, A. L., Ireland, M. J., Martinache, F., and Hillenbrand, L. A. (2011). Mapping the Shores of the Brown Dwarf Desert. II. Multiple Star Formation in Taurus-Auriga. *ApJ*, 731:8.

Kraus, A. L., Shkolnik, E. L., Allers, K. N., and Liu, M. C. (2014). A Stellar Census of the Tucana-Horologium Moving Group. *AJ*, 147:146.

Kroupa, P. (1995). Star cluster evolution, dynamical age estimation and the kinematical signature of star formation. *MNRAS*, 277:1522.

Kroupa, P. (2011). The universality hypothesis: binary and stellar populations in star clusters and galaxies. In Alves, J., Elmegreen, B. G., Girart, J. M., and Trimble, V., editors, *Computational Star Formation*, volume 270 of *IAU Symposium*, pages 141–149.

Kroupa, P. and Bouvier, J. (2003). The dynamical evolution of Taurus-Auriga-type aggregates. *MNRAS*, 346:343–353.

Lada, C. J. and Lada, E. A. (2003). Embedded Clusters in Molecular Clouds. *ARA&A*, 41:57–115.

Lafrenière, D., Doyon, R., Marois, C., Nadeau, D., Oppenheimer, B. R., Roche, P. F., Rigaut, F., Graham, J. R., Jayawardhana, R., Johnstone, D., Kalas, P. G., Macintosh, B., and Racine, R. (2007). The Gemini Deep Planet Survey. *ApJ*, 670:1367–1390.

Lafrenière, D., Jayawardhana, R., Brandeker, A., Ahmic, M., and van Kerkwijk, M. H. (2008). A Multiplicity Census of Young Stars in Chamaeleon I. *ApJ*, 683:844–861.

Lagrange, A.-M., Meunier, N., Chauvin, G., Sterzik, M., Galland, F., Lo Curto, G., Rameau, J., and Sosnowska, D. (2013). Planets around stars in young nearby associations. Radial velocity searches: a feasibility study and first results. *A&A*, 559:A83.

Larson, R. B. (1969). Numerical calculations of the dynamics of collapsing proto-star. *MNRAS*, 145:271.

Larson, R. B. (1995). Star formation in groups. *MNRAS*, 272:213–220.

Lasker, B. M., Lattanzi, M. G., McLean, B. J., Bucciarelli, B., Drimmel, R., Garcia, J., Greene, G., Guglielmetti, F., Hanley, C., Hawkins, G., Laidler, V. G., Loomis, C., Meakes, M., Mignani, R., Morbidelli, R., Morrison, J., Pannunzio, R., Rosenberg, A., Sarasso, M., Smart, R. L., Spagna, A., Sturch, C. R., Volpicelli, A., White, R. L.,

Wolfe, D., and Zacchei, A. (2008). The Second-Generation Guide Star Catalog: Description and Properties. *AJ*, 136:735–766.

Lawson, W. A., Crause, L. A., Mamajek, E. E., and Feigelson, E. D. (2001). The η Chamaeleontis cluster: photometric study of the ROSAT-detected weak-lined T Tauri stars. *MNRAS*, 321:57–66.

Leighton, R. B. (1959). Observations of Solar Magnetic Fields in Plage Regions. *ApJ*, 130:366.

Leinert, C., Zinnecker, H., Weitzel, N., Christou, J., Ridgway, S. T., Jameson, R., Haas, M., and Lenzen, R. (1993). A systematic approach for young binaries in Taurus. *A&A*, 278:129–149.

Lépine, S., Hilton, E. J., Mann, A. W., Wilde, M., Rojas-Ayala, B., Cruz, K. L., and Gaidos, E. (2013). A Spectroscopic Catalog of the Brightest (J $<$ 9) M Dwarfs in the Northern Sky. *AJ*, 145:102.

Lindegren, L., Babusiaux, C., Bailer-Jones, C., Bastian, U., Brown, A. G. A., Cropper, M., Høg, E., Jordi, C., Katz, D., van Leeuwen, F., Luri, X., Mignard, F., de Bruijne, J. H. J., and Prusti, T. (2008). The Gaia mission: science, organization and present status. In Jin, W. J., Platais, I., and Perryman, M. A. C., editors, *IAU Symposium*, volume 248 of *IAU Symposium*, pages 217–223.

Looper, D. L., Bochanski, J. J., Burgasser, A. J., Mohanty, S., Mamajek, E. E., Faherty, J. K., West, A. A., and Pitts, M. A. (2010). A Widely Separated, Highly Occluded Companion to the Nearby Low-mass T Tauri Star TWA 30. *AJ*, 140:1486–1499.

Lopez Martí, B., Jimenez Esteban, F., Bayo, A., Barrado, D., Solano, E., and Rodrigo, C. (2013). Proper motions of young stars in Chamaeleon. I. A Virtual Observatory study of spectroscopically confirmed members. *A&A*, 551:A46.

López-Santiago, J., Montes, D., Crespo-Chacón, I., and Fernández-Figueroa, M. J. (2006). The Nearest Young Moving Groups. *ApJ*, 643:1160–1165.

Lowrance, P. J., Becklin, E. E., Schneider, G., Kirkpatrick, J. D., Weinberger, A. J., Zuckerman, B., Dumas, C., Beuzit, J.-L., Plait, P., Malumuth, E., Heap, S., Terrile, R. J., and Hines, D. C. (2005). An Infrared Coronagraphic Survey for Substellar Companions. *AJ*, 130:1845–1861.

Luhman, K. L. (2004). A Census of the Chamaeleon I Star-forming Region. *ApJ*, 602:816–842.

Luhman, K. L., Stauffer, J. R., Muench, A. A., Rieke, G. H., Lada, E. A., Bouvier, J., and Lada, C. J. (2003). A Census of the Young Cluster IC 348. *ApJ*, 593:1093–1115.

Macintosh, B., Graham, J. R., Ingraham, P., Konopacky, Q., Marois, C., Perrin, M., Poyneer, L., Bauman, B., Barman, T., Burrows, A. S., Cardwell, A., Chilcote, J., De Rosa, R. J., Dillon, D., Doyon, R., Dunn, J., Erikson, D., Fitzgerald, M. P., Gavel, D.,

Goodsell, S., Hartung, M., Hibon, P., Kalas, P., Larkin, J., Maire, J., Marchis, F., Marley, M. S., McBride, J., Millar-Blanchaer, M., Morzinski, K., Norton, A., Oppenheimer, B. R., Palmer, D., Patience, J., Pueyo, L., Rantakyro, F., Sadakuni, N., Saddlemyer, L., Savransky, D., Serio, A., Soummer, R., Sivaramakrishnan, A., Song, I., Thomas, S., Wallace, J. K., Wiktorowicz, S., and Wolff, S. (2014). First light of the Gemini Planet Imager. *Proceedings of the National Academy of Science*, 111:12661–12666.

Malaroda, S., Levato, H., and Galliani, S. (2006). Stellar radial velocities bibliographic catalog (Malaroda+, 2006). *VizieR Online Data Catalog*, 3249:0.

Maldonado, J., Martínez-Arnáiz, R. M., Eiroa, C., Montes, D., and Montesinos, B. (2010). A spectroscopy study of nearby late-type stars, possible members of stellar kinematic groups. *A&A*, 521:A12.

Malkov, O. Y., Oblak, E., Snegireva, E. A., and Torra, J. (2006). A catalogue of eclipsing variables. *A&A*, 446:785–789.

Malo, L., Artigau, É., Doyon, R., Lafrenière, D., Albert, L., and Gagné, J. (2014). BANYAN. III. Radial Velocity, Rotation, and X-Ray Emission of Low-mass Star Candidates in Nearby Young Kinematic Groups. *ApJ*, 788:81.

Malo, L., Doyon, R., Lafrenière, D., Artigau, É., Gagné, J., Baron, F., and Riedel, A. (2013). Bayesian Analysis to Identify New Star Candidates in Nearby Young Stellar Kinematic Groups. *ApJ*, 762:88.

Malogolovets, E. V., Balega, Y. Y., Rastegaev, D. A., Hofmann, K.-H., and Weigelt, G. (2007). GJ 900: A new hierarchical system with low-mass components. *Astrophysical Bulletin*, 62:117–124.

Mamajek, E. E. (2009). Initial Conditions of Planet Formation: Lifetimes of Primordial Disks. In Usuda, T., Tamura, M., and Ishii, M., editors, *American Institute of Physics Conference Series*, volume 1158 of *American Institute of Physics Conference Series*, pages 3–10.

Mamajek, E. E., Meyer, M. R., and Liebert, J. (2006). Erratum: "Post-T Tauri Stars in the Nearest OB Association" (¡A href="/abs/2002AJ.124.1670M"¿AJ, 124, 1670 [2002]¡/A¿). *AJ*, 131:2360–2360.

Marks, M., Leigh, N., Giersz, M., Pfalzner, S., Pflamm-Altenburg, J., and Oh, S. (2014). Revisiting the universality of (multiple) star formation in present-day star formation regions. *MNRAS*, 441:3503–3512.

Martin, E. L. (1997). Quantitative spectroscopic criteria for the classification of pre-main sequence low-mass stars. *A&A*, 321:492–496.

Masciadri, E., Mundt, R., Henning, T., Alvarez, C., and Barrado y Navascués, D. (2005). A Search for Hot Massive Extrasolar Planets around Nearby Young Stars with the Adaptive Optics System NACO. *ApJ*, 625:1004–1018.

Mason, B. D., Wycoff, G. L., Hartkopf, W. I., Douglass, G. G., and Worley, C. E. (2001). The 2001 US Naval Observatory Double Star CD-ROM. I. The Washington Double Star Catalog. *AJ*, 122:3466–3471.

Mathieu, R. D., Ghez, A. M., Jensen, E. L. N., and Simon, M. (2000). Young Binary Stars and Associated Disks. *Protostars and Planets IV*, page 703.

Mayor, M. and Mermilliod, J. C. (1984). Orbit Circularization Time in Binary Stellar Systems. In Maeder, A. and Renzini, A., editors, *Observational Tests of the Stellar Evolution Theory*, volume 105 of *IAU Symposium*, page 411.

McCarthy, K. and White, R. J. (2012). The Sizes of the Nearest Young Stars. *AJ*, 143:134.

McCaughrean, M. J. and Stauffer, J. R. (1994). High resolution near-infrared imaging of the trapezium: A stellar census. *AJ*, 108:1382–1397.

Melo, C. H. F. (2003). The short period multiplicity among T Tauri stars. *A&A*, 410:269–282.

Mermilliod, J. C. (2006). VizieR Online Data Catalog: Homogeneous Means in the UBV System (Mermilliod 1991). *VizieR Online Data Catalog*, 2168:0.

Messina, S., Desidera, S., Lanzafame, A. C., Turatto, M., and Guinan, E. F. (2011). RACE-OC project: rotation and variability in the ϵ Chamaeleontis, Octans, and Argus stellar associations. *A&A*, 532:A10.

Messina, S., Desidera, S., Turatto, M., Lanzafame, A. C., and Guinan, E. F. (2010). RACE-OC project: Rotation and variability of young stellar associations within 100 pc. *A&A*, 520:A15.

Messina, S., Monard, B., Biazzo, K., Melo, C. H. F., and Frasca, A. (2014). Evidence from stellar rotation of enhanced disc dispersal. I. The case of the triple visual system BD-21 1074 in the β Pictoris association. *A&A*, 570:A19.

Messina, S., Monard, B., Worters, H. L., Bromage, G. E., and Sanchez, R. Z. (2016). On the rotation periods of the components of the triple system TYC 9300-0891-1AB/TYC 9300-0529-1 in the Octans Association. *New A*, 42:29–37.

Metchev, S. A. and Hillenbrand, L. A. (2009). The Palomar/Keck Adaptive Optics Survey of Young Solar Analogs: Evidence for a Universal Companion Mass Function. *ApJS*, 181:62–109.

Moeckel, N. and Bate, M. R. (2010). On the evolution of a star cluster and its multiple stellar systems following gas dispersal. *MNRAS*, 404:721–737.

Montes, D., López-Santiago, J., Crespo-Chacón, I., and Fernández-Figueroa, M. J. (2005). Flare stars among K dwarfs members of young stellar kinematic groups. In Favata, F., Hussain, G. A. J., and Battrick, B., editors, *13th Cambridge Workshop on Cool Stars, Stellar Systems and the Sun*, volume 560 of *ESA Special Publication*, page 825.

Montes, D., López-Santiago, J., Gálvez, M. C., Fernández-Figueroa, M. J., De Castro, E., and Cornide, M. (2001). Late-type members of young stellar kinematic groups - I. Single stars. *MNRAS*, 328:45–63.

Montet, B. T., Bowler, B. P., Shkolnik, E. L., Deck, K. M., Wang, J., Horch, E. P., Liu, M. C., Hillenbrand, L. A., Kraus, A. L., and Charbonneau, D. (2015). Dynamical Masses of Young M Dwarfs: Masses and Orbital Parameters of GJ 3305 AB, the Wide Binary Companion to the Imaged Exoplanet Host 51 Eri. *ApJ*, 813:L11.

Moór, A., Szabó, G. M., Kiss, L. L., Kiss, C., Ábrahám, P., Szulágyi, J., Kóspál, Á., and Szalai, T. (2013). Unveiling new members in five nearby young moving groups. *MNRAS*, 435:1376–1388.

Morin, J., Donati, J.-F., Petit, P., Delfosse, X., Forveille, T., Albert, L., Aurière, M., Cabanac, R., Dintrans, B., Fares, R., Gastine, T., Jardine, M. M., Lignières, F., Paletou, F., Ramirez Velez, J. C., and Théado, S. (2008). Large-scale magnetic topologies of mid M dwarfs. *MNRAS*, 390:567–581.

Motte, F., Andre, P., and Neri, R. (1998). The initial conditions of star formation in the rho Ophiuchi main cloud: wide-field millimeter continuum mapping. *A&A*, 336:150–172.

Mould, J. R. (1976). M dwarfs: band strengths in halo and disk populations. *ApJ*, 207:535–544.

Murphy, S. J. and Lawson, W. A. (2015). New low-mass members of the Octans stellar association and an updated 30-40 Myr lithium age. *MNRAS*, 447:1267–1281.

Murphy, S. J., Lawson, W. A., and Bessell, M. S. (2013). Re-examining the membership and origin of the ϵ Cha association. *MNRAS*, 435:1325–1349.

Neuhäuser, R., Briceño, C., Comerón, F., Hearty, T., Martín, E. L., Schmitt, J. H. M. M., Stelzer, B., Supper, R., Voges, W., and Zinnecker, H. (1999). Search for X-ray emission from bona-fide and candidate brown dwarfs. *A&A*, 343:883–893.

Neuhäuser, R., Guenther, E. W., Alves, J., Huélamo, N., Ott, T., and Eckart, A. (2003). An infrared imaging search for low-mass companions to members of the young nearby β Pic and Tucana/Horologium associations. *Astronomische Nachrichten*, 324:535–542.

Nguyen, D. C., Brandeker, A., van Kerkwijk, M. H., and Jayawardhana, R. (2012). Close companions to young stars. i. a large spectroscopic survey in chamaeleon i and taurus-auriga. *The Astrophysical Journal*, 745(2):119.

Nielsen, E. L. and Close, L. M. (2010). A Uniform Analysis of 118 Stars with High-contrast Imaging: Long-period Extrasolar Giant Planets are Rare Around Sun-like Stars. *ApJ*, 717:878–896.

Nordström, B., Mayor, M., Andersen, J., Holmberg, J., Pont, F., Jørgensen, B. R., Olsen, E. H., Udry, S., and Mowlavi, N. (2004). The Geneva-Copenhagen survey of the Solar neighbourhood. Ages, metallicities, and kinematic properties of 14 000 F and G dwarfs. *A&A*, 418:989–1019.

Offner, S. S. R., Kratter, K. M., Matzner, C. D., Krumholz, M. R., and Klein, R. I. (2010). The Formation of Low-mass Binary Star Systems Via Turbulent Fragmentation. *ApJ*, 725:1485–1494.

Oliva, E., Origlia, L., Baffa, C., Biliotti, C., Bruno, P., D'Amato, F., Del Vecchio, C., Falcini, G., Gennari, S., Ghinassi, F., Giani, E., Gonzalez, M., Leone, F., Lolli, M., Lodi, M., Maiolino, R., Mannucci, F., Marcucci, G., Mochi, I., Montegriffo, P., Rossetti, E., Scuderi, S., and Sozzi, M. (2006). The GIANO-TNG spectrometer. In *Society of Photo-Optical Instrumentation Engineers (SPIE) Conference Series*, volume 6269 of *Proc. SPIE*, page 626919.

Padoan, P. and Nordlund, Å. (2002). The Stellar Initial Mass Function from Turbulent Fragmentation. *ApJ*, 576:870–879.

Padoan, P. and Nordlund, Å. (2004). The "Mysterious" Origin of Brown Dwarfs. *ApJ*, 617:559–564.

Parker, R. J. and Goodwin, S. P. (2012). The same, but different: stochasticity in binary destruction. *MNRAS*, 424:272–281.

Parker, R. J., Goodwin, S. P., Kroupa, P., and Kouwenhoven, M. B. N. (2009). Do binaries in clusters form in the same way as in the field? *MNRAS*, 397:1577–1586.

Parker, R. J. and Meyer, M. R. (2014). Binaries in the field: fossils of the star formation process? *MNRAS*, 442:3722–3736.

Pasquini, L., Avila, G., Blecha, A., Cacciari, C., Cayatte, V., Colless, M., Damiani, F., de Propris, R., Dekker, H., di Marcantonio, P., Farrell, T., Gillingham, P., Guinouard, I., Hammer, F., Kaufer, A., Hill, V., Marteaud, M., Modigliani, A., Mulas, G., North, P., Popovic, D., Rossetti, E., Royer, F., Santin, P., Schmutzer, R., Simond, G., Vola, P., Waller, L., and Zoccali, M. (2002). Installation and commissioning of FLAMES, the VLT Multifibre Facility. *The Messenger*, 110:1–9.

Pecaut, M. J. and Mamajek, E. E. (2013). Intrinsic Colors, Temperatures, and Bolometric Corrections of Pre-main-sequence Stars. *ApJS*, 208:9.

Perryman, M. A. C., Lindegren, L., Kovalevsky, J., Hoeg, E., Bastian, U., Bernacca, P. L., Crézé, M., Donati, F., Grenon, M., Grewing, M., van Leeuwen, F., van der Marel, H., Mignard, F., Murray, C. A., Le Poole, R. S., Schrijver, H., Turon, C., Arenou, F., Froeschlé, M., and Petersen, C. S. (1997). The HIPPARCOS Catalogue. *A&A*, 323:L49–L52.

Phillips, N. M., Greaves, J. S., Dent, W. R. F., Matthews, B. C., Holland, W. S., Wyatt, M. C., and Sibthorpe, B. (2010). Target selection for the SUNS and DEBRIS surveys for debris discs in the solar neighbourhood. *MNRAS*, 403:1089–1101.

Pineda, J. E., Goodman, A. A., Arce, H. G., Caselli, P., Longmore, S., and Corder, S. (2011). Expanded Very Large Array Observations of the Barnard 5 Star-forming Core: Embedded Filaments Revealed. *ApJ*, 739:L2.

Pojmanski, G. (2002). The All Sky Automated Survey. Catalog of Variable Stars. I. 0 h - 6 hQuarter of the Southern Hemisphere. *Acta Astron.*, 52:397–427.

Pourbaix, D., Tokovinin, A. A., Batten, A. H., Fekel, F. C., Hartkopf, W. I., Levato, H., Morrell, N. I., Torres, G., and Udry, S. (2004). $S_{B⁹}$: The ninth catalogue of spectroscopic binary orbits. *A&A*, 424:727–732.

Quast, G. R., Torres, C. A. O., de La Reza, R., da Silva, L., and Mayor, M. (2000). V4046 Sgr, a key young binary system. In *IAU Symposium*, volume 200 of *IAU Symposium*, page 28P.

Queloz, D. (1995). Echelle Spectroscopy with a CCD at Low Signal-To-Noise Ratio. In Philip, A. G. D., Janes, K., and Upgren, A. R., editors, *New Developments in Array Technology and Applications*, volume 167 of *IAU Symposium*, page 221.

Raghavan, D., McAlister, H. A., Henry, T. J., Latham, D. W., Marcy, G. W., Mason, B. D., Gies, D. R., White, R. J., and ten Brummelaar, T. A. (2010). A Survey of Stellar Families: Multiplicity of Solar-type Stars. *ApJS*, 190:1–42.

Rameau, J., Chauvin, G., Lagrange, A.-M., Klahr, H., Bonnefoy, M., Mordasini, C., Bonavita, M., Desidera, S., Dumas, C., and Girard, J. H. (2013). A survey of young, nearby, and dusty stars conducted to understand the formation of wide-orbit giant planets. VLT/NaCo adaptive optics thermal and angular differential imaging. *A&A*, 553:A60.

Raskin, G., van Winckel, H., Hensberge, H., Jorissen, A., Lehmann, H., Waelkens, C., Avila, G., de Cuyper, J.-P., Degroote, P., Dubosson, R., Dumortier, L., Frémat, Y., Laux, U., Michaud, B., Morren, J., Perez Padilla, J., Pessemier, W., Prins, S., Smolders, K., van Eck, S., and Winkler, J. (2011). HERMES: a high-resolution fibre-fed spectrograph for the Mercator telescope. *A&A*, 526:A69.

Ratzka, T., Köhler, R., and Leinert, C. (2005). A multiplicity survey of the ρ Ophiuchi molecular clouds. *A&A*, 437:611–626.

Reggiani, M. and Meyer, M. R. (2013). Universality of the companion mass-ratio distribution. *A&A*, 553:A124.

Reid, I. N., Hawley, S. L., and Gizis, J. E. (1995). The Palomar/MSU Nearby-Star Spectroscopic Survey. I. The Northern M Dwarfs -Bandstrengths and Kinematics. *AJ*, 110:1838.

Reiners, A. and Basri, G. (2009). A Volume-Limited Sample of 63 M7-M9.5 Dwarfs. I. Space Motion, Kinematic Age, and Lithium. *ApJ*, 705:1416–1424.

Reipurth, B., Clarke, C. J., Boss, A. P., Goodwin, S. P., Rodríguez, L. F., Stassun, K. G., Tokovinin, A., and Zinnecker, H. (2014). Multiplicity in Early Stellar Evolution. *Protostars and Planets VI*, pages 267–290.

Reipurth, B., Guimarães, M. M., Connelley, M. S., and Bally, J. (2007). Visual Binaries in the Orion Nebula Cluster. *AJ*, 134:2272–2285.

Reipurth, B. and Mikkola, S. (2012). Formation of the widest binary stars from dynamical unfolding of triple systems. *Nature*, 492:221–224.

Reipurth, B., Mikkola, S., Connelley, M., and Valtonen, M. (2010). Orphaned Protostars. *ApJ*, 725:L56–L61.

Riaz, B., Gizis, J. E., and Harvin, J. (2006). Identification of New M Dwarfs in the Solar Neighborhood. *AJ*, 132:866–872.

Riedel, A. R., Finch, C. T., Henry, T. J., Subasavage, J. P., Jao, W.-C., Malo, L., Rodriguez, D. R., White, R. J., Gies, D. R., Dieterich, S. B., Winters, J. G., Davison, C. L., Nelan, E. P., Blunt, S. C., Cruz, K. L., Rice, E. L., and Ianna, P. A. (2014). The Solar Neighborhood. XXXIII. Parallax Results from the CTIOPI 0.9 m Program: Trigonometric Parallaxes of Nearby Low-mass Active and Young Systems. *AJ*, 147:85.

Riviere-Marichalar, P., Elliott, P., Rebollido, I., Bayo, A., Ribas, A., Merín, B., Kamp, I., Dent, W. R. F., and Montesinos, B. (2015a). Herschel-PACS observations of discs in the Eta Chamaeleontis association. *ArXiv e-prints*.

Riviere-Marichalar, P., Elliott, P., Rebollido, I., Bayo, A., Ribas, A., Merín, B., Kamp, I., Dent, W. R. F., and Montesinos, B. (2015b). Herschel-PACS observations of discs in the η Chamaeleontis association. *A&A*, 584:A22.

Robin, A. C., Reylé, C., Derrière, S., and Picaud, S. (2003). A synthetic view on structure and evolution of the Milky Way. *A&A*, 409:523–540.

Rocha-Pinto, H. J., Flynn, C., Scalo, J., Hänninen, J., Maciel, W. J., and Hensler, G. (2004). Chemical enrichment and star formation in the Milky Way disk. III. Chemodynamical constraints. *A&A*, 423:517–535.

Rodriguez, D. R., Bessell, M. S., Zuckerman, B., and Kastner, J. H. (2011). A New Method to Identify Nearby, Young, Low-mass Stars. *ApJ*, 727:62.

Rodriguez, D. R., Duchêne, G., Tom, H., Kennedy, G. M., Matthews, B., Greaves, J., and Butner, H. (2015). Stellar multiplicity and debris discs: an unbiased sample. *MNRAS*, 449:3160–3170.

Rodriguez, D. R., Kastner, J. H., Wilner, D., and Qi, C. (2010). Imaging the Molecular Disk Orbiting the Twin Young Suns of V4046 Sgr. *ApJ*, 720:1684–1690.

Rodriguez, D. R., Zuckerman, B., Kastner, J. H., Bessell, M. S., Faherty, J. K., and Murphy, S. J. (2013). The GALEX Nearby Young-Star Survey. *ApJ*, 774:101.

Roeser, S., Demleitner, M., and Schilbach, E. (2010). The PPMXL Catalog of Positions and Proper Motions on the ICRS. Combining USNO-B1.0 and the Two Micron All Sky Survey (2MASS). *AJ*, 139:2440–2447.

Ruge, J. P., Wolf, S., Demidova, T., and Grinin, V. (2015). Structures in circumbinary disks: Prospects for observability. *A&A*, 579:A110.

Salpeter, E. E. (1955). The Luminosity Function and Stellar Evolution. *ApJ*, 121:161.

Sana, H., de Koter, A., de Mink, S. E., Dunstall, P. R., Evans, C. J., Hénault-Brunet, V., Maíz Apellániz, J., Ramírez-Agudelo, O. H., Taylor, W. D., Walborn, N. R., Clark, J. S., Crowther, P. A., Herrero, A., Gieles, M., Langer, N., Lennon, D. J., and Vink, J. S. (2013). The VLT-FLAMES Tarantula Survey. VIII. Multiplicity properties of the O-type star population. *A&A*, 550:A107.

Sana, H. and Evans, C. J. (2011). The multiplicity of massive stars. In Neiner, C., Wade, G., Meynet, G., and Peters, G., editors, *IAU Symposium*, volume 272 of *IAU Symposium*, pages 474–485.

Sartori, M. J., Lépine, J. R. D., and Dias, W. S. (2003). Formation scenarios for the young stellar associations between galactic longitudes l = 280degr - 360degr. *A&A*, 404:913–926.

Schlieder, J. E., Lépine, S., Rice, E., Simon, M., Fielding, D., and Tomasino, R. (2012a). The Na 8200 Å Doublet as an Age Indicator in Low-mass Stars. *AJ*, 143:114.

Schlieder, J. E., Lépine, S., and Simon, M. (2012b). Likely Members of the β Pictoris and AB Doradus Moving Groups in the North. *ApJ*, 144:109.

Schmitt, J. H. M. M., Fleming, T. A., and Giampapa, M. S. (1995). The X-Ray View of the Low-Mass Stars in the Solar Neighborhood. *ApJ*, 450:392.

Schneider, A. C., Windsor, J., Cushing, M. C., Kirkpatrick, J. D., and Wright, E. L. (2016). WISEA J114724.10-204021.3: A Free-Floating Planetary Mass Member of the TW Hya Association. *ArXiv e-prints*.

Scholz, R.-D., McCaughrean, M. J., Zinnecker, H., and Lodieu, N. (2005). SSSPM J1102-3431: A probable new young brown dwarf member of the TW Hydrae Association. *A&A*, 430:L49–L52.

Schulz, N. (2005). *From Dust To Stars: Studies of the Formation and Early Evolution of Stars*. Springer-Praxis books in astrophysics and astronomy. Springer London, Limited.

Schütz, O., Meeus, G., and Sterzik, M. F. (2005). Mid-IR observations of circumstellar disks. I. Pre-main sequence objects. *A&A*, 431:165–174.

Scott, D. W. (2009). *Multivariate density estimation: theory, practice, and visualization*, volume 383. John Wiley & Sons.

Sestito, P., Palla, F., and Randich, S. (2008). An assessment of Li abundances in weak-lined and classical T Tauri stars of the Taurus-Auriga association. *A&A*, 487:965–973.

Shkolnik, E. L., Anglada-Escudé, G., Liu, M. C., Bowler, B. P., Weinberger, A. J., Boss, A. P., Reid, I. N., and Tamura, M. (2012). Identifying the Young Low-mass Stars within 25 pc. II. Distances, Kinematics, and Group Membership. *ApJ*, 758:56.

Shkolnik, E. L., Hebb, L., Liu, M. C., Reid, I. N., and Collier Cameron, A. (2010). Thirty New Low-mass Spectroscopic Binaries. *ApJ*, 716:1522–1530.

Shkolnik, E. L., Liu, M. C., Reid, I. N., Dupuy, T., and Weinberger, A. J. (2011). Searching for Young M Dwarfs with GALEX. *ApJ*, 727:6.

Sicilia-Aguilar, A., Bouwman, J., Juhász, A., Henning, T., Roccatagliata, V., Lawson, W. A., Acke, B., Feigelson, E. D., Tielens, A. G. G. M., Decin, L., and Meeus, G. (2009). The Long-Lived Disks in the η Chamaeleontis Cluster. *ApJ*, 701:1188–1203.

Siebert, A., Williams, M. E. K., Siviero, A., Reid, W., Boeche, C., Steinmetz, M., Fulbright, J., Munari, U., Zwitter, T., Watson, F. G., Wyse, R. F. G., de Jong, R. S., Enke, H., Anguiano, B., Burton, D., Cass, C. J. P., Fiegert, K., Hartley, M., Ritter, A., Russel, K. S., Stupar, M., Bienaymé, O., Freeman, K. C., Gilmore, G., Grebel, E. K., Helmi, A., Navarro, J. F., Binney, J., Bland-Hawthorn, J., Campbell, R., Famaey, B., Gerhard, O., Gibson, B. K., Matijevič, G., Parker, Q. A., Seabroke, G. M., Sharma, S., Smith, M. C., and Wylie-de Boer, E. (2011). The RAdial Velocity Experiment (RAVE): Third Data Release. *AJ*, 141:187.

Siess, L., Dufour, E., and Forestini, M. (2000). An internet server for pre-main sequence tracks of low- and intermediate-mass stars. *A&A*, 358:593–599.

Skrutskie, M. F., Cutri, R. M., Stiening, R., Weinberg, M. D., Schneider, S., Carpenter, J. M., Beichman, C., Capps, R., Chester, T., Elias, J., Huchra, J., Liebert, J., Lonsdale, C., Monet, D. G., Price, S., Seitzer, P., Jarrett, T., Kirkpatrick, J. D., Gizis, J. E., Howard, E., Evans, T., Fowler, J., Fullmer, L., Hurt, R., Light, R., Kopan, E. L., Marsh, K. A., McCallon, H. L., Tam, R., Van Dyk, S., and Wheelock, S. (2006). The Two Micron All Sky Survey (2MASS). *AJ*, 131:1163–1183.

Slesnick, C. L., Carpenter, J. M., and Hillenbrand, L. A. (2006). A Large-Area Search for Low-Mass Objects in Upper Scorpius. I. The Photometric Campaign and New Brown Dwarfs. *AJ*, 131:3016–3027.

Soderblom, D. R., Hillenbrand, L. A., Jeffries, R. D., Mamajek, E. E., and Naylor, T. (2014). Ages of Young Stars. *Protostars and Planets VI*, pages 219–241.

Song, I., Bessell, M. S., and Zuckerman, B. (2002). Lithium Depletion Boundary in a Pre-Main-Sequence Binary System. *ApJ*, 581:L43–L46.

Song, I., Zuckerman, B., and Bessell, M. S. (2012). New Members of the Scorpius-Centaurus Complex and Ages of Its Sub-regions. *AJ*, 144:8.

Stamatellos, D. and Whitworth, A. P. (2009). The properties of brown dwarfs and low-mass hydrogen-burning stars formed by disc fragmentation. *MNRAS*, 392:413–427.

Stauffer, J. R., Hartmann, L. W., Prosser, C. F., Randich, S., Balachandran, S., Patten, B. M., Simon, T., and Giampapa, M. (1997). Rotational Velocities and Chromospheric/Coronal Activity of Low-Mass Stars in the Young Open Clusters IC 2391 and IC 2602. *ApJ*, 479:776–791.

Strassmeier, K., Washuettl, A., Granzer, T., Scheck, M., and Weber, M. (2000). The Vienna-KPNO search for Doppler-imaging candidate stars. I. A catalog of stellar-activity indicators for 1058 late-type Hipparcos stars. *A&AS*, 142:275–311.

Teixeira, R., Ducourant, C., Chauvin, G., Krone-Martins, A., Song, I., and Zuckerman, B. (2008). SSSPM J1102-3431 brown dwarf characterization from accurate proper motion and trigonometric parallax. *A&A*, 489:825–827.

Tobin, J. J., Looney, L. W., Li, Z.-Y., Chandler, C. J., Dunham, M. M., Segura-Cox, D., Sadavoy, S. I., Melis, C., Harris, R. J., Kratter, K., and Perez, L. (2016). The VLA Nascent Disk and Multiplicity Survey of Perseus Protostars (VANDAM). II. Multiplicity of Protostars in the Perseus Molecular Cloud. *ArXiv e-prints*.

Tokovinin, A. (2005). Designation of Multiple-star Components. *Highlights of Astronomy*, 13:992.

Tokovinin, A. (2014a). From Binaries to Multiples. I. Data on F and G Dwarfs within 67 pc of the Sun. *AJ*, 147:86.

Tokovinin, A. (2014b). From Binaries to Multiples. II. Hierarchical Multiplicity of F and G Dwarfs. *AJ*, 147:87.

Tokovinin, A. (2015). Spectroscopic Subsystems in Nearby Wide Binaries. *AJ*, 150:177.

Tokovinin, A. and Kiyaeva, O. (2016). Eccentricity distribution of wide binaries. *MNRAS*, 456:2070–2079.

Tokovinin, A., Thomas, S., Sterzik, M., and Udry, S. (2006). Tertiary companions to close spectroscopic binaries. *A&A*, 450:681–693.

Toomre, A. (1964). On the gravitational stability of a disk of stars. *ApJ*, 139:1217–1238.

Torres, C. A. O., Quast, G., de La Reza, R., Gregorio-Hetem, J., and Lepine, J. R. D. (1995). Search for T Tauri Stars Based on the IRAS Point Source Catalog. II. *AJ*, 109:2146.

Torres, C. A. O., Quast, G. R., da Silva, L., de La Reza, R., Melo, C. H. F., and Sterzik, M. (2006). Search for associations containing young stars (SACY). I. Sample and searching method. *A&A*, 460:695–708.

Torres, C. A. O., Quast, G. R., Melo, C. H. F., and Sterzik, M. F. (2008). *Young Nearby Loose Associations*, volume 2, page 757.

Turon, C., Creze, M., Egret, D., Gomez, A., Grenon, M., Jahreiß, H., Requieme, Y., Argue, A. N., Bec-Borsenberger, A., Dommanget, J., Mennessier, M. O., Arenou, F., Chareton, M., Crifo, F., Mermilliod, J. C., Morin, D., Nicolet, B., Nys, O., Prevot, L., Rousseau, M., Perryman, M. A. C., and et al. (1993). Version 2 of the HIPPARCOS Input Catalogue. *Bulletin d'Information du Centre de Donnees Stellaires*, 43:5.

van Dessel, E. and Sinachopoulos, D. (1993). CCD astrometry and instrumental Delta-V photometry of wide visual double stars. III - Differential measurements of often observed southern pairs. *A&AS*, 100:517–520.

van Leeuwen, F. (2007). Validation of the new Hipparcos reduction. *A&A*, 474:653–664.

Vanderplas, J., Connolly, A., Ivezić, Ž., and Gray, A. (2012). Introduction to astroml: Machine learning for astrophysics. In *Conference on Intelligent Data Understanding (CIDU)*, pages 47 –54.

Vaytet, N., Audit, E., Chabrier, G., Commerçon, B., and Masson, J. (2012). Simulations of protostellar collapse using multigroup radiation hydrodynamics. I. The first collapse. *A&A*, 543:A60.

Viana Almeida, P., Santos, N. C., Melo, C., Ammler-von Eiff, M., Torres, C. A. O., Quast, G. R., Gameiro, J. F., and Sterzik, M. (2009). Search for associations containing young stars (SACY). II. Chemical abundances of stars in 11 young associations in the solar neighborhood. *A&A*, 501:965–971.

Vigan, A., Patience, J., Marois, C., Bonavita, M., De Rosa, R. J., Macintosh, B., Song, I., Doyon, R., Zuckerman, B., Lafrenière, D., and Barman, T. (2012). The International Deep Planet Survey. I. The frequency of wide-orbit massive planets around A-stars. *A&A*, 544:A9.

Voges, W., Aschenbach, B., Boller, T., Braeuninger, H., Briel, U., Burkert, W., Dennerl, K., Englhauser, J., Gruber, R., Haberl, F., Hartner, G., Hasinger, G., Kuerster, M., Pfeffermann, E., Pietsch, W., Predehl, P., Rosso, C., Schmitt, J. H. M. M., Truemper, J., and Zimmermann, H. U. (1999). VizieR Online Data Catalog: ROSAT All-Sky Bright Source Catalogue (1RXS) (Voges+ 1999). *VizieR Online Data Catalog*, 9010.

Voges, W., Aschenbach, B., Boller, T., Brauninger, H., Briel, U., Burkert, W., Dennerl, K., Englhauser, J., Gruber, R., Haberl, F., Hartner, G., Hasinger, G., Pfeffermann, E., Pietsch, W., Predehl, P., Schmitt, J., Trumper, J., and Zimmermann, U. (2000). VizieR Online Data Catalog: ROSAT All-Sky Survey Faint Source Catalog (Voges+ 2000). *VizieR Online Data Catalog*, 9029.

Vyssotsky, A. N. (1956). Dwarf M stars found spectrophotometrically . *AJ*, 61:201–213.

Wahhaj, Z., Liu, M. C., Nielsen, E. L., Biller, B. A., Hayward, T. L., Close, L. M., Males, J. R., Skemer, A., Ftaclas, C., Chun, M., Thatte, N., Tecza, M., Shkolnik, E. L., Kuchner, M., Reid, I. N., de Gouveia Dal Pino, E. M., Alencar, S. H. P., Gregorio-Hetem, J., Boss, A., Lin, D. N. C., and Toomey, D. W. (2013). The Gemini Planet-finding Campaign: The Frequency Of Giant Planets around Debris Disk Stars. *ApJ*, 773:179.

Walter, F. M. (1986). X-ray sources in regions of star formation. I - The naked T Tauri stars. *ApJ*, 306:573–586.

Walter, F. M., Brown, A., Mathieu, R. D., Myers, P. C., and Vrba, F. J. (1988). X-ray sources in regions of star formation. III - Naked T Tauri stars associated with the Taurus-Auriga complex. *AJ*, 96:297–325.

Wang, J., Fischer, D. A., Horch, E. P., and Xie, J.-W. (2015). Influence of Stellar Multiplicity On Planet Formation. III. Adaptive Optics Imaging of Kepler Stars With Gas Giant Planets. *ArXiv e-prints*.

Watson, M. G., Schröder, A. C., Fyfe, D., Page, C. G., Lamer, G., Mateos, S., Pye, J., Sakano, M., Rosen, S., Ballet, J., Barcons, X., Barret, D., Boller, T., Brunner, H., Brusa, M., Caccianiga, A., Carrera, F. J., Ceballos, M., Della Ceca, R., Denby, M., Denkinson, G., Dupuy, S., Farrell, S., Fraschetti, F., Freyberg, M. J., Guillout, P., Hambaryan, V., Maccacaro, T., Mathiesen, B., McMahon, R., Michel, L., Motch, C., Osborne, J. P., Page, M., Pakull, M. W., Pietsch, W., Saxton, R., Schwope, A., Severgnini, P., Simpson, M., Sironi, G., Stewart, G., Stewart, I. M., Stobbart, A.-M., Tedds, J., Warwick, R., Webb, N., West, R., Worrall, D., and Yuan, W. (2009). The XMM-Newton serendipitous survey. V. The Second XMM-Newton serendipitous source catalogue. *A&A*, 493:339–373.

Weinberger, A. J., Anglada-Escudé, G., and Boss, A. P. (2013). Distance and Kinematics of the TW Hydrae Association from Parallaxes. *ApJ*, 762:118.

Weinberger, A. J., Boss, A. P., Keiser, S. A., Anglada-Escudé, G., Thompson, I. B., and Burley, G. (2016). Trigonometric Parallaxes and Proper Motions of 134 Southern Late M, L, and T Dwarfs from the Carnegie Astrometric Planet Search Program. *ArXiv e-prints*.

Weintraub, D. A. (1990). A catalog of pre-main-sequence emission-line stars with IRAS source associations. *ApJS*, 74:575–594.

Welsh, W. F., Orosz, J. A., Carter, J. A., Fabrycky, D. C., Ford, E. B., Lissauer, J. J., Prša, A., Quinn, S. N., Ragozzine, D., Short, D. R., Torres, G., Winn, J. N., Doyle, L. R., Barclay, T., Batalha, N., Bloemen, S., Brugamyer, E., Buchhave, L. A., Caldwell, C., Caldwell, D. A., Christiansen, J. L., Ciardi, D. R., Cochran, W. D., Endl, M., Fortney, J. J., Gautier, III, T. N., Gilliland, R. L., Haas, M. R., Hall, J. R., Holman, M. J., Howard, A. W., Howell, S. B., Isaacson, H., Jenkins, J. M., Klaus, T. C., Latham, D. W., Li, J., Marcy, G. W., Mazeh, T., Quintana, E. V., Robertson, P., Shporer, A., Steffen, J. H., Windmiller, G., Koch, D. G., and Borucki, W. J. (2012). Transiting circumbinary planets Kepler-34 b and Kepler-35 b. *Nature*, 481:475–479.

Wenger, M., Ochsenbein, F., Egret, D., Dubois, P., Bonnarel, F., Borde, S., Genova, F., Jasniewicz, G., Laloë, S., Lesteven, S., and Monier, R. (2000). The SIMBAD astronomical database. The CDS reference database for astronomical objects. *A&AS*, 143:9–22.

White, R. J., Gabor, J. M., and Hillenbrand, L. A. (2007). High-Dispersion Optical Spectra of Nearby Stars Younger Than the Sun. *AJ*, 133:2524–2536.

Worley, C. E. and Douglass, G. G. (1996). The Washington Visual Double Star Catalog, 1996.0 (Worley+, 1996). *VizieR Online Data Catalog*, 1237:0.

Wright, E. L., Eisenhardt, P. R. M., Mainzer, A. K., Ressler, M. E., Cutri, R. M., Jarrett, T., Kirkpatrick, J. D., Padgett, D., McMillan, R. S., Skrutskie, M., Stanford, S. A., Cohen, M., Walker, R. G., Mather, J. C., Leisawitz, D., Gautier, III, T. N., McLean, I., Benford, D., Lonsdale, C. J., Blain, A., Mendez, B., Irace, W. R., Duval, V., Liu, F., Royer, D., Heinrichsen, I., Howard, J., Shannon, M., Kendall, M., Walsh, A. L., Larsen, M., Cardon, J. G., Schick, S., Schwalm, M., Abid, M., Fabinsky, B., Naes, L., and Tsai, C.-W. (2010). The Wide-field Infrared Survey Explorer (WISE): Mission Description and Initial On-orbit Performance. *AJ*, 140:1868–1881.

Xmm-Newton Survey Science Centre, C. (2013). VizieR Online Data Catalog: XMM-Newton Serendipitous Source Catalogue 3XMM-DR4 (XMM-SSC, 2013). *VizieR Online Data Catalog*, 9044.

Zacharias, N., Finch, C., Subasavage, J., Bredthauer, G., Crockett, C., Divittorio, M., Furguson, E., Harris, F., Harris, H., Henden, A., Kilian, C., Munn, J., Rafferty, T., Rhodes, A., Schultheiss, M., Tilleman, T., and Wieder, G. (2015). VizieR Online Data Catalog: URAT1 Catalog (Zacharias+ 2015). *VizieR Online Data Catalog*, 1329:0.

Zacharias, N., Finch, C. T., Girard, T. M., Henden, A., Bartlett, J. L., Monet, D. G., and Zacharias, M. I. (2012). VizieR Online Data Catalog: UCAC4 Catalogue (Zacharias+, 2012). *VizieR Online Data Catalog*, 1322:0.

Zacharias, N., Monet, D. G., Levine, S. E., Urban, S. E., Gaume, R., and Wycoff, G. L. (2005). VizieR Online Data Catalog: NOMAD Catalog (Zacharias+ 2005). *VizieR Online Data Catalog*, 1297:0.

Zhao, B., Li, Z.-Y., and Kratter, K. M. (2013). Effect of Magnetic Misalignment on Protobinary Evolution. *ArXiv e-prints*.

Zhu, Z., Hartmann, L., Nelson, R. P., and Gammie, C. F. (2012). Challenges in Forming Planets by Gravitational Instability: Disk Irradiation and Clump Migration, Accretion, and Tidal Destruction. *ApJ*, 746:110.

Zinnecker, H. and Preibisch, T. (1994). X-ray emission from Herbig Ae/Be stars: A ROSAT survey. *A&A*, 292:152–164.

Zuckerman, B., Rhee, J. H., Song, I., and Bessell, M. S. (2011). The Tucana/Horologium, Columba, AB Doradus, and Argus Associations: New Members and Dusty Debris Disks. *ApJ*, 732:61.

Zuckerman, B., Song, I., and Bessell, M. S. (2004). The AB Doradus Moving Group. *ApJ*, 613:L65–L68.